SUNNICA ENERGY FARM

EN010106

Applicant's Response to BESS Safety Issues Raised During ISH3

Planning Act 2008

Infrastructure Planning (Examination Procedure) Rules 2010



16 December 2022
Version number: 00

Planning Act 2008

The Infrastructure Planning (Examination Procedure) Rules 2010

Sunnica Energy Farm

Applicant's Response to BESS Safety Issues Raised During ISH3

Planning Inspectorate Scheme Reference	EN010106
Application Document Reference	EN010106/APP/8.69
Author	Sunnica Energy Farm Project Team

Version	Date	Status of Version
Rev 00	16 December 2022	Submitted Version

1. Introduction

1.1.1 This document, and associated Annexes, sets out the Applicant's response to battery safety energy storage system (BESS) safety issues raised at Open Floor Hearings, Issue Specific Hearings and comments on applicant's responses to Examining Authority's First Written Questions (ExQ1).

2. Summary of Applicant's Response

2.1.1 As outlined by Paul Gregory, on behalf of the Applicant at Issue Specific hearing 3: the Outline Battery Fire Safety Management Plan (OBFSMP) is not a standard document that is produced for most BESS projects. The OBFSMP is a preliminary analysis of safety issues outlining how they will be addressed at the detailed design stage. The document was originally drafted in 2020 and amended in consultation with the Fire & Rescue Service (FRS) before publication in 2021. Mr Gregory's peer review for the Applicant established that whilst the content and methodology were generally sound based on information known at the time of original drafting, a significant volume of new safety codes, standards and testing requirements for BESS systems will come into force (2023-2024) between the grant of any DCO and the detailed design process which will take place prior to the commencement of development. The revised OBFSMP establishes a safety framework, commitments to BESS codes, standards and testing requirements, engagement with FRS and all relevant organisations and identifies key considerations that are required to be taken into account for the BESS design. It also establishes a framework for the development of an emergency response plan.

2.1.2 Mr Gregory's peer review recommends that the Applicant commits to annual updates of the OBFSMP to integrate the latest BESS standards and codes to ensure that by the detailed design stage the highest safety standards are enshrined. This will have direct relevance for the current safety standards and Risk Mitigation Method content. New full scale BESS fire and explosion tests are already being conducted in North America and UL 9540A 5th Edition testing requirements will be published in early 2023. As with previous new BESS testing programs, it is Mr Gregory's expectation that lessons learned during early testing leads to iterative improvements to protocols, methodology and data capture techniques over a 12-18 month period. Mr Gregory has no doubt that a BESS system design tested in 2023-24 will have undergone a far more rigorous testing and validation program than a BESS system tested in 2021-22.

2.1.3 Due to time constraints at the hearing there was not time to cover emergency response planning (ERP) issues for Sunnica. Paul Gregory, on behalf of the Applicant, sits on the ISO / UL BESS first responders working group to establish an ISO template for first responder incident planning. As stated in the revised OBFSMP an emergency response plan (ERP) will be drafted based on local, national and international input and best practice recommendations, including CRFS, SFRS, UK National Fire Chiefs Council, NFPA 855 and Electric Power Research Institute (EPRI). An ERP should be developed to facilitate effective and safe emergency response and should include:

(1) How the fire service will be alerted and incident communications & monitoring capabilities

(2) Facility description, including infrastructure details, operations, number of personnel, and operating hours

(3) Site plan depicting key infrastructure:

(1) Site access points, internal roads, agreed access routes, observation points, turning areas, etc

(2) Firefighting facilities (water tanks, pumps, booster systems, fire hydrants, fire hose reels etc)

(3) water supply locations & capacity

(4) drainage and water capture design & locations

(4) Up-to-date contact details for facility personnel, and any relevant off-site personnel that could provide technical support during an emergency.

(5) Site evacuation procedures.

(6) Emergency procedures for all credible hazards and risks, including building, infrastructure and vehicle fire, wildfires, impacts on local respondents, impacts on transport infrastructure

(7) The operator should develop a post-incident recovery plan that addresses the potential for reignition of ESS and de-energizing the system, as well as removal and disposal of damaged equipment.

2.1.4 There is an expectation that templates will become more standardized during 2023-24. EPRI is producing a new template and there is a UL / ISO working group to develop a BESS first responder ISO standard. The Sunnica ERP drafted at the detailed design stage will integrate content referencing UK and International best practice. A required ERP content framework, which is secured through the OBFSMP, will be agreed with the FRS and relevant authorities before the detailed design stage and a template will be produced during an annual OBFSM update (2023 or 2024).

2.1.5 A useful BESS fire & explosion testing glossary is included (Annex 1) which clarifies terminology and provides a brief insight into the latest fire & explosion testing protocols.

2.1.6 Examples of new or upcoming revisions to BESS standards and codes are included (Annex 2). These standards will be reviewed and integrated into the OBFSMP. Key safety areas included are:

a. Cybersecurity

b. BMS standards

c. Standards for BESS best practice from installation through to decommissioning

d. BESS enclosure design and construction

e. New BESS fire & explosion testing

f. IEC revisions to BESS test protocols and acceptance testing protocols

g. 12 new IEC standards for Energy Storage Systems

2.1.7 As mentioned during the hearing, significant resources are currently being devoted to BESS system research and testing. Key BESS fire safety improvements expected during the next two years are mapped out in the EPRI BESS Fire Safety Roadmap (Annex 3). The document provides useful insights into risk analysis techniques for BESS and specific safety solutions which will significantly reduce BESS incident risks and consequences. This information clarifies the Applicant's position that BESS design safety concerns will be better addressed once the raft of new codes, standards and test programs are fully embedded and understood.

2.1.8 EPRI BESS working group has identified 9 key areas for hazard mitigation of common root causes – prevention is the top priority with many new standards and tools in development:

1. Cell abuse tolerance - UL 1973, UL 9540A, 3rd party fire & explosion testing

2. Electrical controls (SCADA, EMS, BMS) - IEEE 1815, IEEE 2686, IEEE 2688

3. Thermal controls (module cooling system, HVAC)

4. Gas venting designs (module, rack, BESS enclosure) - UL 9540A, 3rd party fire & explosion testing, NFPA 69

5. Fire suppression system – UL 9540A, 3rd party fire & explosion testing

6. Deflagration protection – NFPA 68, UL 9540A, 3rd party fire & explosion testing

7. Response plans – NFPA 855 (2023), National Fire Chiefs Council (2023), EPRI (2023)

8. System design & FMEA (Failure modes & effects analysis) - IEEE 2962, EPRI template, Independent Fire Protection Engineer review

9. BESS system certification – UL 9540, IEC 62933

2.1.9 The Applicant considers the safety of first responders to be a top priority. The Sunnica site indicative plans released with the revised OBFSMP [REP2-032] illustrate key FRS emergency response requirements i.e. observation points, ingress and egress routes, bunded lagoons, water tanks, etc. A variety of issues were raised in representations, Annex 4 contains materials which answer many of these queries. Materials cover the latest strategies (2022) for BESS incident response and management from the International Association of Fire Chiefs, UL and New York Fire Department who are at the forefront tactical research and training. There are additional resources and training programs being developed for BESS incident response which will also be shared with the Sunnica Fire & Rescue Service teams and integrated into the ERP documentation. The Applicant will directly engage with the UK National Fire Chiefs Council to ensure that response planning and incident management training content meets with their approval. Site familiarisation and training drills will be a key part of this shared learning and engagement process. Subject Matter Experts (SMEs) who can assist first responders with BESS data analysis and incident response tactics and

decommissioning are usually provided by the BESS integrator or operator, all key stakeholders will have an opportunity to evaluate the role SMEs will play in incident response at the detailed design stage.

2.1.10 The Applicant has collated a portfolio of illustrative materials to expand on subjects covered in the hearing. As stated at the hearing, much of this type of data is proprietary but a range of free source materials has been provided to showcase the type of BESS hazard and risk analysis and consequence modelling which will take place at the detailed design stage. It should be noted that BESS HMEA and Hazard mitigation analysis are usually provided by the BESS integrator. All hazard and risk analysis reports and consequence modelling will be reviewed by an independent Fire Protection Engineer. The Applicant wishes to re-emphasise that it is not possible to conduct this type of risk assessment and consequence modelling before the BESS detailed design stage. A separate response clarifying the purpose and methodology of the Appendix 16D Emissions document has been provided within the Written Summary of Applicant's Oral Submissions at the ISH3 [EN010106/APP/8.58].

2.1.11 BESS example materials include:

a. FMEA (Failure Modes and Effects Analysis) and BESS Hazard Mitigation analysis (Annex 5)

b. Toxic gas emission consequence modelling (Annex 6). Data covers actual BESS system emissions and references a range of battery toxic gas studies.

c. Fire & explosion modelling (Annex 7)

d. Community risk assessment and modelling (Annex 8)

e. Hazard Consequence Analysis (Annex 9)

2.1.12 As discussed at the hearing, generalisations about battery chemistry are not the basis to form any specific safety conclusions without rigorous testing of a BESS system; from cell to installation level assessing a variety of failure modes. Two recent papers covering battery separator materials and cathode coating materials are included (Annex 10), giving an insight into how thermal runaway reactions and gas production can vary within chemistry types even when cells are at identical form factors at identical States of Charge (SOC).

2.1.13 The final range of materials covers battery system fire and explosion test programs and protocols. The Applicant has reviewed a variety of responses which express concerns about BESS system safety questioning how fire and explosion risks can be quantified and mitigated. Much of this type of information is highly proprietary but free source data has been collated to help educate interested parties on how this process has evolved and is rapidly improving:

a. UL 9540A testing data (Annex 11) – a sample report template and outdoor container testing with free burn and suppression system data is provided. UL built the battery systems themselves to allow for free sharing of data. The container testing presentation contains extremely useful data on detection, fire suppression, firefighting tactics, gas emissions, deflagration / explosion safety.

b. Tesla BESS system testing information (Annex 12) shows how Tesla was a pioneer in the development of test programs to sit alongside UL 9540A to assess fire and explosion risks, establish equipment spacing distances through free burn testing and to accurately quantify toxic gas emissions at significant scale (rack level)

c. Annex 13 showcases the ground-breaking US Navy fire and mitigation test program and resulting battery system design hazard analyses and validation testing program. These tools and protocols are being integrated into the latest BESS testing, validation, and certification standards (battery OEM, UL, NFPA 855 3rd party fire & explosion testing). The fire and mitigation test report is the most comprehensive analysis of a significant range of lithium-ion battery fire & explosion hazards, toxic gas production across chemistries, mitigation & suppression solutions for a range of application produced to date (albeit 70% of results were redacted for public consumption due to data proprietary issues). These materials showcase how BESS system hazards can be accurately quantified and effectively mitigated.

Annex 1 BESS fire & explosion testing glossary

Annex 2 New or upcoming revisions to BESS standards and codes

Annex 3 EPRI BESS Fire Safety Roadmap

Annex 4 Latest strategies (2022) for BESS incident response and management

Annex 5 FMEA (Failure Modes and Effects Analysis) and BESS Hazard Mitigation analysis

Annex 6 Toxic gas emission consequence modelling

Annex 7 Fire & explosion modelling

Annex 8 Community risk assessment and modelling

Annex 9 Hazard Consequence Analysis

Annex 10 Battery separator materials and cathode coating materials

Annex 11 UL 9540A testing data

Annex 12 Tesla BESS system testing information

Annex 13 US Navy fire and mitigation test program

Annex 1 BESS fire & explosion testing glossary

BESS fire & explosion risk glossary + BESS testing



December '22

1

FIRE AND EXPLOSION HAZARD GLOSSARY

Fires and gas explosions require fuel, oxygen & ignition source (heat or spark). Flammable gases generated across all LIB chemistries generally have autoignition (ignition from heat) temperatures in 400-800C range

- **Volatile Organic Compounds (VOCs)** generally carbonate based organic electrolyte solvents: Ethylene Carbonate (EC), Diethyl Carbonate (DEC), Dimethyl Carbonate (DMC), Ethyl Methyl Carbonate (EMC), Propylene Carbonate (PC) – autoignition temperatures typically 400-500C
- **Electrolyte:** Lithium salts e.g. Lithium hexafluorophosphate, dissolved in organic solvents
- **Explosion:** Sudden violent release of energy usually accompanied by the genera ion of high temperatures and release of high-pressure gas. Types include: **Deflagration**; subsonic propagation of the combustion zone – **Detonation**; supersonic propagation of the combustion zone
- **Overpressure**: Transient air pressure, such as the shock wave from an explosion which is greater than the surrounding atmospheric pressure.
- **Lower flammability limit (LFL)**: Minimum concentration of fuel that can support a flame; fuel/air mixtures below the LFL are too lean to propagate a flame.
- **Upper flammability limit (UFL):** Maximum concentration of fuel that can support a flame; fuel/air mixtures above the UFL are too rich to propagate a flame.
- **Stoichiometric concentration:** Concentration where fuel is balanced wi h the oxygen in the available air to allow for complete combustion. The stoichiometric concentration is between the LFL and UFL.
- **Enclosure:** for BESS applica ions enclosure refers to a confined space i.e. battery module, an enclosed rack, a container, a room, or an entire building. Sunnica OBFSM uses the terminology **container** for BESS structure

2

Battery Cell glossary

Cell: single lithium-ion battery
Secondary cell: another term for lithium-ion cell i.e. it is rechargeable
Electrodes: a) Cathode (dictates voltage) – positive electrode typically aluminium foil b) Anode - negative electrode typically copper foil
Electrode designs (sheet area dictates capacity): jelly roll, flat wound jelly roll, flat plate stacked structure (book / sheet)
Electrolyte: typically lithium salt dissolved in organic solvents
Typical Cathode coating materials i.e. "chemistry": Nickel, Iron, Manganese, Cobalt, Aluminium, Lithium Oxide
Anode coating materials: alloys i.e. tin, magnesium, aluminium, graphite, lithium titanate, silicon, metal oxides i.e. iron, cobalt, nickel, zinc
Cathode coating materials: alumina oxide, polymers such as PEDOT / PANI / PVP, zirconium dioxide, magnesium oxide, titanium dioxide, zinc oxide, silicon dioxide, cerium oxide, iron oxide, iron sulphate, lithium fluoride, magnesium difluoride, zirconium tetrafluoride, iron trifluoride, lithium phosphate, manganese phosphate, iron phosphate, aluminium phosphate, nickel phosphate, lithium aluminate, lithium titanate, lithium zirconate,
Separator materials: polymers i.e. Polypropylene and / or polyethylene, ceramic coating on polymer membrane

3

Cell level failure glossary

Thermal runaway: rapid internal heat generation

Cell types: cylindrical, pouch, prismatic

Failure responses:
1. Venting / Off gassing electrolyte – flammable & toxic
2. Burning – significant variations in overpressure and flame speeds
3. Deflagration / explosion

Impacts on failure responses:
1. Chemistry (this includes all internal cell materials – significant variations within same chemistry)
2. Cell construction: cell type, vent design (pouch cells no vent), cell case materials, cell capacity, internal design structure
3. State of charge (SOC): significantly influences failure response

Cell type construction typical behaviours:
1. Cylindrical cell – pressure vessel behaviours (significant overpressures can be generated)
2. Pouch cell – flamethrower behaviour (electrolyte ejected as liquid / vapour mixture)
3. Prismatic cell – pressure vessel behaviours (significant overpressures can be generated)

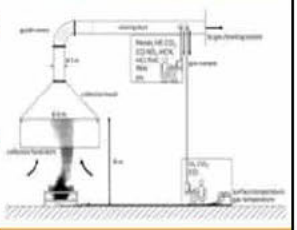
4

Gas & particle quantification at BESS cell & module level

- In internal battery OEM & UL 9540A testing @ cell & module level both **battery gas and particle production defined**.

- Total volume gas production (gas chromatography) and FTIR (Fourier Transform Infrared Spectroscopy) testing (PPM) for organic compounds (toxic gases):
- Carbon Monoxide
- Carbon Dioxide
- Hydrogen
- Sulphur Dioxide
- Nitrogen Oxides
- Hydrogen Fluoride, Hydrogen Cyanide, Hydrogen Chloride
- Hydrocarbon gases (THC content)
- PAHs, etc.





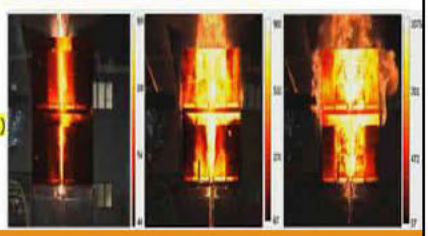
Particle capture by XRF (X-ray fluorescence) analysis checks for – particle size range 10 - 0.5 Microns:
- Phosphorus, Aluminium, Nickel, Silicon, Calcium, etc.

5

Testing multi-module / part rack in representative scale BESS enclosure

BESS multi-module / part rack testing data capture

- Cell propagation rates
- Average module temperatures during TR events
- Overpressure data
- Module venting performance evaluation
- Establish worst case scenario for cell TR initiation position resulting in fastest module-to-module propagation times
- Worst case scenario for cell TR initiation position for quickest cell-to-cell propagation times within the initiating module often varies to cell initiation position for fastest module-to-module propagation times
- Arcing observations
- Electrical integrity performance
- Passive protection design performance
- Active cooling design performance
- Assess BESS structural integrity problems (deflagrations, flaming through walls, flaming through roof)
- Assess BESS enclosure venting / exhaust design
- Module and battery rack heat retention data
- Timings for modules to be fully consumed
- Rack heat flux data
- BESS heat flux data
- BESS detection products evaluation (Pre TR/during TR/post TR)
- Suppression system evaluation vs free burn data
- Establish safe decommissioning protocols



6

5th Edition UL 9540A should be published early 2023

NFPA 855 (2023) Fire & Explosion testing requirement

UL developing new protocols to integrate into UL 9540A

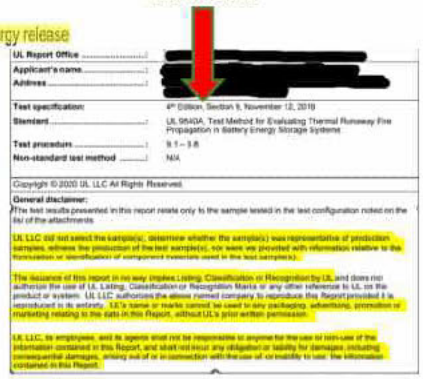
Enclosure Explosion Safety Test Method Development

UL clamping down on UL 9540A test gaming - China lab test data not accepted by many AHJs and insurers

Methodology under development to evaluate explosion hazards:

- ESS enclosure rupture
- Blast waves and projectiles
- Direction of energy release





UL Report Office .....
Applicant's name.....
Address .....

Test specification: 4th Edition, Section 9, November 12, 2019
Standard .....: UL 9540A, Test Method for Evaluating Thermal Runaway Fire Propagation in Battery Energy Storage Systems
Test procedure .....: 9.1 – 9.6
Non-standard test method .....: N/A

Copyright © 2020 UL LLC All Rights Reserved.

General disclaimer:
The test results presented in this report relate only to the sample tested in the test configuration noted on the list of the attachments

UL LLC did not select the sample(s), determine whether the sample(s) was representative of production samples, witness the production of the test sample(s), nor were we provided with information relative to the manufacture or specification of component materials used in the test sample(s).

The issuance of this report in no way implies Listing, Classification or Recognition by UL and does not authorize the use of UL Listing, Classification or Recognition Marks or any other reference to UL on the product or system. UL LLC authorizes the above named company to reproduce this Report provided it is reproduced in its entirety. UL's name or marks cannot be used in any packaging, advertising, promotion or marketing relating to the data in this Report, without UL's prior written permission.

UL LLC, its employees, and its agents shall not be responsible to anyone for the use or non-use of the information contained in this Report, and shall not incur any obligation or liability for damages, including consequential damages, arising out of or in connection with the use of, or inability to use, the information contained in this Report.

7

NFPA 855 (2023) explosion detection and prevention recommendations

NFPA 855 (2023) detection and explosion prevention stipulations

NFPA 855 - Ventilation and Detection

- Exhaust Ventilation
  - 1ft³/min/ft²
  - Designed to keep flammable gasses under 25% of LFL
  - Exhaust away from openings

4.9



- Smoke and Fire Detection
  - Gas detection activates ventilation
  - Smoke detection per NFPA 72

4.10

NFPA.ORG | © National Fire Protection Association. All rights reserved.

8

NFPA 855 explosion control design and testing options

US DOE summary NFPA 855 (2023) explosion control focus

Pacific Northwest NATIONAL LABORATORY

NFPA 855 Explosion Control

Three options for meeting requirement in room, building, cabinets*, or walk-in enclosures:

1. NFPA 68 – Deflagration Venting.
   - Blow-out panels to protect structure from explosion based on max gas production in cell tests. **Explosion risks remain.**
2. NFPA 69 – Deflagration Prevention.
   - Exhaust system designed to keep below 25% of LEL in area.
3. Performance Based – Where Large Scale Fire Test has shown that no pressure waves will occur and no projectiles can be ejected.







PNNL-SA-171280

*TIA 29-2 Published 8/21 adds cabinets to requirements

1

9

Annex 2 New or upcoming revisions to BESS standards and codes

BESS codes & standards update



1

UL changes 2022 - 2023

UL Standards and testing recently updated and / or undergoing revision

UL 1973, 3rd Edition (2022):

- 2022 revisions include more rigorous abuse testing
- More revisions likely in the near future

UL 9540, 2nd Edition (2020):

- Revision underway – 20 revisions agreed – further revisions to be agreed before the end of 2022
- 3rd Edition to be published in 2023

UL 9540A, 4th Edition (2019):

- 4th edition testing at cell, module, unit level is **minimum requirement** - protocols & gas capture were not adequate in earlier test editions
- Test results must be provided for the **specific cell and module used** in the BESS system
- **Multiple proposals for revision are being considered** and preliminary review was conducted in November 2022
- 5th Edition I kely to be published @ end of January 2023

2

IEC changes 2023 - 2024

IEC Standards undergoing revision (12 standards under development)

IEC 62933-5-2 (2020):

- New edition will be published in 2023
- **Test method protocol clarifications / amendments**
- **Greater clarity on when Type / FAT / SAT testing should be conducted**

IEC 62933-5-3 (2020):

- New edition will be published in 2023
- Prospective changes will be shared January 2023

IEC 62933 – standard development:

- **12 standards in development for ESS**
- Likely to play a greater role in Global EES requirements moving forward
- Unclear whether there will be a greater integration with UL standards

3

IEEE standards 2023 - 2024

- **IEEE 1679.1 (2017): Guide for the Characterization and Evaluation of Lithium-Based Batteries in Stationary Applications**
- Active working group to update document - document references existing standards & regulatory requirements updates likely to be major revisions
- **IEEE 1815 (2012): Standard for EPS Communications-Distributed Network Protocol (DNP3)**
- Standard specifies the DNP3 protocol structure, functions, cyber security features and interoperable application options at subset levels, which defines the functionality implemented in each device. This is a useful reference for ES systems that will communicate with utility SCADA using DNP3.0 protocol.
- **IEEE P2686: Battery Management Systems in Energy Storage Applications**
- New standard likely to be published in 2023 - this recommended practice includes information on the design, installation, and configuration of battery management systems (BMS) in stationary applications, including both grid-interactive, standalone cycling and standby modes. The document covers all battery technologies using a BMS, with added emphasis on lithium-ion and flow batteries.

4

IEEE standards 2023 - 2024

- **IEEE P2688: Recommended Practice for Energy Storage Management Systems (ESMS) in Energy Storage Applications**
- New standard in development provides reference for ESMS designers and integrators regarding best practices in ESMS development and deployment. ESMS covers a range of systems: (PMS) power-plant controllers, (PPC) microgrid controllers, (EMS) energy management systems. The document includes software functions and hardware capabilities of ESMS relating to the operation of energy storage systems in grid applications.
- **IEEE P2962: Recommended Practice for Installation, Operation, Maintenance, Testing, and Replacement of Lithium-ion Batteries for Stationary Applications**
- New standard in development seeks to provide guidance on installation, testing, and O&M for stationary lithium-ion ESS. References KEPIC 1400 from Korea + IEEE standards
- **IEEE P3189: Recommended Practice for the Design and Construction of Prefabricated and Modular Outdoor Battery Enclosures**
- New standard in development covers the design and construction of prefabricated and modular enclosures for diverse environments, both indoors and outdoors. These enclosures house batteries and related equipment that may include chargers, inverters, distribution panels, protective devices, and ancillary systems.

5

NFPA 855 (2023) edition

- **NFPA 855 (2023) -** key areas for BESS projects:
- **Fire & gas detection**
- **EMS + system monitoring requirements**
- **ERP drafting**
- **Fire & explosion testing**
- **Fire suppression system guidelines**

Fire & explosion testing - explosion modelling from cell level test data for BESS deflagration design (NFPA 68) should not be accepted:

1. 3rd Party Fire & Explosion testing referenced in new code addresses key problems with current UL 9540A testing
2. Testing already conducted by Fluence & Powin to this scale – this involved TR module initiation (all cells). Test aims were to a) establish deflagration threats b) demonstrate BESS design structural integrity c) confirm / establish safe spacing to adjacent BESS enclosures / PCS equipment
3. Fire suppression system testing performance should be evaluated against this baseline fire & explosion testing free burn data
4. UL 9540A testing changes scheduled for publication January 2023 are likely to compliment this approach and stipulate that BESS enclosure designs and fire suppression systems must be subjected to full scale testing

6

Annex 3 EPRI BESS Fire Safety Roadmap

EPRI

BATTERY STORAGE FIRE SAFETY ROADMAP

EPRI's Immediate, Near, and Medium-Term Research Priorities to Minimize Fire Risks for Energy Storage Owners and Operators Around the World



July 2021



Battery Storage Fire Safety Roadmap: *EPRI's Immediate, Near, and Medium-Term Research Priorities to Minimize Fire Risks for Energy Storage Owners and Operators Around the World*

TABLE OF CONTENTS

Executive Summary 2
BACKGROUND 2
EPRI'S EXPERTISE IN ENERGY STORAGE SAFETY 3
SAFETY ROADMAP: RESEARCH TOPICS 4
BATTERY STORAGE FIRE SAFETY ROADMAP:
EPRI RESEARCH PRIORITIZATION 5
Group 1, Immediate Actions: High-Impact,
Low-Effort for Exisitng Systems 5
Group 2, Near-Term Actions: High-Impact,
Moderate Effort for Systems in Development 6
Group 3, Medium-Term Actions: System Design and Research Guidance for Future Systems 6
Remaining Ungrouped Topics 7
CONCLUSIONS 7
APPENDIX: EPRI BATTERY STORAGE FIRE SAFETY ROADMAP – DETAILED TOPIC DESCRIPTIONS 8
TOPIC: ETD – EXAMPLE TASK DESCRIPTION 8
RESPONSE PLANS 9
DESIGN AND REVIEW TOOLS 10
RESEARCH AND TECHNOLOGY DEVELOPMENT 12

EXECUTIVE SUMMARY

This roadmap provides necessary information to support owners, operators, and developers of energy storage in proactively designing, building, operating, and maintaining these systems to minimize fire risk and ensure the safety of the public, operators, and environment.

The investigations described will identify, assess, and address battery storage fire safety issues in order to help avoid safety incidents and loss of property, which have become major challenges to the widespread energy storage deployment. The research topics identified in this roadmap should be addressed to increase battery energy storage system (BESS) safety and reliability. The roadmap processes the findings and lessons learned from eight energy storage site evaluations and meetings with industry experts to build a comprehensive plan for safe BESS deployment.

BACKGROUND

Owners of energy storage need to be sure that they can deploy systems safely. Over a recent 18-month period ending in early 2020, over two dozen large-scale battery energy storage sites around the world had experienced failures that resulted in destructive fires. In total, more than 180 MWh were involved in the fires. For context, Wood Mackenzie, which conducts power and renewable energy research, estimates 17.9 GWh of cumulative battery energy storage capacity was operating globally in that same period, implying that nearly 1 out of every 100 MWh had failed in this way.[1]

For up-to-date public data on energy storage failures, see the EPRI BESS Failure Event Database.[2] The *Energy Storage Integration Council (ESIC) Energy Storage Reference Fire Hazard Mitigation Analysis* (ESIC Reference HMA),[3] illustrates the complexity of achieving safe storage systems. It shows the large number of threats and failure pathways that may lead to the central hazard of thermal runaway as well as the large number of possible mitigations available in the pursuit of safe outcomes. To further compound the difficulty, codes and standards have provided new tools and procedures, but they are still trying to catch up with a fast-growing industry deploying multiple chemistries and exploring a multitude of configurations. How can operators of energy storage be certain that the systems they have deployed or will deploy are safe, considering today's best practices?

1 Wood McKenzie, Energy Storage Data Hub [redacted]

2 [redacted]

3 [redacted]



Battery Storage Fire Safety Roadmap: *EPRI's Immediate, Near, and Medium-Term Research Priorities to Minimize Fire Risks for Energy Storage Owners and Operators Around the World*

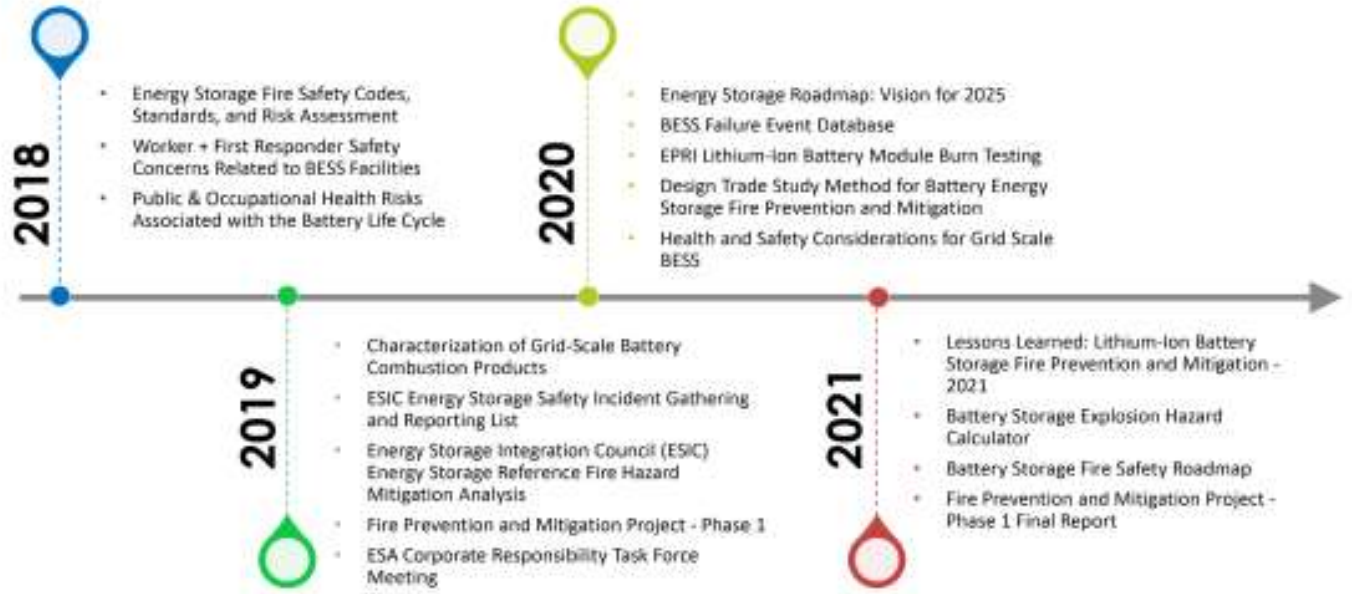


Figure 1 – EPRI energy storage safety research timeline

EPRI'S EXPERTISE IN ENERGY STORAGE SAFETY

For several years, EPRI has conducted a significant effort that addresses battery fire safety and related health, safety, and environmental issues. This work, conducted in collaboration with member utilities, battery solution providers, and other stakeholders, has facilitated the development of best practices and standards, with the aim of ensuring that needs for energy storage can be met in a safe and reliable way.

In 2019, EPRI began the Battery Energy Storage Fire Prevention and Mitigation – Phase 1 research project, convened a group of experts, and conducted a series of energy storage site surveys and industry workshops to identify critical research and development (R&D) needs regarding battery safety. Five utilities deploying the most energy storage in the world joined in the effort and gave EPRI access to their energy storage sites and design data as well as safety procedures and guides. In 2020 and 2021, eight BESS installations were evaluated for fire protection and hazard mitigation using the ESIC Reference HMA.

Each survey included a site review, workshop, and evaluation report comprising the following tasks:

- Site review:
  - Review specifications, design drawings, performance data, and operations and maintenance documentation provided by the site host participant.
  - Document important safety-relevant features (and lack thereof).
- Site workshop:
  - Discuss the Hazard Mitigation Analysis with the site engineering and operations personnel.
  - Document outcomes of the discussion, answering the following questions: Which threats, barriers, and consequences apply to this site? How do they apply? Why do they apply? What recommendations could improve the safety of system operations?
- Site evaluation report:
  - Draft the site evaluation report for member review.
  - Revise and finalize the evaluation report.



At the sites analyzed, system size ranges from 1–8 MWh, and both nickel manganese cobalt (NMC) and lithium iron phosphate (LFP) chemistries are represented. All systems except one are installed in a container or in a dedicated building that functions similarly and appears similar to a container. Six of the eight systems are either 1) installed in locations where all nearby areas have controlled access and are dedicated to the purpose of electrical power production and distribution, or 2) located in extremely remote areas.

For each site, EPRI analyzed safety measures using nine broad categories, as illustrated in Figure 2.

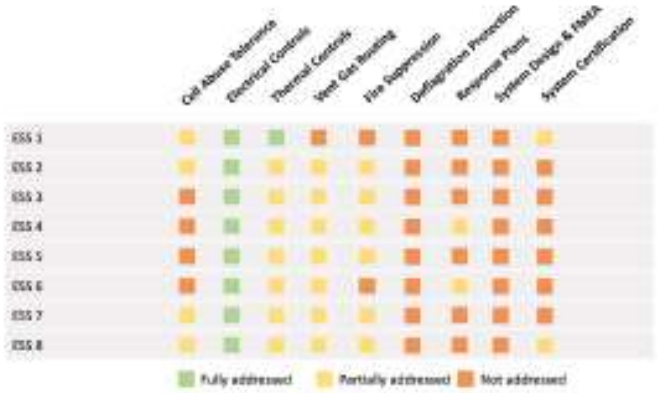


Figure 2 – Summary of system safety barriers at surveyed sites

Electrical controls were found to be the safety measure most commonly present across the eight surveyed sites. Cell abuse tolerance and thermal controls were present, but their level of effectiveness was hard to gauge from the available data. Similarly, it was not possible to assess the level to which system design efforts and failure modes and effects analysis (FMEA) addressed safety. Response plans were another area where there was minimal available data and an indication of insufficient levels of safety.

SAFETY ROADMAP: RESEARCH TOPICS

In order to develop and deploy energy storage safely, many tools and resources are needed. After compiling the results of the industry workshops and site surveys, 22 research topics were identified as industry needs. These have been categorized into four groups: 1) special topics, 2) response plans, 3) design tools, and 4) technology development, as shown in Table 1. A clickable link to the detailed description of each topic is provided in the right column.

Table 1 – Battery Storage Fire Safety Roadmap research topics

Category	Topic	Link
ST: Special Topics	ST1 Addressing the common explosion hazard	ST1
RP: Response Plans	RP1 Response plan guidelines for existing and future BESS	RP1
	RP2 Response plan standardization	RP2
	RP3 Hazard state identification and communication	RP3
	RP4 Contamination management	RP4
DT: Design Tools	DT1 Improving availability and application of 9540A testing	DT1
	DT2 Inclusion of gas prediction and deflagration protection tools in BESS design processes	DT2
	DT3 Expansion of 9540A testing to address statistical variation and multiple cell failures	DT3
	DT4 Guidelines for selection and design of suppression systems	DT4
	DT5 Standardized electrical controls reporting	DT5
	DT6 Failure modes and effects analysis (FMEA) guidance	DT6
	DT7 Integrated system design tools	DT7
	DT8 Adequacy and inclusion of thermal runaway propagation prediction tools in BESS design processes	DT8
TD: Technology Development	TD1 Robust electrical controls	TD1
	TD2 Detection of state of thermal reaction	TD2
	TD3 Detection of future thermal runaway events	TD3
	TD4 Detection of deflagration and toxicity risks	TD4
	TD5 Limitation of propagation using thermal controls	TD5
	TD6 Minimization of thermal runaway using thermal controls	TD6
	TD7 Safe cells with no thermal runaway potential	TD7
	TD8 Thermal runaway vent gas routing management during failure	TD8
	TD9 Ignition control	TD9



These research topics were then evaluated for their relative impact on safety, the effort required to address them, and the time horizon for the work. A graphical representation of the topics was developed for visualization and prioritization. To orient the reader to that overview chart, Figure 3 shows the methodology of representation with estimated potential improvement to safety of a single system (the size of the circle), estimated required effort to complete (Y-axis), and time frame of applicability (X-axis).

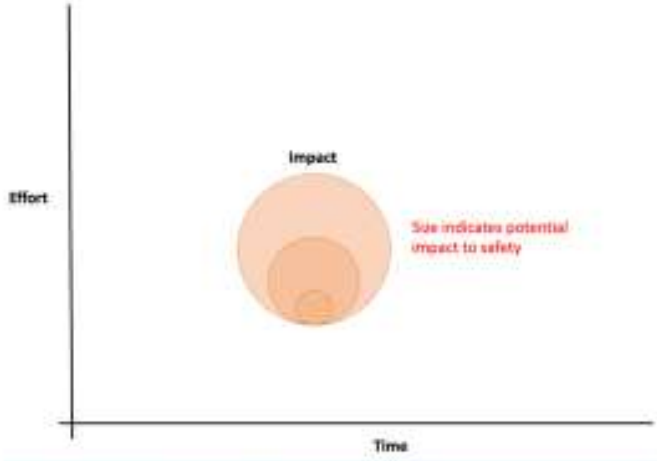


Figure 3 – Orientation guide for overview chart

All topics were plotted using the methodology in Figure 4. Note that the required effort to complete a task can vary largely, depending on who is tasked with the work. For example, select automotive companies that have invested many years in pursuing propagation-resistant lithium ion battery packs may more efficiently complete the task of preventing propagation in stationary systems than BESS integrators just entering the market. Large circles in the lower left corner of the plot represent the best return on investment, as this will significantly impact all existing and future systems for minimal investment.

These battery storage safety topics form the broad landscape of R&D efforts that need to be undertaken to address the safety concerns identified by EPRI's research. The type of effort and engagement required from stakeholders to address those challenges can further be used to determine the actors and organizations best positioned to advance the state of the art.

BATTERY STORAGE FIRE SAFETY ROADMAP: EPRI RESEARCH PRIORITIZATION

The selection and prioritization of these topics for EPRI's planned research have been evaluated based on EPRI's specific role and position within the industry. Some of the identified topics could be beneficially pursued by other organizations such as vendors, original equipment manufacturers (OEMs), Department of Energy (DOE) national laboratories, and other entities.

There are effectively two principal near-term recommendations that have arisen from EPRI's energy storage safety research and roadmapping effort:

- Address the common explosion hazard present in many existing systems.
- Develop the knowledge and tools necessary to conduct improved system-level safety analyses prior to system installation.

Both are attainable in the relatively near term and will provide significant improvements to the safety of present and future storage systems, which will enable continued rapid growth of the industry.

Of the 22 topics, 11 have been identified as priorities for future EPRI research, divided into three groups. The applicable and relevant stakeholders should also pursue further technology development efforts and long-term safety strategies. The EPRI-focused topics are outlined below.

Group 1, Immediate Actions: High-Impact, Low-Effort for Exisitng Systems

The most pressing needs identified in Table 2 in this effort are to address the common deflagration failure mode and poor response plans believed to be present in many energy storage systems operating today. These issues pose an immediate risk to life and property, particularly for first responders, and guidance for rectifying these issues can be developed with relatively little effort. Efforts here will benefit all future installations as well.installations.

Table 2 – Group 1 research topics

Category	Topic	Link
ST: Special Topics	ST1 Addressing the common explosion hazard	ST1
RP: Response Plans	RP1 Response plan guidelines for existing and future BESS	RP1
	RP2 Response plan standardization	RP2
DT: Design Tools	DT1 Improving availability and application of 9540A testing	DT1
	DT2 Inclusion of gas prediction and deflagration protection tools in BESS design processes	DT2

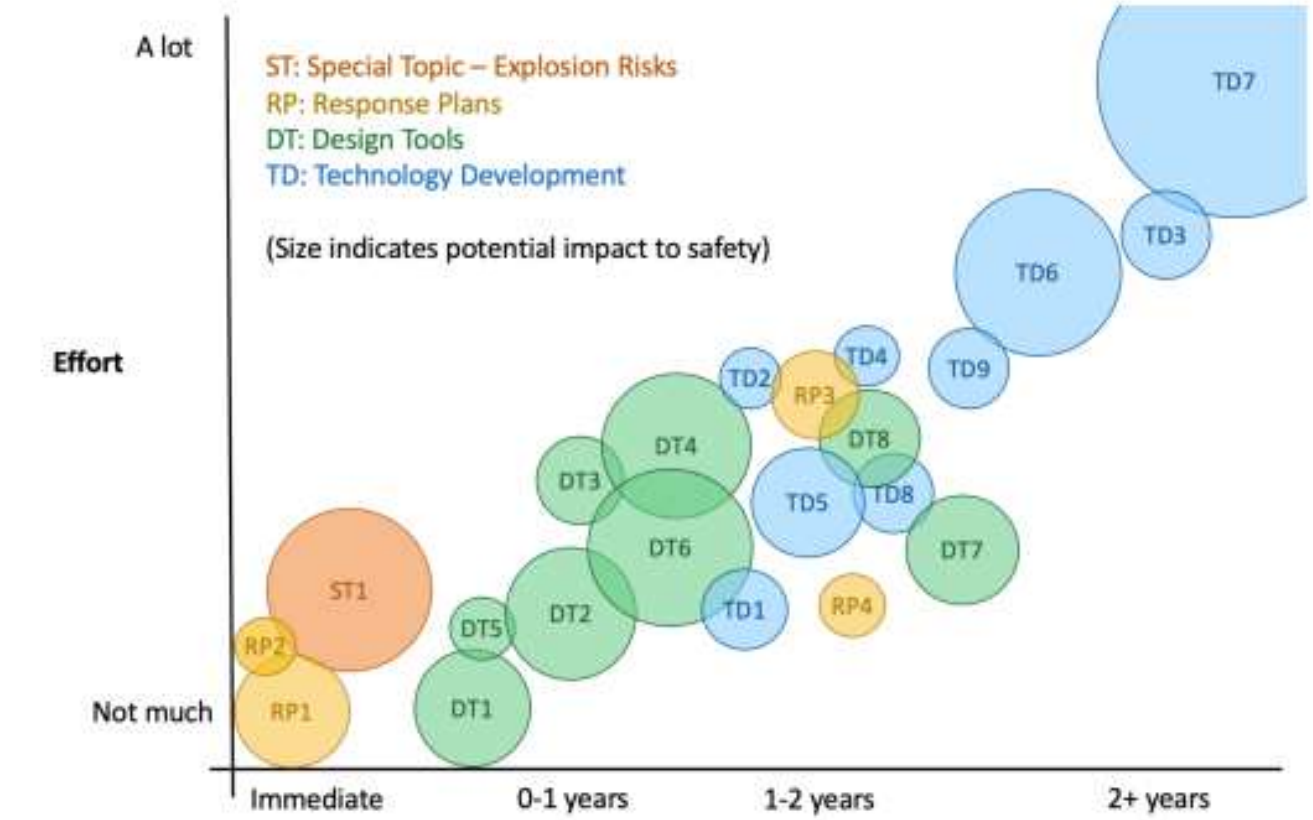


Figure 4 – Battery Storage Fire Safety Roadmap

Group 2, Near-Term Actions: High-Impact, Moderate Effort for Systems in Development

A large number of BESSs are anticipated to be installed in the near future. The medium-effort tasks in Group 2, shown in Table 3, can be completed relatively quickly. They address well-known industry concerns, and their results can be used to improve the safety of the many systems being installed in the near term.

Table 3 – Group 2 research topics

Category	Topic	Link
DT: Design Tools	DT3 Expansion of 9540A testing to address statistical variation and multiple cell failures	DT3
	DT4 Guidelines for selection and design of suppression systems	DT2
TD: Technology Development	TD1 Robust electrical controls	TD1

Group 3, Medium-Term Actions: System Design and Research Guidance for Future Systems

The last group addresses three topics, two of which (FMEA Guidance and Integrated System Design Tools) treat BESS safety from a wholistic systems-level vantage point. This work not only would create direct value by providing these tools to the industry but also could be used for identifying future safety research directions. For example, using the system design and FMEA tools together, research organizations can identify and encourage the safest system configurations, identify presently unknown failure methods, establish high-value barrier opportunities, and then develop targeted future R&D programs.



Table 4 – Group 3 research topics

Category	Topic	Link
DT: Design Tools	DT5 Standardized electrical controls reporting	DT5
	DT6 Failure modes and effects analysis (FMEA) guidance	DT6
	DT7 Integrated system design tools	DT7

Remaining Ungrouped Topics

As shown in Table 5, 11 remaining topics were not chosen for the near-term EPRI roadmap. As noted earlier, these topics are still relevant and could be pursued by vendors, integrators, OEMs, and other government and private entities.

For more information on the roadmap, research groupings, and specific topic details, the full, expanded Battery Storage Fire Safety Roadmap is below in the appendix.

Table 5 – Ungrouped research topics

Category	Topic	Link
RP: Response Plans	RP3 Hazard state identification and communication	RP3
	RP4 Contamination management	RP4
DT: Design Tools	DT8 Adequacy and inclusion of thermal runaway propagation prediction tools in BESS design processes	DT8
TD: Technology Development	TD2 Detection of state of thermal reaction	TD2
	TD3 Detection of future thermal runaway events	TD3
	TD4 Detection of deflagration and toxicity risks	TD4
	TD5 Limitation of propagation using thermal controls	TD5
	TD6 Minimization of thermal runaway using thermal controls	TD6
	TD7 Safe cells with no thermal runaway potential	TD7
	TD8 Thermal runaway vent gas routing management during failure.	TD8
	TD9 Ignition control	TD9

CONCLUSIONS

The research described in this report demonstrates that battery safety is a topic that touches all actors in the ecosystem and requires immediate and reinforced action. Cell suppliers, module and rack suppliers, suppression suppliers, systems integrators, operators, regulators, and first responders need to work together to build a cohesive responsibility for safety. Every stakeholder has a role to play in its respective purview.

- BESS suppliers need to address safety from the cell to the module, to the rack – all the way to the integrated systems. Identifying and addressing the true tolerance of a cell will require additional efforts from a variety of actors, including standards organizations.
- Integrators and battery suppliers should address the issues that emerge from the complex interactions between the different elements of a storage system and continue to innovate with safety technology. The significant coupling between design variables increases the complexity of this task. In addition, rigorous hazard analyses, such as the ESIC Reference HMA (EPRI report 30020017136) or FMEAs, appear to be effective strategies for identifying and improving system-level safety.
- BESS owners, maintenance, and operations staff need to be provided with the right tools to address safety hazards, assess potential environmental impact, and prepare effective, site-specific response plans for first responders to ensure the safety of the public, operators, and environment during a failure event.

If not correctly addressed, these hazards put the entire industry at risk. Technical safety staff, firefighters, and other professionals dealing with battery fires will be exposed to the greatest risk. However, if these near-term research topics are pursued, there is a future where energy storage can be deployed in a way that ensures the safety of the public, operators, and the environment. EPRI is committed to providing the research to enable tools and resources that support owners, operators, and developers of energy storage to ensure a safer future for energy storage.

Contact EPRI's Energy Storage and Distributed Generation Program to learn more about how to partner with EPRI's ongoing safety research.



APPENDIX: EPRI BATTERY STORAGE FIRE SAFETY ROADMAP – DETAILED TOPIC DESCRIPTIONS

In the subsequent sections, each research topic is explained in more detail. Each topic section includes the task name, applicability, impact, effort level, actors, and a detailed description as organized below.

TOPIC: ETD – EXAMPLE TASK DESCRIPTION

Applicability: The applicability of the task on given systems
Impact: High, medium, or low, as used in Figure 4
Effort: High, medium, or low, as used in Figure 4
Actors: Industry entities that are best suited to act on the task outlined
Description: A detailed description and explanation of the task intent and notes on the approach to execution 0

Special Topic – Explosion Risk

Six of the eight examined systems pose a possible explosion risk via the same failure mode. The behavior of these systems has four elements that contribute to this risk:

- They utilize a clean-agent suppression system that prevents ignition, thus encouraging the accumulation of hazardous gases.
- They have no ventilation, further encouraging the accumulation of hazardous gases.
- They have no deflagration protection to control a deflagration should one occur.
- They do not have a first-responder plan that addresses the possibility of explosion.

The explosion failure mode has not been addressed by the cell- and module-level UL listings. While UL 9540A does address explosion risk, most existing systems were installed prior to publication of 9540A, and the industry's experience with 9540A to date is still limited, meaning it may not always be implemented properly. Furthermore, there is statistical variability in thermal runaway events, and it may be necessary to conduct multiple texts per UL 9540A to confidently address this failure mode.

As shown in Figure 5, specific effort is recommended to advise on how to manage explosions due to the high suspected occurrence rate, potential loss of life should an explosion occur, and obvious industry benefits from a quick, coordinated response to this issue.

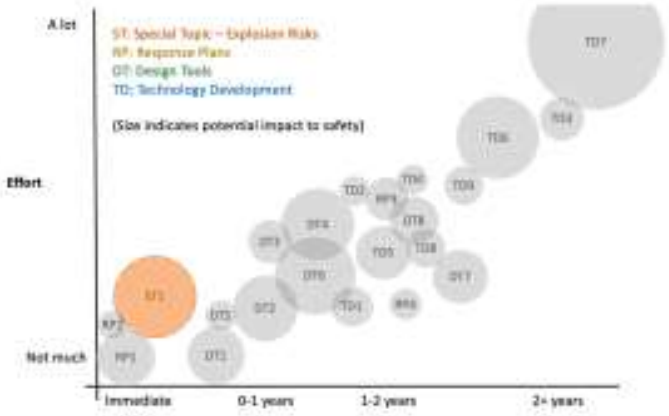


Figure 5 – Special topic – explosion risk

Topic: ST1 – Addressing the Common Explosion Hazard

Applicability: Existing and all future systems
Impact: High
Effort: Low to medium
Actors: BESS developers, BESS owners and operators, safety experts, first responders
Description: Immediate action is necessary on the many existing systems that include gaseous suppression systems without ventilation to eliminate deflagration risks, which threaten bystanders and first responders. At a minimum, a response plan must be made that specifically addresses how to deal with a system post-fault when it contains a dangerous amount of toxic and flammable gases that could explode if disturbed. The ability to retrofit deflagration panels and/or alternative suppression and ventilation systems should also be considered. One particular challenge to these efforts is that many of these older systems are no longer in production, and test-based design methods such as UL 9540A may not be applicable. An industry task force is recommended to create and distribute guidance to owners and operators as well as authorities having jurisdiction (AHJs) and first responders.

This information should also be applied to systems presently under development and to all future system builds. Ideally, recommendations to codes will be made that prevent this risk from occurring in the future



RESPONSE PLANS

Review of site surveys found that response plans were often lacking or missing entirely. Industry workshops raised additional challenges regarding response plan availability and content. As an improper response to a BESS fault can pose a potentially life-threatening risk to first responders and bystanders, response plan topics presented herein are generally high-impact, near-term tasks, as shown in Figure 6. In many cases, the effort needed to complete these tasks is relatively low.

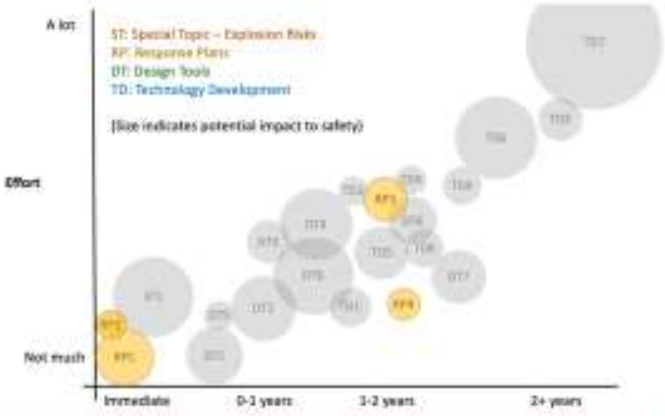


Figure 6 – Response plan tasks

Topic: RP1 – Response Plan Guidelines for Existing and Future BESS

Applicability: Existing and all future systems
Impact: Medium-high
Effort: Low
Actors: First responders, BESS owners and operators, BESS developers, safety experts
Description: Many installed BESSs are believed to not have an adequate response plan in place that covers the known risks of such systems. Further, where response plans do exist, they may not be readily available to first responders. Finally, signage on many BESSs leaves significant room for improvement. An effort should be made to create informative guidelines for response plan writing and delivery as well as improved site signage. The goal is to limit risks to first responders and bystanders while also minimizing financial impact where possible.

Topic: RP2 – Response Plan Standardization

Applicability: Existing and all future systems
Impact: Low
Effort: Low
Actors: First responders, BESS owners and operators, BESS developers, safety experts
Description: The complexity and uniqueness of many operational BESSs have motivated a view in the industry that each BESS requires a unique response plan. This position is justified in that failure modes can vary broadly by BESS design. It is also true that first responders have a multitude of hazards to address and that many first responders are volunteers. Thus, a large diversity of BESS response plans could become counterproductive to enhanced safety. This task would address the question, "Can we create a minimal number of BESS hazard categories and response plans that would safely cover all systems?""

Topic: RP3 – Hazard State Identification and Communication

Applicability: Near-term future and subsequent systems
Impact: Medium
Effort: Medium
Actors: First responders, BESS owners and operators, BESS developers, research scientists, technology developers
Description: An optimal response to a system failure may entail first responders acting if, and only if, the failure event has overcome or threatens to overcome the installed barriers. Understanding the status of these barriers will likely require real-time system state knowledge to best minimize risks. Examples of this knowledge include whether more cells than planned have gone into thermal runaway, the concentration of gases accumulating in the system, and the temperature of different elements within the system. An optimal response requires 1) an understanding of failure modes and how to best assess their state based on real-time system properties, 2) the technology to reliably measure and report the appropriate indicators throughout the entirety of a failure event, and 3) a standardized means to communicate this information to first responders. This task must therefore address all three of these needs. Note that both new science and technology may be required; thus, this could become a long-term task. (Task RP3 requires completion of task TD2 and overlaps with tasks TD3 and TD4.)



Topic: RP4 – Contamination Management

Applicability: Near-term future and subsequent systems
Impact: Low
Effort: Low-medium
Actors: First responders, environment health and safety (EHS) experts, BESS owners and operators, BESS developers, research scientists, technology developers
Description: Where a system's installed fire suppression system is water-based, or when first responders are expected to inject water into a system, there is a risk of contaminating the surrounding environment. This task would seek to quantify the level of contamination possible, assess available strategies for mitigating such contamination, and recommend a best practice to minimize contamination risks.

DESIGN AND REVIEW TOOLS

Industry workshop discussions highlighted the need for improved design and review methodologies on several occasions. Site survey findings also suggested areas where enhanced ability of owners, operators, and AHJs to review designs could improve opportunities for catching and resolving safety problems prior to installation.

Eight design and review tool topics have been created from this data and are presented in Figure 7. They primarily address solutions that improve the industry's ability to predict system response to faults via either test- or model-based methods. There are needs here both in specific domains (such as thermal modeling and suppression system performance) and at the system level.

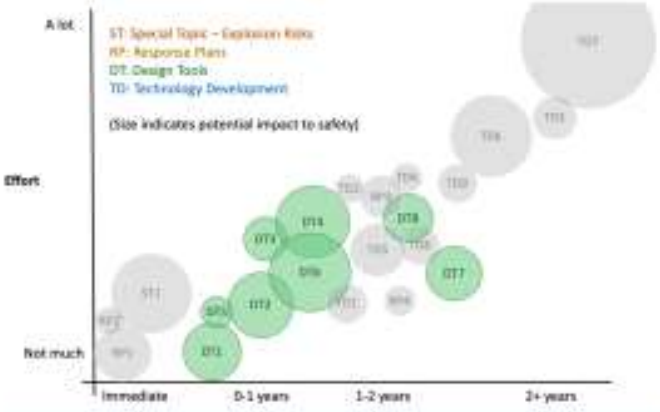


Figure 7 – Design and review tool tasks

Topic: DT1 – Improving Availability and Application of 9540A Testing

Applicability: Under-development and future systems
Impact: Medium-high
Effort: Low
Actors: First responders, BESS owners and operators, BESS developers, codes and standards organizations
Description: UL 9540A test procedures are a powerful tool that enables the design and construction of BESSs with significantly reduced safety risks relative to past systems. However, early findings suggest that developers are 1) not sharing test results from 9540A, 2) sharing inconsistent and/or questionable data from 9540A, and/or 3) applying 9540A data to their designs in unintended ways that do not create the intended levels of risk reduction. Reviewers of 9540A data are often not well informed as to what to look for – as they may not be energy storage experts – and/or the use of 9540A data is relatively new to the industry. In this task, guidelines and tools would be created and shared both for developers and reviewers to improve the consistency and quality of 9540A data usage..

Topic: DT2 – Inclusion of Gas Prediction and Deflagration Protection Tools in BESS Design Processes

Applicability: Near-term future and later systems
Impact: Medium-high
Effort: Low-medium
Actors: BESS developers, gas modeling experts, deflagration protection experts
Description: Deflagration risk caused by accumulation of excess vent gases is reasonably well understood today. The empirical, analytical, and simulation tools necessary to predict the concentration of gases due to a fault – as well as the design tools needed to size adequate deflagration protection systems given gas concentrations – are also well established and will soon be available to BESS developers. However, there is no widespread requirement that these calculations be performed or reviewed. This task would therefore focus on 1) providing widespread access to the necessary tools and knowledge for BESS developers to predict gas concentration and size deflagration protection systems, 2) ensuring understanding of these methods by BESS developers, AHJs, and other BESS reviewers, and optionally 3) standardizing review of the application of these methods to support the safe deployment of future BESSs.



Topic: DT3 – Expansion of 9540A Testing to Address Statistical Variation and Multiple Cell Failures

Applicability: Near-term future and later systems
Impact: Medium
Effort: Medium
Actors: UL, research scientists
Description: UL 9540A test procedures are a powerful tool that enables BESS design and construction with significantly reduced safety risks relative to past systems. However, two key improvement areas have been identified: 1) addressing statistical variation in cell response to fault events, and 2) properly specifying the level of thermal runaway propagation to be achieved in specific tests. The latter requires consideration of the failure modes to address in combination with the level of propagation resistance present in a specific storage device. The fourth edition of UL 9540A has made improvements in this regard, but the need for continued improvement is anticipated

Topic: DT4 – Guidelines for Selection and Design of Suppression Systems

Applicability: Near-term future and later systems
Impact: High
Effort: Medium
Actors: BESS developers, safety experts, suppression system suppliers
Description: The question, "Which suppression system should I choose for my BESS?" is far from answered. Gaseous and clean-agent systems do not address thermal propagation and pose a deflagration risk; in addition, post-event management is unclear. Water-based systems are often infeasible when an unlimited water supply is not available. These systems also might not suppress fires, generally result in a total loss of a system, and pose questions around hydrogen gas generation and environmental contamination. Other options have yet to be fully vetted for BESS applications. This task would focus on collecting available data from past suppression system testing, conducting new testing where necessary, and comparing the benefits and drawbacks of all extant suppression technologies. A design guide would result, enabling BESS developers to choose the right suppression system for their specific installation.

Topic: DT5 – Standardized Electrical Controls Reporting

Applicability: Under-development and future systems
Impact: Low-medium
Effort: Low
Actors: BESS developers, safety experts
Description: Electrical controls are often the first line of defense to failing and failed cells; they are also the most mature and most frequently implemented of all barriers. However, assessing the level of safety provided by a specific installation's electrical controls is difficult without detailed review of electrical schematics, software, and firmware. Many manufacturers are hesitant to disclose the information necessary for an informed assessment of system safety. This task seeks to develop a solution (for example, a standard questionnaire) that enables system developers to disclose adequate information needed for safety assessments without revealing sensitive intellectual property or requiring expert review of detailed design information.

Topic: DT6 – Failure Modes and Effects Analysis (FMEA) Guidance

Applicability: Near-term future and later systems
Impact: High
Effort: Low-medium
Actors: BESS developers, safety experts, FMEA experts
Description: The quality of FMEAs conducted for BESS development is unclear, but the site surveys and continued failures of BESSs suggest there is considerable room for improvement, which could significantly reduce system risks. This task would focus on two main items to improve BESS FMEA effectiveness: 1) create and provide FMEA creation guidelines for BESS developers – as well as FMEA review guidelines for AHJs, owners, and operators – to ensure that the most common and hazardous failure modes are addressed, and 2) convene a task force of BESS safety and FMEA experts to perform a deep FMEA of a generalized BESS to identify presently unknown high-risk failure modes. While this guidance is predominantly intended for future systems where there is opportunity to affect the design process, it could also be applied to existing systems, identifying presently unrecognized failure modes and incentivizing modifications to operational procedures and/or response plans that can improve safety.



Topic: DT7 – Integrated System Design Tools

Applicability: Medium-term future and later systems
Impact: Medium-high
Effort: Low-medium
Actors: BESS developers, safety experts, model-based design experts
Description: BESS complexity and potential design variability are high, with significant coupling between many design variables. An integrated, systemwide design approach is therefore necessary to optimize safety while minimizing cost. However, it appears that today's industry design practices often leave optimal risk mitigation as a missed opportunity. Design tools that seek to capture this opportunity are needed. It is anticipated that fault block size will be a key variable in risk mitigation designs, impacting requirements for thermal protection and suppression, ventilation, and deflagration systems, with a strong overall impact on system cost. EPRI has developed the foundations of this work in *Design Trade Study Method for Battery Energy Storage Fire Prevention and Mitigation*.[4] In this task, that work would be extended to a higher level of fidelity, leveraging improved gas and thermal prediction tools as well as learnings from the suppression systems study. The result would be a design method/tools/guide for informing BESS subsystem choices that maximize safety and minimize lifetime costs.

Topic: DT8 – Adequacy and Inclusion of Thermal Runaway Propagation Prediction Tools in BESS Design Processes

Applicability: Near-term future and later systems
Impact: Medium-high
Effort: Low-medium
Actors: BESS developers, safety experts, thermal modeling experts
Description: It is suspected that properly sized deflagration protection will be challenging to install in many containerized systems due to limited availability of wall and ceiling space. Achieving adequate levels of safety may therefore require strict limitations on the amount of battery energy that is allowed to enter a thermal runaway state and generate gas. Increased usage of thermal analysis tools will be required to design to such limits. Use of simulation tools for thermal runaway prediction is not uncommon in other industries, and similar practices can be adopted. However, there may be a need to improve modeling methods to account for heat transfer from vented gases and flames in the specific setting of stationary storage systems. This task would therefore 1) assess the capability of existing thermal modeling tools and methods, 2) develop improved modeling methods where necessary, and 3) deploy these tools and methods to industry

4 https://www.epri.com/research/products/000000003002020772

RESEARCH AND TECHNOLOGY DEVELOPMENT

Site surveys and industry workshops have highlighted many areas where improved technology and understanding of failure modes are needed to improve BESS safety, as shown in Figure 8. The emphasis here is on R&D of new and improved barriers to hazards, which could be further categorized by barrier type.

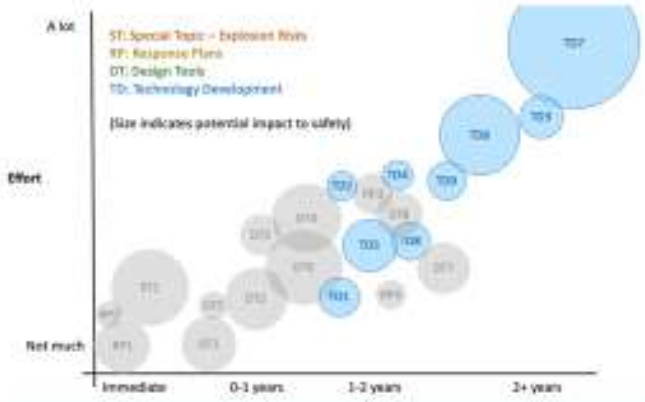


Figure 8 – Research and technology development tasks

The largest opportunity for guaranteeing a safe system response to a fault is, has been, and will continue to be the development of safer lithium ion cells. Such cells would have higher thermal runaway onset temperatures, release lower amounts of heat in thermal runaway, and release smaller amounts of less toxic, less flammable gas during such an event. Reaching this goal could remove much of the barrier complexity throughout the system. However, this goal has long been pursued by the lithium ion battery industry and is a challenging long-term task.

Compared to the mobile applications that have historically driven cell-level safety improvements (such as consumer and automotive), stationary storage applications present unique opportunities for ensuring system-level safety (such as access to water supplies for fire suppression and lower risks of significant mechanical deformation). Therefore, it is recommended that investments to improve BESS safety focus on these areas.



Topic: TD1 – Robust Electrical Controls

Applicability: Near-term future and later systems
Impact: Medium
Effort: Low-medium
Actors: Technology developers, safety experts
Description: While it is believed that most BESSs include effective electrical controls, the robustness of these systems is unclear. For example, what is the likelihood that a single measurement will fail, and what would be the effect of failure on system safety? What is the likelihood that a contactor will fail to isolate a battery exposed to a short circuit? This task would seek to 1) evaluate multiple systems in detail to determine the level of robustness of battery management system and other electrical controls, 2) identify the circuits, devices, and failure modes where redundancy and robustness are most valuable, and 3) publish findings and issue guidance to both BESS developers and AHJs/reviewers.

Topic: TD2 – Detection of State of Thermal Reaction

Applicability: Near-term future and later systems
Impact: Low-medium
Effort: Medium
Actors: Technology developers, cell developers, research scientists, BESS developers
Description: Understanding the state of a thermal runaway reaction may be critical for activation of suppression systems and actions of first responders. This task would pursue the development of technologies that can predict future propagation, heat release, and gas release after a thermal runaway event has begun and would include sensor efficacy testing, which is required for task RP3.

Topic: TD3 – Detection of Future Thermal Runaway Events

Applicability: Far-term future and later systems
Impact: Medium
Effort: High
Actors: Technology developers, cell developers, research scientists
Description: The ability to predict some future runaway events presents the opportunity to limit incurred damage and safety risks, though such an ability will not eliminate the need for other safety systems as some failure modes will not be predictable. This task would pursue the development of technologies that can predict future thermal runaway events based on measurements of system response during nominal operation (such as voltage, current, and temperature). (This task overlaps with task RP3.)

Topic: TD4 – Detection of Deflagration and Toxicity Risks

Applicability: Near-term future and later systems
Impact: Low-medium
Effort: Medium
Actors: Technology developers, safety experts, deflagration protection experts
Description: Detection of deflagration and toxicity risks, most readily via gas concentrations, is critical in certain systems for venting and suppression system activation as well as supporting first-responder actions. Technical challenges include maintaining function throughout the entirety of a safety event, addressing heterogeneity of gas concentrations throughout a system, and minimizing response time. (This task overlaps with task RP3.)

Topic: TD5 – Limitation of Propagation Using Thermal Controls

Applicability: Medium-term future and later systems
Impact: Medium-high
Effort: Medium
Actors: Technology developers, thermal modeling and system design experts
Description: As discussed previously, it is anticipated that the ability to control the propagation of thermal runaway to a limited number of cells will be critical to ensuring desired safety levels are achieved. This task would explore different methods of limiting propagation in stationary systems, drawing on past work in other applications. The result of this task would be data on the ability of various methods to limit propagation and recommendations on when to use which approaches.

Topic: TD6 – Minimization of Thermal Runaway Using Thermal Controls

Applicability: Far-term future systems and later
Impact: High
Effort: High
Actors: Technology developers, cell developers, research scientists, thermal modeling and system design experts
Description: If the heat and/or gas released by a single cell during thermal runaway could be minimized and propagation to neighboring cells prevented entirely, then safety risks could be decreased dramatically as could the requirements for additional safety systems. This task would pursue the development of such thermal control technologies and report on their viability.



Topic: TD7 – Safe Cells with No Thermal Runaway Potential

Applicability: Far-term and later systems
Impact: Very high
Effort: Very high
Actors: Cell developers, research scientists, safety experts
Description: The battery industry has long pursued the development of safer cells, which could eliminate the need for all of the other safety systems and precautions associated with BESSs. This task is a large one, however, and it carries considerable technological risk. It is included in this discussion primarily for completeness, and it is not recommended that EPRI and its members directly invest in this effort.

Topic: TD8 – Thermal Runaway Vent Gas Routing Management During Failure

Applicability: Medium-term future and later systems
Impact: Medium
Effort: Medium
Actors: Technology developers, gas prediction experts, safety experts
Description: The effectiveness and practicality of gas routing for the prevention of ignition and propagation have not been extensively explored in stationary systems. However, gas routing is considered in other industries, and its implementation may be well suited to stationary systems. This task would complete a feasibility study on the use of gas routing for stationary systems.

Topic: TD9 – Ignition Control

Applicability: Medium-term future and later systems
Impact: Medium
Effort: Medium
Actors: Technology developers, safety experts
Description: To date, the industry has favored the prevention of vent gas ignition on the premise that fire will lead to increased propagation and heat release. However, the realization that common fire suppression methods can lead to increased risk of deflagration brings this premise into question. Allowing gases to burn can reduce the risk that sufficient quantities of flammable gases will accumulate to present a deflagration risk. This task would answer the question of when gas ignition should be suppressed and when it should be encouraged.

DISCLAIMER OF WARRANTIES AND LIMITATION OF LIABILITIES

THIS DOCUMENT WAS PREPARED BY THE ORGANIZATION(S) NAMED BELOW AS AN ACCOUNT OF WORK SPONSORED OR COSPONSORED BY THE ELECTRIC POWER RESEARCH INSTITUTE, INC. (EPRI). NEITHER EPRI, ANY MEMBER OF EPRI, ANY COSPONSOR, THE ORGANIZATION(S) BELOW, NOR ANY PERSON ACTING ON BEHALF OF ANY OF THEM:

(A) MAKES ANY WARRANTY OR REPRESENTATION WHATSOEVER, EXPRESS OR IMPLIED, (I) WITH RESPECT TO THE USE OF ANY INFORMATION, APPARATUS, METHOD, PROCESS, OR SIMILAR ITEM DISCLOSED IN THIS DOCUMENT, INCLUDING MERCHANTABILITY AND FITNESS FOR A PARTICULAR PURPOSE, OR (II) THAT SUCH USE DOES NOT INFRINGE ON OR INTERFERE WITH PRIVATELY OWNED RIGHTS, INCLUDING ANY PARTY'S INTELLECTUAL PROPERTY, OR (III) THAT THIS DOCUMENT IS SUITABLE TO ANY PARTICULAR USER'S CIRCUMSTANCE; OR

(B) ASSUMES RESPONSIBILITY FOR ANY DAMAGES OR OTHER LIABILITY WHATSOEVER (INCLUDING ANY CONSEQUENTIAL DAMAGES, EVEN IF EPRI OR ANY EPRI REPRESENTATIVE HAS BEEN ADVISED OF THE POSSIBILITY OF SUCH DAMAGES) RESULTING FROM YOUR SELECTION OR USE OF THIS DOCUMENT OR ANY INFORMATION, APPARATUS, METHOD, PROCESS, OR SIMILAR ITEM DISCLOSED IN THIS DOCUMENT.

REFERENCE HEREIN TO ANY SPECIFIC COMMERCIAL PRODUCT, PROCESS, OR SERVICE BY ITS TRADE NAME, TRADEMARK, MANUFACTURER, OR OTHERWISE, DOES NOT NECESSARILY CONSTITUTE OR IMPLY ITS ENDORSEMENT, RECOMMENDATION, OR FAVORING BY EPRI.

THE ELECTRIC POWER RESEARCH INSTITUTE (EPRI) PREPARED THIS REPORT.

Note

For further information about EPRI, call the EPRI Customer Assistance Center [redacted]

The Electric Power Research Institute, Inc. (EPRI, www.epri.com) conducts research and development relating to the generation, delivery and use of electricity for the benefit of the public. An independent, nonprofit organization, EPRI brings together its scientists and engineers as well as experts from academia and industry to help address challenges in electricity, including reliability, efficiency, affordability, health, safety and the environment. EPRI also provides technology, policy and economic analyses to drive long-range research and development planning, and supports research in emerging technologies. EPRI members represent 90% of the electricity generated and delivered in the United States with international participation extending to nearly 40 countries. EPRI's principal offices and laboratories are located in Palo Alto, Calif.; Charlotte, N.C.; Knoxville, Tenn.; Dallas, Texas; Lenox, Mass.; and Washington, D.C.

Together...Shaping the Future of Electricity

EPRI RESOURCES

Dirk Lange, *Senior Technical Leader*
[redacted]

Energy Storage

3002022540 July 2021

Electric Power Research Institute
3420 Hillview Avenue, Palo Alto, California 94304-1338 • PO Box 10412, Palo Alto, California 94303-0813 USA
[redacted]

© 2021 Electric Power Research Institute (EPRI), Inc. All rights reserved. Electric Power Research Institute, EPRI, and TOGETHER...SHAPING THE FUTURE OF ELECTRICITY are registered service marks of the Electric Power Research Institute, Inc.

Annex 4 Latest strategies (2022) for BESS incident response and management

Recommended Fire Department Response to Energy Storage Systems (ESS) Part 1

Events involving ESS Systems with Lithium-ion batteries can be extremely dangerous. All fire crews must follow department policy, and train all staff on response to incidents involving ESS. Compromised lithium-ion batteries can produce significant amounts of flammable gases with potential risk of deflagration and fire.

1. If a commercial or utility install, follow pre-plan and do not enter structure.
2. Residential setting response, control power to the unit, ventilate the area, and protect exposures.
3. In all cases contact manufacture technical support as soon as possible.

This guide serves as a resource for emergency responders with regards to safety surrounding lithium ion Energy Storage Systems (ESS). Each manufacturer has specific response guidelines that should be made available to first responders prior to activation.

ESS systems come in many shapes and sizes. They may be affiliated with renewable systems (wind, photovoltaic systems, etc) or used as standby power. ESS Systems can be installed in single family homes too large commercial and utility applications.

Pre-Incident

Modify or establish your department policy or standard response guideline to ESS incidents. Include guidelines for mitigation of the event which may include a defensive operations such as non-intervention and manage fire propagation or protect exposures.

Review installation procedures for systems with the various code officials including Building, Fire, and Electrical

ESS systems must be installed per the adopted fire and building codes in the region.

For the 2015 editions of the International Fire Code and NFPA 1 Fire Code and earlier editions the necessary safety requirements are not present (Consider language in 2021 Fire Codes or NFPA 855).

Ensure pre-incident plans are covering location, type, disconnect, and other contact information

Pre-incident plans should provide rapid response resources for company officers specific to your area and region including OEM emergency contact information

Train on department policy and perform practical scenarios which support the response plan

INCIDENT ACTIONS

The fire crew should allow the battery to burn itself out, during which it is recommended to apply water spray to neighboring battery enclosures and exposures to further mitigate the spread of the hazards rather than directly onto the burning unit.

Applying water directly to the affected enclosure will not stop the thermal runaway event, as the fire will be located behind several layers of steel material, and direct application of water has shown to only delay the eventual combustion of the entire unit.

- Firefighters must wear full personal protective equipment, including SCBA with face-piece.
- If identified in pre-incident plan, shut off the unit/system by operating any visible disconnects or E-stops (shutting off the disconnect does not remove the energy from the battery). To isolate any PV system and ESS in an emergency, multiple disconnects may need to be shut off. This could include circuit breakers, knife-blade disconnects, or other switches.
- Lithium ion batteries that are in thermal runaway or off gasing will create hazardous atmospheres. Firefighters must stay out of the vapor cloud and not rely on gas monitors (without consideration of cross contamination of the gas sensors)
- Due to construction of the unit, thermal imaging cameras may not give true thermal conditions.

Events can occur from damage, exterior fire, or a malfunction. Smoke or suspicious odor from an ESS system can be an indication of a hazardous condition. When batteries or cells enter thermal runaway, there is typically a period of smoke (may be under pressure). The smoke is most likely flammable and may ignite at any time.

Responding to a venting ESS product

- Evacuate the area. Never open any doors or remove panels to ESS units.
- Contact vendor-specific technical support for assistance including BMS data.
- Residential units that are located inside a dwelling unit or garage, the space should be properly ventilated with charged hand-lines in place.
- Maintain a safe distance from the ESS and monitor. A remote FDC may be present on larger commercial or utility ESS to support a sprinkler system inside the enclosure.
- Each manufacturer will have a recommended time for a battery pack to cool down. This can be near a full work cycle of 12 hours or more.
- Defensive Firefighting. Water spray is the preferred agent for response to lithium-ion battery fires (*Lithium-ion is not water reactive*).
    - If a fire has not developed and only smoke is visible, take a defensive stance toward the system and be prepared to apply water spray.
    - If a fire develops, take a defensive stance toward the burning unit and apply water spray to neighboring battery enclosures and exposures.
- Maintaining a safe distance from the unit involved (large commercial systems, at least 300').
- Response crews should allow the battery to burn out. Water should be applied to adjacent battery enclosures and exposures (building).

Fire Service Considerations

Investigation of AZ Li-Ion ESS Incident

Mark McKinnon & Steve Kerber

UL Firefighter Safety Research Institute

Underwriters Laboratories

© 2020 Underwriters Laboratories Inc. UL and the UL logo are trademarks of UL LLC.

UL FSRI is dedicated to increasing firefighter knowledge to reduce injuries and deaths in the fire service and in the communities they serve.



FEMA-funded Assistance to Firefighters Grant project focused on studying firefighter line-of-duty injuries and near misses.

- The goal of this project is to enhance the safety and situational awareness of the fire service with high quality interactive training materials developed from applying fire dynamics research results to significant near miss or line of duty injury fire incidents.
- NIOSH's Fire Fighter Fatality Investigation and Prevention Program investigates Line of Duty Deaths but lacks the resources for near misses.
- There are voluntary programs to share near misses but in-depth investigations are rarely conducted.



ELECTRICAL GRID ISSUES

- Aging infrastructure and demand growth outpacing supply
- Electrical grids not designed for peak demand
- Renewable energy sources produce electricity intermittently

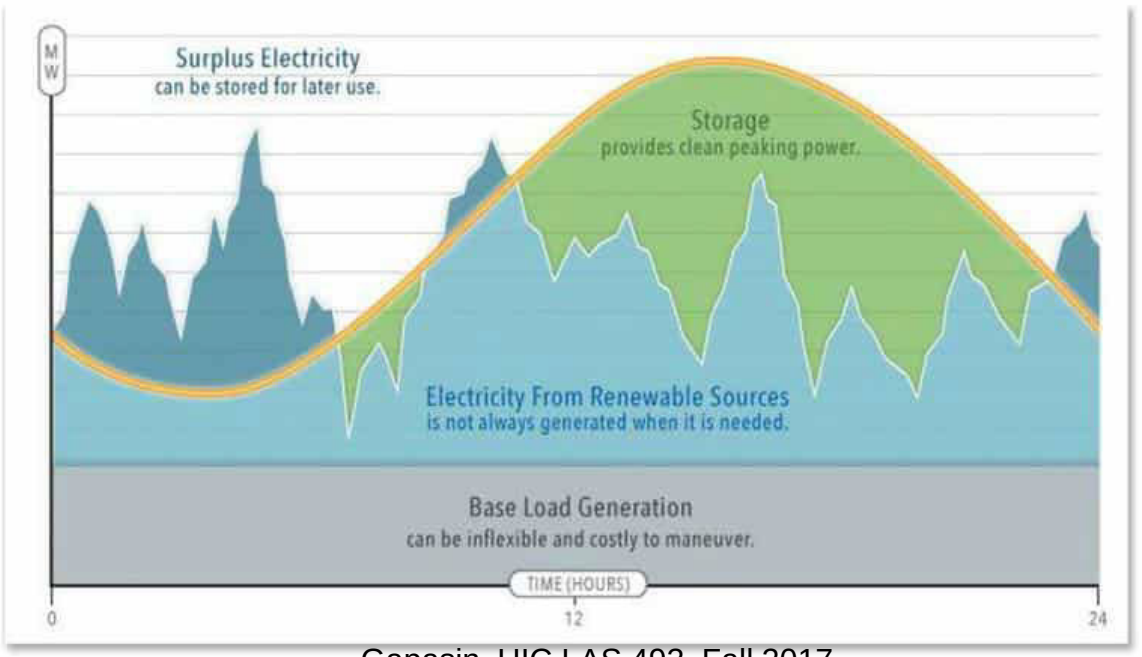




WHY ENERGY STORAGE?

- ESS are a reliable source of energy during peak usage
- Mitigate the variability in renewable energy sources
- Low cost alternative to increasing base load generation capacity





LITHIUM-ION BATTERIES

- Excellent Energy Density
- The Current Battery of Choice
- Batteries and Systems are Readily Available
- Majority of ESS Market is Li-ion



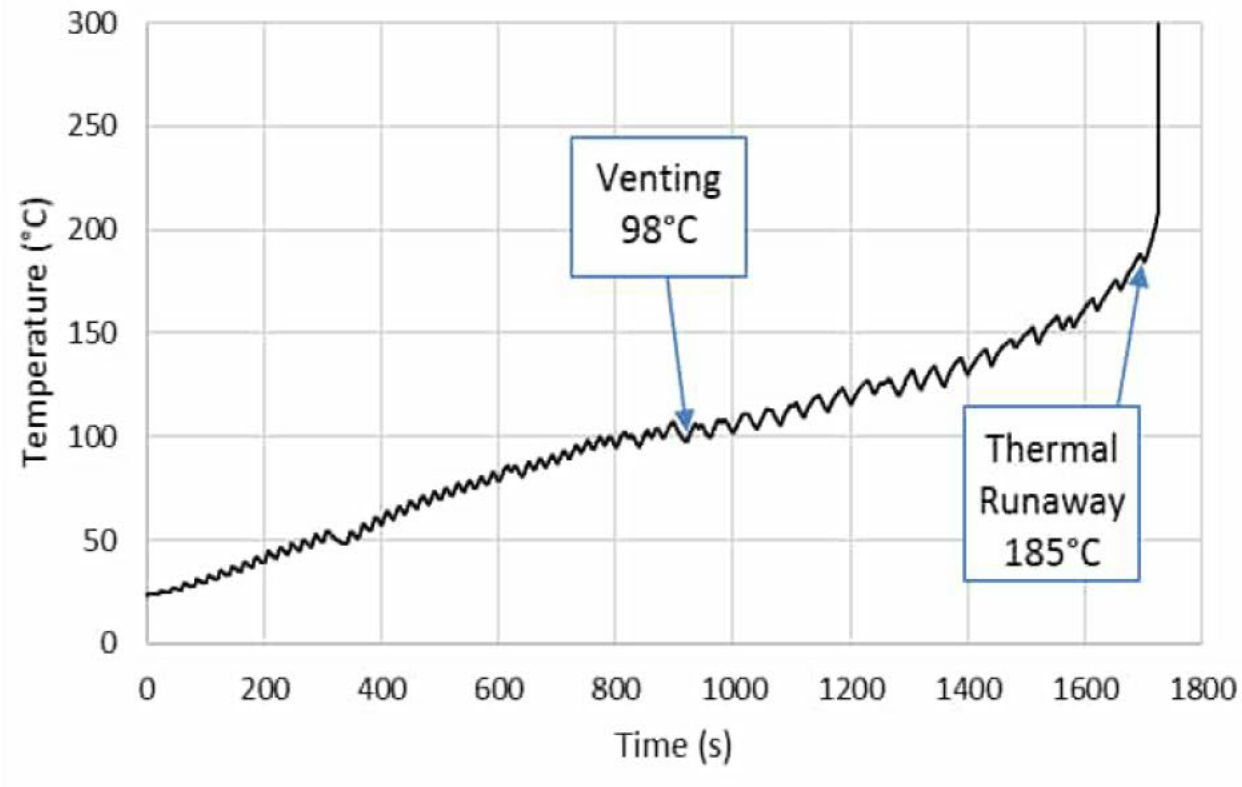


CELL LEVEL MOCKUP TEST



CELL LEVEL MOCKUP TEST

Example of generic li-ion cell heated to thermal runaway.
Cell venting and thermal runaway temperature are documented.



Gas	Composition (Vol %)
CO	36.2
CO_2	22.1
H_2	31.7
Hydrocarbons	~10%

Lower Flammability Limit: ~8.5%
Burning Velocity: 35 cm/sec

RECENT LITHIUM-ION BATTERY INCIDENTS

Over the last year, there have been several major Lithium-Ion Battery ESS incidents.

- September 15, 2020 – Liverpool (20 MW)
- December 1, 2020 – France
- April 6, 2021 - South Korea
- April 16, 2021 – Beijing (25 MWh)

  - 2 firefighters died in suppression efforts



Hongseong, S.K.



Perles et Castelet, France



Liverpool, UK

Surprise, AZ ESS Incident

Background

2 MW/2.16 MWh Lithium-Ion Battery ESS

- Capacity to power 60 average AZ homes for a full day
- ESS owned by local electric utility (APS)
- Batteries manufactured by LG Chem
- ESS designed by integrator (Fluence)
- ESS maintained by contractors to the integrator (Sturgeon)

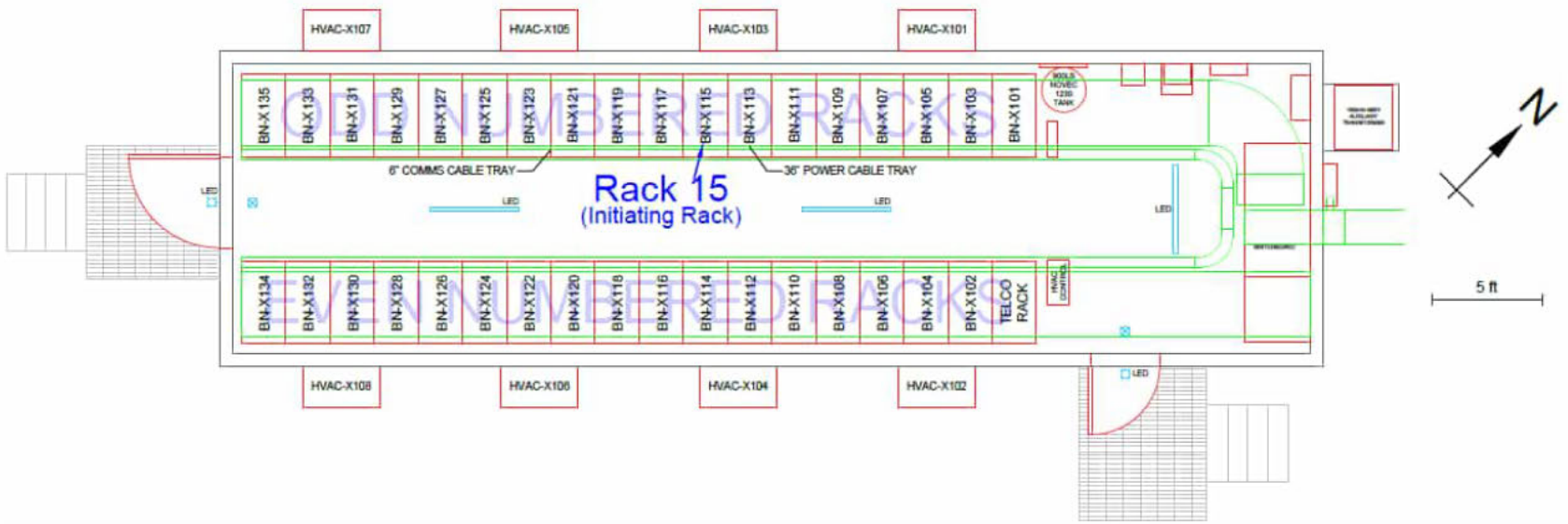
Four firefighters (Peoria HAZMAT team) seriously injured

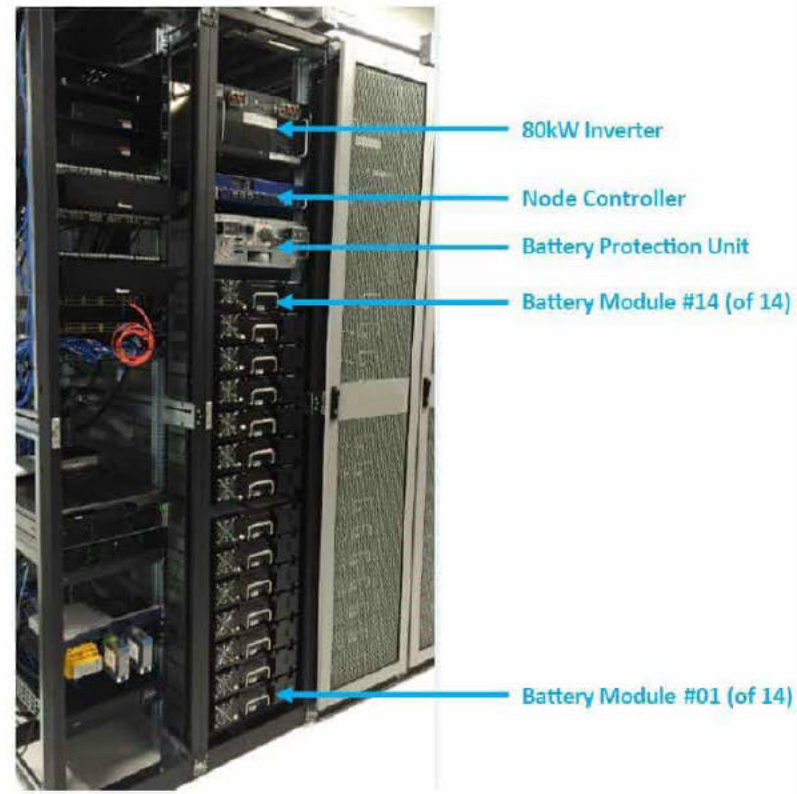
Four firefighters (Surprise E304) held overnight for suspected exposure to HCN



Energy Storage System

- 27 Racks of battery modules
- 14 modules per rack
- 28 lithium-ion NMC pouch cells per module (2P14S)
- 10,584 cells total
- 8 HVAC Units (75 °F ± 5 °F)
- VESDA smoke detector system
- Novec 1230 total flooding clean agent suppression





Timeline



16:54:30 – Minimum battery cell voltage in Rack 15 began to decrease

16:54:44 – Air temperature measurements started to rapidly increase

16:55:20 – VESDA smoke detector registered an alarm condition

- All breakers and contactors opened

16:55:38 – Air temperature measurements peaked at 121.6°F

16:55:50 – Suppression system discharged

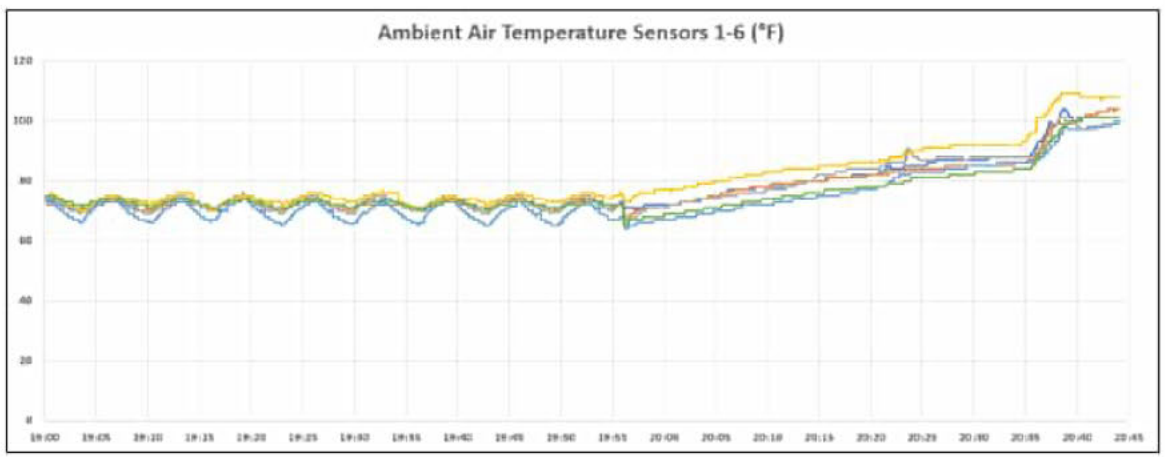
Timeline

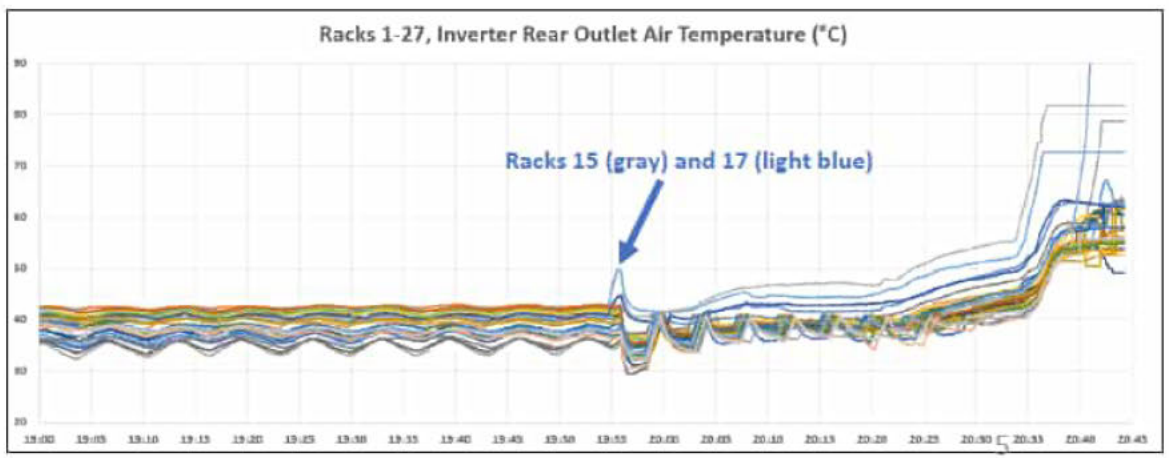


17:41:54 – Phoenix Metro dispatch received a call for smoke and a bad smell near an electric substation and Surprise FD E304, BR304, and T304 were dispatched

17:44:08 – All communication from the ESS was lost

- Air and module temperatures reported prior to 17:44:08





Timeline



17:48:52 – 17:49:12 – Surprise FD E304, BR304, and T304 arrived on the scene

18:04:21 – E304 Capt elevated to HAZMAT operation – Peoria FD E193 HAZMAT team dispatched to call.





Timeline



18:18:30 – Surprise BC 301 arrived on the scene

18:28:21 – Peoria FD E193 and HM193 arrived on the scene





Timeline



18:37:00 – HAZMAT team conducted 360-degree size-up and defined hot zone

18:51:21 – HAZMAT team made second entry into hot zone

19:10:00 – HAZMAT team made third entry into hot zone

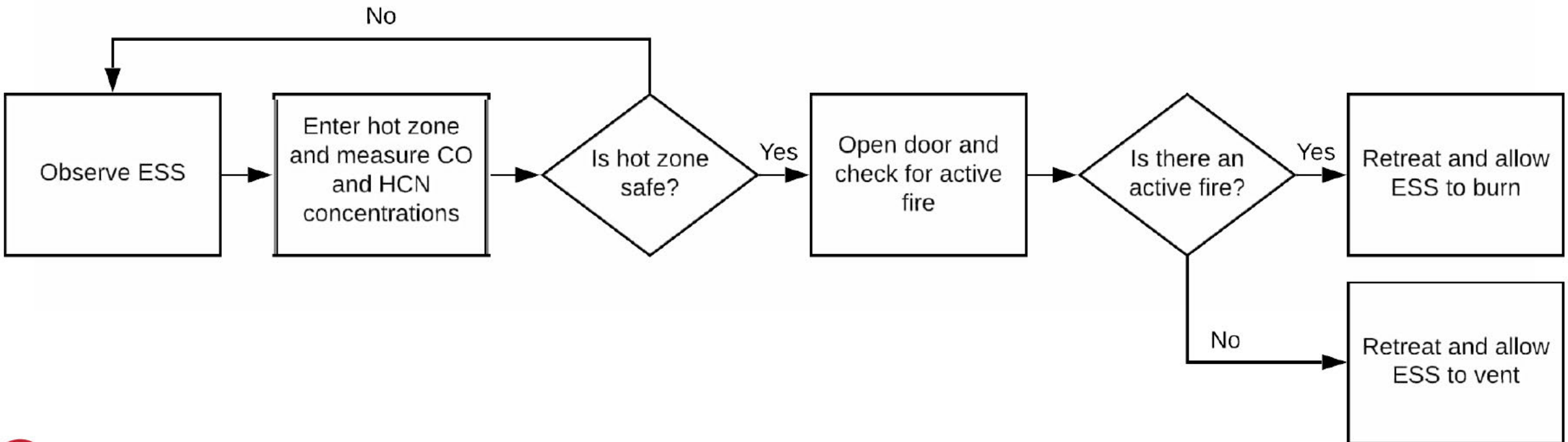




Timeline



19:15 – 19:50 – HAZMAT team conferenced with senior fire department officers and developed a plan to render the ESS and hot zone safe



Timeline



19:50 – The visible gas/vapor mixture was no longer leaking out of the ESS

19:52:24 – HAZMAT team made final entry into the fenced area around the ESS

19:58:03 – HAZMAT team pulled hoseline to ESS to prepare to open door





Timeline



20:00:54 – HAZMAT team opened the door to the ESS

20:03:49 – Mayday call













Contributing Factors and Recommendations

Contributing Factors

- Core HAZMAT training curricula for First Responder and Technician Level do not yet cover basic ESS hazards.
- Extra-curricular ESS-specific training opportunities do not comprehensively address ESS hazards.

Recommendations

- Basic Firefighter, Officer, and HAZMAT training should emphasize ESS safety, the potential explosion hazard from lithium-ion batteries, vapor cloud formation and dispersion, and the dynamics of deflagrations.
- Research that includes full-scale testing should be conducted to understand the most effective and safest tactics for the fire service in response to lithium-ion battery ESS incidents.
- Until definitive tactics can be established, it is recommended that fire service personnel define a conservative blast radius to remain outside of while treating the gas/vapor mixture in the ESS as if it is above the LEL until proven otherwise.
- An online education tool should be developed to proliferate the appropriate base knowledge about lithium-ion battery ESS hazards and fire service tactical considerations.

Contributing Factors

- The ESS did not include sensors that provided information about the presence of flammable gases.
- There was no way for the HAZMAT team to monitor toxic gas concentrations, LEL, or any other conditions inside the ESS from a physically secure location.

Recommendations

- Lithium-ion ESSs should incorporate gas monitoring that may be accessed remotely.
- Research that includes multi-scale testing should be conducted to evaluate the effectiveness and limitations of stationary gas monitoring systems for lithium-ion battery ESSs.

Contributing Factor

- The ESS communication system failed early in the incident.

Recommendation

- ESS communications systems should be more robust to ensure communication remains uninterrupted through a conservative estimate of the duration of a thermal runaway incident.

Contributing Factors

- The emergency response plan was not provided to the responding fire service personnel prior to the incident.
- The emergency response plan that was provided was inadequate.

Recommendations

- Owners and operators of ESS should developed an emergency operations plan in conjunction with local fire service personnel and the AHJ and hold a comprehensive understanding of the hazards associated with lithium-ion battery technology.
- Signage that identifies the contents of an ESS should be required on all ESS installations to alert fire responders to the potential hazards associated with the installation.

Contributing Factors

- The ESS did not have deflagration venting panels (NFPA 68) or adequate ventilation to prevent accumulation of flammable gases (NFPA 69).
- The total flooding clean agent suppression system likely contributed to the deflagration.

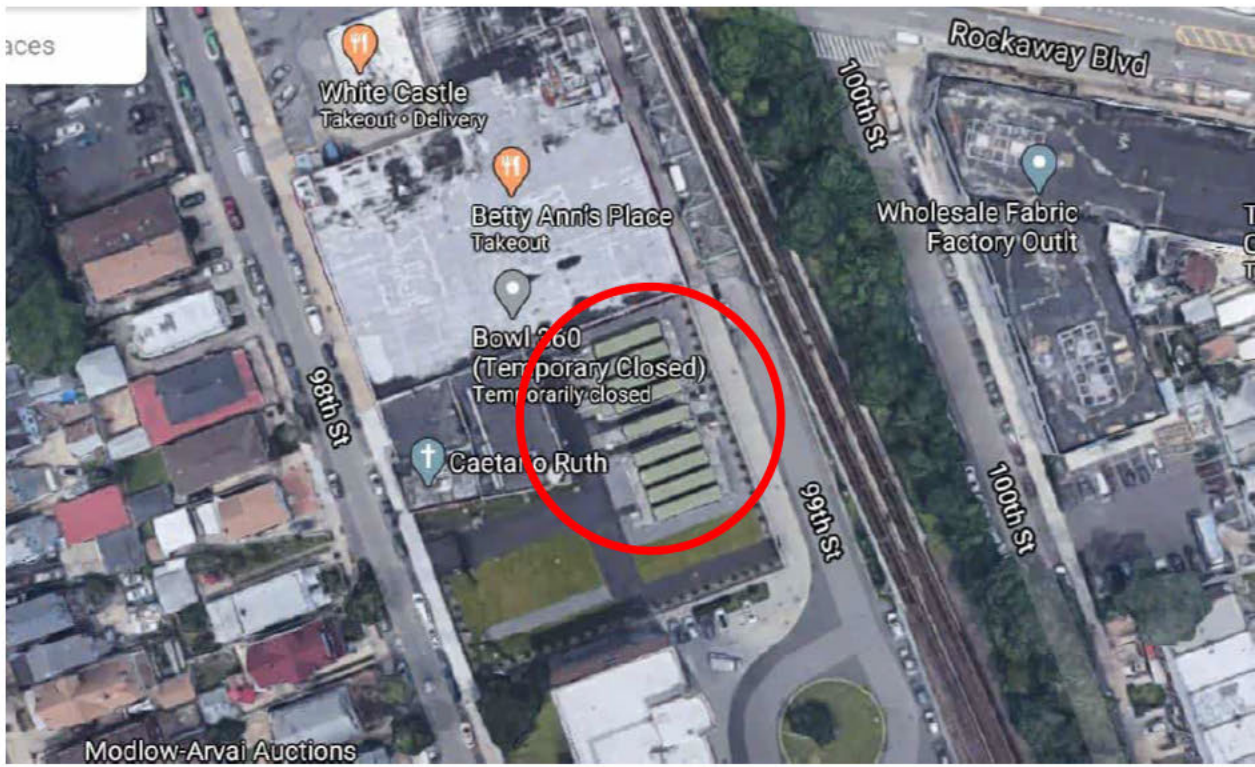
Recommendations

- Lithium-ion battery ESSs should incorporate adequate explosion prevention protection as required by consensus standards in coordination with the emergency operations plan.
- Research that includes full-scale testing should be conducted to determine the most effective fire suppression and explosion prevention systems for lithium-ion battery ESSs.

Additional Recommendation

- Research focused on emergency decommissioning best practices and the role of the fire service in an emergency situation should be conducted.





UL9540A Test Method

Codes, Standards, and Test Methods for ESS

Model Codes: Building and Life Safety	■ NFPA 1 (Chapter 52) — 2018 Fire Code[32] ■ NFPA 70 (Article 706), National Electrical Code, 2017[33] ■ International Fire Code (IFC, Section 1206), 2018[34] ■ International Residential Code (IRC, Section R327), 2018[35] ■ IEEE C2, National Electric Safety Code, 2017[36]
ESS Installation Standards	■ NFPA 855, Standard for the Installation of Stationary Energy Storage Systems[30] ■ UL 9540A, Test Method for Evaluating Thermal Runaway Fire Propagation in Battery Energy Storage Systems*[37]
ESS Design	■ UL 9540, Energy Storage Systems and Equipment[38] ■ ASME TES-1, Safety Standard for Thermal Energy Storage Systems (DRAFT)[39]
ESS Components	■ UL 1973, Batteries for Use in Light Electric Rail and Stationary Applications[40] ■ UL 1974, Evaluation for Repurposing Batteries[41] ■ UL 810A, Electrochemical Capacitors[42] ■ UL 1741, Standard for Inverters, Converters, Controllers and Interconnection System Equipment for Use with Distributed Energy Resources[43]

Updated Since Surprise, AZ Incident

- IFC 2021, Section 1207
- NFPA 855 (2020)
- UL 9540 - 2nd Edition (2020)
- UL 9540A 4th Edition (2019)

Barowy, A. 'True Grid: Standards for Fire, Explosion, and Electrical Safety of Battery Energy Storage Systems'. Fire Protection Engineering. 84. 2019.

UL 9540A Test Method

Scope

Evaluate fire characteristics of a battery energy storage system that undergoes thermal runaway. Data generated will be used to determine the fire and explosion protection required for an installation of a battery energy storage system.

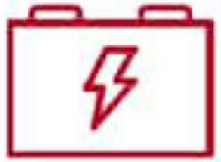
Match Fire Protection of Installation to Performance of BESS





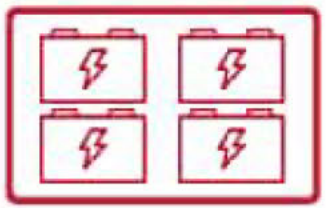


Structure of UL 9540A and Deflagration Hazard Characterization



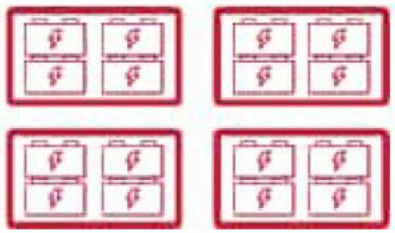
Cell Level Test

- Whether cell can exhibit thermal runaway
- Gas composition
- Explosibility parameters of gas mixture (LFL, P_{max}, Burning Velocity)



Module Level Test

- Gas release rates and total volumes



Unit Level Test

- Gas release rates and total volumes
- Deflagration hazards resulting from confinement



Installation Level Test

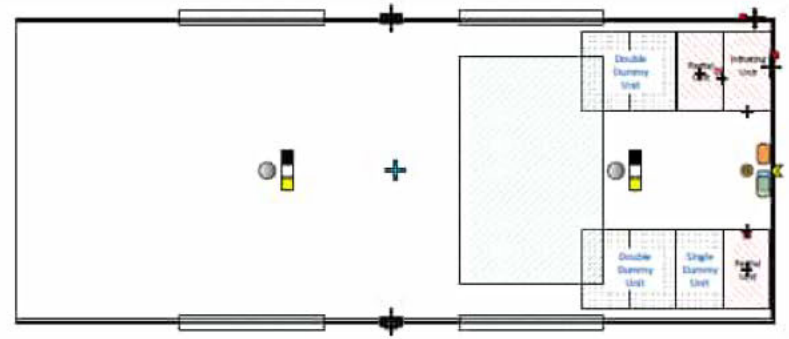
- Effectiveness of fire protection system(s)
- Gas release rates or accumulated gas composition
- Deflagration hazards resulting from confinement

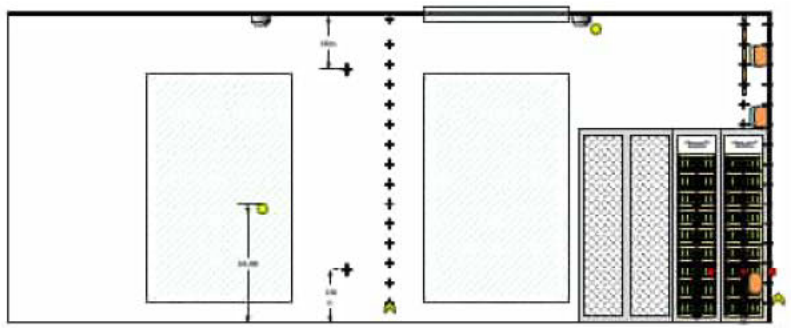
UL 9540A Installation Level Demonstration

Objectives

- Develop non-proprietary UL 9540A installation level data with representative Li-ion chemistry batteries with and without active fire protection systems

- Develop fire service size-up and operational and tactical considerations.









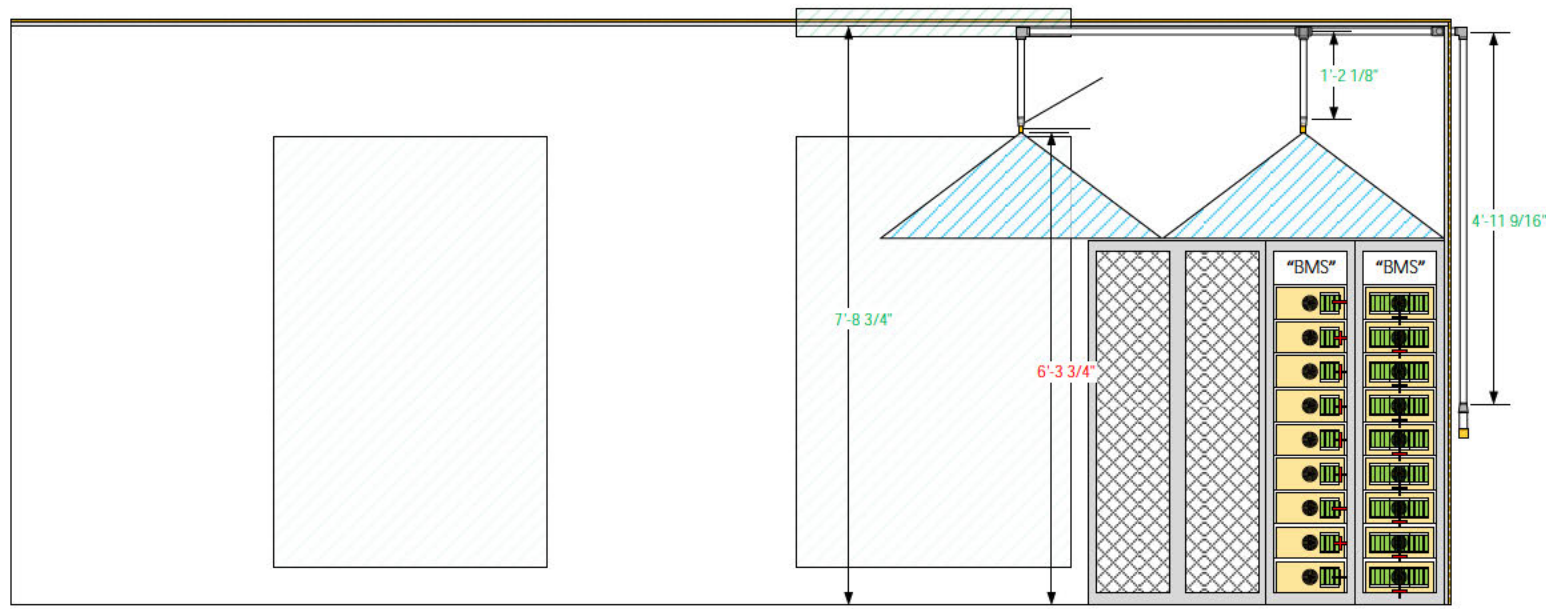




Test Setup - Installation Level Test Configurations

- Test 1 – Without any provision for fire protection.
- Test 2 – With Novec 1230 total flooding clean agent system (8 v% concentration).
- Test 3 – With 0.5 gpm/ft^2 density water spray system (from ceiling).





Operation pressure 0.5 psig; vent area calculation based on NFPA 68, *Standard on Explosion Protection by Deflagration Venting*

UL 9540A Installation Level Demonstration



Smoke accumulation at second smoke detector activation [TR + 00:00:55]



Novec 1230 discharge [TR + 00:00:58]



Smoke stratification before ignition [TR + 00:26:51]



Ignition [TR + 00:28:32]



Partial volume deflagration [TR + 00:44:39]



Continued thermal runaway propagation [TR + 00:46:26]



Smoke plume from open door [TR + 02:09:27]



Flashover and flaming from open door [TR + 02:09:48]

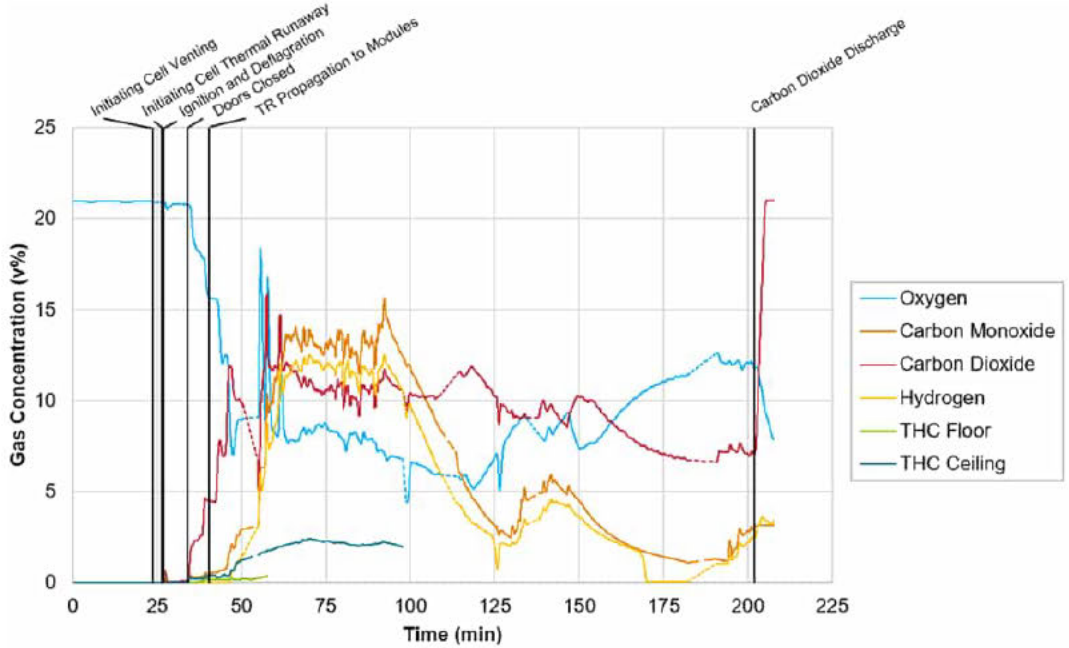
Reports Available [redacted]

UL9540A Test Method

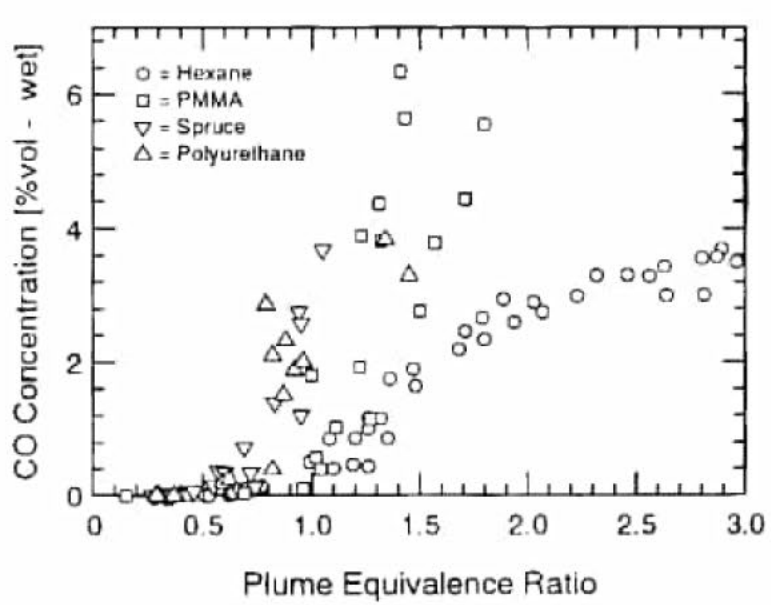
Key Findings

Key Findings – Comparison to Room and Content Fires

Propagating thermal runaway events generate more severe flammability and toxicity hazards than typical room and content fires.



- THC: ~3 v%
- H_2: > 10 v%
- CO: 12 v% - 15 v%
- CO_2: ~10%



- H_2 = 0 v%
- CO: ~6 v%
- CO_2: ~10%

D. Gottuk, et al. J. of Fire Prot Eng. 4, 4, 1992

Key Findings – Gas Detection

Common combustible gas/hydrogen detectors:

1) **Effective for detecting that thermal runaway has occurred.**
2) **Not reliable for ongoing hazard assessment.**

Advantages:

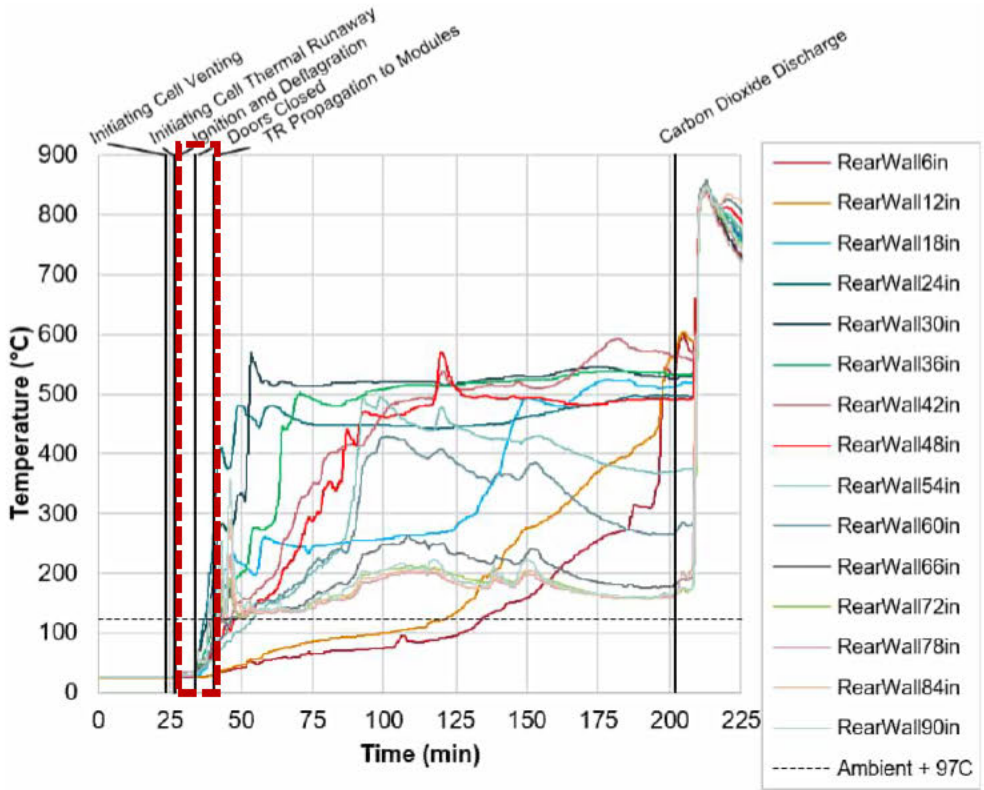
- All detectors responded within seconds when exposed to battery gas.
- Nuisance activation unlikely given measurands (e.g., H_2, CO, LEL).

Limitations:

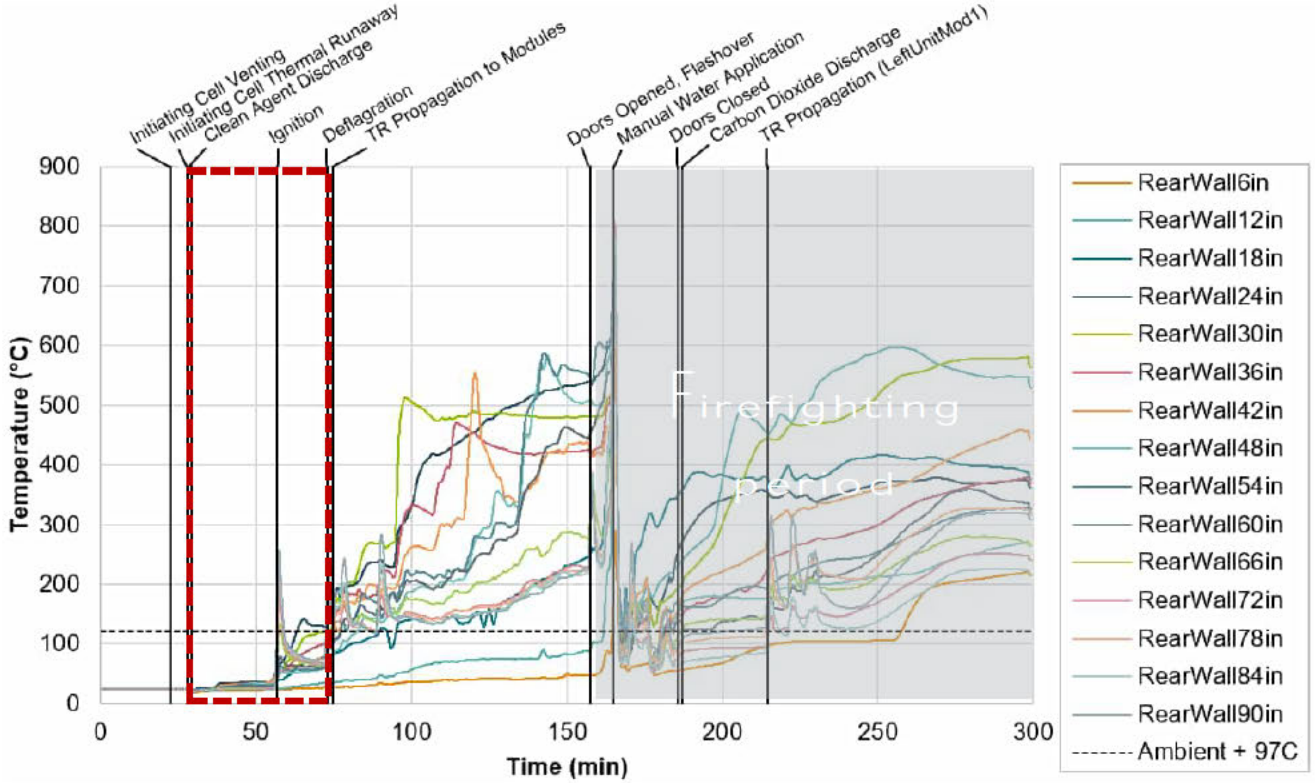
- Detection time dependent on positioning. These tests did not seek to determine optimal locations.
- Cross sensitivity diminishes electrochemical sensor accuracy
- Catalytic bead:
  - Imprecise measurements of flammable gas mixtures,
  - Requires > 10% O_2 for proper operation,
  - "Poisoned" by halogen exposure.

Key Findings – Novec 1230 Total Flooding System

When simulating a total flooding system approach, Novec 1230 did not deliver sufficient cooling to prevent propagation of thermal runaway or to prevent thermal exposure to combustible construction materials.



Rear Wall – No Novec 1230

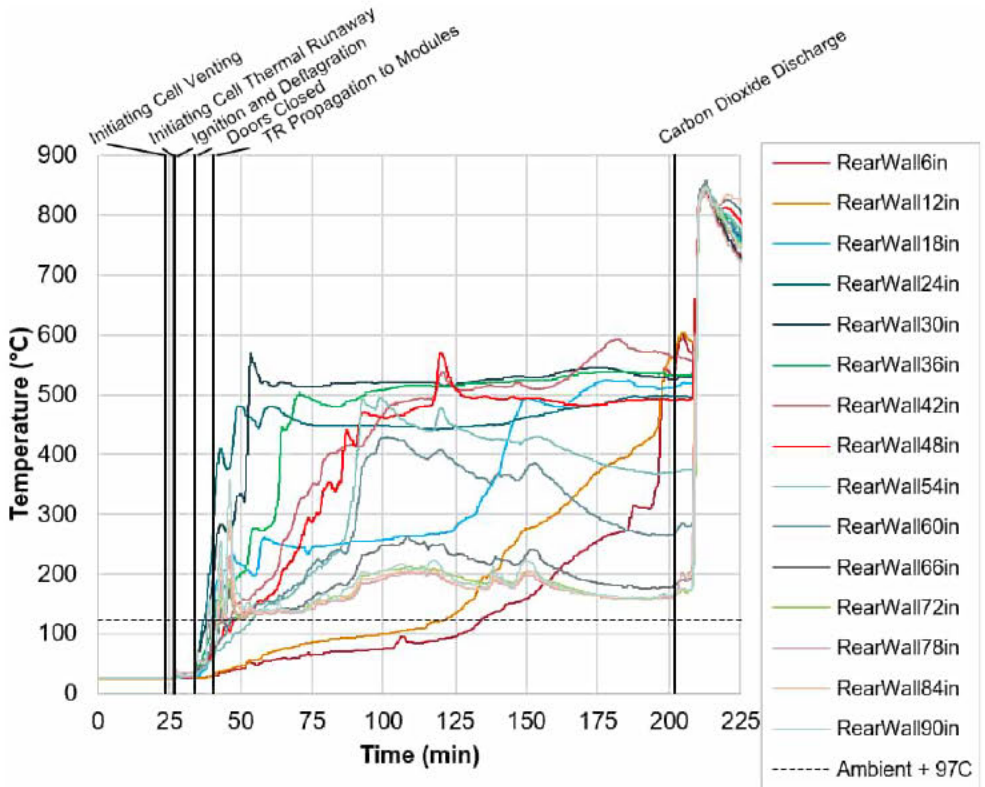


Rear Wall – w/ Novec 1230

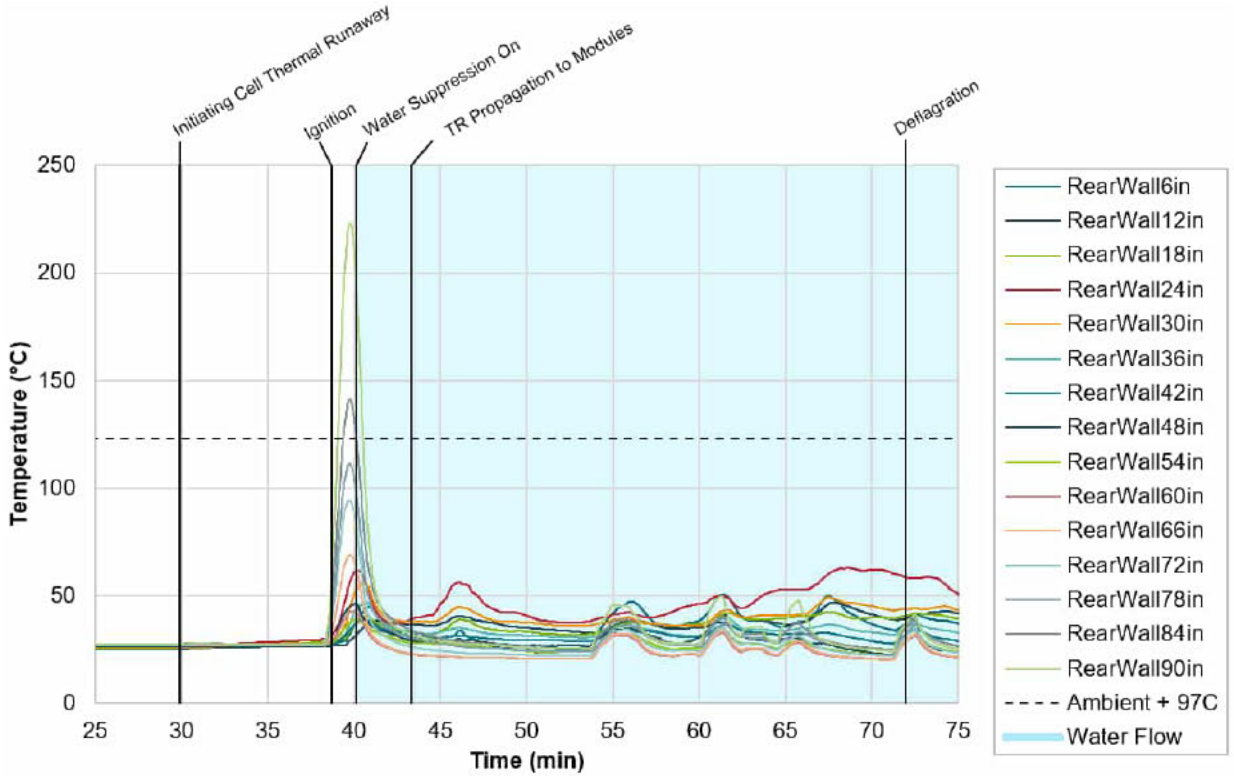
Key Findings – Water Spray Suppression System

Ceiling-based water spray suppression system prevented unit-to-unit propagation and cooled surfaces adjacent to initiating ESS unit.

Demonstrated limited effectiveness to prevent module-to-module thermal runaway propagation within initiating unit.



Rear Wall – No Water



Rear Wall – w/ Water

Key Findings – Deflagration Protection System

The generation and accumulation of battery gases created an explosion hazard and was mitigated with an engineered deflagration protection system.







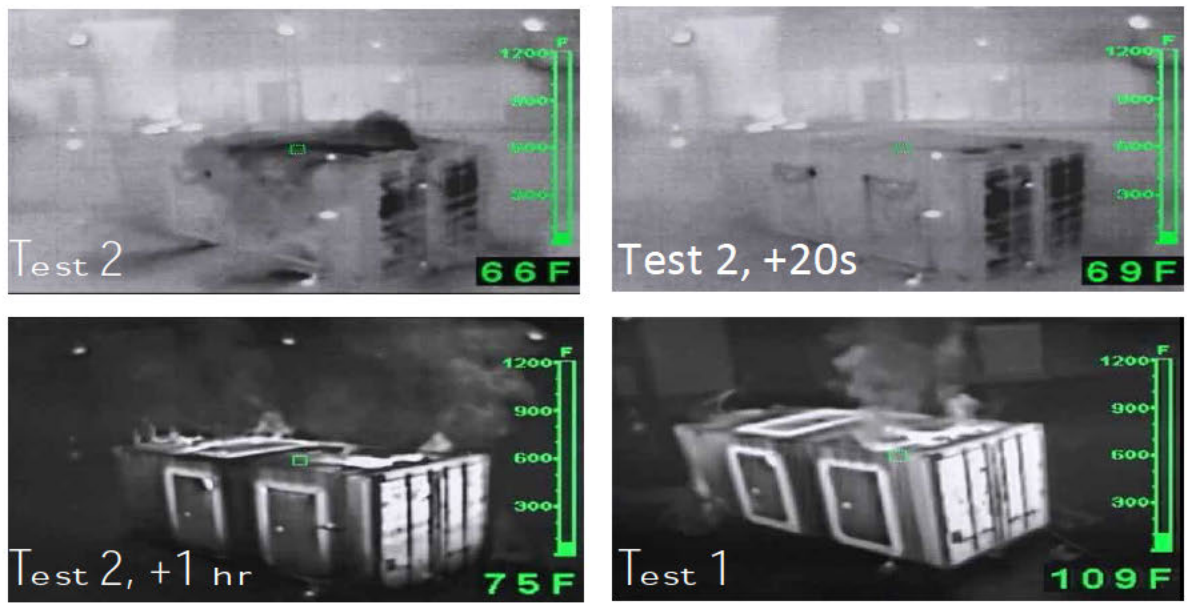
UL9540A Test Method

Tactical Considerations

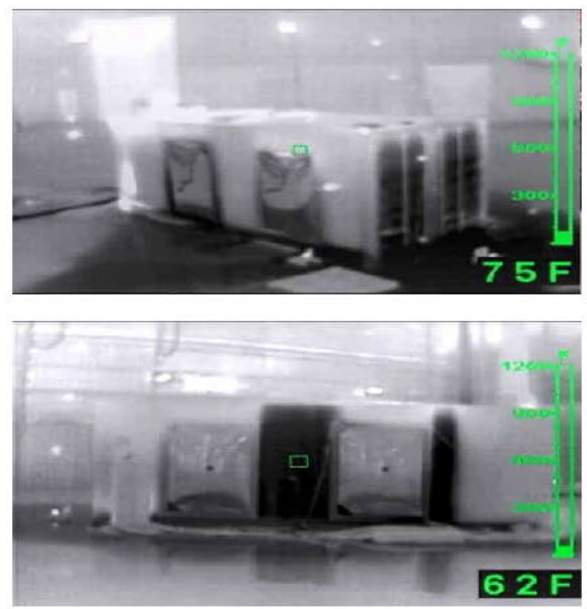
Tactical Consideration – Thermal Imaging Cameras

Thermal imaging cameras enable a limited ability to determine whether a suppression system has operated or is operating.

Thermal Imaging Cameras are not a viable tool for determining the nature of visible vapors (e.g. battery gas, steam, Novec 1230).



Novec discharge evident for short time, likely prior to FD arrival.

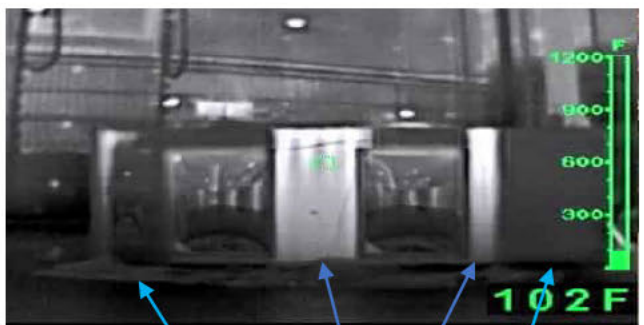


Sprinkler operation visible while water flowing.

Tactical Consideration – Thermal Imaging Cameras

Thermal imaging cameras do not enable evaluation of the number or location of ESS units in thermal runaway.

Wall construction influenced thermal image.

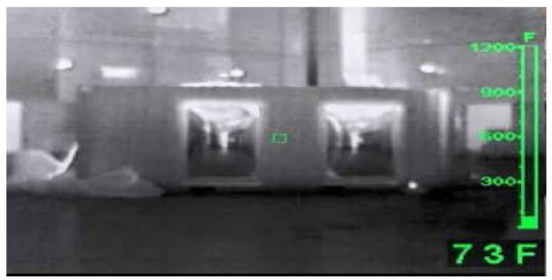


Bare

Insulated

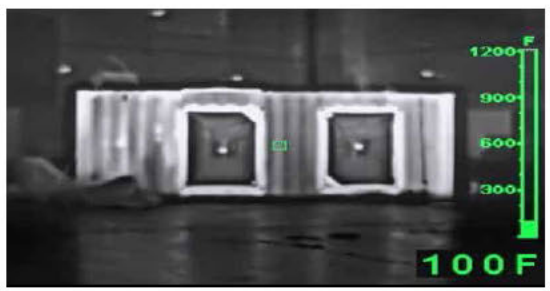
Heat sources not identifiable.

Built up/insulated wall



t= 15 min

Built up/insulated wall



t= 95 min

Bare/insulated wall



t= 95 min

Tactical Consideration – Continuous Gas Monitoring

First responders should consider the practicality of continuous monitoring of the interior and exterior gas environment near the ESS.

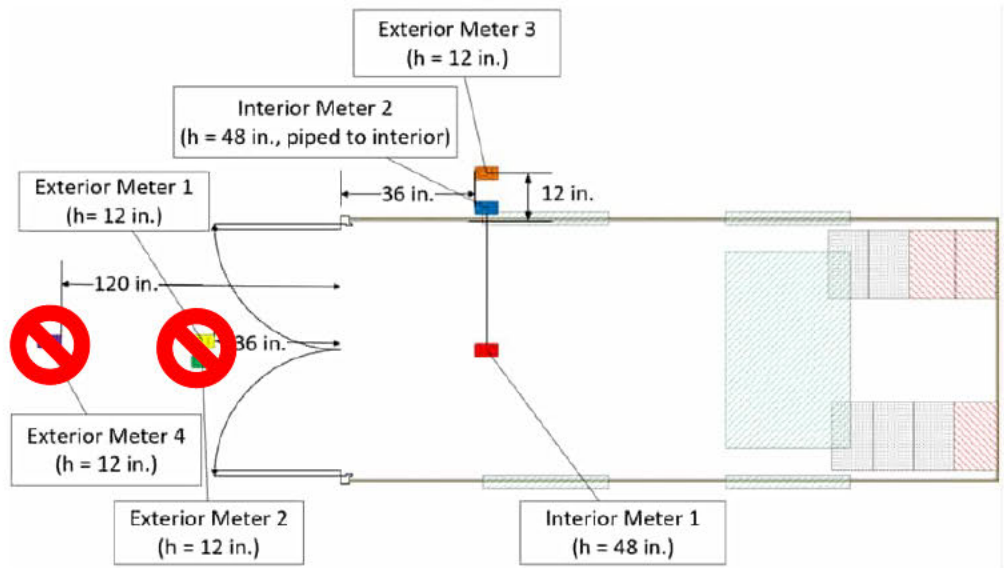
- Firefighters may need to create an opening into container to insert gas meter probe – proximate to potential explosion hazard.
- Soot accumulation clogged pump style meter shortly after the onset of thermal runaway in all three tests.
- CO and H_2 v% measured was often several orders of magnitude higher than the upper measurement limit of the portable gas meters.



Tactical Consideration – Portable Gas Meters

Portable gas meters have limited effectiveness to evaluate the potential for explosive atmosphere within the ESS container.

- Deflagration may occur before flammable gas detectable at exterior of the container for measurement.
- Flammable gas only detected/measured 1 ft from container:
  - FF may be dangerously close to the container before an explosion hazard via "LEL" measurement is identified.
- Exterior gas concentrations were approximately equal to interior gas concentrations:
  - Remotely monitored gas meters may safely provide insight into continued or halted thermal runaway activity, but subject to factors like wind, terrain, etc.



Tactical Consideration – Portable Gas Meters

Fire service portable gas meters have limitations in a battery gas environment.

Electrochemical sensor cross-sensitivity

RAE Systems				
Cross-Sensitivity %	Gas			
Sensor	CO	H_2S	HCN	H_2
CO	100%	0%	N/A	40%
CO-H_2 Compensated	100%	N/A	N/A	1%
H_2S	1%	100%	N/A	N/A
HCN	5%	600%	100%	N/A
H_2	20%	20%	30%	100%
MSA				
Cross-Sensitivity %	Gas			
Sensor	CO	H_2S	HCN	H_2
CO	100%	0%	-5%	48%
H_2S	1%	100%	-3%	0%
HCN	0%	400%	100%	0%
Ventis				
Cross-Sensitivity %	Gas			
Sensor	CO	H_2S	HCN	H_2
CO	100%	5%	15%	22%
H_2S	1%	100%	-1%	0%
HCN	0%	10%	100%	0%

Catalytic bead sensitivity

Compound	LEL Relative Sensitivity[1]	LEL CF
Acetone	45	2.2
Ammonia	125	0.8
Benzene	40	2.5
Carbon monoxide	83	1.2
Cyclohexane	40	2.5
Ethanol	59	1.7
Ethyl acetate	45	2.2
Hydrogen	83	1.2
Isobutylene	67	1.5
Isopropanol	38	2.6
Leaded gasoline	42	2.4
Methane	100	1
Methanol	67	1.5
Methyl ethyl ketone	38	2.6
n-Butane	63	1.6
n-Heptane	37	2.7
n-Hexane	40	2.5
n-Octane	34	2.9
n-Pentane	50	2
Phosphine	385	0.26
Propane	63	1.6
Propene	59	1.7
Toluene	33	3
Turpentine	34	2.9

Note: Interior measurements peaked at 80% LEL, despite several deflagrations.

Tactical Consideration – Ventilation

Ventilation of an ESS installation may result in a deflagration or rapid transition to flashover.

UL Tests - Flashover



Δt = 21 s

Surprise, AZ - Deflagration



Δt ≈ 3 min

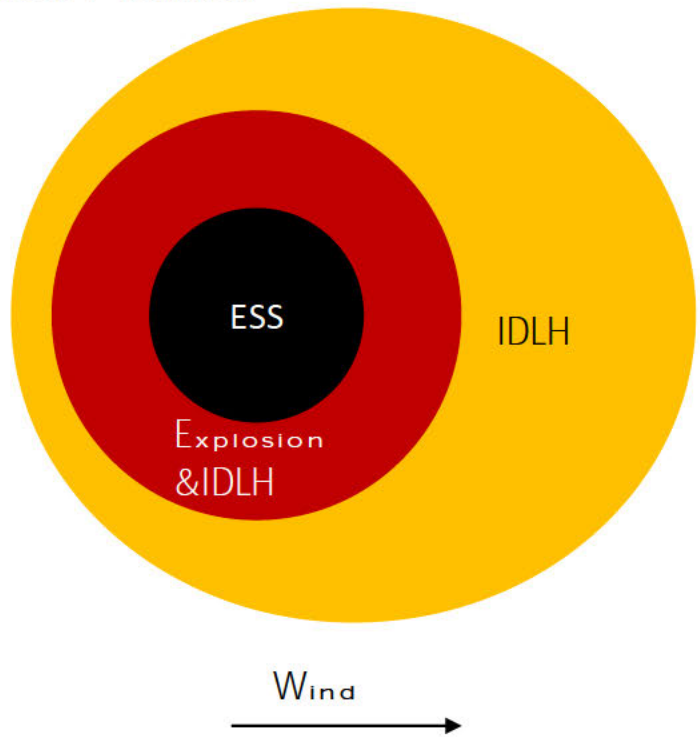
Tactical Consideration – Personal Protective Equipment

Gas meters and visual observations should be utilized for defining the "hot zone" or "exclusion zone" at ESS incidents.

Full structural PPE (Level D Ensemble) with full SCBA should be donned before performing size-up or operating within the hot zone.

Hazards during size-up:

1. CO concentrations above IDLH - SCBA
2. Deflagration, flash fire, flashover hazard – Level D





Questions?

© 2020 Underwriters Laboratories Inc. UL and the UL logo are trademarks of UL LLC.

Incident Management

Failure Modes of ESS

- All Chemistries
  - Over charge
  - HEAT
  - Component failure
  - Environmental issues
  - Mechanical\Impact
  - Factory Defects
  - END OF LIFE
  - Lack of maintenance
  - Improper Installation





Lead Acid and Ni Cad Hazards

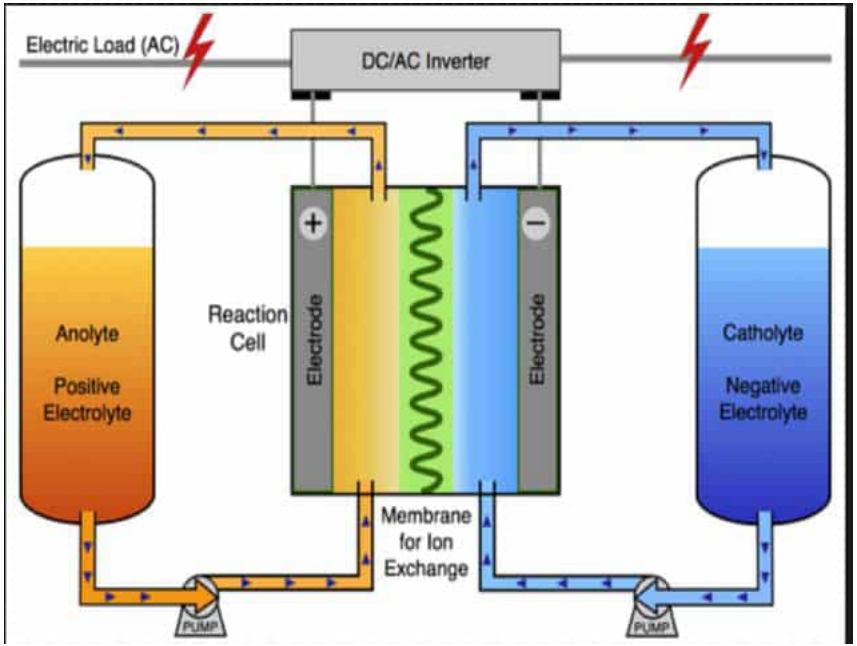
- Corrosive spills
- Toxic gases
- Hydrogen Gas
- Explosion
- Arc Flash
- Stranded Energy





Flow Batteries Hazards

- Corrosive spills
- Hydrogen gases releases
- Very little fire concerns
- Explosion if not vented probably
- Arc flash
- Wires degradation
- Stranded Energy



Lithium Ion Failure

- Thermal Abuse
  - (thermal runaway)
- Electric Abuse
  - (over/under charge)
- Mechanical abuse
  - Separator puncture
- Factory defects
  - Dendrites
- Components





Lithium Ion Hazards

Preliminary testing data

- Toxic/Corrosive gases liberated
- Flammable cocktail
- Deep Seated Fire
- Delayed ignition
- Re-ignition Concerns
- Stored\Stranded Energy after burn

No Fire Showing



- Alarms
  - Smoke Alarm
  - Other Alarm
- Electrolyte vapor released?
- Overheated batteries?
- Environmental= floods or earthquake
- Ventilation needed?
- SME reach back



If there is fire or smoke present

Initial Actions

- Control fire spread
- Smoke no fire = explosion concern
- Keep away from container
- Proper PPE and reduce smoke exposure
- Find a water source
- Make sure no life hazards exist
- Do not open or enter container/cabinet
- Do not stand in front of doors or openings
- Call SME/Help Line



If there is fire or smoke present

Control fire

- Use a hand line fog nozzle 10 degree
- Stop the spread of fire
- Use reach of the stream
- Do not use foam or additives
- Keep your distance
- Do not stand in water pool
- Watch water run off
- Water Environmental issues
- NO LITH X



Ventilation and Exhaust

Exhaust container or cabinet *

- Wait for SME to respond if possible
- Remote access switch
- Removes clean agent
- Introduce O2
- Delayed explosion is possible
- Stay away doors or openings
- Ventilation + Sprinkler
- Building air inlet concerns



* May not exist as part of installation

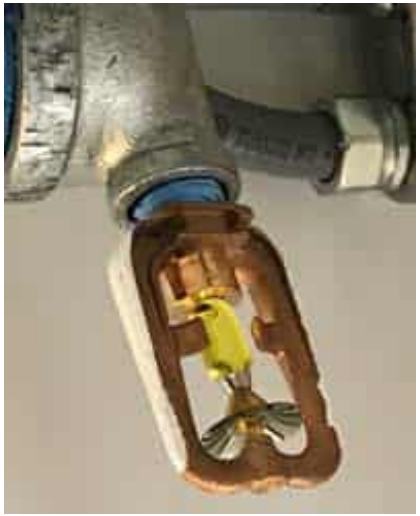
Extinguishment Agents

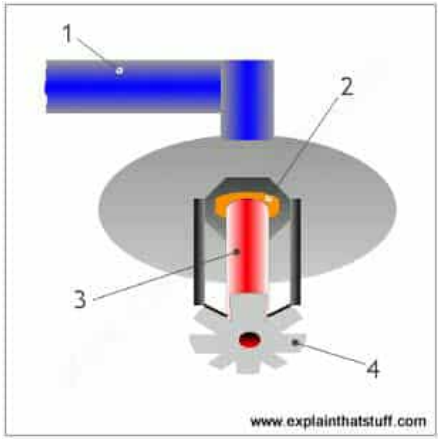
Clean Agent

- Displaces O2
- Does not stop reaction
- Hold time is important

Sprinkler system

- Automatic
- Dry Pipe Systems
- Closed heads
- NONE





Water under pressure in a pipe (1) is held in place by a small plug (2) itself held in place by a glass bulb filled with glycerin (3) When a fire breaks out the bulb breaks releasing the plug allowing the water to hit the flower shaped deflector which spreads it around in a spray

Shut Down

Shut Down (E-Stop)

- Remote and labeled
- Arc Flash
- Shuts down entire system
- Loss of data
- HVAC off

Shut down (BMS Automatic)

- Part of safety
- Isolates the container\Cabinet
- No charging or discharging



Subject Matter Expert

- Signage
- Telephone #
- May respond
- Will advise on shut down procedures
- Will advise on ventilation
- Shall call the decommissioning company
- Advise the Incident Commander



Incident Management

Indoor installations



Inside buildings

- **Fire/Smoke**
  - Evacuate Building
  - DO NOT ENTER ROOM
    - When LEL sensor is sounding
    - When smoke and no fire
    - During ventilation of room
  - Make sure sprinkler is working
  - Check Exhaust exit ports
  - Call SME
  - Stay out of doorway



Dedicated Use Building

- Ensure no life hazards
- Only enter for KNOWN VIABLE LIFE
- Fire/Smoke do not enter
- Information from battery company
- Call SME to respond
- Water extinguisher system



Rooftops Install

- Shut down system
- Exhaust if available
- FD roof access
- Water access at roof
- Hand line off Standpipe
- Automatic sprinkler
- Augment the water supply water run off (weight)



Residential

- Extinguish immediately
- Locations
  - Inside Garage
  - Outdoors
  - Indoors
  - Away from the house
- Can be several ESS
- No fire suppression
- May need smoke alarm or IR



Post Fire Event Concerns

- What do I need to be concerned about?
- Who is going to safe guard the scene?
- When can we investigate the origin?
- What's my role as a Fire Commander
- When can we re-occupy a building?
- How will this be transported?
- How do you remove these systems from a building safely?



Post Fire Considerations

- Re-ignition
- Compromised safety features
- Stranded energy
  - Assume SOC 100%
  - How can we remove the SOC safely?
  - What is needed for safety?
  - Monitoring devices
  - Right type of PPE
  - What is the BMS saying ?
    - On or OFF
  - What's a safe way to transport the ESS?



Post Fire

Fire Chief Responsibilities

- Review the decommissioning procedures
- Acceptance criteria
- Review the transportation plan
- Acceptance criteria
- Inquire about the recovery location
- Proper protections in your jurisdiction



Post Fire Decommissioning

- Fire Commander Role
- Narrative of removal process
- Listing of contingencies
- Fire Mitigation personnel
  - Safe guard of scene
  - Continuously on duty
  - Keep watch for fire
  - Contact FD if needed
  - Follow Decommissioning plan
  - Evacuate public structures
  - Stays till full removal
  - Must be qualified



Post Fire Removal

- Considerations
  - Salt bath for modules for safety
  - Remove to outdoor after each module removal
- Proper packaging for transport
  - Should be secured
- DOT Regulations
- What type of vehicle
  - Open back Transport
  - Closed back Transport



Energetic Hazardous Material

- DOT > Transport Haz Mat
- OSHA > Worker Safety
  - SDS > needed ?
- EPA > Environment
  - Water runoff
  - Similar to structure fires for corrosive



SAMSUNG SDI Co., LTD
Date: Dec. 10, 2015 Revision no.: 02
MODEL : BM13C

SAMSUNG SDI

- The International Air Transport Association (IATA) Dangerous Goods Regulations, Packing Instruction 965, Section I & or II (56th Edition, 2015)
- The International Maritime Dangerous Goods (IMDG) Code (2014 Edition), (Special provision 188, 230)
- US Hazardous Materials Regulations 49 CFR(Code of Federal Regulations) Sections 173.185 Lithium batteries and cells.
- The UN Recommendations on the Transport of Dangerous Goods, Manual of Tests and Criteria 38.3 Lithium batteries, Revision 3, Amendment 1 or any subsequent revision and amendment applicable at the date of the type (latest version is Revision 5, Amendment 2)
- UN No. 3480

If those lithium-ion batteries are packed with or contained in an equipment, then it is the responsibility of the shipper to ensure that the consignment are packed in compliance to the latest edition of the IATA Dangerous Goods Regulations section II. of either Packing Instruction 966 or 967 in order for that consignment to be declared as NOT RESTRICTED (non-hazardous/non-Dangerous). If those lithium-ion batteries are packed with or contained in an equipment, UN No. is UN3481

Our products are properly classified, described, packaged, marked, and labeled, and are in proper condition for transportation according to all the applicable international and national governmental regulations, not limited to the above mentioned. We further certify that the enclosed products have been tested and fulfilled the requirements and conditions in accordance with UN Recommendations (T1 ~ T8) on the Transport of Dangerous Goods Model Regulations and the Manual of Testes and Criteria.

Test results of the UN Recommendation on the Transport of Dangerous Goods

Manual of Test and Criteria (38.3 Lithium battery)		Test Results	Remark
No	Test item		
T1	Altitude Simulation	Pass	
T2	Thermal Test	Pass	
T3	Vibration	Pass	
T4	Shock	Pass	
T5	External Short Circuit	Pass	
T6	Impact/Crush	Pass	
T7	Overcharge	Pass	For pack and single cell battery only
T8	Forced Discharge	Pass	

15. Regulatory Information

U.S. Regulations

National Inventory TSCA
All of the components are listed on the TSCA inventory.

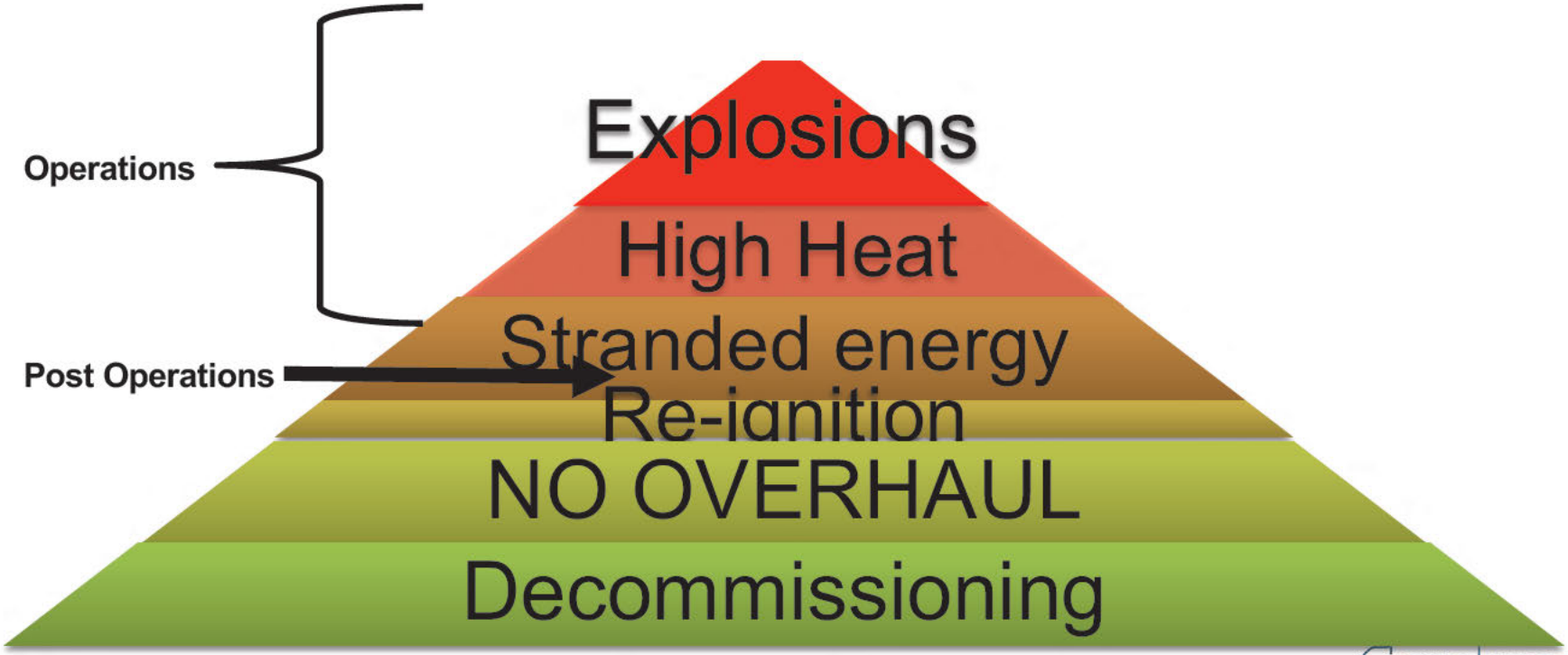
SARA
To the best of our knowledge this product contains no toxic chemicals subject to the supplier notification requirements of Section 313 of the Superfund Amendments and Reauthorization Act (SARA/EPCRA) and the requirements of 40 CFR Part 372.

Regulatory information EU

Labeling

Page 7 of 8

Operational Review



ESS installation



Case Study Arizona APS

- 8 firefighters hurt
- 2 critical
- Response information
- What they saw on arrival
- What they were told on the scene
- Size up information
  - 2 hours
  - Hose line stretched
- Door opened to the structure
- Explosion
  - FF thrown
  - Debris thrown
- Post fire Events



Questions?

For additional questions, please contact:

CleanEnergyHelp@nyserda.ny.gov



Annex 5 FMEA (Failure Modes and Effects Analysis) and BESS Hazard Mitigation analysis

B
DETAILED THREAT BARRIER DESCRIPTIONS

Each barrier in these models is more indicative of a concept that may include a single approach or may consist of a complex series of combined measures. This list does not contain all possible solutions and in some designs, these barriers may not exist at all. Many of the same barriers apply to a number of threats. For each barrier description, the associated top-level hazard model(s) and threat category are listed.

Active Cell Protections

Active cell protections which may mitigate thermal runaway such as module fans, liquid cooling systems, module scale suppression systems, or other mitigation measures.

A wide-ranging category that includes any type of actively monitored or controlled mechanism intended to protect against the effects of thermal runaway, whether it be actively preventing the cell from entering thermal runaway or actively mitigating thermal runaway once it occurs. This could include liquid cooling systems, direct injection suppression systems, fans, or other types of active protection schemes.

Adequate Sensing and Control

Aggregate of the ability of the BMS to detect cell imbalance and to properly return system to balance if possible, including adequately sized passive or active balancing scheme.

This covers the overall "resolution" of data acquisition within a battery system including the ability of the system to reliably detect voltages and verify those measurements for the purpose of avoiding false positives. Sensors can be sensitive to ground faults and other errors. Therefore, the inability to identify a failure and initiate response can result in extremely adverse consequences such as over charge, over discharge, and improper balancing.

Arc Design Protections

Design considerations intended to limit the ability of arc flash to occur in the system. Also includes proper design and selection of components which are capable of handling such events.

Protections in the system, as required by local codes and safety best practice, to avoid arc flash or mitigate the effects if it occurs. While arc flash poses a greater risk to humans, the energy released could cause adverse damage which may further drive other failure modes.

BMS Balancing Algorithm/Circuit Sizing

Ability of the BMS and balancing system to adequately balance the circuit including sizing of the balancing resistors or transistors.

Similar to *Adequate Sensing and Control*, BMS balancing is related to the effectiveness of the balancing circuitry to manage balance of voltage between cells, modules, and racks. Unlike the previous barrier though, this barrier is related to the actual balancing algorithm itself, as well as the effectiveness of the hardware to balance the system. As an example, some systems possess

DRAFT

passive resistors for balancing, but these resistors are capable of balancing less than .05% SOC in an hour, which would be critically ineffective in the case where a cell started degrading quickly.

BMS Control

Includes monitoring and shutdown/isolation capabilities of the affected BMS/module or system.

BMS Control includes aspects of ***BMS Shutdown/Disconnect*** but also includes overall effectiveness of monitoring such that proactive measures may be taken, or warnings given, indicating imminent failure or adverse conditions. Utilized as a barrier on multiple threats, it is likely this barrier would be evaluated differently in each case based on the algorithmic response to the threat or failure in question.

BMS Shutdown/Disconnect

Ability of the BMS to isolate affected modules or strings without shutting down the entire system, if unneeded.

BMS shutdown and disconnect is focused primarily on the ability of the system, while still active, to isolate itself or effected components while maintaining normal operation. Rather than rapid opening of emergency contactors and shutting down the entire system as in ***System Shutdown/Disconnect***, a BMS shutdown may be thought of as a soft shutdown, or standby state where the only affected modules or racks are isolated. Ideally, the BMS, while maintaining function, should return these components to function when the event has been cleared or corrected.

Cell Electrical Abuse Tolerance

Ability of the cell to withstand electrical abuse such as overcharge, over discharge, high currents, or other adverse electrical abuse.

The ability of the individual cells to withstand electrical abuse such as short circuit, overcharge, and overcurrent events without resulting in adverse conditions. This should not be considered a strong barrier. This barrier may include passive elements within the cells, as well as the cells' electrochemical ability to withstand these events. While some chemistries have shown more resilient to thermal exposure than others, it is less clear how those same chemistries withstand electrical abuse. As no testing standard yet exists to quantify the ability of the cell to withstand electrical abuse, this barrier, without consideration for passive elements, should typically be evaluated as weak.

Cell Physical Abuse Tolerance

Ability of the cell to withstand thermal, physical, or mechanical abuse.

This barrier considers the ability of a cell to withstand physical, thermal, or mechanical damage without resulting in an adverse condition. As all lithium ion battery chemistries have shown susceptibility to physical damage such as penetration and crush, this barrier is likely to be considered weak, depending on the threat faced. Some consideration may be given to the cell casing (e.g., cells comprised of hardened cases such as prismatic cells compared to a softer

DRAFT

pouch cell). However, the threat faced will ultimately determine the effectiveness of the case as even many prismatic cells will not survive ballistic penetration, vehicle impact, or crush.

Cell Quality Control

Overall quality of the cell such that internal defects are minimized and cells maintain rigidity and shape during operations. Also includes tight tolerances with respect to degradation and new capacity.

This barrier is intended as a catch all for considerations related to cell quality. This is likely to be outside the control of the end user of the system but covers the overall reliability of the cells with respect to internal failures and faults that may result in adverse conditions. In many cases, this barrier may be represented as a failure rate, such as 1 in 100 million. It is an exercise for the end user and their suppliers to determine how best to quantify this barrier.

Cell Thermal Abuse Tolerance

Ability of the cells to withstand thermal abuse without going into failure themselves.

Thermal abuse tolerance applies to the ability of the chemistry in question to fail when exposed to high temperatures. It is typically not considered a strong barrier without sufficient testing to demonstrate. Case by case results suggest some cells of a certain chemistry may resist high temperatures better than other chemistries, but this should not be assumed that this applies to the chemistry as a whole. Additionally, even more thermally tolerant chemistries may not withstand the temperatures of a fire or extreme heating during failure.

Cell Thermal Management

Active and passive controls put in place to manage cell temperature. Includes passive materials like Phase change material, module fans, liquid cooling system or passive systems dependent on system HVAC.

Effectiveness of cell temperature management, be it active or passive. Intended to cover the overall effectiveness of all (if any) methods employed by the system to manage individual cell temperatures. This could include liquid cooling, conductive or convective active cooling such as thermally regulated plates, or more passive approaches like simple air cooling.

Container Conditions Monitoring

Monitoring within the container which may detect high humidity, water condensation, water leakage, salinity in humidity, and other adverse water conditions.

In addition to the sensors, this barrier includes intelligence in the measurements which allows for prompt determination of adverse conditions, such as high humidity or dust, which poses a corrosion or electrical risk.

Container HVAC

Heating, ventilation, and air conditioning for the overall container designed to maintain overall system temperature and humidity levels.

DRAFT

HVAC failures have proven to be one of the most common failure modes in ESS and have been identified as the root cause for several of the battery fires in South Korea. While this barrier typically focuses primarily on temperature and managing heating from the electrical load, it should also account for high exterior temperatures and include humidity management and ventilation when the air conditioning is not running. It does not include emergency exhaust ventilation for managing the buildup of explosive gas or deflagration venting.

Depending on the HVAC design, the loss of a single unit may result in adverse temperature conditions. Redundant HVAC is an additional barrier to mitigate the impact of the loss of a unit.

Further consideration for the effectiveness of the barrier should include evaluation of the restriction of airflow through the unit. A lumped parameter model of heat generation that does not take into account the constricted nature of ESS racks and modules is likely to be inadequate for evaluating performance.

Container Structural Resiliency

Resiliency of the system and container of the system to withstand impacts or strikes.

While this depends on the threat and Facility Siting and Design, the enclosure envelope should be effective to protect against basic vandalism or low speed, accidental vehicle impacts such as construction equipment as well as high winds, hail, seismic vibrations, and other environmental forces.

Design Review and Engineering Best Practice

In addition to analysis required by product standards, good engineering practice should require design review such that design mistakes and weaknesses are identified and corrected in a timely and efficient manner.

This catchall barrier includes any and all engineering best practices, recommended best practices, standards of care, review process and analysis which are used to ensure a system is engineered to the best possible state based on realistic or practical expectations.

Emergency Response Plan/First Responders

System operator plan to handle any and all emergency events. Effectiveness based on level of SME / first responder training, knowledge of the specific ESS undergoing failure, coordination with fire department, etc.

First responders refer to site personnel, corporate employees, local technicians, and subject matter experts (SMEs) who may be the first to detect or respond to failure or fault in the system and alert fire services. The term first responders in this case does not refer to fire fighters or other fire service personnel, but to those who will be reporting the event or directing the fire service in regard to the risks posed by the system. The guidance from these individuals, as well as the information contained in the emergency response plan, will serve as the initial human response to the incident and have the greatest chance of containing the incident, if it is containable, to a reduced state. Depending on time to detection, time to first response and fire service response, the incident may have progressed through multiple consequence pathways, as single cell failure can propagate to adjacent modules and beyond in a matter of minutes.

DRAFT

The emergency response plan should address how these first responders, as well as the fire service, react to emergencies within the system. This may include a separate alarm management plan to address which information is essential for responders, critical thresholds of parameters, and potential hazards indicated by the alarms. The first responders' familiarity with the document as well as the overall effectiveness of the document may add or remove minutes or seconds to the response. Therefore, both the emergency response plan as well as the competence of the SME should be evaluated with respect to their effectiveness in interacting with the fire service. First responders may lack experience both with the technology and emergency response.

Facility Design and Siting

Placement of the facility such that adverse environmental effects such as flooding, vehicle impact, and fire impingement are mitigated or avoided. Likewise, placement such that adverse effects from the system are limited to exposures.

A broad barrier depending on threat or consequence pathway that is intended to include analysis of the system in its location with respect to localized environmental hazards, adjacent structures, fire loads, and personnel exposures, and other generic environmental threats either to the system as posed by the environment or to the environment as posed by the system. While a specific spacing may be suitable for most ESS, it may not be sufficient spacing from a large fuel storage depot or an ambulatory care facility. Further, this should include the type of environment the system is built in such as a flood plain, a high traffic area, a wetland, or an area prone to fire.

Fire Service Response

Fire department response including active firefighting suppression. Effectiveness based on level of department knowledge and training to effectively respond both offensively and defensively during an ESS incident.

This barrier includes all aspects of the fire service response including the personnel, resources, knowledge, and overall comfort level brought to bear on the scene. Current industry training and emergency response planning point toward automatic dispatch of multiple trucks or departments/stations for ESS emergencies or multiple alarms in some jurisdictions. In these cases, clear incident command is necessary to ensure that departments properly trained on the system are able to drive response. Further, fire service response will be supported by SMEs, whose own knowledge can drastically impact the fire service response. Finally, availability of data from the BMS, FACP, and any additional detection systems will act as the final multiplier, resulting in decisions which may save the currently impacted or adjacent systems or result in the loss of the entire project.

Fire Suppression

Fire suppression inside battery compartment which may address BoS fire without adverse effect on batteries. Potentially separate from battery fire suppression.

Fire suppression as a threat management barrier deals with management of non-battery fires and the effective suppression of these fires before they can impact the battery itself. Further, it deals with the ability of this suppression approach to manage the non-battery fire in a way that does not compromise the battery, such as by dousing it with saltwater or exposing it to caustic

DRAFT

substances which may cause degradation. However, fire suppression system discharge may be grounds for voiding the warranty, depending on the specific contract language.

See *Gas Phase Suppression System* and *Water Based Suppression System* for fire suppression as a consequence barrier.

Human Factors and Process Control

Quality control or other processes put in place to prevent mishandling of systems that may result in adverse or hazardous conditions or mishandling.

A catchall barrier that includes all possible failures and adverse conditions brought about by human interaction with the system. It also includes failures related to process and flow separate from the control system of ESS itself. This could be as simple as a technician dropping a wrench across the terminals or as complex as sophisticated maintenance procedure which fails to adequately address an otherwise trivial detail, such as failure to check the tightness of unreachable bolts or clean unexposed terminals.

Insulation Monitoring

Continual, or active, monitoring of insulation integrity, ground versus float voltage, and other practices to prevent insulation or isolation degradation.

Insulation monitoring is a common electrical maintenance best practice. Degradation of insulation for any reason runs the risk of current related failures anywhere in the system. This includes not just wire insulation but isolation on components and effectiveness of ground isolation during normal operation.

Inverter/PCS Controls

Includes monitoring, shutdown/isolation capabilities, and transient protections.

For electrical risks, this covers much of the inverter's ability to a manage adverse conditions as tested in UL1741 and less about the ability of the inverter or PCS' intelligence to detect adverse related to controls (such as an adverse current condition which is otherwise within an acceptable current range).

Module Resiliency

Resiliency of the individual modules to withstand impacts, shocks, or other mechanical abuse.

Similar to cell abuse tolerance, this barrier covers the overall strength and rigidity of a battery module as it relates to the ability of the module to withstand both impacts and shocks as well as the noise, vibration, and harshness which may be encountered over an ocean voyage or transportation in a semi-truck. Unlike cell abuse tolerance, which shouldn't be considered a strong barrier, module resiliency may be built in as part of commissioning with confidence that the modules should withstand transportation, maintenance, and construction without requiring reinspection. Regulations provide certification under UN38.3 that can be referenced for levels of resiliency during transportation for a certified product.

DRAFT

Module Thermal Management

Thermal management at the module scale including effectiveness of system HVAC at this level, passive materials, fans, and liquid cooling.

This barrier is intended to cover any active or passive mechanisms which manage the thermal properties of the modules. This could be a module-wide conductive cooling scheme, liquid cooling interfaces within the module, module fans, or other measures which are intended to cool the module as a whole more so than individual cells. Module thermal management may interact with or depend upon an enclosure-wide thermal management scheme.

Passive Arc Flash Protection

Physical protections and hardware designed to protect against or to limit arc flash.

Passive arc flash protection is common design feature used to protect against arc flash in the AC and DC equipment and could be based on NFPA 70E requirements or other local or organizational electrical protection codes. While the supporting equipment (switchgear, contactors, balance of plant subsystems) may withstand the heat and current of an arc flash (blowing fuses and throwing breakers), the batteries themselves may be adversely affected by heat and potential projectiles should the arc flash occur near the batteries. Further, the current event itself, which may be on the order of several thousand or tens of thousands of amps may also unduly stress the batteries.

Passive Cell Protections

Current interrupt devices, fuses, or other passive elements which may open the circuit in the case of failure and general resilience of design to withstand adverse electrical conditions.

In cases where the circuit is unable to adequately isolate itself, such as when no physical disconnect exists, the final barrier to avoiding catastrophic failure is passive circuit elements which may open the circuit at a number of locations. These would include breakers, fuses, current interrupt devices (CIDs), and pressure fuses or diaphragms which open individual cells prior to failure.

Depending on the nature of the failure, these elements may have mixed success in achieving these goals. For example, an inverter failure resulting in a short circuit or ground fault may draw sufficient current to trip a fuse or breaker, but an inverter which has lost voltage sensing capabilities may not result in the trip or failure of breakers or fuses because the batteries charge at their normal current rate. In the second scenario, the system could operate well beyond their safe voltage (assuming no active monitoring or control from the batteries) which may drive the cells into thermal runaway if left unchecked. The final passive cell protection barrier resides in the cells themselves, where pressure activated fuses or CIDs would open the individual cell circuits when a pressure increases as a result of gas generation from overcharge tripped the pressure device. These devices are only found in certain cell types.

Passive Circuit Protection and Design

Breakers, fuses, or other passive surge arresting elements which may open the circuit in the case of failure and general resilience of design to withstand adverse electrical conditions. Note hazard condition and component and that not all protections apply to a certain failure.

DRAFT

Passive circuit design considerations at this level aim to minimize pathways between modules or racks in which energy from one may bleed into another during failure, unlike Passive Cell Protections where the holistic design of the system is considered at the cell level. Passive elements under this barrier are likely purely current driven, only capable of protecting against over current events by way of breakers and fuses. Passive design considerations at this level may include circuit design such that the failure of a BMS in one module does not result in an adverse condition in others. An example may include a BMS whose balancing system fails, resulting in short circuits. A poorly designed system may allow for excessive energy to be dissipated through this short by having a common ground that allows energy from other modules to also be dissipated through this failure.

This failure mode was identified as a cause of the South Korea fires in 2018 and 2019. As a result of a design failure at the rack level, a ground fault in the rack was discharging the entire serial system, putting thousands of amps through a system designed for a few hundred amps.

Preventative Maintenance and Commissioning

Proper maintenance and monitoring of the system in conjunction with adequate commission and site acceptance testing to reduce likelihood of loose connections or other transportation or construction defects.

Preventative Maintenance consists of the normally scheduled preplanned maintenance required for operation such as periodic inspections for function and operating limits, replacement of expendable parts such as air filters, and the necessary upkeep required for continued operation as well as the prompt repair of failures and failing components. Commissioning refers to the process of bringing the system online, performing inspections of the built system to ensure proper compliance with operating parameters, and the shakedown of "bugs" and issues from construction to normal operation. Through these processes, the system is brought to and maintained in good working order. These processes, along with real time monitoring during operation are critical to the error and fault free operation of the system and should be evaluated based on their effectiveness at maintaining such conditions.

Redundant Failure Detection/System Intelligence

Ability of system to determine a sensor has failed, to operate safely without that sensor to shut down, or operate safely indefinitely without sensor. This may include Checksums, additional sensors, or the ability to pull data from other sensors.

This barrier is highly dependent on the sensor in question as well as the design, architecture, and operation of the system as a whole and the evaluation of the data collected within the confines of the system. As referenced in the definition, the loss of a cell level voltage sensor could be made up by comparing the known surviving voltage sensors with the total module voltage, allowing for the calculation of the cell voltage in question. While less than ideal, this method could be used to keep the system online during emergency situations or until maintenance can be performed.

In another circumstance, rather than risk shutting down the system for a potential false negative, false positive, or other failed signal, redundant detection compared against similar sensors may allow sensor failure to be ignored and operation to continue. As an example, a high temperature

DRAFT

signal without an accompanying high voltage signal could indicate a thermocouple failure, but a third sensor, such as an off-gas detector, IR, or additional voltage sensor could alert the system to a sensor failure and allow continued safe operation. This barrier may actually exist as multiple barriers in some systems, where both redundant sensors act as a hardware backup while intelligent software may also detect this failure digitally and devise a method for working around it safely.

If the system is poorly designed, lacking such redundant capability with no mitigating protection, a BMS failure, whether hardware or software, may equally result in the Top Hazard

Failures at the EMS level are unlikely to be mitigated by redundant sensors or detection systems. At this level, failure of this controller is likely handled by the balance of system PLC or the fire control panel which would issue a shutdown signal to the entire system, attempt to isolate the AC-DC circuit, and potentially open any utility connection such as a re-closer.

Redundant HVAC

Design, sizing, and hardware physical redundancy of the HVAC system such that failure of one or multiple units does not result in adverse conditions within the container or system.

Additional HVAC can be added such that a single HVAC failure or a temperature event does not result in an adverse temperature condition. Multiple HVAC condensers or air handlers not always function as redundant HVAC. If the number of units installed is the number to maintain 100% of the required cooling load, redundancy has not been achieved. Likewise, if HVAC units feed directly into rack or specific modules, then redundant HVAC is unlikely to be effective as a single unit loss still results in a single point of failure unless the effected racks/modules can be isolated.

Too much HVAC, however, can pose other issues. For example, an oversized system without proper controls can overcool the batteries (which could result in condensation or other adverse conditions) or at a minimum, result in excessive cycling and auxiliary power consumption by the HVAC.

Subject Matter Expertise/Training Adequacy

Proper training procedures, availability of subject matter expertise and system competence, and clear jurisdictional hierarchy for managing situations.

Though required by fire codes such as NFPA 855, subject matter expert (SME) remains an undefined term and the quality and title of SMEs across the industry varies wildly. In addition to the undefined term, there is no nationally recognized standard or methodology for training or credentialing subject matter experts. In some cases, the SME may be more critical to the response of an ESS emergency than the first service, because the safety of the first responders and fire fighters also depends on the SME. This role should be evaluated carefully by all stakeholders when selecting an SME.

Systems Certification and Standards Compliance

Risk assessment and functional safety are key processes for safe deployment of ESS.

DRAFT

Throughout UL1973, UL9540, UL1741 and other US standards are a number of requirements for product analysis and review including failure mode and effects analysis (FMEA), safety integrity level (SIL)/layer of protection analysis (LOPA), and other failure modes and safety analysis. While the product standards themselves usually cover the minimum requirements for safety, the analysis required by the standard may serve as a basis for additional review and may indicate additional failure modes not tested for in the standards or covered exhaustively by this guide. Compliance with these standards, by fire code and best practice, shall be requisite for operation of an ESS and while compliance with those standards does not ensure strong barriers where relevant, data from the tests may be used to inform this analysis.

System Design and Quality Control

Protections, design considerations, and manufacturing QC such that system may withstand such shocks.

A catchall barrier related to the overall quality of the build of the container, the integration of the system into the container, the ability of the system to withstand noise, vibration, and harshness (NVH) during transport and the overall design of the system for maintenance, construction, and transportation. This may also include container coatings and durability against degradation due to UV exposure, weather, and corrosion.

System Electrical Abuse Tolerance

Refers to ability of the overall system collectively to withstand adverse electrical abuse such as overcharge or dead shorts without failure.

This considers passive design, any additional technologies or approaches which may manage adverse electrical behavior, and overall resiliency of the design such that hazardous or adverse conditions within the electrical system are mitigated prior to becoming hazardous to the batteries.

System Shutdown/Disconnect

Ability of system to actively shut itself down or disconnect itself. This is the aggregate of the BMS or inverter's shutdown ability as well as physical disconnects and the BoS controller's ability to shut down.

In many of the threat pathways, system shutdown and disconnect are provided as barriers against cell failure. In this case, this barrier may be approached from two perspectives, with the first the ability of the system to truly shut off only the affected and responsible operations, namely the battery itself, when such conditions are detected. This shutdown will stop ohmic and electrochemical heating thus stopping heat generation and may also increase the temperature at which thermal runaway would occur (by stopping internal heat generation). The second approach involves shutting down the entire system, including thermal management or cooling systems, when such an issue is detected. Though the coordination of thermal management systems offers benefits to managing system temperature, this coordination, if done improperly, results in the shutdown of the same systems necessary to manage the issue. While ceasing heat generation may be sufficient in many cases for reducing, or stopping, the risk of thermal runaway, deactivating the protection system along with the protected system may result in spreading of the heat and continued exposure to hazardous conditions.

DRAFT

An Inverter Failure may trigger physical and electrical isolation of the power electronics from the energy storage system. This can be done by way of a mechanical switch/relay/contactor or any other active hardware component which will physically open the circuit. Electrical components such as FETs, IBGT's, or other power elements in the failed device may not reliably open the circuit as a failure of the device itself may result in failure of other components tied directly to the inverter. System shutdown and disconnect should be done automatically without human intervention, however manual switches may also exist in this protection scheme manual throw switches on individual racks or modules inside the container, E-stop buttons or switches, and remotely activated switches without automatic onsite control should only be considered for this barrier if manned 24/7 and if an alarm indicates a failure requiring response. Many vendors offer switches with view windows to visually verify physical disconnection and hasp mechanisms to lock out the equipment during maintenance, though these may be optional.

Beyond the existence of physical disconnect points, the following actuating factors should be considered: Can a module level high voltage alarm result in a disconnect? Does the failure of the inverter result in the opening? If a physical disconnect point exists, but it cannot detect the inverter failure and instead relies on a cell failure before opening, the barrier may not prove effective.

While there are likely few if no circumstances in which it is safe to operate without a functioning BMS (BMS Failure), isolation of the affected module in parallel systems or of the rack in serial configurations would allow the remainder of the ESS to operate without the need to shut down the entire system. This may only be accomplished in systems which possess the appropriate degree of control.

The shutdown and isolation required following a Sensor Failure can be more complex than an electronic component. The loss of a sensor itself does not guarantee a system behavior that may lead to catastrophic failure, and in many cases the system could continue to operate safely without it. As such, it may not be necessary to shut down an entire ESS container following the loss of a single thermistor if intelligent software and redundant hardware make up for the loss of the input. Further, a complicated isolation or shut down schema may allow for the affected module to be removed from the circuit. While not practical in serially installed systems, multiple parallel racks or modules may allow such isolation depending on system design and the nature of the failure.

More in line with inverter failure than BMS failure, a breakdown in function at the system or subsystem level operating on a single inverter is likely to result in the need for full system isolation from the power electronics in addition to isolation of individual strings or racks if power management between them cannot be managed or monitored as needed. It is unlikely isolation of individual strings or racks may correct the problem or result in adequate mitigation of it, and the entire system should be opened to prevent power transfer between racks if maintenance or emergency response is required.

Temperature Monitoring and Alarms

Thermal monitoring within the container including BMS, fire alarm thermal monitoring, and any BoS temperature monitoring.

This barrier is the ability of the battery system or BMS to detect adverse thermal conditions within itself and alarm those issues outward. While many systems claim thermal protection, the

DRAFT

presence of a single thermocouple or thermistor within a module may prove insufficient at detecting hot spots. Effective temperature monitoring would include high "resolution" detection of hot spots within a module. While measurement of every cell may not be required, monitoring should be done in a manner which offers an ability to detect high temperature zones within the battery.

Thermal Isolation Cascading Protection

Thermal protections inside the battery compartment which would limit module fire/thermal exposure.

As a threat barrier, Thermal Isolation/Cascading Protection consists of passive barriers, insulating materials and passive thermal materials such as intumescent and phase change materials which may protect the cells of an ESS from adverse thermal conditions within and outside of the ESS.

For more, see Error! Reference source not found. below in Consequence Barriers.

Voltage Monitoring

Overall effectiveness of the voltage monitoring scheme of the system. Includes resilience to errors, error checking, and other measurement intelligence.

This includes adequate measurement of voltage throughout the system coupled with checks or redundant measurements such that a sensor failure cannot drive the system to an adverse condition. This includes monitoring of module, rack, and bus levels DC voltages as well as AC line voltages and any intermediary voltages.

Voltage Monitoring and SOC Estimation

This may apply at the cell, module, and rack level. While voltage monitoring may be useful, more advanced methods such as coulomb counting may be used as well.

Voltage monitoring or other techniques at the cell, module, and rack level may be used to measure SOC. Voltage and SOC measurements are key to the safe and efficient operation of the system, therefore the ability to determine this state reliably is necessary for operation. SOC estimation is essential for monitoring capacity of the system and for de-rating the system should temperature conditions require such a response. Rapid, unexpected changes in capacity could also be indicative of failures in the system. Should SOC estimation be a function purely of voltage, failures of the voltage sense would also result in inaccurate SOC estimation, potentially allowing the system to exceed certain protection limits again depending on the architecture of the system.

DRAFT

C
DETAILED CONSEQUENCE DESCRIPTIONS

Consequences are the results of a threat pathway reaching and exceeding its Top Event. In these cases, barriers intended to mitigate the threat have failed, and the repercussions or consequences of those failures must now be dealt with directly. For the models described here, the Top Events were selected as the event in which proactive protections give way to reactive measures mostly related to fire protection systems and direct response. As the Top Event then is defined as either "cell failure" or propagating cell failure, the consequences in the models described assume a condition exists in which flammable gas is being released into the system or a fire is burning within the system. Further, the endpoint of a consequence is itself not the end of the event, and a single cell failure resulting in off-gas can easily evolve to a multicell failure with fire and ultimately a multi-module fire or worse. Thus, with consequences, as with threats, common barriers may be evaluated differently depending on the consequence they are associated with, and consequence pathways should not be assumed to be similar despite being comprised of similar barriers. As an example, though situational awareness, ventilation, and suppression are barriers in almost all the Consequences, situational awareness may increase or become less critical as the fire grows in scale. It may also decrease in effectiveness depending on the scale and the design of the system. As a further example, water-based suppression may not prove effective at a single cell failure while a gas phase agent may suppress combustion and limit the convective failure. As the scale of the fire increases though, gas-phase agents may only exacerbate the situation while water-based agents may more effectively manage the heat transfer. Ultimately, each consequence pathway should be evaluated separately and uniquely based on the consequence condition.

Accumulation of Off-Gas/Explosion Risk

Cell failure which may or may not have propagated has resulted in the accumulation of potentially explosive off-gas within the containment.

Even with a single cell, long after the risk of propagating failure has passed, off-gas may continue to linger in the area, especially in confined, poorly ventilated spaces. This gas may continue to pose deflagration risk. Even cooled or extinguished batteries may emit gas several hours following an event. The lack of ventilation observed in some systems means the ability to exhaust this gas may be lacking or nonexistent. The quantity of the gas itself, coupled with some common suppression methods, may result in oxygen depleted environments which make emergency response challenging or dangerous without adequate situational awareness.

Battery Damage or Excessive Degradation/Impact to Life

As a result of adverse conditions, batteries are subject to increased rate of or excessive degradation which will result in premature end of life.

SOH degradation and imbalance or any drastic change in electrical performance of the battery as a result of damage could create a number of problems with the operation of the battery.

DRAFT

Cell Failure Results in Balance of System Fire

A fire from a cell or multiple cells which results in a balance of system fire such as wire insulation or plastic inside the system.

In this instance, a small fire, results in damage to the balance of system, including wiring insulation, bus bars, plastic containment or other component or material. Such damage may pose significant risk as compromised wiring or components may result in arcing, shorting, or other high energy event or act as ignition source causing delayed fire or explosion.

Fire Spread Beyond Containment

A fire within the system has spread beyond the system containment, be it the container, room, or purpose-built structure.

In this case, fire has likely compromised the entire interior space of the enclosure or container and has now breached the container, posing immediate risk to adjacent equipment or facilities. Defensive firefighting is required while the nature of the breach is assessed to determine ability to use the opening to get suppressant into the container. A fire of this scale may burn for several hours.

Multicell/Module Failure – Combustion

Multiple cells have failed or entered thermal runaway, resulting in a propagating fire or combustion up to a full module fire.

Similar to a single cell fire, a multicell or module failure resulting in combustion poses a significant fire risk which must be dealt with immediately. At this scale, the likelihood of propagation, or continuing propagation is high. It is at this point where suppression likely has its best chance of controlling the fire, though dependent on a number of factors. Ultimately it is at this stage where changes in combustion patterns or oxygen content may still result in buildup of explosive gas and may generate sufficient heat to stay above autoignition temperature for several hours, even if the fire fails to propagate further.

Multiple/Module Failure – Off-gas

Multiple cells up to an entire module have failed, resulting in gas production.

Similar to single cell failure with off-gas, an explosive mixture is likely to exist in the container. While this event may not directly result in module-to-module thermal runaway propagation, preliminary modeling in some systems has shown that a single module failure may still result in a uniformly explosive vapor cloud in a containerized system. As such, this failure may pose one of the greatest risks to first responders as the failure mode will create an explosive, oxygen depleted atmosphere potentially lacking the heat required for exterior detection or to drive smoke out of the system and provide warning of the environment inside.

Multi Module/Rack Fire

Multiple modules have begun burning, resulting in a growing fire which may overcome internal suppression capabilities.

DRAFT

Fire within multiple modules or racks. Fire at this scale may be the result of propagation from a smaller event and may indicate failure of the suppression systems to contain it. As such, fire at this scale will be more dependent on the fire fighter response. Defensive postures may be needed to protect external exposures if firefighters struggle to reach the affected systems and manage the fire directly. Depending on system size, this fire may burn for several hours.

Physical Damage to Batteries

Batteries are subject to thermal, electric, or physical abuse which would make their continued use subject to higher risk.

In this case, physical damage includes mechanical, thermal, or electrical which may compromise the cell, leading to any of the failure modes discussed above.

Single Cell Failure – Combustion

A single cell has failed and is now producing flame or combusting.

A single cell failure resulting in combustion and flame is likely the result of thermal runaway. While several mitigating barriers exist to prevent this scenario from reaching its natural conclusion, should those barriers fail, it is possible this consequence will continue, evolving into any of the consequences listed in this section.

Single Cell Failure – Off-gas

A single cell has failed or entered thermal runaway and is now producing off-gas.

Battery off-gas is often highly flammable and typically consists of hydrogen, carbon monoxide, methane, and other flammable hydrocarbons. As such, this event may pose even greater risk than a single cell combustion, as the ability of batteries to maintain high temperatures in excess of autoignition temperatures for hours is well documented and the electrical nature of the systems adds additional ignitions sources. Poor air management may also result in delayed ignition scenarios when oxygen rich air is introduced into the space later. While small cylindrical cells may pose reduced risk by nature of their size, large format cells may possess enough electrolyte, and ultimately gas generation potential, to create a highly flammable environment from only a single cell.

Unknown Failure

A system or cell failure of unknown nature in which the environment inside the system is unknown and poses unknown risks to first responders, the fire service, and potentially the public.

Though large-scale fire testing and commitment of considerable resources to the study of energy storage safety issues has drastically improved the industry's knowledge of failure modes, threats, consequences, and general safety, many failure modes and corresponding responses remain uncharacterized. Preparing for the unexpected is always advised. Further, this consequence may cover emergency scenarios where a fire department has a lack of situational awareness.

DRAFT

D
DETAILED CONSEQUENCE BARRIER DESCRIPTIONS

Consequence pathways include barriers that may help to manage or prevent the consequence event.

Cell Physical Abuse Tolerance

Ability of the cell to withstand thermal, physical, or mechanical abuse.

This barrier considers the ability of a cell to withstand physical, thermal, or mechanical damage without resulting in an adverse condition. Some consideration may be given to the cell casing (e.g., cells comprised of hardened cases such as prismatic cells compared to a softer pouch cell) when assessing the strength of this barrier. However, the threat faced will ultimately determine the effectiveness of the case as even many prismatic cells will not survive ballistic penetration, vehicle impact, or crush.

Deflagration Protection

NFPA 68, NFPA 69, or other deflagration protection.

Deflagration or explosion as a result of combustion, expansion, or detonation, poses severe risks to life and property near an ESS. The off-gas emitted by all lithium ion batteries with an organic electrolyte is composed primarily of hydrogen, carbon monoxide, carbon dioxide and flammable hydrocarbons. Therefore, the release of gas from even a small number of cells can pose significant danger. As a result, many fire codes now require deflagration protection designed with system-specific test results from product standards tests such as UL 9540a. While systems going into the field in compliance with this code should have this barrier as a strength, many systems in the field today lack even a basic ability to protect themselves from this buildup of explosive gas or ability to withstand the actual deflagration itself.

Detection Systems / FACP

Includes heat, smoke, and gas detection systems, as well as other Fire Alarm Control Panel (FACP) / NFPA 72 devices. Effectiveness based on what is detected and how well, how information is conveyed, and robustness of sensors in case of failure.

This is an example of a barrier that is less a physical barrier and more a multiplier to the other barriers in the pathway. The effectiveness is based on the ability of the system and site to provide information and clarity of the failure. Poor situational awareness may weaken subsequent barriers in the same manner. As an example, firefighter response hampered by a lack of data may result in excessive propagation of a fire when earlier intervention may have saved greater portions of the system.

This barrier consists of whatever data is available from within the energy storage system, (e.g., temperature, system voltage, SOC, currents, and connection status), as well as information from the fire control panel (e.g., smoke alarm status, thermal alarm status, gas detection, off-gas

DRAFT

detection, and suppression status), and information from any third-party monitoring systems including separate gas and visual monitoring systems. In all cases. it is dependent on proper annunciation of this data on site or the availability of this data to first responders and operations personnel. It also includes knowledge available at the site in the form of subject matter experts (SMEs), site personnel, emergency response experts available via phone, and any additional knowledge which may be gained from within the system visually or digital documentation.

All of this information is necessary for maximizing the efficiency of each subsequent barrier, whether it is automated or driven by human factors.

Emergency Response Plan/First Responders

System operator plan to handle any and all emergency events. Effectiveness based on level of SME / first responder training, knowledge of the specific ESS undergoing failure, coordination with fire department, etc.

First responders refer to site personnel, corporate employees, local technicians, and subject matter experts (SMEs) who may be the first to detect or respond to failure or fault in the system and alert fire services. The term first responders in this case does not refer to fire fighters or other fire service personnel, but to those who will be reporting the event or directing the fire service in regard to the risks posed by the system. The guidance from these individuals, as well as the information contained in the emergency response plan, will serve as the initial human response to the incident and have the greatest chance of containing the incident, if it is containable, to a reduced state. Depending on time to detection, along with time to first response and fire service response, the incident may have progressed through multiple consequence pathways, as single cell failure can propagate to adjacent modules in beyond in a matter of minutes.

The emergency response plan should address how these first responders, as well as the fire service, react to emergencies within the system. This may include a separate alarm management plan to address which information is essential for responders, critical thresholds of parameters, and potential hazards indicated by the alarms. The first responder's familiarity with the document as well as the overall effectiveness of the document may add or remove minutes or seconds to the response. Therefore, both the emergency response plan as well as the competence of the SME should be evaluated with respect to their effectiveness in interacting with the fire service. First responders may lack experience both with the technology and emergency response and the industry currently lacks best practices in formalized training and standard curriculum.

Exhaust Ventilation

Effectiveness of exhaust ventilation to remove battery off-gas, heat, and smoke which may result in adverse atmospheric conditions.

ESS failures often produce an immense quantity of gas. While numbers vary as additional data comes available, proprietary testing to date has shown the gas produced per unit of energy is approximately on the order of 1-3 liters/Ah during pre-combustion thermal runaway. The concern is the explosive nature of this gas, which is oxygen depleting (based on volumetric ratio) due to the quantity released, especially in confined spaces. This gas is prone to stratification as well depending on failure mode, temperature, and ventilation effectiveness. This explosive risk is compounded by the fact that pre-combustion off-gas is composed heavily of hydrogen gas,

DRAFT

which becomes explosive at 4% concentration and is prone to high-pressure deflagration and potentially detonation. As a result, these events have proven difficult to manage, and even labs and test facilities, staffed by experts in safety and destructive testing, have still experienced explosions and other loss of control situations despite best efforts and past experiences.

With these facts considered, exhaust ventilation is critical to managing an energy storage incident. Many jurisdictions require compliance with NFPA 68 (Standard on Explosion Protection by Deflagration Venting), and best practice would suggest that designs also incorporate measures to reduce the level of flammable gas in the enclosure via ventilation to avoid the explosion, It should be noted that even with ventilation, the tight confines within an ESS can create areas of poor air flow, and localized explosions within a system are possible where small pockets of gas build up from even a single cell failure. Further, while not yet demonstrated via additional large-scale testing, preliminary test results indicate that automated, water-based suppression may be more effective at managing energy storage fire when used in conjunction with effective exhaust ventilation.

Effective exhaust barriers require right-sized penetrations in the container designed with consideration for the specific chemistry and failure test results of the specific energy storage product for that site. The solution may require self-opening mechanical louvers, small exhaust fans used for temperature control, and pressure relief louvers directed outward and upward from of the container capable of handling the high flow rates needed during wider scale failure.

Facility Design and Siting

Placement of the facility such that adverse environmental effects such as flooding, vehicle impact, and fire impingement are mitigated or avoided. Likewise, placement such that adverse effects from the system are limited to exposures.

This barrier is intended to include analysis of the system in its location with respect to localized environmental hazards, adjacent structures, fire loads, and personnel exposures, and other generic environmental threats either to the system as posed by the environment or to the environment as posed by the system. While a specific spacing may be suitable for most ESS, it may not be sufficient spacing from a large fuel storage depot or an ambulatory care facility. Further, proper siting should include the type of environment the system is built in such as a flood plain, a high traffic area, a wetland, or an area prone to fire.

Fire Service Response

Fire department response including active firefighting suppression. Effectiveness based on level of department knowledge and training to effectively respond both offensively and defensively during an ESS incident.

This barrier includes all aspects of the fire service response including the personnel, resources, knowledge, and overall comfort level brought to bear on the scene. Current industry training and emergency response planning point toward automatic dispatch of multiple trucks or departments/stations for ESS emergencies or multiple alarms in some jurisdictions. In these cases, clear incident command is necessary to ensure that departments properly trained on the system are able to drive response. Further, fire service response will be supported by SMEs, whose own knowledge can drastically impact the fire service response. Finally, situational

DRAFT

awareness (e.g. Detection Systems / FACP) will act as the final multiplier, resulting in decisions which may save the currently impacted or adjacent systems or result in the loss of the entire project.

Gas Phase Suppression Systems

Novec, FM-200, inert gas, or aerosolized gas-based agent designed for fire suppression.

Gas phase suppression systems have been installed, many at the factory, in a number of systems deployed around the world. The intent is to provide fire suppression capability in lieu of installing a water-based system which would require additional, and potentially costly, plumbing. The "tradition" of installing these systems has persisted even after initial test data suggested they may not properly address fire in the batteries themselves in their current configurations. Gas based systems, which may be effective against "balance of system" or non-battery fires, may be backed up by water-based suppression for fire in the batteries and supported by adequate ventilation to promptly remove the agent if it is ineffective at suppression (i.e., the system continues to increase in temperature).

The concern around gas phase agents, is the explosion risk they introduce. Suppressing combustion with a gas phase suppressant without controlling thermal runaway propagation allows for off-gas generation while depleting oxygen levels. Affected batteries, which may remain hot for hours, could provide an ignition source if oxygen is reintroduced back into the space.

Without large-scale fire testing to support it, gas phase agents should not be considered a strong or effective barrier against battery fires. However, they are expected to perform adequately against other fires in the battery space and may, in limited cases, manage convective heat propagation. Additionally, gas-based system discharge may be grounds for voiding the warranty, depending on the specific contract language.

Redundant Failure Detection/System Intelligence

Ability of system to determine a sensor has failed, to operate safely without that sensor to shut down, or operate safely indefinitely without sensor. This may include Checksums, additional sensors, or the ability to pull data from other sensors.

This barrier is highly dependent on the sensor in question as well as the design, architecture, and operation of the system as a whole and the evaluation of the data collected within the confines of the system. As referenced in the definition, the loss of a cell level voltage sensor could be made up by comparing the known surviving voltage sensors with the total module voltage, allowing for the calculation of the cell voltage in question. While less than ideal, this method could be used to keep the system online during emergency situations or until maintenance can be performed.

In another circumstance, rather than risk shutting down the system for a potential false negative, false positive, or other failed signal, redundant detection compared against similar sensors may allow sensor failure to be ignored and operation to continue. As an example, a high temperature signal without an accompanying high voltage signal could indicate a thermocouple failure, but a third sensor, such as an off-gas detector, IR, or additional voltage sensor could alert the system to a sensor failure and allow continued safe operation. This barrier may actually exist as multiple

DRAFT

barriers in some systems, where both redundant sensors act as a hardware backup while intelligent software may also detect this failure digitally and devise a method for working around it safely.

System Shutdown and Disconnect

Ability of system to actively shut itself down or disconnect itself. This is the aggregate of the BMS or inverter's shutdown ability as well as physical disconnects and the BoS controller's ability to shut down.

See *System Shutdown/Disconnect* above in Error! Reference source not found..

While this barrier is technically equivalent to the same barrier on the Threat side, and in most cases will be evaluated for effectiveness the same way, its role on the consequence path is to shut down and isolate the system for the safety of first responders during an emergency event. On the Threat side, its effectiveness is weighed to its ability to isolate the system and stop failure or mitigate its propagation. Therefore, while the effectiveness of the two should align, there may be slight differences that lead to variations in analysis and ultimately the possibility that the effectiveness of each side may vary based on the failure and consequence.

Thermal Isolation/Cascading Protection

Thermal protections inside the battery compartment which would limit module fire/thermal exposure.

This includes all protections between battery modules and/or racks which would limit the propagation of a fire outward to other modules/racks and likewise protect modules/racks in the case of external (or internal) fire which may impinge on the batteries. This does not include active suppression systems but instead covers things like passive barriers and materials, nonflammable plates, intumescent materials, and intelligent designs which include gas routing and other design features which manage heat release and absorption.

Water Based Suppression Systems

Water based suppression system includes systems covered under NFPA standards NFPA 13 for sprinklers, NFPA 15 for sprayers, deluge systems, or NFPA 750 for water mist systems designed to suppress fire.

This suppression agent is the only suppression methodology prescriptively called out in the fire code. Automated water-based suppression has been shown to be capable of managing the heat exposure which can reduce the risk posed to adjacent exposures and objects. Recent testing by FM Global[1] showed that while the sprinkler did not extinguish, or even suppress, the system itself, it did protect nearby walls and systems.

While test data is lacking, preliminary research shows that suppression systems may more effectively manage battery fires by spraying water directly into the effected systems. Though the

[1] [redacted]

DRAFT

heat released by lithium ion battery systems is high, it is the gas production, deep seated nature of the fire, and the tight, densely packed, and protected structure of the systems that makes extinguishment difficult. While not 100% effective as reignitions have occurred in preliminary testing, water has been shown to be the most effective agent for managing ESS fires by removing the heat generated. Additional large-scale testing and data is needed to determine effective, prescriptive water flow rate requirements and the effectiveness of automated water systems.

DRAFT

Exhibit I:
Hazard Mitigation Analysis

FIRE & RISK ALLIANCE

Scout Energy Storage Facility, Wattsville, VA
Hazard Mitigation Analysis for Outside Ground Mounted Battery Energy Storage Systems

DRAFT REPORT – REVISION 0

DRAFT

Jupiter POWER

Prepared by:

Fire & Risk Alliance, LLC
Derwood, MD 20855

November 5, 2021

TABLE OF CONTENTS

Executive Summary 4

1.0 Report Description 6

2.0 Report Definitions 6

3.0 Applicable Codes and Standards 8

4.0 Maximum Allowable Quantity (MAQ) 8

4.1 VFPC/IFC 2018 Maximum Allowable Quantity 8

4.2 NFPA 855 Maximum Allowable Quantity 9

4.3 Electrical Energy Storage System Design 9

4.3.1 Samsung Cell Specifications 10

4.3.2 Samsung Module Specifications 10

4.3.3 Samsung Unit specifications 11

5.0 Proposed Battery Energy Storage System Designs 12

5.1 Model ST2752UX-US ESS 12

6.0 Hazard Mitigation Analysis 14

6.1 UL 9540A Test Method 15

6.1.1 Samsung SDI UL 9540A Cell Level Test Summary 15

6.1.2 Samsung UL 9540A Module Level Test Summary 18

6.1.3 Samsung UL 9540A Unit Level Test Summary 18

6.2 Off Gassing IDLH and Explosion Hazard Analysis 26

6.2.1 Flammable Gas Generation 26

6.2.2 Analysis of IDLH Gas Concentrations 27

6.2.3 Ventilation Requirements 28

6.3 Failure Modes and Effects Analysis 29

6.3.1 Thermal Runaway 29

6.3.2 Failure of ESMS 30

6.3.3 Failure of Ventilation or Exhaust System 30

6.3.4 Voltage Surge on Primary Electric Supply 30

6.3.5 Short Circuit on Load Side of Battery Storage System 30

6.3.6 Failure of Fire Detection and Suppression System 31

6.3.7 Spill Neutralization 31

6.4 Mitigations 31

7.0 Conclusions 31

8.0 References 33

DRAFT

TABLE OF FIGURES AND TABLES

Figure 1. Samsung SDI CS1000RT001A Cell 10
Figure 2. Samsung Module Assembly 11
Figure 3. Unit Assembly 12
Figure 4. ST2752UX-US ESS Exterior View 13
Figure 5. ST2752UX-US ESS Plan View 13
Figure 6. Samsung Cell Testing Configuration 16
Figure 7. Samsung Cell Test Temperature Data 17
Figure 8. Samsung Cell after UL 9540A Testing 18
Figure 9. Module Location in Unit Testing 19
Figure 10. Location of Thermocouples inside the Initiating Module 20
Figure 11. Temperature Measurements in the Initiating Module (Odd Numbered Cells) 21
Figure 12. Temperature Measurements in the Initiating Module (Even Numbered Cells) 21
Figure 13. Unit Testing Configuration 22
Figure 14. Temperature Measurements at the Front of the Initiating Unit 23
Figure 15. Temperature Measurements at the Rear of the Initiating Unit 23
Figure 16. Damage to the Initiating Module 24
Figure 17. Damage to Module 26 in Target Unit 1 24
Figure 18. Damage to Module 54 in Target Unit 3 25
Figure 19. Gas Flow Rates Measured during the Unit Level Test 25

Table 1. Battery Capacity Threshold and MAQ per the IFC 9
Table 2. Battery Capacity Threshold and MAQ per NFPA 9
Table 3 ST2752UX-US System Specifications 14
Table 4. Samsung Cell Off Gas Composition 16
Table 5. Samsung Cell Level Test Data 16
Table 6. Hydrogen Off Gassing Volume Needed to Reach the LEL 26
Table 7. Carbon Monoxide Off Gassing Volume Needed to Reach the LEL 27
Table 8. Cell Vent Gas Volume Needed to Reach the LEL 27
Table 9. Carbon Monoxide Volume Needed to Reach the IDLH Threshold 28
Table 10. Ventilation Requirements for Each Gas Species 29

DRAFT

EXECUTIVE SUMMARY

Jupiter Power (Jupiter) is installing an outdoor stationary storage battery system in Wattsville, VA. The battery energy storage systems (BESS) are integrated turnkey designs in an outdoor cabinet or container configuration. Fire & Risk Alliance, LLC. (FRA) was contracted to perform a Hazard Mitigation Analysis (HMA) for the proposed BESS system provided by Sungrow-Samsung SDI Energy Storage Power Supply Co, Ltd. (Sungrow). The proposed BESS is Model ST2752UX-US with nameplate battery capacity of 2752 kWh comprised of Lithium Iron Phosphate (LFP) batteries. The report is applicable to installations involving one or more of these outdoor ESS on a site.

The HMA was prepared in accordance with International Fire Code (IFC) and National Fire Protection Association (NFPA) requirements. UL (Underwriters Laboratories) 9540A testing was conducted in accordance with the UL 9540A Test Method for Evaluating Thermal Runaway Fire propagation in Battery Energy Storage Systems.

A Failure Mode and Effects Analysis (FMEA) was conducted which illustrated that there are numerous protections in place at the cell, module, and unit level to minimize the likelihood of a thermal runaway event within the cells from occurring. The UL testing was performed to demonstrate that, in the unlikely event that a thermal runaway event does occur, that the risk is minimal.

Cell level testing determines the method for initiating thermal runaway and characterizes the flammable gases that are vented during the event. The Samsung cells underwent thermal runaway via the use of thin film heaters applied to the cells per UL 9540A. The cells also generated flammable and toxic gases, which results in the need for module level testing.

Module level testing indicated that thermal runaway propagates to all cells within the Samsung module when thermal runaway is induced within multiple cells. Propagation of thermal runaway of the cells within the module and the presence of visible flames resulted in the need for unit level testing to be conducted.

Unit level testing demonstrated that thermal runaway does not propagate beyond the initiating module. The maximum recorded heat flux to the neighboring target modules was XX kW/m^2 and the maximum temperature measured at target modules was XX °C. This indicates that thermal runaway of a single module does not generate sufficient heat to induce thermal runaway in neighboring units. Ultimately, the UL 9540A unit level test demonstrated that thermal runaway is contained within the module of initiation. Thermal runaway does not propagate to neighboring modules or units, preventing a cascading fire event.

The units being proposed for installation meet the criteria listed in IFC §1206.2.3.2 and NFPA 855 §4.1.4.3 pertaining to fire development. Heat flux measured at the target walls and egress path recorded a maximum value of XX kW/m^2 during the test. Therefore, there is no thermal hazard to any container construction elements located at the distances measured or beyond. The effects of thermal runaway are localized to the initiating module and do not produce thermal energy hazardous to occupants or first responders.

Based on the results of the UL 9540A test off gassing in the event of thermal runaway may lead to flammable gas concentrations presenting an explosion hazard and carbon monoxide concentrations

DRAFT

exceeding the IDLH threshold. Accordingly, XX cfm of ventilation must be provided to run continuously or activate upon gas detection to prevent flammable and untenable gas concentrations in the container. Assuming that this mitigation feature is provided, the potential explosion and toxic exposure risks will be appropriately managed.

Although the UL9450A unit level testing indicates that propagation of thermal runaway will not occur, each of the BESS containers will be equipped with a manually activated dry pipe suppression system and detection of thermal runaway and fire conditions is via smoke and heat gas detectors installed within the container. The BESS cabinets are located outdoors and are not designed for walk-in use. Walkways are outside the containers.

The UL 9540A testing does not account for the protections provided by the BMS or ESMS that provide multiple layers of protection and detection for the batteries. The BMS monitors the cell voltage, temperature, discharging power, overvoltage protection, cell impedance, and fuse detection. In the event of an abnormal reading for any of the listed conditions, the BMS prevents the affected module from charging or discharging. The ESMS also prevents the affected module from charging or discharging, if required, as a supplementary safety measure.

In summary, the lithium ion battery energy storage systems being proposed by Jupiter meet all the criteria listed by the IFC and NFPA 855 for approval of the HMA, contingent on the provision of ventilation. XX cfm of ventilation must be provided to run continuously or activate upon gas detection to prevent flammable and untenable gas concentrations in the container in the unlikely event of thermal runaway.

DRAFT

1.0 REPORT DESCRIPTION

Jupiter Power, LLC. (hereafter referred to as Jupiter) is installing an outdoor stationary storage battery system in Wattsville, VA. The battery energy storage system (BESS) are integrated turnkey designs in an outdoor cabinet or container configuration. Fire & Risk Alliance, LLC. (FRA) was contracted to perform a Hazard Mitigation Analysis (HMA) for Jupiter on the proposed BESS system enclosure design to be provided by Sungrow Model ST2752UX-US.

This report is applicable to the Sungrow Model ST2752UX-US BESS and similar configurations provided that the same size enclosures are used with the same internal volumes. Additionally, the following configurations are acceptable:

- The number of cells per module and number of modules per rack is less than or equal to those evaluated in this report. The enclosures may be de-populated with fewer cells per module, fewer modules per rack, or fewer racks.
- The enclosure may have a different inverter model provided that the system remains UL9540 compliant.
- One or more of the applicable BESS enclosure systems may be used on the same site.

The HMA is prepared in accordance with International Fire Code (IFC) and National Fire Protection Association (NFPA) requirements. The UL (Underwriters Laboratories) 9540A testing was conducted in accordance with the UL 9540A Test Method for Evaluating Thermal Runaway Fire propagation in Battery Energy Storage Systems.

2.0 REPORT DEFINITIONS

The following terms are defined in the National Fire Protection Association (NFPA), Underwriters Laboratories (UL) 9540A, and International Fire Code (IFC).

Battery Energy Storage System (BESS) [UL 9540A §4.2]: Stationary equipment that receives electrical energy and then utilizes batteries to store that energy to supply electrical energy at some future time. The BESS, at a minimum consists of one or more modules, a power conditioning system (PCS), battery management system (BMS) and balance of plant components. (Underwriters Laboratories, 2019)

Battery Management System (BMS) [NFPA 855§ 3.3.3]: A system that monitors, controls, and optimizes performance of an individual or multiple battery modules in an energy storage system and has the ability to control the disconnection of the module(s) from the system in the event of abnormal conditions. This system can be completely independent of the ESMS. (National Fire Protection Association, 2020)

Cell [UL 9540A §4.3]: The basic functional electrochemical unit containing an assembly of electrodes, electrolyte, separators, container, and terminals. It is a source of electrical energy by direct conversion of chemical energy. (Underwriters Laboratories, 2019)

Combustible: Readily or easily ignitable material. Specific definitions vary depending on material; dust, fibers, liquids.

Combustible Liquid, Class II [IFC §202]: Liquids having a closed cup flash point at or above 100 degrees F, and below 140 degrees F. [E.G. Diesel Fuel] (International Code Council, 2018)

DRAFT

Emergency Alarm System [IFC §202]: A system to provide indication and warning of emergency situations involving hazardous materials.

Energy Storage Management System (ESMS) [NFPA 855 §3.3.8]: A system that monitors, controls, and optimizes the performance of an energy storage system and has the ability to control the disconnection of the energy storage system in the event of abnormal conditions.

Energy Storage Systems (ESS) [NFPA 855 §3.3.9]: One or more devices, assembled together, capable of storing energy in order to supply electrical energy at a future time to the local power loads, to the utility grid, or for grid support. (National Fire Protection Association, 2020)

Energy Storage System Cabinet [NFPA 855 §3.3.9.2]: A cabinet containing components of the energy storage system that is included in the UL 9540A listing for the system where personnel cannot enter the enclosure (National Fire Protection Association, 2020)

Fire Resistance [IFC §202]: That property of materials or their assemblies that prevents or retards the passage of excessive heat, hot gases or flames under conditions of use. (International Code Council, 2018)

Fire Resistance Rating [IFC §202]: The period of time a building element, component or assembly maintains the ability to confine a fire, continues to perform a given structural function, or both, as determined by the tests, or the methods based on tests prescribed in Section 703 of the International Building Code. (International Code Council, 2018)

Flammable Gas [IFC §202]: A material that is a gas at 68° F (20° C) or less at 14.7 pounds per square inch atmosphere (psia) (101 kPa) of pressure [a material that has a boiling point of 68° F (20° C) or less at 14.7 psia (101 kPa) which:

1. Is ignitable at 14.7 psia (101 kPa) when in a mixture of 13 percent or less by volume with air; or
2. Has a flammable range at 14.7 psia (101 kPa) with air of at least 12 percent, regardless of the lower limit.

The limits specified shall be determined at 14.7 psi (101 kPa) of pressure and a temperature of 68° F (20° C) in accordance with ASTEM E681. (International Code Council, 2018)

Lithium-ion battery [IFC §202]: A storage battery with lithium ions serving as the charge carriers of the battery. The electrolyte is a polymer mixture of carbonates with an inorganic salt and can be in a liquid or a gelled polymer form. Lithiated metal oxide is typically a cathode and forms of carbon or graphite typically form the anode. (International Code Council, 2018)

Module [UL 9540A §4.9]: A subassembly that is a component of a BESS that consists of a group of cells or electrochemical capacitors connected together either in a series and/or parallel configuration (sometimes referred to as a block) with or without protective devices and monitoring circuitry. (Underwriters Laboratories, 2019)

Occupancy Classifications: For the purposes of this report certain occupancies are defined as follows:

Factory Industrial Group F [IFC §306]: Factory Industrial Group F occupancy includes, among others, the use of a building or structure, or a portion thereof, for assembling, disassembling, fabricating, finishing, manufacturing, packaging, repair or processing operations that are not classified as a Group H hazardous or Group S storage occupancy.

DRAFT

> High-hazard Group H-2 [IFC §307]: Buildings and structures containing materials that pose a deflagration hazard or a hazard from accelerated burning shall be classified as Group H-2. (International Code Council, 2018)

Stationary Energy Storage System [NFPA 855 §3.3.9.7]: An energy storage system that is permanently installed as fixed equipment. (National Fire Protection Association, 2020)

Thermal runaway [UL 9540A §4.11]: The incident when an electrochemical cell's temperature increases at an accelerating rate in an uncontrollable fashion sufficient to result in damage to the cell. The thermal runaway progresses when the cell's generation of heat is at a higher rate than the heat it can dissipate. This may lead to fire, explosion and gas and smoke evolution. (Underwriters Laboratories, 2019)

Unit [UL 9540A §4.12]: A frame, rack, or enclosure that consists of a functional BESS which includes components and subassemblies such as cells, modules, battery management systems, ventilation devices and other ancillary equipment. (Underwriters Laboratories, 2019)

3.0 APPLICABLE CODES AND STANDARDS

The following fire protection codes and standards are anticipated to apply to this report:

- 2018 Virginia Construction Code (VCC) (Adopts the International Building Code (IBC), 2018 edition with amendments)
- 2018 Virginia Statewide Fire Prevention Code (VFPC) (Adopts the International Fire Code (IFC), 2018 edition with amendments)

The following standards are also considered for this evaluation:

- NFPA 855, *Standard for the Installation of Stationary Energy Storage Systems*, 2020 edition
- UL 9540A Test Method for Evaluating Thermal Runaway Fire Propagation in Battery Energy Storage Systems, Edition 4, March 29, 2019.

4.0 MAXIMUM ALLOWABLE QUANTITY (MAQ)

Electrical Energy Storage Systems are recognized by the building and fire codes as posing a potential hazard. Lithium-ion batteries are the primary technology being considered. The following sections provide information on the MAQ's as defined by the IFC and NFPA.

4.1 VFPC/IFC 2018 Maximum Allowable Quantity

The VFPC has modified the 2018 IFC to remove references to MAQ's, thus there is no limits that have been formally adopted by the state for outdoor stationary storage battery systems. Nonetheless the following guidance from the IFC is provided for reference.

Section 1206.2 of the IFC states *"stationary storage battery systems having capacities exceeding the values shown in table 1206.2 shall comply with Section 1206.2.1 through 1206.2.12.6, as applicable."* As the capacity of each BESS design evaluated in this report exceeds the 20-kWh threshold, the provisions of 1206.2.1 through 1206.2.12.6 apply.

The IFC defines a Maximum Allowable Quantity (MAQ) above which stored energy batteries must:

DRAFT

a) Comply with the requirements of Chapter 12 (Energy Systems); and,

b) Be considered a Hazardous Occupancy.

These requirements are provided in Tables 1206.2 and 1206.2.9 and are captured below in Table 1. The IFC includes an exception for the AHJ to consider areas containing stationary storage batteries exceeding the MAQ as an incidental occupancy instead of a Group H occupancy based on an HMA conducted in accordance with §1206.2.3. (International Code Council, 2018)

Table 1. Battery Capacity Threshold and MAQ per the IFC

Battery Type	Table 1206.2 Threshold	Table 1206.2.9 MAQ
Lithium-ion	20 kWh	600 kWh

It should further be noted that IFC §1206.2.8.7 addresses requirements for outdoor installations. Per the IFC stationary storage battery systems located outdoors must comply with IFC Sections 1206.2.8.7 through 1206.2.8.7.4 in addition to all applicable requirements of §1206.2. *"Installations in outdoor enclosures or containers that can be occupied for servicing, testing, and maintenance must be treated as battery storage rooms."* However, the MAQ in Table 1206.2.9 is only applicable to fire areas within buildings. As such, the BESS evaluated in this report are not required to be meet the requirements related to MAQ.

4.2 NFPA 855 Maximum Allowable Quantity

Virginia has not adopted NFPA 855 however the following information on MAQ's is provided for reference.

Section 4.8.1 NFPA 855 states *"Where approved by the AHJ, fire areas in non-dedicated use buildings containing ESS that exceed the amounts in Table 4.8 shall be permitted based on a hazardous mitigation analysis in accordance with 4.1.4 and large-scale fire testing complying with 4.1.5."* As the capacity of the batteries in each BESS design exceeds the 20-kWh threshold, the provisions of 4.1.4 and 4.1.5 apply.

NFPA defines a Maximum Allowable Quantity (MAQ) above which stored energy batteries must:

a) Comply with the requirements of Chapter 4; and,

b) Be considered a Hazardous Occupancy.

These requirements are provided in Tables 1.3 and 4.8 and are captured below in Table 2. NFPA includes an exception for the AHJ to consider non-Dedicated-Use buildings exceeding the MAQ based on an HMA conducted in accordance with §4.1.4 and §4.1.5.

Table 2. Battery Capacity Threshold and MAQ per NFPA

Battery Type	Table 1.3 Threshold	Table 4.8 MAQ
Lithium-Ion	20 kWh	600 kWh

4.3 Electrical Energy Storage System Design

DRAFT

Jupiter is installing the BESS to provide peak shaving, uninterruptible power in the event of a utility power outage, and power smoothing. Jupiter has requested a Hazard Mitigation Analysis to support the project.

NOTE: The following sections utilize information from a prior iteration of the Sungrow BESS product. The approach outlined below will remain the same, however when additional information becomes available the analysis and this report will be updated appropriately. It is anticipated that the results in general and conclusions will remain the same, however the specific information related to system voltage, Ah, and energy may be altered somewhat.

4.3.1 Samsung Cell Specifications

The cells used in the battery modules are Samsung SDI CS1000RT001A. These cells are rated for 100 Ah capacity, 3.8 V, and 0.38 kWh.

$$0.38\ kWh = \frac{100\ Ah * 3.8V}{1000}$$

Each cell measures 6.8" (173.9 mm) x 1.8" (45.6 mm) x 4.9" (125.7 mm). (Underwriter Laboratories, 2020) Figure 1 shows the Samsung SDI CS1000RT001A cell.

Figure 1. Samsung SDI CS1000RT001A Cell



4.3.2 Samsung Module Specifications

Each module (EM1762AL001A or EM8831AE001A) contains 48 or less CS1000RT001A cells. Each module with 48 cells is rated for 200 Ah, 88.32 V, and 17.664 kWh.

$$17.664\ kWh = \frac{200\ Ah * 88.32\ V}{1000}$$

Each module is enclosed in a metal case with a polycarbonate cover with vent openings and mica sheets between each cell. There are also compressed Novec (i.e., clean agent for fire suppression) sheets installed underneath the top cover. Each module measures 14.8" (377 mm) wide x 50.4" (1281 mm) long x 6.2" (158 mm) tall. (Underwriters Laboratories, 2020) Figure 2 below shows the module assembly setup for UL 9540A testing.

DRAFT

Figure 2. Samsung Module Assembly



4.3.3 Samsung Unit specifications

Each rack contains a battery management system and up to 14 modules (EM1762AL001A or EM8831AE001A) with each module utilizing 48 or less CS1000RT001A cells. (Underwriters Laboratories, 2020) A typical rack consisting of 14 modules with 48 cells in each module (Samsung SDI PHR0000-004AE3D) is rated for 200 Ah, 1236.5V, and 247.3 kWh and measures 18.3" **(465 mm) wide x** 54.8" **(1392 mm) deep x** 105.9" **(2690 mm) tall.**

$$247.3\ kWh = \frac{200Ah * 1236.5V}{1000}$$

Figure 3 below shows the test configuration for 14-module racks per UL 9540A. Three racks are shown in the figure. Thermocouples and heat flux gauges are installed throughout the unit for the UL 9540A test; however, these devices are not present in the installed configuration.

DRAFT

Figure 3. Unit Assembly



5.0 PROPOSED BATTERY ENERGY STORAGE SYSTEM DESIGNS

The HMA presented in this report evaluates an integrated turnkey BESS design for use in an outdoor container configuration, based on the Model ST2752UX-US battery cabinet. The 2752 designation following the battery cabinet enclosure number (e.g., ST2752) specifies the maximum power in kW per battery cabinet size and may be less as required by the application. Each BESS design utilizes the same cells and incorporates modules with 24 or less cells. The number of racks in each BESS varies but all designs utilize racks with 14 modules or less. The following sections of this report discuss the relevant features of each BESS design.

5.1 Model ST2752UX-US ESS

The Model ST2752UX-US battery energy storage system is an integrated outdoor cabinet design with a total battery capacity of 2752 kWh. The ST2752UX-US based cabinet measures 181.1" (4.6 m) wide x 94.5" (2.4 m) tall x 39.4" (1.0 m) deep and houses 8 racks or less and an Energy Storage Management System (ESMS). Figure 4 shows an exterior view of the cabinet while Figure 5 shows a plan view illustrating the layout of the cabinet interior.

DRAFT

Figure 4. ST2752UX-US ESS Exterior View

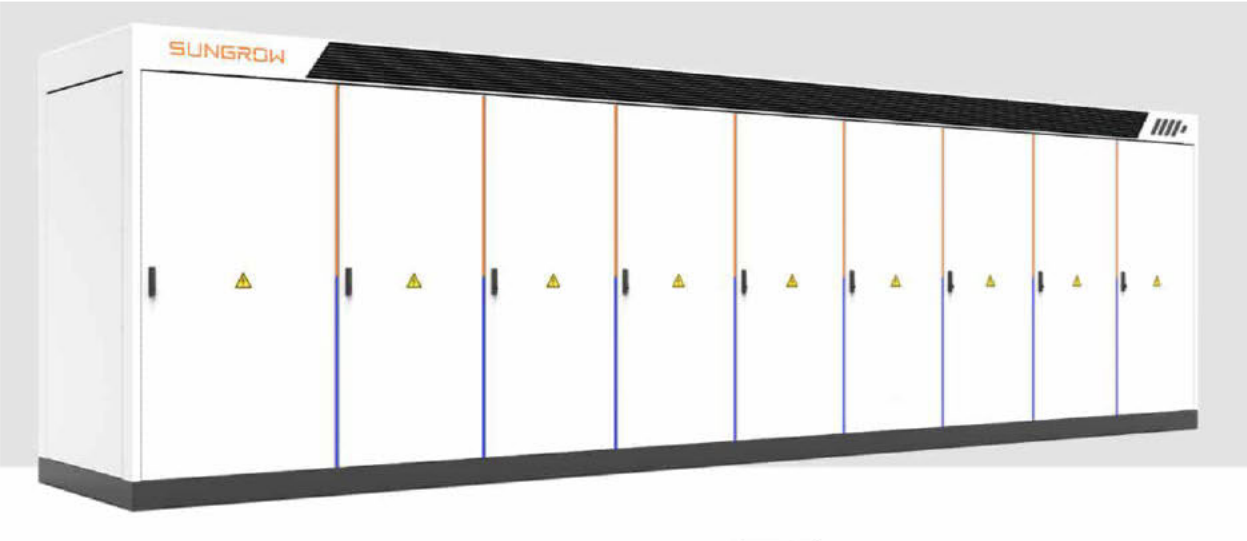


Figure 5. ST2752UX-US ESS Plan View

The system utilizes and intelligent liquid cooling system to improve system efficiency and battery life cycle. The ESS comes pre-assembled and does not require handling of battery modules on site, the ESS can be dropped onto a pad and the associated electrical and other system connections can be made immediately reducing the hazards associated with the field installation of cabinets. Detailed system specifications are provided below.

DRAFT

Table 3 ST2752UX-US System Specifications

Type designation	ST2752UX-US
Battery Data	
Cell type	LFP
Battery capacity (BOL)	2752 kWh
Battery voltage range	1370 ~ 1500 V
General Data	
Dimensions of battery unit (W * H * D)	9,300 * 2,620 * 1,700 mm 366.1''*103.1''*66.9''
Weight of battery unit	26,000 kg 57320.2 lbs
Degree of protection	NEMA 3R
Operating temperature range	-30 to 50 ℃ (> 45 ℃ derating) -22 to 122 ℉ (> 113 ℉ derating)
Relative humidity	0 ~ 95 % (non-condensing)
Max. working altitude	1,000 m (standard) / > 1,000 m (optional) (3280.8 ft (standard) / > 3280.8 ft (optional)
Cooling concept of battery chamber	Liquid cooling
Fire safety	Deluge sprinker heads (standard), fused sprinkler heads (optional), NFPA69 explosion prevention and ventilation IDLH gases (optional)
Communication interfaces	RS485, Ethernet
Communication protocols	Modbus RTU, Modbus TCP
Compliance	UL9540, UL9540A/NFPA 855
2 HOURS APPLICATION-ST2752UX*4-5000UD-MV-US	
BOL kWh(DC/AC LV Side)	11,008 kWh DC / 10,369 kWh AC
ST2752UX Quantity	4
PCS Model	SC5000UD-MV-US
4 HOURS APPLICATION-ST2752UX*8-5000UD-MV-US	
BOL kWh(DC/AC LV Side)	22,016 kWh / 21,425 kWh
ST2752UX Quantity	8
PCS Model	SC5000UD-MV-US
Grid Connection Data	
Max. THD of current	< 3 % (at nominal power)
DC component	< 0.5 % (at nominal power)
Power factor	> 0.99 (at nominal power)
Adjustable power factor	1.0 leading ~ 1.0 lagging
Nominal grid frequency	50 / 60 Hz
Grid frequency range	45 ~ 55 Hz / 55 ~ 65 Hz
Transformer	
Transformer rated power	5,000 kVA
LV/MV voltage	0.95 kV / 34.5 kV
Transformer cooling type	ONAN (Oil Natural Air Natural)
Oil type	Mineral oil (PCB free) or degradable oil on request

6.0 HAZARD MITIGATION ANALYSIS

As noted above VFPC has stricken most of the provisions of the IFC with regards to ESS, however this HMA is being prepared using the guidance provided by IFC§1206.2.3. The HMA evaluates the findings of the UL 9540A cell, module, and unit level testing pertaining to thermal runaway and off gassing. A FMEA has also been prepared and is reviewed to assess the adequacy of planned mitigating provisions and need for any additional mitigating features.

NOTE: The following sections utilize information from a prior iteration of the Sungrow BESS product. The approach outlined below will remain the same, however when additional information becomes available the analysis and this report will be updated appropriately. It is anticipated that the results in general and conclusions will remain the same, however the specific information related to Temperature, Heat Flux, etc. will likely be altered somewhat.

6.1 UL 9540A Test Method

UL 9540A is the Test Method for Evaluating Thermal Runaway Fire Propagation in Battery Energy Storage Systems.

Initially, the cells are tested to determine if further testing is required. Module level testing is required if the following observations are recorded:

- Thermal runaway is induced in the cell; and,
- The cell vent gas is flammable in air when tested in accordance with ASTM E918.

Module level testing examines the module design, heat release rate, gas generation, external debris, and flying debris hazards. Unit level testing is required if the following observations are recorded:

- Module design is unable to contain thermal runaway; and,
- Cell vent gas is flammable.

Unit level testing assesses the BESS design of the unit, heat release rate, gas generation and composition, deflagration and flying debris hazards, BESS and wall surface temperatures, heat flux at the target walls, and reignition. Installation level testing is required if the following observations are recorded during unit level testing:

- Flaming is observed outside the initiating BESS unit;
- Surface temperature of the modules in the adjacent BESS unit exceeds the temperature at which cell level gas venting occurred;
- Surface temperatures of wall surfaces increases more than 175 °F (79.4 °C) from ambient; and,
- Explosion hazards are recorded.

Installation level testing assesses the effectiveness of fire protection systems installed as mitigation methods for the BESS in its intended installation configuration. UL 9540A states "installation level testing in section 10 is not required if the following performance conditions outlined in Table 9.1 are met during the unit level test." (Underwriters Laboratories, 2019)

The units did not exhibit flaming outside the initiating BESS unit, surface temperatures of the modules adjacent to the initiating module did not induce thermal runaway, venting of gases did not generate an explosion hazard, surface temperatures of wall surfaces did not exceed 73.4 °F (23 °C), and the heat flux on the wall surfaces did not exceed 1.66 kW/m^2. Details are provided in section 6.1.3 of this report.

6.1.1 Samsung SDI UL 9540A Cell Level Test Summary

Cell level testing was conducted per UL 9540A. The cell was heated by applying a flexible film heater to the cell. Thermal runaway was induced in the cell by increasing heat at a rate of 7.2 °F/min (4 °C/min) to 12.6 °F/min (7 °C/min). Thermocouples recorded the cell surface temperature throughout the test. The testing configuration of the cell level test is shown in Figure 6. Thermal runaway is established when the heating rate of the cell exceeds the 7.2 – 12.6 °F/min rate (4-7 °C/min). (Underwriters Laboratories, 2019) Thermal runaway was induced in the Samsung cell

DRAFT

and the gases produced by thermal runaway of the cell were collected and analyzed. The results of the gas analysis are provided in Table 4 for the Samsung cells.

The Samsung cells were observed venting gas between 24 and 32 minutes, at 324 ºF (162 ºC). Thermal runaway for the Samsung cells occurred between 43 and 51 minutes, at 327 ºF (164 ºC). (Underwriter Laboratories, 2020) Table 5 contains the cell level test data for tests 1-4. Test five was conducted in a gas composition chamber and was not included in Table 6, as the environment inside the gas test chamber is purged to contain less than 1% Oxygen by volume.

Figure 6. Samsung Cell Testing Configuration



Table 4. Samsung Cell Off Gas Composition

Gas	Concentration %	Volume of Gas (ft^3)	Volume of Gas (m^3)
CO	16.6 %	1.41	0.04
CO_2	25.2 %	2.14	0.06
H_2	39.6 %	3.36	0.095
Hydrocarbons	18.7 %	1.59	0.045
TOTAL	100%	8.48	0.24

Table 5. Samsung Cell Level Test Data

Test	Venting Time	Venting Temperature ºF (ºC)	Thermal Runaway Time	Thermal Runaway Temperature ºF (ºC)
1	0:32:14	323.6 °F (162 °C)	0:49:26	330.8 °F (166 °C)
2	0:27:16	325.4 °F (163 °C)	0:50:44	327.2 °F (164 °C)
3	0:24:00	325.4 °F (163 °C)	0:42:59	327.2 °F (164 °C)
4	0:26:26	323.6 °F (162 °C)	0:46:22	327.2 °F (164 °C)

Figure 7 shows the surface temperature of the cell throughout the second Samsung test. In all tests, a period of gas venting ranging from approximately 17 to 23 minutes preceded thermal runaway.

Three of the four thermal runaway methodology tests resulted in ignition of vent gases. In one test, sparks were observed coming from the cell vent. Figure 8 shows the Samsung SDI CS1000RT001A cell after thermal runaway was induced. The cell casing in each test exhibited signs of thermal damage but remained intact. Venting in each test occurred from the top of the cell.

Figure 7. Samsung Cell Test Temperature Data

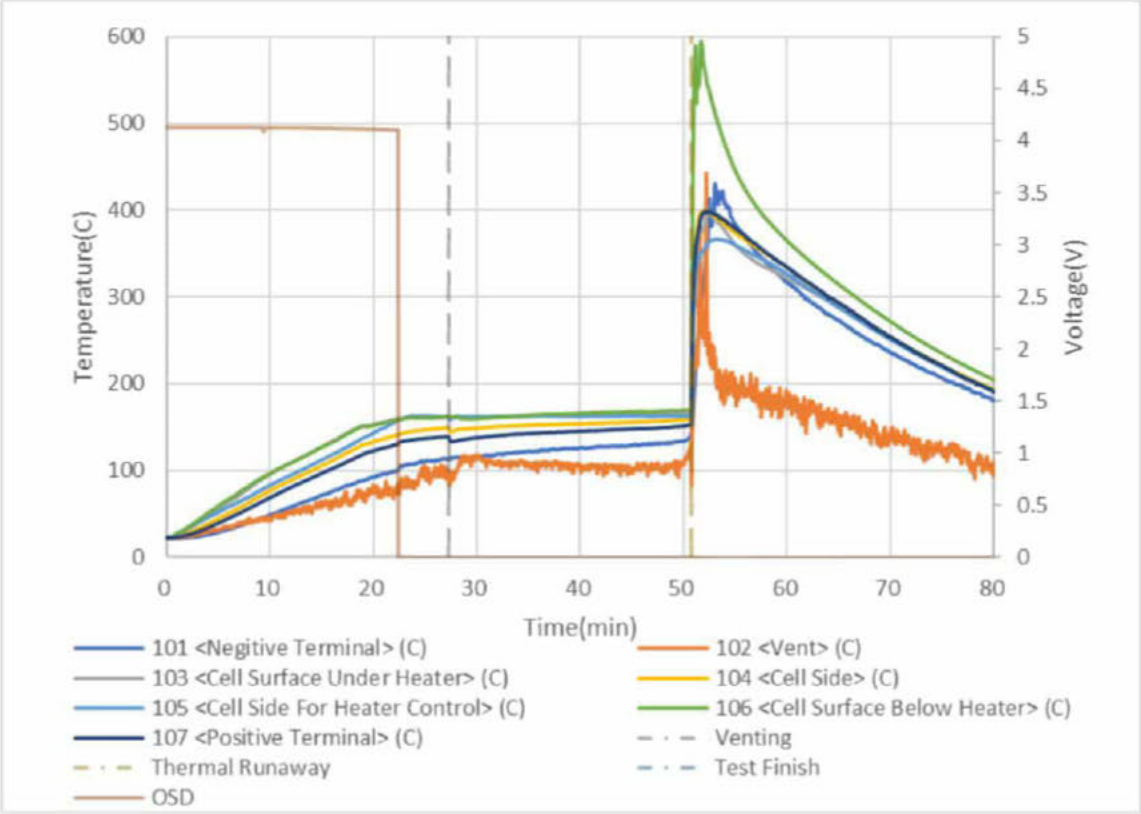


Figure 8. Samsung Cell after UL 9540A Testing



6.1.2 Samsung UL 9540A Module Level Test Summary

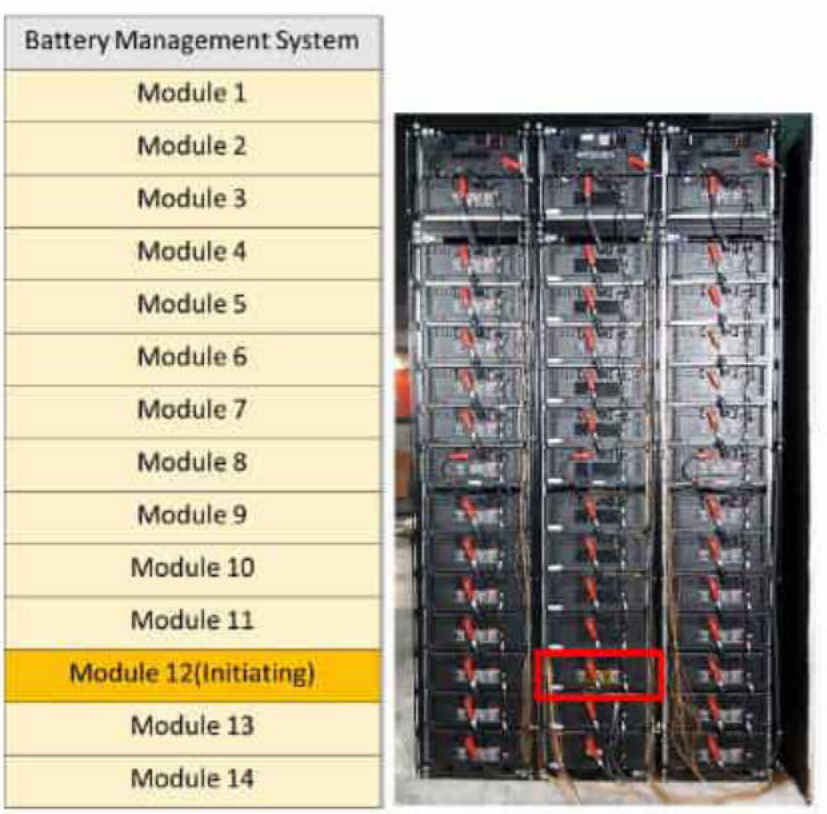
The modules were tested by inducing thermal runaway in multiple cells of a module. The initiating cells were heated using the same heating method as the cell level test. Thermal runaway propagated through all cells in the test module. External flame was observed in the form of flame jetting vertically and horizontally from the cells resulting in a peak heat release rate of 1000 kW. Flying debris was also observed in each thermal runaway event. Vent gasses after flaming were comprised of CO (2.4%) and unburned hydrocarbons (97.6%). The total vent gas volume was measured to be 29 ft^3 (0.82 m^3).

6.1.3 Samsung UL 9540A Unit Level Test Summary

Unit level testing was conducted on four Samsung SDI PHR0000-00AE3D racks with 14 modules each. Thermal runaway was initiated in one cell in a single module. Figure 9 shows the location of the initiating module. The module location was selected to analyze upward and downward propagation of thermal runaway due to wiring and flammable materials.

DRAFT

Figure 9. Module Location in Unit Testing

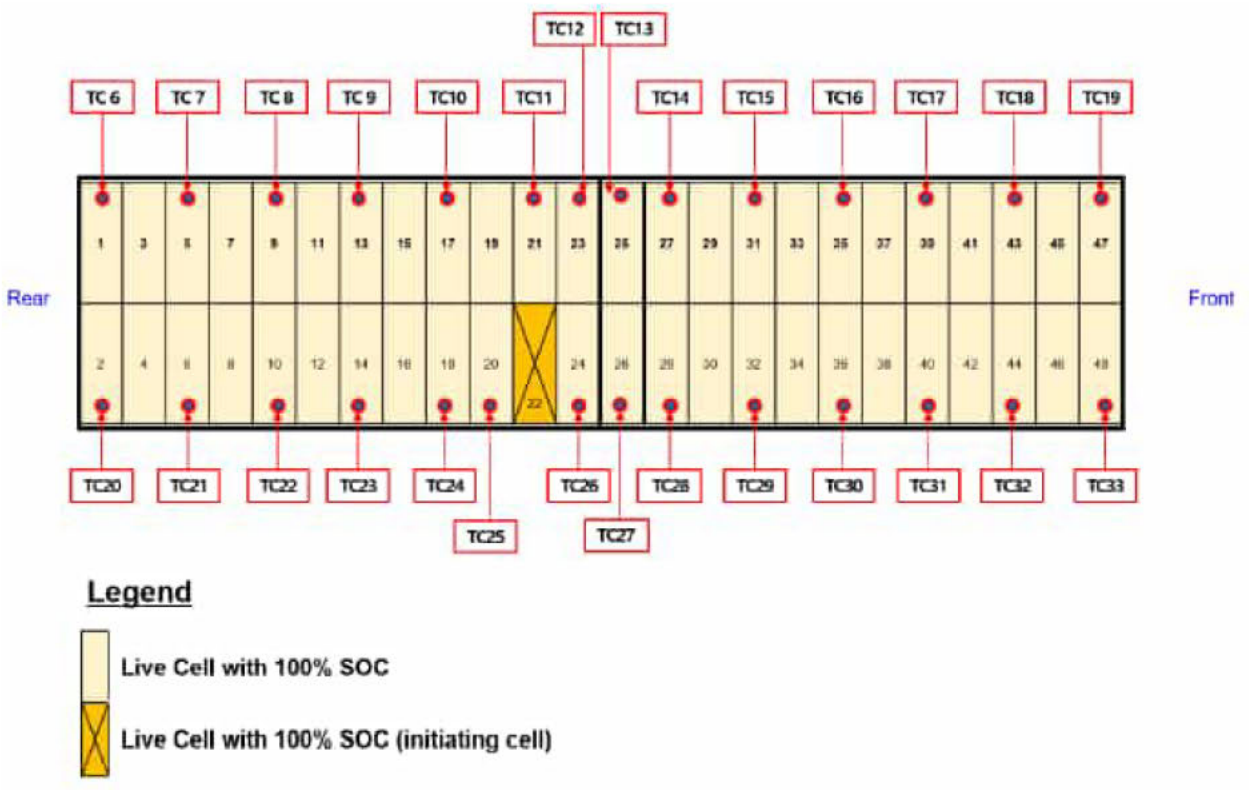


The initiating module begins to vent gases at 32:34 and thermal runaway was observed at 36:25 with a recorded cell surface temperature of 458.6 ºF (237 ºC). Gas venting was observed between the initiating unit and the front wall at this time. A second venting event occurred at 1:03:56 between the initiating unit and the front wall.

Although thermal runaway occurred in the initiating cell, thermal runaway did not propagate through the initiating module. Temperatures measured throughout the initiating module illustrated that there was not enough temperature increase to cause thermal runaway. Figure 10 shows the location of thermocouples inside the initiating module while Figure 11 and Figure 12 illustrate the evolution of temperature measurements for odd and even numbered cells, respectively. Review of Figure 12 demonstrates that thermal runaway in the initiating cell (i.e., spikes in temperature starting at 32:34) caused the even numbered cells adjacent to the initiating cell (cells 20 and 24) to show a marked increase in temperature; however, thermal runaway did not occur. Temperatures at all other odd and even numbered cells were considerably lower.

DRAFT

Figure 10. Location of Thermocouples inside the Initiating Module



DRAFT

Figure 11. Temperature Measurements in the Initiating Module (Odd Numbered Cells)

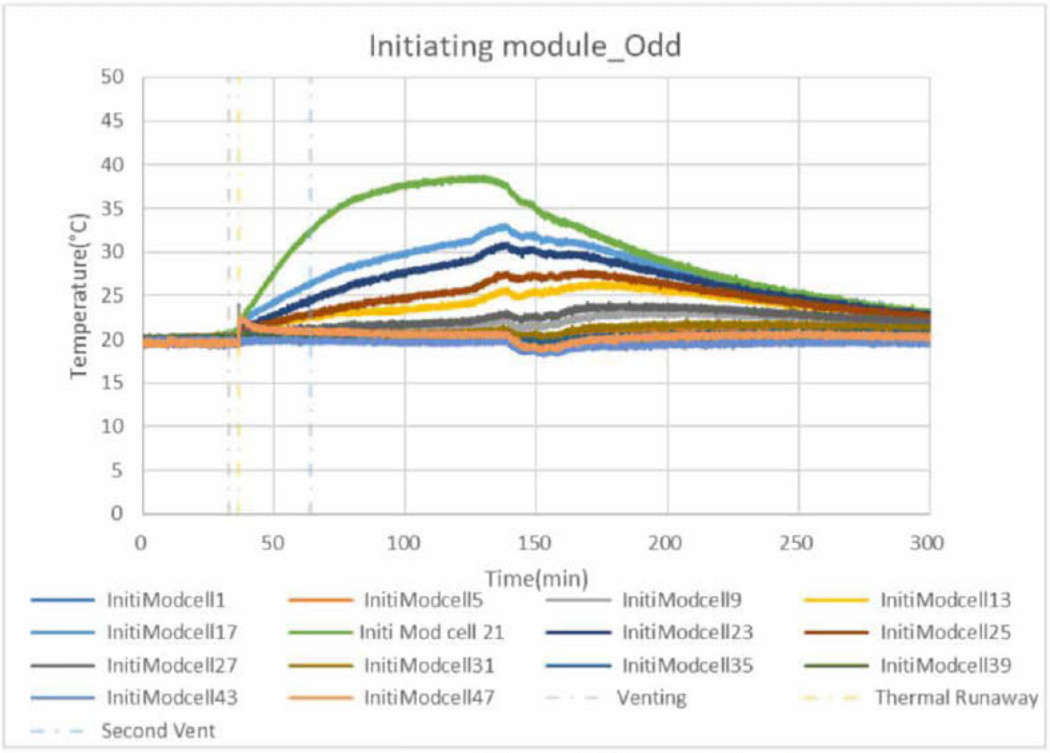
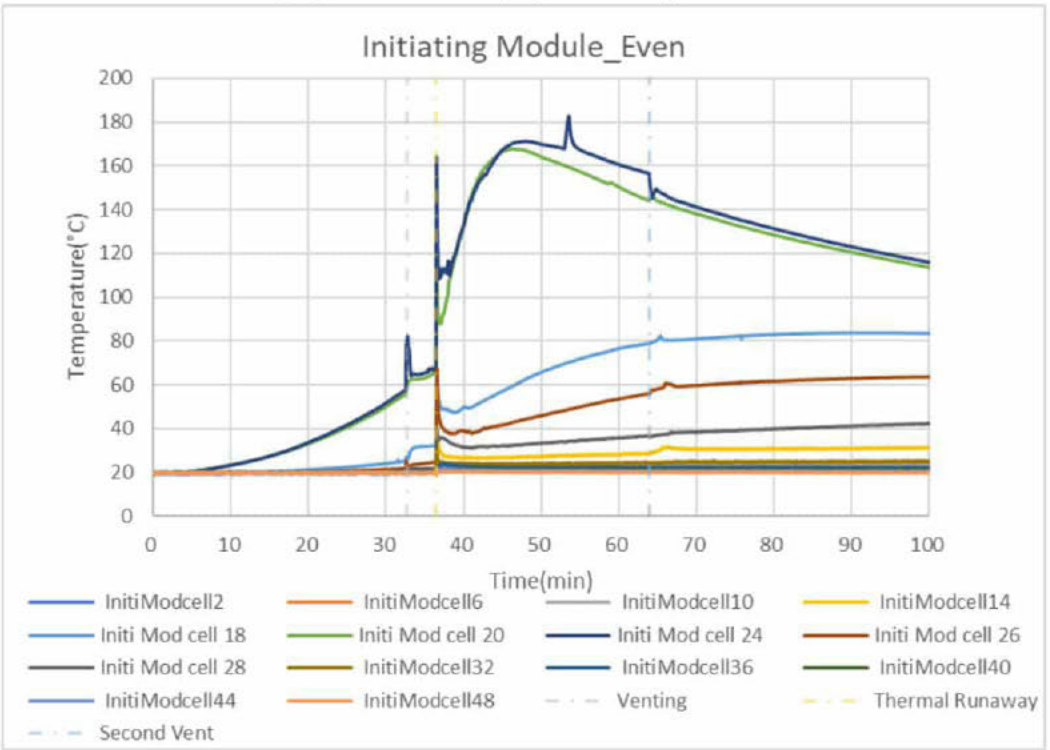


Figure 12. Temperature Measurements in the Initiating Module (Even Numbered Cells)



Throughout the duration of the test, fire did not extend beyond the initiating module. Thermal runaway did not propagate to the neighboring modules, damage did not extend past the initiating module, and target temperatures adjacent to the initiating module were well below those necessary for the onset of thermal runaway. Vent gases did not ignite during the unit level testing. (Underwriters Laboratories, 2020)

Temperature and heat flux was measured at multiple spots that are required per UL 9540A. See Figure 13 for a diagram of the test configuration. The three target racks represent neighboring units were used to examine the increase in temperature and heat flux during thermal runaway. Target rack 1 recorded a maximum temperature of 82.4 ºF (28 ºC), target rack 2 recorded a maximum temperature of 77 ºF (25 ºC), and target rack 3 recorded a maximum temperature of 77 ºF (25 ºC). The max temperature of the target racks indicate that any neighboring units to the unit undergoing thermal runaway will not be exposed to sufficient heat to propogate thermal runaway.

Figure 13. Unit Testing Configuration

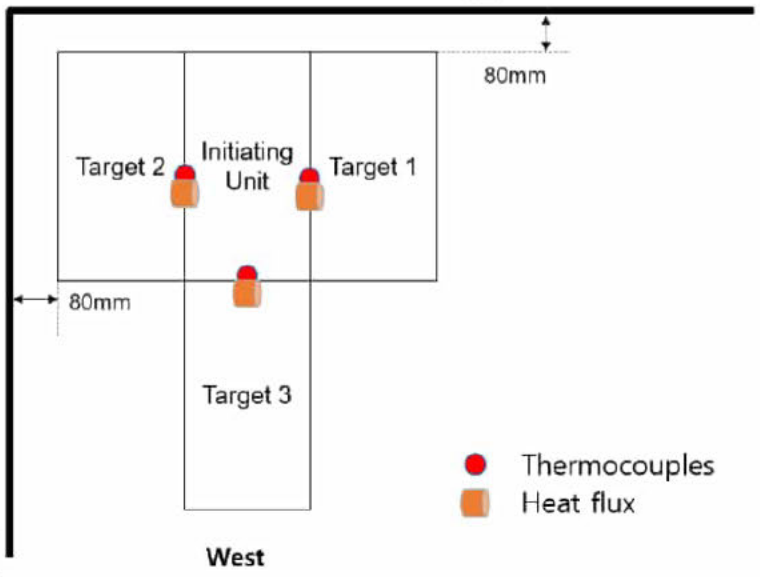


Figure 14 and Figure 15 provide the surface temperatures of the modules in the initiating unit during the unit test. As the temperature data illustrates, the modules adjacent to the initiating module did not exceed the venting temperature from the cell test. No rapid and significant temperature increase was observed beyond the initiating module.

DRAFT

Figure 14. Temperature Measurements at the Front of the Initiating Unit

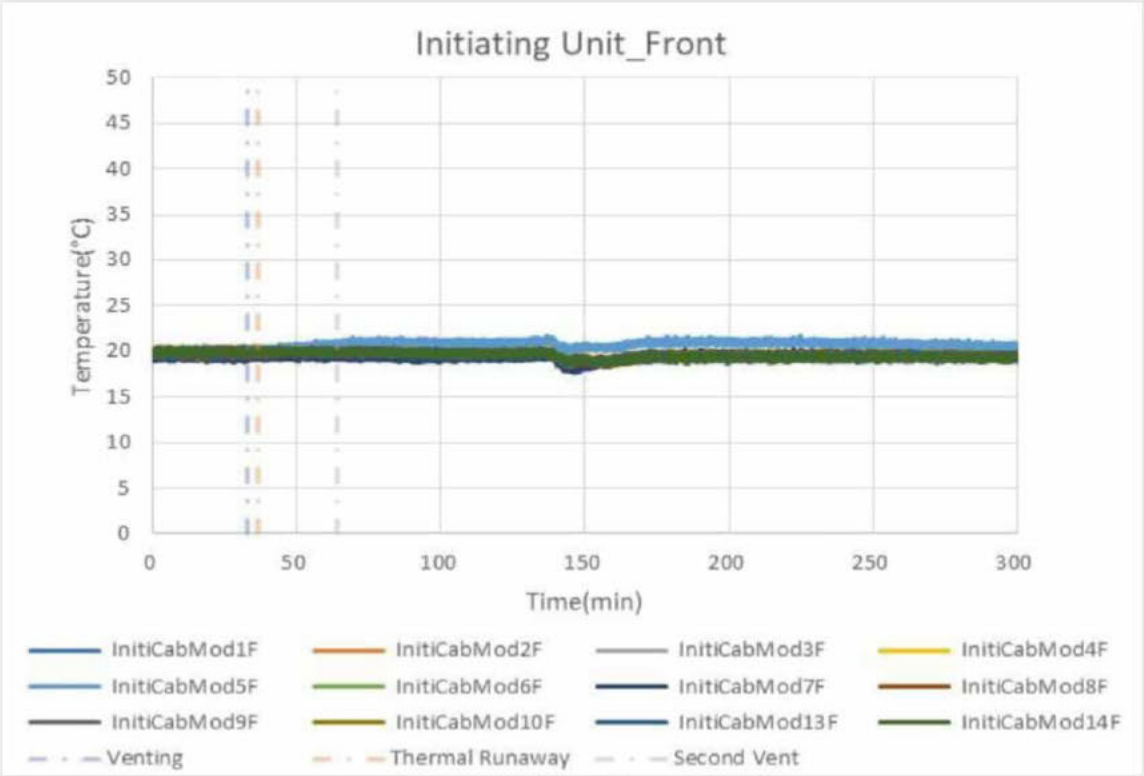
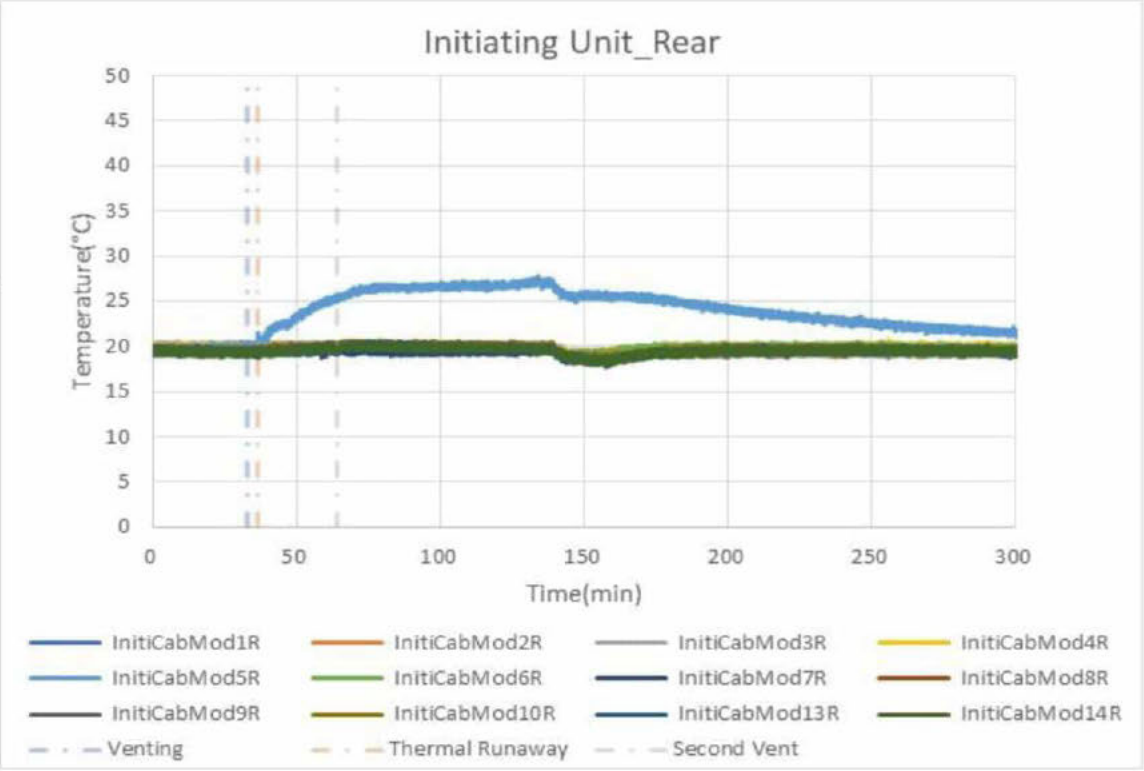


Figure 15. Temperature Measurements at the Rear of the Initiating Unit



An explosion (deflagration or detonation) was not observed during the test. (Underwriters Laboratories, 2020) In addition, there was no evidence of external flaming or flying debris noted in the room at the conclusion of the test. Physical damage was primarily limited to the initiating module as shown in Figure 16. The polycarbonate cover of the initiating module was breached during the test; however, only minor thermal damage (i.e., light charring) occurred in adjacent target modules. Figure 17 and Figure 18 show photographs of the damage to adjacent modules in target units 1 and 2, respectively. No fire was observed on adjacent modules and the target wall was void of damage. A maximum temperature of 73.4 °F (23 °C) and peak heat flux of 1.66 kW/m^2 was measured on the target wall.

Figure 16. Damage to the Initiating Module



Figure 17. Damage to Module 26 in Target Unit 1

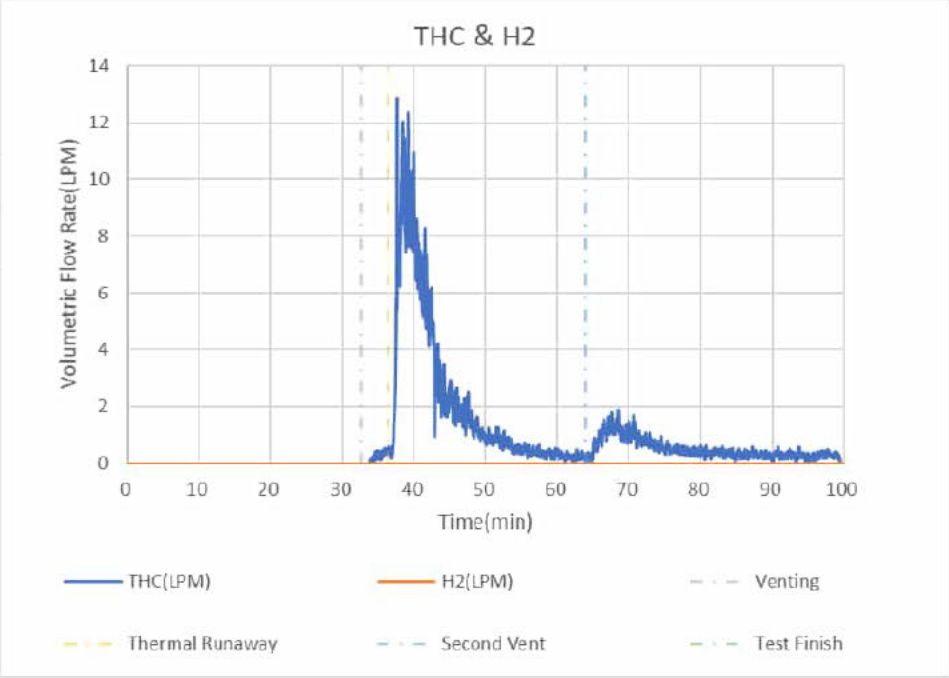


Figure 18. Damage to Module 54 in Target Unit 3



Gas generation and composition during the unit level testing was measured via the calorimetry measurement system. Hydrogen, total unburned hydrocarbons, carbon monoxide, and carbon dioxide gas species were measured. During the test, hydrogen, carbon monoxide, and carbon dioxide were not generated in measurable quantities. However, unburned hydrocarbons were generated following thermal runaway in the initiating cell and the second venting event. Figure 19 shows a plot of the total hydrocarbon (THC) generation rate during the test. In total, 80 L of THC was generated during the unit level test.

Figure 19. Gas Flow Rates Measured during the Unit Level Test



6.2 Off Gassing IDLH and Explosion Hazard Analysis

The Samsung CS1000RT001A cells generated toxic and flammable gasses during the cell level, module level, and unit level tests. The analysis provided in this section of the report is based on recorded levels of gases in the cell level tests as a bounding (worst-case) off gassing scenario. While the cabinets are non-walk in units (i.e., they are not normally occupied), a conservative analysis approach is taken to ensure the safety of bystanders and first responders. Section 6.2.1 evaluates the potential to develop a flammable concentration of gas within an outdoor BESS cabinet / container. Section 6.2.2 evaluates the potential that gas concentrations reach immediately dangerous to life and health (IDLH) thresholds during a thermal runaway event. Section 6.2.3 discusses requirements for ventilation to prevent off gas concentrations from reaching flammable or IDLH thresholds.

6.2.1 Flammable Gas Generation

The BESS has been tested to UL 9540A standards as required by IFC §1206.2.10.1. (International Code Council, 2018) The UL testing does not take into account any ventilation that would be present in the outdoor BESS cabinet / station during the test. Thermal runaway was induced at the cell level. Table 4 shows the composition of gases generated during off gassing during the Samsung cell level test. The total gas volume collected from the cell was 8.48 ft^3 (0.24 m^3). Flying debris was not observed during the test.

6.2.1.1 Hydrogen

Hydrogen (H_2) gas has a lower explosive limit (LEL) of 4% in air. During the cell level test, 39.6% of the total generated gas volume, or 3.36 ft^3 (0.095 m^3), was comprised of H_2. Accordingly, the total H_2 generation from a module is 80.6 ft^3 (2.28 m^3).

$$80.6\ ft^3 H_2\ per\ module = 39.6\% H_2 * 8.48\ ft^3 * 24\ cells$$

The interior air volume of each outside ground mounted BESS being analyzed was conservatively estimated (i.e., neglecting air space above in between racks) to range from approximately 140 to 983 ft^3. Table 6 provides a summary of the number of cells and modules in each BESS that would need to off gas to reach the LEL for H_2.

Table 6. Hydrogen Off Gassing Volume Needed to Reach the LEL

BESS Container Design	Interior Air Volume (ft^3 / m^3)	Volume of H_2 to Reach the LEL (ft^3 / m^3)	No. of Cells to Reach the LEL	No. of Modules to Reach the LEL
ST0556KWH	139.93 / 3.96	5.6 / 0.16	1.67	0.069

Assuming there is no ventilation, the LEL calculations indicate that the LEL for H_2 can be reached by the off gassing of approximately 2 to 12 cells depending on the BESS container design. In all cases, thermal runaway leading to the off gassing from less than 1 module may exceed the LEL.

DRAFT

6.2.1.2 Carbon Monoxide

Carbon Monoxide (CO) has a LEL of 12.5% in air. (Center for Disease Control and Prevention, n.d.) During the cell level test, 16.6% of the total generated gas volume, or 1.41 ft^3 (0.04 m^3), was comprised of CO. Accordingly, the total CO generation from a module is 33.78 ft^3 (0.96 m^3).

$$33.78\ ft^3 CO\ per\ module = 16.6\% H_2 * 8.48\ ft^3 * 24\ cells$$

Table 7 provides a summary of the number of cells and modules in each BESS that would need to off gas to reach the LEL for CO.

Table 7. Carbon Monoxide Off Gassing Volume Needed to Reach the LEL

BESS Container Design	Interior Air Volume (ft^3 / m^3)	Volume of CO to Reach the LEL (ft^3 / m^3)	No. of Cells to Reach the LEL	No. of Modules to Reach the LEL
ST0556KWH	139.93 / 3.96	17.49 / 0.5	12.41	0.518

Assuming there is no ventilation, the LEL calculations indicate that the LEL for CO can be reached by the off gassing of approximately 13 to 88 cells depending on the BESS container design. For the smaller volume container (ST0556KWH based ESS), the LEL can be exceeded during thermal runaway of less than 1 module. The larger containers would require thermal runaway of multiple modules which is not considered to be credible based on the results of the unit level testing.

6.2.1.3 Cell Vent Gas

The cell vent gas composition was determined using Gas Chromatography. The cell vent gas has a LEL of 5.97% in accordance with ASTM E918. A module discharges 203.52 ft^3 (5.76 m^3) of vent gas. Table 8 provides a summary of the number of cells and modules in each BESS that would need to off gas to reach the LEL.

Table 8. Cell Vent Gas Volume Needed to Reach the LEL

BESS Container Design	Interior Air Volume (ft^3 / m^3)	Volume of Vent Gas to Reach the LEL (ft^3 / m^3)	No. of Cells to Reach the LEL	No. of Modules to Reach the LEL
ST0556KWH	139.93 / 3.96	8.35 / 0.24	0.99	0.041

Assuming there is no ventilation, the LEL calculations indicate that the LEL for vent gas can be reached by the off gassing of approximately 1 to 7 cells depending on the BESS container design. In all cases, thermal runaway leading to the off gassing from less than 1 module may exceed the LEL.

6.2.2 Analysis of IDLH Gas Concentrations

Table 4 shows that a cell generates 16.6% Carbon Monoxide (CO) during thermal runaway. The IDLH of CO is listed as 1500 parts per million. This corresponds to a 0.15% IDLH. (Center for Disease Control and Prevention, n.d.) A cell generates 1.41 ft^3 (0.04 m^3) of CO which equates to 33.78 ft^3 (0.96 m^3) per module. Table 9 provides a summary of the number of cells and modules in each BESS that would need to off gas to reach the LEL.

DRAFT

Table 9. Carbon Monoxide Volume Needed to Reach the IDLH Threshold

BESS Container Design	Interior Air Volume (ft^3 / m^3)	Volume of CO to Reach the IDLH (ft^3 / m^3)	No. of Cells to Reach the IDLH	No. of Modules to Reach the IDLH
ST0556KWH	139.93 / 3.96	0.21 / 0.01	0.15	0.006

Assuming there is no ventilation, the IDLH for CO can be reached by the off gassing of approximately 1 cell or less in all cases.

6.2.3 Ventilation Requirements

The UL 9540A unit test demonstrates that thermal runaway is limited to the initiating cells within a module and module to module propagation does not occur. While this is the most likely outcome in the event a single cell undergoes thermal runaway, the LEL calculations presented in Section 6.2.1 indicate that there is a limited margin of safety for reaching the LEL without ventilation. In the limiting case involving cell vent gas (Section 6.2.1.3), the LEL may be reached by the off gassing of 1 cell in the smallest container and approximately 7 cells in the largest containers. Furthermore, the IDLH calculations for CO presented in Section 6.2.2 indicate that the IDLH can be reached without ventilation in all container designs during the off gassing of 1 cell. Accordingly, ventilation is required to maintain vent gasses to safe levels in the event of thermal runaway.

To ensure safe conditions in the event of thermal runaway, ventilation must be designed to:

1. *Maintain the concentration of flammable gasses below 25% of the LEL (IFC §1206.2.11.3); and,*
2. *Maintain a CO concentration below 50% of the IDLH (IFC §1206.2.11.4).*

The gas flow rates measured during the unit level test (see Figure 19) illustrate that the peak rate of off gassing occurs over a period of approximately 4 minutes following thermal runaway of the initiating cell. Assuming that the total volume of gas released from a cell (8.48 ft^3 measured during the cell level testing) occurs during this 4-minute period, the peak gas generation rate is 2.12 cfm.

$$2.12\ ft^3 per\ minute = 8.48\ ft^3 / 4\ minutes$$

Table 10 provides a summary of the minimum ventilation rates (i.e., outside makeup air and exhaust) rates required to achieve the ventilation design objectives for each gas species. The results confirm that maintaining CO concentrations below 50% of the IDLH is the limiting design case. Accordingly, each BESS cabinet design must be configured to provide at least 500 cfm (0.24 m^3/s) of outside makeup air and exhaust.

DRAFT

Table 10. Ventilation Requirements for Each Gas Species

Gas Species	Ventilation Rate to Maintain Concentration below 25% of the LEL (cfm / m^3/s)	Ventilation Rate to Maintain Concentration below 50% of IDLH (cfm / m^3/s)
H_2	84 / 0.04	N/A
CO	12 / 0.006	470 / 0.22
Cell vent gas	142 / 0.07	N/A

Ventilation is not required during normal operation as the lithium ion cells do not produce off gasses during normal operation. Accordingly, 500 cfm (0.24 m^3/s) of ventilation may either be provided continuously or activated by a gas detection system configured to activate at 25% of the LEL or 50% of the IDLH, whichever occurs first. Ventilation must also be designed to provide uniform airflow movement through the entire volume of the BESS container as off gasses produced during venting consist of constituents that are both heavier and lighter than air.

6.3 Failure Modes and Effects Analysis

An FMEA was conducted, examining the following items as required by the IFC §1206.2.3.1. (International Code Council, 2018)

- Thermal runaway condition in a single-battery storage rack, module, or array
- Failure of any energy storage management system (ESMS)
- Failure of any required ventilation or exhaust system
- Voltage surges on the primary electric supply
- Short Circuits on the load side of the stationary battery storage system
- Failure of the smoke detection, fire detection, fire-extinguishing, or gas detection system
- Spill neutralization not being provided or failure of the secondary containment system

A Risk Priority Number (RPN) was assigned to each failure mode based on the probability of occurrence, detection reliability, and severity of event. The three items were ranked on a scale of 1-10 and the three values were then multiplied to establish the RPN. Higher RPN values represent a severe event with a high probability of occurrence and low probability of detection. (Sungrow, 2020)

6.3.1 Thermal Runaway

Thermal runaway in a single battery storage rack was tested in accordance with the UL 9540A test method for unit level testing. A single battery storage module in thermal runaway does not induce thermal runaway in the neighboring modules. The fire event of a single module in thermal runaway does not create an explosion hazard.

The FMEA identified an internal short in a cell as the primary failure mode capable of causing thermal runaway leading to a fire. Potential causes include a manufacturing defect (presence of contaminant), damage during handling, excessively high temperature, and low temperature charging. Direct effects for each of these causes include a high probability of thermal runaway and fire and second order effect that a fault internal to the battery cell would be uninterruptable.

DRAFT

The RNP for an internal short is 10. The ESMS monitors the voltage and will quickly respond to trigger undervoltage protection. The severity is listed as a 10, due to the high potential for thermal runaway and fire. However, the occurrence and detection are both listed as a 1 because the layers of protection provided by the ESMS are considered a reliable means of preventing an internal short. Further mitigating provisions include rigorous quality controls in the manufacturing process (e.g., X-ray screening and OCV/IR readings).

6.3.2 Failure of ESMS

Failure of the ESMS may result in overcharge, overheating, or other abnormal conditions. With the exception of an overcharge condition, the FMEA identified that ESMS by itself is unlikely to cause a fire unless there is prolonged operation with the fault and/or subsequent failures occur. Overcharging is a direct effect of a failure in the ESMS software logic that allows continuous operation. The ESMS control incorporates multiple trip setpoints that would detect this fault along with the inverter operating limits. Mitigating provisions include ESMS logic safety review and data integrity checks of preconfigured values.

The ESMS monitors cell voltage, temperature, discharging power, overvoltage protection, cell impedance, and fuse detection. In the event of an abnormal reading for any of the listed conditions the ESMS prevents the affected module from charging or discharging. Loss of the ESMS will disconnect the affected module from operation, preventing thermal runaway of a faulty module.

The UL 9540A testing demonstrates that thermal runaway does not lead to fire propagation outside of a single module. Loss of the ESMS is mitigated by the design of the battery backup units. The UL 9540A test method states in §9.8.1 that further testing is not required if the performance criteria in table 9.1 of the Test Method are met. (Underwriters Laboratories, 2019)

6.3.3 Failure of Ventilation or Exhaust System

There is no release of gasses during normal operation thus ventilation for dilution of gases during operation is not needed. During a thermal runaway event ventilation is required to maintain gas concentrations below 25% of the LEL and 50% of the IDLH. Refer to Section 6.2 for additional information.

6.3.4 Voltage Surge on Primary Electric Supply

The FMEA did not identify failure modes on the electric supply side of the battery modules. If such failures were to occur, they result in external failure of the modules requiring replacement of the modules. The detection of this condition by the ESMS and low frequency of these events helps to minimize the risk of initiating thermal runaway.

6.3.5 Short Circuit on Load Side of Battery Storage System

As discussed in Section 6.3.1, four potential causes were identified as potentially leading to an internal short. For all causes, the occurrence and detection are both listed as a 1 because the layers of protection provided by the ESMS are considered a reliable means of preventing an internal short. Further mitigating provisions include rigorous quality controls in the manufacturing process (e.g., X-ray screening and OCV/IR readings).

DRAFT

6.3.6 Failure of Fire Detection and Suppression System

The modules are equipped with compressed Novec sheets installed underneath the top cover. The UL 9540A unit level test was conducted with these sheets in place; therefore, the results of the test are contingent on this protection feature. Assuming the Novec sheets are in place, the UL 9540A unit level test demonstrated that thermal runaway is contained within the module, mitigating the need for an automatic fire suppression system. As such, the automatic fire suppression systems planned for installation in the BESS cabinets are considered an additional, redundant layer of protection.

6.3.7 Spill Neutralization

The Samsung SDI CS1000RT001A cells do not require spill neutralization per IFC §1206.2.12.3.

6.4 Mitigations

The UL 9540A testing does not account for the protections provided by the BMS or ESMS that provide multiple layers of protection and detection for the batteries. The BMS monitors the cell voltage, temperature, discharging power, overvoltage protection, cell impedance, and fuse detection. In the event of an abnormal reading for any of the listed conditions, the BMS prevents the affected module from charging or discharging. The ESMS also prevents the affected module from charging or discharging, if required, as a supplementary safety measure.

Although the UL9450A unit level testing indicates that propagation of thermal runaway does not occur. The suppression and mitigation systems provide a redundant layer of protection to control a fire should one occur. The BESS cabinets are located outdoors and are not occupiable. They are reach in only for inspection, testing, and maintenance activities.

Based on the results of the UL 9540A test, the battery modules being installed in the racks do not pose a propagating fire risk to the other equipment. However, off gassing in the event of thermal runaway may lead to flammable gas concentrations presenting an explosion hazard and carbon monoxide concentrations exceeding the IDLH threshold. Accordingly, ventilation must be provided to run continuously or activate upon gas detection to prevent flammable and untenable gas concentrations in the container. Assuming that this mitigation feature is provided, the potential explosion and toxic exposure risks will be appropriately managed.

7.0 CONCLUSIONS

A HMA was performed on an outdoor stationary BESS container design planned for installation in Wattsville, VA. The design utilizes LFP batteries installed in racks. As demonstrated by the UL 9540A unit level tests, the modules limit the propagation of cells in thermal runaway to the initiating module where thermal runaway is expected to be limited to the initiating cell.

Section §1206.2.3.2 of the IFC and §4.1.4.3 of NFPA 855 list the criteria that must be met in order to gain approval of the HMA by the AHJ:

1. *Fires or explosions will be contained within unoccupied battery storage rooms for the minimum duration of the fire-resistance-rated specified:* This has been demonstrated to be met through the UL 9540A testing, in particular the unit level testing which showed that a

DRAFT

fire did not propagate beyond the initiating module. There was no indication of reignition at the conclusion of the test. (IFC §1206.2.3.2. #1 and NFPA 855 §4.1.4.3 #1)

2. *Suitable deflagration protection is provided where required:* a minimum of 500 cfm of ventilation must be provided to run continuously or activate upon gas detection to prevent flammable concentrations in the container during a thermal runaway event. Assuming that this mitigation feature is provided, the potential explosion and toxic exposure risks will be appropriately managed. (NFPA 855 §4.1.4.3 #2)
3. *Fires and explosions in battery cabinets in occupied work centers will be detected in time to allow occupants within the room to evacuate safely:* This will be accomplished via smoke and heat detection and ESMS. It also should be noted that these containers are not occupiable spaces. Access to the BESS containers is via the doors, will be reach in only, and further will be limited to inspection, testing, and maintenance. Based on the results of the UL 9540A testing, fires will be contained within a single module of a BESS rack. (IFC §1206.2.3.2. #2 and NFPA 855 §4.1.4.3 #3)
4. *Toxic and highly toxic gases released normal operations shall not exceed the PEL in the area of the energy storage system:* There are no toxic gas releases during normal operation. (NFPA 855 §4.1.4.3 #4)
5. *Toxic and highly toxic gases released during fires and other fault conditions shall not reach concentrations in excess of Immediately Dangerous to Life or Health (IDLH) levels in the building or adjacent means of egress routes during the time deemed necessary to evacuate from that area.:* There are no toxic gas releases during normal operation. During a thermal runaway event, off gassing may lead to flammable gas concentrations presenting an explosion hazard and carbon monoxide concentrations exceeding the IDLH threshold. Accordingly, ventilation must be provided to run continuously or activate upon gas detection to prevent flammable and untenable gas concentrations in the container. Assuming that this mitigation feature is provided, the potential explosion and toxic exposure risks will be appropriately managed. (IFC §1206.2.3.2. #3 and NFPA 855 §4.1.4.3 #5)
6. *Flammable gases released from batteries during charging, discharging and normal operation shall not exceed 25 percent of their lower flammability limit (LFL):* Flammable gases are not released from the batteries during normal operation, charging, or discharging. (IFC §1206.2.3.2. #4 and NFPA 855 §4.1.4.3 #6)
7. *Flammable gases released from batteries during fire, overcharging and other abnormal conditions shall not create an explosion hazard that will injure occupants or emergency responders:* Ventilation must be provided to run continuously or activate upon gas detection to prevent flammable and untenable gas concentrations in the container. Assuming that this mitigation feature is provided, the potential explosion and toxic exposure risks will be appropriately managed. (IFC §1206.2.3.2. #5)

In summary, the lithium-ion battery energy systems being proposed meet the Hazard Mitigation Analysis criteria laid out in IFC 2018 and NFPA 855 and as outlined above.

DRAFT

8.0 REFERENCES

Center for Disease Control and Prevention. (n.d.). *Carbon monoxide IDLH*. Retrieved 2020, [redacted]

International Code Council. (2018). *International Building Code*. (International Code Council) Retrieved from [redacted]

International Code Council. (2018). *International Fire Code*. (International Code Council) Retrieved from https://codes.iccsafe.org/content/OFC2019P1/chapter-12-energy-systems

National Fire Protection Association. (2020). *NFPA 855 Standard for the Installation of Stationary Energy Storage Systems*. NFPA.

New York City Fire Department. (2019). *Fire Department Rule 3 RCNY 608-01, Outdoor Stationary Storage Battery Systems*.

Panasonic. (2020). *AWS_BBU FMEA Panasonic_20200210*. Panasonic.

Sungrow. (2020). *FMEA Samsung E3 1.00*.

Underwriter Laboratories. (2020). *Cell Level Test Report Number 4788881139*.

Underwriters Laboratories. (2019). *9540A Module 4 cell FINAL Report_01_10_20*. UL.

Underwriters Laboratories. (2019). *9540A Unit Report FINAL Amazon_01_10-20*. UL.

Underwriters Laboratories. (2019). *UL 9540A Test Method for Evaluating Thermal Runaway Fire Propogation in Battery Energy Storage Systems*. UL.

Underwriters Laboratories. (2020). *9540A AWS Module Panasonic Cell Final report_05_13_20*. Underwriters Laboratories.

Underwriters Laboratories. (2020). *9540A Panasonic Cell Report Final_04-26-20*. Underwriters Laboratories.

Underwriters Laboratories. (2020). *9540A TP_Cell Level Report_Final_02-13-20*. Underwriters Laboratories.

Underwriters Laboratories. (2020). *9540A Unit Level Test Report Number 4789231760*. UL.

Underwriters Laboratories. (2020). *9540A Unit Report Panasonic Draft Amazon_05-07-20*. Underwriters Laboratories.

DRAFT

Annex 6 Toxic gas emission consequence modelling

Public Health Risk Assessment

Final Report

Ventura Energy Storage Project

Prepared for:
Ventura Energy Storage, LLC

Prepared by:
MRS Environmental
1306 Santa Barbara Street
Santa Barbara, CA 93101

Date:

September 16, 2019

Table of Contents

1.0 Introduction 1
2.0 Project Description 1
3.0 Environmental and Regulatory Setting 3
4.0 Assessment Methodology 4
5.0 Environmental Consequences 9
5.1 Exposure Assessment 9
5.2 Significance Criteria 10
5.3 Toxic Impacts 10
5.4 Flammable Impacts 11
6.0 Summary of Impacts and Conclusions 11
7.0 References 11

List of Tables

Table 1 Potential Toxic Pollutants from Battery Malfunctions 6
Table 2 Studies on Emissions from Battery Malfunctions 6
Table 3 Potential Flammable Components from Battery Off Gassing 7
Table 4 Tesla Manufacturer Battery Off Gassing Primary Flammable Components 8
Table 5 CAPCOA Risk Prioritization Results 11

List of Figures

Figure 1 Project Location 2

Attachments

Attachment A Calculations
Attachment B Emergency Response Guide

List of Acronyms

Acronym	Definition
Ah	Amp hour
APCD	Air Pollution Control District
ARB	Air Resources Board
BMS	Battery Management System
BSS	Battery Storage System
CAPCOA	California Air Pollution Control Officers Association
CGA	Compressed Gas Association
CFC	California Fire Code
CPUC	California Public Utilities Commission
EPA	Environmental Protection Agency
ESS	Energy Storage Systems
HVAC	Heating Ventilation and Air Conditioning
IDLH	Immediately Dangerous to Life and Health
IEEE	Institute of Electrical and Electronics Engineers
MWhr	Megawatt hour
NCA	Lithium Nickel Cobalt Aluminum
NFPA	National Fire Protection Association
NIOSH	National Institute for Occupational Safety and Health
OEHHA	Office of Environmental Health Hazard Assessment
REL	Reference Exposure Level
TS	Toxic Score
UL	Underwriters Laboratory
VCAPCD	Ventura County Air Pollution Control District
Whr	Watt hour

1.0 Introduction

Ventura Energy Storage, LLC. proposes to install a 102MW, 4-hour battery energy storage system near the town of Saticoy in the unincorporated area of Ventura County, CA. The Battery Storage Project (Project) would provide additional capacity to the electrical grid during periods when the solar arrays and other sources of electrical generation are not generating power. The Project would provide increased electrical reliability and stability to the local grid by storing electricity in the battery systems from the solar arrays and other grid-based systems and then releasing the power into the grid during periods when electricity is needed, thereby reducing the need to operate fossil-fuel-powered power systems and reducing the consumption of fossil-fuels and the emissions of greenhouse gasses.

This report examines the potential upset and malfunction scenarios that could occur at the facility that could result in health risk and flammable gas production and potential resulting impacts on public receptors. During normal operations the facility would not have any health risk or flammable impacts. Impacts to onsite personnel or emergency response personnel are outside the scope of this analysis.

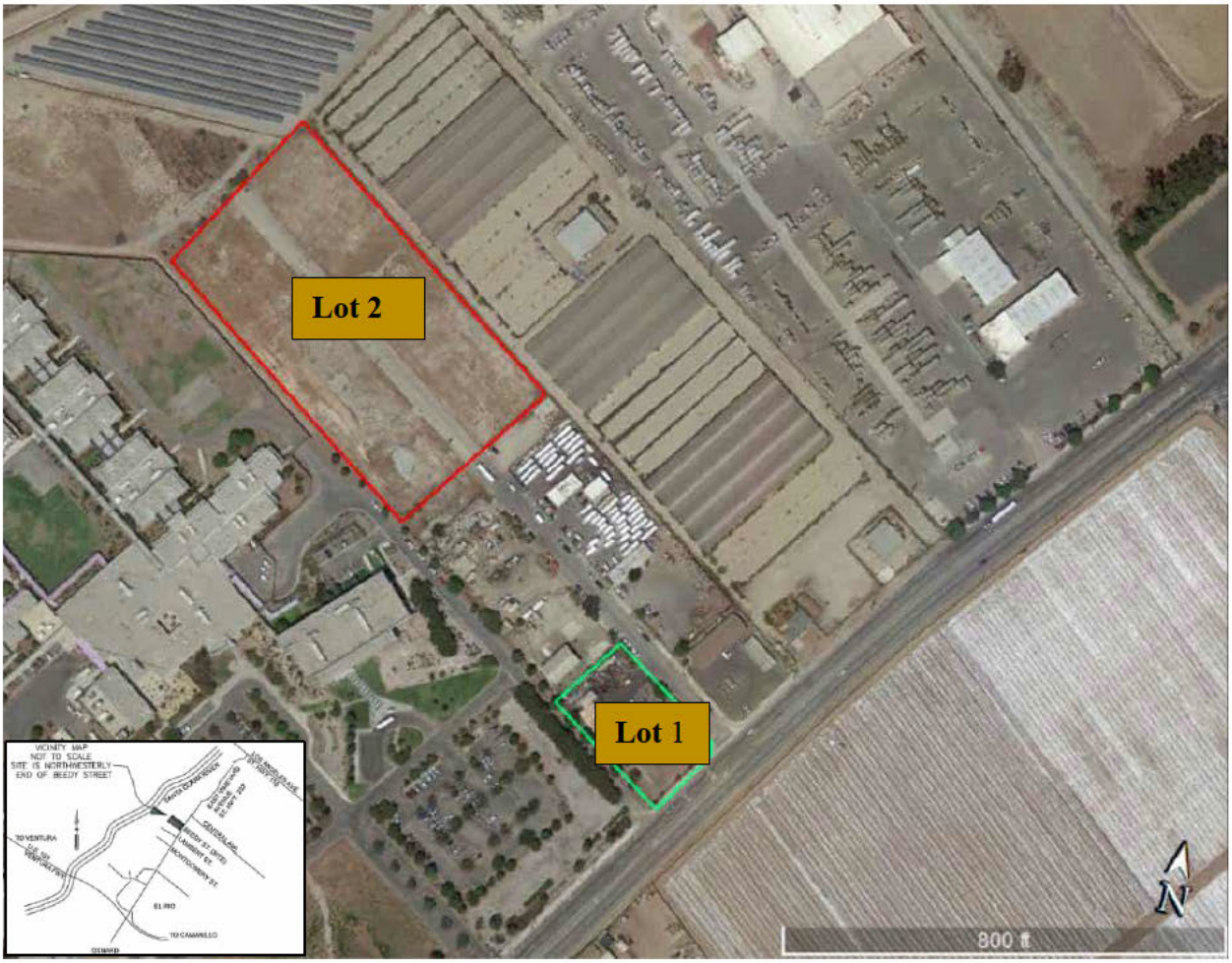
2.0 Project Description

The Project site would be located along Beedy Street near East Vineyard Avenue in the unincorporated area of Ventura County, just outside the Oxnard City limits. For the purposes of this report, the Project construction would be described as follows: Lot 1 and Lot 2. Lot 1 is a substation and single breaker line tap. Lot 2 contains the battery energy storage system. Although fires and potential risks are associated with the Lot 1 substation and single breaker line tap, this analysis only addresses the potential for health risks from the battery installation. Only Lot 2 includes batteries and therefore Lot 1 is not discussed further as the installation of substations are relatively common and the risks are well known and within normal fire response capabilities. Battery installations are relatively new technology and therefore additional analysis on the potential risks is warranted.

The proposed Project location Lot 2 would be located immediately north and east of the Perren Ventura County Juvenile Justice Complex, south of agricultural and industrial uses, north and west of Pegasus Transit storage areas and other industrial facilities, and south and east of the Santa Clara River and solar panel arrays. Figure 1 shows the location of the proposed battery storage facility. The site is currently undeveloped with some utilities (power, sewage and water) available.

The project would involve the installation of 142 self-contained energy storage and management cabinets (called a Megapack) containing battery modules designed and manufactured by Tesla. Each cabinet would hold 17 modules of batteries, with each module holding about 12,636 battery cells. An operations and maintenance control enclosure would also be located on the project site. The cabinets would be placed at the site outdoors. There will be no walk-in or inhabitable facilities in the proposed project design.

Figure 1 Project Location



Source: Google Maps

The proposed battery cell type would be Lithium Nickel Cobalt Aluminum (NCA) manufactured by Tesla. This analysis assumed an NCA-type battery.

The facility would be equipped with inverters to convert the DC electricity of the battery systems into AC current used by the electrical grid. There would also be a liquid thermal cooling system integrated into the cabinets to provide cooling to the batteries and power electronics.

Fire prevention systems would include proposed cabinets designed to limit or eliminate the threat of the spread of fire from one cabinet to another, infrared camera monitoring at the site and onsite hydrants.

The Battery Management System (BMS) would monitor all cell voltages, currents and temperatures and shut down equipment if unsafe conditions are detected.

3.0 Environmental and Regulatory Setting

There are a number of different lithium battery types including the following:

- Lithium Nickel Cobalt Aluminum (NCA)
- Lithium Nickel Manganese Cobalt (NMC)
- Lithium Manganese Oxide (LMO)
- Lithium Titanate Oxide (LTO)
- Lithium-Iron Phosphate (LFP, proposed for this project)

This study assumed the use of the NCA battery type.

Battery Testing Requirements and Regulations
Batteries are subject to several codes and standards. Some of the relevant ones are discussed below.

UL9540A: Test Method for Evaluating Thermal Runaway Fire Propagation in Battery Energy Storage Systems – this test methodology evaluates the fire characteristics of a battery energy storage system that undergoes thermal runaway. The data generated can be used to determine the fire and explosion protection required for an installation of a battery energy storage system

UL1973: Standard for Batteries for Use in Stationary, Vehicle Auxiliary Power and Light Electric Rail (LER) Applications - These requirements cover battery systems as defined by this standard for use as energy storage for stationary applications such as for PV, wind turbine storage or for UPS, etc. applications. This standard evaluates the battery system's ability to safely withstand simulated abuse conditions. This standard evaluates the system based upon the manufacturer's specified charge and discharge parameters. Requires that an ESS is not allowed to be an explosion hazard when exposed to an external fire source and that a single cell failure will not result in a cascading thermal runaway of cells.

IEEE C2: This Code covers basic provisions for safeguarding of persons from hazards arising from the installation, operation, or maintenance of (1) conductors and equipment in electric supply stations, and (2) overhead and underground electric supply and communication lines. It also includes work rules for the construction, maintenance, and operation of electric supply and communication lines and equipment. The Code is applicable to the systems and equipment operated by utilities, or similar systems and equipment, of an industrial establishment or complex under the control of qualified persons.

International Fire Code: Specifies limits on sizing for battery systems (Lithium all type, 50 kwh each array), seismic and structural design, spacing (minimum 3 feet separation of arrays), vehicle impact protection, testing, maintenance and repairs, maximum quantities within a building of 600 kwh, BMS monitoring, shutdown and notification requirements, automatic smoke detector requirements.

NFPA 1: The General NFPA Fire Code addressing extracts from other NFPA codes.

NFPA 13: Standard for the Installation of Sprinkler Systems, addresses sprinkler system design approaches, installation, and component options.

NFPA 70: National Electrical Code, addresses electrical design, installation, and inspection

NFPA 550: Guide to Fire Safety Concepts Tree for Protecting Energy Systems - addresses issues such as utilizing BMS and compatible equipment, ventilation as needed, fire resistive separation, array spacing, signage.

NFPA 855: Standard for the Installation of Stationary Energy Storage Systems - establishes criteria for minimizing the hazards associated with ESS (under development).

Health Protective Regulations

The California Air Pollution Control Officers Association (CAPCOA) in consultation with the California Air Resources Board (ARB) and Office of Environmental Health Hazard Assessment (OEHHA) implements the Air Toxics "Hot Spots" Information and Assessment Act of 1987 (Air Toxics "Hot Spot" Act, Health and Safety Code §44344.4(c).). The Hot Spots regulation requires the assessment of the potential acute, chronic and cancer health risks associated with facilities. OEHHA also publishes the reference exposure levels (REL) for a range of pollutants, which defines the concentration levels at which pollutants start to generate health effects.

The National Institute for Occupational Safety and Health (NIOSH) defines the immediately dangerous to life and health (IDLH) standard for pollutants.

In 2016, a technical working group comprised of utility and industry representatives worked with the California Public Utilities Commission Safety & Enforcement Division's Risk Assessment and Safety Advisory (RASA) section to develop a set of guidelines for documentation and safe practices at ESS co-located at electric utility substations, power plants or other facilities (CPUC 2017). The guidelines require a safety plan and inspection procedures.

4.0 Assessment Methodology

During normal operation there will be no emissions from the battery systems associated with the Project. However, in the unlikely event of a battery cell malfunction, such as a runaway reaction or external impact event, the Project could emit pollutants to the atmosphere. For these types of battery cell malfunctions, emissions could be generated due to elevated temperatures within a single storage cell or group of storage cells caused by a runaway reaction.

This analysis is limited to a reasonable worst-case event. A catastrophic event, such as an airplane impact, run-away vehicle impact, terrorist incident or nearby construction equipment collapse causing impact, could cause multiple megapacks to be destroyed, causing substantial emissions associated with a large-scale fire. A reasonable worst-case event is more limited in scope, defined as a control system failure or a puncture of a module, similar to that conducted as part of the UL 1973 testing, which could cause a runaway reaction in a group of cells. Generally, a reasonable worst-case scenario is more appropriate for a planning scenario as any development project could produce substantial fires and cause impacts to neighboring facilities under the catastrophic scenario.

The Battery Storage System (BSS) will be equipped with monitoring and control systems that will prevent and/or control battery cell malfunctions. However, to determine an unlikely, but reasonable worst-case public health impacts for this analysis, it is assumed that these control systems fail and do not control the battery cell malfunction. For this unlikely event, it is assumed that the battery cell malfunction continues until the fire department arrives onsite.

Different manufacturers have developed various studies examining the potential scenarios related to battery malfunctions, although most of these studies are proprietary. Some studies have been independently performed for agencies, including by Det Norske Veritas (DNVGL 2017) conducted for the New York State Energy Research & Development Authority (NYSERDA) and Consolidated Edison. Other studies include Anderson 2015, Blum 2016, Larsson 2017 and LG Chem (another battery manufacturer) where batteries were exposed to external heat sources and off gases were measured. In addition, the battery manufacturer Tesla, has conducted some testing conducted by DNVGL (DNVGL 2019) where external heat was added and forced a burn of the entire enclosure.

Different battery cell malfunctions could produce emissions. These include: (1) an elevated temperature situation due to a runaway reaction with no combustion (venting with no combustion); (2) combustion of the battery due to an elevated temperature situation from a runaway. Studies have shown (Rincon 2017, and proprietary UL9540A testing) that a localized runaway reaction with combustion produces the greatest emissions and is therefore the reasonable worst-case scenario and the scenario analyzed in this report.

The BSS will be enclosed in cabinets that have venting. It is assumed that the emissions caused by these malfunction scenarios will be vented during the malfunction scenario. As per the DNVGL 2019 testing, emission occurred over a period of a few hours. Therefore, for all malfunction scenarios, it is assumed that the release of pollutants to the atmosphere would occur within one hour as a reasonable worst case.

In addition, as part of the UL 1973 requirements, battery malfunctions and punctures are required to have limited cascading capabilities. Therefore, it is highly unlikely that an entire module or groups of modules would be involved in a single event. Therefore, as a reasonable worst-case, it is assumed that only 10 percent of the cells in a single module would be involved in the battery malfunction.

Battery malfunctions can result in the release of toxic materials and/or the release of a flammable gas mixture and subsequent flammable gas vapor cloud with subsequent fire or explosion.

Toxic Pollutants

Toxic pollutants emitted from battery malfunctions are partially dependent on the battery type. For lithium ion batteries, studies indicate that the primary toxic pollutants are as listed in Table 1.

Generally, the battery cell will start to off gas if the temperature exceeds 120 ^{o}C (DNVGL 2017).

Several studies have examined the emissions of toxic pollutants from battery off gassing situations, with some studies examining only the concentration of toxic pollutants and others also examining emission rates. The relevant studies are listed in Table 2.

Table 1 Potential Toxic Pollutants from Battery Malfunctions

Pollutant	OEHHA Reference Exposure Level (REL), µg/m3 (ppm)	IDLH
Carbon monoxide (CO)	23,000/26.7	1,200 ppm
Hydrogen Chloride (HCL)	2100/3.2	50 ppm
Hydrogen Cyanide (HCN)	340/0.4	50 ppm
Hydrogen Fluoride (HF)	240/0.2	30 ppm
Methanol	28,000/36.7	6,000 ppm
Nitrogen Oxide (NO_x)	470/0.9	13 ppm
Phosphine (PH_3)**	400/0.6	50 ppm
Phosphorous Pentafluoride (PF_5)	240/0.2*	50 ppm***
Phosphoryl Fluoride (POF_3)	240/1.0*	50 ppm
Styrene	21,000/89.5	700 ppm
Sulfur Dioxide (SO_2)	660/1.8	100 ppm
Toluene	37,000/140	500 ppm

* Utilized the acute REL for hydrogen fluoride as per OEHHA REL tables for Fluorides chronic are very similar

** OEHHA does not have REL for acute PH3. Estimated based on NIOSH values.

*** The National Institute for Occupational Safety and Health (NIOSH) does not have a listing for PF_5. PF_5 and POF_3 estimated based on general fluorides.

Sources: see Table 2

Table 2 Studies on Emissions from Battery Malfunctions

Study	Description	Results
Anderson 2015	Exposure of battery to heat source, off gasses tested. LFP battery, 1.2 kg, 35 Ah	HF: 30-50ppm peak POF_3: 1-2ppm peak HF Rate: 0.01 g/s
Blum 2016	Modules tested with heat exposure until thermal runaways. 100kwh unit by Tesla.	HF: 100 ppm peak
Larsson 2017	External propane burner to heat batteries, measured toxic gasses. Examined different battery types	HF: up to 145 ppm peak HF rate: 50 mg/s peak HF rate: 200mg/whr peak POF_3 rate: 22 mg/whr peak
LG Chem	Proprietary data on LFP battery tests. NMC battery type.	HF: 4.7e-7 g/hr PH_3: 2.4e-4 g/hr Up to 244 L gas per cell at: HF-0.2ppm and PH_3-1.0ppm

Table 2 Studies on Emissions from Battery Malfunctions

Study	Description	Results
DNVGL 2017	Measured characteristics of a wide range of battery types and failures	kg/s release rates per kg of battery weight: HF: 1.7e-7 kg/s-kg
DNVGL 2019	Measure characteristics of a Tesla powerpack thermal runaway scenario	Maximum Values: HCL: 538 ppm HF: 183 ppm HCN: 67 ppm
Tesla	Proprietary studies	HF: 500 ppm HCL: 1,000 ppm HCN: 1,600 ppm Methanol: 32 ppm Styrene: 1 ppm Toluene: 3,500 ppm

Some of the key findings from these studies include the following:

- HF was found to be produced by all battery types.
- For NCA batteries, HCL, HF and HCN are produced (DNVGL 2019).
- PH_3 was only identified by LG Chem for the NMC battery type, not the NCA proposed for this project. No other studies identified PH_3 as an issue for the NCA battery.
- PF_5 rapidly decomposes to HF and was therefore generally not detected (Anderson 2013).
- POF_3 was found to be not be produced by NCA batteries (Larsson 2017).

It was also found that the average emission rate of HF in a plastics fire can be higher than the average emission rate of a battery fire (DNVGL 2017), indicating that potentially a majority of the toxic emissions from a battery fire are a result of the combustion of the plastic components.

Flammable Components and Flammability

Flammable components are also emitted from a battery malfunction. Based upon the studies listed in Table 2, the flammable components could include any the following:

Table 3 Potential Flammable Components from Battery Off Gassing

Component	Lower Flammability Limit (LFL), vol%
Acetylene (C_2H_2)	2.5
Butanes (C_4)	1.8
Carbon monoxide (CO)	12.5
Ethane (C_2H_6)	3.0
Ethanol (C2H6O)	3.3
Ethylene (C_2H_4)	2.7
Hydrogen (H_2)	4.0
Methane (CH_4)	5.0

Table 3 Potential Flammable Components from Battery Off Gassing

Component	Lower Flammability Limit (LFL), vol%
Methanol (CH4O)	6.0
Pentanes (C_5)	1.4
Propane (C_3H_8)	2.1
Propene (C_3H_6)	2.0

Sources: See Table 2.

Depending on the combination of these flammable materials, the off gasses could have varying degrees of flammability.

The Tesla manufacturer provided information on the composition of battery off gassing as part of battery testing. These are shown below:

Table 4 Tesla Manufacturer Battery Off Gassing Primary Flammable Components

Component	Mole Percent
Hydrogen (H_2)	24
Carbon monoxide (CO)	34
Methane (CH_4)	4
Ethylene (C_2H_4)	5
Propane (C_2H_8) +	< 1

Note: based on Telsa proprietary testing, worst-case level encountered (most flammable), for single cell level testing. Other components, such as nitrogen and carbon dioxide, are produced also but are not shown due to not being flammable.

The Compressed Gas Association (CGA) Publication P-23 provides algorithms for estimating the level of flammability of gas mixtures. The application of this technique to the off gassed materials as provided by the manufacturer as part of the testing (shown in Table 4) indicates that the released vapor/gas would be flammable, with a Q value of over 6.0 and an estimated lower flammability limit of 5.4 percent. (This exceeds the Q value flammability limit of 1.0, established by the CGA, indicating the materials is flammable. See Attachment A) (CGA 2015).

Screening and Modeling

In order to estimate the impacts of the off gassing from toxic and flammable emissions, a screening and a modeling approach were used. The Ventura County APCD screening approach for health risks was used for the acute impact of toxic emissions. The screening approach uses the prioritization method developed by the California Air Pollution Control Officers Association (CAPCOA) in consultation with the California Air Resources Board (ARB) and Office of Environmental Health Hazard Assessment (OEHHA) as part of the implementation of the Air Toxics "Hot Spots" Information and Assessment Act of 1987 (Air Toxics "Hot Spot" Act, Health and Safety Code §44344.4(c).). The criteria used by the prioritization method is based on a Total Score (TS) for acute impacts. These score thresholds are as follows:

- High priority facilities with TS greater than 10.0
- Intermediate priority facilities with TS between 1.0 and 10.0
- Low priority facilities with TS less than 1.0

The criteria are based on the application of several conservative air dispersion modeling scenarios coupled with air pollutant toxicities as reported by OEHHA and the Environmental Protection Agency (EPA). For scores falling in the High or Intermediate Priority category, other factors that should be considered that could affect the results may include:

- Population density near the facility,
- Proximity of sensitive receptors to the facility,
- Receptor proximity less than 50 meters,
- Elevated receptors/complex terrain,
- Frequency of nuisance violations,
- Importance of non-inhalation pathway for substance(s) emitted by the facility,
- Presence of non-stack (fugitive) emissions, and
- Stack temperatures and release source terms.

The prioritization utilized guidelines developed by the Air District (VCAPCD 2016). For intermediate and high priority facilities, additional analysis utilizing modeling with source and receptor specific factors may be required.

For flammable impacts, the Canary© model was used to determine the distances that flammable vapor clouds could travel with a resulting battery malfunction scenario under different meteorological conditions. The Canary© model was also used to examine vapor cloud explosion impacts to 1 psi overpressure. The Canary© model is a computerized model developed by Quest Consulting to estimate the thermodynamic properties of gas mixtures and estimate impact distances of thermal exposure, explosions, vapor clouds and toxic effects.

5.0 Environmental Consequences

The consequences associated with battery malfunctions are discussed below based on the methodology presented above.

5.1 Exposure Assessment

Project emissions to the air would consist of combustion and vent products from the burning and/or venting of the battery cells due to a battery cell malfunction under the reasonable worst-case scenario. Inhalation is the main pathway by which air pollutants could potentially cause public health impacts.

Flammable impacts could be produced by vapor cloud deflagrations or explosions for the reasonable worst-case scenario.

5.2 Significance Criteria

A prioritization method was developed by the California Air Pollution Control Officers Association (CAPCOA) as well as detailed in the Ventura County APCD Air Toxics "Hot Spots" Prioritization Procedure (VCAPCD 2016) are utilized to access the potential impacts associated with toxic emissions based on Total Score (TS) for acute impacts. A TS of below 1.0 is considered less than significant, with a TS of above 1.0 requiring additional analysis in order to determine significance.

Flammable impacts are determined to be less than significant if vapor cloud fires or explosions do not impact sensitive areas, with additional analysis required to determine significance if flammable vapors could impact sensitive receptors (including the use of a quantitative risk analysis).

5.3 Toxic Impacts

Potential human health impacts associated with the project stem from exposure to air emissions from the battery cell malfunction reasonable worst-case scenario discussed above. The reasonable worst-case scenario would involve the battery malfunctions associated with combustion. The battery manufacturer provided information on primary and toxic pollutants from the battery combustion malfunction are utilized. It is assumed that these emissions are released over a period of 1 hour.

Detailed calculations are provided in Attachment A. Included in Attachment B is a copy of the Emergency Response Guide provided by the battery vendor Tesla. The compounds and the associated mass emission rates were determined by proprietary testing performed by the battery vendor.

As per UL requirements tests, in the event of a single cell undergoing thermal runaway there was no propagation to surrounding cells. In addition, the tests showed that when an entire module was ignited, there was no propagation to surrounding modules. While the entire BSS will be comprised of many modules, because the malfunction events discussed above are unlikely to occur and, if such an event does occur, it will only likely occur within a single or limited number of battery cells, the analysis conservatively assumed that only 10 percent of the cells within a module would be affected as a reasonable worst-case analysis (i.e. a multicell malfunction).

As the emissions would occur over a short period of time, only the public health impacts associated with acute exposure to short term releases were analyzed for the reasonable worst-case battery cell malfunction. The acute impact prioritization scores for the reasonable worst-case battery cell malfunction scenario is provided in Table 5, and detailed calculations can be found in Attachment A. Each score is well below a TS of 1.0, indicating that all of the modeled release scenarios receive a low priority classification. Therefore, the public health impacts from toxic pollutants associated with the reasonable worst-case battery cell malfunction would be less than significant.

Table 5 CAPCOA Risk Prioritization Results

Scenario	CAPCOA Total Score (TS)
Single Cell malfunction, reasonable worst case	0.0005
Multiple Cell malfunction (10% of cells), reasonable worst case	0.69

5.4 Flammable Impacts

The off gassed materials could generate a flammable vapor cloud and may produce a flammable gas mixture (see above). The Canary© computer model was utilized to estimate the distance that the flammable vapor cloud could reach (see Attachment A for the Canary© model outputs and assumptions). The lower flammability limit (LFL) and the ½ LFL are used as an estimate of the potential impacts from flammable vapors. Distances for the LFL and the ½ LFL are estimated to be 10 and 18 feet, respectively. Explosion distances to a 1 psi overpressure assumed a high level of material reactivity (due to the presence of hydrogen) and a high obstacle density (due to the location of multiple cabinets together) in order to be conservative. Vapor cloud explosion impacts are estimated to be less than the ½ LFL distance. This distance would not extend outside of the project site boundaries and would not impact any offsite receptors. Therefore, the flammable vapor impacts would be less than significant.

6.0 Summary of Impacts and Conclusions

Results from the prioritization analysis indicate that the reasonable worst-case battery cell malfunction scenario would result in maximum acute impacts for toxic pollutant exposure below the significance threshold of 1.0 TS for the CAPCAO screen health risk. Flammable component impacts within the LFL and ½ LFL and explosion impacts (to 1 psi overpressure) would remain on the facility site. Therefore, the maximum potential public health impacts for the battery facility are considered less than significant.

7.0 References

Anderson 2013, Investigation of fire emissions from Li-ion batteries

Blum 2016, Lithium Ion Battery Energy Storage System Fires

CAPCOA 2016, CAPCOA Air Toxic "Hot Spots" Program Facility Prioritization Guidelines

CPUC 2017, SED Safety Inspection Items for Energy Storage Ratified by D.17-04-039, April 27, 2017 (Finding of Fact #24)

DNVGL 2017, Considerations for ESS Fire Safety

DNVGL 2019, Live Fire Test of Tesla Powerpacks Tesla, Inc. DNV GL Doc. No.: 10118434-HOU-R-02-D Issue: D; Status: Release Issue Date: April 17th, 2019

ESN 2019, Energy Storage News, Korea's ESS fires: Batteries not to blame but industry takes hit anyway, 19 June, 2019

FDNY 2015, Workshop on Energy Storage Systems and the Built Environment

Hopper 2017, Energy Storage Systems – Fire Safety Concepts in the 2018 International Fire and Residential Codes

Larsson 2017, Toxic Fluoride Gas Emissions from Lithium-Ion Battery Fires

NFPA 2017, Technical Committee on Stationary Energy Storage Systems Minutes of Meeting

NIOSH 2019, The National Institute for Occupational Safety and Health (NIOSH), Immediately Dangerous To Life or Health (IDLH) Values: Table of IDLH Values, [redacted]

OEHHA 2019, REL listing, [redacted]

Rincon 2017, NRG Ellwood Battery Storage Project Final Initial Study – Mitigated Negative Declaration Case #15-145-CUP (LG Chem batteries)

Ronken 2017, Lithium-Ion Batteries – A New Fire Risk

Tesla 2019, Tesla "Cell and unit level assessment of gas release composition from Tesla ESS"

VCAPCD 2016, Ventura County Air Pollution Control District (APCD) Air Toxics "Hot Spots" Prioritization Procedure

Attachment A

Calculations

Tesla Battery System
NCA Toxic Emission Calcs

Pollutant	Vol %	Volume (Liter)	MW (g/mol)	Single Cell Emissions (grams)	Single Cell Rate (g/s)	Single Cell Rate (lbs/hr)	Multicell Rate (g/s)	Multicell Rate (lbs/hr)
Primary Compounds								
H2	24	1.5	2.0	0.1	0.0000	0.0003	0.0419	0.3328
CO	34	2.1	28.0	2.6	0.0007	0.0057	0.9078	7.2047
CO2	28	1.7	44.0	3.3	0.0009	0.0074	1.1748	9.3237
CH4	4	0.2	16.0	0.2	0.0000	0.0004	0.0610	0.4843
C2H4	5	0.3	28.1	0.4	0.0001	0.0008	0.1340	1.0633
C2H6	0	0.0	30.1	0.0	0.0000	0.0000	0.0000	0.0000
C3H6	0.004	0.0	42.1	0.0	0.0000	0.0000	0.0002	0.0013
C3H8	0	0.0	44.1	0.0	0.0000	0.0000	0.0000	0.0000
C4	0	0.0	58.1	0.0	0.0000	0.0000	0.0000	0.0000
C5	0	0.0	72.2	0.0	0.0000	0.0000	0.0000	0.0000
Nitrogen	5	0.3	28.0	0.4	0.0001	0.0008	0.1335	1.0595
Total	100.0	6.1	25.8	7.0	0.0019	0.0154	2.4570	19.5000
Trace compounds	**ppm**	**MW**						
HF	500	20.0		2.7E-03	7.5E-07	6.0E-06	9.5E-04	7.6E-03
HCL	1,000	36.4		9.9E-03	2.7E-06	2.2E-05	3.5E-03	2.8E-02
HCN	1,600	27.0		1.2E-02	3.3E-06	2.6E-05	4.1E-03	3.3E-02
Methanol	32	27.0		2.3E-04	6.5E-08	5.2E-07	8.2E-05	6.5E-04
Styrene	1	104.0		2.8E-05	7.8E-09	6.2E-08	9.9E-06	7.9E-05
Toluene	3,500	92.0		8.7E-02	2.4E-05	1.9E-04	3.1E-02	2.4E-01

Assumes: Atmospheric Normal Temperature and Pressure (298.15K and 100.3 kpa)
Vol % and single cell emissions total provided by manufacturer
Standard temperature and pressure (STP) is defined as 0°C (273.15 K) and 1 atm of pressure
Number of cells in multicell event 1264
Time of event, minutes 60
Gas compsitions based on Tesla and DNVGL studies, maximum values measured.

Tesla Battery Cell Malfunction Toxic Emissions
CAPCOA health Risk Screening Prioritization Score

Single Cell

Pollutant	Name	TAC?	Max lbs/hr	Acute normalization Factor	Proximity Factor	Acute REL (ug/m3)	Prioritization Score
H2	Hydrogen	No	-	1500	1	-	-
CO	Carbon monoxide	Yes	5.7E-03	1500	1	23,000	3.7E-04
CO2	Carbon Dioxide	No	-	1500	1	-	-
CH4	Methane	No	-	1500	1	-	-
C2H4	Ethylene	No	-	1500	1	-	-
C2H6	Ethane	No	-	1500	1	-	-
C3H6	Propene	No	-	1500	1	-	-
C3H8	Propane	No	-	1500	1	-	-
C4	Butanes	No	-	1500	1	-	-
C5	Pentanes	No	-	1500	1	-	-
HF	Hydrogen Fluoride	Yes	6.0E-06	1500	1	240	3.7E-05
HCL	Hydrochloric acid	Yes	2.2E-05	1500	1	2100	1.6E-05
HCN	Hydrogen cyanide	Yes	2.6E-05	1500	1	340	1.1E-04
Methanol	Methanol	Yes	5.2E-07	1500	1	28000	2.8E-08
Styrene	Styrene	Yes	6.2E-08	1500	1	21000	4.4E-09
Toluene	Toluene	Yes	1.9E-04	1500	1	37000	7.8E-06
Total							0.0005

Multi-Cell

Pollutant	Name	TAC?	Max lbs/hr	Acute normalization Factor	Proximity Factor	Acute REL (ug/m3)	Prioritization Score
H2	Hydrogen	No	-	1500	1	-	-
CO	Carbon monoxide	Yes	7.2E+00	1500	1	23,000	4.7E-01
CO2	Carbon Dioxide	No	-	1500	1	-	-
CH4	Methane	No	-	1500	1	-	-
C2H4	Ethylene	No	-	1500	1	-	-
C2H6	Ethane	No	-	1500	1	-	-
C3H6	Propene	No	-	1500	1	-	-
C3H8	Propane	No	-	1500	1	-	-
C4	Butanes	No	-	1500	1	-	-
C5	Pentanes	No	-	1500	1	-	-
HF	Hydrogen Fluoride	Yes	7.6E-03	1500	1	240	4.7E-02
HCL	Hydrochloric acid	Yes	2.8E-02	1500	1	2100	2.0E-02
HCN	Hydrogen cyanide	Yes	3.3E-02	1500	1	340	1.4E-01
Methanol	Methanol	Yes	6.5E-04	1500	1	28000	3.5E-05
Styrene	Styrene	Yes	7.9E-05	1500	1	21000	5.6E-06
Toluene	Toluene	Yes	2.4E-01	1500	1	37000	9.9E-03
Total							0.69

Notes: Assumes worst case proximity factor of 1.0 (0-100 meters)
Spreadsheets as per VCAPCD 2016 Guidance for risk prioritization

Battery Malfunction Flammability Analysis: pg 2 of Tesla "Cell and unit level assessment of gas release composition from Tesla ESS"

CGA P-23 Method

Component	Mole %	MW	Wt %	LEL	NFN2: Non-Flamm in Nitrogen*	Mole% x NFN2
H2	24	2	4.01	4.0	5.7	4.21
N2	5	28	11.69	-		
CO2	28	44	102.87	-		
CO	34	28	79.49	12.5	20	1.70
Ch4	4	16	5.34	5	14.3	0.28
C2	5	30	12.53	3	12	0.42
C3	0.004	44	0.01	2.1	6.5	0.00
C4	0	58	0.00	1.8	5.6	0.00
C5+	0	72	0.00	1.4	4.4	0.00
Total	100	25.9	215.9491	5.56	Q factor =	6.61
Frac flamm	67.00		101.39			

* From CGA P-23 Table 1

```
+------------------------------------------------------------+
|                CANARY by Quest - Version 4.6.2             |
|                       CANARY Case Input                    |
|                     Case Name - B-1revised                 |
|                    Mon Sep 16 13:48:14 2019                |
|          Quest Consultants Inc., Norman, Oklahoma, USA     |
|          [redacted]          canary@questconsult.com       |
|        telephone (405) 329-7475     fax (405) 329-7734     |
+------------------------------------------------------------+
```

Title: Battery Malfunction

```
Case Type           : Vapor Dispersion
Case Name           : B-1revised
User ID             : GC
Project Number      :
Type of Units       : English Units
```

NOTES:

MATERIAL MENU

Materials Released	Number	Formula	Name	Fraction
Component 1	51	H2	Hydrogen(equilibrium)	0.250878
Component 2	43	CO	Carbon Monoxide	0.355411
Component 3	17	CO2	Carbon Dioxide	0.292691
Component 4	1	CH4	Methane	0.041813
Component 5	2	C2H6	Ethane	0.052266
Component 6	3	C3H8	Propane	0.000042
Component 7	50	HF	Hydrogen Fluoride	0.000523
Component 8	26	HCl	Hydrogen Chloride	0.001045
Component 9	103	CHN	Hydrogen Cyanide	0.001673
Component 10	281	C7H8	Toluene	0.003659

```
Temperature         :        77.00 °F
Pressure            :        29.40 psia
The material is GAS
```

NOTES:

ENVIRONMENT MENU

```
Wind speed                                    3.36 mph
Wind speed measurement height                 32.8 feet
Stability class <A-F>                            F
Relative humidity                               70 %
Air temperature                               77.0 °F
Spill surface temperature                     77.0 °F

Substrate name                          Soil
  Substrate thermal conductivity         1.0000 Btu/hr-ft-F
  Substrate density                         100 lb/cu.ft
  Substrate heat Capacity                  0.24 Btu/lb-F
  Substrate delay time                       60 sec
Surrounding terrain                     Long grass or crops > 15 cm (6 in)
```

NOTES:

Case continued on page 2.

Page 2 Title: Battery Malfunction

RELEASE MENU
Type of release: Regulated, Continuous release

Release duration	60 min
Regulated flow rate	0.01 lb/sec
Pipe inner diameter	12.00 inches
Equivalent release diameter	12.00 inches
Height of release point	6.0 feet
Angle of release from horizontal	0.0 degrees

NOTES:

IMPOUNDMENT MENU
Unconfined

NOTES:

VDVE MENU
Vapor generation, dispersion and cloud explosion - Flammable calculation

Concentration endpoint 1	LFL mol%
Concentration endpoint 2	1/2 LFL mol%
Concentration endpoint 3	1/2 LFL mol%

Dispersion coefficient averaging time	1 min

Baker-Strehlow-Tang parameters

Fuel reactivity	High
Obstacle density	High
Flame expansion	3-D

Overpressure values

Overpressure endpoint 1	3.00 psi
Overpressure endpoint 2	1.00 psi
Overpressure endpoint 3	1.00 psi

NOTES:

```
+-------------------------------------------------------------+
|                CANARY by Quest - Version 4.6.2              |
|              Momentum Jet Vapor Dispersion Model            |
|                     Case Name - B-1revised                  |
|                   Mon Sep 16 13:48:14 2019                  |
|         Quest Consultants Inc., Norman, Oklahoma, USA       |
|         [redacted]          canary@questconsult.com         |
|         telephone (405) 329-7475    fax (405) 329-7734      |
+-------------------------------------------------------------+

TITLE: Battery Malfunction


concentration limits

concentration 3 (highest) =    0.082931 mole fraction
concentration 2 (middle)  =    0.041466 mole fraction
concentration 1 (lowest)  =    0.041466 mole fraction
```

downwind distance x(ft)	centerline conc. c(mole frac.)	ground conc. c(mole frac.)	y(c1) 1/2 width (ft)	y(c2) 1/2 width (ft)	y(c3) 1/2 width (ft)	centerline height (ft)
0	1.000000	0.000000	1.0	1.0	0.9	6.0
0.3	0.827153	0.000000	1.0	1.0	0.9	6.0
0.5	0.718949	0.000000	1.0	1.0	0.8	6.0
0.8	0.636307	0.000000	1.0	1.0	0.8	6.1
1.0	0.569857	0.000000	1.0	1.0	0.8	6.1
1.3	0.514734	0.000000	1.0	1.0	0.8	6.1
1.5	0.468452	0.000000	1.0	1.0	0.8	6.2
1.7	0.428986	0.000000	1.0	1.0	0.9	6.2
2.0	0.394974	0.000000	1.0	1.0	0.9	6.3
2.3	0.365183	0.000000	1.0	1.0	0.9	6.3
2.5	0.339175	0.000000	1.1	1.1	0.9	6.4
2.8	0.316004	0.000000	1.1	1.1	0.9	6.4
3.0	0.295519	0.000000	1.1	1.1	0.9	6.5
3.3	0.277149	0.000000	1.1	1.1	0.9	6.5
3.5	0.260479	0.000000	1.1	1.1	0.9	6.5
3.7	0.245684	0.000000	1.1	1.1	0.9	6.6
4.0	0.232150	0.000000	1.1	1.1	0.9	6.6
4.3	0.219724	0.000000	1.1	1.1	0.9	6.7
4.5	0.208394	0.000000	1.1	1.1	0.9	6.7
4.8	0.198089	0.000000	1.1	1.1	0.9	6.7
5.0	0.188554	0.000000	1.2	1.2	0.8	6.8
5.3	0.179713	0.000000	1.2	1.2	0.8	6.8
5.5	0.171603	0.000000	1.2	1.2	0.8	6.9
5.8	0.163996	0.000000	1.2	1.2	0.8	6.9
6.0	0.156984	0.000000	1.2	1.2	0.8	7.0
6.3	0.150489	0.000000	1.2	1.2	0.8	7.0
6.5	0.144285	0.000000	1.2	1.2	0.8	7.0
6.8	0.138550	0.000000	1.2	1.2	0.8	7.1
7.0	0.133253	0.000000	1.2	1.2	0.8	7.1
7.3	0.128238	0.000000	1.2	1.2	0.7	7.1
7.5	0.123539	0.000000	1.2	1.2	0.7	7.2
7.8	0.119105	0.000000	1.2	1.2	0.7	7.2
8.0	0.114931	0.000000	1.2	1.2	0.7	7.3
8.3	0.111000	0.000000	1.2	1.2	0.6	7.3
8.5	0.107233	0.000000	1.2	1.2	0.6	7.3

downwind distance x(ft)	centerline conc. c(mole frac.)	ground conc. c(mole frac.)	y(c1) 1/2 width (ft)	y(c2) 1/2 width (ft)	y(c3) 1/2 width (ft)	centerline height (ft)
8.8	0.103678	0.000000	1.2	1.2	0.6	7.4
9.0	0.100344	0.000000	1.2	1.2	0.5	7.4
9.3	0.097146	0.000000	1.2	1.2	0.5	7.4
9.5	0.094178	0.000000	1.2	1.2	0.5	7.5
9.8	0.091271	0.000000	1.2	1.2	0.4	7.5
10.0	0.088541	0.000000	1.2	1.2	0.3	7.5
10.3	0.085962	0.000000	1.2	1.2	0.3	7.6
10.5	0.083452	0.000000	1.1	1.1	0.1	7.6
10.8	0.081086	0.000000	1.1	1.1	0.0	7.6
11.0	0.078822	0.000000	1.1	1.1	0.0	7.7
11.3	0.076666	0.000000	1.1	1.1	0.0	7.7
11.5	0.074586	0.000000	1.1	1.1	0.0	7.7
11.8	0.072599	0.000000	1.1	1.1	0.0	7.7
12.0	0.070721	0.000000	1.1	1.1	0.0	7.8
12.3	0.068898	0.000000	1.1	1.1	0.0	7.8
12.5	0.067161	0.000000	1.1	1.1	0.0	7.8
12.8	0.065488	0.000000	1.0	1.0	0.0	7.9
13.0	0.063885	0.000000	1.0	1.0	0.0	7.9
13.2	0.062322	0.000000	1.0	1.0	0.0	7.9
13.5	0.060825	0.000000	1.0	1.0	0.0	8.0
13.8	0.059409	0.000000	1.0	1.0	0.0	8.0
14.0	0.058024	0.000000	0.9	0.9	0.0	8.0
14.3	0.056690	0.000000	0.9	0.9	0.0	8.0
14.5	0.055403	0.000000	0.9	0.9	0.0	8.1
14.8	0.054197	0.000000	0.9	0.9	0.0	8.1
15.0	0.052992	0.000000	0.8	0.8	0.0	8.1
15.3	0.051846	0.000000	0.8	0.8	0.0	8.2
15.5	0.050728	0.000000	0.8	0.8	0.0	8.2
15.7	0.049651	0.000000	0.7	0.7	0.0	8.2
16.0	0.048623	0.000000	0.7	0.7	0.0	8.2
16.3	0.047615	0.000000	0.7	0.7	0.0	8.3
16.5	0.046655	0.000000	0.6	0.6	0.0	8.3
16.8	0.045728	0.000000	0.6	0.6	0.0	8.3
17.0	0.044833	0.000000	0.5	0.5	0.0	8.3
17.3	0.043954	0.000000	0.5	0.5	0.0	8.4
17.5	0.043110	0.000000	0.4	0.4	0.0	8.4
17.8	0.042294	0.000000	0.3	0.3	0.0	8.4
18.0	0.041506	0.000000	0.0	0.0	0.0	8.4

The downwind distance to c3 is 10.55 ft after about 5 seconds
The downwind distance to c2 is 18.01 ft after about 7 seconds
The downwind distance to c1 is 18.01 ft after about 7 seconds

+--+
| CANARY by Quest - Version 4.6.2 |
| Momentum Jet Vapor Cloud Explosion |
| Case Name - B-1revised |
| Mon Sep 16 13:48:14 2019 |
| Quest Consultants Inc., Norman, Oklahoma, USA |
| [redacted] canary@questconsult.com |
| telephone (405) 329-7475 fax (405) 329-7734 |
+--+

Title: Battery Malfunction

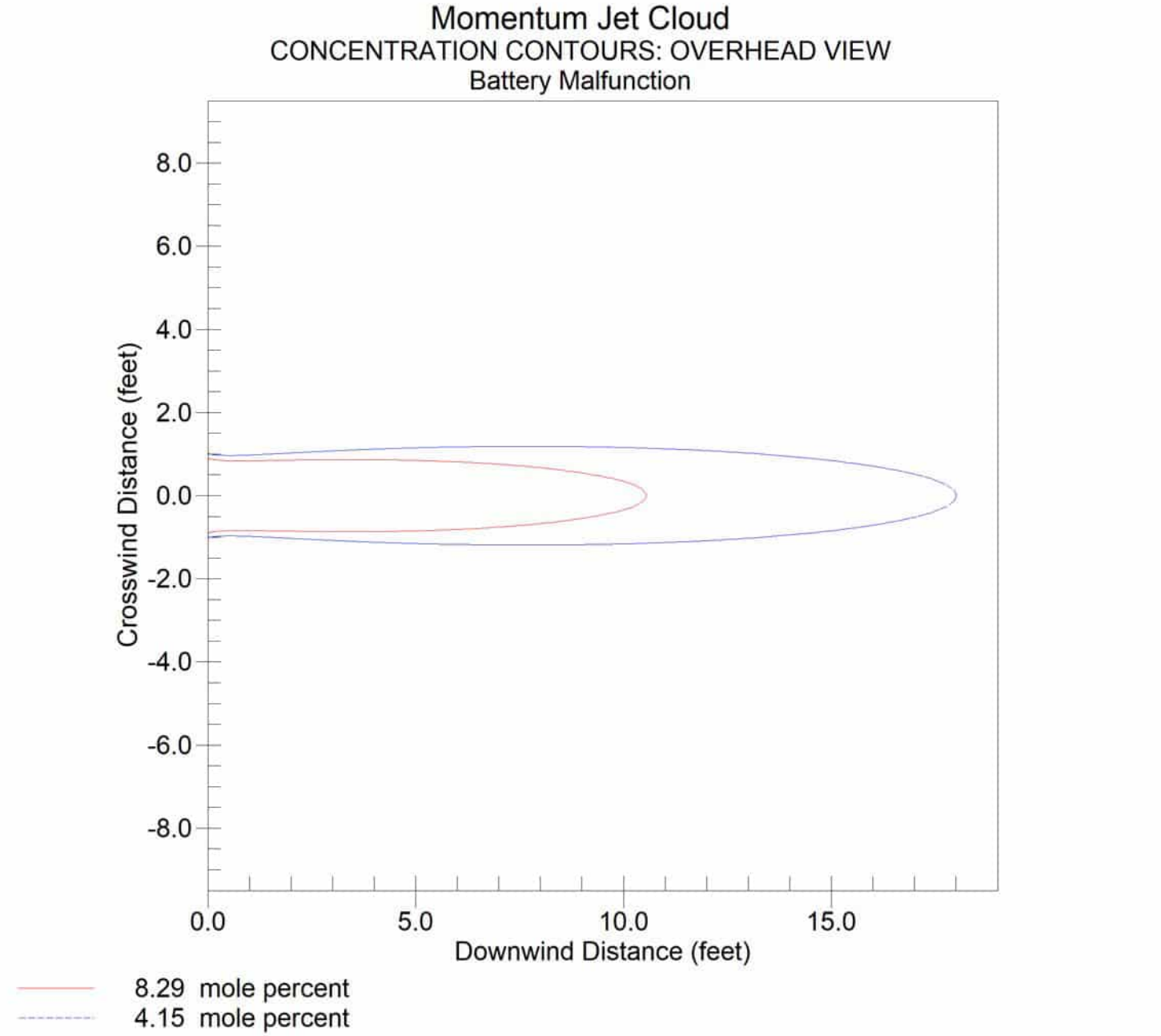
Fuel Reactivity: High Obstacle Density: High
Flame Expansion: 3-D Flame Speed: 5.20

Overpressure levels:
---
dp3 = 3.00 psi gauge
dp2 = 1.00 psi gauge
dp1 = 1.00 psi gauge

Mass of released material in explosive range: 0.0153819 lbs.

Distance from Center of Flammable Cloud (feet)	Overpressure (psi gauge)	Impulse (psi-s)
0.0	308.61	0.0114
0.3	308.61	0.0114
0.3	308.61	0.0107
0.3	308.61	0.0100
0.4	308.61	0.0094
0.4	308.61	0.0088
0.4	308.61	0.0082
0.4	308.61	0.0077
0.5	302.51	0.0073
0.5	252.54	0.0068
0.5	210.83	0.0064
0.6	176.00	0.0060
0.6	146.93	0.0056
0.7	122.66	0.0053
0.7	102.40	0.0049
0.7	85.48	0.0046
0.8	71.36	0.0043
0.9	59.58	0.0041
0.9	49.74	0.0038
1.0	41.52	0.0036
1.0	34.66	0.0034
1.1	19.27	0.0031
1.2	17.81	0.0029
1.3	16.46	0.0028
13.1	1.00	0.0003

The downwind distance to dp3 is 11.5 feet
The downwind distance to dp2 is 13.1 feet
The downwind distance to dp1 is 13.1 feet


Momentum Jet Cloud
CONCENTRATION CONTOURS: OVERHEAD VIEW
Battery Malfunction
Crosswind Distance (feet)
8.0
6.0
4.0
2.0
0.0
-2.0
-4.0
-6.0
-8.0
0.0
5.0
10.0
15.0
Downwind Distance (feet)
8.29 mole percent
4.15 mole percent
CANARY by Quest
casename=B-1revised
windspeed = 3.4 mph
F stability
Mon Sep 16 13:48:14 2019

Annex 7 Fire & explosion modelling

Modeling the Conditions Produced During a Lithium-ion Battery Reaction



JENSEN HUGHES

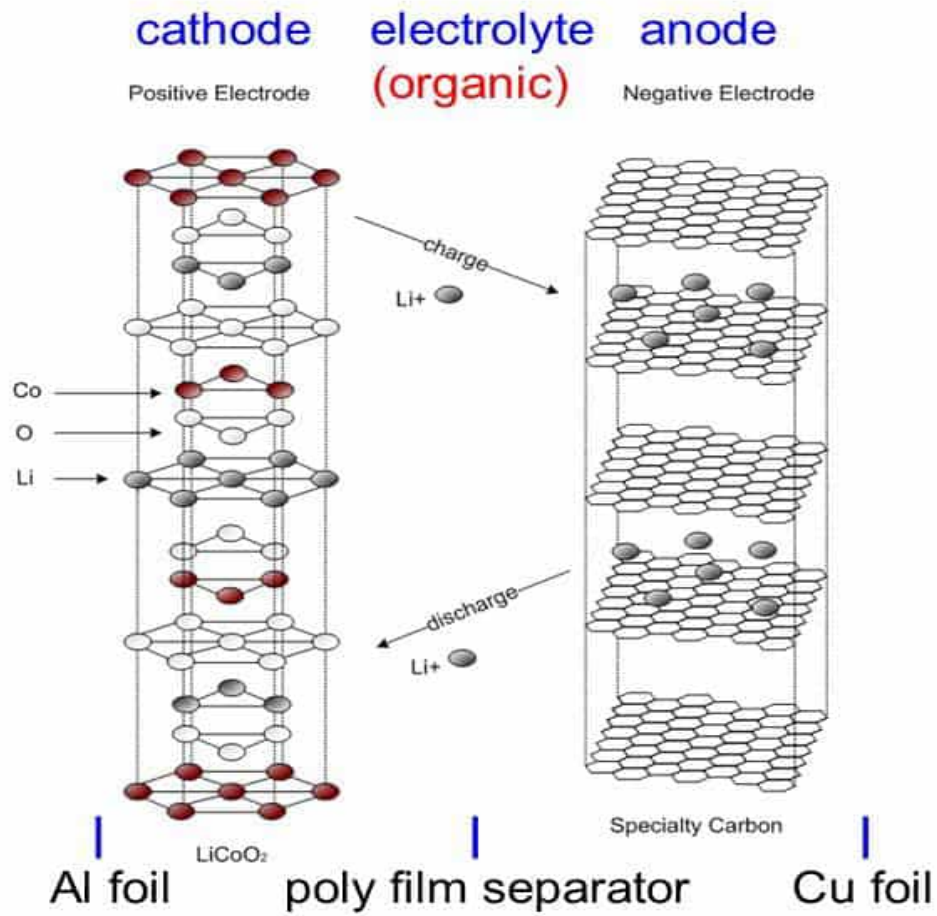
Battery Contents

"Lithium batteries" are family of cells that consist of a lithium anode and a variety of different types of cathodes and electrolytes 3.6-4.2 V

Primary – Non rechargeable (Lithium Batteries)

Secondary – Rechargeable (Lithium Ion Batteries)

Testing and regulations make a distinction between the two but from a fire hazard perspective, my data suggests that there is only a limited difference.



The Hazard – Organic Electrolytes

High energy densities

Plus

Organic electrolytes →

Internal shorts cause electrical energy to vaporize and ignite electrolyte

Vulnerabilities to:

- Physical abuse
- Electrical abuse
- Thermal abuse

Compound	CAS Registry Number	Molecular Formula	Flash Point	Boiling Point	Auto-Ignition Temperature	Heat of Combustion
Diethyl Carbonate (DEC)	105-58-8	$C_5H_{10}O_3$	25°C 77°F	126°C 259°F	445°C 833°F	−20.9 kJ/ml −5.0 kcal/ml
Dimethyl Carbonate (DMC)	616-38-6	$C_3H_6O_3$	18°C 64°F	91°C 195°F	458°C 856°F	−15.9 kJ/ml −3.8 kcal/ml
Ethylene Carbonate (EC)	96-49-1	$C_3H_4O_3$	145°C 293°F	248°C 478°F	465°C 869°F	−17.2 kJ/ml −4.1 kcal/ml
Ethyl Methyl Carbonate (EMC)	623-53-0	$C_4H_8O_3$	25°C 77°F	107°C 225°F	440°C 824°F	−19.2 kJ/ml −4.6 kcal/ml
Propylene Carbonate (PC)	108-32-7	$C_4H_6O_3$	135°C 275°F	242°C 468°F	455°C 851°F	−20.1 kJ/ml −4.8 kcal/ml
Tetrahydrofuran (THF)	109-99-9	C_4H_8O	−14°C 6°F	65°C 149°F	321°C 610°F	−31.2 kJ/ml −7.5 kcal/ml
Dimethylether	115-10-6	C_2H_6O	−41°C −42°F	−23.7°C 11°F	350°C 662°F	−51.3 kJ/ml −12.3 kcal/ml
1,3-Dioxolane	646-06-0	$C_3H_6O_2$	2°C 35°F	75°C 167°F	?	−24.4 kJ/ml −5.8 kcal/ml
1,2-Dimethoxyethane (Ethylene Glycol)	110-11-4	$C_4H_{10}O_2$	104°C 232°F	83°C 197.5°F	400°C 752°F	−21.3 kJ/ml −5.1 kcal/ml
Acetonitrile (Methyl Cyanide)	75-05-8	CH_3CN	6°C 42°F	81.6°C 179°F	524°C 975°F	−23.9 kJ/ml −5.7 kcal/ml
Thionyl Chloride	7719-09-7	$SOCl_2$	?	78.8°C 174°F	?	?

JENSEN HUGHES

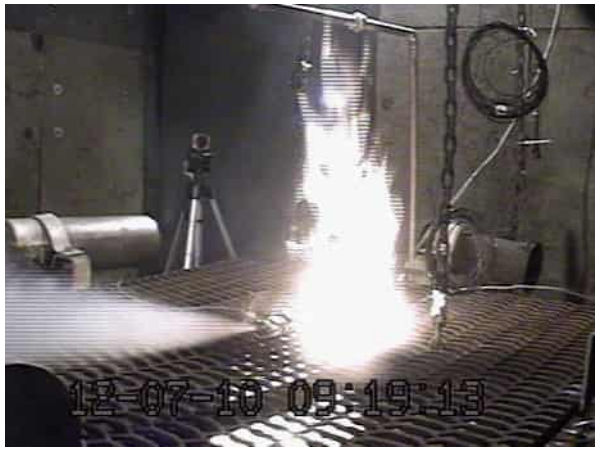
Empirical Data (USN)

Hundreds of tests, millions of dollars in batteries

Over 30 different manufacturers/cell types
- 25+ Commercial cells
(A123, Panasonic, Sony, E-one Moli, Ultralife, K2, etc.)
- 5 Military specific cells (Saft, Dow-Kokam)

Battery casualty characterization tests
- Vulnerability
- Failure response
- Heat Release Rate (HRR)
- Gas production and species

Hazard mitigation tests
- Ventilation
- Passive barriers
- Suppression



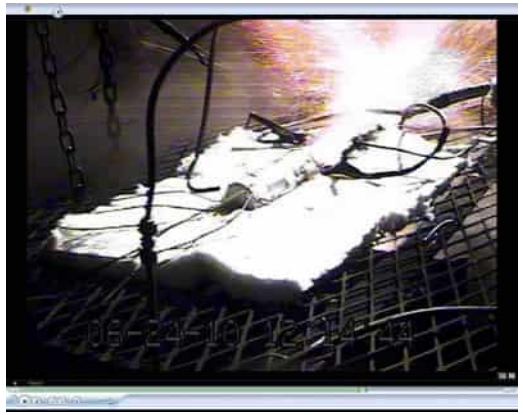


General Battery Reactions

Failure Responses

1. Venting/off gassing electrolyte flammable and toxic
2. Road Flare Effect
3. Steady Burn
4. Flash fireball
5. Explosion





Reactions are driven by

- Chemistry
- Construction
- State of charge





Reaction Products

Testing of reaction products during thermal runaway

Species Formula	Species Name	Average Vol %
N_2	Nitrogen Gas	30
CO	Carbon Monoxide	20
CO_2	Carbon Dioxide	20
H_2	Hydrogen Gas	20
C_xH_y	Hydrocarbons	10

Venting Scenario

Gas volume is proportion to electrical energy

- 160 L of gas per MJ of electrical energy

Lower Flammable Limit (LFL) ~10% by volume

- Ventilation system design
- Explosion protection

Burning Scenario

- Mostly CO_2 ,N_2 & H_2O, (HF)





USN primary concern is explosive gas mixtures and toxicity

Heat Release Rates

Combustion energy is proportional to the electrical energy/capacity

Combustion energy is 6 – 10 times electrical energy/capacity

Shrink wrapping of individual cells can add 40%

Battery pack casings can add 200% shrink wrap to thin plastic

1000% heavy plastic cases





Modeling

Fluids - Fire Dynamics Simulator (FDS)

gas/fluid heat transfer and gas concentrations

Solids - Heating and Abacus

internal cell temperatures

Modeling Objectives

- Quantify the hazard
- Assess mitigation (passive barriers and suppression)
- Design explosive gas extraction systems

Cell Level Reactions / Model Inputs











Cell to Cell Propagation / Model Parameters







- Vent gas temperatures: 400°C – 800°C based on chemistry
- Gas thermal properties – average of products table
- Cell properties (density, specific heat, conductivity) – average of Aluminum, Copper and Steel.
- Cell reaction temperatures: 100°C – 200°C based on chemistry

Case Study 1
UUV Internal Battery Gas Release and Cell Propagation

Modeling thermal conditions and heat transfer inside UUV

Analysis of propagation:

- Cell-to-cell
- Module-to-module
- Tray to tray



Predicting cell-to-cell and tray-to-tray propagation

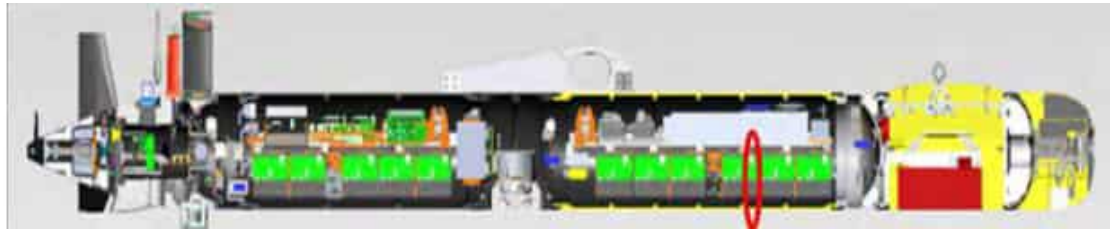
USN Unmanned Underwater Vehicle; MK18 Mod 2

Mine countermeasures

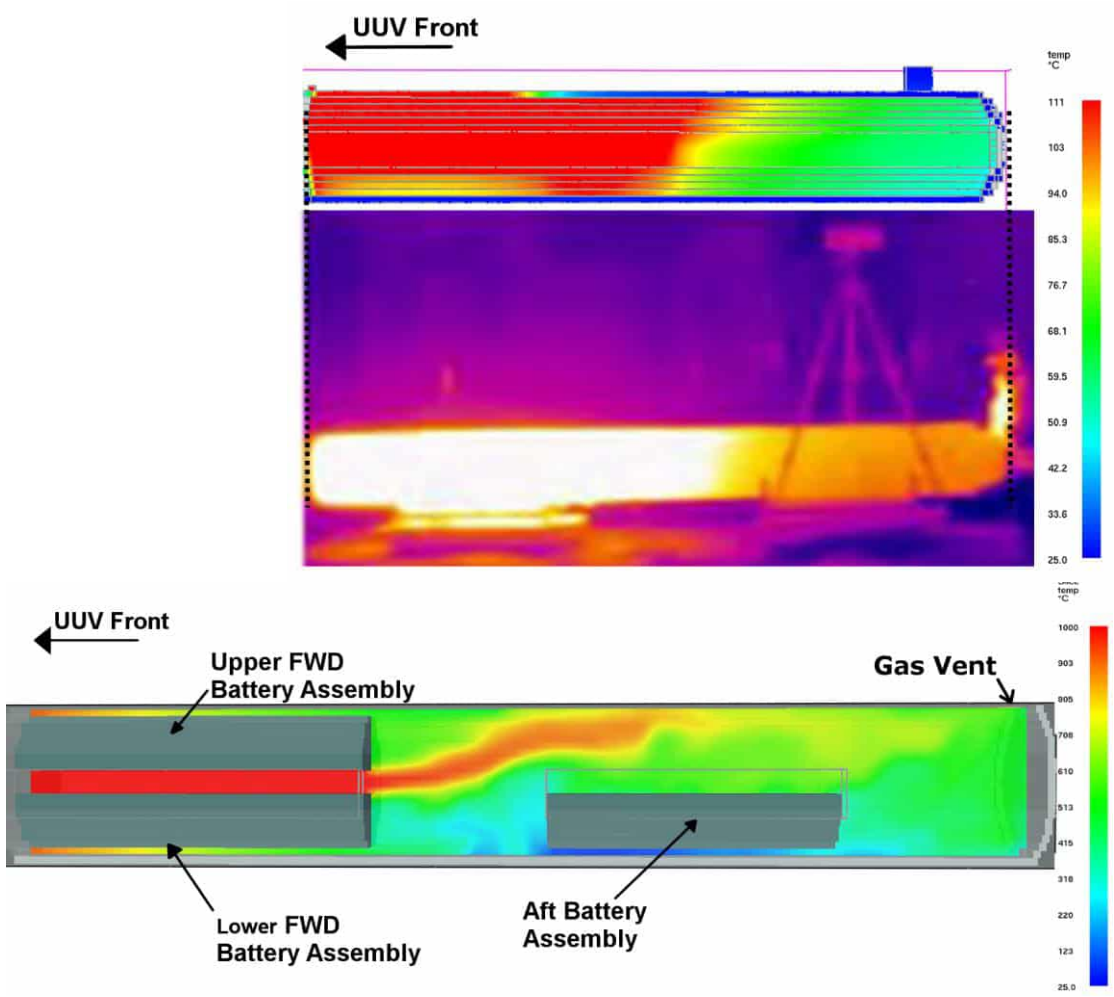
Reconnaissance

Battery Package:

- 5 or 6 module pairs in 2/3 trays
- 63 cells per module
- Over 1890 total cells (18650-size)



Case Study 1
UUV Internal Battery Gas Release and Cell Propagation



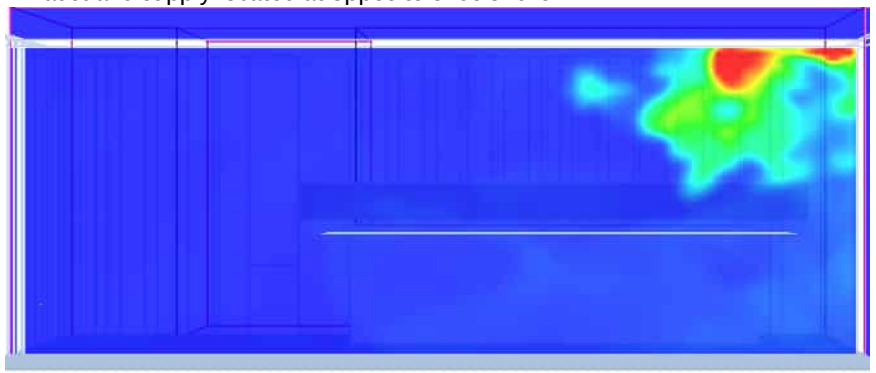
- Calibration of FDS to test data
- Model gas temperature inside UVV during release
- Heat transfer to adjacent batteries
- Cell-to-cell propagation
- Module-to-module propagation
- Tray to tray propagation
- Compare UUV outer skin temperature predictions to FLIR temperature measurements
- Compare internal gas temperature predictions to thermocouple measurements

JENSEN HUGHES

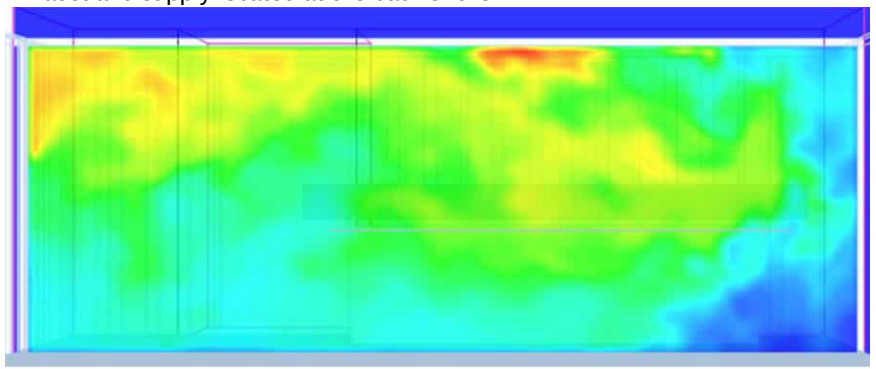
Case Study 2
MILVAN Enclosure Ventilation

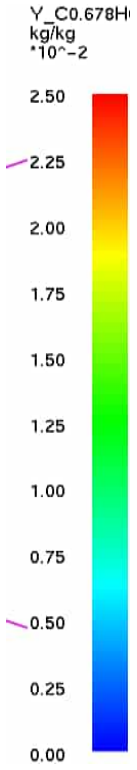
Assess ability of ventilation system to prevent explosive gas concentrations

Exhaust and supply located at opposite ends of the MILVAN



Exhaust and supply located at the back of the MILVAN





- Two configurations
- Predict gas release and mixing
- Evaluate flammable gas concentrations in MILVAN

Poorly configured ventilation results in severe explosion risk

Summary and Conclusions

- Extensive database of battery reactions
- Able to use/adapt this data as input to FDS
- Calibrated model using a range of empirical data
- FDS was used to accurately predict propagation
- FDS worked well to extrapolate data (i.e., sensitivity assessments)
- Quantified the hazard for a range of applications/conditions
- Assessed ventilation, passive barriers and suppression options

Annex 8 Community risk assessment and modelling

2. METHODOLOGY

FRA conducted the CRA utilizing the protocols and methods published by the Center for Chemical Process Safety (CCPS) in their Guidelines for Chemical Process Quantitative Risk Analysis, the Dutch Government in their Guidelines for Quantitative Risk Assessment, known as the "TNO Purple Book", and other relevant guidelines. These guidelines provide the methodologies for:

- Identification of Hazards (HAZID)
- Consequence and Impact Analysis (Phast)
- Likelihood Analysis
- Calculation of Risk
- Presentation of Risk Results

The scope of work for the CRA included the following steps:

- Identification of potential hazard release scenarios
- Conduct consequence modeling using the Phast consequence model
- Assess offsite risk results using Phast and site-specific data
- Develop individual risk contours as appropriate
- Develop societal risk contours based on onsite and offsite population data as appropriate
- Compare BESS risk results to international risk acceptance criteria, where appropriate
- If unmitigated risks are identified, make recommendations to reduce identified risks as reasonably practical

The approach was to conduct a site-specific analysis, using the commercially available Process Hazards Analysis Software Tool (Phast) version 8.2. Phast has been selected for this analysis because it is well established, has been validated and is widely used in the energy, industrial, and chemical industries.

This analysis is performed under site specific conditions for the proposed BESS site in Wattsville, VA. ***Therefore, these results are specific to this location and facility design at the time of the study and as a result the consequence and risk results should not be applied to any other location***.

2.1 Facility Information

The proposed facility will be an integrated turnkey BESS design for use in an outdoor container configuration, based on the Model ST2752UX-US battery cabinet, with a maximum power of 2752 kW per battery cabinet. All BESS cabinets shall utilize racks with 14 modules or less. The BESS facility will be located to the southwest of the Route 175 and Route 679 intersection.

The BESS facility includes fifty two (52) battery storage units (containers) grouped into 26 blocks, twenty-four (24) inverter/transformers (INV/XFMR), auxiliary equipment, and a substation.

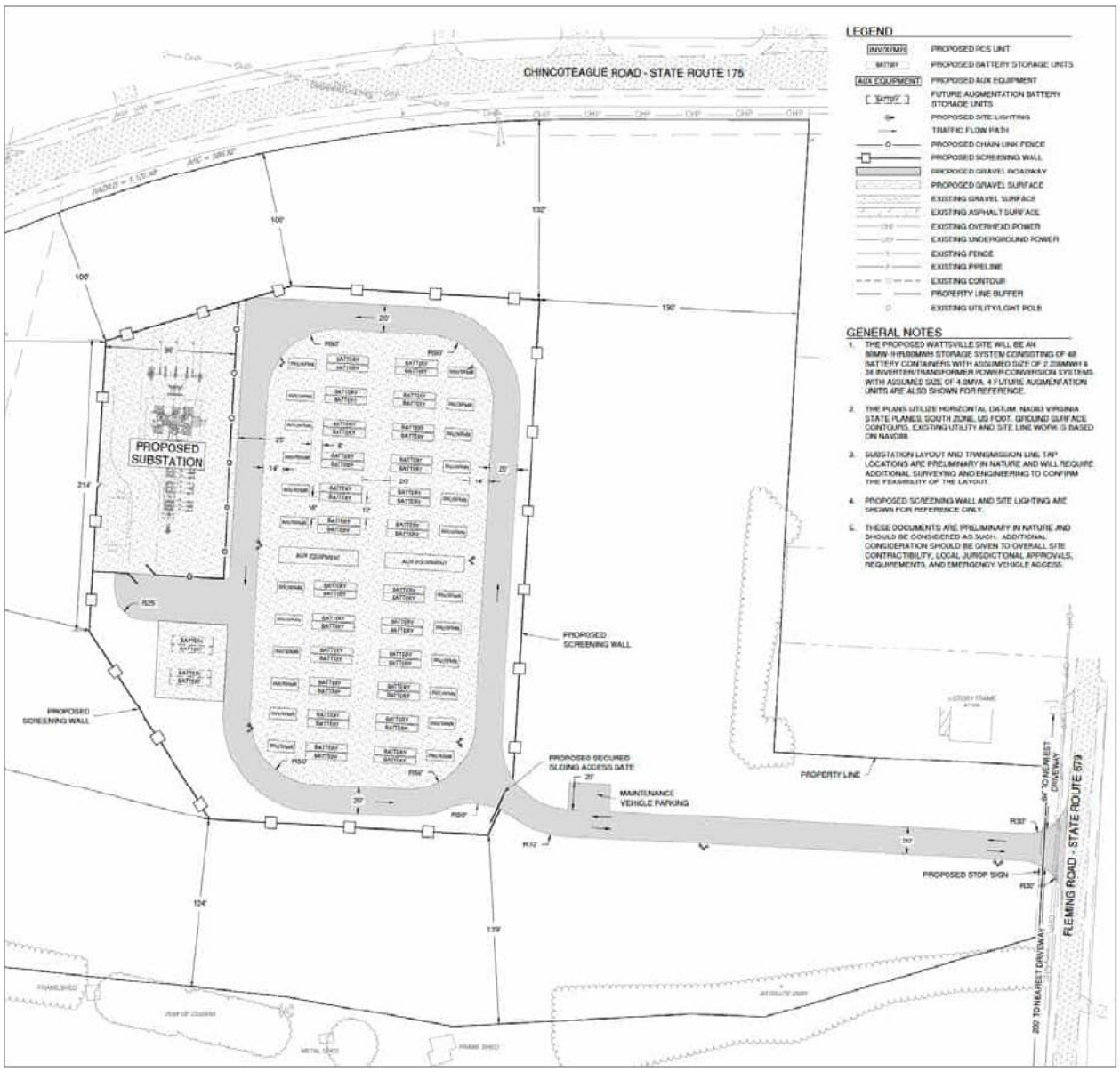


Figure 1 Wattsville Battery Energy Site Facility Plan

2.2 Data Collection

This analysis was performed using site specific weather conditions for the proposed Wattsville BESS site.

The data that was collected provides the basis for the assumptions applied in the CRA. This information includes the following (with section references within the CRA report, which detail the specific assumptions):

- BESS Layout and Locations
- Consequence Modeling
- BESS Module Failure Rate Data

- Meteorological Data
- Offsite Population
- Vulnerability to toxic exposures, fire, and explosion overpressure
- Risk Criteria

2.3 HAZID

To identify the potential vent gas release scenarios for the CRA, FRA reviewed the provided calculations, based on lab testing, to identify the potential for hazardous scenarios. Based on the small volumes of the vent gasses, the greatest potential hazard to off-site populations is from exposure to flammable gas clouds and potential thermal radiation and explosion overpressures.

While the toxicity of CO is well known in confined or unventilated spaces, releases of CO at the BESS site are limited by the small volume of release occurring into open atmosphere. Additionally, the volume and/or reactivity of flammable gasses are inadequate to cause an explosion generating harmful overpressures. Thus, the primary focus of the risk analysis is the potential thermal radiation hazard from flash fires or fireballs outside the site property boundaries.

2.4 Release Scenario Development

The goal of scenario selection is to limit the total number of incident outcome cases to be studied to a manageable size, without introducing bias or losing resolution through overlooking significant incidents or incident outcomes. Based on the HAZID, the final set of hazard release scenarios/conditions for the BESS CRA were as follows:

- Module based Total Cell Vent Gas release of 203.52 ft^3 to atmosphere from the BESS container vent fan for a 4-min duration (flammable & toxic)
- Module based H_2 Cell Vent Gas release of 80.59 ft^3 to atmosphere from the BESS container vent fan for a 4-min duration
- Module based CO Cell Vent Gas release of 33.78 ft^3 to atmosphere from the BESS container vent fan for a 4-min duration
- Module based Total Cell Vent Gas continuous release of 81,414 ft^3 to atmosphere from the BESS container vent fan
- Results shall be evaluated based on flammable and toxic endpoints

A release was considered to be equally likely to occur from a module within any of the BESS containers located onsite.

2.5 Consequence Analysis

Consequence analysis is the methodology used to determine the potential for damage or injury from specific incidents. A single incident (e.g., BESS module gasses vented to atmosphere) can have many distinct incident outcomes [e.g. fireball, flash fire, toxic exposure]. These outcomes are analyzed using source and dispersion models and explosion and fire models within the software tool Phast.

In this analysis, consequence is defined as the hazard distance or hazard area to various endpoints. For the identified BESS vent gas release scenarios, the consequences were modeled using the Phast model. The specific consequences considered include:

- Flammable Gas Dispersion
- Toxic Gas Dispersion
- Fires (flashfire, fireball)

2.6 Frequency Analysis

The initiating event failure frequency for a release of BESS vent gas was based on the potential for thermal runaway to occur within an individual cell and carry forward to all cells within the affected module. For the purposes of this analysis the failure frequency of an individual cell was given a 1, indicating the underlying study assumption of the occurrence of a runaway event.

The initiating event frequency is used to determine the range of potential risks which may vary depending on the associated hazard (e.g. flashfire, fireball, explosion, or toxic exposure).

2.7 Risk Integration

To assess offsite risks as a result of potential consequences- offsite population data, consequence modeling results, likelihood calculations, and weather data are combined to generate a geographical rating of Individual and Societal risk, as defined below:

- **Individual Risk**: Individual Risk represents the frequency of an individual dying due to loss of containment events (LOCs) while in a specific location. The individual is assumed to be unprotected and to be present during the total exposure time.
- **Societal Risk**: Defined as the risk to a group of people to a hazard. The hazard can be a single incident, or a collection of incidents (e.g., the release scenarios developed for the PCF site). Thus, societal risk evaluated the scale of the incident in terms of the number of people that could be impacted from the hazard(s). Societal risk is expressed as the cumulative risk to a group(s) of people who might be affected by accidental release events. The calculation for societal risk uses the same consequence and frequency results as the individual risk calculation, but uses information about the number, geographical distribution, occupied building construction and occupancy levels of the population group(s) to determine the risk level.

If there are no consequences found to impact occupied offsite properties or public access areas, then there can be no impact to individuals or communities and as such, the Individual Risk and Societal Risk shall be 0%.

3. CONSEQUENCE ANALYSIS SCENARIOS

The following Consequence Scenarios were utilized in the consequence modeling for the assessment of offsite risks for the CRA.

Table 1. Consequence Analysis Scenarios

Description	Volume (ft^3)	Peak Gas Release Rate (cfm)	25% LEL	IDLH
Total Module Vent Gas	203.52	5.763	1.49%	-
H2 Module Vent Gas	80.59	0.84	1%	-
CO Module Vent Gas	33.78	0.3525	3.13%	0.08%
Continuous Release of Total Module Vent Gas	81,414	1,357	1.49%	-

The CRA considers a release of gas to atmosphere incorporating the entire volume released over the peak 4-minute duration identified and described in client provided vent gas release calculations. The continuous release of total module vent gas is when the peak gas release rate is increased to 1,357 cfm and flows continuously. This is the minimum flowrate and volume at which the ¼ LFL (lower flammability limit) threshold is reached at ground level. In addition, it is likely the maximum non-fire release rate, as heat must spread from one module to the next through conduction. Based on testing, the duration would be limited to 4-minutes making it unlikely that more than 2 modules involved in an incident at any single time. Scenarios were assessed in accordance with guidance from the TNO Purple Book.

4. CONSEQUENCE ANALYSIS

Accidents begin with an incident, which usually results in a release of hazardous/toxic/or flammable material from a storage site or process facility. A consequence analysis evaluates the expected outcome of an event and is measured or expressed as a hazard distance, hazard zone, or a hazard value at a specific location. A quantitative consequence analysis is carried out using mathematical models and computer software addressing the physical and chemical phenomenon.

Before conducting a consequence analysis, it is necessary to identify events that could follow the release of a hazardous material. The consequence analysis considers a range of potential hazards. In general, a hazardous material release may exhibit one or more of the following types of hazards:

- Flammable exposure (thermal radiation, flame impingement)
- Explosions (blast overpressure)
- Toxic exposure

A site-specific consequence analysis of the accidental release scenarios was conducted using the commercially available Process Hazards Analysis Software Tool (Phast) consequence modeling software. Phast was used to determine the fire, toxic, and blast overpressure hazard consequences. The TNO Multi-Energy methodology within the Phast tool was used to evaluate any potential vapor cloud explosions.

4.1 Dispersion Modeling

The Phast Unified Dispersion Model (UDM) was used to calculate the downwind dispersion distance, concentration profile, and the width of flammable releases of vent gasses.

Dispersion models use an average time to calculate the maximum concentration and the plume width. The values used in this QRA are detailed below and consistent with the Phast default parameters. All toxic dispersion models used an averaging time of 600 seconds (Phast default). All flammable dispersion models used an averaging time of 18.75 seconds (Phast default).

4.2 Toxic Hazards

The release of carbon monoxide, a toxic gas, may have the potential to impact the surrounding offsite population. In general, toxic vapor dispersion hazard zones are characterized by the following parameters:

- Release Quantity
- Duration of Release
- Source Elevation
- Surrounding Terrain
- Prevailing Atmospheric Conditions
- Chemical Toxicity

Each of the parameters above is discussed below with special emphasis on their influence on estimating downwind dispersion distances.

Release Quantity or release rate refers to the quantity of (or the rate at which) a hazardous chemical is released in the event of an accident. The quantity (or rate) is the single most important parameter in determining the dispersion hazard distances. In general, larger quantities lead to larger dispersion distances. However, the dispersion distance does not increase linearly with quantity or release rate. For gaseous and high-vapor-pressure liquid releases, the vapor release rate will be the same as the discharge rate. However, for non-flashing liquids, the vapor release rate is governed by the evaporation rate of the liquid and will always be less than the liquid release rate.

Duration of Release is dependent on the release mode. For example, a safety valve release may not last for more than a few minutes whereas a tank puncture may continue to discharge for several hours. Simple dispersion models use one of the two extreme cases, i.e., continuous release or instantaneous release. In the case of instantaneous release, the duration of release is very short (e.g., pressurized storage tank rupture) and the total quantity of the chemical released during the accident contributes to the dispersion hazard. Further, the dispersion takes place in longitudinal (along wind), and lateral (across wind) and vertical directions. In the case of a continuous release, the release lasts a relatively long time and the release rate is the most important parameter. The dispersion model used in this study is encoded in Phast and takes into account the actual duration of release.

Source Elevation is attributed to the physical height of the release. For this study, all scenarios have been modeled at a representative release height based on equipment location. A higher source elevation will increase the distance to cloud touchdown. This is particularly important for buoyant and neutrally buoyant clouds.

Surrounding Terrain affects the dispersion process greatly. For example, rough terrains involving trees, shrubs, buildings and structures usually enhance air entrainment. This leads to shorter dispersion distances than that if predicted using a flat terrain. However, rough terrain may lead to localized regions of high concentrations.

Prevailing Atmospheric Conditions include a representative wind speed and atmospheric stability. The neutral or unstable (typical daytime) weather conditions generally leads to shorter dispersion distances than stable (nighttime) weather. For neutrally buoyant releases, increased wind speed reduces the dispersion distance. For heavy gases, dispersion distance increases with wind speed. Since the weather conditions at the time of an accident cannot be controlled, it is important to evaluate the release scenarios for both typical and worst-case weather conditions.

Chemical Toxicity affects the extent of the hazard zone. In this analysis, a probit equation is used to equate the exposure dosage of a toxic chemical to percent fatality. Dosage at a fixed position is the integral of concentration over time at that position. Lower dosage levels lead to larger dispersion distances. As with release quantity, the effect is not linear. In other words, a reduction in dosage by a factor of 100 may result in an increase in the dispersion distance by a factor of 20. The probit equations used in this analysis are in the public domain and were input into the Phast model. Since dosage is a function of concentration and exposure duration, both parameters can significantly alter the calculated hazard zone.

A review of the hazardous gasses contained in the potential release of BESS vent gasses shows that the predominant risk to offsite locations is posed by flammable gas dispersal and ignition.

5. FREQUENCY ANALYSIS

An important component of risk analysis is the estimation of the likelihood or frequency of each failure case or release scenario. Based on the base assumption of this study, that a runaway thermal event occurs in one individual cell of a BESS module, *the frequency of occurrence for the release of vent gasses to atmosphere shall be assumed to be equal to 1 (i.e. a 100% likelihood).*

5.1 Weather Conditions

The likelihood of the eight (8) wind speed and Pasquill stability class combinations were developed from local climactic data. The resulting probabilities were input to the model to determine the probabilities of various wind direction, wind speed and stability class combinations.

Atmospheric stability and wind speed are important factors for consequence analysis. The six most common Pasquill stability classes are given in Table 2 with their conditions defined in Table 3. Stability Class F is the most conservative for vapor dispersion distances since there is limited mixing of the released gas with air under these stable atmospheric conditions, and therefore the flammable gas cloud can travel a significantly long distance before it is diluted to the Lower Flammability Limit (LFL), or a toxic concentration of interest.

Table 2 Pasquill Stability Class

Stability Class	Definition	Stability Class	Definition
A	Very Unstable	D	Neutral
B	Unstable	E	Slightly Stable
C	Slightly Unstable	F	Stable

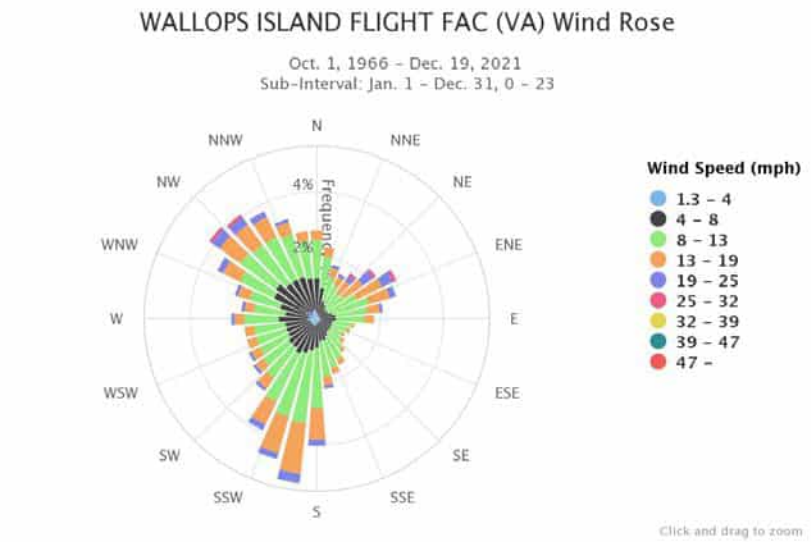
Table 3. Conditions Defining Atmospheric Stability Classes

Surface Windspeed		Daytime Incoming Solar Radiation			Nightime Cloud Cover	
m/s	mph	Strong	Moderate	Slight	>50%	<50%
<2	<5	A	A-B	B	E	F
2-3	5-7	A-B	B	C	E	F
3-5	7-11	B	B-C	C	D	E
5-6	11-13	C	C-D	D	D	D
>6	>13	C	D	D	D	D

For this analysis, representative meteorological data was from the nearby Wallops Island weather station. The meteorological data consists of wind speed, wind direction, and Pasquill stability observations. The wind speed/stability observations have been combined into four representative groups and the probabilities of occurrence summed for day and night time periods. The representative combinations of wind speed and stability class for this location that will be used as input to the Phast model are given in Table 4.

Table 4 Representative Weather Conditions (Wind Speed & Stability Class)

Wind Speed (mph)	Pasquill Stability
3.4	B
3.4	C
7.8	D
7.8	F
11.2	B
11.2	C
18	D
18	F



Other key site specific meteorological parameters used as inputs to the consequence model are:

- Ambient Temperature – 78 °F
- Relative Humidity – 80%
- Surface Roughness Length – .25 meter

6. RISK ANALYSIS

The risks of the proposed facility may be expressed from two perspectives: (1) the risk to individuals and (2) the risk to groups of people. These are referred to, respectively, as individual and societal risk.

This QRA reports individual and societal risk results, and well as the overpressure contours from a vapor cloud explosion.

6.1 Individual Risk

Individual risk is defined as the risk to a single person/ individual to a hazard. The hazard can be a single incident, or a collection of incidents (e.g., the release scenarios developed for the PCF site). The scale of any incident, in terms of the number of people impacted by an event(s), does not affect the individual risk level at a distance from the hazard location(s). The risk contours developed can be used to assess potential risk to the surrounding community for the Wattsville BESS site location.

The risk contours are calculated from the expected frequency of an event capable of causing the specified level of harm at a specified location. Thus, individual risk contour maps are generated by calculating individual risk at every geographic location assuming that somebody will be present, unprotected (e.g., outdoors), and subject to the risk 100% of the time that they are present (i.e., annual exposure of 2,000 hours per year). Individual risk results are associated with a particular location rather than a particular person. The individual risk results are expressed as a likelihood (e.g., fatalities per year) or expressed as a recurrence period (e.g., 1 fatality in X years).

The calculation of individual risk is made with the understanding that the contributions of all incident outcome cases (i.e., event sequences) are additive.

6.2 Societal Risk

The societal risk is defined as the risk to a group of people to a hazards. The hazard can be a single incident, or a collection of incidents (e.g., the release scenarios developed for the PCF site). Thus, societal risk evaluated the scale of the incident in terms of the number of people that could be impacted from the hazard(s). Societal risk is expressed as the cumulative risk to a group(s) of people who might be affected by accidental release events (for the Wattsville CRA societal risk only refers to the offsite community as the site is unmanned). The calculation for societal risk uses the same consequence and frequency results as the individual risk calculation, but uses information about the number, geographical distribution, occupied building construction and occupancy levels of the population group(s) to determine the risk level.

Societal risk expresses the cumulative risk to groups of people who might be affected by release events. The calculation uses the same consequence and frequency results as the individual risk calculation, but uses information about the number, geographical distribution, building construction and occupancy levels of the population to determine the level of risk.

Societal risk is expressed using an F-N curve, which is the most common method of depicting societal risk results. The F-N curve indicates the expected frequency (F) of release scenarios occurring which result in the number of N or more fatalities. The x-axis of the F-N curve represents the number of fatalities, N. The number of fatalities is depicted on a logarithmic axis with a

minimum value of 1. The y-axis of the F-N curve represents the cumulative frequency of the release scenarios with the number of fatalities equal to N or more.

6.3 Risk Criteria

In most locations worldwide, including the United States, there is no legally mandated risk acceptance criteria for facilities handling hazardous chemicals. In lieu of legally mandated criteria, published risk acceptance criteria from foreign governments and trade associations are available for interpreting risk results. As a standard industry practice, risk analysts and facility operators defer to these guidelines in the absence of any legally mandated risk criteria.

From the definition above, individual risk is the level of risk at a distance from a hazard(s). The risk is measured as the risk of fatality to a single person, assuming the person is always present at the location. This CRA uses risk acceptance criteria published by the Health and Safety Executive of the United Kingdom (UK HSE), as the basis of comparison. The UK HSE risk acceptance criteria details the individual risk criteria and is illustrated in Table 5.

Table 5 Individual Risk Criteria

Individual Risk Criteria	Recurrence Period
Maximum tolerable risk to workers	1 fatality in 1,000 years
Maximum tolerable risk to the public	1 fatality in 10,000 years
Broadly acceptable (or negligible) risk to workers and public	1 fatality in 1,000,000 years

Using the UK-HSE criteria, the individual risk levels for the onsite populations can be classified as follows:

- **Unacceptable** (≥ 1 fatality in 1,000 years)
  - Level where further risk assessment or risk mitigation is required.

- **Broadly Acceptable** (≤ 1 fatality in 1 million years)
  - Level where further risk reduction is not required.

- **Tolerable** (1 fatality between 1,000 and 1 million years.
  - Level where further, prudent risk reduction should be considered. Region is typically referred as the As Low as Reasonably Practicable (ALARP) zone.

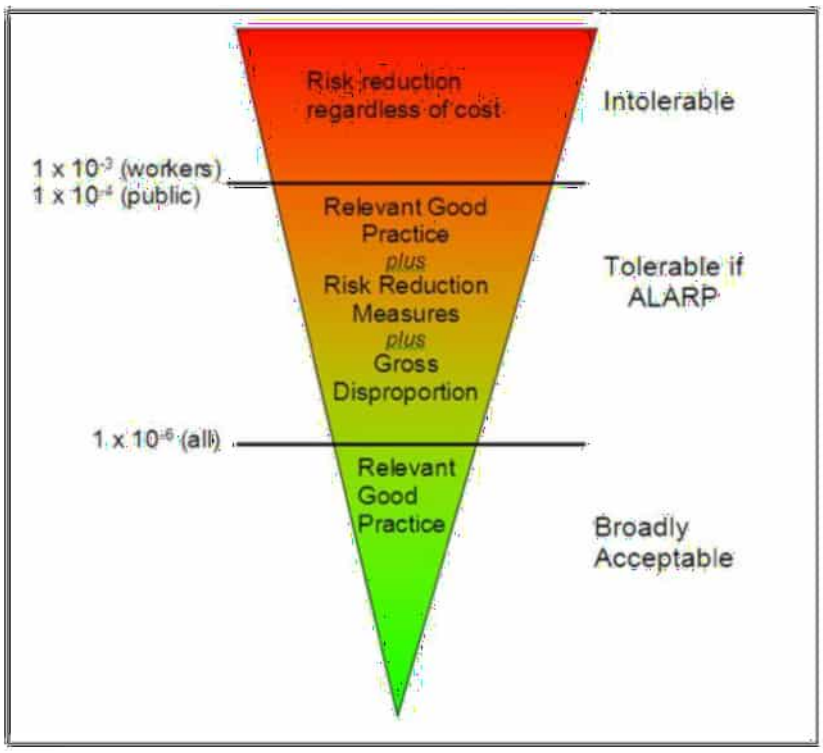


Figure 2 Individual Risk Criteria

Societal risk compares the risk to the onsite and offsite populations to the UK-HSE societal risk criteria. As with individual risk, the societal risk criteria include a broadly acceptable, intolerable and ALARP regions.

The consequence of an event can only be realized if the event occurs and there are individuals that are exposed to the hazard, thus it is important to understand the population density and nature of the population that may be exposed to any potential release. Table 6 provides a summary of estimated populations in the vicinity of the facility.

Table 6 Population, Building Category, and Distance

Description	Building Category	Population
Census Block- A	C	83
Census Block- B	C	221
Census Block- C	B, C	68
Census Block- D	B, C	65
Census Block- E	C	3

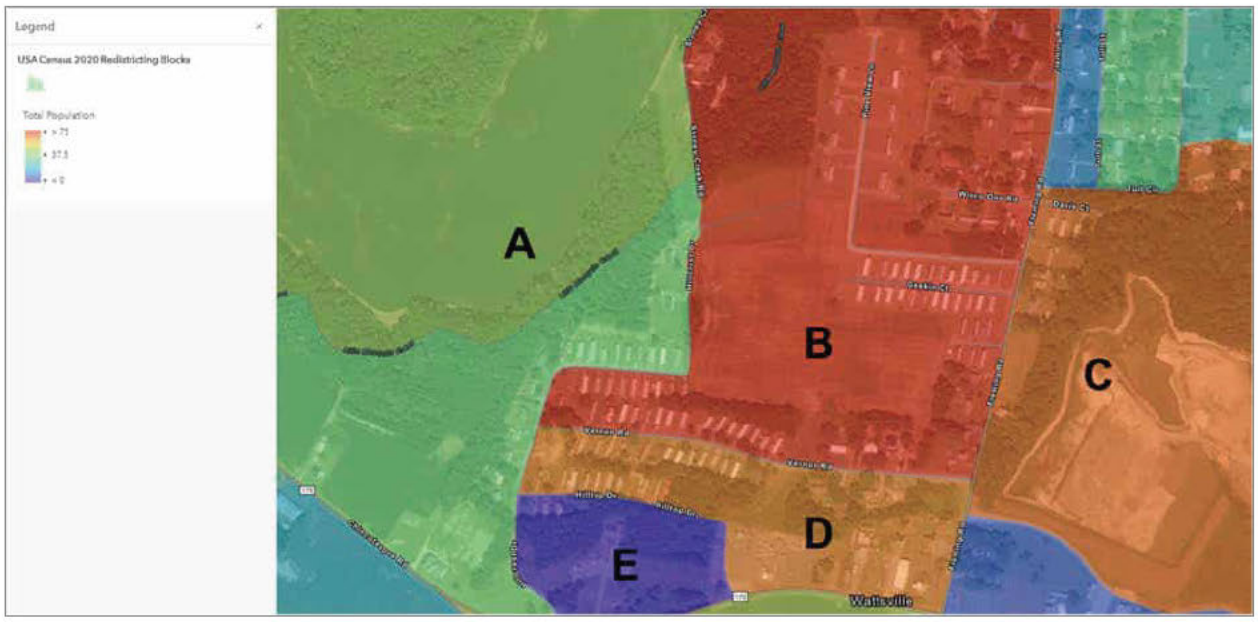


Figure 3 Population map (taken from 2020 Census Data)

7. SUPPRESSION RUNOFF

Based on a typical BESS SDS, the constituents that may be present after a fire include lithium, fluoride, iron, and phosphate compounds. Graphite and heavy metals such as aluminum and copper are present in components of the BESS; however, these will likely be present as less soluble, oxidized solids in low concentrations. The plastic components may burn to form polycyclic aromatic hydrocarbons (PAHs). For the purposes of this analysis benzo(a)pyrene was used due to its greater toxicity than most other PAHs. The greatest potential impact to the environment would result from runoff to ponds and waterways downgradient of the BESS unit after a fire.

Several best management practices, including crushed stone yards and channeling sheet flow to on site infiltration and detention basins, can be implemented to collect and treat potential pollutants to groundwater or surface water following a fire event. If warranted, the runoff after a fire event can be collected and removed to minimize any introduction of pollutants to the environment. Through these measures, the operation and maintenance of battery energy storage facilities will not result in adverse impacts to groundwater or surface water resources.

It should be noted that the primary components of BESS systems are similar in nature to those in commercial and residential structures, thus the runoff is not anticipated to be significantly different than that of a residential or commercial fire.

8. CONSEQUENCE ANALYSIS RESULTS

Results of the consequence analysis for the consequence scenarios are presented in the subsections below.

There were no toxic hazards associated with the release scenarios for total vent gas, H_2 gas, or CO gas, due to the low volume and short duration of releases.

The primary potential for hazards on and offsite were from a release and ignition of flammable gasses. As such, the flammable hazards are summarized in the section below as they constitute the only hazard associated with the facility. The summary demonstrates that the flammable hazards are limited in scope and do not impact any areas offsite. Potential impacts to BESS units adjacent to the initiating unit are similarly limited to exposure to a short duration flash fire or to thermal radiation in the event of a BESS fire.

8.1 Flammable Vapor Dispersion

8.1.1 Total Vent Gas

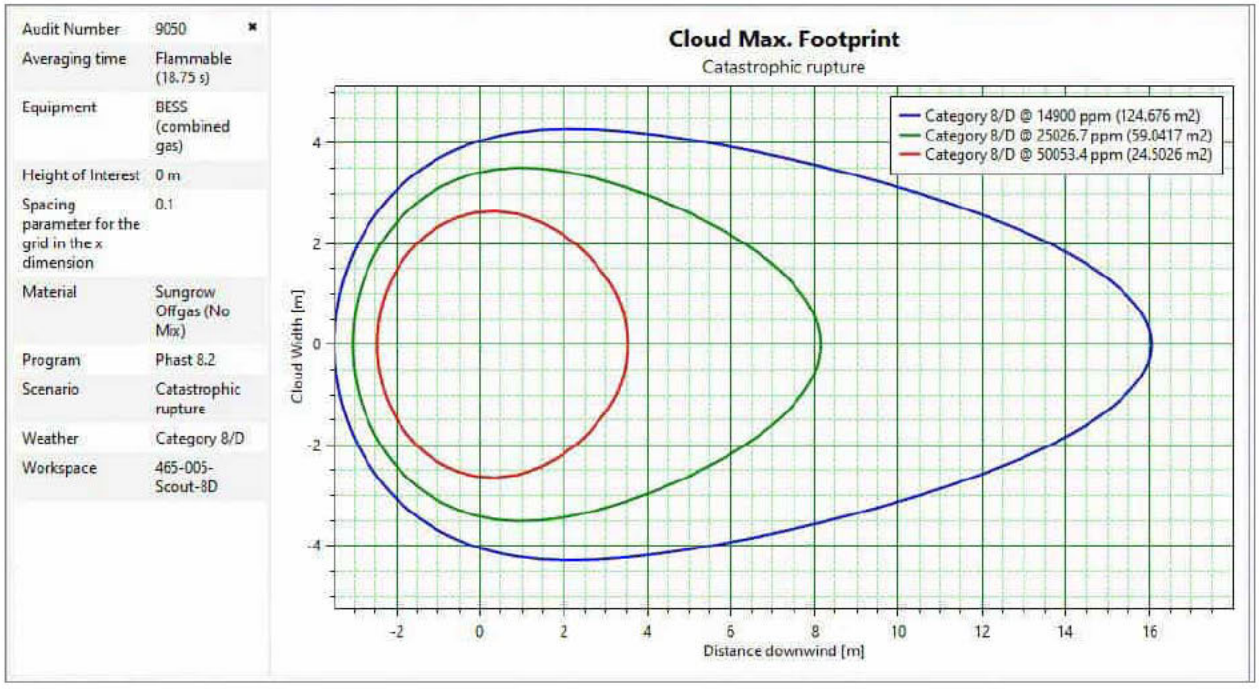


Figure 4 Maximum extent of flammable vapor showing LEL, ½ LEL, and ¼ LEL

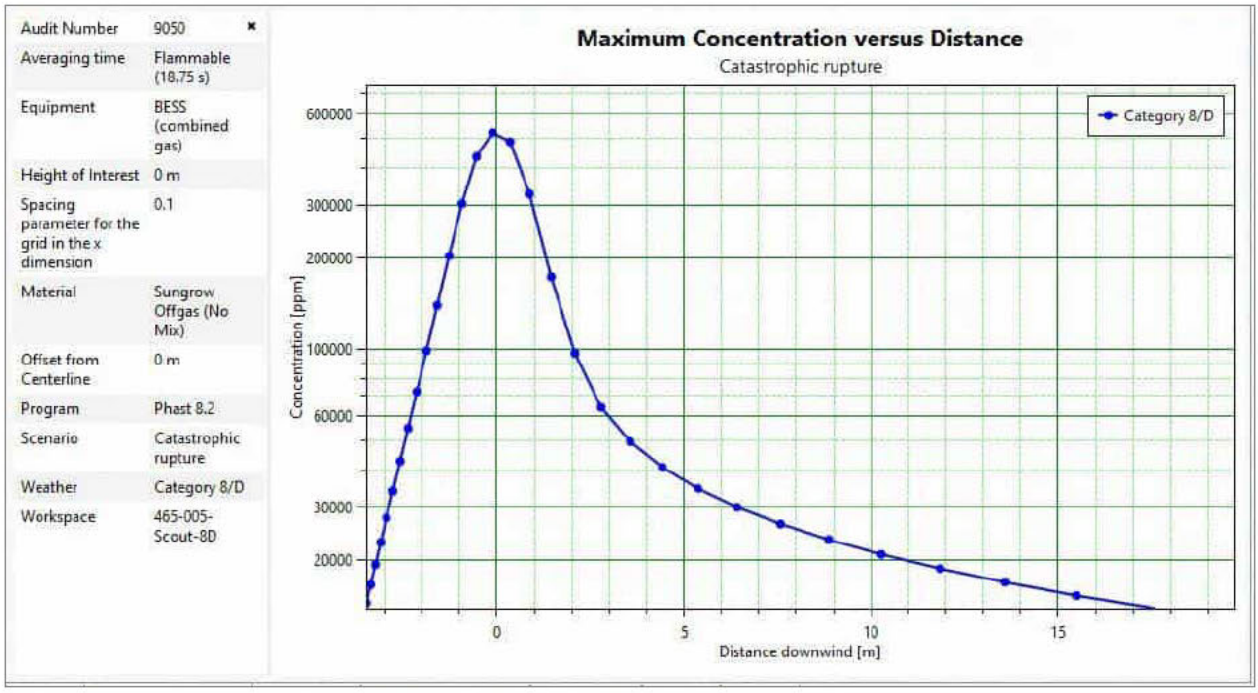


Figure 5 Maximum gas concentration vs distance downwind

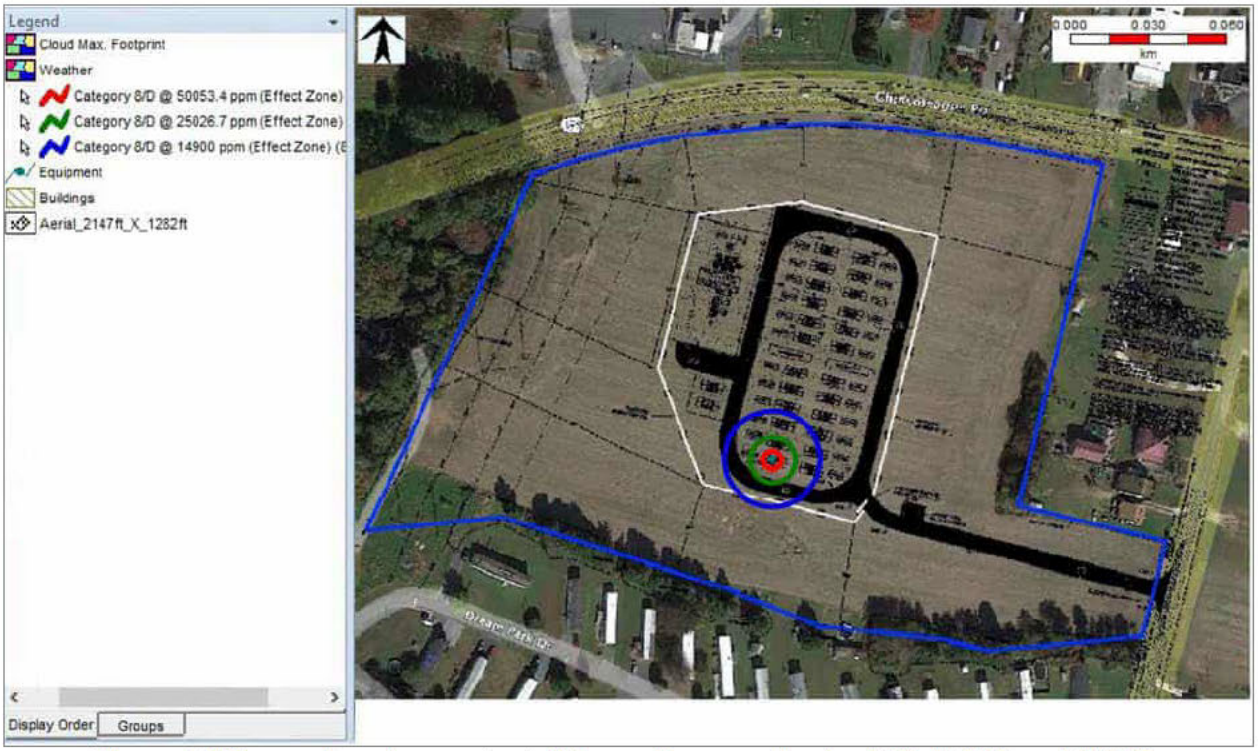


Figure 6 GIS map of maximum extent of flammable vapor showing LEL, ½ LEL, and ¼ LEL

8.1.2 H2 Vent Gas (Individual Species)

Audit Number	9050
Averaging time	Flammable (18.75 s)
Equipment	BESS (H2)
Height of Interest	0 m
Spacing parameter for the grid in the x dimension	0.1
Material	HYDROGEN
Material to track	Sungrow H2
Program	Phast 8.2
Scenario	Catastrophic rupture
Weather	Category 8/D
Workspace	465-005-Scout-8D

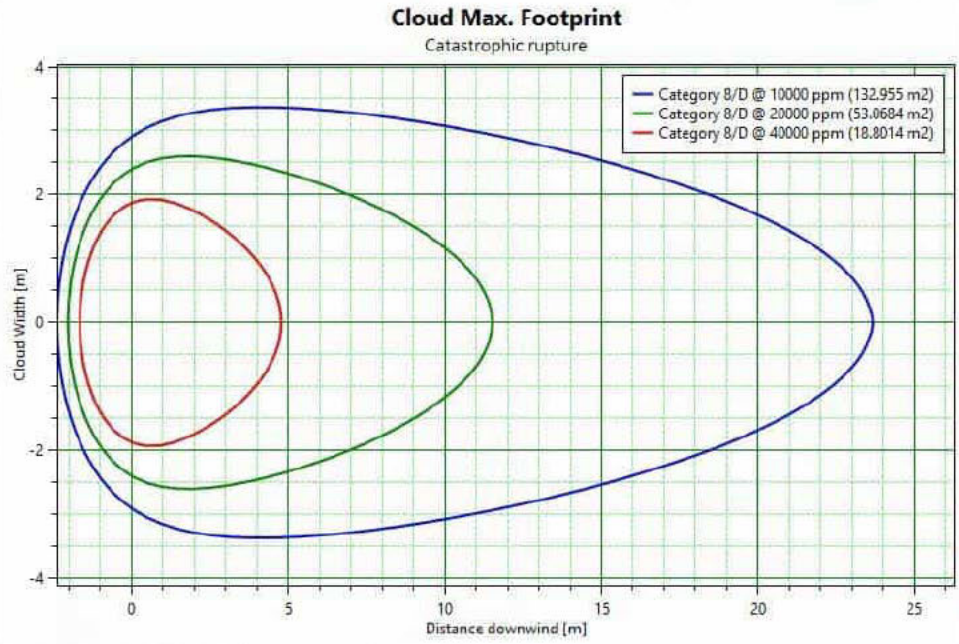


Figure 7 Maximum extent of flammable vapor showing LEL, ½ LEL, and ¼ LEL

Audit Number	9050
Averaging time	Flammable (18.75 s)
Equipment	BESS (H2)
Height of Interest	0 m
Spacing parameter for the grid in the x dimension	0.1
Material	HYDROGEN
Material to track	Sungrow H2
Offset from Centerline	0 m
Program	Phast 8.2
Scenario	Catastrophic rupture
Weather	Category 8/D
Workspace	465-005-Scout-8D



Figure 8 Maximum gas concentration vs distance downwind

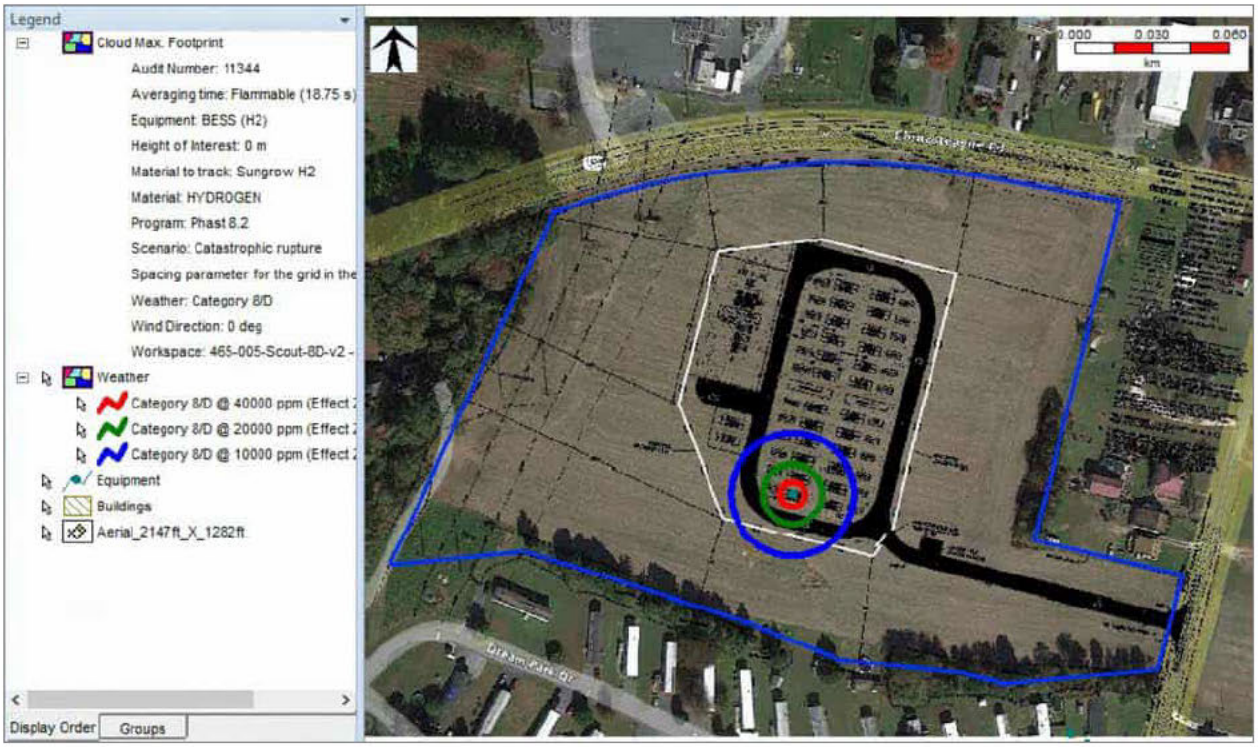


Figure 9 GIS map of maximum extent of flammable vapor showing LEL, ½ LEL, and ¼ LEL

8.1.3 CO Vent Gas (Individual Species)

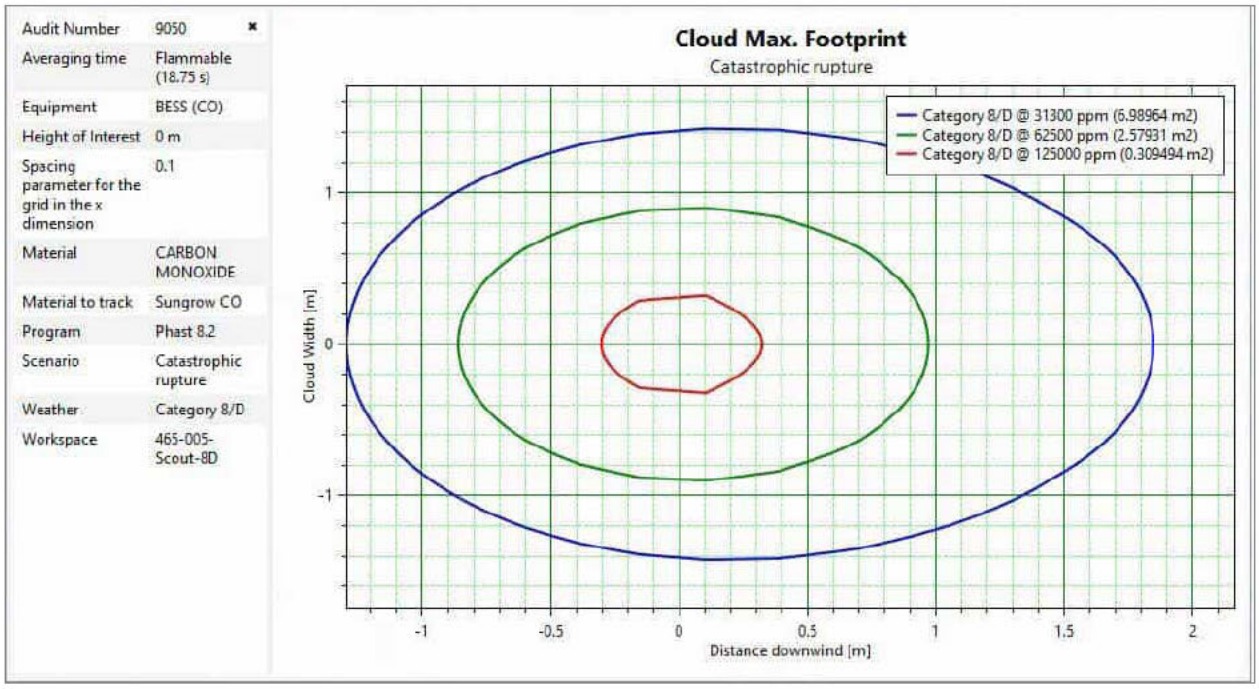


Figure 10 Maximum extent of flammable vapor showing LEL, ½ LEL, and ¼ LEL

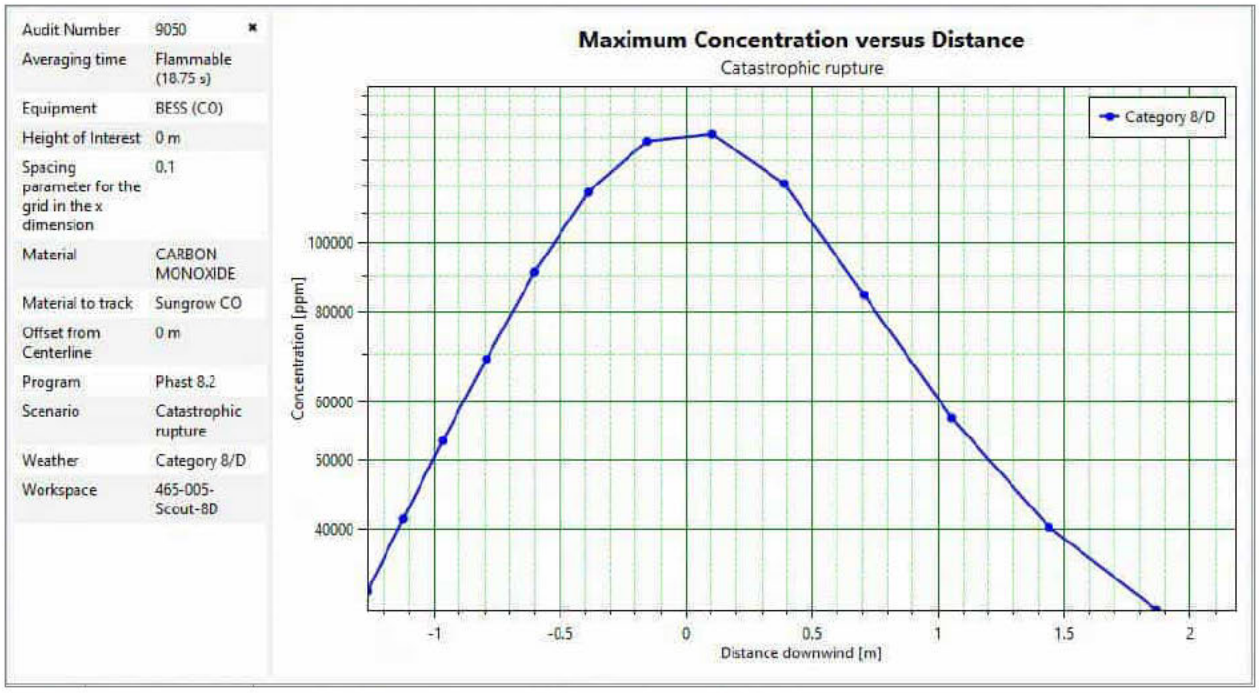


Figure 11 Maximum gas concentration vs distance downwind

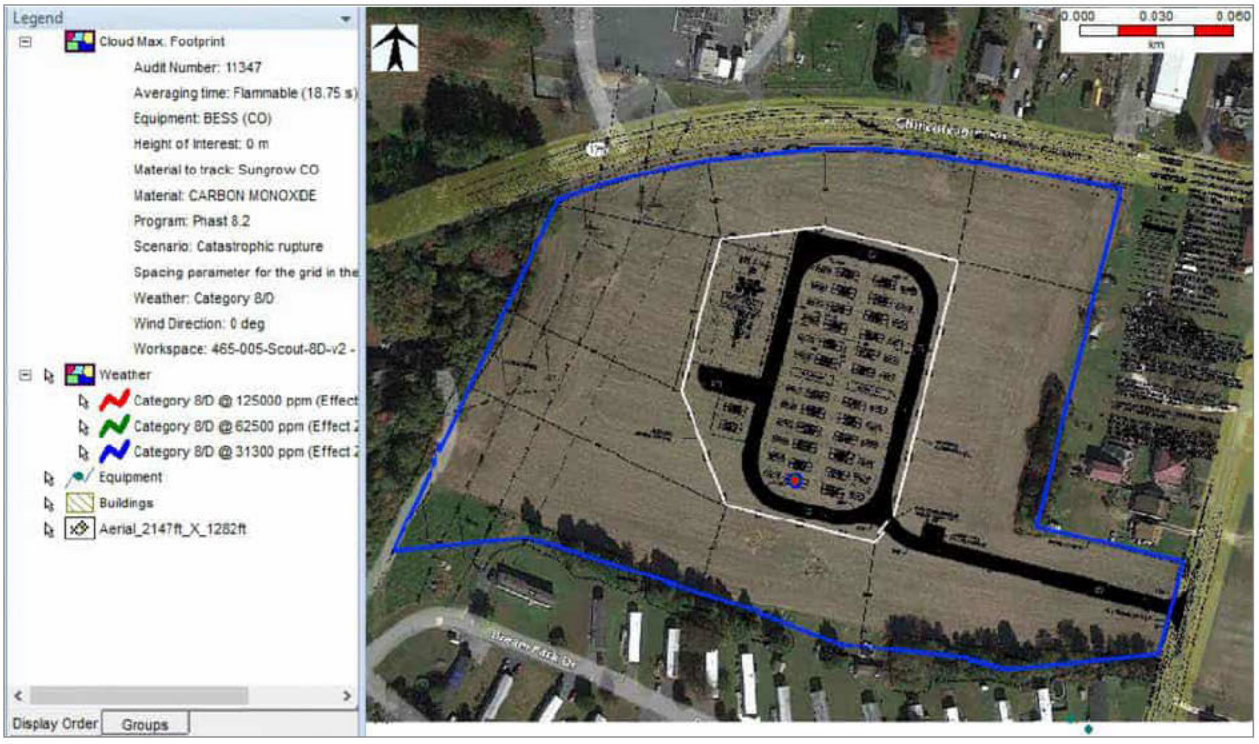


Figure 12 GIS map of maximum extent of flammable vapor showing LEL, ½ LEL, and ¼ LEL

8.1.4 Continuous Release of Total Vent Gas

Audit Number	10467
Averaging time	Flammable (18.75 s)
Equipment	BESS (combined gas) MIN
Height of Interest	0 m
Spacing parameter for the grid in the x dimension	0.1
Material	Sungrow Offgas (No Mix)
Material to track	Sungrow Offgas (No Mix)
Program	Phast 8.2
Scenario	Leak
Weather	Category 8/D
Workspace	465-005-Scout-8D-v2 - Copy

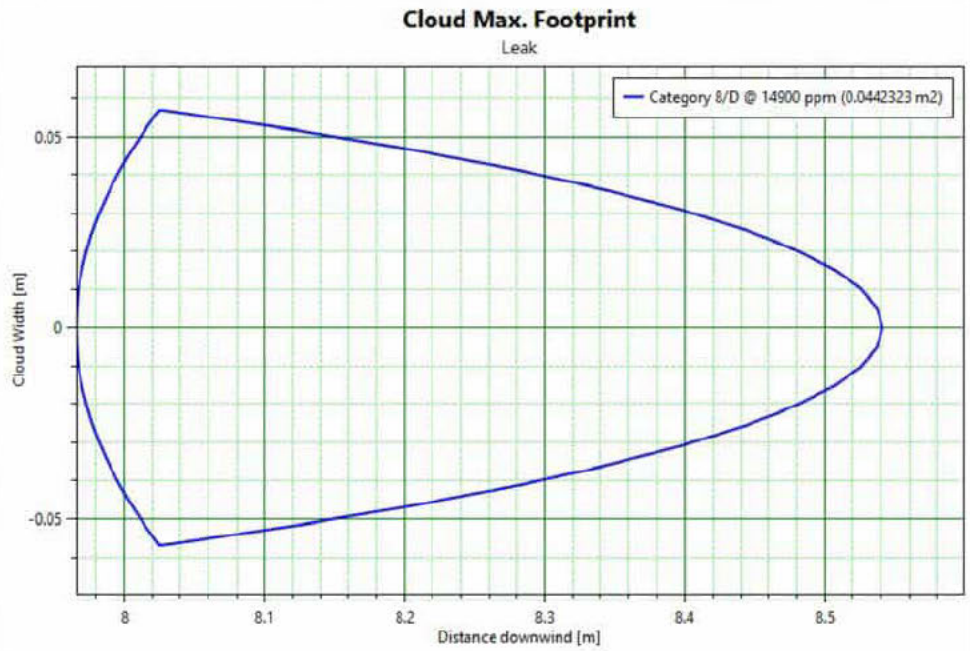


Figure 13 Maximum extent of flammable vapor showing ¼ LEL

Audit Number	10467
Averaging time	Flammable (18.75 s)
Equipment	BESS (combined gas) MIN
Height of Interest	0 m
Spacing parameter for the grid in the x dimension	0.1
Material	Sungrow Offgas (No Mix)
Material to track	Sungrow Offgas (No Mix)
Offset from Centerline	0 m
Program	Phast 8.2
Scenario	Leak
Weather	Category 8/D
Workspace	465-005-Scout-8D-v2 - Copy

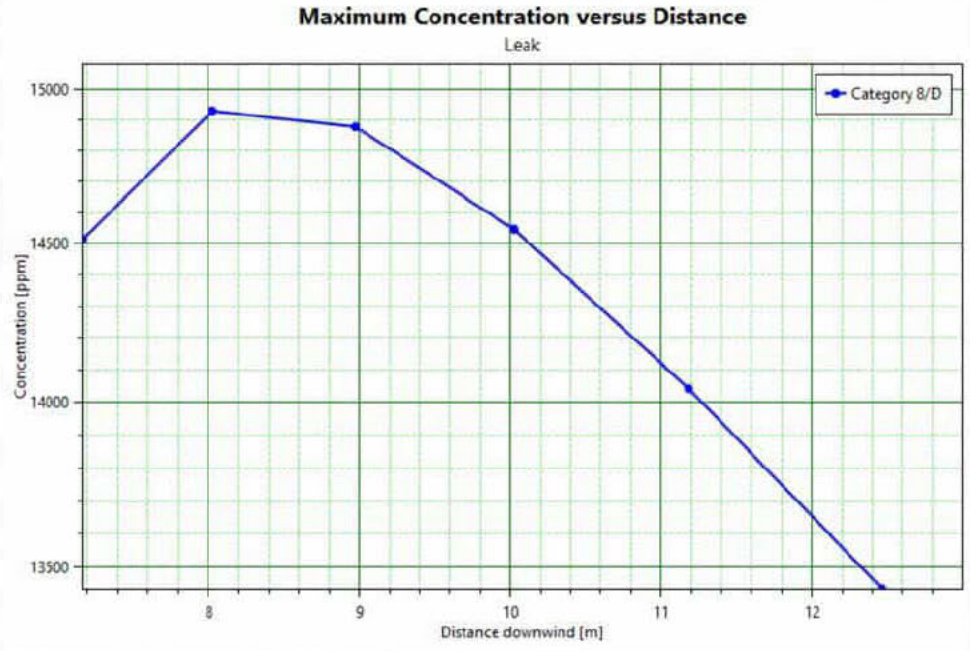


Figure 14 Maximum gas concentration vs distance downwind

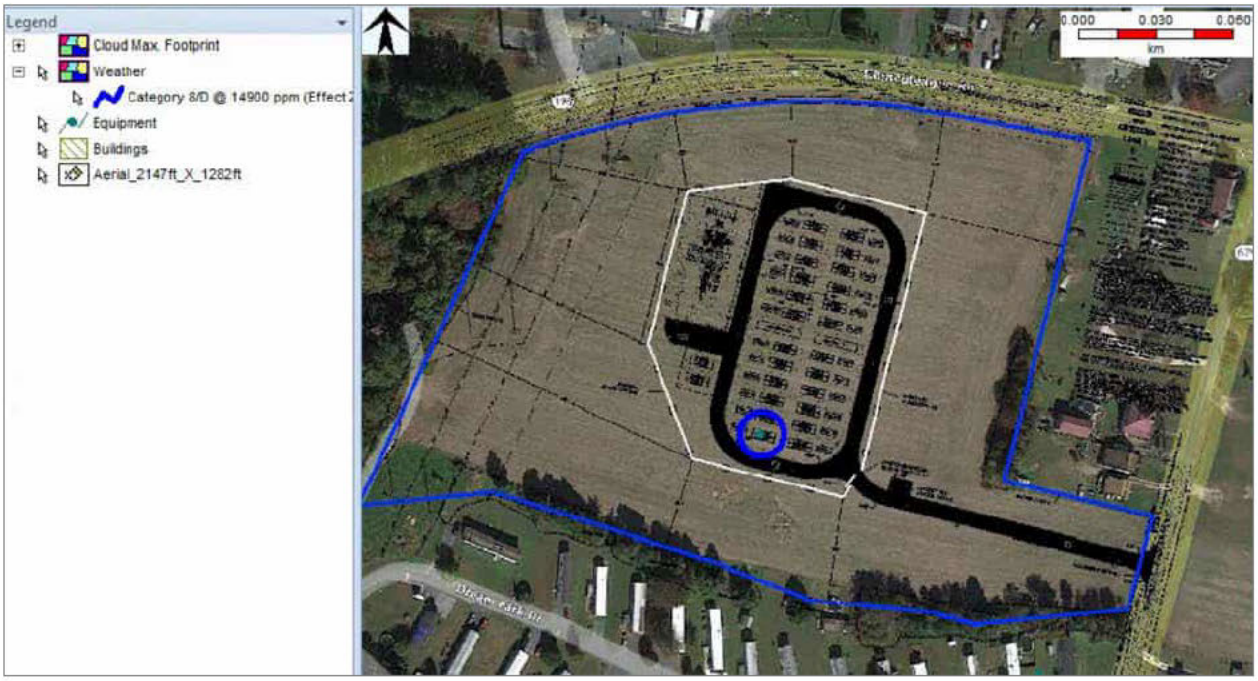


Figure 15 GIS map of maximum extent of flammable vapor showing ¼ LEL

8.2 Flashfire and Fireball Flame Extent and Thermal Radiation

8.2.1 Total Vent Gas

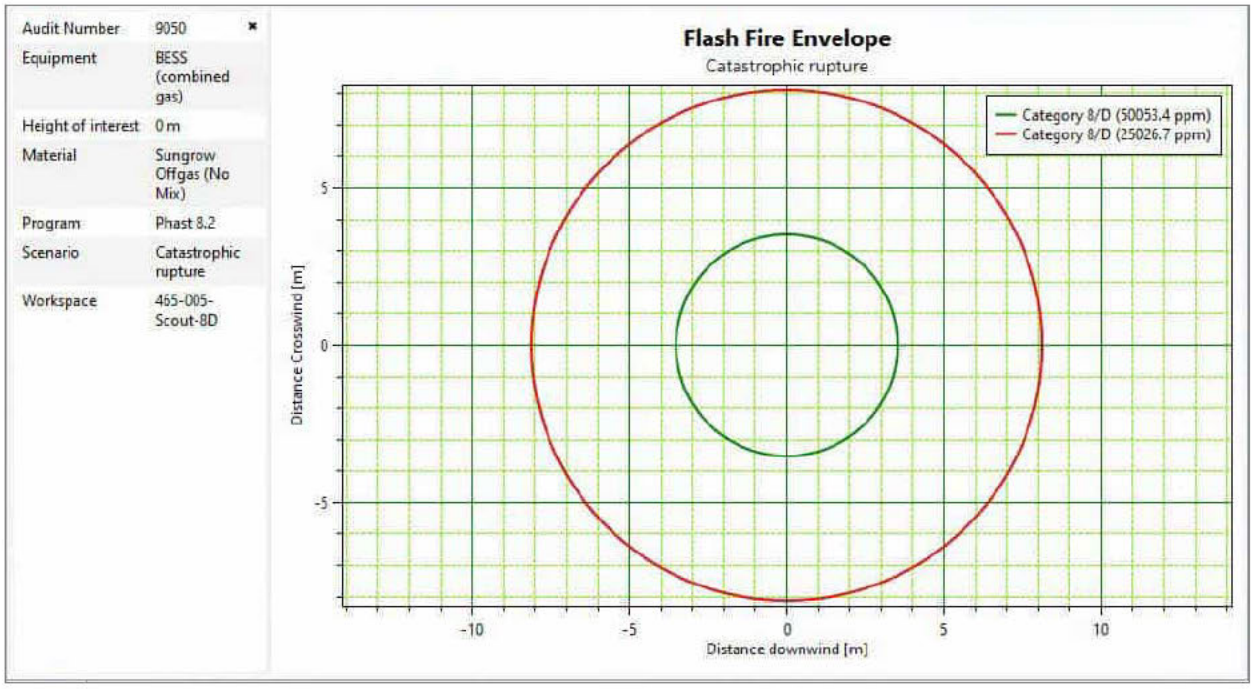


Figure 16 Flashfire envelope for LEL and ½ LEL vapor cloud ignition

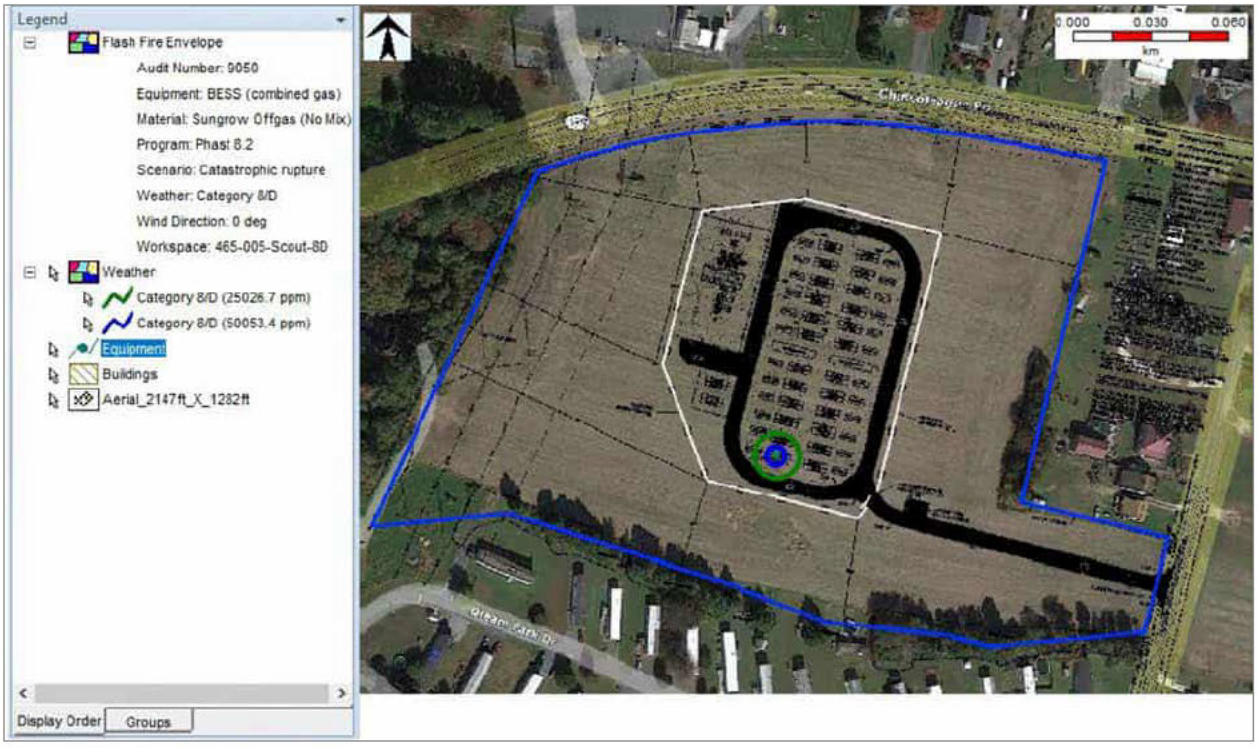


Figure 17 GIS map of flashfire envelope for LEL and ½ LEL vapor cloud ignition

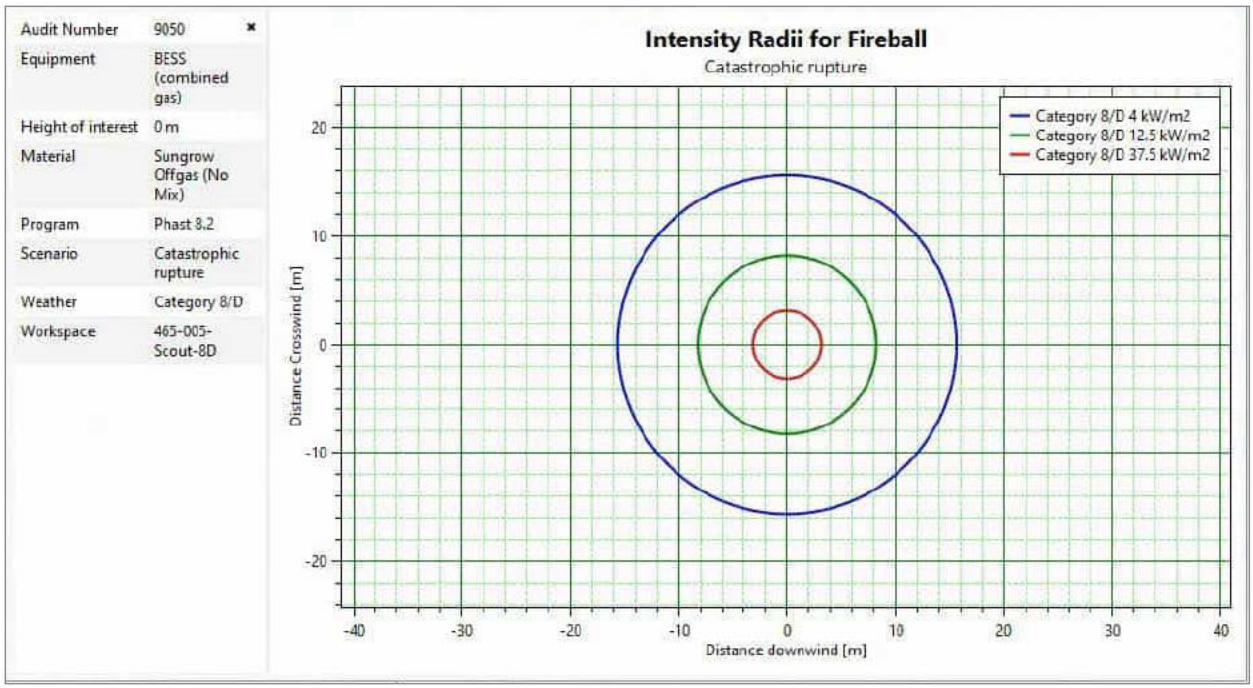


Figure 18 Fireball thermal radiation intensity radii

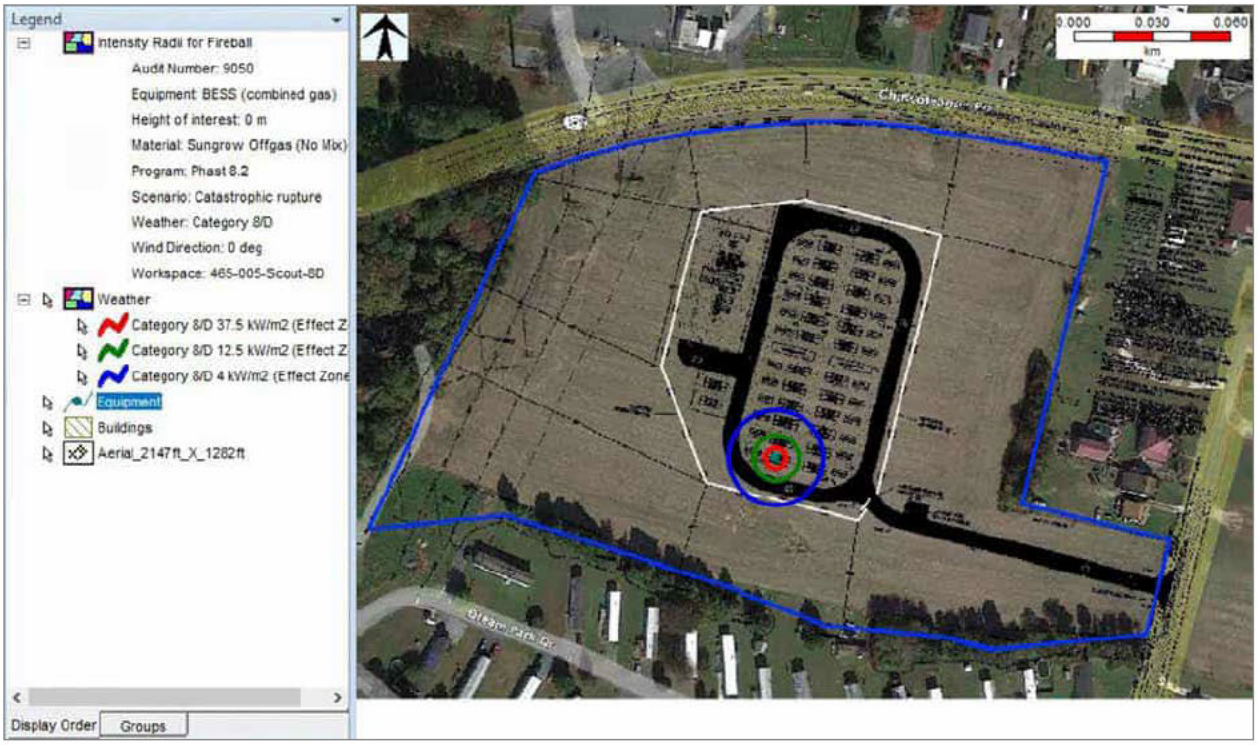


Figure 19 GIS map of fireball thermal radiation intensity radii

8.2.2 H_2 Vent Gas (Individual Species)

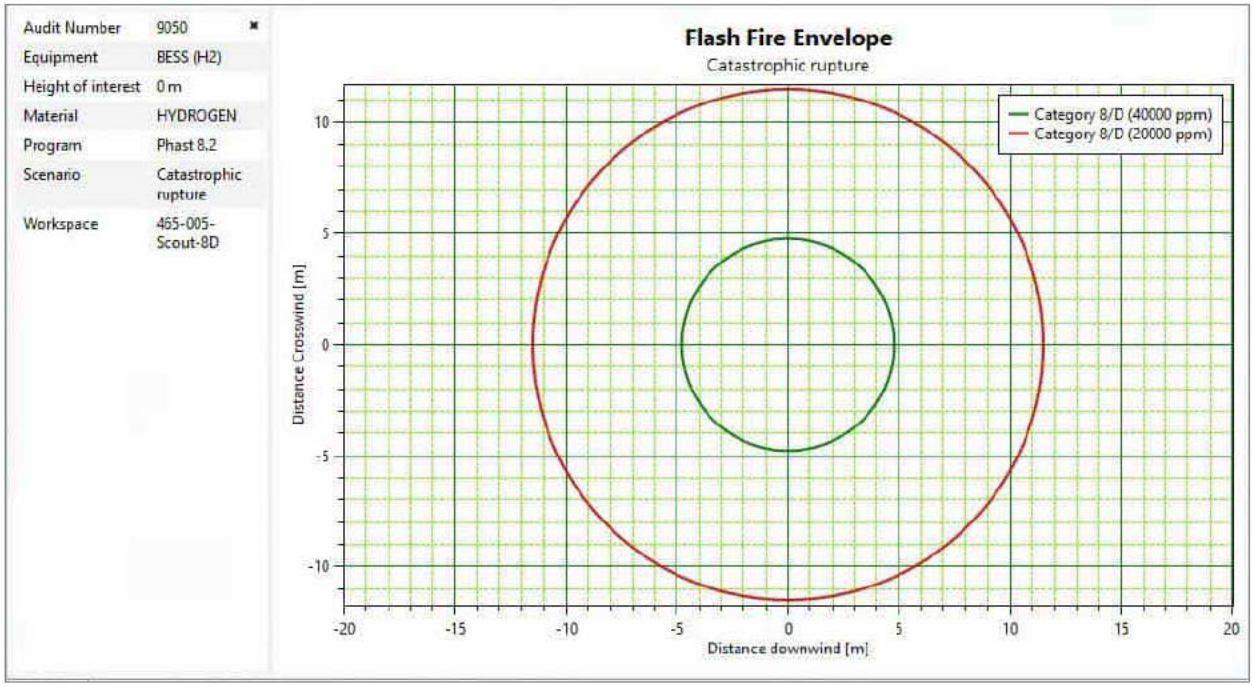


Figure 20 Flashfire envelope for LEL and ½ LEL vapor cloud ignition

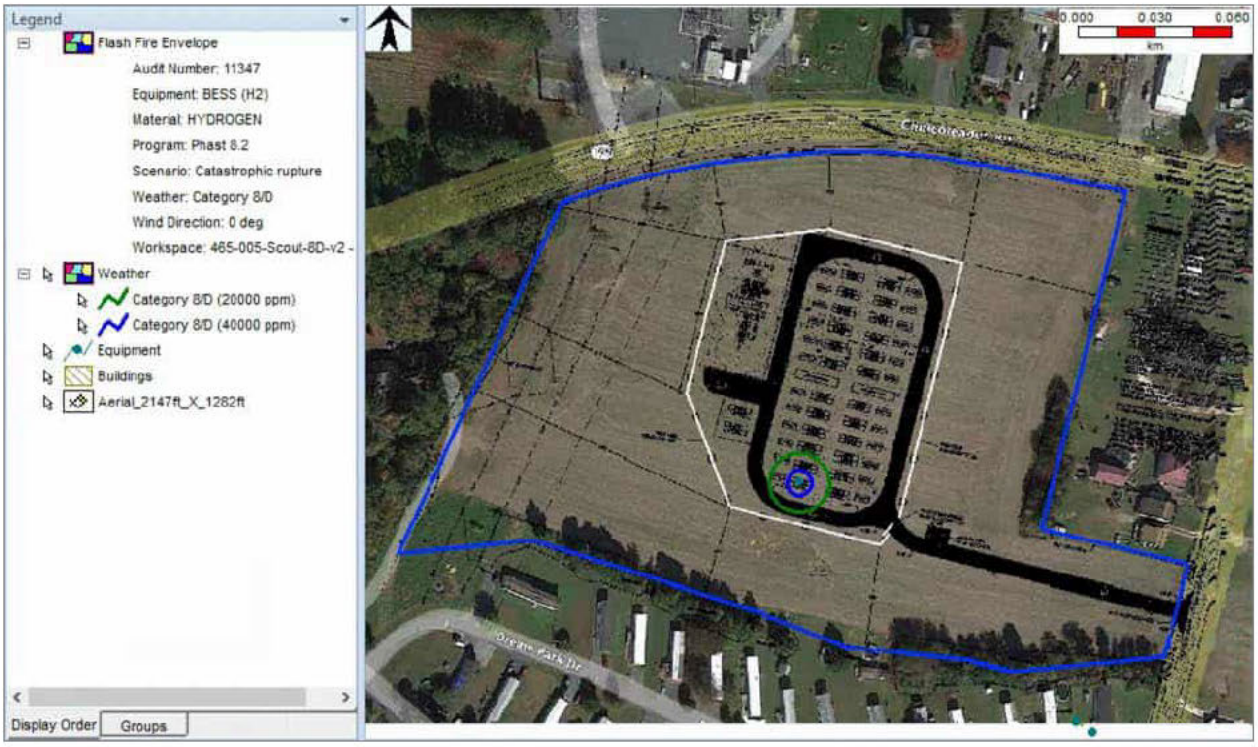


Figure 21 GIS map of flashfire envelope for LEL and ½ LEL vapor cloud ignition

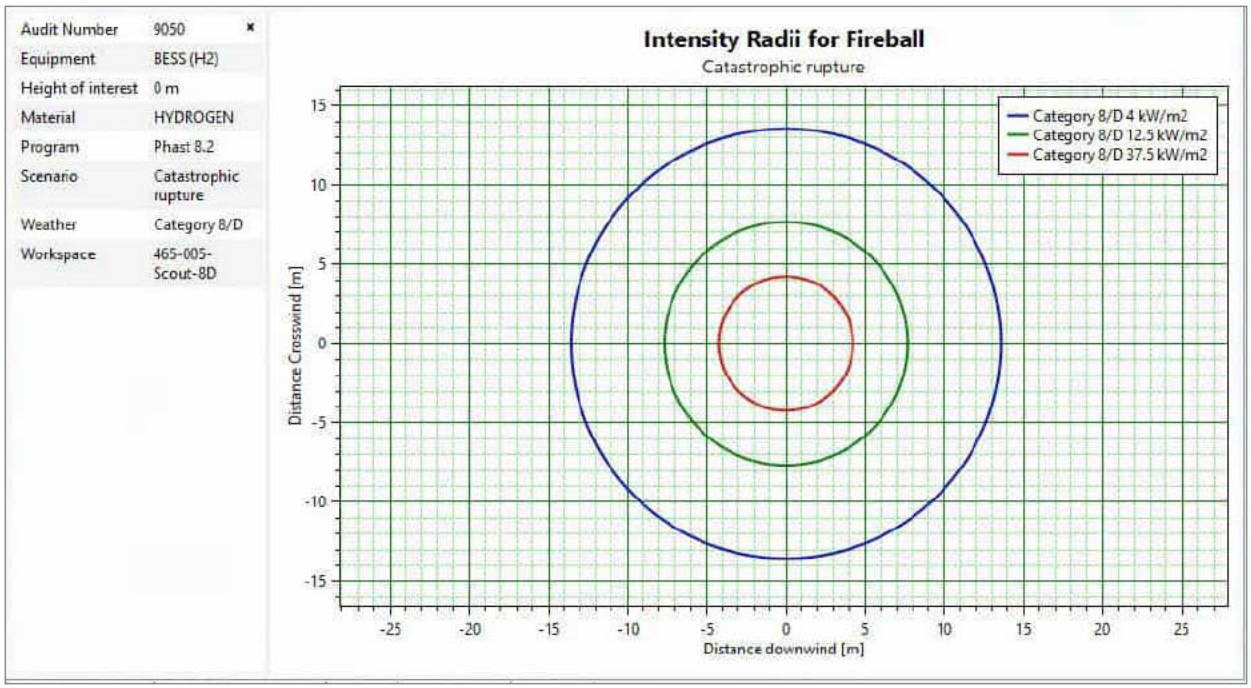


Figure 22 Fireball thermal radiation intensity radii

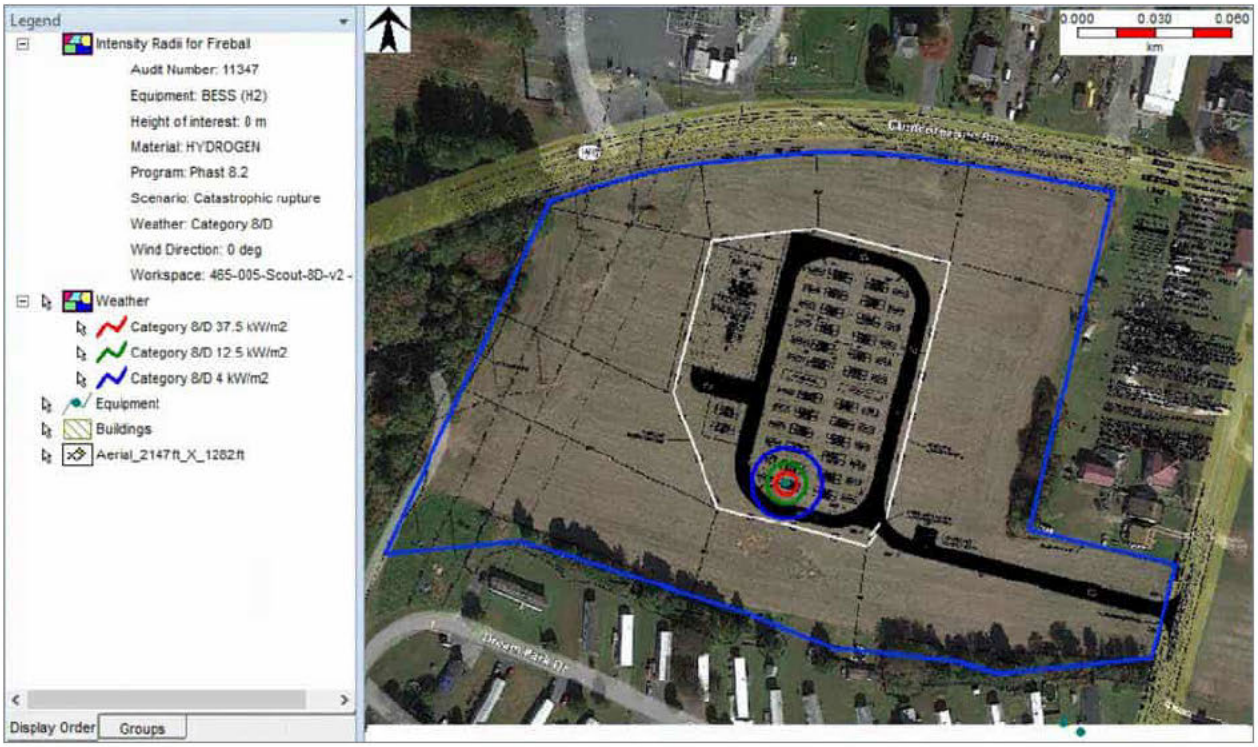


Figure 23 GIS map of fireball thermal radiation intensity radii

8.2.3 CO Vent Gas (Individual Species)

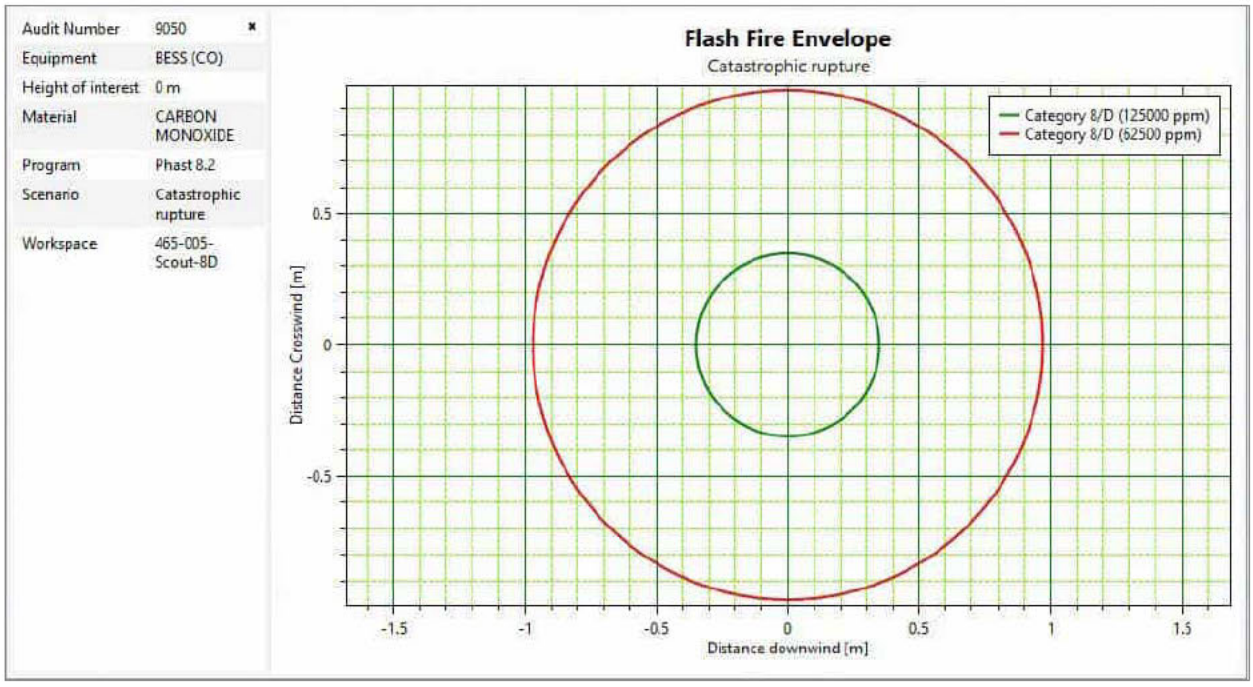


Figure 24 Flashfire envelope for LEL and ½ LEL vapor cloud ignition

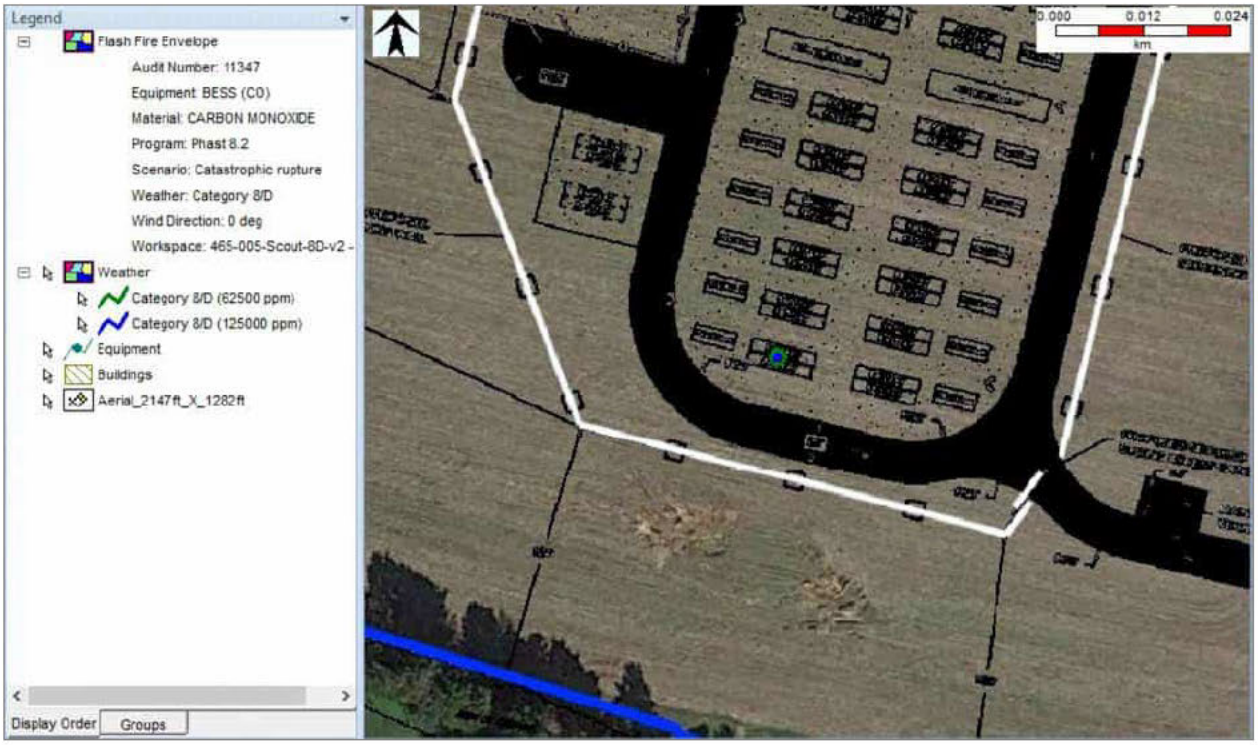


Figure 25 GIS map of flashfire envelope for LEL and ½ LEL vapor cloud ignition

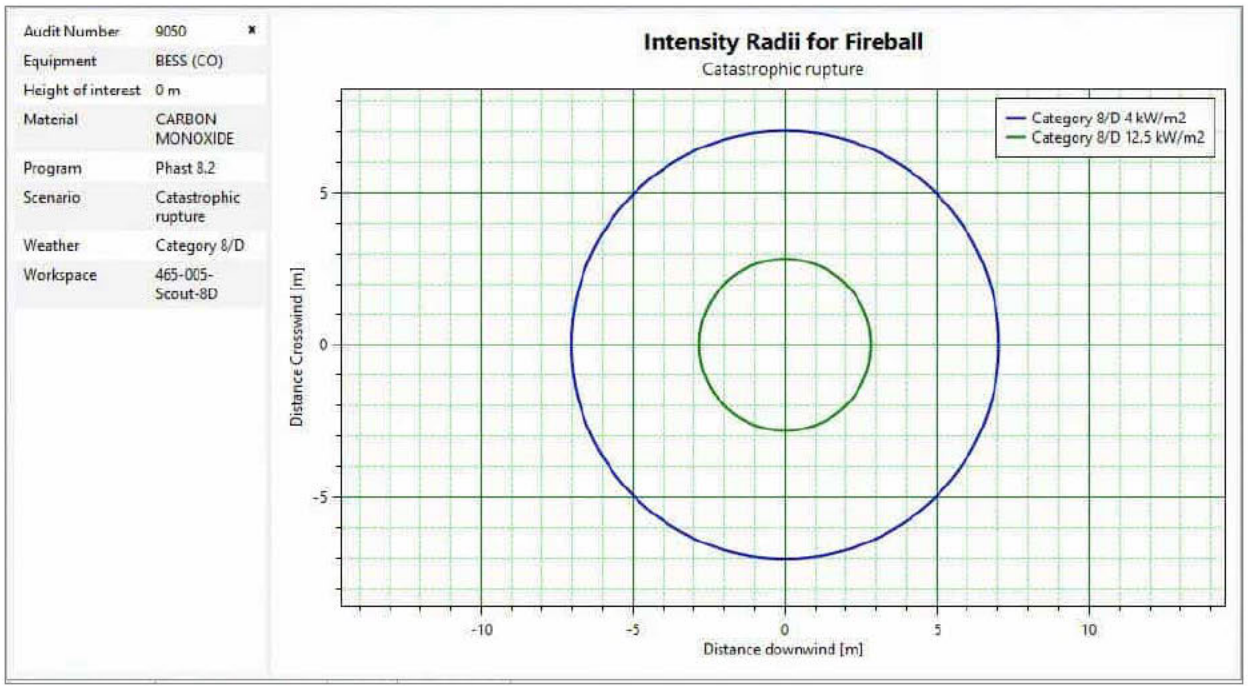


Figure 26 Fireball thermal radiation intensity radii

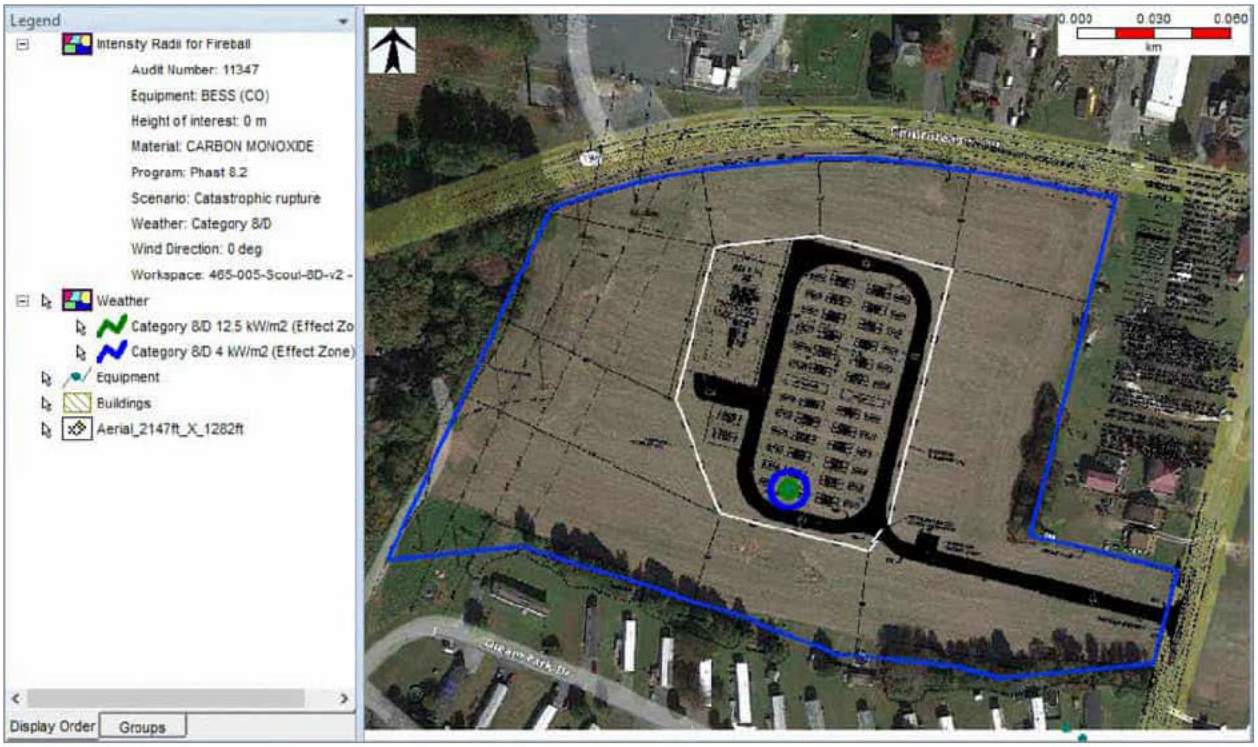


Figure 27 GIS map of fireball thermal radiation intensity radii

8.3 Risk Results

Risk results for the Wattsville BESS facility are detailed below. As described above, the societal risk is compared to the guidance provided by UK HSE which has devised generally acceptable risk criteria that has been widely accepted. The societal risk should fall beneath the UK risk curve, which indicates that fewer predicted fatalities are expected to occur than would be acceptable. Individual risk is computed and presented geographically.

8.3.1 Societal Risk Results

As described above, societal risk is the cumulative risk associated with all potential loss scenarios.

As is clearly shown in the results for all consequence scenarios reported in Sections 7.1 and 7.2, there are no hazards that extend beyond the immediate release location. No areas outside of the site boundaries are impacted and as such there is no risk to individuals or the surrounding community. This takes into account all potential release scenarios, consequence extents, and the population.

8.3.2 Individual Risk Results

Individual risk is calculated as described above and shows the risk of fatality that an individual may have when in a specific location.

As is clearly shown in the results for all consequence scenarios reported in Sections 7.1 and 7.2, there are no hazards that extend beyond the immediate release location. No areas outside of the site boundaries are impacted and as such there is no risk to individuals or the surrounding

community. This takes into account all potential release scenarios, consequence extents, and the population.

9. CONCLUSIONS

This CRA was completed to address any potential risks to individuals or the community associated with a release of vent gas from a BESS module at the Wattsville site. While the Wattsville BESS facility proposed and not currently built, the CRA evaluates the risk assuming the facility is built and in operation.

It should be noted that all observations, conclusions and recommendations are relevant only to this CRA project and the proposed operations at the Wattsville BESS facility. These include, and are not limited to:

- Facility plot plan BESS container type and design
- Inverters/Transformers and auxiliary equipment
- Meteorological data
- Onsite buildings
- Surrounding offsite residences, businesses, and community

The conclusion of the CRA is that the proposed Wattsville BESS facility poses no risks of any kind (flammable vapor, flashfires, fireballs, explosion overpressures, or toxic exposure) to any individual on the immediately adjacent properties, as well as to the surrounding community at large.

As there are no onsite personnel, there is no risk onsite to individuals.

Annex 9 Hazard Consequence Analysis

HAZARD CONSEQUENCES ANALYSIS
VALLEY CENTER STORAGE PROJECT
29523 VALLEY CENTER ROAD
VALLEY CENTER, SAN DIEGO COUNTY, CALIFORNIA



by
Haley & Aldrich, Inc.
San Diego, California

for
Chambers Group, Inc.
San Diego, California

File No. 134940-002
June 2020

HALEY & ALDRICH, INC.
5333 Mission Center Road
Suite 300
San Diego, CA 92108
619.280.9210

SIGNATURE PAGE FOR

HAZARD CONSEQUENCES ANALYSIS
VALLEY CENTER STORAGE PROJECT
29523 VALLEY CENTER ROAD
VALLEY CENTER, SAN DIEGO COUNTY, CALIFORNIA

PREPARED FOR
CHAMBERS GROUP, INC.
SAN DIEGO, CALIFORNIA

DRAFT

PREPARED BY:

[redacted]

Robert Kallin
Senior Technical Specialist
Haley & Aldrich, Inc.

REVIEWED AND APPROVED BY:

[redacted]

Tina Berceli-Boyle, P.E. (MA)
Senior Associate | Chemical Engineer
Haley & Aldrich, Inc.

[redacted]

Table of Contents

Page

List of Figures ii

SECTION 1.0 – Introduction 1

1.1 PROJECT OVERVIEW 2
1.2 PROJECT SITE AND LOCATION 2
1.3 PROJECT DESCRIPTION 3
1.4 PROJECT CONSTRUCTION 4
1.4.1 Construction Schedule, Sequence and Phasing 5
1.4.2 Construction Personnel and Equipment 5
1.5 PURPOSE 6
1.6 PROJECT SETTING 7
1.6.1 Surrounding Area 7
1.6.2 Meteorological Conditions 7

SECTION 2.0 – Design Measures and Fire Mitigation Measu es 9

SECTION 3.0 – Potential Air Toxics Emissions 11

3.1 CHARACTERIZATION OF AIR TOX CS 12
3.1.1 Hydrogen Chloride 12
3.1.2 Hydrogen Fluoride 12
3.1.3 Hydrogen Cyanide 13
3.1.4 Carbon Monoxide 14
3.2 ESTIMATED EMISSIONS 15

SECTION 4.0 – Offsite Consequence Analysis 16

4.1 METHODOLOGY 16
4.2 RESULTS 17

References 18

Figures
Appendix A - ALOHA Modeling Files
Appendix B - Peer Review

AFT

List of Figures

Figure No.	Title
1	Project Location
2	Project Site
3	Wind Rose
4	Wind Frequency Distribution
5	Estimated Maximum Toxic Endpoint

AFT

SECTION 1.0 – Introduction

This Hazard Consequences Analysis (Analysis) presents the results of an offsite consequence analysis associated with the operation of the Valley Center Storage Project; a 140-megawatt (MW) lithium-ion battery energy storage system (BESS) facility proposed by Valley Center ESS, LLC (Developer), in the unincorporated community of Valley Center, San Diego County, California (Project). Under normal operations, BESS do not store or generate hazardous materials in quantities that would represent a risk to offsite receptors. However, this Analysis was conducted to determine potential impacts resulting from the release of toxics from an unlikely but credible fire or thermal runaway event at the Project site. BESS thermal runaway/fire events may generate hazardous substances such as hydrogen chloride, hydrogen fluoride, hydrogen cyanide, and carbon monoxide, which may be released to the environment during such an event.

For the purposes of this Analysis, "offsite" means any activity or receptors located beyond the boundaries of the Project site. The Project is not subject to 40 Code of Federal Regulations Part 68 (EPA's Chemical Accident Prevention Provisions), as there is no regulated substance present above any threshold quantity as defined in the regulation nor is it subject to California Accidental Release Prevention Program (CalARP) regulations. Nevertheless, this Analysis has been conducted consistent with the U.S. Environmental Protection Agency's (EPA) 2009 "Risk Management Program Guidance for Offsite Consequence Analysis" and guidance from CalARP, as suggested in Section 5.1 of the San Diego County's 2007 "Guidelines for Determining Significance, Hazardous Materials and Existing Contamination."

This Analysis was conducted using EPA's "Areal Location of Hazardous Atmospheres" ([ALOHA]; Version 5.4.7, September 2016) hazards modeling program to determine distances to the toxic endpoints for release scenarios. The distance to the toxic endpoints the distance a toxic vapor cloud, heat from a fire, or blast waves from an explosion will travel before dissipating to the point where serious injuries from short-term exposures will no longer occur. The supporting ALOHA hazards modeling program output files for the Analysis are provided in Appendix A.

The evaluation of BESS and air toxic releases during a credible fire event is relatively new, with limited emissions data and limited similar hazards analyses. While available information is recent and subject to ongoing study, this Analysis represents the current understanding of the subject matter, subject to the limitations of available data at the time this Analysis was prepared.

The Project's preventative measures and state-of-the-art fire and safety systems, as more fully described in Section 2 of this Analysis, make a thermal runaway event very rare. Furthermore, in the unlikely event of thermal runaway, the Project's preventative measures and systems are designed to limit the event to a single battery module as well as reduce the duration and intensity of an event if it occurs. The Project is subject to the requirements of Chapter 12 of the 2019 California Fire Code and will utilize pre-engineered battery storage systems and equipment certified under UL 9540, the established Standard for Energy Storage Systems and Equipment. The UL 9540 rating establishes the design limit of a thermal runaway events to a single battery module.

While the design failure event for this Project, pursuant to UL 9540, is a thermal runaway/fire event involving a single battery module, this Analysis studies a conservative case thermal runaway/fire event

DRAFT

involving 1.5 battery racks. As final manufacturer design and vendor has not been completed, a conservative estimate of 30 battery modules per rack was assumed.

.DNV-GL is an internationally recognized testing, certification and advisory service to the energy and BESS industry. Its testing and reports on ESS fire and safety are used throughout the industry. Many of the DNV-GL 2017 Report findings have been incorporated into the NFPA 855 and the UL 9540 standards and the Report (and the 1.5 rack basis for a credible thermal runaway/fire event) has been accepted by the County of San Diego related to Hazards Consequences Analysis for BESS projects similar to the Project. DNV-GL's Report estimated the limit of failure of a BESS as 1.5 battery racks (referred to as modules in their Report) in cases where, like the Project, the system includes adequate separations, cascading protections, and suppression systems to limit failure to a single cell or module or at least a single rack. DNV-GL found that "the probability of failure for multiple racks should be very low for systems with these active and passive barriers to catastrophic failure." The requirements of UL 9540A meets the safety recommendations of DNV GL's Report, making the runaway event of 1.5 racks sufficiently conservative. The Developer is considering a vendor configuration that is characterized by multiple battery cells within isolated "packs." Based on material provided by the vendor, these packs are similar in nature to a single large battery module. As there are few r han eight battery strings per cabinet unit and the strings are electrically similar to a rack, the pack co figuration would have fewer affected packs in a thermal runaway event than modules in the rack config ration. Therefore, this Analysis covering 1.5 racks of 30 modules per rack is more conservative than a similar credible thermal runaway event involving packs.

1.1 PROJECT OVERVIEW

The Developer plans to construct, own and operat the Valley Center Storage Project, a lithium-ion based battery energy storage facility capable of deli ering up to 140 megawatts (MW) for approximately 4 hours on an 8.93-acre parcel and associated utility nd access easement in Valley Center, San Diego County (the Project). The Project will interconnect to the existing, adjacent San Diego Gas & Electric (SDG&E) 69kV Valley Center Substation via an approximately 0.3-mile underground generation tie line (gen-tie line). The Project will be comprised of sets of four battery enclosures (each enclosure approximately 31.6 feet long by 5.7 feet wide by 8.6 feet high) that will house the integrated Battery Energy Storage System (BESS) including battery cells, modules, racks, a fully integrated fire and safety systems, HVAC systems, and other electrical systems. The batteries will be charged from the CAISO (California Independent System Operator) grid via the Project's interconnection to the SDG&E Valley Center Substation. Energy stored in the Project will then be discharged back into the grid when the energy is needed, providing essential electricity reliability services to the local area. The Project plans to start construction in the fourth quarter of 2020 and begin operations by August 1, 2021.

1.2 PROJECT SITE AND LOCATION

The Project site is located at 29523 Valley Center Road, Valley Center, California on a parcel of private land (APN 189-013-20-00) within unincorporated Valley Center in San Diego County (Figure 1). San Diego County (County) identifies land use and zoning of the Project site as Medium Impact Industrial (I-2) and General Impact Industrial (M54) use regulation. Permitted uses in the Medium Impact Industrial zone are manufacturing, processing, and assembly; warehousing and distribution; large equipment supply and sales; and other industrial or commercial activities. The M54 use regulation allows for unenclosed commercial and industrial operations having potential nuisance characteristics such as construction,

AFT

sales and services. The County has identified the Project as a Minor Impact Utility, defined as public utilities which have a local impact on surrounding properties and are necessary to provide essential services. All Minor Impact Utilities, including the Project, are permitted by right within the M54 use regulation (County of San Diego Zoning Ordinance).

Additionally, the Project Area is located in an area under County Special Area Regulations, Designator B: Community Design Review Area, where visual impacts criteria must be met through a limited Site Plan approval process. These regulations are intended to ensure that added consideration is provided to visual impacts in areas of special interest. Surrounding land uses include Limited Impact Industrial to the north, Semi-Rural Residential (SR-4 and SR-2) to the east and south, and Medium Impact Industrial to the west (Figure 2).

The Project site is defined as the 8.93-acre parcel and the Project-controlled access easement. The Project Area is described as the Project site and the off-site underground gen-tie line alignment.

1.3 PROJECT DESCRIPTION

The Project will be comprised of lithium ion battery modules housed in cabinets within up to 58 sets of 4 non-walk-in enclosures on dedicated foundations that will be capable of charging and delivering up to 140MW for approximately 4 hours. Each enclosure will contain integrated battery, heat/fire and safety management systems including electrical and mechanical controls ventilation systems, HVAC, fire alarm detection and heat management systems. From the BESS containers, low voltage cables will connect to low profile, pad- inverter/transformers located adjacent to the BESS units, and to a control center enclosure called a Power Distribution Center (PDC). The Project will meet all criteria pursuant to the municipal and California Fire Code. All Project equipment will be set back at least 30 feet from property boundaries, fire access roads will be a minimum of 24' in width with appropriate turn-around capabilities, among other fire and safety systems and practices.

DRAFT

Major Project equipment and facilities include:

- Up to 58 sets of 4 BESS enclosures including battery modules and integrated battery, fire and safety management systems.
- Up to 58 pad-mounted inverter/transformers located adjacent to each set of BESS enclosures to convert direct current into alternative current and step the units' voltage up to 34.5 kV.
- 2 PDC enclosures which are modular electrical equipment enclosures housing energy management systems, communications/SCADA equipment, and other electrical equipment.
- A BSU (Battery Step-Up Transformer), circuits will enter the BSU from the PDC at 34.5 kV where voltage will be stepped up to 69kV.
- An approximately 0.3-mile 69kV gen-tie line will be constructed from the Project BSU north across Valley Center Road to SDG&E 69kV Valley Center Substation across one of four alignment options (described further below).
- Security lighting and fencing
- Stormwater drainage and retention basins
- Signage

The exact size and quantity of the battery storage containers and inverter transformers may vary depending on the battery and BESS manufacturer(s) selected for the Project.

Access to the Project site is provided from Valley Center Road via a permanent Project-controlled easement. The site access road will comply with County regulations and be stabilized using gravel in order to provide access to operational, fire department, and emergency vehicle access to the facility. Project site equipment and facilities (with the exception of stormwater drainage and retention basins) will be surrounded by a solid, 8-foot tall vinyl fence or a similar solid fence. The fence will be built flush with the ground and have the appearance of a paneled wood fence. Existing fences surrounding the property boundary will remain. Existing fences surrounding and adjacent to the property boundary will remain. The Project design will adhere to County Guidelines, including the Valley Center Design Guidelines. Lighting at the Project site will be installed per County requirements.

The Project will be un-manned during operations, with no buildings or parking areas. The Project would not require restroom facilities. Any operational water that may be required for routine maintenance would be trucked in from offsite or sourced by a new Valley Center Municipal Water District (VCMWD) service. A fire hydrant will be located at or near the site entrance. No groundwater would be used for any purposes during construction or operational phases of the Project.

The Project will interconnect to the existing, adjacent SDG&E 69kV Va ley Center Substation via a Project-constructed underground gen-tie line that, upon leaving the roject site will cross Valley Center Road heading north onto SDG&E property for approximately 0.3 miles. F ur alignment options are being considered and evaluated for the gen-tie line (Figure 1). All f ur options le ve the Project site access easement, cross under Valley Center Road and then:

- Option A: enters SDG&E's property and heads nor adjacent to existing SDG&E underground circuits within SDG&E's property and en rs the subst ion at the point of interconnect.
- Option B: enters SDG&E's property fol wing Option A, but travels across the property in a northwesterly direction until reaching the ubstation.
- Option C: follows the southern and wester property boundaries within SDG&E's property until turning easterly to access the substation from the west.
- Option D: follows the west-bound Valley Center Road right-of-way before entering SDG&E's property, following Option C in the easterly direction to access the substation.

All four options are approximately the same length.

The Project will be operated, monitored and dispatched remotely on a day-to-day basis. Crews of two to four person's will periodically visit the site (approximately twice per month) for routine inspection and maintenance of the facilities and site. The Developer will own and maintain the gen-tie line up to the point where the gen-tie line enters SDG&E property, where ownership and maintenance responsibilities will be transferred to SDG&E.
The facility is anticipated to have a Project life of approximately 30 years. At the end of the Project life, most of the Project's enclosures, batteries, and electrical equipment (breakers, transformers, inverters) would be removed and recycled. Equipment foundations and pads would be demolished and removed.

1.4 PROJECT CONSTRUCTION

Project construction includes site preparation and grading, installation of drainage and retention basins, foundations/supports, setting battery enclosures, wiring and electrical system installation, and assembly of the accessory components including inverter transformers and generation step-up transformers. The Project would require the grading of approximately 3,000 cubic yards of soils, balanced on site (no net

AFT

import or export). The approximately 0.3-mile gen-tie line will be installed underground by the Project to the SDG&E 69kV Valley Center substation.

1.4.1 Construction Schedule, Sequence and Phasing

In accordance with the County Noise Ordinance, Project construction will occur between the hours of 7:00AM and 7:00PM Monday through Saturday. Construction of the Project is anticipated to occur over approximately 6 months, beginning as early as fourth quarter 2020. Project construction would likely occur in two phases:

- Phase 1 – Installation of battery storage enclosures and associated civil, electrical and structural features placed outside of the floodplain. During Phase 1, ancillary features, such as graveled access roads and underground electrical components, that are not considered "encroachment" would be installed within the floodplain.

- Phase 2 – Installation of remaining battery storage enclosures and associated civil, electrical and structural features placed within the floodplain; includes features, such as pad-mounted switchgear, step-up transformer(s), and a control cent r nclosure, that could be considered "encroachment" within the floodplain.

The two construction phases would likely be executed con ecutively; Phase 1 ollowed by Phase 2. However, for the purposes of preparing a worst-case CE A analy is, technical analyses were completed assuming the two construction phases would occur simulta usly over a period of approximately 6-12 months.

The sequence of construction activities for the BESS wo ld ge erally occur as follows (with activities limited within the floodplain as described in Phase nd Phase 2 above):

1. Equipment staging and mobilization
2. Site preparation and grading
3. Preparation of equipment foundations
4. Site compaction and gravel as necessary
5. Excavating footings and pads
6. Pour-in-place concrete footings, pad foundations, and/or piers
7. Install below-ground conduit banks
8. Install PCS, power distribution systems, and pad-mounted transformers
9. Install below-ground and above-ground conduit
10. Install safety features, permanent fencing and security lighting
11. Commissioning

The approximately 9 acre-feet of water required during the duration of construction is expected to be provided by VCMWD through a temporary use agreement.

1.4.2 Construction Personnel and Equipment

Construction personnel are expected to consist of approximately 10 to 15 workers on average, depending on the construction activities. Project laydown and construction staff parking is expected to be located on-site to the extent practicable. The Project may need to utilize an offsite temporary use area, up to approximately 2 acres in size, for equipment storage during construction. Should it be

AFT

needed, the temporary use area would be located within 2 miles of the Project site, on a site that has been previously disturbed, and where temporary equipment storage is an allowable use and compatible with the existing uses on the property. The technical analyses prepared for the Project have been conducted assuming use of a temporary offsite area following these parameters. If it is determined that use of a temporary offsite area is needed during Project construction, the selected location will be submitted to the County and shown to be consistent with the technical analyses performed for the Project.

Typical equipment expected to be used during Project construction and commissioning:

- Excavator (2)
- Backhoe (2)
- Dozer (1)
- Roller/Compactor (1)
- Dump truck (2)
- Concrete mixer (3)
- Flatbed-mounted utility crane (1)
- Portable generator and welding equipment (1)
- Forklift (1)
- Pickup trucks (4)
- Utility line trucks (2)

1.5 PURPOSE

While the Project is not subject to CalARP, this Analysis has been conducted to be consistent with Section 5.1 of the San Diego County's 2007 "Guidelines for Determining Significance, Hazardous Materials and Existing Contamination," which states that facilities that would handle regulated substances subject to CalARP regulations and are located within 0.25-mile from a school or day care are required to prepare a hazard assessment to determine the effects of the regulated substance on surrounding land uses in the event of a release. According to these guidelines, the requirement for a hazard assessment is typically satisfied by preparing an Offsite Consequence Analysis following EPA's 2009 "Risk Management Program Guidance for Offsite Consequence Analysis," as supplemented by guidance from CalARP.

There is a single daycare, located at 29235 Valley Center Road, approximately 0.24-mile from the northwest corner of the Project site. In addition, there are existing residences located to the north, east and west of the Project site. As a result of being within 0.25-mile of a daycare facility, and as part of Site Plan review, San Diego County requested this hazard consequences analysis to evaluate the potential for adverse effects to people or the environment related to hazards and hazardous materials.

The objectives of this Analysis are to:

- Identify Project safety design measures and fire risk mitigation measures.
- Determine the distance from the Project BESS to the nearest sensitive receptors;
- Identify and characterize the quantities and locations of hazardous chemicals that could be released during a thermal runaway/fire event from the Project BESS;

AFT

- Conduct plume dispersion modeling using EPA's ALOHA (Version 5.4.7, September 2016) hazards modeling program to determine distances to the toxic endpoints for the release scenario; and
- Determine potential impacts and safety risks at the nearest receptors to Project BESS.

1.6 PROJECT SETTING

The Project's general location is within the industrial/commercially corridor of the unincorporated community of Valley Center, in northern San Diego County. Figure 1 shows the general Project location.

1.6.1 Surrounding Area

The Project's surrounding industrial/commercial area of unincorporated Valley Center includes several storage facilities, propane gas distributors, and the adjacent SDG&E electrical distribution substation. Adjacent commercial operations are co-located with residences both west and north of the Project site, all located on industrially-zoned parcels. Also located north of the Pr ject site, across Valley Center Road, is the SDG&E 69kV Valley Center Substation. Rural agricul urally z ned properties are located east and south of the Project site.

As stated in Section 1.2 above, a daycare facility is located appro imately 0.24-mile northwest of the Project site. The nearest school to the Project site is Valley nter Elementary School, located approximately 0.4-mile from Project site - outsid of the 0.25- ile study area. The nearest residence to Project BESS is located adjacent to the Project's wester property ine.

1.6.2 Meteorological Conditions

Air impacts are a function of the rate of emissions and source characteristics under the influence of meteorological conditions and topographic features which affect pollutant movement and dispersion. Atmospheric conditions such as wind speed, wind direction, atmospheric stability, and air temperature gradients interact with the physical features of the landscape to determine the movement and dispersal of air pollutants and consequently affect air quality. Climate within the San Diego Air Basin area often varies dramatically over short geographical distances with cooler temperatures on the western coast gradually warming to the east as prevailing winds from the west heats up. Most of southern California is dominated by high-pressure systems for much of the year, which keeps San Diego County mostly sunny and warm. Typically, during the winter months, the high-pressure system drops to the south and brings cooler, moister weather from the north. It is common for inversion layers to develop within high-pressure areas, which mostly define pressure patterns over the air basin. These inversions are caused when a thin layer of the atmosphere increases in temperature with height.

An inversion acts like a lid preventing vertical mixing of air through convective overturning. This type of inversion is typically thousands of feet above the ground, too high to affect a dispersing gas cloud. While some low-level inversions, which may be indicated by the presence of ground level fog, may occur in the Project area, it is exceedingly rare to have an inversion height below 1,000 feet, which even at that height would not have an effect on adjacent receptors.

AFT

Meteorological trends within the Valley Center area are generally similar to that of Escondido daytime highs ranging between 65ºF in the winter to approximately 88ºF in the summer with August usually being the hottest month. Median temperatures range from approximately 57ºF in the winter to approximately 78ºF in the summer. Precipitation is generally about 16.2 inches per year (WRCC, 2018). Prevailing wind patterns for the area vary during any given month during the year and also vary depending on the time of day or night. The predominant pattern though throughout the year is usually from the west or westerly (WRCC, 2018).

To estimate the average wind speed and direction, hourly surface data was reviewed. Neither Valley Center nor Escondido have hourly surface weather stations. The nearest hourly surface weather stations to the project are the McClellan Palomar Airport and the Ramona Airport. The Ramona Airport, while not the nearest station, is considered most representative because of its proximity and similar inland distance. Based on hourly meteorological data from the Ramona Airport from 2009 through 2014[1], the wind is predominantly calm, with wind speeds of less than 0.5 meters per second recorded about 41 percent of the time. When the wind is blowing it is primarily from the west and west-northwest (about 28 percent of recorded hours, or about 47 percent of all non-calm hours) with a high frequency of low wind conditions (2.1 to 5.7 meters per second [m/s] or 4.7 to 12.7 miles per hour [mph]).

San Diego County is also subject to periodically subject to Santa Ana win conditions. Santa Ana winds consist of strong down slope winds that blow through the m untain passes n southern California. These winds, which can easily exceed 40 miles per hour (18 m/s) are warm and dry. Stronger wind speeds typically enhance dispersion and dissipate releases more apidly than low-wind conditions. However, as the Santa Ana wind is a frequent and period condition, this enario is included in this analysis.

Figure 3 displays the wind rose during this period and t freque cy distribution is depicted graphically as shown in Figure 4.

AFT

[redacted]

SECTION 2.0 – Design Measures and Fire Mitigation Measures

The 2019 California Fire Code was published July 1, 2019, with an effective date of January 1, 2020. The 2019 California Fire Code, Title 24, Part 9, Chapter 12, Energy Systems, requires prepackaged and pre-engineered stationary storage battery systems to be listed in accordance with UL 9540, Standard for Energy Storage Systems and Equipment. This standard was developed for energy storage systems and are intended for installation and use in accordance with the National Electrical Code, NFPA 70, the Canadian Electrical Code, Part I Safety Standard for Electrical Installations, CSA C22.1, the National Electrical Safety Code, IEEE C2, the International Fire Code, ICC IFC, the International Residential Code, ICC IRC, the National Fire Code of Canada, NRC NFC, the Fire Code, NFPA 1, and the Standard for the Installation of Stationary Energy Storage Systems, NFPA 855.

The Project is subject to the requirements of Chapter 12 of the 2019 California Fire Code and will utilize pre-engineered battery storage systems listed under UL 9540. UL 9540 serves as the system certification and does so by incorporating and making references to ma y other codes. It references over 60 other rules, including UL 1973 (batteries), UL 1741 (inverters), ASME B31 (power piping), ASME B & PV (boiler & pressure vessel), ASHRAE 62.1 (ventilation), NFPA 70 (electrical). Aspects of the code relevant to this Project are summarized below.

UL 9540 contains safety standards for the system's const uction (e g., frame and enclosure, including mounting, supporting materials, barriers and more); the i sulat on, wiring, switches, transformers, spacing and grounding; safety standards for performance of ver twenty different elements, such as tests for temperature, volatility, impact, overloa of switches, a d an impact drop test; and standards for manufacturing, ratings, markings, and instruc on ma ls In addition to the many individual standards referenced, UL 9540 compliance require a Failure Mode and Effects Analysis (FMEA) be performed and requires a test to ensure safe compa bility of the system's parts. Hence, the standard embodies both a "forest and trees" approach, ensuring that the components are certified, that the system as a whole is certified as safe, and that an FMEA has identified the set of things that might still go wrong, and taken action to mitigate those risks.

Chapter 12 of the 2019 California Fire Code also requires the use of an Energy Management System, for monitoring and balancing cell voltages, currents and temperatures. The system must transmit an alarm signal if potentially hazardous temperatures or other conditions such as short circuits, over voltage or under voltage are detected. The fire code also requires the use of appropriate fire-extinguishing and smoke detection systems, which will be incorporated into each of the Project's BESS enclosures.

UL 9540 incorporates the UL 1973 standard, in which a battery manufacturer must prove that a failed cell inside will not cause a fire outside the system. The Project will meet the UL 9540 and industry standards for adequate separations, cascading protections, and suppression systems to limit failure to a single cell. As described above, the design thermal runaway/fire event for batteries compliant with UL 9540 was determined to involve one (1) battery module. However, for the purposes of this Analysis is a more conservative 1.5 battery rack was studied per DNV GL's 2017 Report "Considerations for ESS Fire Safety." The DNV-GL Report is recognized throughout the industry and many of the recommendations of DNV GL's 2017 Report have been incorporated into NFPA 855 and the UL 9540A standard, supporting this scenario as a credible thermal runaway event.

AFT

UL has also introduced a comprehensive testing method, UL 9540A, Test Method for Evaluating Thermal Runaway Fire Propagation in Battery Energy Storage, designed to subject battery technologies to a variety an adverse conditions in order to determine if a thermal runaway event is achievable at the cell, unit, enclosure, and installation level and the impact of the event and ensuing fire at those levels. The results from the UL 9540A Test Method can also be used to address building code and fire safety concerns involving BESS installation, ventilation requirements, effectiveness of protection, and fire response methods. While UL 9540A has not been adopted by the California Fire Code, it provides technology specific data that can be used to determine appropriate fire protection measures. All BESS technologies proposed for the facility will either meet the UL 9540 standard or incorporate technology appropriate mitigation measures as informed by the UL 9540A Test Method.

AFT

SECTION 3.0 – Potential Air Toxics Emissions

Based upon testing data in available publications (the DNV GL Report, National Fire Protection Association studies), there are four hazardous substances that are potentially released during an accidental event within a BESS that may have an impact on nearby receptors. The hazardous substances include hydrogen chloride (HCl), hydrogen fluoride (HF), hydrogen cyanide (HCN), and carbon monoxide (CO).

The following describes the potential air toxics, potential effects from acute inhalation exposure, Emergency Response Planning Guidelines (ERPG) values, and Acute Exposure Guideline Levels (AEGLs). The descriptions of health effects are summarized from the National Institute of Health PubChem database. ERPGs are developed by the Emergency Response Planning committee of the American Industrial Hygiene Association (AIHA). AEGLs are developed by the National Academy of Sciences. Both the ERPGs and AEGLs have three levels, categorized by severity of impact.

The ERPG values are defined as follows:

- ERPG-1 is the maximum airborne concentration below which ne ly all individuals could be exposed to for up to one hour without experiencing more than mild transient adverse health effects or without perceiving a clearly defined ob ectionable odor.
- ERPG-2 is the maximum airborne concentration be w which nearly all individuals could be exposed to for up to one hour without experiencing o developing irreversible or other serious health effects or symptoms which could mpa an individual's ability to take protective action.
- ERPG-3 is the maximum airborne concentr tio below which nearly all individuals could be exposed to for up to one hour without expe encing or developing life-threatening health effects.

The AEGL values are defined as:

- AEGL-1 is the airborne concentration (expressed as ppm or mg/m3) of a substance above which it is predicted that the general population, including susceptible individuals, could experience notable discomfort, irritation, or certain asymptomatic non-sensory effects. However, the effects are not disabling and are transient and reversible upon cessation of exposure.
- AEGL-2 is the airborne concentration (expressed as ppm or mg/m3) of a substance above which it is predicted that the general population, including susceptible individuals, could experience irreversible or other serious, long-lasting adverse health effects or an impaired ability to escape.
- AEGL-3 is the airborne concentration, expressed as parts per million (ppm) or milligrams per cubic meter (mg/m3), of a substance above which it is predicted that the general population, including susceptible individuals, could experience life-threatening health effects or death.

The distance of toxic endpoints (See Section 4) uses the ERPG-2 and AEGL-2 values per EPA guidance to evaluate potential risk to nearby receptors or first responders.

AFT

3.1 CHARACTERIZATION OF AIR TOXICS

3.1.1 Hydrogen Chloride

HCl is a colorless, corrosive gas with a pungent, suffocating odor. It is heavier than air and may accumulate in low-lying areas. When exposed to air it forms white fumes due to condensation with atmospheric moisture. These fumes consist of hydrochloric acid which forms when HCl dissolves in water. HCl forms corrosive hydrochloric acid on contact with body tissue. Inhaling the fumes can cause coughing, choking, inflammation of the nose, throat, and upper respiratory tract, and in severe cases, pulmonary edema, circulatory system failure, and death.

Inhalation is an important exposure route to HCl. Its odor and highly irritating properties generally provide adequate warning for acute, high-level exposures. Concentrated HCl can be corrosive to the skin, eyes, nose, mucous membranes, and respiratory and gastrointestinal tracts. Inhaling HCl can lead to pulmonary edema. Other effects of exposure include shock, circulatory collapse, metabolic acidosis, and respiratory depression. HCl gas is intensely irritating to the mucous membranes of the nose, throat, and respiratory tract. Brief exposure to 35 parts per million (ppm) cau es throat irritation and levels of 50 to 100 ppm are barely tolerable for 1 hour. The greatest impact s n the upper respiratory tract; exposure to high concentrations can rapidly lead to swelling and spasm f the throat and suffocation.

Most seriously exposed persons have immediate onset of apid breathing, blue coloring of the skin, and narrowing of the bronchioles. Patients who have massive expos res may develop an accumulation of fluid in the lungs. Exposure to HCl can lead to Reactive Airw Dysfunction Syndrome, a chemically- or irritant-induced type of asthma. Children may be ore vulnera le to corrosive agents than adults because of the relatively smaller diameter of the airways Children may also be more vulnerable to gas exposure because of increased minute ventilation er k ogram and failure to evacuate an area promptly when exposed. EPA has not classified HCl or hydroc oric acid for carcinogenicity.

The ERPG values for HCl are:

- ERPG-1: 3 ppm;
- ERPG-2: 20 ppm; and
- ERPG-3: 150 ppm.

The AEGL 30-minute values for HCl are:

- AEGL-1: 1.8 ppm;
- AEGL-2: 43 ppm; and
- AEGL-3: 210 ppm.

3.1.2 Hydrogen Fluoride

HF is a colorless, corrosive gas or liquid (it boils at 19.5 degrees Celsius [°C]) that is made up of a hydrogen atom and a fluorine atom. It fumes strongly, readily dissolves in water, and both the liquid and vapor will cause severe burns upon contact. HF is also a very irritating gas, not as dangerous as fluorine, but large amounts of it can also cause death. The dissolved form is called hydrofluoric acid, a colorless

AFT

fuming mobile aqueous solution with a pungent odor. It is corrosive to metals and tissue and highly toxic by ingestion and inhalation. Exposure to fumes or very short contact with liquid may cause severe painful burns; it penetrates skin to cause deep-seated ulceration that may lead to gangrene.

Hydrofluoric acid is a clear, colorless liquid, miscible with water, with an acrid, irritating odor. It is an extremely corrosive liquid and vapor that can cause severe injury via skin and eye contact, inhalation, or ingestion. Dilute solutions deeply penetrate before dissociating, thus causing delayed injury and symptoms. Skin contact results in painful deep-seated burns that are slow to heal. Burns from dilute (less than 50 percent) hydrogen fluoride solutions do not usually become apparent until several hours after exposure. Hydrofluoric acid and HF vapor can cause severe burns to the eyes, which may lead to permanent damage. At 10 to 15 ppm, HF vapor is irritating to the eyes, skin, and respiratory tract. Exposure to higher concentrations can result in serious damage to the lungs. Hydrofluoric acid has not been reported to be a human carcinogen.

Acute inhalation exposure to gaseous HF can cause severe respiratory damage in humans, including severe irritation and pulmonary edema. Irritation of the eyes, nose, and upper and lower respiratory tract, lacrimation, sore throat, cough, chest tightness, and wheezing have been reported. Damage to the lungs, liver, and kidneys has been observed in animals acutely exposed to HF by inhalation. Acute animal tests in rats, mice, guinea pigs, and monkeys have demonstrated HF to h ve moderate to high acute toxicity from inhalation exposure. EPA has not classified hyd ogen fluoride r hydrofluoric acid for carcinogenicity.

AFT

The ERPG values for HF are:

- ERPG-1: 2 ppm;
- ERPG-2: 20 ppm; and
- ERPG-3: 50 ppm.

The AEGL 30-minute values for HF are:

- AEGL-1: 1.0 ppm;
- AEGL-2: 34 ppm; and
- AEGL-3: 62 ppm.

3.1.3 Hydrogen Cyanide

HCN is a colorless, extremely poisonous gas above temperature at 26° C. It is a chemical asphyxiant as it interferes with the normal use of oxygen by nearly every organ of the body. Exposure to HCN can be rapidly fatal. It has whole-body (systemic) effects, particularly affecting those organ systems most sensitive to low oxygen levels: the central nervous system (brain), the cardiovascular system (heart and blood vessels), and the pulmonary system (lungs). It is used commercially for fumigation, electroplating, mining, chemical synthesis, and for producing synthetic fibers, plastics, dyes, and pesticides. HCN gas has a distinctive bitter almond odor (others describe a musty "old sneakers smell"), but a large proportion of people cannot detect it; the odor does not provide adequate warning of hazardous concentrations.

HCN is extremely toxic to humans. Acute inhalation exposure to 100 milligrams per cubic meter or more of HCN will cause death in humans. Acute exposure to lower concentrations (6 to 49 milligrams per cubic meter) of HCN will cause a variety of effects in humans, such as weakness, headache, nausea, increase rate of respiration, and eye and skin irritation.

Tests involving acute exposure of rats and mice have shown HCN to have extreme acute toxicity from inhalation exposure. EPA has not classified HCN or hydrocyanic acid for carcinogenicity.

The ERPG values for HCN are:

- ERPG-1: Not Appropriate;
- ERPG-2: 10 ppm; and
- ERPG-3: 25 ppm.

The AEGL 30-minute values for HCN are:

- AEGL-1: 2.5 ppm;
- AEGL-2: 10 ppm; and
- AEGL-3: 21 ppm.

3.1.4 Carbon Monoxide

CO is a poisonous, colorless, odorless, and tastel ss ga It is the product of the incomplete combustion of carbon-containing compounds, notably in inter al combus n engines. It consists of one carbon atom covalently bonded to one oxygen atom and is a gas room temperature. CO is a significantly toxic gas and is the most common type of fatal poisoning in m ny countries. Exposures can lead to significant toxicity of the central nervous system and heart.

When CO is not ventilated, it binds to hemoglobin, which is the principal oxygen-carrying compound in blood; this produces a compound known as carboxyhemoglobin. The traditional belief is that carbon monoxide toxicity arises from the formation of carboxyhemoglobin, which decreases the oxygen-carrying capacity of the blood and inhibits the transport, delivery, and use of oxygen by the body. The affinity between hemoglobin and CO is approximately 230 times stronger than the affinity between hemoglobin and oxygen, so hemoglobin binds to carbon monoxide in preference to oxygen. The resultant oxygen deprivation causes headache, dizziness, decreased pulse and respiratory rates, unconsciousness, and death. EPA has not classified CO for carcinogenicity.

The ERPG values for CO are:

- ERPG-1: 200 ppm;
- ERPG-2: 350 ppm; and
- ERPG-3: 500 ppm.

The AEGL 30-minute values for CO are:

AFT

- AEGL-1: N/A;
- AEGL-2: 150 ppm; and
- AEGL-3: 600 ppm.

3.2 ESTIMATED EMISSIONS

The modeled release assumes a constant emission rate in kilograms per second for a thermal runaway event lasting 30 minutes, after which it is assumed that the event would be controlled. For the purpose of evaluating potential risk to first responders in a controlled event, the DNV GL Report identified a 30-minute release rate as conservative, accounting for an average of emissions rate that is higher than the low-level emissions leading up to peak failure, and lower than the peak emissions. DNV GL's calculated average 30-minute release rate was identified in Table 2 of the DNV GL Report. The release rate was calculated per battery module. Fire testing showed that even small battery modules had residual mass remaining after a burn event, indicating that the number of cells involved in a fire event had a greater impact on total emissions than the size of an individual module.

The DNV GL Report "Considerations for ESS Fire Safety" (as Table 2 w thin publication), documents the average release rate (in kilograms per second) of the air toxics describe above for thermal runaway events and fires involving battery materials over a 30-minute period. The DNV GL Report evaluated several types and manufacturers of battery systems includ ng lithium ion batt ries. These values were used to estimate the toxics release rate of a credible fire vent Consistent with "Considerations for ESS Fire Safety", it was assumed that the event would involve 1 5 ingle battery racks (Table 3). As final manufacturer design and vendor has not been completed, a co servative estimate of 30 battery modules per rack was assumed.

AFT

Table 3. Emissio Release Rates

Materials	30-minute Release Rate (kg/s) for 1 Battery Module	30-minute Release Rate (kg/s) for 1.5 Battery RACKS (45 Modules)
HCl	2.36E-07	1.06E-05
HF	1.74E-07	7.83E-06
HCN	1.74E-07	7.83E-06
CO	2.00E-07	9.00E-06

kg/s = kilograms per second

SECTION 4.0 – Offsite Consequence Analysis

An offsite consequence analysis was conducted using emission rate estimates as described in Section 2.5 and the ALOHA model as described in the sections below.

4.1 METHODOLOGY

The EPA's "Risk Management Program Guidance for Offsite Consequence Analysis" and the CalARP both recommend conducting an offsite consequence analysis to represent release scenarios that are possible (although unlikely) to occur under a variety of weather and wind conditions to determine the distance to a toxic or flammable endpoint. Modeling assumptions and meteorological conditions that were used for conducting this offsite consequence analysis are specified in the California Code of Regulations, Title 19, Chapter 4.5, Article 2735.1 et seq.

The offsite consequences analysis was conducted based on the following conditions:

- The credible fire event involves the toxic release from 1.5 battery modules over a 30-minute period.
- Nighttime conditions - wind speed of 1.5 m/s (3.4 mph) from the west and atmospheric stability class F (very stable atmospheric conditions).
- Daytime conditions - wind speed of 3.9 m/s (8.7 mph) from the west and atmospheric stability class C (slightly unstable atmospheric conditions), representative of normal windy daytime conditions.
- Santa Ana wind conditions of 18 m/s (40 mph) from the east and atmospheric stability class
- Default release temperature of 77 degrees Fahrenheit (°F) for toxic gas releases.
- No ambient temperature inversion was included in the consequence analysis; although the San Diego County area does periodically experience inversions with mixing heights of less than 3,000 feet.
- Humidity of 50 percent, except during Santa Ana winds, where humidity is assumed to be 5 percent.
- Height of release – ground level.
- Surface roughness – rural; as determined based on the density and height of obstructions.
- Passive mitigation, such as the release inside of the container, was considered. Active mitigation measures, such as fire suppression, were also considered.

ALOHA uses location and elevation information to estimate sun angle using the location's latitude and longitude and the time of day and atmospheric pressure using the location's elevation. Site-specific project location data were used for input into ALOHA.

ALOHA allows the user to specify up to three toxic Levels of Concern. Modeling was conducted to identify maximum estimated distances to the ERPG-2 and AEGL-2. As ALOHA only automatically imports values for 60-minute AEGLs, the 30-minute AEGLS were input manually.

AFT

The offsite consequence analysis was conducted according to EPA's "Risk Management Program Guidance for Offsite Consequence Analysis" and guidance from the CalARP. Plume analysis and exposure impacts were conducted using USEPA's ALOHA hazards modeling program. Based on information about a chemical release, ALOHA estimates how quickly the chemical will escape from containment and form a hazardous gas cloud, and also how that release rate may change over time. ALOHA can then model how that hazardous gas cloud will travel downwind, including both neutrally buoyant and heavy gas dispersion. Additionally, if the chemical is flammable, ALOHA simulates pool fires, boiling liquid expanding vapor explosions, vapor cloud explosions, jet fires, and flammable gas clouds (where flash fires might occur). ALOHA evaluates different types of hazards (depending on the release scenario); toxicity, flammability, thermal radiation, and overpressure. ALOHA produces a threat zone estimate, which shows the area where a particular hazard (such as toxicity or thermal radiation) is predicted to exceed a specified level of concern at some time after the release begins. ALOHA is able to determine a threat zone under different weather and wind scenarios.

4.2 RESULTS

The nighttime release scenario is under more stable meteorological c nditions and represents the more conservative release scenario. A daytime release scenario and Santa na wind condition were also evaluated as an alternative release scenarios.

A toxic release from 1.5 battery racks (45 modules) was a sumed to be triggered by a fire event and result in a release of HCl, HF, HCN, and CO:

- Using nighttime meteorological conditions, modeling esults indicate that the distance to the toxic endpoint at ERPG-2 and AEGL-2 would e less than 17 yards (51 feet) with HCN's release controlling.
- Using daytime meteorological conditions, m deling results indicate that the distance to the toxic endpoint at ERPG-2 and AEGL-2 would be les than10.9 yards (33 feet), which is the minimum distance the model can produce.
- Under Santa Ana conditions, modeled only for the controlling pollutant, HCN, modeling results indicate that the distance to the toxic endpoint at ERPG-2 and AEGL-2 would be less than10.9 yards (33 feet), which is the minimum distance the model can produce.

The results of the offsite consequence analysis show that potential concentrations at the ERPG-2 or AEGL-2 thresholds may extend to a toxic endpoint distance of approximately 51 feet from the toxic release during the unlikely but credible fire event during the nighttime scenario and may require shelter in place and/or evacuation of receptors within this toxic endpoint distance. The first 30 feet are entirely within the project boundary. No schools or daycares are located within the potential impact area. The extent of the estimated maximum toxic endpoint is depicted in Figure 5.

This report has been peer reviewed by an independent third party and their verification letter is presented in Appendix B.

AFT

References

1. 2019 California Fire Code, [redacted]

2. California Accidental Release Prevention Program, Administering Agency Guidance, January 31, 2005, [redacted]

3. County of San Diego "Guidelines for Determining Significance, Hazardous Materials and Existing Contamination," July 30, 2007.

4. DNV GL, Considerations for ESS Fire Safety, February 9, 2017, [redacted]

5. DNV GL, Technical Guidance Note on Considerations for ESS ire Safety, 2019.

6. National Fire Protection Association, Hazard Assessm nt of Lithium Ion Battery Energy Storage Systems, February 26, 2016, [redacted]

7. National Fire Protection Association, Lith um n Batterie Hazard and Use Assessment - Phase III, November 2016, [redacted] t

8. New York Department of State, 2019 Energy Storage Supplement, September 2019.

9. U.S. Environmental Protection Agency, *Areal Location Hazardous Atmospheres Technical Documentation*, September 2016 [redacted]

10. U.S. Environmental Protection Agency, *Risk Management Program Guidance for Offsite Consequence Analysis*, March 2009 [redacted]

11. U.S. Environmental Protection Agency, *Acute Exposure Guideline Levels*, April 2020, [redacted]

12. UL 9540, Standard for Energy Storage Equipment and Systems. [redacted]

13. WRCC. (2018). ESCONDIDO, CALIFORNIA (042862). Retrieved from [redacted]

DRAFT

FIGURES

AFT

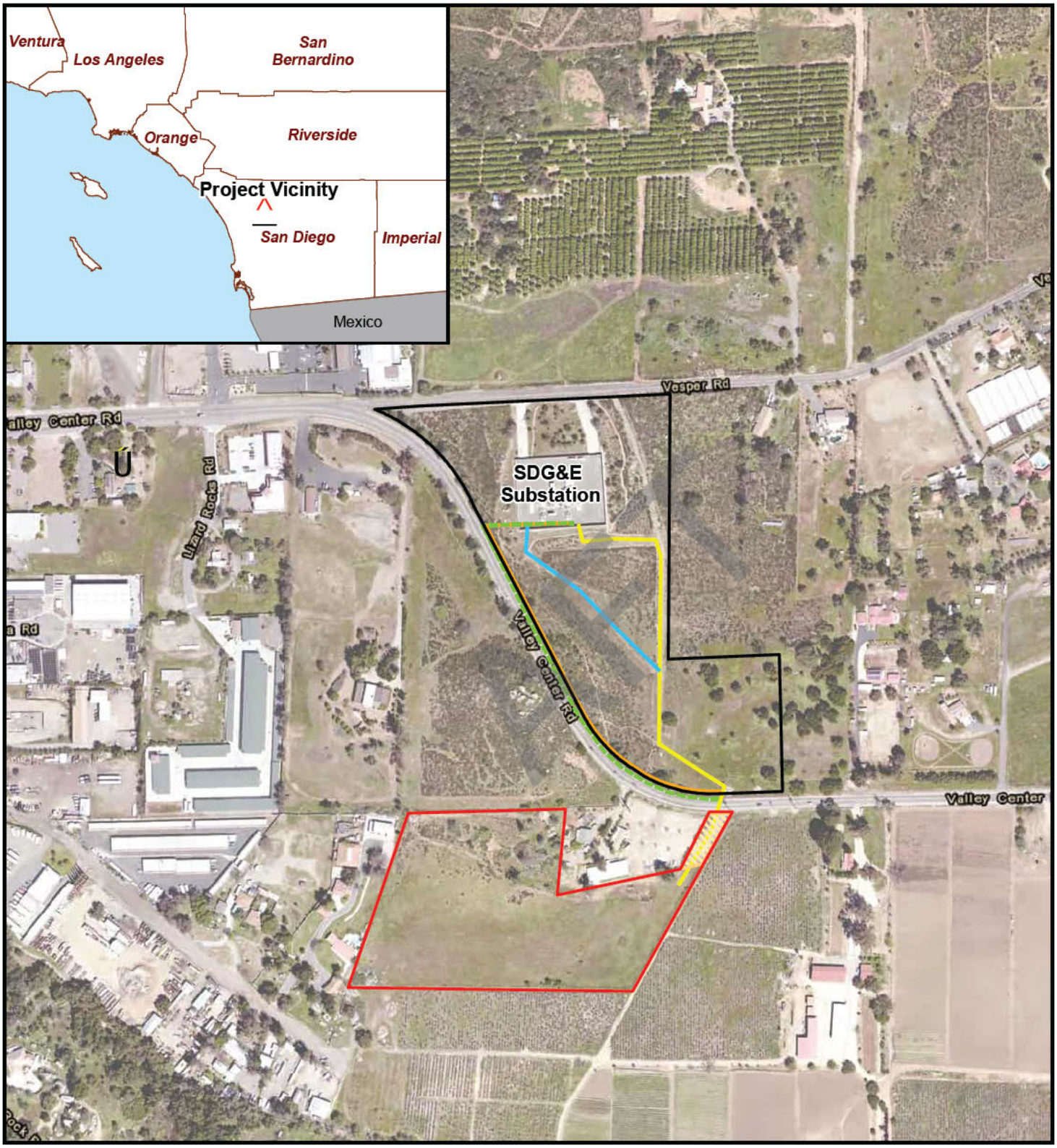


Figure 1
Valley Center Storage Project
Project Site

Name: 21206 PLAN Fig 1 Project Site.Mxd
Print Date: 4/28/2020, Author: pcarlos

CHAMBERS GROUP

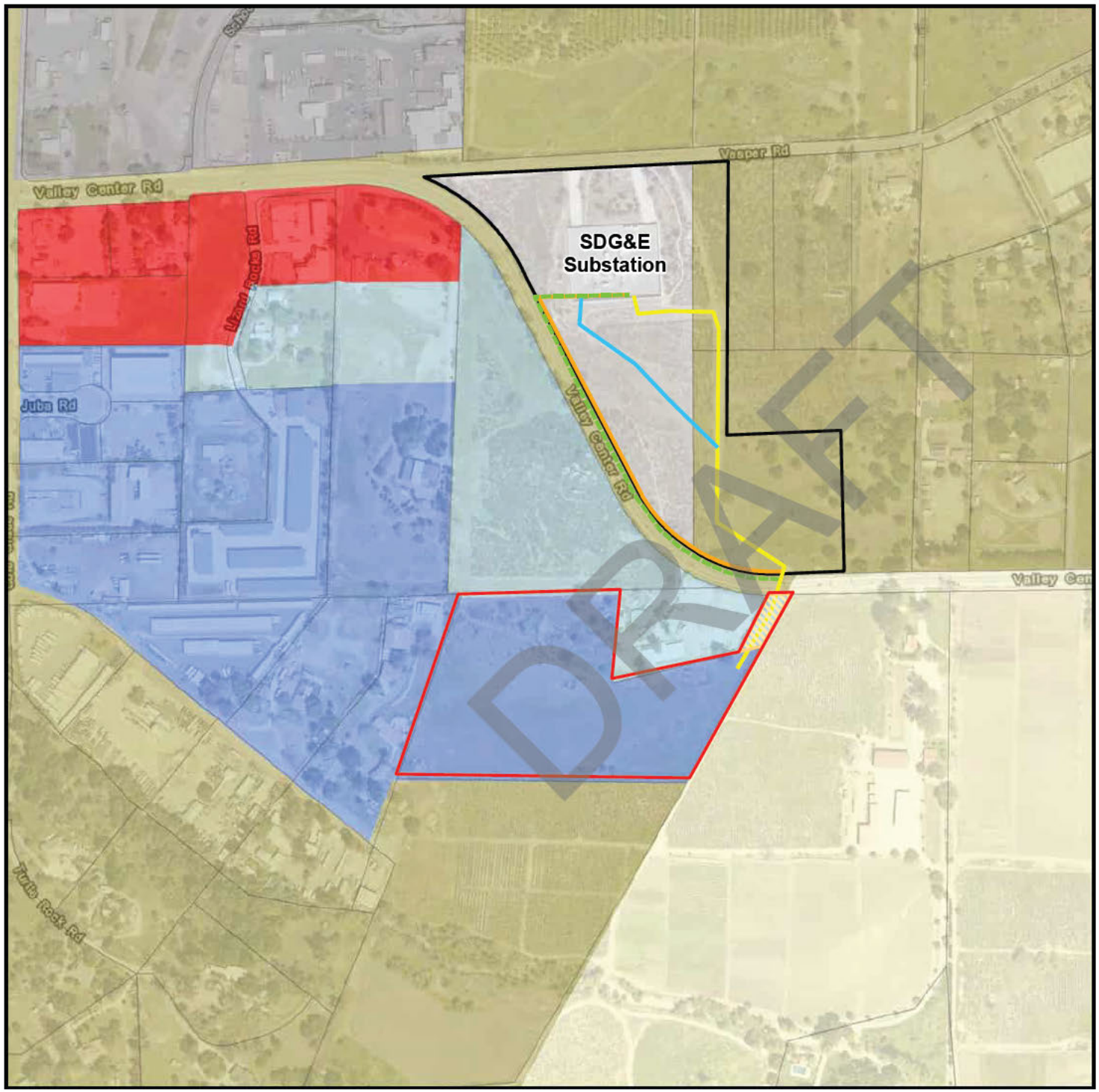


Figure 2
Valley Center Storage Project
Land Use Zoning

- Project Site
- SDG&E Property Boundary
- Private Access Easement

Preliminary Underground 69kV Alignment

- Option A
- Option B
- Option C
- Option D

Zoning Designation

- Semi-Rural Residential (SR-2)
- Semi-Rural Residential (SR-4)
- General Commercial
- Limited Impact Industrial
- Medium Impact Industrial
- Public/Semi-Public Facilities
- Public Agency Lands

0 150 300 600

Feet

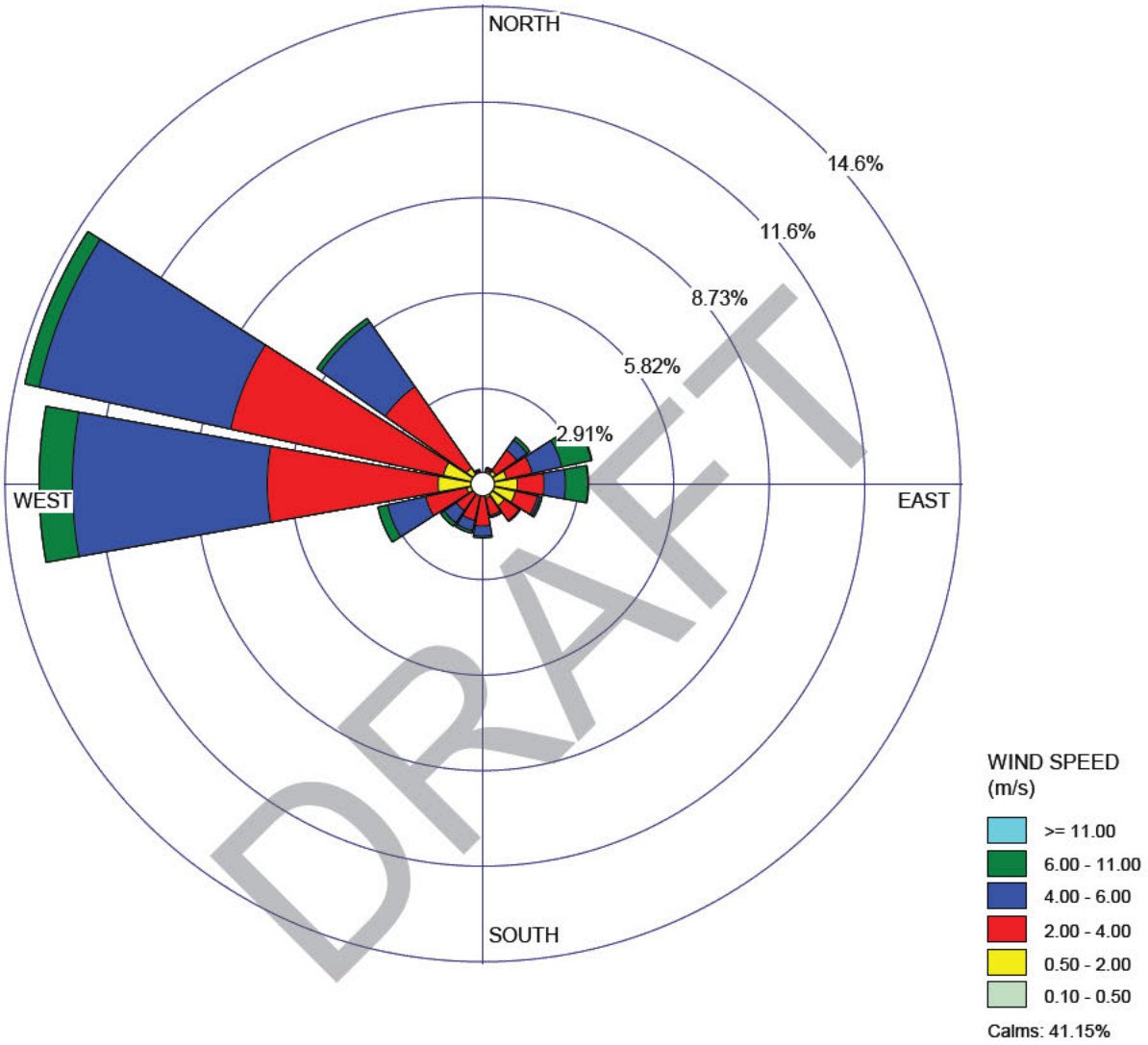
Name: 21206 PLAN Fig 2 Land Use Zoning.Mxd
Print Date: 4/28/2020, Author: pcarlos

CHAMBERS GROUP

W ND ROSE PLOT:

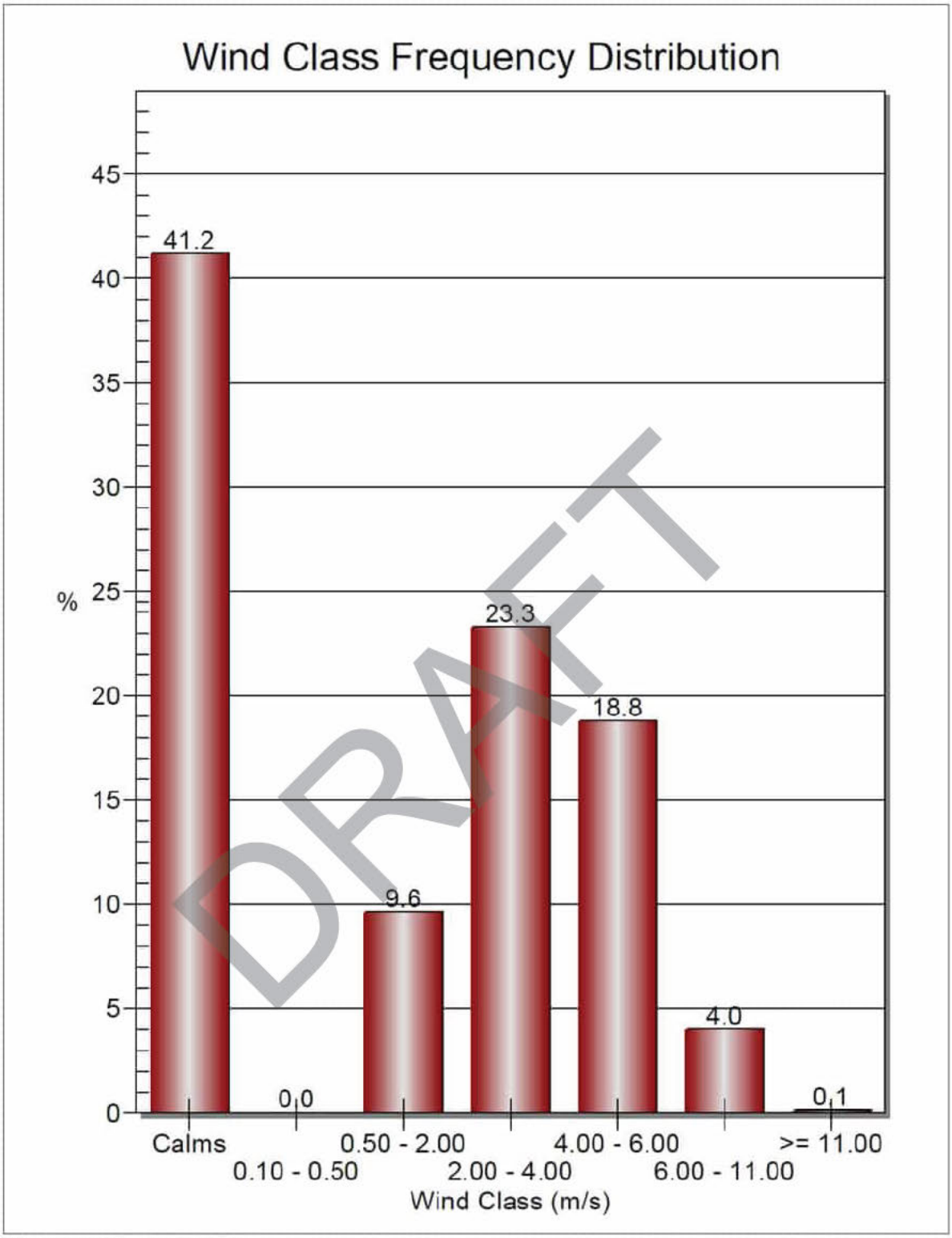
Windrose for Ramona Airport
2009-2014

DISPLAY:
Wind Speed
Direction (blowing from)



DRAFT

COMMENTS:	DATA PERIOD: **Start Date: 1/1/2009 - 00:00** **End Date: 1/2/2014 - 23:59**		
	CALM W NDS: **41.15%**	TOTAL COUNT: **42481 hrs.**	HALEY ALDRICH
	AVG. W ND SPEED: **2.19 m/s**	DATE: **3/27/2020**	PROJECT NO.:



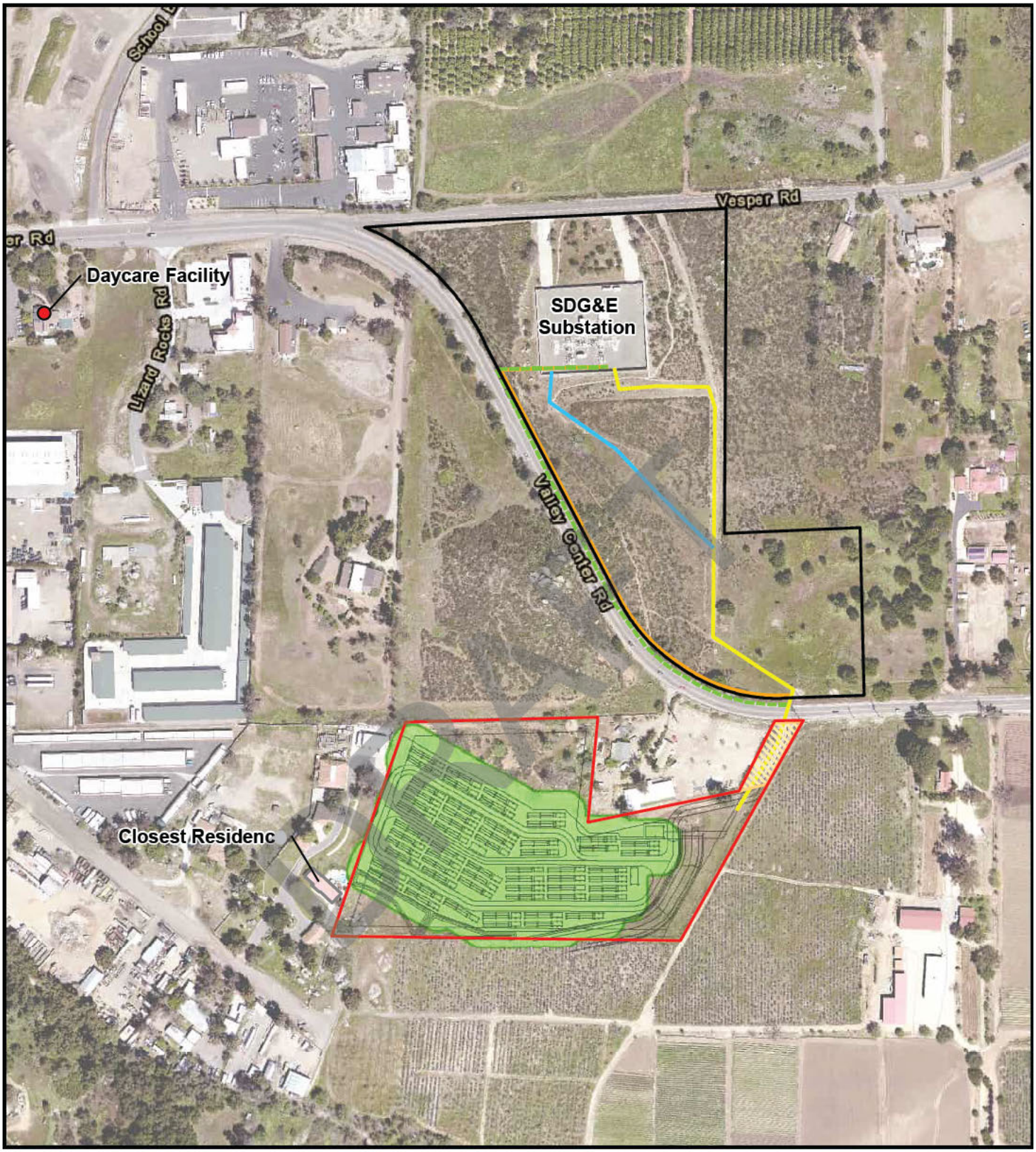
WRPLOT View 9.7.0 - Lakes Environmental Software

HALEY ALDRICH

Valley Center Battery Storage

Wind Class Frequency Distribution

FIGURE 4



Project Site
SDG&E Property Boundary
Private Access Easement
Estimated Maximum Toxic Endpoint (51 ft)

Preliminary Underground 69kV Alignment

Option A
Option B
Option C
Option D

0 100 200 400
Feet

Figure 5
Valley Center Storage Project
Estimated Maximum Toxic Endpoint

Representative of modeling results using nighttime meteorological conditions

Name 21206 PLAN Fig 1 Estimated Maximum Toxic Endpoint.Mxd
Print Date 6/12/2020, Author pcarlos

CHAMBERS GROUP

APPENDIX A

ALOHA Mod ling Files

DRAFT

```
SITE DATA:
  Location: VALLEY CENTER, CALIFORNIA
  Building Air Exchanges Per Hour: 0.85 (unsheltered single storied)
  Time: March 27, 2020  1212 hours PDT (user specified)

CHEMICAL DATA:
  Warning: HYDROGEN CHLORIDE can react with water and/or water vapor.  This
  can affect the evaporation rate and downwind dispersion.  ALOHA cannot
  accurately predict the air hazard if this substance comes in contact with
  water.
  Chemical Name: HYDROGEN CHLORIDE
  CAS Number: 7647-1-0                    Molecular Weight: 36.46 g/mol
  AEGL-1 (60 min): 1.8 ppm   AEGL-2 (60 min): 22 ppm   AEGL-3 (60 min): 100 ppm
  IDLH: 50 ppm
  Ambient Boiling Point: -122.7° F
  Vapor Pressure at Ambient Temperature: greater than 1 atm
  Ambient Saturation Concentration: 1,000,000 ppm or 100.0%

ATMOSPHERIC DATA: (MANUAL INPUT OF DATA)
  Wind: 3.9 meters/second from W at 3 meters
  Ground Roughness: open country          Cloud Cover: 5 tenths
  Air Temperature: 77° F                  Stability Class: C
  No Inversion Height                     R lative Humidity: 50%

SOURCE STRENGTH:
  Direct Source: 1.06e-5 kilograms/se
  Source Height: 0
  Release Duration: 30 minutes
  Release Rate: 0.0014 pounds/mi
  Total Amount Released: 0.042 pounds
  Note: This chemical may flash bo l and/ r result in two phase flow.

THREAT ZONE:
  Model Run: Gaussian
  Red   : less than 10 meters(10.9 yards) --- (20 ppm = ERPG-2)
  Note: Threat zone  as not drawn because effects of near-field patchiness
     make dispersion p edictions less reliable for short distances.
  Orange: less than 10 m ters(10.9 yards) --- (43 ppm)
  Note: Threat zone was n t drawn because effects of near-field patchiness
     make dispersion predictions less reliable for short distances.
```

DRAFT

SITE DATA:
Location: VALLEY CENTER, CALIFORNIA
Building Air Exchanges Per Hour: 0.38 (unsheltered single storied)
Time: June 8, 2020 0000 hours PDT (user specified)

CHEMICAL DATA:
Warning: HYDROGEN CHLORIDE can react with water and/or water vapor. This can affect the evaporation rate and downwind dispersion. ALOHA cannot accurately predict the air hazard if this substance comes in contact with water.
Chemical Name: HYDROGEN CHLORIDE
CAS Number: 7647-1-0 Molecular Weight: 36.46 g/mol
AEGL-1 (60 min): 1.8 ppm AEGL-2 (60 min): 22 ppm AEGL-3 (60 min): 100 ppm
IDLH: 50 ppm
Ambient Boiling Point: -122.7° F
Vapor Pressure at Ambient Temperature: greater than 1 atm
Ambient Saturation Concentration: 1,000,000 ppm or 100.0%

ATMOSPHERIC DATA: (MANUAL INPUT OF DATA)
Wind: 1.5 meters/second from W at 3 meters
Ground Roughness: open country Cloud Cover: 5 tenths
Air Temperature: 77° F Stability Class: F
No Inversion Height R lative Humidity: 50%

SOURCE STRENGTH:
Direct Source: 1.06e-5 kilograms/se
Source Height: 0
Release Duration: 30 minutes
Release Rate: 0.0014 pounds/mi
Total Amount Released: 0.042 pounds
Note: This chemical may flash bo l and/ r result in two phase flow.

THREAT ZONE:
Model Run: Gaussian
Red : 12 yards -- (20 pp = ERPG-2)
Note: Threat zone as not drawn because effects of near-field patchiness make dispersion p edictions less reliable for short distances.
Orange: less than 10 m ters(10.9 yards) --- (43 ppm)
Note: Threat zone was n t drawn because effects of near-field patchiness make dispersion predictions less reliable for short distances.

DRAFT

```
SITE DATA:
  Location: VALLEY CENTER, CALIFORNIA
  Building Air Exchanges Per Hour: 0.85 (unsheltered single storied)
  Time: March 27, 2020  1212 hours PDT (user specified)

CHEMICAL DATA:
  Warning: HYDROGEN FLUORIDE can react with water and/or water vapor.  This
  can affect the evaporation rate and downwind dispersion.  ALOHA cannot
  accurately predict the air hazard if this substance comes in contact with
  water.
  Chemical Name: HYDROGEN FLUORIDE
  CAS Number: 7664-39-3                    Molecular Weight: 20.01 g/mol
  AEGL-1 (60 min): 1 ppm   AEGL-2 (60 min): 24 ppm   AEGL-3 (60 min): 44 ppm
  IDLH: 30 ppm
  Ambient Boiling Point: 64.8° F
  Vapor Pressure at Ambient Temperature: greater than 1 atm
  Ambient Saturation Concentration: 1,000,000 ppm or 100.0%

ATMOSPHERIC DATA: (MANUAL INPUT OF DATA)
  Wind: 3.9 meters/second from W at 3 meters
  Ground Roughness: open country           Cloud Cover: 5 tenths
  Air Temperature: 77° F                   Stability Class: C
  No Inversion Height                      R lative Humidity: 50%

SOURCE STRENGTH:
  Direct Source: 7.83e-6 kilograms/se
  Source Height: 0
  Release Duration: 30 minutes
  Release Rate: 0.00104 pounds/m
  Total Amount Released: 0.031 pounds
  Note: This chemical may flash bo l and/ r result in two phase flow.
     Use both dispersion mod les  o i   stigate its potential behavior.

THREAT ZONE:
  Model Run: Gaussian
  Red   : less than  0 meters( 0.9 yards) --- (20 ppm = ERPG-2)
  Note: Threat zone wa  not drawn because effects of near-field patchiness
     make dispersion predictions less reliable for short distances.
  Orange: less than 10 mete s(10.9 yards) --- (34 ppm)
  Note: Threat zone was not drawn because effects of near-field patchiness
     make dispersion predictions less reliable for short distances.
```

DRAFT

```
SITE DATA:
  Location: VALLEY CENTER, CALIFORNIA
  Building Air Exchanges Per Hour: 0.38 (unsheltered single storied)
  Time: June 8, 2020  0000 hours PDT (user specified)

CHEMICAL DATA:
  Warning: HYDROGEN FLUORIDE can react with water and/or water vapor.  This
  can affect the evaporation rate and downwind dispersion.  ALOHA cannot
  accurately predict the air hazard if this substance comes in contact with
  water.
  Chemical Name: HYDROGEN FLUORIDE
  CAS Number: 7664-39-3                  Molecular Weight: 20.01 g/mol
  AEGL-1 (60 min): 1 ppm   AEGL-2 (60 min): 24 ppm   AEGL-3 (60 min): 44 ppm
  IDLH: 30 ppm
  Ambient Boiling Point: 64.8° F
  Vapor Pressure at Ambient Temperature: greater than 1 atm
  Ambient Saturation Concentration: 1,000,000 ppm or 100.0%

ATMOSPHERIC DATA: (MANUAL INPUT OF DATA)
  Wind: 1.5 meters/second from W at 3 meters
  Ground Roughness: open country         Cloud Cover: 5 tenths
  Air Temperature: 77° F                 Stability Class: F
  No Inversion Height                    R lative Humidity: 50%

SOURCE STRENGTH:
  Direct Source: 7.83e-6 kilograms/se
  Source Height: 0
  Release Duration: 30 minutes
  Release Rate: 0.00104 pounds/m
  Total Amount Released: 0.031 pounds
  Note: This chemical may flash bo l and/ r result in two phase flow.
     Use both dispersion mod les  o i   stigate its potential behavior.

THREAT ZONE:
  Model Run: Gaussian
  Red   : 14 yards - - (20 ppm = ERPG-2)
  Note: Threat zone wa  not drawn because effects of near-field patchiness
     make dispersion predictions less reliable for short distances.
  Orange: less than 10 mete s(10.9 yards) --- (34 ppm)
  Note: Threat zone was not drawn because effects of near-field patchiness
     make dispersion predictions less reliable for short distances.
```

DRAFT

```
SITE DATA:
  Location: VALLEY CENTER, CALIFORNIA
  Building Air Exchanges Per Hour: 0.85 (unsheltered single storied)
  Time: March 27, 2020  1212 hours PDT (user specified)

CHEMICAL DATA:
  Chemical Name: HYDROGEN CYANIDE
  CAS Number: 74-90-8                    Molecular Weight: 27.03 g/mol
  AEGL-1 (60 min): 2 ppm   AEGL-2 (60 min): 7.1 ppm   AEGL-3 (60 min): 15 ppm
  IDLH: 50 ppm       LEL: 56000 ppm      UEL: 400000 ppm
  Ambient Boiling Point: 75.8° F
  Vapor Pressure at Ambient Temperature: greater than 1 atm
  Ambient Saturation Concentration: 1,000,000 ppm or 100.0%

ATMOSPHERIC DATA: (MANUAL INPUT OF DATA)
  Wind: 3.9 meters/second from W at 3 meters
  Ground Roughness: open country         Cloud Cover: 5 tenths
  Air Temperature: 77° F                 Stability Class: C
  No Inversion Height                    Relative Humidity: 50%

SOURCE STRENGTH:
  Direct Source: 7.83e-6 kilograms/sec
  Source Height: 0
  Release Duration: 30 minutes
  Release Rate: 0.00104 pounds/min
  Total Amount Released: 0.031 pounds

THREAT ZONE:
  Model Run: Gaussian
  Red   : less than 10 meters(10.9 yards  --- (10 ppm = ERPG-2)
  Note: Threat zone was not drawn because effects of near-field patchiness
     make dispersion predict ons  ess  liable for short distances.
  Orange: less than 10 meters(  .9 yards) --- (10 ppm)
  Note: Threat zone was not draw  because effects of near-field patchiness
     make dispersion predicti ns less reliable for short distances.
```

DRAFT

```
SITE DATA:
  Location: VALLEY CENTER, CALIFORNIA
  Building Air Exchanges Per Hour: 0.38 (unsheltered single storied)
  Time: June 8, 2020  0000 hours PDT (user specified)

CHEMICAL DATA:
  Chemical Name: HYDROGEN CYANIDE
  CAS Number: 74-90-8                    Molecular Weight: 27.03 g/mol
  AEGL-1 (60 min): 2 ppm   AEGL-2 (60 min): 7.1 ppm   AEGL-3 (60 min): 15 ppm
  IDLH: 50 ppm       LEL: 56000 ppm      UEL: 400000 ppm
  Ambient Boiling Point: 75.8° F
  Vapor Pressure at Ambient Temperature: greater than 1 atm
  Ambient Saturation Concentration: 1,000,000 ppm or 100.0%

ATMOSPHERIC DATA: (MANUAL INPUT OF DATA)
  Wind: 1.5 meters/second from W at 3 meters
  Ground Roughness: open country         Cloud Cover: 5 tenths
  Air Temperature: 77° F                 Stability Class: F
  No Inversion Height                    Relative Humidity: 50%

SOURCE STRENGTH:
  Direct Source: 7.83e-6 kilograms/sec
  Source Height: 0
  Release Duration: 30 minutes
  Release Rate: 0.00104 pounds/min
  Total Amount Released: 0.031 pounds

THREAT ZONE:
  Model Run: Gaussian
  Red   : 17 yards --- (10 ppm = ERPG-2)
  Note: Threat zone was not drawn because effects of near-field patchiness
     make dispersion predict ons  ess   liable for short distances.
  Orange: 17 yards --- (10 ppm
  Note: Threat zone was not draw  because effects of near-field patchiness
     make dispersion predicti ns less reliable for short distances.
```

DRAFT

```
SITE DATA:
  Location: VALLEY CENTER, CALIFORNIA
  Building Air Exchanges Per Hour: 3.77 (unsheltered single storied)
  Time: June 8, 2020  1200 hours PDT (user specified)

CHEMICAL DATA:
  Chemical Name: HYDROGEN CYANIDE
  CAS Number: 74-90-8                    Molecular Weight: 27.03 g/mol
  AEGL-1 (60 min): 2 ppm   AEGL-2 (60 min): 7.1 ppm   AEGL-3 (60 min): 15 ppm
  IDLH: 50 ppm       LEL: 56000 ppm      UEL: 400000 ppm
  Ambient Boiling Point: 75.8° F
  Vapor Pressure at Ambient Temperature: greater than 1 atm
  Ambient Saturation Concentration: 1,000,000 ppm or 100.0%

ATMOSPHERIC DATA: (MANUAL INPUT OF DATA)
  Wind: 18 meters/second from E at 3 meters
  Ground Roughness: open country         Cloud Cover: 0 tenths
  Air Temperature: 77° F                 Stability  lass: C
  No Inversion Height                    Relative Humidity: 5%

SOURCE STRENGTH:
  Direct Source: 7.83e-6 kilograms/sec
  Source Height: 0
  Release Duration: 30 minutes
  Release Rate: 0.00104 pounds/min
  Total Amount Released: 0.031 pounds

THREAT ZONE:
  Model Run: Gaussian
  Red   : less than 10 meters(10.9 yards  --- (10 ppm = ERPG-2)
  Note: Threat zone was not drawn because effects of near-field patchiness
     make dispersion predict ons  ess   liable for short distances.
  Orange: less than 10 meters(  .9 yards) --- (10 ppm)
  Note: Threat zone was not draw  because effects of near-field patchiness
     make dispersion predicti ns less reliable for short distances.
```

DRAFT

```
SITE DATA:
  Location: VALLEY CENTER, CALIFORNIA
  Building Air Exchanges Per Hour: 0.85 (unsheltered single storied)
  Time: March 27, 2020  1212 hours PDT (user specified)

CHEMICAL DATA:
  Chemical Name: CARBON MONOXIDE
  CAS Number: 630-8-0                    Molecular Weight: 28.01 g/mol
  AEGL-1 (60 min): N/A   AEGL-2 (60 min): 83 ppm   AEGL-3 (60 min): 330 ppm
  IDLH: 1200 ppm     LEL: 125000 ppm     UEL: 742000 ppm
  Ambient Boiling Point: -313.5° F
  Vapor Pressure at Ambient Temperature: greater than 1 atm
  Ambient Saturation Concentration: 1,000,000 ppm or 100.0%

ATMOSPHERIC DATA: (MANUAL INPUT OF DATA)
  Wind: 3.9 meters/second from W at 3 meters
  Ground Roughness: open country         Cloud Cover: 5 tenths
  Air Temperature: 77° F                 Stability  lass: C
  No Inversion Height                    Relative Humidity: 50%

SOURCE STRENGTH:
  Direct Source: 9e-6 kilograms/sec      Source Height: 0
  Release Duration: 30 minutes
  Release Rate: 0.00119 pounds/min
  Total Amount Released: 0.036 pounds
  Note: This chemical may flash boil  nd/or res lt in two phase flow.
     Use both dispersion modules to invest gate its potential behavior.

THREAT ZONE:
  Model Run: Gaussian
  Red   : less than 10 meters(10.9 yards) --- (350 ppm = ERPG-2)
  Note: Threat zone was not  rawn bec   e effects of near-field patchiness
     make dispersion predictio  less reliable for short distances.
  Orange: less than 10 mete s(10 9 yards) --- (150 ppm)
  Note: Threat zone was not d awn because effects of near-field patchiness
     make dispersion predictions less reliable for short distances.
```

DRAFT

```
SITE DATA:
  Location: VALLEY CENTER, CALIFORNIA
  Building Air Exchanges Per Hour: 0.38 (unsheltered single storied)
  Time: June 8, 2020  0000 hours PDT (user specified)

CHEMICAL DATA:
  Chemical Name: CARBON MONOXIDE
  CAS Number: 630-8-0                    Molecular Weight: 28.01 g/mol
  AEGL-1 (60 min): N/A   AEGL-2 (60 min): 83 ppm   AEGL-3 (60 min): 330 ppm
  IDLH: 1200 ppm     LEL: 125000 ppm     UEL: 742000 ppm
  Ambient Boiling Point: -313.5° F
  Vapor Pressure at Ambient Temperature: greater than 1 atm
  Ambient Saturation Concentration: 1,000,000 ppm or 100.0%

ATMOSPHERIC DATA: (MANUAL INPUT OF DATA)
  Wind: 1.5 meters/second from W at 3 meters
  Ground Roughness: open country         Cloud Cover: 5 tenths
  Air Temperature: 77° F                 Stability  lass: F
  No Inversion Height                    Relative Humidity: 50%

SOURCE STRENGTH:
  Direct Source: 9e-6 kilograms/sec      Source Height: 0
  Release Duration: 30 minutes
  Release Rate: 0.00119 pounds/min
  Total Amount Released: 0.036 pounds
  Note: This chemical may flash boil  nd/or res lt in two phase flow.
     Use both dispersion modules to invest gate its potential behavior.

THREAT ZONE:
  Model Run: Gaussian
  Red   : less than 10 meters(10.9 yards) --- (350 ppm = ERPG-2)
  Note: Threat zone was not  rawn bec   e effects of near-field patchiness
     make dispersion predictio  less reliable for short distances.
  Orange: less than 10 mete s(10 9 yards) --- (150 ppm)
  Note: Threat zone was not d awn because effects of near-field patchiness
     make dispersion predictions less reliable for short distances.
```

DRAFT

APPENDIX **B**

Peer Re iew

DRAFT

Stantec

Memo

To:	Robert Kallin	From:	Eric Clark, P.E.
	[redacted]		[redacted]
File:	185804813	Date:	June 18, 2020

Reference: Stantec Review of Hazard Consequences Analysis Valley Center Storage Project

Mr. Kallin:

Haley & Aldrich requested that Stantec provide peer review on the methods and findings of the Hazard Consequences Analysis for the Valley Center Storage Project. Stantec reviewed a draft of the report dated 18 June 2020 and provided comments. My comments have been satisfactorily addressed in the final report dated 19 June 2020.

Stantec Consulting Services Inc.

[redacted]

Eric Clark P.E.
Project Engineer
[redacted]

DRAFT

Annex 10 Battery separator materials and cathode coating materials

MOLECULES

MDPI

Review

A Review on Lithium-Ion Battery Separators towards Enhanced Safety Performances and Modelling Approaches

Ao Li [1], Anthony Chun Yin Yuen [1,*], Wei Wang [1], Ivan Miguel De Cachinho Cordeiro [1], Cheng Wang [1], Timothy Bo Yuan Chen [1], Jin Zhang [1], Qing Nian Chan [1] and Guan Heng Yeoh [1,2]

[1] School of Mechanical and Manufacturing Engineering, University of New South Wales, Sydney, NSW 2052, Australia [redacted]

[2] Australian Nuclear Science and Technology Organization (ANSTO), Locked Bag 2001, Kirrawee DC, NSW 2232, Australia

* Correspondence: [redacted]

Abstract: In recent years, the applications of lithium-ion batteries have emerged promptly owing to its widespread use in portable electronics and electric vehicles. Nevertheless, the safety of the battery systems has always been a global concern for the end-users. The separator is an indispensable part of lithium-ion batteries since it functions as a physical barrier for the electrode as well as an electrolyte reservoir for ionic transport. The properties of separators have direct influences on the performance of lithium-ion batteries, therefore the separators play an important role in the battery safety issue. With the rapid developments of applied materials, there have been extensive efforts to utilize these new materials as battery separators with enhanced electrical, fire, and explosion prevention performances. In this review, we aim to deliver an overview of recent advancements in numerical models on battery separators. Moreover, we summarize the physical properties of separators and benchmark selective key performance indicators. A broad picture of recent simulation studies on separators is given and a brief outlook for the future directions is also proposed.

Keywords: lithium-ion battery; separator; numerical modelling; battery safety

check for updates

Citation: Li, A.; Yuen, A.C.Y.; Wang, W.; De Cachinho Cordeiro, I.M.; Wang, C.; Chen, T.B.Y.; Zhang, J.; Chan, Q N.; Yeoh, G.H. A Review on Lithium-Ion Battery Separators towards Enhanced Safety Performances and Modelling Approaches. *Molecules* **2021**, *26*, 478. [redacted]

Academic Editor: Gaëlle Fontaine
Received: 14 December 2020
Accepted: 14 January 2021
Published: 18 January 2021

Publisher's Note: MDPI stays neutral with regard to jurisdictional claims in published maps and institutional affiliations.

Copyright: © 2021 by the authors. Licensee MDPI, Basel, Switzerland. This article is an open access article distributed under the terms and conditions of the Creative Commons Attribution (CC BY) license [redacted]

1. Introduction

Pioneered by Yoshino in 1985 [1,2], lithium-ion (Li-ion) batteries have been commercialized and used ever since in the industry as an alternative source of energy. It is usually applied as an energy storage reservoir for renewable energies and commonly used in portable electronics and electric vehicles. Nonetheless, a Li-ion battery is less thermally stable in comparison with other battery systems. This has caused a significant amount of battery fires in recent years, which occurred in mobile phones, electric vehicles, and airplanes [3–6]. The Li-ion battery separator is one of the crucial factors affecting fire safety performance since it directly contributes to the thermal stability of the entire battery system.

As one of the most important components in Li-ion batteries, the separator is placed between the anode and cathode [7]. The schematic diagram about a common separator applied in Li-ion batteries is shown in Figure 1, with the function of preventing physical contact between electrodes while serving as the electrolyte reservoir to enable ionic transport. There are no direct cell reactions in the separator, but the structure and properties of the separator play an essential role in determining the battery performance, including cycle life, safety, energy density, and power density, through influencing the cell kinetics [8]. A wide variety of factors should be considered while selecting appropriate separators for use in Li-ion batteries. Table 1 summarizes the general requirements that should be considered for Li-ion battery separators, and the detailed discussion has been provided

by previous studies, such as development of membrane separators by Lee et al. [8], production process of separators by Deimede et al. [9], characterization and performance evaluation of separators by Lagadec et al. [10], and so on. These early reviews focused on the characterization methods for separator properties and manufacturing techniques for separators through experimental methods. Moreover, the application of the separator increases electrical resistance and takes up limited space inside the battery, which has a negative impact on battery performance. Therefore, reasonable utilization of a separator is of vital importance to improving the battery performance, which includes energy density, cycle life, power density, and fire safety.

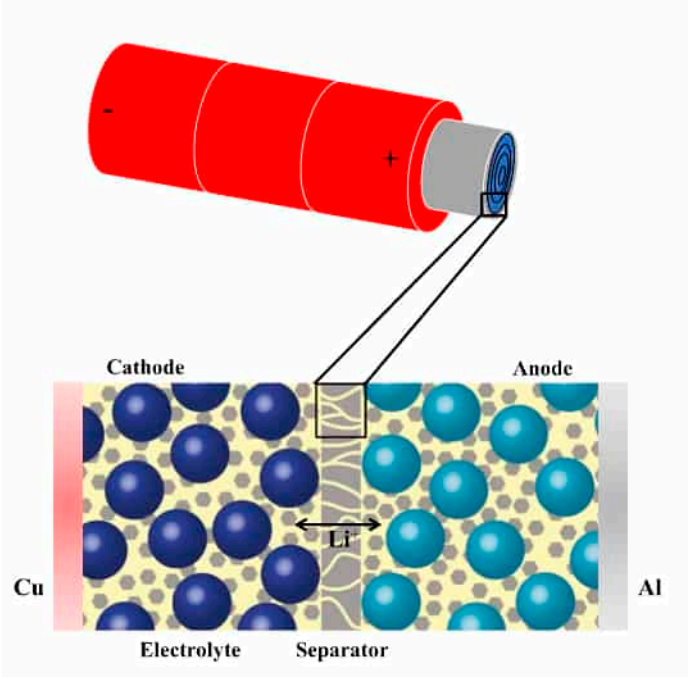


Figure 1. Schematic image of a separator in cylindrical Li-ion battery cell and a zoomed-in cross-section of the layered structure.

Table 1. General requirements for separators used in Li-ion batteries [8].

Parameter	Requirement
Chemical and electrochemical stabilities	Stable for a long period of time
Wettability	Wet out quickly and completely
Mechanical property	>1000 kg·cm^{-1} (98.06 MPa)
Thickness	20–25 μm
Pore size	<1 μm
Porosity	40–60%
Permeability (Gurley)	<0.025 s·μm^{-1}
Dimensional stability	No curl up and lay flat
Thermal stability	<5% shrinkage after 60 min at 90 °C
Shutdown	Effectively shut down the battery at elevated temperatures

In view of battery safety, the separator must be able to act as a blocking interface between the electrodes when an internal short circuit occurs, so that the thermal runaway is avoided [11]. Chemical and thermal stability, as well as shutdown function at the set temperature, should be the requirement for the separator. Considering the material price, current technology, and the trade-off relationship of the above properties, a comprehensive evaluation of the separator properties is required for separator selection. In order to improve the performance of separators and enhance the safety of Li-ion batteries, researchers have thus performed a lot of research work in recent years [12–14]. Furthermore, numerical modelling on the design and test of separators for improving battery abuse tolerance and performance

is deemed a practical compromise in optimizing the separator in future battery systems. Compared with the experimental investigation on separators, numerical modelling is treated as an efficient and economic tool for the study of separators. Both the separator material properties and the various performances of the separator are able to be simulated and predicted by numerical models. In this paper, the current numerical studies of separators will be reviewed in terms of mathematical models, finite element analysis (FEA), and computational fluid dynamic (CFD) models, and molecular dynamic (MD) models. From the perspective of numerical study, we describe the separator performance based on its influence on the battery performance, including microstructure of separators, stress analysis for the separators, thermal and ion transport of separators, as well as degradation process of separators. Moreover, the relationship between separator properties and battery safety will be discussed based on the separator shutdown and separator breakdown. Based on this review, future research directions on the Li-ion battery separators will be discussed in detail.

2. Numerical Study of Separators

Separators must be chemically and electrochemically stable to the electrolyte and electrode materials in Li-ion batteries since the separator itself does not participate in any cell reactions. As a critical component inside Li-ion batteries under strongly oxidizing and reducing conditions when the battery is fully discharged and charged, separators should also be mechanically strong to withstand the high tension during the battery assembly operation. In terms of the properties and performances of the separator, related numerical studies of battery fire safety can be divided into separator shutdown and separator breakdown, which are reviewed in this section.

2.1. Numerical Methods

With the development of computer science, numerical simulations are gradually applied in many assessments of separator safety designs. Compared to standard experiments, numerical simulation validates experiment results with less physical resources and also reveals in-depth key performance parameters including temperature, pressure, electrochemical properties. Furthermore, we are able to visualize the battery system internally to effectively diagnose the problems that may lead to potential battery failures. The development of numerical battery models has facilitated better understanding of the underlying principles of the battery circuit and its associated influence towards the ambient environment. Figure 2 summarizes the reviewed numerical studies in this paper.

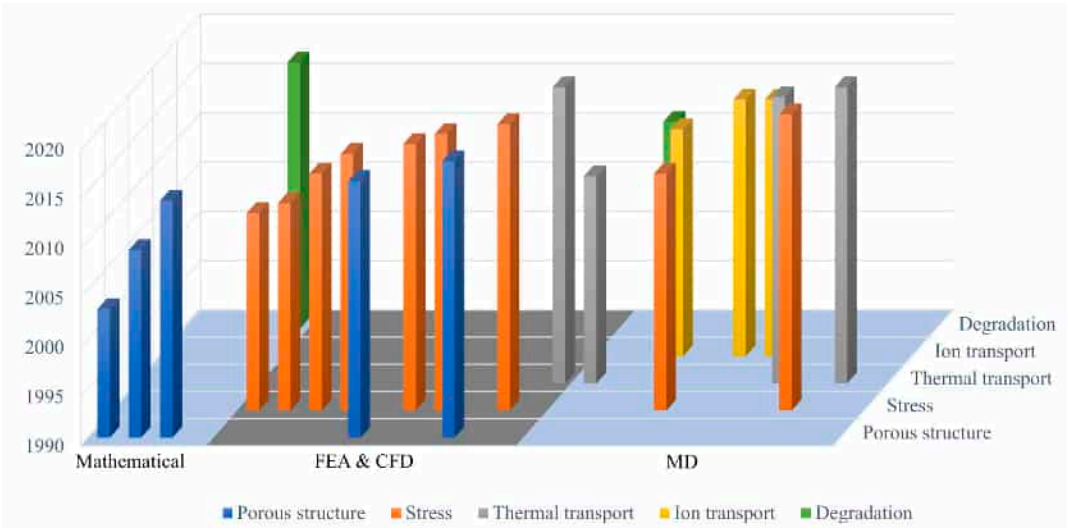


Figure 2. Summary of the reviewed papers for separators categorized by numerical methods and performances.

Mathematical models have been widely used in the battery property investigation and battery working procedure [15–17]. The development of a detailed mathematical model

is important to design and optimize the batteries. Simulation results provide intuitive data on the performance of the battery. A suitable mathematical model can describe a few parameters which are not known experimentally and regulate parameter adjustment. For example, the direct experimental data for tortuosity or liquid-phase transport resistance is lacking, which can be simulated from mathematical models [18,19].

Finite Element Analysis (FEA) theories and methods originate from the need to solve complex elasticity and structural analysis problems in engineering [20]. This method has been developed and applied in studying the mechanical properties, and many FEA packages such as ABAQUS, LS-DYNA, RADIOSS were used to model the material structure. Computation fluid dynamics (CFD) is a practical tool to study different thermal fluid dynamic parameters and simulate multiple physics fields [21–23], and CFD makes it possible to use the equations governing a fluid motion for an extensive range of complex situations, providing both insight and quantitative predictions. CFD simulation can provide detailed information about the electrical and thermal field inside the battery that is often difficult to be assessed by experimental means. Model-based investigations promote theoretical understanding of battery physics beyond what is possible from experiments only.

Molecular dynamics (MD) simulations have been applied to understand the properties at the molecular-level and design chemical structures with high performance. There are variations of MD simulation models utilizing different chemical force-field based on their characterizing phenomena, for instance, pyrolysis [24], nucleation [25], material thermal/electrical properties [26], and so on. Moreover, MD simulations are used to predict the chemical interactions between different materials and understand numerous membrane properties. Table 2 summarized the numerical studies associated with separators, which are applied with numerical simulations, including mathematical models, FEA and CFD simulations, MD simulations, and so on.

Table 2. The summary of the reviewed numerical studies for separators with model parameters.

Numerical Method	Model Parameters	Year	Ref
Mathematical model	Bruggeman exponent α	2003	[27]
	Tortuosity	2009	[19]
	Distance map, spatial distribution map, and histogram	2014	[28]
	Capacity loss, temperatures, and SOC	2017	[29]
FEA and CFD	Packing pattern, thickness variation, stress, and viscoelastic relaxation	2010	[30]
	Stress distribution, thermal effect, friction, particle radius, separator thickness	2011	[31]
	Principal stresses and Von Mises stress	2014	[32]
	Stress-strain curves and force-displacement curves	2016	[33]
	Porosity ε, tortuosity τ, and effective transport coefficient δ	2016	[34]
	Stress-strain curves, deformed shapes, and pores diameter	2017	[35]
	Strain, stress, node angle, voltage drop, and C-rate	2018	[36]
	Porosity, TP tortuosity, separator thickness, and connectivity density	2018	[37]
	Stress-strain curves	2019	[38]
	Thickness, porosity, energy density, heat generation rate, temperature, thermal conductivity, and heat capacity	2020	[39]
MD	Tip temperature, current density, and tip aspect ratio	2011	[40]
	Li density, SEI thickness, component ratio	2011	[41]
	Free energy, radial distribution functions, and proton transfer coordinate	2013	[42]
	Young's modulus and density	2014	[43]
	Proton concentration (i.e., C_{H+})	2016	[44]
	Proton conductivity and ion exchange capacity value	2016	[45]
	Temperature, density, heat flux, and thermal conductivity	2019	[46]
	Young's modulus	2020	[47]
	Interfacial thermal conductance	2020	[48]

2.2. Separator Shutdown

As shown in Figure 1, the location of the separator decides its primary function is to separate the anode and the cathode. The mechanical properties of separators are therefore very important for maintaining separation and Li-ion battery safety. Polyethylene (PE), polypropylene (PP), and PE/PP separators with pore sizes in the range of micrometres have been commercialized and widely used in Li-ion battery technology [49]. These microporous separators play a protective role during cell abuse. For example, if the temperature of the battery cell rises abnormally, separator shutdown occurs, which indicates that separators can provide a margin of safety to the device instead of leading to thermal runaway caused by the direct contact of electrodes. Numerical simulations can be carried out to study the microstructure and mechanical properties of the separator and to predict battery safety.

2.2.1. Porous Structure

Microporous membranes are normally characterized by pore sizes in the micrometre scale and are mainly manufactured based on polyolefin materials, such as PE, PP, and their blends such as PE–PP, as they afford both excellent chemical stability and mechanical properties. High-density polyethylene (HDPE) and ultrahigh molecular polyethylene (UHMWPE) are also used for preparing microporous membranes [50]. Therefore, numerical study as a simplified analysis has been employed to evaluate the effect of separators in practice [16]. In mathematical modelling, the following empirical equation has been widely used.

$$R_s = \varepsilon^{-\alpha} \cdot R_0 \quad (1)$$

where R_s is the resistance of the separator filled with liquid electrolyte, R_0 is the resistance of the native liquid electrolyte, ε is the void volume fraction in a separator, and α is the Bruggeman exponent. Separator morphology plays an important role in battery design and battery safety; therefore, numerical studies can provide better justification for the morphological parameters of separators for design and optimization.

Patel et al. [27] demonstrated models of porous networks to investigate the influence of particle shape and overall porosity on the liquid phase conductivity inside electrodes or separators used for Li-ion batteries. These models demonstrate that for batteries with high-rate performance, spherical or slightly prolate ellipsoidal particles should be preferred. Porous networks based on other particle morphologies however increase the tortuous path for ionic conductivity and result in either a significant increase of the exponent α, or a complete deviation from the power law.

Thorat et al. [19] applied a mathematical model for an empirical relationship between porosity and the tortuosity of the porous structures. They concluded that the tortuosity-dependent mass transport resistance in porous separators and electrodes is significantly higher than that predicted by the often-used Bruggeman relationship. Moreover, Chen-Wiegart et al. [28] proposed a distance propagation method for calculating tortuosity with relatively low computation time from three-dimensional (3D) tomographic data.

Lagadec et al. [34] built an electrolyte-soaked separator model and studied the influences of the separator microstructure on the battery performance. The porosity ε and tortuosity τ of the polyethylene separators directly influence the transport properties (the concentration-dependent electrolyte D_l and the concentration-dependent electrolyte σ_l, calculated according to Nyman et al. [51]). The electrolyte conductivity decreased with the separator microstructure, and the potential drop can be thereby increased across the electrolyte-soaked separator. Based on their simulations, it is clearly illustrated that increasing the electrolyte conductivity and the transference number in separator membranes can improve the Li-ion battery performance, particularly at high current rates. Lagadec et al. [37] delivered an analysis of tomographic data of commercial separators. They demonstrated the extent to which Li-ion concentration gradients can be induced or smoothed by the separator structure. This is linked to the pore space connectivity, i.e., a parameter that can be determined by topological or network-based analysis of separators.

2.2.2. Stress Analysis

It is well recognized by the Li-ion battery community that stress plays an essential role in the performance of the separator. To enhance the battery separator's performance, the stresses upon the separator in situ must be fully understood. Young's modulus, which is a physical quantity parameter evaluating the anti-deformability of elastic materials subjected to external force, is applied to evaluate the mechanical performance of separators. In view of battery safety for Li-ion batteries, a larger elastic modulus enables the separator to sustain internal or external pressure and local stress. In order to evaluate the intercalation and thermal mismatch induced stresses in the separator, multi-scale multi-physics models have been proposed and developed [30,31,52]. Testing the mechanical properties of a separator in situ in a battery is one of the tasks in improving the performance of battery separators [53]. For an isotropic material, the mechanical stress has a constitutive relationship for the strain, which is given as [30]:

$$\varepsilon_{ij} = \frac{1}{E}\left((1+\nu)\sigma_{ij} - \nu\sigma_{kk}\delta_{ij}\right) \quad (2)$$

where ε_{ij} is the strain component, E is Young's modulus, ν is the Poisson's ratio of the material, and δ_{ij} is the Dirac delta function. Moreover, with the understanding of the mechanical properties of separators, battery safety performance can be estimated and optimized. Table 3 summarizes the numerical stress analysis results in this section.

Table 3. Stress analysis summary for separators used in Li-ion batteries.

Materials	Young's Modulus (GPa)	Poisson's Ratio	Average Strain (%)	Ref.
Polyolefin Poly(vinylidene fluoride) (PVDF)	0.2 0.05	0.35	−0.14 −0.035	[30]
A homogeneous solid medium	0.5	0.35	−0.40	[31]
PP separator Celgard 2400	0.1	-	-	[32]
PE microstructure PP microstructure	1.2 1.5	0	−0.40	[36]
PP	In vacuum/In DMC Crystalline fiber: 43.4/46.5 Infinitely long chain fiber: 0.66/0.07 Finite chain fiber: 0.29/0.01	-	-	[43]
Cellulose/lignin	Dry/Wet Pure cellu: 3.38/2.50 Lignin 2.5%: 3.90/3.58 Lignin 5%: 4.10/3.25 Lignin 7.5%: 4.23/2.98 Lignin 10%: 4.78/2.88	-	-	[47]

Xiao et al. [30] developed a multi-physics, multi-scale model of a lithium-ion battery cell by using COMSOL. Their simulation results illustrate that the stress is affected by Young's modulus of the separator, electrode particle size, separator wrapping patterns, and the pressure of the cell, and the local strain at the indented areas was much higher than the nominal strain of the separator.

Shi et al. [31] investigated the influences of some adjustable design parameters, including the effective friction, electrode particle radii, and thickness of the separator, on the stresses in the separator. It is concluded that the maximum Von Mises stress increased as increasing the thickness of the separator and the effective frictions between the separator and its adjacent electrodes. The stress analysis showed that the maximum stress in the separator always emerged at the area around the inner corner of the separator. In this case, the cell voltage at 4.2 V was assumed to be fully charged. The schematic of the structure represents the macro-scale 2D model with separator thickness of 25 μm and

anode thickness of 45 µm. When the Li-ion battery was fully charged, the maximum stress was wrapped around the edge of the anode, as shown in Figure 3. In addition, with the same volume fractions of active materials, the particle radii had a negligible effect on the stress in the separator.

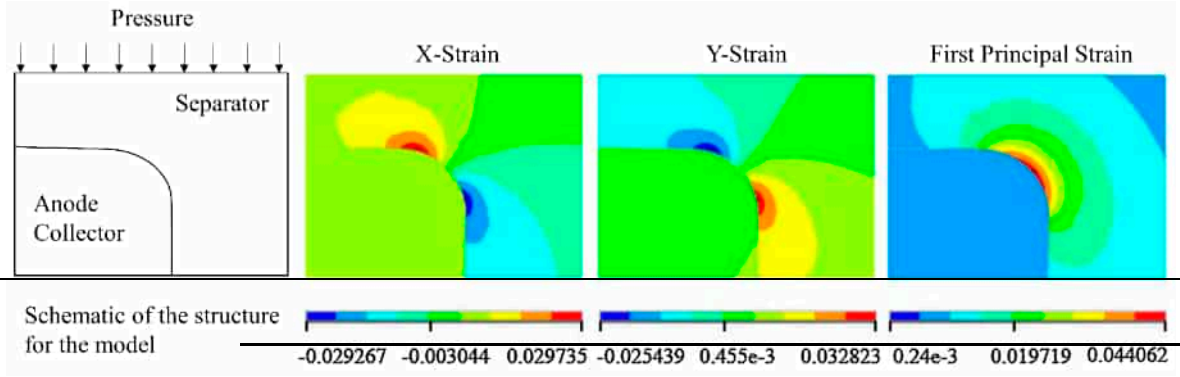


Figure 3. Schematic and contours of strain [m m^{-1}] components in the separator near the corner [31].

A multi-physics model was built by Wu et al. [32] to analyze the stress in the PP separator via COMSOL. The results showed that the effects of the intercalation and thermal expansion are coupled summations and hence must be considered concurrently. The type ~~of the constitutive relationship of the separator affects the stress values. The calculated~~ stresses in the separator with a viscoelastic material law were about a half of that estimated with an elastic law.

A finite element model of PE separator was developed in LSDYNA by Zhang et al. [33] based on the uniaxial tensile and through-thickness compression test data. The model succeeded in predicting the response of PE separator under punch tests with different sizes of punch head, including 1 inch (25.4 mm), 1/2 inch (12.6 mm), 1/4 inch (6.35 mm), and 1/8 inch (3.175 mm), which is shown in Figure 4. The model also correctly predicted the effect of anisotropic material on the shape and curvature of deformation in two planes of anisotropy. Furthermore, the anisotropic mechanical behaviour of the material can be analyzed by FEA models as well. Bulla et al. [54] developed a model to predict the anisotropic response of the PE separator due to deformation and failure by combining the novel failure criterion with Hill's yield surface and a Swift–Voce hardening rule.

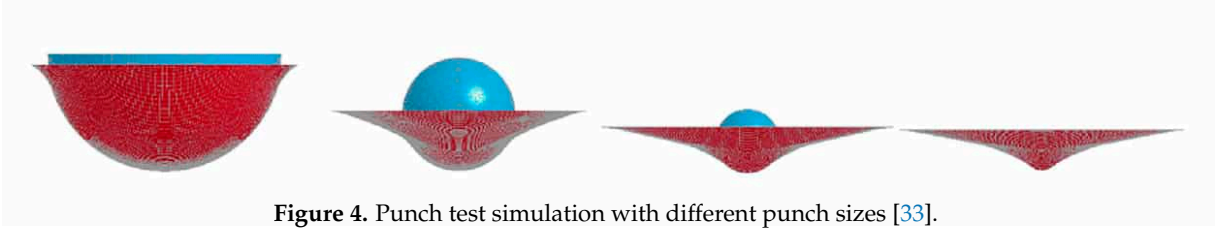


Figure 4. Punch test simulation with different punch sizes [33].

An image-based microstructure representative volume element (RVE) modelling method was applied by Xu et al. [35], which facilitates the understanding of the separators' complex macro mechanical behaviour as a result of microstructural features. The proposed method successfully captures the anisotropic behaviour of the separator under tensile test and provides insights into microstructure deformation, such as the growth of voids. In this study, the imaging processing method and finite element simulation are successfully coupled to analyze the stress-strain relation of battery separators. Furthermore, Xu et al. [55] developed a microstructure modelling method to investigate the deformation patterns of the battery separator. Based on their results, the reason why the separator film turns transparent has two folds was explained. One is the material-level instability, and the other is the structure-level instability.

Lagadec et al. [36] characterized how the microstructural properties (including porosity, tortuosity, and permeability) of the separators change as a function of compressive

strain and predicted the influence of these changes on the Li-ion transport through the separator by mechanical simulations. They also concluded that a given compressive strain negatively impacts the microstructure of PE separator more than that of a PP separator, because PE has a lower Young's modulus, smaller pore sizes, and a more isotropic structure.

Xu and Bae [38] proposed a stochastic reconstruction algorithm to generate random but statistically equivalent 3D microstructure models for mechanical property analysis and uncertainty quantification. The proposed modelling method provides a tool to establish the "microstructure-property" relation, which can be considered as important separator design variables.

In addition, from the molecular level, investigations of atomic interactions provide a deep understanding of the stress of separators in Li-ion batteries. Yan et al. [43] mapped the separator microstructure into discrete atomistic models of bulk crystalline phases and oriented amorphous nanofibers at different conditions such as in vacuum, water, and dimethyl carbonate (DMC) by using MD (See Figure 5). The mechanical responses of a porous PP separator in different media were found, which indicates that DMC can penetrate into the amorphous nanofiber and result in Young's modulus reduction to one-tenth of its original value, while a polar solvent (e.g., water) can increase Young's modulus by slightly squeezing the amorphous fibre due to the repulsive interaction.

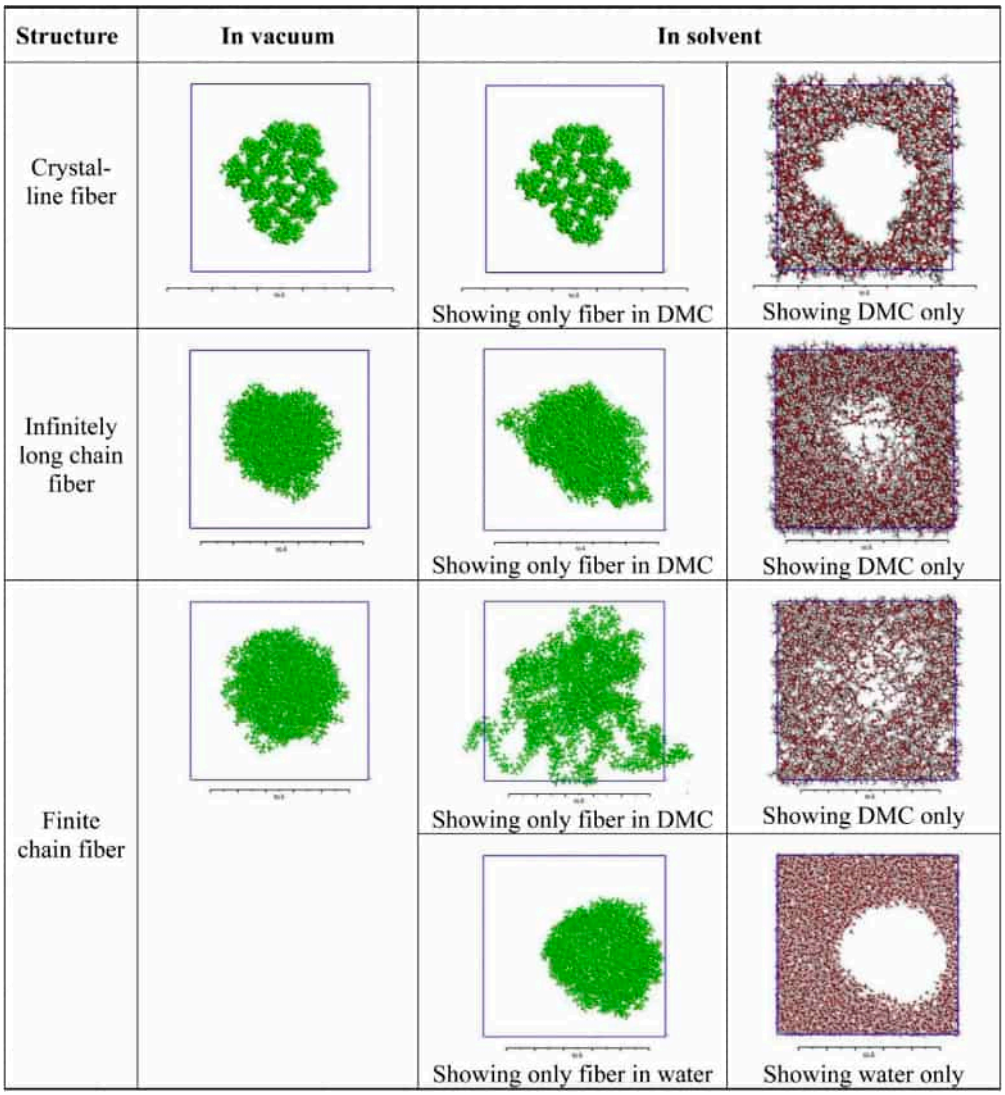


Figure 5. Relaxed structure for crystalline fibre, infinitely long chain fibre and finite chain fibre in vacuum, in DMC, and in water at zero strain [43].

Xie et al. [47] successfully applied molecular simulation to unveil that the weakening of cellulose separator submerged in the electrolyte results from the deformed cellulose amorphous region and the promoting effect of adding lignin. The addition of lignin generates new hydrogen bonds between the cellulose and lignin molecules and subsequently form a larger fibrous network. The weakening phenomenon of cellulose separator immersed in the electrolyte is mainly caused by the deformation of the cellulose amorphous region, shown in Figure 6.

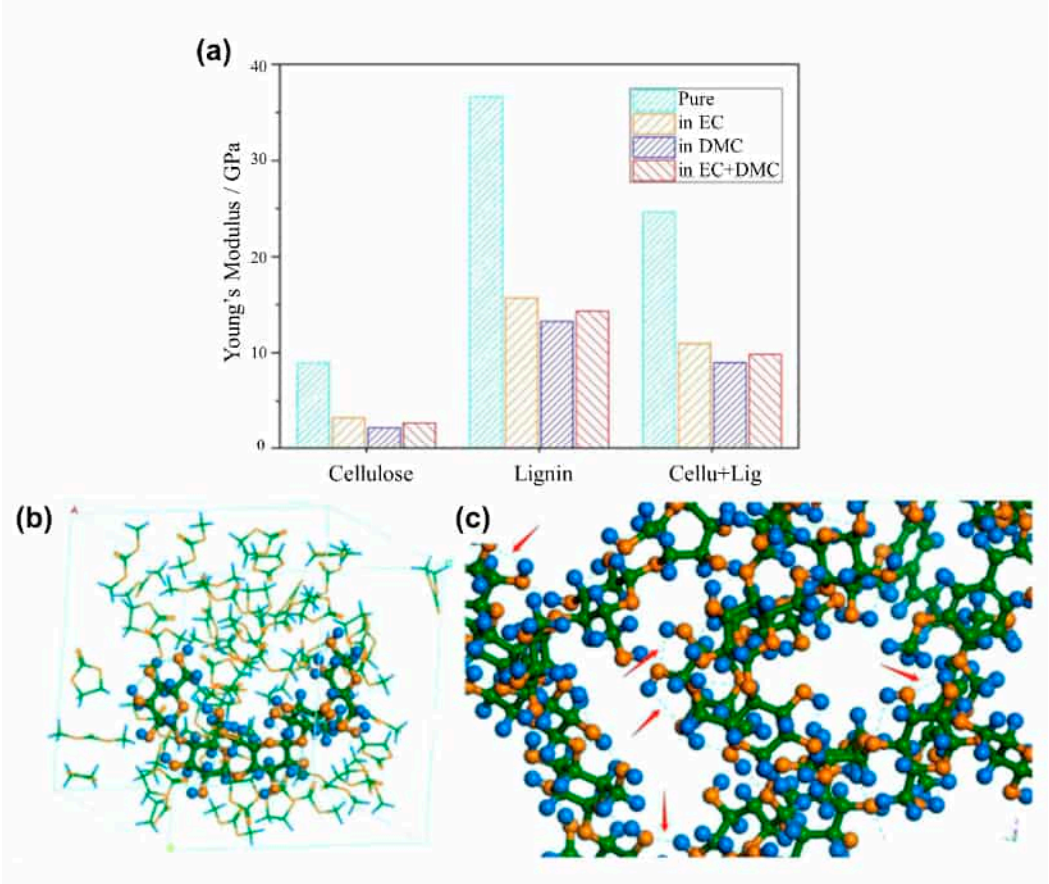


Figure 6. Simulation results from Xie et al. [47] (**a**) simulated Young's modulus of molecular models under different environments, and distinct details in blended models: (**b**) deformed cellulose amorphous model in electrolyte solvents and (**c**) generated hydrogen bonds between cellulose and lignin molecules.

2.3. Separator Breakdown

During the battery working progress, it is possible that due to thermal inertia the temperature can continue to rise until the separator would melt and short the electrodes, leading to violent reactions and heat generation [56]. This phenomenon is called separator breakdown, which is one step of the Li-ion battery thermal runaway process. Therefore, the thermal properties of separators have a strong influence on battery safety. Numerical studies in this field can provide a better understanding of the separator breakdown mechanism and give reliable prediction results. Other related performances such as ion transport and the solid electrolyte interphase (SEI) degradation can be modelled as well by numerical methods.

2.3.1. Thermal Transport

As mentioned in the Introduction, the separator acts as an essential role in improving battery safety performance. Low thermal transport in Li-ion cells and battery packs has been widely recognized as a critical technological concern that limits the use of Li-ion batteries [49,57,58]. Therefore, the focus for the current development of advanced Li-ion

battery separators is to enhance the safety performance of the separator and/or facilitate the ionic flow through the separator during battery operation.

Standard MD simulation studies thermal transport and heat conduction across the molecular interfaces at the given length-scales (~a few nms). For example, MD simulations have been employed to model thermal transport across a variety of material pairs such as graphene-semiconductor heterostructures [59], Si/Ge interfaces [60], silicene/silica interfaces [61], graphene/phosphorene interfaces [62], etc. The thermal conductivity study on the electrodes and solid electrolytes have also been carried out, including equilibrium molecular dynamics [63] and nonequilibrium molecular dynamics simulation method [64].

Parviainen et al. [40] developed a new model, based on an existing MD code, to include resistive heating and electronic thermal conduction. The model accounts for dynamic changes of both tip geometry and temperature and gives an accurate and detailed view of the temperature development, including the temperature gradient in tips. For nanosized field emitters, it is critical to account for finite-size effects since both electric and thermal conductivity have a strong size dependence at this scale (height 13.1 nm and diameter 2 nm).

Non-equilibrium MD simulations were performed by Kawagoe et al. [46] on bulk amorphous polyacrylic acid with three polymer chain lengths to investigate the molecular mechanism of thermal energy transfer in heat conduction. The simulation results showed that the dominant mechanism of thermal energy transfer in polyacrylic acid (PAA) was intramolecular interaction. Consequently, the intramolecular interaction caused the thermal conductivity to increase as the polymer chain length elongated, which also increased the total thermal conductivity. The relation between thermal conductivity and the polymer chain length results in a saturation curve, which will lead to the characterization of thermal energy transfer in more complicated materials such as the layer-by-layer membranes.

Dhakane et al. [48] applied MD simulations for the calculation of thermal conductance across the cathode-separator interface with the interface force field in Figure 7. It is shown that molecular bridging at the interface results in up to 250% improvement in interfacial thermal conductance for the 3-Aminopropyl triethoxysilane (APTES) case. These results quantify the crucial role of the cathode-separator interface on thermal transport within the Li-ion cell, as well as the potential improvement in interfacial thermal transport by molecular bridging.

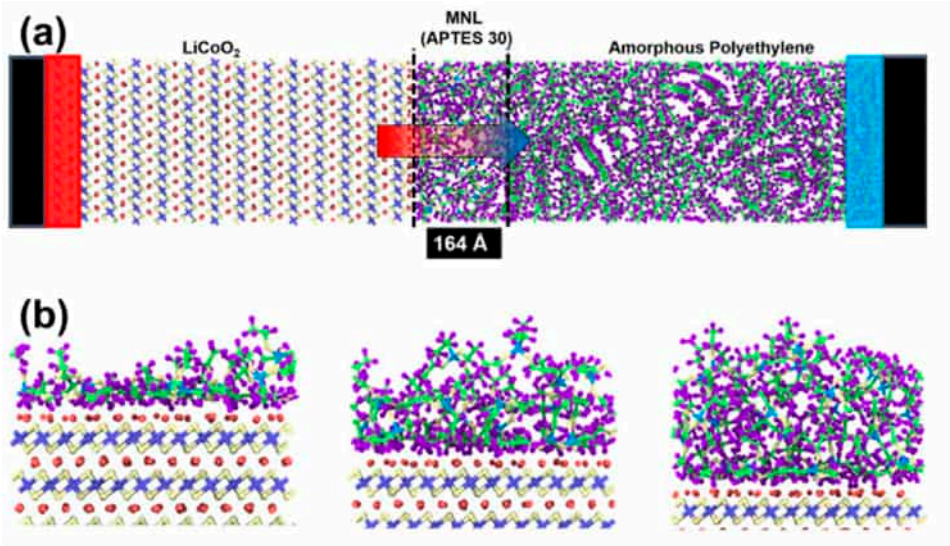


Figure 7. Representative images of the molecular assembly from Dhakane et al. [48]. (**a**) Molecular structure for simulation of a case with a bridging molecular layer (30 APTES molecules) at the $LiCoO_2$-polyethylene interface. Hot reservoir (red rectangle on the left) and cold reservoir (blue rectangle on the right) maintained at 350 K and 250 K respectively are shown. (**b**) Schematics of the cathode-APTES interface for simulations with 10, 20, and 30 molecules.

A two-dimensional electrochemical-thermal coupled model was developed by Li and Tan [39] for a 38120-type $LiFePO_4$ Li-ion battery. Modeling results showed that the separator thickness strongly impacted battery energy density: the battery energy density dropped from 148.8 W h/kg to 110.6 W h/kg, while the separator thickness increased from 5 μm to 100 μm. The battery temperature rise and temperature difference dropped when both the separator thermal conductivity and heat capacity increased to 1 W m^{-1} K^{-1} and 3500 J kg^{-1} K^{-1}, respectively.

2.3.2. Ion Transport

During the working procedure of the Li-ion batteries, the transportation of ions plays an important role in battery performance. A separator membrane offers ion-conducting routes between electrodes and also electronically isolates the electrodes to prevent internal short-circuit failure, which eventually results in cell fire or explosion [65]. MD simulations have been developed in this area to explore the transport mechanisms and previous numerical studies investigated ion transport in the solid electrolyte [66], cathodes [67], and SEI [68,69]. The numerical simulations applied for separators will be reviewed in this section.

Vilčiauskas et al. [42] performed first-principles MD simulations to study proton conductivity at the fundamental molecular level, which represents a first step towards a more detailed understanding of the proton conduction mechanisms in realistic phosphoric acid-based polymer electrolyte materials. The solvation shell characteristics of the H-bond network are significantly over coordinated as compared to those in pure phosphoric acid. However, the lower density of H-bonds slightly increases the local molecular mobilities and artificially increases the proton diffusion coefficient.

Xu et al. [44] investigated ionic microporous zeolite membranes to overcome the challenge of the trade-off between ion selectivity and conductivity associated with conventional polymeric ion separators. They used the open-source software Packmol to construct the model and applied the LAMMPS package for running the simulations. The proton concentration in the zeolite structure (i.e., C_{H+}) was determined to assist with understanding ion diffusion behaviour in the zeolite pores since the equilibrium values of C_{H+} are difficult to measure experimentally. This type of separator showed the ability to drastically reduce the self-discharge rates and enhance energy efficiencies.

Kim et al. [45] demonstrated the effect of the functional groups on the hydronium and hydroxide ions in hydrated poly(ether ether ketone) (PEEK) using MD simulations. The hydronium ion and hydroxide conductivity of the PEEK ion exchange membranes increased as the mole ratio of the functionalized moiety in PEEK increased. The diffusivity of the hydronium and hydroxide ions were calculated using their mean squared displacement in the simulation process via the COMPASS force field.

2.3.3. Degradation

The most popular separator materials for Li-ion batteries with organic electrolytes are polyolefin materials [70]. However, the low melting point of polyolefins (135 °C for PE and 165 °C for PP) qualifies their utilization as a thermal fuse to shut down the cell by losing porosity and permeability if an over-temperature condition occurs. The main causes regarding separator degradation are typically traced to the lithium dendrite growth caused by separator pores, attack through the electrolyte, blockage of passageways in the separator over cycling, and structural degradation arising from elevated temperature or high cycle number [71].

A reduced-order capacity-loss model was applied by Jin et al. [29] to improve computational efficiency without sacrificing model fidelity. This model captures the two primary degradation mechanisms that occur in the graphite anode of a typical Li-ion cell: (a) capacity loss due to SEI layer growth, and (b) capacity loss due to isolation of active material. The model matches experimental capacity degradation results within a 20% error and 2400× faster than currently existing more complex physically-based electrochemical models.

Kim et al. [41] studied the formation and growth of SEI for the case of ethylene carbonate (EC), DMC, and mixtures of these electrolytes using molecular dynamics simulations. The simulation studied the distribution of organic and inorganic salts as a function of the distance from the anode surface in Figure 8, and the results show that inorganic salts are found closer to the anode surface while the region near the electrolyte–SEI interface is rich in organic salts.

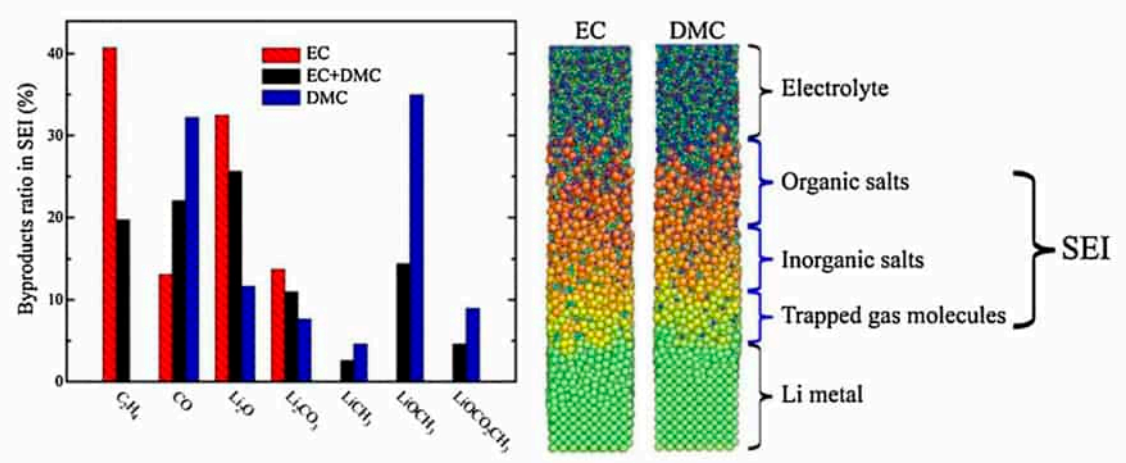


Figure 8. Distribution of the SEI components for different electrolytes (**left** chart). Atomic configurations from MD simulations; the components of the SEI are identified (**right**) [41].

3. Summary and Outlook

The separator is a crucial component in Li-ion batteries with the function of preventing physical contact between the positive and negative electrodes of the battery and stopping internal short while serving as the electrolyte reservoir to enable ionic transport. The ideal separator should not only have large electrolyte uptake for lowering the cell internal resistance but also have extremely thin thickness with strong mechanical strength, being electrochemically and structurally stable, as well as having a highly porous structure with great tortuosity to prevent the growth of dendritic lithium. In addition, the separator should be able to shut the battery down when overheating occurs for battery safety, as well as being cost-effective through the manufacturing process. However, it is challenging for practical separators to possess these ideal properties simultaneously, and therefore it becomes essential to balance different separator properties to achieve high-performance batteries. Moreover, the safety issue is still another obstacle for the separator and Li-ion battery applications.

In this paper, we have reviewed the recent numerical model advancements for Li-ion battery separators. It included mathematical and mechanical analytical-based simulation approaches such as FEA, CFD, and MD models. Through our summary, numerical simulation can be applied in the investigation of the properties of a separator and the prediction for the performance of the separators. Meanwhile, numerical studies not only provide a time-efficient and cost-effective way but also show a comprehensive understanding of the primary mechanism of the separator performance. Mathematical models describe certain parameters which are not known experimentally and provide the capacity of parameter adjustment. Mechanical models show a detailed microstructure of separators, and combining with FEA and CFD models, the properties of separators can be simulated and predicted. MD models demonstrate a more detailed view of the mechanisms, such as thermal propagation, ion transportation, and degradation. Furthermore, key mechanical design parameters such as Young's modulus and average strain rate for various types of separator materials (i.e., polyolefin, PVDF, PP, PE, Cellulose/lignin, homogeneous solid medium) were analyzed through numerical simulation and characterization approaches. The development of robust, effective numerical tools to address the needs of fire safety of

separators will be beneficial to the battery industry, providing a complementary design tool for safety engineering design and performance studies.

With the increasing demand of Li-ion batteries with high charge/discharge efficiency and energy density in the future, battery separators with high performances are required for both industrial and research purposes. Currently, the investigation on the separator materials and performances is mainly based on experiments. Numerical simulations can provide reliable results compared to experiments and contribute to study the mechanism of some effects, meanwhile, numerical simulations provide an efficient and economical way to develop the separator and battery system. To provide safer, more functional, and powerful separators, developing a novel Li-ion battery or battery system and optimizing the manufacturing process is critical. The following numerical investigations and development of models are recommended in the future: (i) an effective pre-system failure numerical tool that is able to diagnose the thermal propagation, short-circuiting, separator degradation; (ii) a novel thermal-runaway model for Li-ion battery systems that is able to incorporate multiple battery separator materials with different mechanical and physical properties; (iii) coupling of multi-scale simulation models to study the all-inclusive coupled internal/external phenomena of Li-ion battery fires; and (iv) the simulation findings can be inputted as useful parameters for machine learning algorithms.

Author Contributions: Conceptualization, A.L. and A.C.Y.Y.; methodology, A.L. and W.W.; formal analysis, C.W.; investigation, I.M.D.C.C.; resources, T.B.Y.C.; writing—original draft preparation, A.L.; writing—review and editing, A.C.Y.Y., Q.N.C. and J.Z.; visualization, A.L.; supervision, G.H.Y.; project administration, A.C.Y.Y.; funding acquisition, G.H.Y. All authors have read and agreed to the published version of the manuscript.

Funding: This research was funded by the Australian Research Council (ARC Industrial Transformation Training Centre IC170100032), the Australian Government Research Training Program Scholarship and the Tactical Research Fund, Bushfire and Natural Hazard Cooperative Research Centre in Australia. All financial and technical supports are deeply appreciated by the authors.

Acknowledgments: The author sincerely thank Hu Long for assisting with the image format suggestions.

Conflicts of Interest: The authors declare no conflict of interest.

References

1. Yoshino, A. The birth of the lithium-ion battery. *Angew. Chem. Int. Ed.* **2012**, *51*, 5798–5800. [CrossRef] [PubMed]
2. Etacheri, V.; Marom, R.; Elazari, R.; Salitra, G.; Aurbach, D. Challenges in the development of advanced Li-ion batteries: A review. *Energy Environ. Sci.* **2011**, *4*, 3243–3262. [CrossRef]
3. Kong, L.; Li, C.; Jiang, J.; Pecht, M.G. Li-ion battery fire hazards and safety strategies. *Energies* **2018**, *11*, 2191. [CrossRef]
4. Ouyang, D.; Chen, M.; Huang, Q.; Weng, J.; Wang, Z.; Wang, J. A review on the thermal hazards of the lithium-ion battery and the corresponding countermeasures. *Appl. Sci.* **2019**, *9*, 2483. [CrossRef]
5. Wang, Q.; Mao, B.; Stoliarov, S.I.; Sun, J. A review of lithium ion battery failure mechanisms and fire prevention strategies. *Prog. Energy Combust. Sci.* **2019**, *73*, 95–131. [CrossRef]
6. Sun, P.; Bisschop, R.; Niu, H.; Huang, X. A review of battery fires in electric vehicles. *Fire Technol.* **2020**, *56*, 1–50. [CrossRef]
7. Huang, X. Separator technologies for lithium-ion batteries. *J. Solid State Electrochem.* **2011**, *15*, 649–662. [CrossRef]
8. Lee, H.; Yanilmaz, M.; Toprakci, O.; Fu, K.; Zhang, X. A review of recent developments in membrane separators for rechargeable lithium-ion batteries. *Energy Environ. Sci.* **2014**, *7*, 3857–3886. [CrossRef]
9. Deimede, V.; Elmasides, C. Separators for lithium-ion batteries: A review on the production processes and recent developments. *Energy Technol.* **2015**, *3*, 453–468. [CrossRef]
10. Lagadec, M.F.; Zahn, R.; Wood, V. Characterization and performance evaluation of lithium-ion battery separators. *Nat. Energy* **2019**, *4*, 16–25. [CrossRef]
11. Zhang, H.; Zhou, M.-Y.; Lin, C.-E.; Zhu, B.-K. Progress in polymeric separators for lithium ion batteries. *RSC Adv.* **2015**, *5*, 89848–89860. [CrossRef]
12. Cho, J.; Jung, Y.-C.; Lee, Y.S.; Kim, D.-W. High performance separator coated with amino-functionalized SiO_2 particles for safety enhanced lithium-ion batteries. *J. Membr. Sci.* **2017**, *535*, 151–157. [CrossRef]
13. Liu, J.; Liu, Y.; Yang, W.; Ren, Q.; Li, F.; Huang, Z. Lithium ion battery separator with high performance and high safety enabled by tri-layered SiO2@ PI/m-PE/SiO2@ PI nanofiber composite membrane. *J. Power Sources* **2018**, *396*, 265–275. [CrossRef]
14. Wang, S.; Zhang, D.; Shao, Z.; Liu, S. Cellulosic materials-enhanced sandwich structure-like separator via electrospinning towards safer lithium-ion battery. *Carbohydr. Polym.* **2019**, *214*, 328–336. [CrossRef] [PubMed]

15. Fuller, T.F.; Doyle, M.; Newman, J. Simulation and optimization of the dual lithium ion insertion cell. *J. Electrochem. Soc.* **1994**, *141*, 1. [CrossRef]
16. Doyle, M.; Newman, J.; Gozdz, A.S.; Schmutz, C.N.; Tarascon, J.M. Comparison of modeling predictions with experimental data from plastic lithium ion cells. *J. Electrochem. Soc.* **1996**, *143*, 1890. [CrossRef]
17. Doyle, M.; Fuller, T.F.; Newman, J. Modeling of galvanostatic charge and discharge of the lithium/polymer/insertion cell. *J. Electrochem. Soc.* **1993**, *140*, 1526. [CrossRef]
18. Stephenson, D.E.; Hartman, E.M.; Harb, J.N.; Wheeler, D.R. Modeling of particle-particle interactions in porous cathodes for lithium-ion batteries. *J. Electrochem. Soc.* **2007**, *154*, A1146. [CrossRef]
19. Thorat, I.V.; Stephenson, D.E.; Zacharias, N.A.; Zaghib, K.; Harb, J.N.; Wheeler, D.R. Quantifying tortuosity in porous Li-ion battery materials. *J. Power Sources* **2009**, *188*, 592–600. [CrossRef]
20. Bi, Z. Overview of Finite Element Analysis. In *Finite Element Analysis Applications A Systematic and Practical Approach*; Katey Birtcher: London, UK, 2018; pp. 1–29.
21. Tu, J.; Yeoh, G.H.; Liu, C. *Computational Fluid Dynamics: A Practical Approach*; Butterworth-Heinemann: Oxford, UK, 2018.
22. Yuen, A.C.Y.; Chen, T.B.Y.; Yang, W.; Wang, C.; Li, A.; Yeoh, G.H.; Chan, Q.N.; Chan, M.C. Natural ventilated smoke control simulation case study using different settings of smoke vents and curtains in a large Atrium. *Fire* **2019**, *2*, 7. [CrossRef]
23. Yuen, A.C.; Yeoh, G.H.; Timchenko, V.; Cheung, S.C.; Chan, Q.N.; Chen, T. On the influences of key modelling constants of large eddy simulations for large-scale compartment fires predictions. *Int. J. Comput. Fluid Dyn.* **2017**, *31*, 324–337. [CrossRef]
24. Chen, T.; Yuen, A.; Lin, B.; Liu, L.; Chan, Q.; Zhang, J.; Cheung, S.; Yeoh, G. Characterisation of Pyrolysis Kinetics and Detailed Gas Species Formations of Engineering Polymers via Reactive Molecular Dynamics (ReaxFF). *J. Anal. Appl. Pyrolysis* **2020**, *153*, 104931. [CrossRef]
25. Sosso, G.C.; Chen, J.; Cox, S.J.; Fitzner, M.; Pedevilla, P.; Zen, A.; Michaelides, A. Crystal nucleation in liquids: Open questions and future challenges in molecular dynamics simulations. *Chem. Rev.* **2016**, *116*, 7078–7116. [CrossRef] [PubMed]
26. Sangha, A.K.; Petridis, L.; Smith, J.C.; Ziebell, A.; Parks, J.M. Molecular simulation as a tool for studying lignin. *Environ. Prog. Sustain. Energy* **2012**, *31*, 47–54. [CrossRef]
27. Patel, K.K.; Paulsen, J.M.; Desilvestro, J. Numerical simulation of porous networks in relation to battery electrodes and separators. *J. Power Sources* **2003**, *122*, 144–152. [CrossRef]
28. Chen-Wiegart, Y.-C.K.; DeMike, R.; Erdonmez, C.; Thornton, K.; Barnett, S.A.; Wang, J. Tortuosity characterization of 3D microstructure at nano-scale for energy storage and conversion materials. *J. Power Sources* **2014**, *249*, 349–356. [CrossRef]
29. Jin, X.; Vora, A.; Hoshing, V.; Saha, T.; Shaver, G.; García, R.E.; Wasynczuk, O.; Varigonda, S. Physically-based reduced-order capacity loss model for graphite anodes in Li-ion battery cells. *J. Power Sources* **2017**, *342*, 750–761. [CrossRef]
30. Xiao, X.; Wu, W.; Huang, X. A multi-scale approach for the stress analysis of polymeric separators in a lithium-ion battery. *J. Power Sources* **2010**, *195*, 7649–7660. [CrossRef]
31. Shi, D.; Xiao, X.; Huang, X.; Kia, H. Modeling stresses in the separator of a pouch lithium-ion cell. *J. Power Sources* **2011**, *196*, 8129–8139. [CrossRef]
32. Wu, W.; Xiao, X.; Huang, X.; Yan, S. A multiphysics model for the in situ stress analysis of the separator in a lithium-ion battery cell. *Comput. Mater. Sci.* **2014**, *83*, 127–136. [CrossRef]
33. Zhang, X.; Sahraei, E.; Wang, K. Deformation and failure characteristics of four types of lithium-ion battery separators. *J. Power Sources* **2016**, *327*, 693–701. [CrossRef]
34. Lagadec, M.F.; Ebner, M.; Zahn, R.; Wood, V. Communication—technique for visualization and quantification of lithium-ion battery separator microstructure. *J. Electrochem. Soc.* **2016**, *163*, A992. [CrossRef]
35. Xu, H.; Zhu, M.; Marcicki, J.; Yang, X.G. Mechanical modeling of battery separator based on microstructure image analysis and stochastic characterization. *J. Power Sources* **2017**, *345*, 137–145. [CrossRef]
36. Lagadec, M.F.; Zahn, R.; Wood, V. Designing polyolefin separators to minimize the impact of local compressive stresses on lithium ion battery performance. *J. Electrochem. Soc.* **2018**, *165*, A1829. [CrossRef]
37. Lagadec, M.F.; Zahn, R.; Müller, S.; Wood, V. Topological and network analysis of lithium ion battery components: The importance of pore space connectivity for cell operation. *Energy Environ. Sci.* **2018**, *11*, 3194–3200. [CrossRef]
38. Xu, H.; Bae, C. Stochastic 3D microstructure reconstruction and mechanical modeling of anisotropic battery separators. *J. Power Sources* **2019**, *430*, 67–73. [CrossRef]
39. Li, Y.; Tan, Z. Effects of a Separator on the Electrochemical and Thermal Performances of Lithium-Ion Batteries: A Numerical Study. *Energy Fuels* **2020**, *34*, 14915–14923. [CrossRef]
40. Parviainen, S.; Djurabekova, F.; Timko, H.; Nordlund, K. Electronic processes in molecular dynamics simulations of nanoscale metal tips under electric fields. *Comput. Mater. Sci.* **2011**, *50*, 2075–2079. [CrossRef]
41. Kim, S.-P.; Van Duin, A.C.; Shenoy, V.B. Effect of electrolytes on the structure and evolution of the solid electrolyte interphase (SEI) in Li-ion batteries: A molecular dynamics study. *J. Power Sources* **2011**, *196*, 8590–8597. [CrossRef]
42. Vilčiauskas, L.; Tuckerman, M.E.; Melchior, J.P.; Bester, G.; Kreuer, K.-D. First principles molecular dynamics study of proton dynamics and transport in phosphoric acid/imidazole (2:1) system. *Solid State Ion.* **2013**, *252*, 34–39. [CrossRef]
43. Yan, S.; Xiao, X.; Huang, X.; Li, X.; Qi, Y. Unveiling the environment-dependent mechanical properties of porous polypropylene separators. *Polymer* **2014**, *55*, 6282–6292. [CrossRef]

44. Xu, Z.; Michos, I.; Cao, Z.; Jing, W.; Gu, X.; Hinkle, K.; Murad, S.; Dong, J. Proton-selective ion transport in ZSM-5 zeolite membrane. *J. Phys. Chem. C* **2016**, *120*, 26386–26392. [CrossRef]
45. Kim, D.J.; Park, C.H.; Nam, S.Y. Molecular dynamics simulations of modified PEEK polymeric membrane for fuel cell application. *Int. J. Hydrog. Energy* **2016**, *41*, 7641–7648. [CrossRef]
46. Kawagoe, Y.; Surblys, D.; Kikugawa, G.; Ohara, T. Molecular dynamics study on thermal energy transfer in bulk polyacrylic acid. *Aip Adv.* **2019**, *9*, 025302. [CrossRef]
47. Xie, W.; Dang, Y.; Wu, L.; Liu, W.; Tang, A.; Luo, Y. Experimental and molecular simulating study on promoting electrolyte-immersed mechanical properties of cellulose/lignin separator for lithium-ion battery. *Polym. Test.* **2020**, *90*, 106773. [CrossRef]
48. Dhakane, A.; Varshney, V.; Liu, J.; Heinz, H.; Jain, A. Molecular dynamics simulations of separator-cathode interfacial thermal transport in a Li-ion cell. *Surf. Interfaces* **2020**, *21*, 100674. [CrossRef]
49. Xiang, Y.; Li, J.; Lei, J.; Liu, D.; Xie, Z.; Qu, D.; Li, K.; Deng, T.; Tang, H. Advanced separators for lithium-ion and lithium-sulfur batteries: A review of recent progress. *ChemSusChem* **2016**, *9*, 3023–3039. [CrossRef]
50. Ihm, D.; Noh, J.; Kim, J. Effect of polymer blending and drawing conditions on properties of polyethylene separator prepared for Li-ion secondary battery. *J. Power Sources* **2002**, *109*, 388–393. [CrossRef]
51. Nyman, A.; Behm, M.; Lindbergh, G. Electrochemical characterisation and modelling of the mass transport phenomena in LiPF6–EC–EMC electrolyte. *Electrochim. Acta* **2008**, *53*, 6356–6365. [CrossRef]
52. Wu, W.; Xiao, X.; Shi, D. Heat Transfer and Thermal Stress in a Lithium-Ion Battery. In Proceedings of the ASME International Mechanical Engineering Congress and Exposition, Vancouver, BC, Canada, 12–18 November 2010; pp. 343–351.
53. Sheidaei, A.; Xiao, X.; Huang, X.; Hitt, J. Mechanical behavior of a battery separator in electrolyte solutions. *J. Power Sources* **2011**, *196*, 8728–8734. [CrossRef]
54. Bulla, M.; Kolling, S.; Sahraei, E. An Experimental and Computational Study on the Orthotropic Failure of Separators for Lithium-Ion Batteries. *Energies* **2020**, *13*, 4399. [CrossRef]
55. Pan, Z.; Zhu, J.; Xu, H.; Sedlatschek, T.; Zhang, X.; Li, W.; Gao, T.; Xia, Y.; Wierzbicki, T. Microstructural deformation patterns of a highly orthotropic polypropylene separator of lithium-ion batteries: Mechanism, model, and theory. *Extrem. Mech. Lett.* **2020**, *37*, 100705. [CrossRef]
56. Balakrishnan, P.; Ramesh, R.; Kumar, T.P. Safety mechanisms in lithium-ion batteries. *J. Power Sources* **2006**, *155*, 401–414. [CrossRef]
57. Shah, K.; Vishwakarma, V.; Jain, A. Measurement of multiscale thermal transport phenomena in Li-ion cells: A review. *J. Electrochem. Energy Convers. Storage* **2016**, *13*, 030801. [CrossRef]
58. Bandhauer, T.M.; Garimella, S.; Fuller, T.F. A critical review of thermal issues in lithium-ion batteries. *J. Electrochem. Soc.* **2011**, *158*, R1. [CrossRef]
59. Wang, X.; Zhang, J.; Chen, Y.; Chan, P.K. Investigation of interfacial thermal transport across graphene and an organic semiconductor using molecular dynamics simulations. *Phys. Chem. Chem. Phys.* **2017**, *19*, 15933–15941. [CrossRef]
60. Feng, T.; Zhong, Y.; Shi, J.; Ruan, X. Unexpected high inelastic phonon transport across solid-solid interface: Modal nonequilibrium molecular dynamics simulations and Landauer analysis. *Phys. Rev. B* **2019**, *99*, 045301. [CrossRef]
61. Zhang, J.; Hong, Y.; Tong, Z.; Xiao, Z.; Bao, H.; Yue, Y. Molecular dynamics study of interfacial thermal transport between silicene and substrates. *Phys. Chem. Chem. Phys.* **2015**, *17*, 23704–23710. [CrossRef]
62. Zhang, Y.-Y.; Pei, Q.-X.; Mai, Y.-W.; Lai, S.-K. Interfacial thermal conductance in multilayer graphene/phosphorene heterostructure. *J. Phys. D Appl. Phys.* **2016**, *49*, 465301. [CrossRef]
63. Meng, H.; Yu, X.; Feng, H.; Xue, Z.; Yang, N. Superior thermal conductivity of poly (ethylene oxide) for solid-state electrolytes: A molecular dynamics study. *Int. J. Heat Mass Transf.* **2019**, *137*, 1241–1246. [CrossRef]
64. Bedoya-Martinez, O.; Barrat, J.-L.; Rodney, D. Computation of the thermal conductivity using methods based on classical and quantum molecular dynamics. *Phys. Rev. B* **2014**, *89*, 014303. [CrossRef]
65. Oh, Y.S.; Jung, G.Y.; Kim, J.H.; Kim, J.H.; Kim, S.H.; Kwak, S.K.; Lee, S.Y. Janus-Faced, Dual-Conductive/Chemically Active Battery Separator Membranes. *Adv. Funct. Mater.* **2016**, *26*, 7074–7083. [CrossRef]
66. Borodin, O.; Smith, G.D. Mechanism of ion transport in amorphous poly (ethylene oxide)/LiTFSI from molecular dynamics simulations. *Macromolecules* **2006**, *39*, 1620–1629. [CrossRef]
67. Li, L.; Pascal, T.A.; Connell, J.G.; Fan, F.Y.; Meckler, S.M.; Ma, L.; Chiang, Y.-M.; Prendergast, D.; Helms, B.A. Molecular understanding of polyelectrolyte binders that actively regulate ion transport in sulfur cathodes. *Nat. Commun.* **2017**, *8*, 1–10. [CrossRef] [PubMed]
68. An, S.J.; Li, J.; Daniel, C.; Mohanty, D.; Nagpure, S.; Wood III, D.L. The state of understanding of the lithium-ion-battery graphite solid electrolyte interphase (SEI) and its relationship to formation cycling. *Carbon* **2016**, *105*, 52–76. [CrossRef]
69. Wang, A.; Kadam, S.; Li, H.; Shi, S.; Qi, Y. Review on modeling of the anode solid electrolyte interphase (SEI) for lithium-ion batteries. *npj Comput. Mater.* **2018**, *4*, 1–26. [CrossRef]
70. Arora, P.; Zhang, Z. Battery separators. *Chem. Rev.* **2004**, *104*, 4419–4462. [CrossRef]
71. Kabir, M.; Demirocak, D.E. Degradation mechanisms in Li-ion batteries: A state-of-the-art review. *Int. J. Energy Res.* **2017**, *41*, 1963–1986. [CrossRef]

Journal of The Electrochemical Society

The Electrochemical Society
Advancing solid state & electrochemical science & technology

OPEN ACCESS

Review—Surface Coatings for Cathodes in Lithium Ion Batteries: From Crystal Structures to Electrochemical Performance

To cite this article: Gurbinder Kaur and Byron D. Gates 2022 *J. Electrochem. Soc.* **169** 043504

View the article online for updates and enhancements.

This content was downloaded from IP address 86.133.56.127 on 03/12/2022 at 17:00

Journal of The Electrochemical Society, 2022 169 043504

Review—Surface Coatings for Cathodes in Lithium Ion Batteries: From Crystal Structures to Electrochemical Performance

Gurbinder Kaur[z] and Byron D. Gates[*,z]

Department of Chemistry and 4D LABS, Simon Fraser University, Burnaby V5A 1S6, British Columbia, Canada

Lithium ion batteries (LIBs) have dominated the energy industry due to their unmatchable properties that include a high energy density, a compact design, and an ability to meet a number of required performance characteristics in comparison to other rechargeable systems. Both government agencies and industries are performing intensive research on Li-ion batteries for building an energy-sustainable economy. LIBs are single entities that consist of both organic and inorganic materials with features covering multiple length scales. Two vital parameters for LIBs are their stable and safe operation. Critical insights should be made for understanding the structure to property relationships and the behavior of components under the working condition of LIBs. Since, the cathode serves as a central component of LIBs, the overall cell performance is significantly affected by the chemical and physical properties of the cathode. Cathodes tend to react with the electrolytes and, hence, to undergo surface modifications accompanied by degradation. These side-reactions result in an erosion of battery performance, thereby causing a reduced battery life and power capacity. Recently, techniques for preparing surface coatings on cathode materials have been widely implemented as a measure to improve their stability, to enhance their electrochemical performance, and to prevent detrimental surface reactions between the electrode materials and electrolyte. This review will cover different types of surface coatings for cathode materials, as well as a comparison of the changes in electrochemical performance between those materials with and without an applied coating. In addition, a brief outlook is included for different cathode materials and their coatings.
© 2022 The Author(s). Published on behalf of The Electrochemical Society by IOP Publishing Limited. This is an open access article distributed under the terms of the Creative Commons Attribution 4.0 License (CC BY, [redacted] which permits unrestricted reuse of the work in any medium, provided the original work is properly cited. [DOI: 10.1149/1945-7111/ac60f3]

Manuscript submitted February 1, 2022; revised manuscript received March 16, 2022. Published April 8, 2022. This paper is part of the JES Focus Issue on Electrochemical Separations and Sustainability.

The proliferation of petroleum fueled systems for stationary and transportation applications have been tied to concerns that include global warming and an increasing need for methods of clean energy production along with the depletion of fossil fuels. There is a pressing demand to introduce CO_2 emission free energy sources as alternatives to fossil fuels. Though the solar power received by the Earth is enough to fulfill the world's annual energy needs, due to limitations in converting this light into useful energy, losses via energy dissipation, and an inefficient collection and storage of energy, there is an increasing need to focus on developing functional materials that can help satisfy the world's ever-increasing energy demands. [1–3] Lithium ion batteries (LIBs) have emerged as one of the leading choices for energy storage, and remain a popular technology for use in power tools, consumer electronics, and electric vehicles (EV).[4,5]

LIBs are rechargeable batteries with a relatively high energy power densities, long-lifetimes, high charge/discharge rates, and relatively low maintenance.[6–10] Depending on their depth of discharge/charge (DOD) for LIBs, the life-cycle of LIBs can be >10,000 cycles, yielding energy densities of almost 250 $W{\cdot}h{\cdot}kg^{-1}$.[1,11] Li-ions offer several advantages over other elements for their use in rechargeable batteries. These advantages include a relatively low reduction potential, a small ratio of charge to ionic radii, and a high ion mobility. These properties enable the LIBs to yield relatively high volumetric and gravimetric capacities. There are safety concerns with these batteries that include thermal runaway, which is receiving an increased attention from the scientific community. Thermal runaway at a cell level often initiate chain reactions that result in a short circuit forming within the cell. Due to the properties of lithium ions, the growth of Li dendrites and short circuits have a high probability of occurring in LIBs. Ultimately, they are prone to catastrophic failure when used in energy storage devices, including in EVs. Reported failures of LIBs include fires in the batteries of Samsung phones (2016), the batteries in Boeing 787 planes (2013), and the batteries in Tesla S cars (2019).[6–9,12] Such incidents can pose serious safety issues and impose threats to human health and life. It is, therefore, essential to take into consideration the design and safety issues of LIBs for their prolonged uninterrupted functioning in these and other applications.

The cathode is a vital component of LIBs as it serves as the source of Li^+ ion donation in these cells, and is a central factor for determining its specific capacity and overall cost. A significant amount of research has been put into reducing the cost of LIBs by tailoring the choice of precursors and switching from more expensive elements (e.g., Co) to more earth abundant elements (e.g., Mn, Fe). Development of LIBs has focused on the need to extend beyond just the cost-related issues. Including, for example, the other aspects of cathode chemistry (e.g., dendrite formation, surface degradation, and short circuiting) are critical to achieving the long-term performance goals of LIBs. Elements within the cathode tend to undergo side-reactions with the electrolyte that result in surface erosion of the cathode materials and an overall degradation in battery performance.[13–19] Researchers have modified the electrolytes using additives to improve the stability of the interface between the electrolyte and the materials in each of the electrodes. Another approach to stabilizing these materials is to introduce a passivation layer that serves as a physical barrier to unwanted reactions. Surface coatings have emerged as a leading method to modify cathode materials in the search for ways to improve their structural and thermal stabilities, along with providing enhanced mechanical, physical, and chemical properties. This review focuses on different surface coatings of cathode materials for LIBs that include ZrO_2, Al_2O_3, MgO, ZnO, glasses, fluorides, phosphates, lithium composites, and carbon-based materials. Additional topics include evaluating the performance of cathode materials both with and without these coatings, and the technical challenges associated with these materials that still need to be addressed through future research efforts.

Overview of LIBs

Secondary batteries are a rechargeable electrochemical power source that converts chemical energy into electrical energy. In contrast to this, primary batteries (e.g., carbon-zinc/zinc-air batteries) are non-rechargeable and can only be used once, making them less appealing for energy storage applications.[20–23] The first

*Electrochemical Society Member.
[z]E-mail: [redacted]

rechargeable battery was the lead-acid battery invented by Plante in 1857. lead-acid batteries could yield up to 180 $W{\cdot}kg^{-1}$ of specific power with efficiencies from 60 to 90%. A major disadvantage of this type of battery is freezing of the electrolyte in cold weather. In 1899, Jungner invented Ni-Cd batteries with a specific power of 150 $W{\cdot}kg^{-1}$ and efficiencies up to 70 to 90%. This battery was determined to be quite expensive and also involved the use of toxic elements (i.e., cadmium). Additionally, it suffered from issues such as "memory effects" and "thermal runaway." Around 180 years ago, intercalation chemistry for energy storage was exploited by Schauffautl (1841) when he showed the use of sulfate ion intercalation into graphite. The first intercalation-based metal disulfide battery was demonstrated by Whittingham (Exxon Corporation, US) in 1970. The Li-TiS_2 cell exhibited a discharge voltage of $<$2.5 V (vs Li) with a reversibility of one lithium per TiS_2 sub-unit. The Whittingham battery used a TiS_2 cathode, a lithium metal anode, and a liquid electrolyte [i.e., a Li salt dissolved in a mixture of tetrahydrofuran (THF) and dimethoxyethane]. These batteries posed safety issues that included dendrite formation on the lithium-anodes, which lead to short-circuiting of the cells. In 1970, Besenhard prepared a battery system with an oxide-based cathode and a graphite anode. Research efforts in LIBs continued to seek batteries that could reach higher cell voltages and that exhibited improved safety performance. In the 1980s, Goodenough and coworkers investigated various cathodes materials as a substitute to sulfide electrodes. In a parallel route, Yoshino demonstrated carbon-based materials as anodes for LIBs, and focused on creating non-aqueous electrolytes for secondary batteries. The 2019 Nobel Prize in Chemistry was awarded to Goodenough, Whittingham, and Yoshino for developing LIBs, a technology that ushered in a revolution in energy storage applications. LIBs were able to achieve specific powers of up to 340 $W{\cdot}kg^{-1}$ and efficiencies of 90%, which are considerably higher than alternative rechargeable battery technologies.

Electrochemical potential considerations.—The primary functions of LIBs are depicted in Fig. 1. LIBs consist of an anode, cathode, electrolyte, and porous separator. During charging of the battery, lithium ions are extracted from the cathode and pass through the electrolyte and separator before they are intercalated within the anode. At the same time, an equivalent number of electrons flow into the anode through an external circuit. During the reverse process (i.e., the discharge process), Li^+ ions are extracted from the anode and move through the separator towards the cathode where these ions re-intercalate within the cathode materials. After charging, the potential of the anode relative to the cathode indicates the storage of electric energy that can be released during the discharge process. The process of discharging is thermodynamically favored and, hence, will be determined by enthalpically (ΔH) and entropically (ΔS) driven forces.[4–6] Some solid-state mass diffusion will also occur during Li^+ ion transport across the porous membranes. In an ideal situation, the total concentration of Li^+ ion is maintained at a relatively constant level within the electrolyte, although the mass balance of Li species will shift from the cathode to the anode when charging the battery as Li-ions migrate through the separator. The mass balance subsequently shifts from the anode to the cathode during the discharge of the battery. The storage of Li species in the batteries can take place through three mechanisms: (i) chemical intercalation; (ii) chemical transformation; and (iii) formation of alloys. Reactions associated with chemical transformations have a limited reversibility, whereas the formation of alloys can result in relatively large volume expansion although alloys can offer a larger specific capacity. The intercalation mechanism requires the host electrode to exhibit enough space to accommodate the Li species and either the transportation of or the transformation of a charged counter ion species for maintaining charge neutrality within the system. Lithium vacancies are created by lithium ion deintercalation, which can lead to oxygen release at high states of charge (SoCs). This furthermore enables the migration of transition metal ions and, concurrently, the formation of new phases like the cation disordered phases. Intercalation reactions have been exploited to a wide extent as they have been thought to yield the required parameters for enhancing the output of LIBs.

Two imperative parameters for LIBs are power density and energy density, which are ultimately dependent on the cell potential. The overall cell voltage is given by[24,25]

$$V = \frac{\mu_A - \mu_C}{e} \quad [1]$$

where μ_A and μ_C are the chemical potentials of the anode and cathode, respectively, and e is the electronic charge. Equation 1 implies that the energy of the anode should be as high as possible and cathode energy should be as low as possible to maximize the stored energy. In other words, anodes would require stabilization of lower oxidation states (at a higher energy band) and cathodes should be stabilized for higher oxidation states (at a lower energy band). Goodenough expanded upon this insight when he proposed that the top of O^{2-}: 2p bands lie lower than the S^{2-}: 3p bands.[21] For a cathode material, the chemical potential can be significantly reduced by accessing lower energy bands through the use of higher oxidation state species such as the transformation between Co^{3+}/Co^{4+} that leads to an increase in the overall cell voltage up to 4 V (Fig. 2a). Therefore, the working voltage of the cell is limited by the electrochemical window or range of the electrochemical stability of the components (including the electrolyte). Figure 2b illustrates that the electrochemical window is a limiting factor for solid-state batteries.

Energy gap considerations.—The energy gap (E_g) of a cell is represented by the difference between the HOMO (highest occupied molecular orbital) and the LUMO (lowest unoccupied molecular orbital) of the electrolyte. Two important points to take into consideration are to ensure that: (i) μ_C of the cathode is higher than the HOMO of the electrolyte; and (ii) μ_A of the anode is lower than the LUMO of the electrolyte.[15,26,27] If the anode and cathode do not satisfy this condition, the electrolyte would be oxidized at the cathode and reduced at the anode. This degradation will otherwise result in the formation of a passivating solid electrolyte interphase (SEI). A space charge layer (SCL) is formed when two materials with different chemical potentials are brought into close contact with one another, which leads to a lack of local charge neutrality due to a limited migration of ions and/or electrons.[28,29] These space charge layers can have beneficial effects such as increasing ionic diffusion especially within solid-solid dispersions, but can have detrimental effects such as increasing the internal resistance of the cell.[30,31] The electronic structure of the electrodes will be modified after coming into contact with the electrolyte (Fig. 2c). The electrolyte initially possesses a higher chemical potential for Li^+, which results in a migration of Li^+ ions into the electrolyte and towards the cathode. This process aligns the electrochemical potentials of the system and results in the formation of a heterojunction.[15] Consequently, the Fermi level of the system will be readjusted and the energy level of each component changes due to band bending and formation of inner electric fields. Both electrodes also have current collectors that are essential for electron transport to and from the anode and cathode. The current collectors for the anode and cathode are copper and aluminum, respectively. These materials are largely considered to be non-reactive and highly conductive materials for some systems, but their stability towards the chemical and electrochemical changes in the system are important considerations.

LIBs should be operated within a reliable and safe potential window (≈2 to 4 V). Their operating conditions are limited by their voltage and temperature as demonstrated in Fig. 3. Generally, the operating voltage of LIBs is between 1.5 to 4.2 V (e.g., for C/$LiNi_xMn_yCo_zO_2$, C/$LiNi_{0.8}Co_{0.15}Al_{0.05}O_2$, C/$LiCoO_2$, C/$LiFePO_4$) and the charging and discharging temperatures are between 0 to 45 °C and 20 to 55 °C, respectively.[5] Some

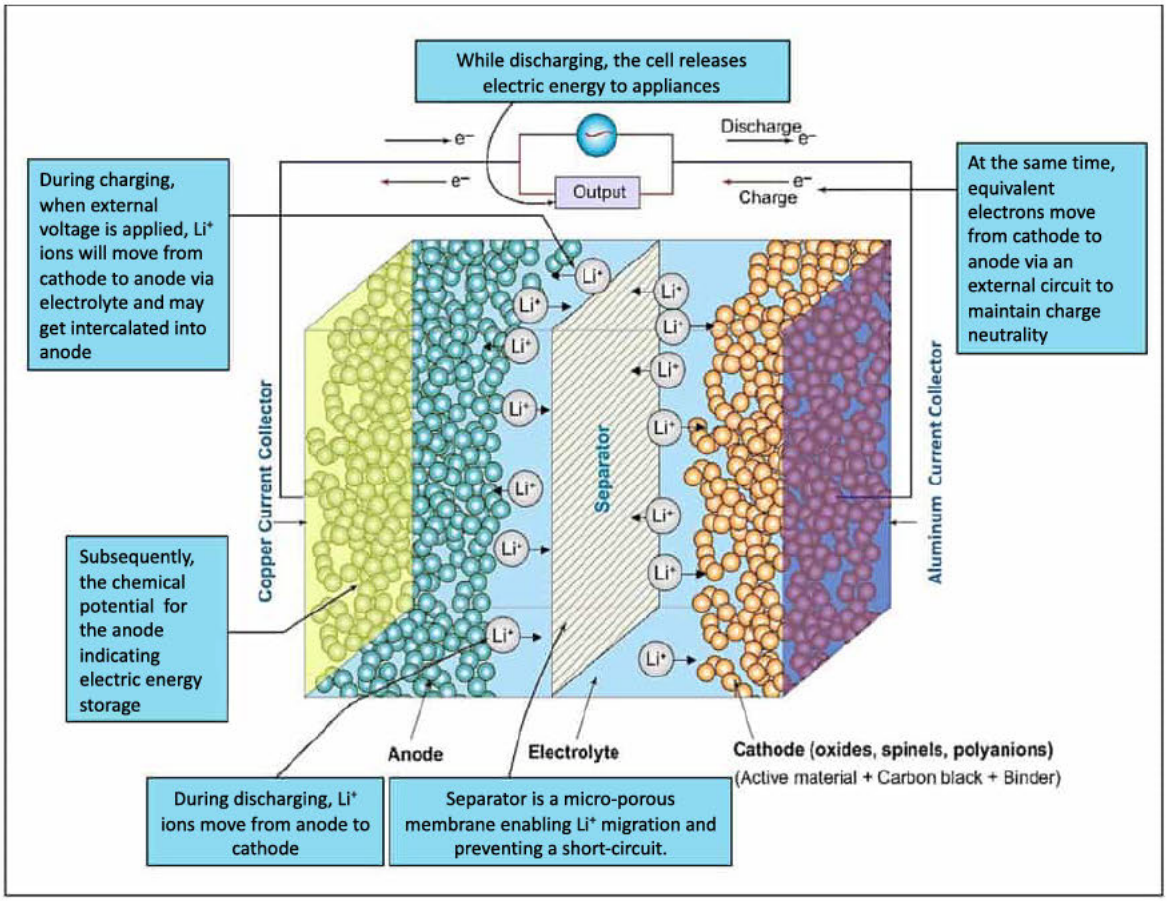


Figure 1. Schematic of LIBs and overview of their primary components and their functions.

electrolyte systems start to decompose around 70 °C, and the SEI decomposes between 90 to 120 °C.[32–35] Above 120 °C, the SEI films are unable to protect the anode from further side reactions with the surrounding electrolyte, which could result in the production of flammable gases. The cell also stops functioning properly when the separator starts to melt above 130 °C. At temperatures above 150 °C, the cathode materials start to decompose. For instance, $LiCoO_2$ breakdowns at 150 °C, $LiNi_{0.8}Co_{0.15}Al_{0.05}O_2$ breakdowns at 160 °C, and $LiMn_2O_4$ and $LiNi_xMn_yCo_zO_2$ decompose at 265 °C and 210 °C, respectively. Decomposition of $LiFePO_4$ occurs around 310 °C. Oxygen can also be produced during the decomposition of these cathode materials.[5] If the heat that is produced accumulates within the cell (e.g., from side reactions of the electrodes with the electrolytes), thermal runaway can occur. Thermal runaway can result in a self-heating rate of 10 °C min^{-1} or higher as a result of a large scale short-circuit within the cell, which leads to overheating of the system.[36]

The cell might explode because of the release of gases following the decomposition of active components and combustion of the gaseous by-products. It is important to fully recognize the safety issues with LIBs. Potential solutions that improve their safety include the selection of cell materials, the fabrication processes, and introducing physical barriers and protective layers on the electrodes. There are many challenges to the design and safe operation of LIBs as depicted in Fig. 4. Adverse interactions can include graphite exfoliation, structural disordering, particle cracking, internal short-circuiting, binder decomposition, dendrite formation, and transition metal dissolution are some prominent causes of a loss in capacity. Cathode materials of LIBs tend to react with the electrolytes and, hence, undergo surface modifications accompanied by degradation. These side-reactions can be detrimental as they can result in an erosion of battery performance, formation of thick SEI layers and fading of capacity, thereby, causing a reduction of both battery life and power capacity. These are concerns that continue to be addressed by the scientific community.[37]

It is difficult to address all the potential issues with regards to the safe operation of LIBs in one report. Hence, the present review will focus on coating materials being sought after for the cathode. The reason for selecting cathode materials as a focus is due to these materials being a limiting factor in terms of cell performance and cost. This review will cover details of the coating materials being sought for cathodes, the techniques to prepare these coatings, and cell performance behavior prior to and after applying these coatings. Before reviewing these areas in detail, it is important to gain further insight into the crystal structures and design of the microstructure within cathode materials, and to review their electrochemical performance.

Cathodes: Microstructure, Crystal Structure, and Performance

There remain several challenges to improving the performance of cathodes in LIBs. Some challenges exist because these materials undergo severe changes during lithiation and delithiation. When an external current is applied to charge the battery, the lithium ions diffuse from the cathode to the anode via the electrolyte. This process of lithium extraction from the cathode is known as delithiation. In contrast, during discharge of the battery, lithium ions diffuse from the anode and migrate back towards the cathode via the electrolyte. Electrons from the oxidation of the Li species are collected by the copper electrode supporting the anode material. The process of incorporating Li^+ ions within the cathode materials is known as lithiation.[1–4] The overall performance of a cell is affected by the cathode structure (e.g., valence states of the host matrix for Li^+ ions, space available for accommodating Li^+, and reversibility

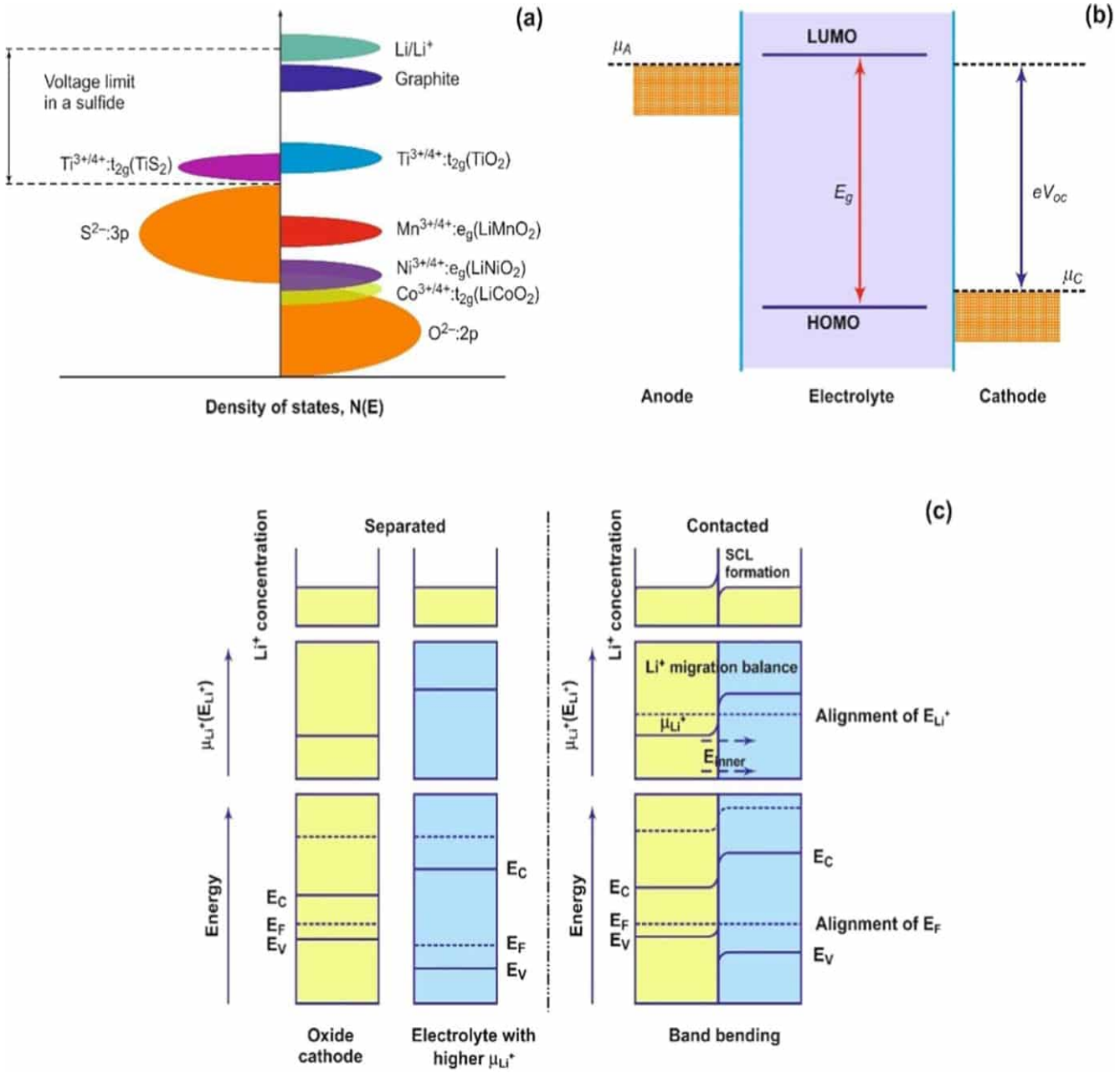


Figure 2. (a) Redox energy potentials relative to the anion bands,[1] (b) relationship between the electrochemical potentials of electrodes, LUMO/HOMO of electrolytes and respective energy gaps (E_g), μ_A and μ_C are the chemical potentials of the anode and cathode,[26] and (c) modification of the band structures when active materials come into contact with each other, E_c (conduction band energy), E_v (valence band energy) and E_f (Fermi level energy); redrawn with permission from Ref. 15.

of the intercalation process). The following sections will review prominent classes of cathode materials, and their microstructure and performance characteristics.

Layered oxides.—Layered oxides are the most commonly used cathode materials in LIBs. These materials have a general formula of $LiMO_2$ where M can be Co, Ni, or Mn. The first layered oxide for Li-ion intercalation was $LiCoO_2$ (LCO), which was invented by Goodenough, Mizoshima and colleagues in 1976. The t_{2g} bands of Co^{3+} are redox active. These bands are completely filled and overlap with the O^{2-}:2p bands.[7,38,39] The Co^{3+} t_{2g} bands lose electron density as the Fermi level shifts toward the top of the O^{2-}:2p band during charging of the cathode. As a result, Co^{3+} is oxidized to Co^{4+} and almost half of the electrons in its t_{2g} orbitals can be removed without hampering the structural integrity of these materials. This process yields a reversible capacity of 140 $mA{\cdot}h{\cdot}g^{-1}$ vs Li/Li^+ at around 4 V. In the $LiMO_2$ structure, Li and M occupy the 3a and 3b sites, respectively, within the lattice. The Li and M form an ABC stacking sequence, occupying alternate octahedral sites between the (111) planes within rock-salt structures that yield a cubic-close packing of oxide ions (space group $R\bar{3}m$). The unit cell for this layered structure consists of sheets of CoO_6 octahedra that are separated by interstitial layers of Li^+ ions. This crystal structure corresponds to an O_3 phase (Fig. 5a).[40] The Li^+ ions migrate during charging and discharging from one octahedral void to another by passing through a neighboring tetrahedral void because this pathway offers a lower energy barrier to Li^+ transport.

From the perspective of orbital overlap and bonding (Fig. 5b), the (n + 1)s, (n + 1)p and nd orbitals of the transition metal (TM) overlap with the s orbitals of O ligands to yield a_{1g}^*, t_{1u}^*, e_g^*

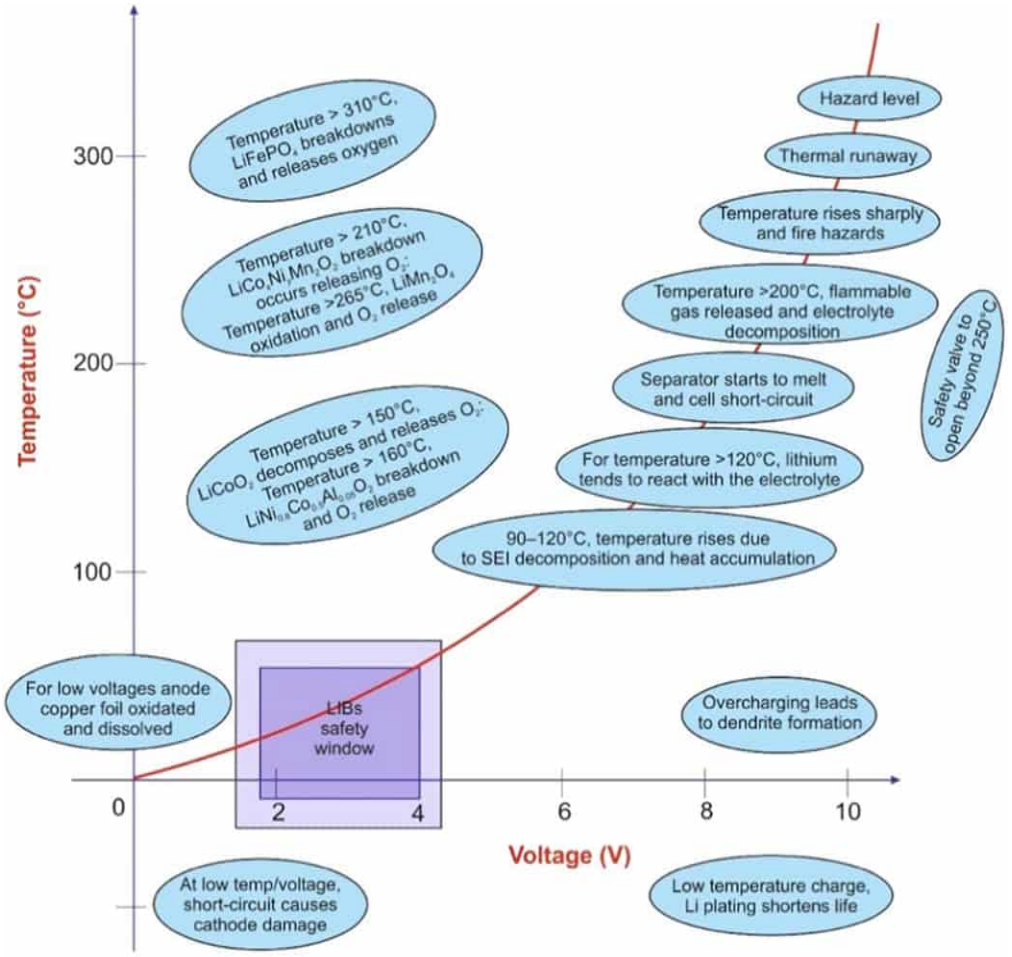


Figure 3. Window for the safe operation of LIBs and processes that result from operating in voltages and temperatures outside of this window (outer square represents threshold, inner square represents desirable limit), redrawn with permission.[32]

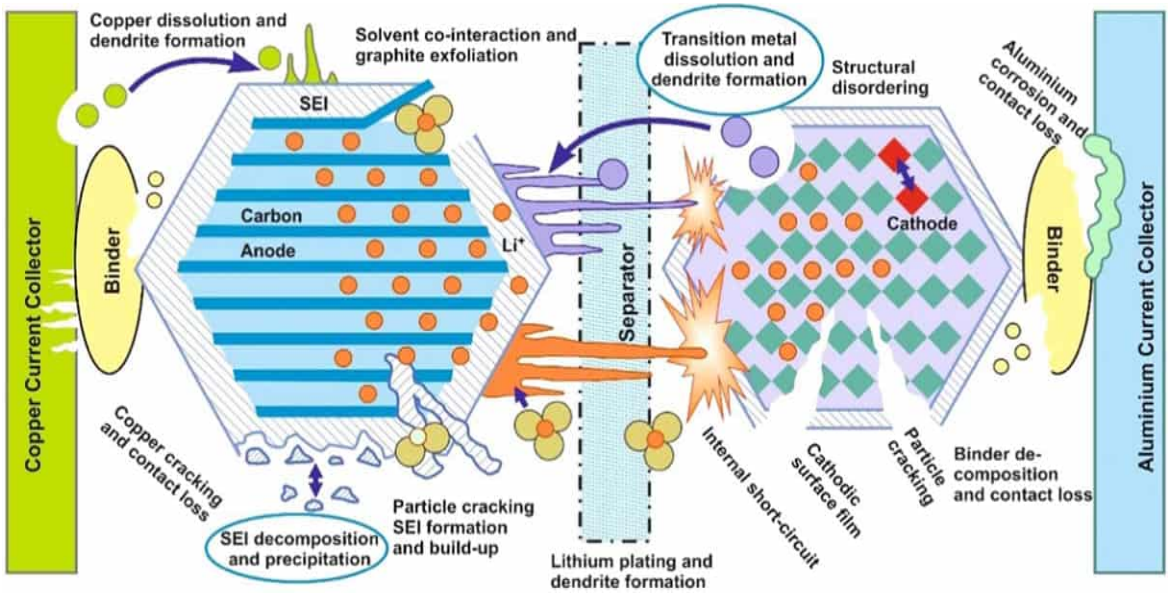


Figure 4. Various areas of research investigation in LIBs, redrawn with permission.[37]

antibonding and a_{1g}, t_{1u}, e_g bonding states.[41] The t_{2g} and t_{2g}^* are completely filled bonding states and partially filled antibonding states, respectively, which form when p orbitals from the O ligands interact with the t_{2g} orbitals of transition metal. The electrochemistry of the metal oxides is controlled by the (M–O)* band formed by the e_g^* and t_{2g}^*. A loss of electrons from the (M–O)* band or the d-band

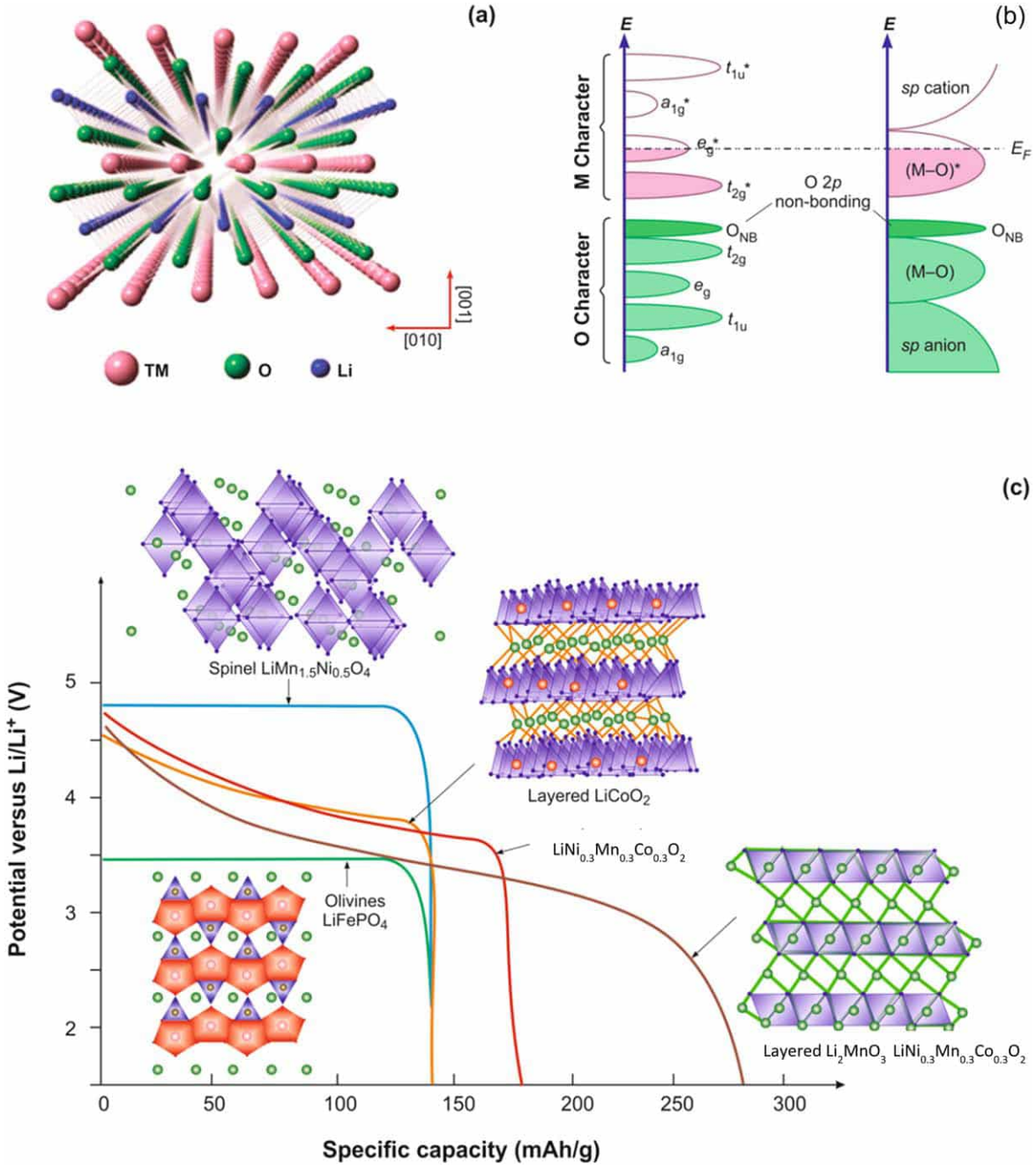


Figure 5. (a) Unit cell for the layered cathode (TM=Co, Ni, Mn),[40] (b) electronic states that contribute to the formation of bands in the density of states due to formation of metal-oxygen bonds within layered metal oxide cathodes,[41] and (c) specific capacities for the layered, spinel and polyanion cathode materials.[42,43] (All Figs. have been redrawn with permission).

contributes to Li^+ insertion during electrochemical charging because the 2p orbitals of the O ligands participate in the M–O band formation.[7,42,43] During charging, the oxidation state of the Co changes (e.g., Co^{3+} to Co^{4+} during charging), which results in charge compensation during Li^+ ion removal and formation of non-stoichiometric $Li_{1-x}CoO_2$ compounds. Though the theoretical capacity for Li_xCoO_2 is 280 $mA{\cdot}h{\cdot}g^{-1}$, degradation of its performance might occur at elevated temperatures. Deep cycling or a steady draw of power from the battery for an extended period of time, can result in thermal or structural instabilities that occur at high voltages.

A structural transformation from hexagonal to monoclinic will occur for $LiCoO_2$ if almost half of the lithium is extracted from the lattice during the discharge cycle. As a result, the practical capacity for LCO is 140 $mA{\cdot}h{\cdot}g^{-1}$ when charging at a voltage of 4.2 V (vs Li/Li^+).[2,7] The Li_xCoO_2 materials offer good electrical conductivity, which is attributed to the ordering of its cations and the direct Co–Co interactions within the planes containing the cobalt species. In addition to this, holes are incorporated into the low spin $Co^{3+/4+}$: t_{2g} bands during the charging process, endowing the Li_xCoO_2 with a metallic character. A significant contribution to the decay in performance of $LiCoO_2$ is structural degradation within its lattice that occurs at high voltages. These changes possibly result from an uneven lithiation and delithiation process within LMO_2 materials. For example, $LiNiO_2$ can attain a capacity of 240 $mA{\cdot}h{\cdot}g^{-1}$ and can be prepared at a lower cost in comparison to $LiCoO_2$.[44–47] But $LiNiO_2$ undergoes structural transformations from rhombohedral to monoclinic to a mixed phase. These transformations compromise the material's thermal stability during cycling and results in a

decomposition of its structure, such as a release of oxygen from its lattice. Nickel cations can also occupy sites within the lithium layers due to cation mixing with Li^+, which obstructs Li^+ migration during the charging and discharging processes. Another layered oxide of potential interest is $LiCo_{1-x}Ni_xO_2$, which can be considered as an amalgam of $LiCoO_2$ and $LiNiO_2$. The $LiCo_{1-x}Ni_xO_2$ has a higher thermal stability and structural integrity than $LiNiO_2$ for $0.1 \leqslant x \leqslant 0.3$ at cutoff voltages from 4.2 to 4.3 V (vs Li/Li^+). It is believed that Mn^{4+} can provide structural stability during the electrochemical process of charging and discharging. $LiNi_{0.5}Mn_{0.5}O_2$ has also been synthesized and exhibits a charge/discharge window of 3.6 to 4.3V associated with the transformation between the Ni^{2+}/Ni^{4+} redox states. Due to the relatively small size of Li^+ (0.71 Å) and Ni^{2+} (0.69 Å), cation exchange can occur and the Li^+ can form flower-like structures where it is surrounded by consecutive rings of $LiMn_6$ and $LiNi_6$. An irreversible capacity of 200 $mA{\cdot}h{\cdot}g^{-1}$ can be obtained for $LiNi_{0.5}Mn_{0.5}O_2$ with a relatively small amount of capacity fade during the cycle. In contrast, although $LiMnO_2$ is relatively structurally stable as the e_g band of high-spin Mn^{3+} lies above the O^{2-}: 2p levels, the Mn^{3+} is octahedrally coordinated and prone to Jahn-Teller distortions. The Jahn-Teller effect is regarded as a geometric distortion that reduces symmetry and energy of a non-linear molecular system, such as for octahedral complexes since their axial and equatorial bonds are unequal.[1–3] These properties result in a transformation of $LiMnO_2$ to a spinel structure upon repeated electrochemical cycling.[48–50]

In 1999, Liu et al. developed a new series of cathode materials containing $LiNi_xMn_{1-x-y}Co_yO_2$ (NMC), which can be visualized as a solid solution of $LiNiO_2/LiMnO_2/LiCoO_2$.[51] Within an ideal NMC structure, the anions occupy 6c sites to form a close-packed geometry with the 3a and 3b sites occupied by Li^+ and transition metals, respectively. A variety of NMC compositions have been reported in the literature. Prominent examples include $LiNi_{1/3}Mn_{1/3}Co_{1/3}O_2$ (NMC 111 or 333), $LiNi_{0.5}Mn_{0.3}Co_{0.2}O_3$ (NMC 532), $LiNi_{0.6}Mn_{0.2}Co_{0.2}O_2$ (NMC 622), $LiNi_{0.4}Mn_{0.4}Co_{0.2}O_2$ (NMC 442) and $LiNi_{0.8}Mn_{0.1}Co_{0.1}O_2$ (NMC 811). For NMC materials, the Mn^{4+} is Jahn-Teller inactive and the Ni^{2+} is energetically favored for the electrochemical transformations because the single high spin Mn^{3+} e_g electron is transferred to Ni^{3+}. The Ni^{3+} has an octahedral site stabilization energy (OSSE) of $-1.35\ \Delta_o$, which is between that of Mn^{3+} ($-0.42\ \Delta_0$) and Co^{3+} ($-2.13\ \Delta_o$), yielding a competitive structural stability.[1] The NMC 111 has exhibited promising properties as a cathode material with a specific capacity of 200 $mA{\cdot}h{\cdot}g^{-1}$ for a voltage range from 2.8 to 4.6 V (vs Li/Li^+) and a reversible capacity of 160 $mA{\cdot}h{\cdot}g^{-1}$ [Fig. 5c].

Spinel oxides.—In 1980, Michael Thackeray reported the formation of $LiMn_2O_4$, the first spinel oxide for use as a cathode material in LIBs.[52,53] This material has a relatively low cost to prepare and possesses relatively fast rates of intercalation and deintercalation of Li^+ ions. The spinel structure contains a face-centered cubic packing created by its anions that occupy Wyckoff position 32e, which includes seven binary and four ternary anion substructures. The tetragonal 8a sites are occupied by lithium ions, and manganese cations occupy 16d sites, whereas the octahedral 16c sites remain empty. These empty 16c sites along with the 8a sites occupied by lithium serve as a three-dimensional (3-D) pathway for the migration of Li^+ ions. These pathways offer the lowest energy barrier to Li^+ transport. The drawback of these pathways is that they suffer from severe capacity fading upon electrochemical cycling at elevated temperatures. If the Mn^{3+} concentration is increased, Jahn-Teller distortions will occur upon changes to the crystal structure from a cubic to a tetragonal structure. Another critical issue associated with capacity fading in $LiMn_2O_4$ cathode materials is the dissolution of Mn from the lattice to the electrolyte (within acidic media), which has been attributed to result from a disproportionation reaction.[54,55] During the disproportionation reaction, the Mn^{3+} ions within the lattice are both reduced and oxidized to Mn^{2+} and Mn^{4+}, respectively, in the presence of H^+. The Mn^{2+} is leached into the electrolyte and Mn^{4+} remains within the solid as follows:[56]

$$2Mn^{3+} \rightarrow Mn^{4+} + Mn^{2+} \quad [2]$$

The dissolution of Mn^{2+} can also cause anode poisoning, thereby limiting the lifetime of the cell. Due to Mn dissolution, Li_2MnO_3 could be obtained from the spinel material as governed by the following reaction at a voltage of 4 V (vs Li/Li^+):[57,58]

$$Li_2Mn_2O_4 \rightarrow Li_2MnO_4 + MnO \quad [3]$$

MnO dissolution into the electrolyte results in an increase in the Li/Mn ratio in the residual structure along with concomitant oxidation of Mn^{3+} to Mn^{4+}. Various methodologies have been implemented to suppress Mn dissolution and to enhance cell performance. Dopants such as Mg, Al, Zn, Ti, Ni, Cu and Li have been believed to disrupt Mn–Mn interactions and to result in an improved reversibility of the charging and discharging of these cathode materials.[13–18] Another approach is to decrease the surface area of the cathode material accessible to the electrolyte by increasing the size of the $LiMn_2O_4$ particles. Although larger particles increase the electrode density and suppress Mn dissolution, it also results in an overall degradation of cell performance. Coating materials such as Al_2O_3, TiO_2, and B_2O_3 have been reported to improve cell characteristics because of the ability of the coating to prevent direct contact between the surfaces of the active cathode materials and the electrolyte.[14–17] A promising spinel composition for use as a cathode material is $LiNi_{0.5}Mn_{1.5}O_4$, which is also referred to as high voltage spinel or HVS.[1–5] Jahn-Teller distortion of Mn^{3+} can be eliminated if $LiMn_2O_4$ is doped with nickel. The inclusion of Ni^{3+} assists in promoting the oxidation of Mn^{3+} to Mn^{4+} during potential cycling. Depending on the conditions for its synthesis, $LiNi_{0.5}Mn_{1.5}O_4$ crystallizes in one of two forms: (i) an ordered lattice with a stoichiometric composition of the space group $P4_332$; and (ii) a disordered lattice with a non-stoichiometric composition of the space group $Fd\bar{3}m$.[7] For the ordered structure, empty sites occupy both the 4a and 12d positions, whereas the Li, Mn, and Ni occupy 8c, 12d and 4b sites, respectively. The Li^+ ions can take two pathways for diffusion: (i) following an 8c to 12d to 8c through the partially occupied 12d sites; or (ii) following a 8c to 4a to 8c pathway through the empty 4a sites. For materials with a disordered lattice, the 16c positions are vacant and Li^+ ions occupy 8a sites, whereas the Ni and Mn occupy 16d octahedral sites but with a random distribution.[59,60] The resulting diffusion pathway in this disordered lattice is 8a to 16c to 8a for lithium migration. The operating window for $LiNi_{0.5}Mn_{1.5}O_4$ is increased to 4.7 V (vs Li/Li^+), in comparison to ~4 V (vs Li/Li^+) for $LiMn_2O_4$, due to the formation of the Ni^{2+}/Ni^{4+} and Mn^{3+}/Mn^{4+} redox couples. The experimentally demonstrated capacity for $LiNi_{0.5}Mn_{1.5}O_4$ is 140 $mA{\cdot}h{\cdot}g^{-1}$. Although its voltage is one of the highest achievable for cathode materials, this voltage is outside of the stability window of the electrolyte. This results in the formation of the SEI and, therefore, affects the reversibility of the cell. It is also difficult to synthesize and to stabilize the high oxidation state of the $M^{3+/4+}$ species in a LiM_2O_4 spinel.

Polyanion compounds.—Polyanion compounds are regarded as a relatively new class of cathode materials, which were initially discovered by Goodenough and Manthiram.[21,24,26,39] Large tetrahedral polyanion groups $(XO_4)^{3-}$ (X = Ar, W, P, Si, Mo) stabilize the structure, and increases the redox potential of these materials by occupying lattice positions. The general formula for the polyanions is $LiM(XO_4)^{3-}$ (M=Fe, Ni, Co, and Mn).[11] Polyanions are relatively safe, environmentally friendly, cost effective to prepare, and stable to electrochemical cycling. Polyanion units share strong covalent bonds with the MO_x polyhedra. Isolated TM-oxygen polyhedral groups are often the determining factor for the electronic structure of polyanions. As a result of this, polyanion groups are primarily responsible for inducing a separation of the TM valence

electrons resulting in a relatively low electrical conductivity. The most extensively investigated polyanion is an ordered olivine structure of $LiMPO_4$ (M=Mn, Co, Ni, and Fe) [Figs. 6a, 6b)]. These phosphates have a slightly distorted hexagonal close packed (hcp) lattice that results in the formation of materials of the D_{2h} space group Pmnb.[61,62]

A representative phosphate based polyanion is $LiFePO_4$ (LFP) with an olivine structure, which can achieve high powers and can exhibit structural and thermal stability [Fig. 6a]. The P atoms are in tetrahedral sites of the lattice, and the Li/Fe^{2+} occupy octahedral sites. $LiFePO_4$ is an attractive cathode material for its superior properties such as its thermal and electrochemical stability at higher operating voltages, its relatively low cost to prepare, its excellent stability to electrochemical cycling, a high theoretical capacity of 170 $mA{\cdot}h{\cdot}g^{-1}$, and a stable redox potential of 3.5 V (vs Li^+/Li). The LFP crystals possess anisotropic features, which suggests that their electrochemical performance can depend on their microstructure.[61–63] The anisotropic structure of LFP is attributed to the one-dimensional channels of lithium ions that form along the [010] direction surrounded by the tetrahedral PO_4. The corners of the unit cell in LFP share FeO_6 and the edges share LiO_4, which propagate along the b-axis in a direction parallel to the c-axis. The FeO_6 octahedra are separated by PO_4 tetrahedra, which interrupt electron conduction through the FeO_6 scaffolding. This structure results in a relatively low electrical conductivity of LFP ($\sim10^{-9}$ S cm^{-1} at room temperature or RT). This low conductivity is one of the main hindrances to a more wide-spread utilization of LFP as a cathode material.[64,65]

To improve the conductivity of these materials three approaches have been used: (i) doping Fe with other conducting elements; (ii) enhancing the available surface area through reducing the particle size; and (iii) applying a conductive coating on the LFP particles. $LiMnPO_4$ can achieve higher operating potentials and energy densities than $LiFePO_4$ [i.e., LMP achieving 4.1 V (vs Li/Li^+) and 700 $W{\cdot}h{\cdot}kg^{-1}$].[64–66] Olivine $LiMnPO_4$ and LFP are isostructural with an almost identical electrochemical capacity. The Mn^{3+} ions can cause significant lattice distortions due to the Jahn-Teller effect, and these materials can also suffer from a low electrical conductivity ($\sim10^{-14}$ S cm^{-1}). In comparison to the volume change between $LiFePO_4$ and $FePO_4$, the $LiMnPO_4$ tends to exhibit a higher volume change of 9.5% between the $LiMnPO_4$ and $MnPO_4$ phases. The $LiCoPO_4$ and $LiNiPO_4$ are also attractive alternatives as cathode materials as they are capable of achieving potentials of 4.8 and 5.1 V (vs Li/Li^+), respectively.[62–66] At these high voltages the electrolyte will decompose and compromise the overall electrochemical performance.

Orthosilicates (Li_2MSiO_4, M = Fe, Co, Ni, Mn) is another class of polyanion cathode material that has attracted interest due to their properties. These properties include their improved safety, lower cost, and enhanced electrochemical performance. Layers of silicates and TMs within orthosilicates share edges, within a Pmn2 structure.[11,67–69] Orthosilicates possesses a framework that improves the reversibility of changes to the oxidation state of the TM [Fig. 6b]. Theoretically the SiO_4^{4-} groups enable the valence of the 3d metals to change between +2 and +4 to accommodate the de-intercalation of two lithium ions per formula unit. For Li_2MSiO_4, the theoretical capacity is $\sim$333 $mA{\cdot}h{\cdot}g^{-1}$ if two Li^+ ions are fully extracted per formula unit.[67,68] Generally, Li_2MSiO_4 compounds exhibit several polymorphs categorized as β and γ phases, which depend upon the distribution of cations within the two available tetrahedral sites. For Li_2FeSiO_4, the theoretical capacity is reported to be 166 $mA{\cdot}h{\cdot}g^{-1}$ because the Fe^{3+}/Fe^{2+} redox couple is relatively difficult to access:[70,71]

$$Li_2FeSiO_4 \rightarrow LiFeSiO_4 + Li^+ + e^- \quad [4]$$

The Li_2MSiO_4 (M=Mn, $Mn_{0.5}Fe_{0.5}$, Fe, Co) materials follow the Curie-Weiss law for their temperature dependence and long-range M–O–Li–O–M interactions give rise to antiferromagnetic ordering at low temperatures.[70–72] The Li_2CoSiO_4 polymorphs (Pmn2, Pbn2, Pmnb, and $P2_1ln$) have relatively poor electrochemical performance and their structural differences do not significantly alter the potentials for lithium insertion and removal. The Li_2MnSiO_4 possess a higher specific capacity (i.e., $\sim$333 $mA{\cdot}h{\cdot}g^{-1}$) and a higher redox potential than Li_2FeSiO_4 because two Li^+ ions can participate in the electrochemical transformation. The redox couples for Li_2MnSiO_4 are Mn^{2+}/Mn^{3+} and Mn^{3+}/Mn^{4+} with transformations at 4.1 and 4.5 V (vs Li/Li^+), respectively. The Li_2MnSiO_4 does, however, suffer from capacity fade and degradation due to its relatively low electrical conductivity ($\sim5 \times 10^{-16}$ S cm^{-1} at room temperature).[72] It has been proposed that the instability of the Co^{4+} and Mn^{4+} species occupying the tetrahedral sites can result in

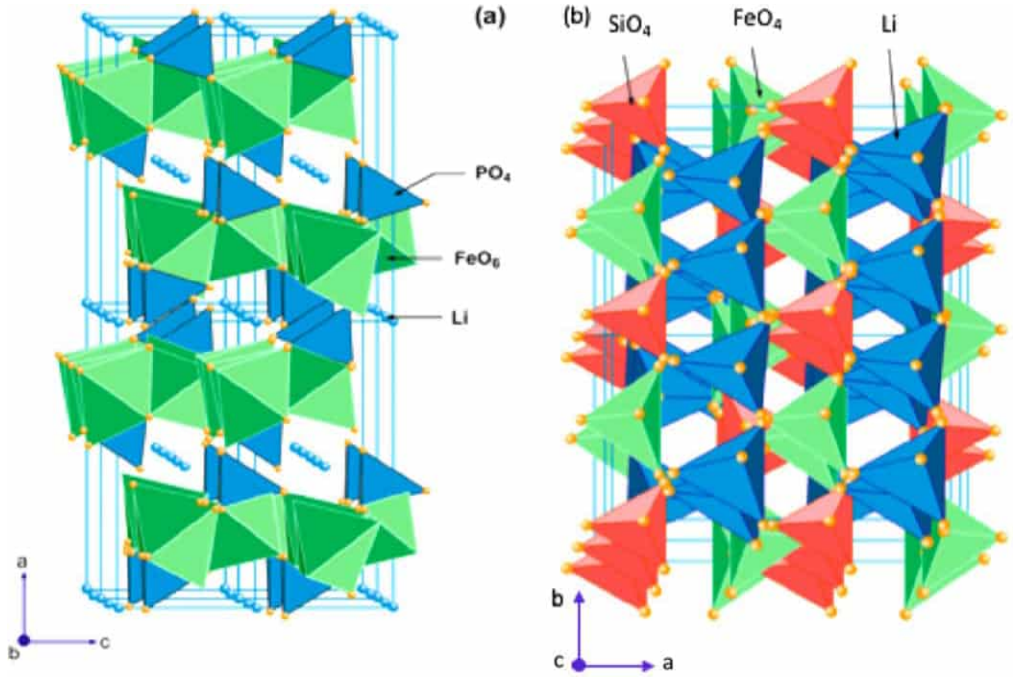


Figure 6. Olivine crystal structures for: (a) $LiFePO_4$; and (b) Li_2FeSiO_4. Redrawn with permission.[11]

a poor performance for the corresponding Li_2MSiO_4 (M = Mn, Co) materials because of the tendency of these metal ions to prefer octahedral coordination.[64–66]

Changes to the electronic structure (orbital filling) of orthovanadate polyanions have been simulated using density function theory (DFT) by substituting SiO_4^{4-} with VO_4^{3-} polyanions.[11] These DFT calculations have indicated that substituting 12.5% of VO_4^{3-} into these sites can significantly enhance their capacity. Fluorophosphates, fluorosulphates, and borates have also been evaluated as potential cathode materials.[73,74] Fluorophosphates (e.g., PO_4F) is assumed to be an amalgam with contributions from the inductive effect of the phosphate and the relatively high electronegativity of the F^- anion. The $LiVPO_4F$ cathode materials can achieve a potential of ~4.2V (vs Li/Li^+) based on the reversibility of the V^{3+}/V^{4+} redox couple. Preliminary investigations have revealed an excellent thermal stability for this material and a capacity of ~155 $mA{\cdot}h{\cdot}g^{-1}$.[74–76] In addition, Li_2CoPO_4F and Li_2NiPO_4F have also been proposed as suitable candidates for cathode materials.[77–79] Although the theoretical capacity is estimated to be around 310 $mA{\cdot}h{\cdot}g^{-1}$, the stability to potential cycling (i.e., charge and discharge cycles) and their specific capacity still need to be validated due to the absence of an electrolyte with an appropriate potential window for these materials. In addition, fluorosulphates such as $LiMgSO_4F$ can achieve Li^+ ion conduction with a reversible capacity of ~140 $mA{\cdot}h{\cdot}g^{-1}$ around 3.6 V (vs Li^+/Li) at a rate of C/10 (C-rates are the determining factor for the charging and discharging capability of the secondary batteries).[80,81] The $LiFeSO_4F$ have a relatively high ionic conductivity (~4×10^{-6} S cm^{-1}) in contrast to that of $LiFePO_4$, which eliminates the need of applying a coating material to the $LiFeSO_4F$.[81] Borate-based polyanion compounds such as $LiMBO_3$ (M = Mn, Fe, Co) can achieve a reversible capacity of ~200 $mA{\cdot}h{\cdot}g^{-1}$ around 3 V (vs Li/Li^+). Initial calculations have indicated that $LiFeBO_3$ cathode materials can suffer from surface poisoning, which will decrease its achievable potential and performance.[82,83]

Why are Surface Coatings Required for Cathode Materials?

Multiple phenomena take place the interfaces within LIBs, including: (i) diffusion of Li^+ with the electrolyte; (ii) charge transfer to and from the lattice sites of the electrodes; (iii) Li^+ diffusion within the electrode materials; and (iv) interfacial or surface reactions of the active components.[13–18] To ensure the long-term stability of the battery, it is desirable that the interfaces therein have smooth surfaces without cracks, pores, or dendritic structures. The evolution of the interface depends on the nature of the electrolyte and the intrinsic properties of the active materials. Both doping and applying coatings have been investigated as a potential means to reduce surface degradation of the cathodes. Doping can include an aliovalent substitution and multivalent substitution with a species that is electrochemically inactive while increasing the electronic and ionic conductivity, whereas a coating introduces a buffer layer between the cathode and the electrolyte to improve the chemical stability of the interface.[16–18] Doping of elements into the cathode materials can lead to a concentration gradient; hence the proper amount of dopant should be considered as a higher or lower concentration might cause poor electrochemical cycling and a capacity decay, specifically for nickel-rich cathode materials. Coatings on other hand can be amorphous or crystalline, and the most important parameter of a coating is to optimize their thickness to enable an efficient Li^+ diffusion. Compared to coatings, dopants can also increase mechanical stresses at the grain boundaries causing particle fracturing.[18–20]

Hence, the introduction of suitable “buffer” layers or coatings between the cathode materials and the electrolyte have been sought to stabilize the interface. Coatings provide a means to prevent side reactions [Fig. 7a]. One of the important advantages of applying a coating is for scavenging of hydrofluoric acid (HF). Surface corrosion in batteries results in part from the formation of HF as a byproduct of the decomposition of $LiPF_6$ in the presence of moisture:

$$LiPF_6 + H_2O \rightarrow POF_3 + 2HF + LiF \quad [5]$$

$$2POF_3 + 3Li_2O \rightarrow 6LiF \downarrow + P_2O_5 \quad [6]$$

LiF is insulating in nature, which hinders the lithium migration and charge transfer, resulting in a deterioration of the performance of the battery [Fig. 7b]. Hence, coatings are sought to help suppress the formation of this insulating phase. In the following sections, we will discuss the compositions and properties of the coatings and the techniques to synthesize these coatings.

Different Types of Coatings

Oxide coatings.—Alumina (Al_2O_3) coatings.—Alumina (Al_2O_3) reacts with LiOH and Li_2CO_3 in Ni-rich cathode materials at elevated temperatures. The Al_2O_3 exhibits a relatively high hardness and a resistance towards chemical attack by acidic and alkaline species. Coatings of Al_2O_3 also improve the chemical stability of the interface along with providing pathways for Li^+ diffusion. Reports indicate that 1.5 wt% Al_2O_3 coated onto over lithiated $Li_{1.17}Ni_{0.135}Mn_{0.56}Co_{0.135}O_2$ cathode material has yielded a higher Li^+ diffusion and a higher specific exchange current at lower temperatures than for the uncoated cathode materials.[84] The uncoated $Li_{1.17}Ni_{0.135}Mn_{0.56}Co_{0.135}O_2$ exhibit a much steeper increase in charge transfer resistance (R_{ct}) as a function of increasing temperature. The coated $Li_{1.17}Ni_{0.135}Mn_{0.56}Co_{0.135}O_2$ achieved a specific capacity >300 $mA{\cdot}h{\cdot}g^{-1}$ when charged to 4.5 V (vs Li/Li^+, C/20). In contrast, the Al_2O_3 created a close interconnectivity between the NMC 532 cathode particles at high sintering temperatures, and indicated a relatively homogeneous lithium doping of the Ni-rich cathode and its coating.[17,85] As the coating content decreases from 2% to 1% and 0.5%, the initial capacity increases from 168.5 to 176.4 and 179.4 $mA{\cdot}h{\cdot}g^{-1}$ (3 to 4.5 V at C/10),respectively. These results indicate that a thinner coating could mitigate the capacity loss. In comparison, an Al_2O_3 coated lithiated LCO/Li yielded a specific capacity of ~190 $mA{\cdot}h{\cdot}g^{-1}$ when charged to 4.5 V at C/9 (vs Li/Li^+).[16,85,86] A separate study investigated the effects of Al_2O_3 and $LiAlO_2$ coatings applied to NMC 622 particles.[87] This study found that ultrathin coatings of $LiAlO_2$ on the NMC 622 cathode particles maintained a reversible capacity up to 149 $mA{\cdot}h{\cdot}g^{-1}$ after 350 cycles. The Al_2O_3 coated NMC 622 exhibited rate capacities of 196.9 $mA{\cdot}h{\cdot}g^{-1}$ and 131.9 $mA{\cdot}h{\cdot}g^{-1}$ at 0.2C and 3C charging rates, respectively.

The effect of applying two distinct types of coatings has also been studied using alumina-based materials. For example, NMC 622 particles have been coated with both Al_2O_3 and a conductive copolymer poly(3,4-ethylenedioxythiophene)-co-poly(ethylene glycol) (or PEDOT-co-PEG).[88] The cycle stability of these cathode materials were significantly enhanced under harsh testing conditions and the coated electrode retained 94% of its initial capacity even after 100 cycles. Another study prepared an NMC 532 cathode material with a coating containing both Al_2O_3 and $AlPO_4$, which were deposited using a wet chemical method outlined in Fig. 8.[89] The NMC 532 particles with a $Al_2O_3/AlPO_4$ coating exhibited a lower polarization resistance (R_p) and a lower contact transfer resistance (R_{ct}) than the uncoated particles or those coated with a single layer, which resulted in improved electrochemical properties of the coated NMC materials.

It is important that the coating sufficiently covers all surfaces of the active cathode materials to realize the benefits and limitations of the coating in contrast to the properties of the pristine materials. In the case of the doubly coated NMC materials with a coating that contained both Al_2O_3 and $AlPO_4$ its thickness was ~20 nm, whereas the singly coated NMC materials had a coating of either Al_2O_3 or $AlPO_4$ with a thickness of ~30 to 40 nm (Fig. 9). Although the double coating produced a thinner film over the NMC particles, this

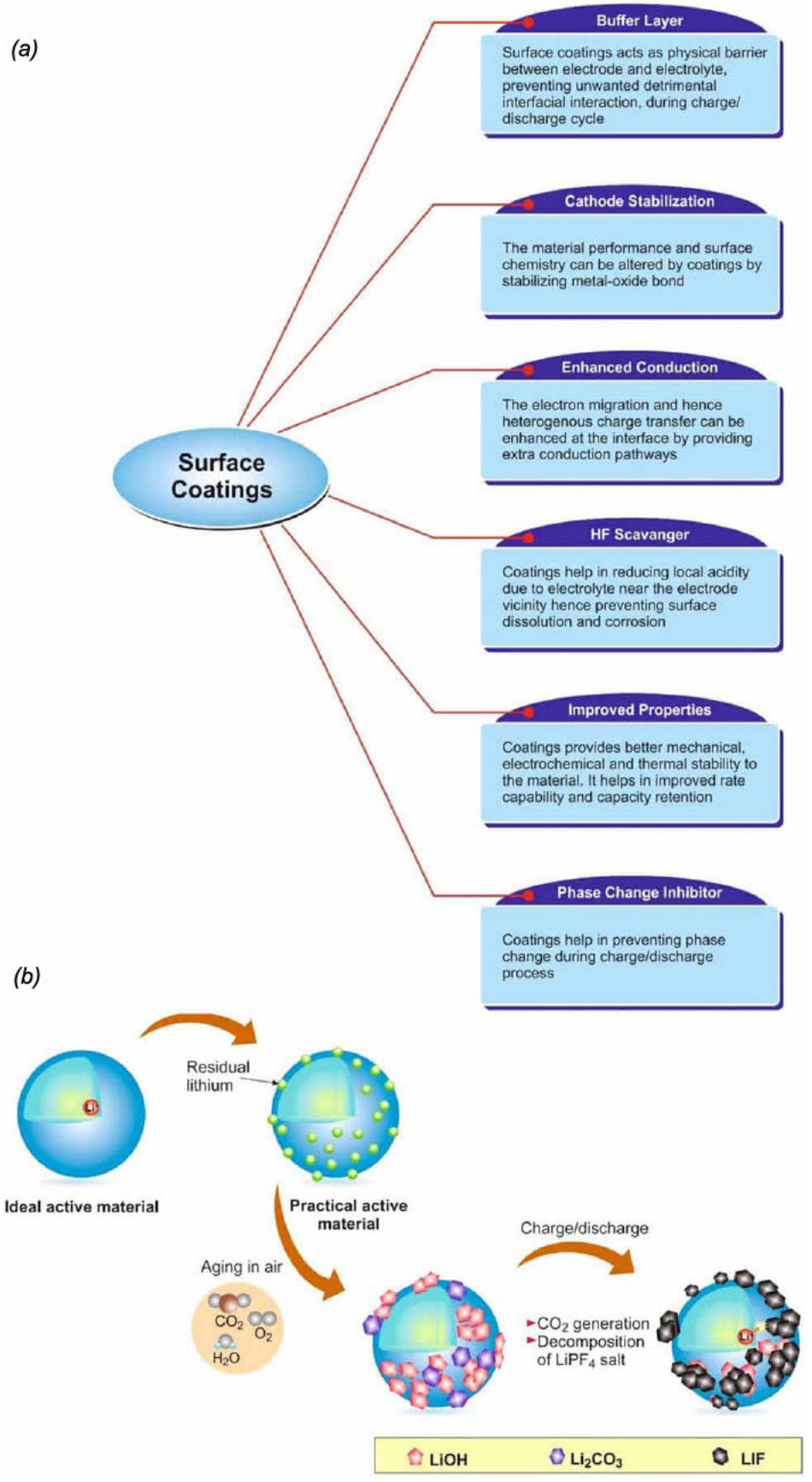


Figure 7. (a) Roles of surface coatings on cathode materials, and (b) formation of an insulating phase on the surfaces of an active materials, redrawn with permission.[19]

coating was also denser than the single coatings. These results suggested that the reactants of the second layer (applied using a solution-based method depicted in Fig. 8) strongly interacted with and potentially penetrated into the first layer. The double coating process was not merely one coating on top of another coating, but instead the combination of the two chemistries altering the properties

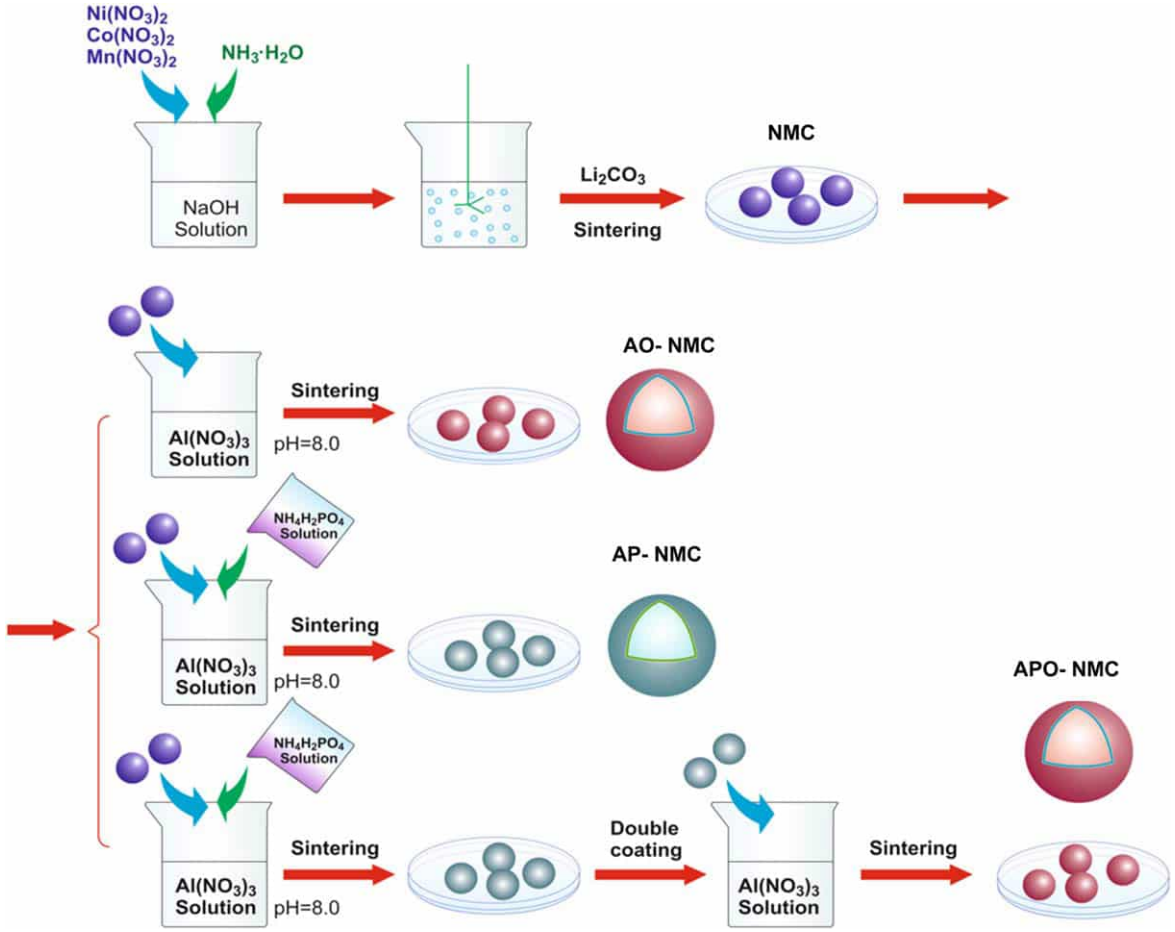


Figure 8. Schematic for depiction of the synthesis of NMC materials and the preparation of double coated NMC particles (AO = Al_2O_3; AP = $AlPO_4$; APO = both AP and AO); redrawn with permission.[89]

of the resulting film. The resulting Al_2O_3/NMC, $AlPO_4$/NMC and Al_2O_3–$AlPO_4$/NMC particles exhibited discharge capacities of 179 $mA{\cdot}h{\cdot}g^{-1}$, 174 $mA{\cdot}h{\cdot}g^{-1}$ and 180 $mA{\cdot}h{\cdot}g^{-1}$, respectively.

In contrast, a discharge capacity of 174 $mA{\cdot}h{\cdot}g^{-1}$ was achieved for the core NMC cathode material in the absence of any coating. The doubly coated materials exhibited a slight improvement in its capacity, which was attributed to combining the properties of both types of coatings. Double layer coatings provide better protection and less reactivity towards the electrolyte hence stabilizing the interface. However, the thickness of the coating material and relative ratios of the components therein should be carefully tailored to minimize the obtain least contact resistance and to enhanced Li^+ transport.

In a recent study, Al_2O_3 coatings were applied to NMC 532 particles using two different methodologies: (i) a solution-based coating method; and (ii) atomic layer deposition (ALD).[90] When the samples were prepared by solution-based processes, the particles were annealed at 800 °C for 8 h to strengthen the interactions between the Al_2O_3 coating and the core NMC 532 particles. This heat treatment likely resulted in the formation of $LiAlO_2$ species at the interface between the cathode particles and their coating. When the alumina loading is decreased from 0.5 wt% to 0.2 wt%, the capacity retention of the samples coated by solution-based techniques exhibited a considerable decrease, which was attributed to a decreased coverage of alumina over the surfaces of the particles. In comparison, the alumina coatings prepared using ALD processes exhibited less influence from the inclusion of a post-coating annealing step. A separate study found that low temperature ALD of Al_2O_3 onto NMC 622 prevented the leaching of transition metals and preserved the bulk lattice structure after potential cycling for 1,400 cycles.[91] Figs. 10a and 10b depict the data from potential cycling that was averaged over at least 4 independent experiments to assess the significance of the results of the ALD-based coating in comparison to the pristine NMC particles. The values of 4 and 10 indicate the number of ALD growth cycles used to prepare the respective coatings.

The ALD-10@NMC-622 and ALD-4@NMC-622 each outperformed the pristine NMC 622 particles with specific discharge capacities of 127.2 ± 0.6 $mA{\cdot}h{\cdot}g^{-1}$, 126.5 ± 0.4 $mA{\cdot}h{\cdot}g^{-1}$ and 123.3 ± 0 $mA{\cdot}h{\cdot}g^{-1}$, respectively. The Coulombic efficiency increased by up to 99.8% within the first 20 cycles for the coated particles, which suggested that the coating increased the energy barrier for the ionic charge transfer. The thin alumina coating was sufficient to suppress unwanted side reactions at the interface with the electrolyte at high voltages.[92] Increasing the C-rate from 0.1C to 2C resulted in a higher polarization and a decrease in the capacity of the Al_2O_3 coated LNMO materials. Some of the initial capacity was recovered after a prolonged process of charging and discharging at 4C. This process likely results in a severe degradation of the core LNMO particles during the charge-discharge cycling [Figs. 10c, 10d].

Additional studies have also indicated that the retention of capacity for cathode materials could be increased with the inclusion of an alumina coating. For example, it has been reported that Al_2O_3 coated NMC 622 exhibited an increase in retention of capacity (relative to pristine NMC 622 cathodes) from 91% to 93% after 100 cycles (at a 0.5C rate).[88] A series of Al_2O_3 coated NMC 532 cathode particles were also prepared by varying the annealing temperature, as well as the selection of precursors, solvents and concentrations of the precursors (e.g., 0.2 to 2 wt%).[93] These precursors included aluminum nitrate, aluminum acetate, aluminum isopropoxide, and

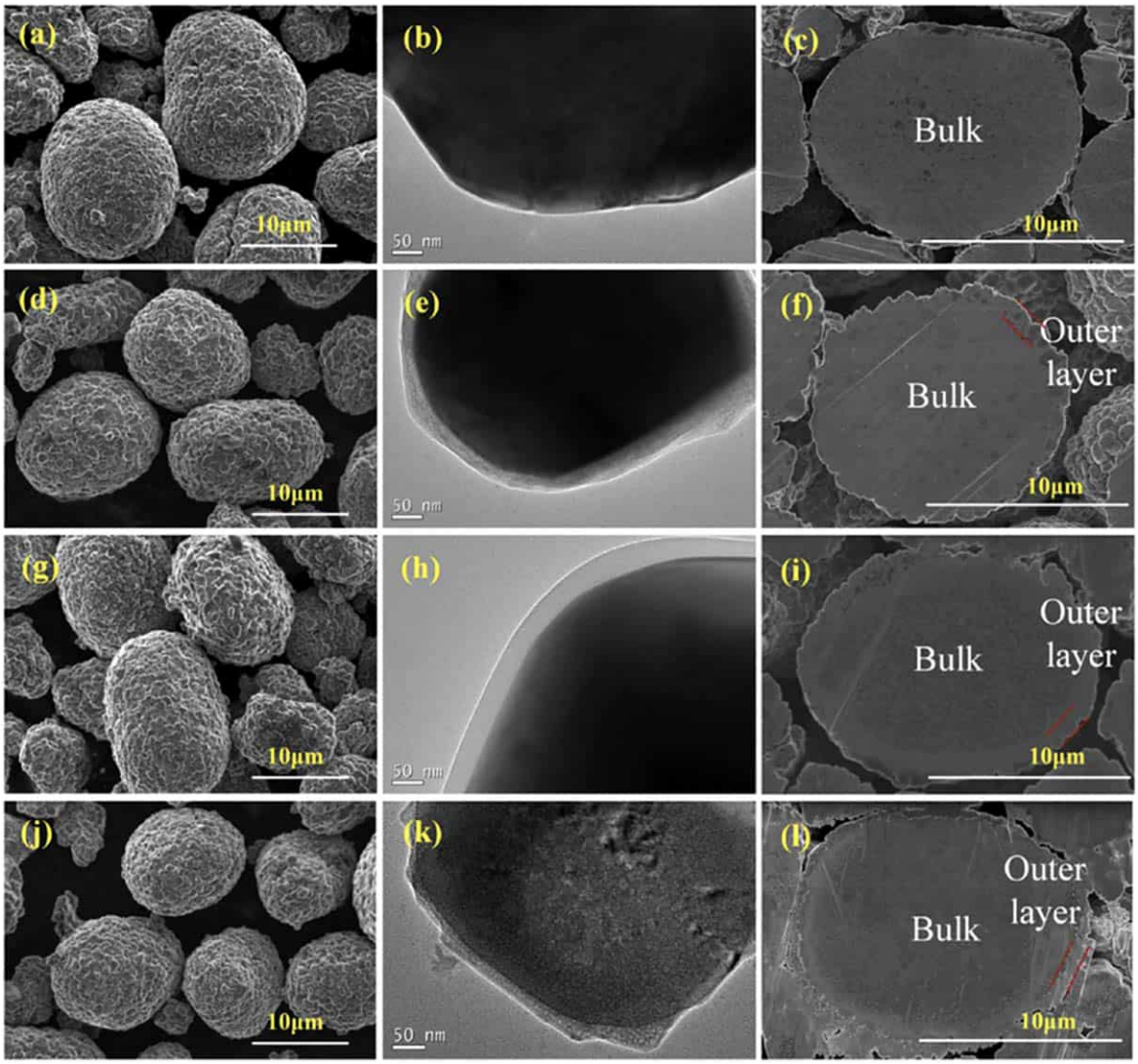


Figure 9. Morphology of cathode particles and, where applicable, an applied coating as seen by SEM of cross-sections of: (a)–(c) pristine NMC 532; (d)–(f) Al_2O_3 coated NMC 532; (g)–(i) $AlPO_4$ coated NMC 532; and (j)–(l) $AlPO_4$ and Al_2O_3 coated NMC 532, reproduced with permission.[89]

aluminum chloride. The solvents evaluated in this study were methanol (MeOH), ethanol (EtOH), xylene and water. Annealing at 800 °C formed additional $LiAlO_2$ phases and resulted in a crystallization of the interface between the coating and the particles regardless of the procedure used to prepare the coatings. This annealing process improved the reversibility of the potential cycling for the 0.2 wt% Al_2O_3 coated NMC 532 when compared to the performance of pristine cathode materials. A related study investigated the effects of changing the composition of transition metals within $LiNi_xMn_yCo_{1-x-y}O_2$ cathode materials along with applying an alumina coating.[94] The alumina coatings diffused into the bulk cathode material after annealing at high temperatures, such as those cathodes prepared from $LiNi_{0.5}Mn_{0.3}Co_{0.2}O_2$ (NMC 532), $LiNi_{0.6}Mn_{0.2}Co_{0.2}O_2$ (NMC 622), and $LiNi_{0.8}Mn_{0.1}Co_{0.1}O_2$ (NMC 811) (Fig. 11). At an Al_2O_3 loading of 0.5 wt%, relatively smooth interfaces were obtained for each of these coated NMC particles after annealing at 800 °C. Upon increasing the loadings to 5 wt%, small particles could be seen on the surfaces of the NMC 532 and NMC 622, possibly due to aggregation of excess Al_2O_3. For NMC 811, the Al_2O_3 coating might have diffused into the bulk particles after annealing such that there were no Al_2O_3 particles observed on their surfaces even at higher loadings up to 5 wt% (Fig. 11). The fundamental understandings on interphase chemistry depict that a careful selection of the preparation method, solvents, precursors, temperature, annealing conditions, coating nature and loadings has a vital impact on the cathode performance.

Zirconium dioxide (ZrO_2) coatings.—A zirconium dioxide (ZrO_2) coating can act as a scavenger of HF and to assist in mitigating the dissolution of Mn, which hinders detrimental phase transformations at the interface between the cathode particle and the electrolyte. Increasing the operating temperature affects the cell performance via two mechanisms: (i) improved lithium ion and electron transport at elevated temperatures, which increases their electrochemical performance; and (ii) a faster Mn dissolution and electrolyte decomposition, which deteriorates their electrochemical performance. Ultrathin films of crystalline ZrO_2 have been deposited onto spinel $LiMn_2O_4$ cathode materials using ALD at 120 °C.[95] The thickness of these layers could be adjusted up to 2.9 Å nm. Over this range of thicknesses, the thickness that maximized the electrochemical performance of these materials was found to be 1.74 nm. The improved performance of the 1.74-nm thick ZrO_2 coating on the cathode particles was attributed to a more uniform transport of both electrons and lithium ions through these surfaces, which led to a lower polarization resistance (transfer resistance between electrodes and electrolyte, R_p). In addition, strong oxygen bonds formed between the ZrO_2 coating and the $LiMn_2O_4$ cathode particles could reduce the Mn^{3+}/Mn^{4+} redox shift at high potentials. It has also

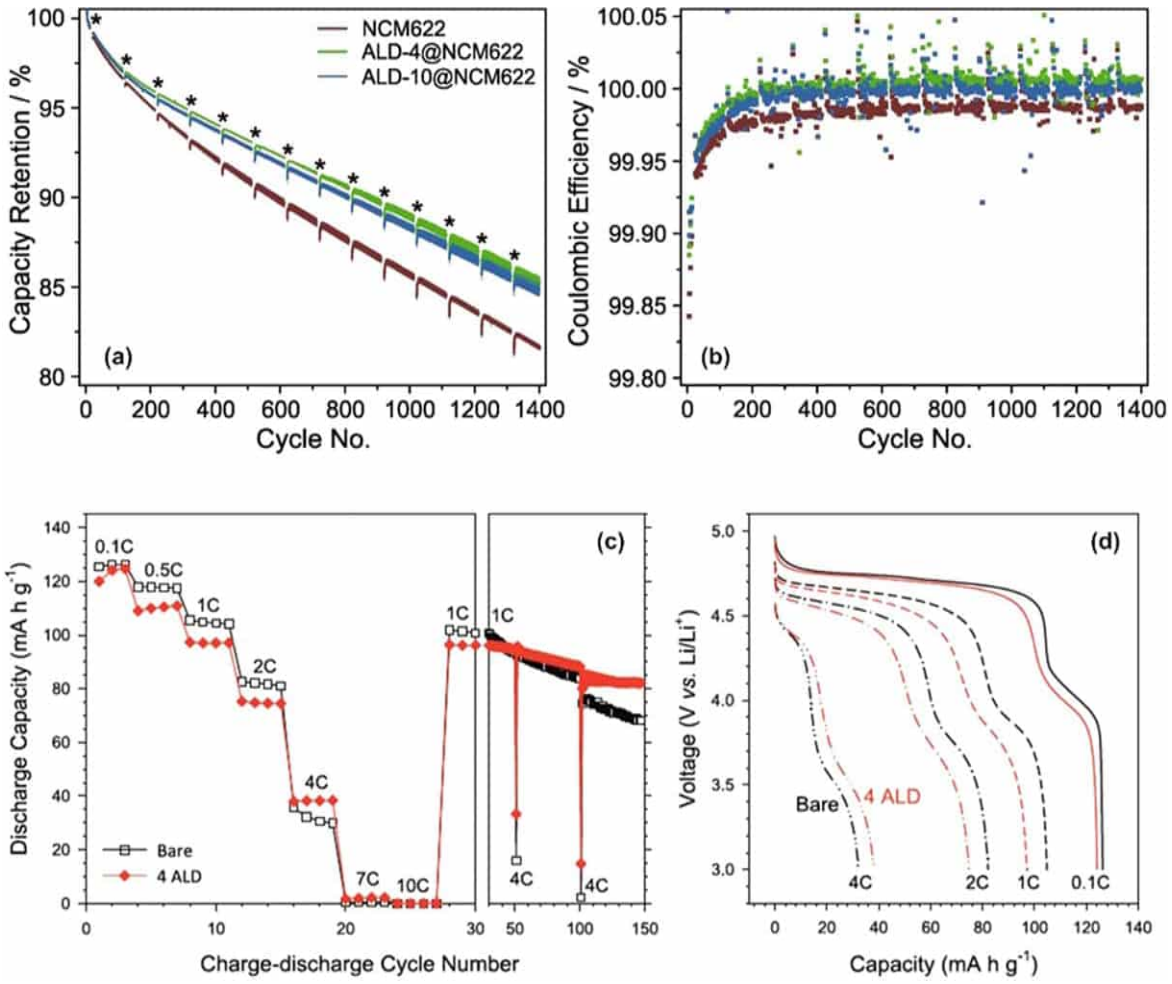


Figure 10. (a) Capacity retention relative to the 5th cycle of the discharge capacity (at a 1C rate) and (b) the Coulombic efficiency of bare NMC 622, ALD-4@NMC 622 (Al_2O_3 coating prepared by 4 cycles of ALD), and ALD-10@NMC 622 (10 cycles of ALD) reproduced with permission.[91] (c) Discharge capacities vs charge-discharge cycle number, and (d) discharge voltage profiles for bare and Al_2O_3 coated (4 cycles of ALD) LNMO cathode particles at different C-rates between 3.0 and 5.0 V (vs Li/Li^+); reproduced with permission.[92]

been found that ZrO_2 coated NMC 111 cathode materials exhibited an enhanced stability towards potential cycling and a high rate capability at a high cut-off voltage of 4.5 V (vs Li/Li^+).[96] The ZrO_2 coated cathode particles had a cell resistance that increased from 70 to 210 Ω between the 2nd and 40th cycle, which are lower values than those of the bare cathode particles. These results supported the observation that thickness of the ZrO_2 coatings affects the performance and can improve the diffusion of lithium during the charging and discharging processes.

A series of reports suggest that Zr can also yield improved performance of cathode materials through doping. For example, the Zr doping of NMC 532 can improve the stability of these cathode materials to potential cycling.[97] The use of Zr doping instead of a coating can increase the number of cycles and capacity achievable for cathode materials like $Li_{1.2}Ni_{0.13}Mn_{0.54}Co_{0.13}O_2$, LCO, and NMC 111, which has been attributed to the high bond energy of the Zr–O bonds.[98–100] For example, $Li(Ni_{0.5}Mn_{0.3}Co_{0.2})_{0.99}Zr_{0.01}O_2$ retained 84% of its capacity after 1C for 100 cycles at 4.6 V in comparison to a retention of 69% of the initial capacity for pristine cathode materials under similar cycling conditions. Discharge values up to 100 $mA{\cdot}h{\cdot}g^{-1}$ (at 8C) have been reported for Zr doped cathode materials due to a decrease of R_p. In addition, significant damage was observed in the undoped particles after 100 cycles up to 4.6 V (vs Li/Li^+). The relative stability of the Zr doped materials was attributed to the more negative value (compared to Ni and Mn) for $\Delta_f G_{ZrO_2}$ = 1042.8 kJ mol^{-1}. The lithium diffusion coefficient (D_{Li+}) for the Zr doped materials was ∼1.14×10^{-10} cm^2 s^{-1}, which was higher than that for the undoped cathode materials (i.e., 1.15×10^{-11} cm^2 s^{-1}) after the first cycle. The improved electrochemical performance of the Zr doped materials could be attributed to a lower degree of cation mixing, better kinetics for lithium transport and a lower overall impedance.

The benefits of Zr doping could extend to thin films applied to cathode materials. The benefits of the Zr incorporation depends upon the techniques used to apply these coatings and the uniformity of these films. A ZrO_2 coating on $LiNi_{0.8}Co_{0.2}O_2$ was investigated as a function of its thickness (including the uniformity of the distribution of the coating material) on the cathode material.[101] The pristine $LiNi_{0.8}Co_{0.2}O_2$ yielded an initial capacity of 181.1 $mA{\cdot}h{\cdot}g^{-1}$ vs 170 $mA{\cdot}h{\cdot}g^{-1}$ for the ZrO_2 coated cathode. Capacity retention did, however, improve through incorporation of the coating as the capacity decreased by ∼3% for the coated cathode in comparison to a decrease of ∼25% in capacity for the uncoated cathode after 50 cycles. The use of a ZrO_2 film also enhanced the structural stability of $Li_{1-x}CoO_2$ ($0 < x < 0.7$) cathode materials by suppressing the c-axis expansion or phase transition, which indicated that the delithiation process did not alter the hexagonal symmetry of this cathode material. Bare $Li_{1-x}CoO_2$ retained ∼30% of its original capacity after 30 cycles, whereas the coated sample did not yield an observable decrease in its capacity even after 70 cycles.[102–104] An NMC 532 cathode material coated with ZrO_2 using ALD techniques (e.g., 5 cycles) exhibited a high Coulombic efficiency, an improved

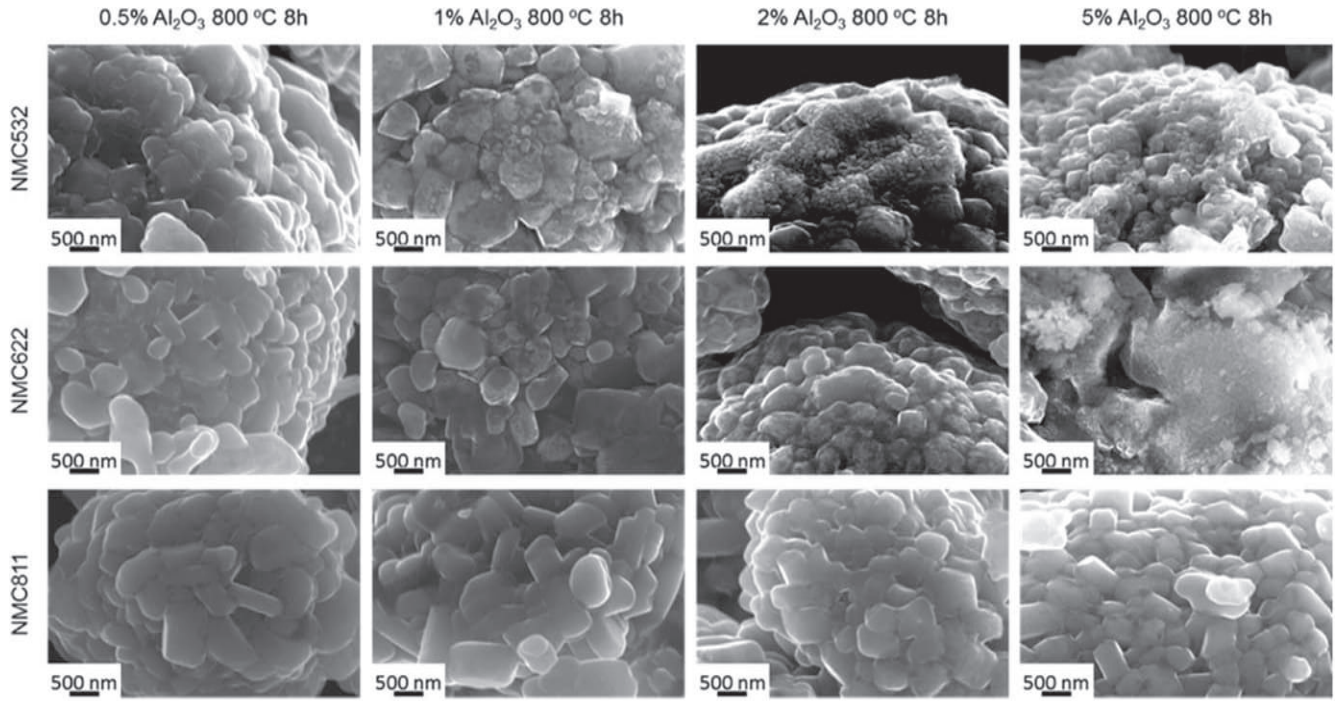


Figure 11. SEM images of alumina (Al_2O_3) coated NMC 532, NMC 622, and NMC 811, with Al_2O_3 loading of 0.5, 1, 2, and 5 wt%. Each of the samples were annealed at 800 °C for 8 h, reproduced with permission.[94]

stability to electrochemical cycling, and an improved range from 2.5 to 4.5 V (vs Li/Li^+).[105] During ALD the metal amide precursor initially interacts with the terminal OH groups on the surfaces of the cathode particles via a chemical absorption process. During this step, the metal nitrogen bond is broken, which results in the formation of a new metal bond along with the release of volatile dialkylamine by-products. In the second step, metal hydroxyl bonds and additional dialkylamines are generated when H_2O reacts with the surface bound metal amide species. Unreacted water and the dialkylamine by-products are purged from the system under an N_2 atmosphere. This process is repeated as necessary to prepare films of a different thickness. The resulting ZrO_2 coated NMC 532 particles had initial discharge capacities of 198.5 $mA{\cdot}h{\cdot}g^{-1}$, 216.5 $mA{\cdot}h{\cdot}g^{-1}$, and 206.1 $mA{\cdot}h{\cdot}g^{-1}$ for ZrO_2 coatings prepared from 2, 5, and 8 ALD cycles, respectively. In comparison, the discharge capacity of the pristine cathode materials was 190.1 $mA{\cdot}h{\cdot}g^{-1}$. The ZrO_2 coating prepared by 5 ALD cycles retained ~89% of its discharge capacity (i.e., 155.3 $mA{\cdot}h{\cdot}g^{-1}$) after 50 cycles, in comparison to a decrease to 101.7 $mA{\cdot}h{\cdot}g^{-1}$ for the pristine, uncoated cathode particles. The Li^+ diffusion constants for these materials can be calculated from their Nyquist plots [Figs. 12a, 12b] using the following equations:

$$D_{Li^+} = \frac{0.5R^2T^2}{n^4F^4\sigma_\omega^2A^2C^2} \quad [7]$$

where R, A, F, T, n and C are the molar gas constant, surface area from BET calculations, Faraday's constant, absolute temperature, number of electrons/molecules in the reaction, and the lithium ion concentration, respectively. The value σ_ω is the Warburg parameter, which is calculated as follows:

$$Z_{img} = k - \sigma_\omega w^{-1/2} \quad [8]$$

Z_{img} = imaginary impedance

w = angular frequency, and k is a constant

R_f and R_{ct} correspond to Li^+ ion diffusion on the surface and interface layer, respectively. R_f is attributed to the insulating solid electrolyte interface (SEI) layer formed at the surface (in the high frequency region). R_f is also formed due to electrolyte decomposition or organic compound breakdown on the electrode surface. R_{ct} is obtained from the semi-circle in the low-frequency region and

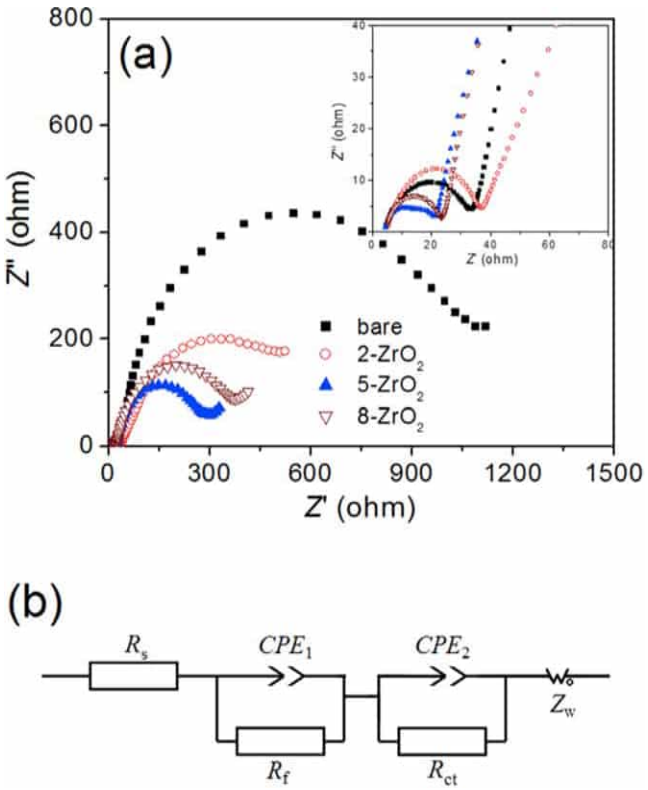


Figure 12. (a) Nyquist plots of uncoated and ZrO_2 coated NMC 532 cathode particles, and (b) a fitted equivalent circuit simulating the EIS results for measurements obtained at 4.3 V (vs Li^+/Li) at 25 °C; reproduced with permission.[105]

corresponds to the resistance to electron transfer processes from one phase to another, such as from liquid to solid or vice versa.

The values for D_{Li+} were found to be 7.38×10^{-9} cm^2 s^{-1}, 9.63×10^{-9} cm^2 s^{-1}, 2.11×10^{-8} cm^2 s^{-1} and 1.69×10^{-8} cm^2 s^{-1} for the pristine NMC, and the NMC coated with ZrO_2 prepared by 2 ALD cycles (2-ZrO_2), 5 ALD cycle (5-ZrO_2), and 8 ALD cycles (8-ZrO_2), respectively. It has been proposed that ultrathin coatings prepared from an amorphous phase can suppress the increases to the cell impedance and favor lithium diffusion due to the short-range order within these structures.

Alternatively, D_{Li}^+ can also be calculated from the relationship between peak current (I_p) and san rate from the cyclic voltammetry curves as follows:

$$I_p = (2.69 \times 10^5)\mathrm{A}\, n^3/2(D_{Li^+})^{1/2}\mathrm{C}\, V^{1/2} \quad [9]$$

where I_p is peak current (mA), A is the area of the electrode (154 mm^2), n is the number of electrons involved in electronic transfer reaction, C is the lithium concentration, and V is scan rate (mV s^{-1}). The epitaxial formation of ZrO_2 coatings on spinel $LiMn_2O_4$ particles using ALD techniques can yield a high degree of conformity and control over film thickness.[106] $LiMn_2O_4$ particles coated with ZrO_2 using 6 ALD cycles exhibited an initial discharge capacity of 136.0 mA·h·g^{-1} at 1C (55 °C), which was higher than the capacity of 124.1 mA·h·g^{-1} observed for the pristine cathode particles. A more distinct effect of the ZrO_2 coating when prepared by ALD techniques was observed for the retention of capacity at high rates of charge and discharge, as well as at elevated temperatures. For example, at a current density of 600 mA·h·g^{-1} (~5C at 55 °C), the ZrO_2 coatings prepared by 2 ALD cycles exhibited a high initial discharge capacity of 123.4 mA·h·g^{-1} in comparison to the discharge capacities of 112.7 mA·h·g^{-1}, 88.5 mA·h·g^{-1}, and 114.6 mA·h·g^{-1} for the ZrO_2 from 6 ALD cycles, 10 ALD cycles, and the pristine (or uncoated) cathode particles, respectively. The application of a ZrO_2 coating to cathode particles can significantly alter their electrochemical stability and the properties of lithium diffusion.

Magnesium oxide (MgO) coatings.—A coating of MgO has been found to have a beneficial impact on battery performance. Studies have shown that MgO coated LCO cathodes can be cycled between 2.5 and 4.7 V (vs Li^+/Li) yielding a high capacity of 210 mA·h·g^{-1} and without material degradation.[107] The MgO coating protected the active, core material from the acidic electrolyte, which prevented Co dissolution from the LCO particles. An Li_2CO_3 insulating phase can form at the LCO/electrolyte interface through a series of electrochemical reactions, but its formation was prevented up to 4.4 V by inclusion of the MgO coating.[108] Additionally, the MgO/LCO interface on the LCO particles also protects against the electrochemical reactivity of adsorbed ethylene carbonate at low voltages.

A coating of MgO prepared at a loading of <1 wt% by ALD methods on NMC 532 cathode materials provides better Li^+ ion diffusion pathways as indicated by a relatively high lithium diffusion coefficient (D_{Li}^+) at a low overpotential.[109] Other studies involved the use of magnesium ethoxide [$Mg(OEt)_2$] as a source of Mg and hydrous ethanol as a solvent to coat NMC 811 cathode particles through solution-based methods, which were followed by heat treatment to form an MgO coating. This route resulted in a change in the crystal structure of the surface states at the interface with the coating and a change in cycling performance.[110] Initial charge and discharge capacities of the MgO coated NMC 811 particles were 225.6 mA·h·g^{-1} and 190.1 mA·h·g^{-1}, respectively, and the Coulombic efficiency was 84.1%. In contrast, the charge and discharge capacities for the uncoated NMC 811 particles were 235.2 mA·h·g^{-1} and 194.2 mA·h·g^{-1}, but the Coulombic efficiency was ~83%. Due to the electrochemical inactive nature of the Mg^{2+} ions, the initial charge and discharge capacities for the coated cathode particles were lower than that of the pristine cathode particles. The enhanced Coulombic efficiency of the MgO coated NMC 811 was attributed to a decrease in the place exchange or mixing of Ni and Li within the NMC lattice. Potential cycling of the MgO coated and uncoated samples [Figs. 13a, 13b)] revealed three pairs of anodic and cathodic peaks around 3.8, 4.0, and 4.2 V (vs Li^+/Li), corresponding to the phase transition from hexagonal to monoclinic ($H_1 \rightarrow M$), monoclinic to hexagonal ($M \rightarrow H_2$), and hexagonal to hexagonal ($H_2 \rightarrow H_3$), respectively. The electrochemical voltage difference, ΔV, between the anodic and cathodic peaks for the first cycle were 0.162 V for the coated particles and 0.173 V for the pristine particles. These results indicated that the MgO coated cathode particles possess a smaller electrochemical polarization (and a higher degree of reversibility) than the pristine NMC 811 particles.

For layered LCO cathode particles, it was determined that the effects of surface modifications with MgO and doping with Mg did not alter the electrochemical potential window between 2.9 to 4.3 V (vs Li/Li^+).[111] The LCO particles were modified by solution-phase processing with $Mg(CH_3COO)$, followed by a heat treatment of the coated particles at 600 °C. After the 30th cycle, the cell capacities for the pristine and MgO modified LCO particles were 113 mA·h·g^{-1} and 135 mA·h·g^{-1}, respectively. The capacity retention for the MgO coated, Mg doped, and pristine LCO particles were 86%, 90%, and 10%, respectively. These results indicate that the replacement of Co by Mg in the LCO lattice has a positive impact on the capacity retention, although Mg did not improve the stability to potential cycling. Thin films of MgO coated on LCO were also prepared by pulsed laser deposition (PLD), which revealed that the MgO

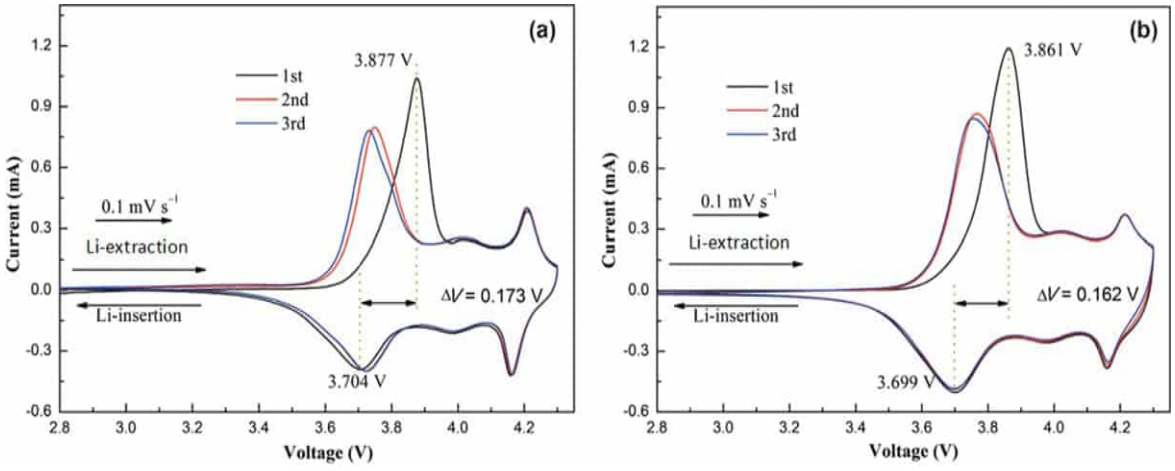


Figure 13. Cyclic voltammetry plots for the first three potential cycles from 2.8 to 4.3 V (vs Li/Li^+) for: (a) pristine NMC 811 particles; and (b) MgO coated NMC 811 cathode particles; reproduced with permissions.[110]

modification suppressed an increase in resistance following repetitive Li^+ insertion and extraction up to 4.2 V (vs Li/Li^+).[112] The charge transfer resistances (R_{ct}) for bare and coated LCO films were found to be 250 Ω and 750 Ω, respectively. A probable reason for the increase in charge transfer resistance for the coated LCO films could be due to the formation of an electrochemically inactive layer. Additional reports in the literature evaluated cobalt dissolution at potentials <4.2 V (vs Li/Li^+), and found that the separation in peak potentials was not due to Co^{4+} dissolution.[113] Another explanation for the enhanced electrochemical properties of the MgO coated cathode is an increased structural stability due to the comparable ionic radii of Mg^{2+} (86 pm) and Li^+ (90 pm). Hence, Mg^{2+} could migrate into the LiO_2 layers and could increase the attraction of adjacent CoO_2 layers and lead to the stabilization of these layers. Nano-crystalline MgO coatings deposited via sol-gel techniques onto layered LCO yielded an improved stability to potential cycling.[114] After the 40th cycle, the pristine LCO had a 13 $mA{\cdot}h{\cdot}g^{-1}$ discharge capacity in comparison to a discharge capacity of 120 $mA{\cdot}h{\cdot}g^{-1}$ for the MgO coated LCO. Pristine LCO exhibited a faster degradation in comparison to the MgO coated LCO possibly due to a mechanical failure of the uncoated electrodes due to the formation of fractures induced by cumulative stresses in these materials. Preparing MgO coatings with >1 mol% of the Mg precursor can, however, compromise the stability of the cathode materials with potential cycling along with an increase in the degradation of the discharge capacity. There was no direct evidence of Mg^{2+} substitution within the LCO materials. Future studies could include a detailed analysis of changes to the structure of the LCO and MgO/LCO interface as a function of annealing temperature for these sol-gel derived coatings.

Additional studies reported the effects of various thermal treatments to MgO coated LCO on their electrochemical performance. For example, MgO coated LCO annealed at 810 °C exhibited a high initial capacity and an ability to retain capacity over the voltage range from 3 to 4.35 V (vs Li/Li^+) at 0.2C.[115] No phase transformations were observed at the interface between the MgO coating and the LCO cathode during the charging and discharging cycles. A separate study provided further insight into the effects of the MgO coating in comparison to an Al_2O_3 coating on layered LCO materials.[116] These materials were evaluated in 18650 li^+ ion cells (18 mm diameter x 65 mm height cylindrical cell). The active cathode material was coated with either a Mg oxide or Al oxide using alkoxide-based solutions followed by their heat treatment between 300 and 500 °C. The ability of these cathode materials to retain their capacity with cycling improved for both coatings, but the Al_2O_3 coating was slightly more effective. In another study, a MgO coating on a cathode composed of a composite of 0.5 li_2MnO_3–0.5 $liNi_{0.5}Mn_{0.5}O_2$ minimizes subsequent reactions between the electrolyte and electrode and also stabilizes the structure of these cathode materials.[117] Their Coulombic efficiency increases from 73 to 75% with the application of the coating. The MgO coated cathode exhibited a discharge capacity of 143 $mA{\cdot}h{\cdot}g^{-1}$ after the 25th cycle, in comparison to 223 $mA{\cdot}h{\cdot}g^{-1}$ for the uncoated cathode material after 20 cycles. This decreased capacity for the MgO coated cathodes was attributed to the lower electronic and ionic conductivities of this coating. These results reveal that the cathode surface modification by MgO is effective to improve the lithium-ion transfer reaction kinetics electrode—electrolyte interface.

Titanium dioxide (TiO_2) coatings.—Titania (TiO_2) is a promising candidate for coating cathode materials and enhancing cell performance.[118–120] Coating the surfaces of NMC 532 cathode particles with nanoscale TiO_2 that contained a low degree of crystallinity resulted in these materials retaining ∼87% of their initial capacity for up to 250 cycles over the potential range from 3.0 to 4.4 V (vs Li/Li^+) and ∼87% of their capacity for up to 100 cycles over an extended potential range of 3.0 to 4.6 V (vs Li/Li^+). In comparison, capacities of ∼76% and 74.1%, respectively, were retained for the uncoated samples.[118] Additionally, the samples coated with nanoscale TiO_2 yielded a smaller degree of polarization and more intense redox peaks as observed in their response to potential cycling. A separate study prepared nanoscale TiO_2 coated LNMO cathode materials by solution-phase methods.[119] These TiO_2 coated LNMO electrodes were able to achieve discharge capacities of 97.6 $mA{\cdot}h{\cdot}g^{-1}$, 88.3 $mA{\cdot}h{\cdot}g^{-1}$, and 74.5 $mA{\cdot}h{\cdot}g^{-1}$ at 7C, 10C, and 15C, respectively. Their retention of capacity at 2C was about ∼89% after 500 cycles, indicating that the TiO_2 coating was effective in suppressing manganese dissolution into the electrolyte. In addition, the coated LNMO had a much higher impedance slope in response to low frequencies in contrast to the pristine LNMO materials, which indicated a better Li^+ conductivity through the coated cathodes. Another study used a co-precipitation technique to prepare coatings of anatase-based TiO_2 nanoparticles on the surfaces of $Li(Li_{0.2}Ni_{0.13}Mn_{0.54}Co_{0.13})O_2$ cathode materials. The TiO_2 nanoparticles adhered strongly to these cathode materials, and exhibited a uniform distribution over their surfaces. The pristine electrode exhibited an initial discharge capacity of 248.0 $mA{\cdot}h{\cdot}g^{-1}$ and a capacity retention of 67% after 100 cycles (0.5C), whereas the nanoscale TiO_2 covering the cathode materials had a discharge capacity of 243.8 $mA{\cdot}h{\cdot}g^{-1}$ and capacity retention of 84% under same potential cycling conditions. The transfer coefficient (α) and $D_{Li}{}^+$ for the TiO_2 coated cathode materials were reported to be 0.126 and 2.7×10^{-12} $cm^2\ s^{-1}$ and for pristine cathode materials were 0.164 and 10×10^{-11} $cm^2\ s^{-1}$, respectively. The transfer coefficient indicates the energy barrier symmetry and its value lies in between 0 to 1 (i.e., if its values is towards 0 side then it is considered to be more like a reactant and if its value is towards 1 this would indicate a more product like nature). This emphasizes that coatings induced more reactant like characteristics to the cathode material, which is favorable to avoid any interfacial degradation. These results indicate a dual character of the semiconducting TiO_2 nanoparticles.

A series of TiO_2 coated Li_2MnO_3 with a varying thickness of the titania layers were prepared using different amounts of a titanium butoxide precursors.[121] The TiO_2 coatings prepared by the addition of 100 ml of titanium butoxide (referred to as TiO_2-100) exhibited an improved electrochemical performance in comparison to the coatings prepared from 50 ml of precursor (TiO_2-50) or 200 ml of titanium butoxide (TiO_2-200). Each of the coated samples exhibited an oxidation peak centered at 4.1 V (vs Li/Li^+) corresponding to the delithiation of the layered electrodes, and with corresponding reduction peaks centered at ∼4.0 V and 2.7 V (vs Li/Li^+). As the coating thickness increased, the discharge capacity decreased, which could have been due to the formation of Li_xTiO_2 within the TiO_2 layer. The $D_{Li}{}^+$ for the films derived from TiO_2-100 were found to be 1.3×10^{-14} $cm^2\ s^{-1}$ after the first cycle, which was higher than the values observed for the other coated samples and the uncoated cathode materials. The discharge capacity and charge retention for the TiO_2-100 sample was found to be 125.2 $mA{\cdot}h{\cdot}g^{-1}$ and 66%, respectively, which were higher than the values observed for the uncoated sample (81.4 $mA{\cdot}h{\cdot}g^{-1}$ and 38.3%), the TiO_2-50 coated sample (99.5 $mA{\cdot}h{\cdot}g^{-1}$ and 48.1%), and the TiO_2-200 sample (97.9 $mA{\cdot}h{\cdot}g^{-1}$ and 54%).

The TiO_2 coating could also be directly sputtered onto the surfaces of layered LCO cathodes, which also enabled a controllable formation of the oxide coating on the surfaces of the electrode.[122] The TiO_2 layer was sputtered for different durations to control the thickness of these films, such as for 3, 5, 7, 10, and 20 s. With an increase in the sputtering time, the difference in potential between the anodic and cathodic peaks became larger, which was attributed to an enhanced electrode polarization with increasing thickness of the TiO_2 coating. A high Coulombic efficiency was observed for the TiO_2 coated electrodes in comparison to the uncoated electrodes, which also indicated the coatings suppressed irreversible electrochemical reactions that can include formation of an SEI and decomposition of electrolyte. The coated electrode could achieve a reversible capacity of 109 $mA{\cdot}h{\cdot}g^{-1}$, which was 47% higher than the capacity of 74 $mA{\cdot}h{\cdot}g^{-1}$ for the uncoated LCO. Additionally, the Li^+ ion diffusion coefficient for the TiO_2 coated electrode was found

to be 3.6×10^{-11} cm^2 s^{-1}, which was larger than that for the pristine cathode material (2.48×10^{-11} cm^2 s^{-1}). It was suggested that a reaction between TiO_2 and the HF by-product formed during cell operation could generate a metal fluoride layer that could resist electrolytic attack and enable Li^+ ion transfer through the interface. Another Ti-based modification to cathode materials has been achieved by doping with Ti.[123,124] It was found that Ti-doped NMC 811 prepared using solution-based methods could achieve a capacity of 196 $mA{\cdot}h{\cdot}g^{-1}$ at 0.5C, and 157 $mA{\cdot}h{\cdot}g^{-1}$ at 2C over a range of potentials from 2.8 to 4.6 V (vs Li/Li^+), which were 5% higher at 0.5C and 15% higher at 2C than those of the pristine NMC 811 materials. In another sample prepared by TiO_2 doping of NMC 811 (i.e., incorporating 0.005 mol TiO_2 into the NMC lattice using a solid-state technique), yielded a capacity of 214.9 $mA{\cdot}h{\cdot}g^{-1}$ at 0.1C with a stability to potential cycling of 77% at 1C for 150 cycles and 86% at 5C for 50 cycles. These doped NMC materials also had a high performance at 1C with a capacity of 165.02 $mA{\cdot}h{\cdot}g^{-1}$, as well as a capacity of 136.9 $mA{\cdot}h{\cdot}g^{-1}$ at a rate of 5C. These TiO_2 doped NMC cathode materials exhibited a diffusion coefficient of 6.8×10^{-12} cm^2 s^{-1}. These well-ordered, TiO_2 doped NMC materials exhibited a decrease in cation disordering with potential cycling and a relative increase in layer spacing for lithium transport.

If the amount of TM that transfers to the anode increased, the gas by-products produced by the cell decreases, which may seem counter intuitive as transition metals can be catalytic towards gas evolution processes under reductive conditions. The influence of titanium-based coatings on NMC 532 cathodes was also evaluated using pouch cells.[125] These coatings improved the capacity retention of cells whose electrolyte were doped with 2% vinylene carbonate. It was elucidated from these studies that the titania coating and the additives in the electrolyte each enhanced the cell performance, and prevented metal dissolution and minimized detrimental reactions with the electrolyte.

Zinc oxide (ZnO) coatings.—The ZnO coatings have been pursued for their potential to suppress cation dissolution from cathode materials by scavenging HF. Coatings on $LiMn_2O_4$ prepared from amphoteric oxides (capable of functioning as either an acid or base), such as ZnO, Al_2O_3, SnO_2, or ZrO_2, have been investigated for their ability to stabilize these cathode materials.[126] Coatings from amphoteric oxides could maintain 97% of initial capacity of the cathode after 50 cycles when compared to retaining 75% capacity in the uncoated electrode after the same electrochemical conditions. The ZnO coating was found to be most effective at scavenging HF followed by Al_2O_3, ZrO_2, and SnO_2. Plasma-enhanced chemical vapor deposition (PECVD) techniques were used to prepare ZnO coatings on LCO with a ZnO loading in the range of 0.08 to 0.49 wt %. The coatings up to 0.21 wt% yielded uniform films of ZnO nanoparticles covering the surfaces of the LCO without any change in the ZnO particle size.[127] The ZnO coatings also proved to be effective against Co dissolution. Extensive agglomeration of the ZnO particles was, however, observed on the surfaces of the cathode materials when the coating content was increased up to 0.49 wt%. The agglomerated ZnO particles could hinder lithium intercalation into the cathode and transport of Li^+ ions to and from the electrolyte. The ZnO coated LCO retained ~65% of its capacity in contrast to a retention of ~37% of the capacity by the bare cathode materials after 30 cycles. A separate study investigated the influence of the ZnO coating (also prepared by PECVD) on LCO when used in a cell that was operated at various temperatures and C rates.[128] At low operating temperatures (e.g., 0 °C), the electrochemical performance of the cathode was not significantly influenced by the thickness of the coating, which was attributed to the slower kinetics of charge transfer at lower temperatures. Increases in the thickness of the coating could suppress the degree of phase transition (and changes in the crystal structure) of the LCO. The ZnO coated LCO prepared with a 0.38 wt% ZnO loading exhibited a relatively poor reversibility at both 25 °C and 50 °C in comparison to the ZnO coated LCO prepared from a 0.20 wt% loading of ZnO. The pristine LCO had a capacity retention of ~0.2% and ~15% following potential cycling at 0 °C and 50 °C, respectively. In contrast, the 0.20 wt% loading of ZnO on LCO retained 44% and 53%, respectively, when operated under the same conditions. On the other hand, a 0.38 wt% loading of ZnO on LCO exhibited a poor performance in comparison to all the other type of electrodes, which was attributed to these thicker layers hindering the processes of inserting and extracting lithium. This effect was more pronounced under the harsh operating conditions of high charge and discharge rates and reduced or elevated temperatures.

An ultrathin layer of amorphous ZnO was deposited onto NMC 532 cathode materials at elevated temperatures using ALD technology.[129] At a low rate of charge and discharge at 0.2C, both the coated and uncoated samples exhibited a reversibility of nearly 100% after 20 cycles. At elevated temperatures the uncoated electrode exhibited a decrease in its discharge capacity with retaining only 87% of its initial capacity after 60 cycles at 2C, whereas the ZnO coated sample retained up to 92% of its capacity under the same electrochemical conditions. Additionally, the ZnO coated NMC 532 yielded a discharge capacity of 256.7 $mA{\cdot}h{\cdot}g^{-1}$ at 1C, which was 30% higher than that achieved by the uncoated sample. In a separate study, a ZnO coating was prepared by co-precipitation on a composite of 0.5 li_2MnO_2–0.5 $liNi_{0.5}Mn_{0.5}O_2$.[130] These coated materials exhibited a high charge and discharge capacity, a faster activation, and an improved rate performance than the uncoated materials. No significant change in the discharge capacity was observed when the C rate was increased from 0.05C to 0.1C for both the ZnO coated and uncoated cathode materials. At a rate of 0.2C the discharge capacities of the ZnO coated cathode and pristine cathode were 206 $mA{\cdot}h{\cdot}g^{-1}$ and 185 $mA{\cdot}h{\cdot}g^{-1}$, respectively. A separate study used reactive magnetron sputtering to prepare a ZnO coating on 0.3 $li_2MnO_{3-0.7}$ $liNi_{5/21}Mn_{11/21}Co_{5/21}O_2$ (LMO-NMC) cathode materials.[131] This sputtering technique achieved ZnO coatings that were ultrathin and dense, and that fully covered the electrodes. The RMS technique achieved low substrate temperatures during the coating process. These coatings were relatively uniform in thickness and exhibited a good adhesion to the substrate. A two-minute process used to coat the LMO-NMC electrodes with a thin layer of ZnO achieved a discharge capacity of 316 $mA{\cdot}h{\cdot}g^{-1}$ at 1.0C and an initial Coulombic efficiency of 89.1%. Additional studies of ZnO coatings prepared on LCO using radio frequency (RF) assisted magnetron sputtering suggested that the ZnO could fully cover the electrode and could also diffuse into the electrode materials due to the intrinsic properties of the electrode.[132] It was determined that these ZnO coatings had an optimal thickness around 17 nm, which retained 81% of its capacity after 200 cycles and exhibited an initial discharge capacity of 191 $mA{\cdot}h{\cdot}g^{-1}$ at 0.2C. These coated LCO materials exhibited a relatively high rate performance with a retained capacity of 106 $mA{\cdot}h{\cdot}g^{-1}$ at 10C. Magnetron sputtered ZnO films were also coated onto $Li_4Ti_5O_{12}$ composites.[133] Additional studies demonstrated that lithium and ZnO can reversibly react:[134,135]

$$ZnO + 2\,Li \leftrightarrow Li_2O + Zn \quad [10]$$

$$Zn + Li \rightarrow \underbrace{ZnLi}_{Zn-Li\ alloy} \quad [11]$$

Both the Zn and the ZnLi alloy have good electrical conductivities. Structural and chemical stabilization of the ZnLi is provided by the Li_2O. The theoretical capacity for this two-step process is 978 $mA{\cdot}h{\cdot}g^{-1}$, which is very high. This alloy serves as a conductive network for the transport of both ions and electrons. This material is of interest for both energy storage and as a coating on cathode materials. The highest rate performance for the magnetron sputtered ZnO films was achieved using a coating that had a thickness of 47.5 nm. This coating was obtained after a 5 min sputtering process and exhibited a relatively good reversibility to potential cycling at rates up to 10C within the potential range from 1 to 3 V (vs Li/Li^+).

Silicon dioxide (SiO_2) coatings.—Silica (SiO_2) have thermal properties that are expected to correlate well with their thermal stability as a coating. This material is also readily available and can serve as an HF scavenger to suppress cathode degradation. The matrix of SiO_2 is created by covalent Si-O bonds, which can be organized in a crystalline or amorphous lattice.[8–10] During its reaction with HF, a barrier layer of $SiO_{2-x}F_{2x}$ species are expected to form based on the following reaction:

$$4HF + SiO_2 \rightarrow SiF_4 + 2H_2O \quad [12]$$

A method of reacting sodium silicate with carbonic acid has been used to deposit a thin layer of SiO_2 onto the surfaces of $LiNi_{0.8}Mn_{0.1}Co_{0.1}O_2$ (NMC 811).[136] The initial discharge capacities were the same for the coated and uncoated NMC 811 cathodes, implying that the SiO_2 layer did not hinder the properties of the bulk cathode. After 300 cycles, the SiO_2 coated sample exhibited a loss in capacity of only 14.6%, in comparison to a loss of 30.2% for the pristine cathode materials. The enhanced cycling performance of the SiO_2 coated NMC 811 cathode is possibly due to the structure of this coating and its ability to serve as a barrier to protect against unwanted interactions with the electrolyte. During potential cycling the anodic peaks for the coated samples appeared at 3.758, 4.02 and 4.218 V (vs Li/Li^+), whereas the cathodic peaks were present at 3.72, 3.98 and 4.156 V. For Ni-based cathode materials, a primary electrochemical transformation within these materials is between Ni^{3+} and Ni^{4+} during Li^+ intercalation and de-intercalation. The observed peaks were attributed to: (i) an oxidative transformation from Ni^{2+} to Ni^{3+} and from Ni^{3+} to Ni^{4+} at 3.785 and 4.02 V, respectively; and (ii) an oxidative transformation from Co^{3+} to Co^{4+} at 4.218 V. In a separate study, it was found that the electrochemical performance during potential cycling of SiO_2 coated NMC 622 (prepared from a solution-phase process) could be greatly enhanced when the coating process was performed at an elevated temperature of 60 °C.[137] Initially, the pristine NMC 622 and the coated NMC 622 both exhibited a similar discharge capacity of ~175 $mA{\cdot}h{\cdot}g^{-1}$. The pristine sample had a capacity retention of 68% in comparison to 92% for the silica coated sample after 48 cycles. The influence of the silica coating can also be observed in the additional thermal stabilization of these materials. For example, the exothermic peak for thermal decomposition of these materials occurs at 275 °C for the pristine NMC 622 material (1882 J g^{-1} of heat generated from this decomposition) and for the silica coated sample this decomposition shifted to 288 °C (releasing 1217 J g^{-1} of heat).

Modifying the surfaces of NMC 811 with different amounts of SiO_2 (e.g., 0.25 to 1 wt%) reveals that a coating of 0.25 wt% of SiO_2 on NMC 811 delivers an initial capacity of 200.7 $mA{\cdot}h{\cdot}g^{-1}$, and retains 87% of its capacity after 100 cycles at 0.5C.[138] Thin layers of SiO_2 were favorable for creating a reversible transport of lithium ions and electrons including at elevated temperatures (e.g., 55 °C). Contact resistance at the interface of the active materials and current collector (R_e) was almost the same for the 0.25 wt% SiO_2 coated NMC 811 sample and the uncoated sample, which indicated the ease with which Li^+ and electrons passed through these coatings. For the pristine NMC 811, the R_e values increased from 31 Ω to 39 Ω due to the formation of an SEI and structural distortion of the materials, which was attributed to Ni dissolution and vacancy formation within the lattice of the cathode particles. Silica provides a sacrificial protection by scavenging HF, and offers the benefit of being an economical material. These attributes make silica a potential coating of interest for the LIBs.

Mixed oxides and composite coatings.—Apart from the aforementioned classifications of coatings on cathode materials, extensive research has been conducted on other oxides and composite systems using various dopants that seek to enhance cell performance. Rare earth oxides have also been considered as good candidates for preparing coatings due to their ability to improve electrical conduction to the supported oxides and to promote electron transfer.[139–142] Cerium oxide has been used as a coating on both NMC 111 and $LiMn_2O_4$. In either case, the coating was observed to improve cyclability of the cathode materials. Coatings of ceria or CeO_2 derived from solution-phase techniques on NMC 532 cathodes could retain a discharge capacity 97.4 $mA{\cdot}h{\cdot}g^{-1}$ and 59.2 $mA{\cdot}h{\cdot}g^{-1}$ following 100 cycles over a voltage range from 2.8 to 4.6 V (vs Li/Li^+) at 10C and 20C, respectively. The pristine NMC 532 retained a capacity of 23.5 $mA{\cdot}h{\cdot}g^{-1}$ and 9.0 $mA{\cdot}h{\cdot}g^{-1}$, respectively, for the same parameters for electrochemical cycling.[143] A coating of ruthenium dioxide (RuO_2) on both $LiFePO_4$ (LFP) and $Li(Li_{0.2}Ni_{0.13}Mn_{0.54}Co_{0.13})O_2$ cathode materials also improved their electrochemical performance in comparison to the pristine, uncoated counterparts.[144–150] Enhanced cell performance was also observed for Ru-doped LFP, $LiNi_{0.5}Mn_{1.5}O_4$, and 0.55 li_2MnO_3–0.45 $liNi_{1/3}Mn_{1/3}Co_{1/3}O_2$.[148–150] Dispersing a small amount of RuO_2 nanoparticles into the carbon layer coated onto a $Li_3V_2(PO_4)_3$ cathode also improves its electrochemical performance.[146] In addition, RuO_2 modified LNMO materials whose coating was prepared by a co-precipitation method, revealed that a coating on the spinel cathode materials that was prepared from a solution containing 2.0 wt% RuO_2 exhibited discharge capacities of 104.5 $mA{\cdot}h{\cdot}g^{-1}$ and 66.1 $mA{\cdot}h{\cdot}g^{-1}$ at 5C and 10C, respectively, after 700 cycles.[151] The discharge capacities were 131.7 $mA{\cdot}h{\cdot}g^{-1}$ at room temperature and 129.7 $mA{\cdot}h{\cdot}g^{-1}$ at 60 °C when cycled at a rate of 0.5C with a corresponding capacity retention of 98% and 97%, respectively, after 100 cycles.

Iron oxide coatings have also been pursued for enhancing the performance of cathode materials. An LCO cathode coated from a 5 wt% Fe_2O_3 achieved an initial capacity of 168.7 $mA{\cdot}h{\cdot}g^{-1}$ at 1C and retained a capacity of almost 93% after 50 cycles.[152] Interestingly, the Fe_2O_3 coated cathodes performed better than when Fe_2O_3 was mixed with the LCO or when Fe was doped into the LCO. These results suggested that a thin coating of Fe_2O_3 decreased the charge transfer resistance of the cell. Additional oxides have also been pursued to improve the performance of cathode materials. For example, a solution-phase method has been used to deposit coatings of Al_2O_3, ZrO_2, and a Li_2O–B_2O_3 glass onto the surfaces of NMC 811.[153] Of these coatings, the NMC coated with the Li_2O–B_2O_3 glass possessed water absorption stability (e.g. when stored at room temperature with a 10% relative humidity for 72 h). This coated cathode had the smallest degree of moisture uptake and retained the most capacity after 50 cycles (i.e., nearly 100%) over a voltage range from 3.5 to 4.3 V (vs Li/Li^+). These glassy coatings exhibited a cathode resistance of 12.2 mΩ, which was significantly less than that of the pristine NMC 811 and their Al_2O_3 or ZrO_2 coated counterparts.

Iron oxides and iron sulphates can catalyze the formation of graphitized carbon from different carbon sources.[154–158] To prepare highly graphitized carbon coatings on cathode particles, the dispersion of both the carbon source and the metal catalyst are critical. The methods to mix these materials and the relative dimensions of the materials are each important. In one example, $LiMn_{0.8}Fe_{0.2}PO_4$ (LMFP) particles were coated with carbon through an iron-assisted process that relied on solvothermal techniques. It was determined that LMFP/Fe/C exhibited a substantially improved discharge capacity in comparison to LMFP/C.[159] A retained capacity of 78.6% at 10C was achieved after 60 cycles for the LMFP/Fe/C, while the retained capacity of the LMFP/C was only 39.1% under the same conditions. In another example, an LFP-carbon nanocomposite with the addition of an excess of a polymer additive followed by thermal annealing and pyrolysis under an inert gas atmosphere at elevated temperatures achieved a discharge capacity of 312 $mA{\cdot}h{\cdot}g^{-1}$ and retained a capacity of 218 $mA{\cdot}h{\cdot}g^{-1}$ after 20 cycles.[160] This performance was attributed to the formation of LFP-based nanocrystallites within the sample that had a high surface area to volume ratio, a low bulk crystallinity, and likely the inclusion of defects within these nanostructured layers, thereby more easily accommodating the transport of lithium ions than that observed for bulk LFP materials.

Coatings have also been prepared from a spinel zinc aluminate ($ZnAl_2O_4$). For example, these coatings have been applied to $Li_{1.2}Ni_{0.2}Mn_{0.6}O_2$ cathodes using a thermal process with a varying amount of $ZnAl_2O_4$ loaded onto these cathode materials (e.g., 0.5, 1, and 2.5 wt%). It was observed from an analysis by selected area electron diffraction (SAED), that the $ZnAl_2O_4$ coating adopts a spinel structure on the lithium rich cathode material.[161] Another type of coating has been the custom preparation of films using two distinct components or from a mixture of materials. These coatings can enhance the electrochemical stability and rate capabilities of cathode materials.[158–160] One example of such custom coatings seeks to combine the advantages of fast ion conductors and electron conductors to boost cell performance at high voltages.[162–165] For example, NMC 622 materials coated with a mixture of Li_3VO_4 and PPy (polypyrole) have been prepared through an in situ chemical polymerization.[166] NMC 622 materials contain lattice spacings of 0.238 nm corresponding to the spacings of (101) planes, and the Li_3VO_4 layers have an interlayer spacing of 0.250 nm corresponding to the (210) planes. These results confirmed a partial crystallization of the Li_3VO_4 on the NMC materials. The TEM analyses also confirmed the formation of a layer of PPy with a thickness of ∼15 nm. The initial discharge capacity of the Li_3VO_4-PPy coated NMC 622 was 185.6 $mA{\cdot}h{\cdot}g^{-1}$ at 0.5C, which was higher that than that achieved for the pristine cathode, the Li_3VO_4 coated NMC 622, and the PPy coated NMC 622. These results indicated that these dual coatings of ion and electron conductive materials were able to inhibit chemical attack and to minimize surface impedance.

In another example of a dual functional coating, a cathode of $LiNi_aCo_bAl_{1-a-b}O_2$ (NCA, with the values of a >0.85) coated with layers of TiO_2 and Li_2CO_3 could protect the surfaces of the cathode from damage caused by contact with H_2O during the production of the NCA.[167] These TiO_2/Li_2CO_3 coated NCA materials retained 95% of its discharge capacity after the 30th cycle between 2.5 and 4.25 V (vs Li/Li^+) in comparison to a retention of 93% of the capacity for the uncoated cathode materials; the discharge capacities were 187 $mA{\cdot}h{\cdot}g^{-1}$ and 186 $mA{\cdot}h{\cdot}g^{-1}$ for coated and uncoated NCA, respectively after potential cycling.

Another approach to improving the functionality of cathode materials is through both doping and coating of the cathode materials. As an example, an LCO sample was coated with ZrO_xF_y and also treated with Mg doping.[152,168] The pristine sample retained only 64% of its initial capacity after 100 cycles over a potential range from 3.0 to 4.5 V (vs Li/Li^+), but for the Mg doped LCO and the Mg doped sample that was also coated with ZrO_xF_y the retained capacities were ∼85% and 91%, respectively, of their original capacity. In another study, a coating of Al metal was applied to LNMO materials using electron beam vapor deposition techniques.[169] Annealing the Al coated sample at 800 °C in air resulted in the formation of Al^{3+} doped LNMO. The Al layer can form a passivation layer of alumina that helps to resist the oxidation of the underlying materials, but the passivation layer for aluminum oxide on Al is relatively thick in comparison to some metals. Regardless, the Al coated and Al doped LNMO exhibited an improved stability to cycling as it retained 96% of its initial capacity after 100C when cycled from 3.0 to 5.0 V (vs Li/Li^+).

An LCO coated with a nanostructured film of CuO was also prepared by a sol-gel method. It was found that the CuO reduced the charge transfer resistance and the coated LCO cathode retained a capacity of 123 $mA{\cdot}h{\cdot}g^{-1}$ at 50C for the potential range from 3.0 to 4.5 V (vs Li/Li^+).[170] A CuO film is a promising coating due to its relatively low toxicity, ease of storage and handling, and its relatively high theoretical capacity. Although this coating did not eliminate the phase transition of hexagonal to monoclinic of the LCO, this coating did enrich the properties of the LCO such as by improving its electrochemical reversibility, enhancing its activity, and reducing its charge transfer resistance.

A composite of nanoscale graphene and TiO_2 derived through a sol-gel methodology were prepared as coatings on NMC 622 cathode materials. These composite coatings yielded an improved rate performance, a higher cut-off voltage, and an improved stability at elevated temperatures. For example, over the voltage range from 3.0 to 4.5 V (vs Li/Li^+), the coated materials retained ∼94% of their capacity at 1C and 89.2% of their capacity at 2C following 150 cycles.[171] The dual functionality obtained by blending two distinct types of materials can also be achieved through the application of these materials within a single layer. For example, Li_xTiO_2 nanoparticles can be embedded within a matrix of SiO_2 as a coating on Ni-rich $LiNi_{1-x-y}Mn_yCo_xO_2$ cathode materials.[172] This strategy sought to improve the performance of the Ni-rich cathode by incorporating a fast ion conductor (Li_xTiO_2) within an amorphous SiO_2 matrix doped with Ti to enhance the Li^+ ion diffusion. Related materials such as $LiVPO_4F$ have been of interest for their relatively high energy density and stability, and for establishing a cut-off voltage between 4.4 and 4.5 V (vs Li/Li^+).[75,76,173,174] Another approach to preparing Mg-doped cathode materials used polymer pyrolysis to synthesize $Li[Li_{0.2-2x}Mg_xNi_{0.13}Mn_{0.54}Co_{0.13})O_2$. This material exhibited a reversible capacity of 272 $mA{\cdot}h{\cdot}g^{-1}$, excellent stability to potential cycling by retaining 93% of this capacity after 300 cycles, and a good rate capability with achieving 114 $mA{\cdot}h{\cdot}g^{-1}$ at 8C. These enhancements were attributed to the structural stability provided by substitution of Li by Mg within the layers of transition metals in the cathode materials, which suppressed unwanted cation mixing within their lattice during potential cycling.[175]

Fluoride coatings.—Fluorides have better ionic and electronic conductivities and an improved resistance to HF attack than oxides. The use of fluorides stems from their intrinsic stability and their ability to yield high energy density as electrodes.[113] Most fluorides are inert and cannot be easily reduced or oxidized under the operating conditions of a battery. It has been found that the addition of the F^- species can improve the rate performance and material cyclability, and also decreases the charge transfer resistance of LIB cathodes.[13,176–178] The high electronegativity of F^- drives the formation of LiF, which can improve the interfacial stability of cathode materials. Lower Gibbs energies relative to their respective oxide counterparts drive the preferential formation of the metal fluorides in the presence of the oxides, which also implies a higher stability of the fluorides over the oxides. Enriching the SEI with lithium fluoride (LiF) has recently gained popularity to improve Li cyclability.[8–11] For example, AlF_3 layer can suppress the decomposition of $LiPF_6$ salts and also prevent Mn dissolution.[1,5] An LNMO coated with a 1 wt% AlF_3 can achieve a capacity retention of up to ∼94% after 50 cycles at 0.5C (over a range of 3.5 to 4.9 V vs Li/Li^+), which was significantly higher than that achieved for the uncoated spinel cathode (i.e., ∼78% after the same potential cycling).[179] Additionally, the 1 wt% AlF_3 coated LNMO exhibited a slow change in its impedance (both real and imaginary components), whereas the bare LNMO spinel exhibited a sharp increase in its impedance upon potential cycling. This change in the impedance of the uncoated LNMO might result from more resistive materials/phases being deposited onto its surfaces. In another study, AlF_3 coated LCO retained ∼91% of its capacity after 500 cycles at voltages up to 4.4 V (vs Li/Li^+).[180] At higher current densities (e.g., 320 mA g^{-1}), the pristine LCO retained only 35% of its capacity, whereas the AlF_3 coated LCO retained up to 85% of its capacity for a potential range of 3.3 to 4.4 V (vs Li/Li^+). When preparing these or other fluoride-based coatings, it is important to keep in mind that the formation of LiF should be minimized as it is highly resistive to Li ion transport. If LiF is formed in excess, it would hinder the transport characteristics of the cell.

Magnesium difluoride, MgF_2, has a good thermal stability, a refractive index of 1.37, a relatively high hardness, and a relatively wide bandgap. The effects of a MgF_2 coating on LCO were studied using MgF_2 films prepared using a chemical deposition technique.[181] The cycling performance of these materials deteriorated as the MgF_2 content increased from 1 wt% to 3 wt%, which indicated that excessive MgF_2 hinders Li^+ ion transport due to the chemical and electrochemical inactivity of the MgF_2 layers. The most effective

performance for the coated LCO materials was obtained from the 1 wt% MgF_2 coating with a retention of 80% of the initial capacity and achieving a discharge capacity of 141 $mA{\cdot}h{\cdot}g^{-1}$ in comparison to the performance of coatings prepared from the 0.5 and 3 wt% loadings of MgF_2. In another study, a solution-phase process was used to prepare a coating of $Al_2O_3/TiO_2/MgF_2$ on LCO. These coated LCO materials were able to retain a capacity to a similar degree as the pristine LCO. In contrast, the TiO_2 coated LCO samples prepared by the same solution-phase method exhibited a capacity of 183 $mA{\cdot}h{\cdot}g^{-1}$, followed by MgF_2 and Al_2O_3 coated LCO.[182,183] In another study, MgF_2 was coated onto LCO by spin casting from a 0.1 M or 0.05 M solution of precursors.[184] The 0.05 M solution of MgF_2 precursors cast onto LCO retained 61.3% of its original capacity in comparison to a retention of 71.0% of the capacity being retained for the LCO coated with MgF_2 that was prepared from a 0.1 M solution of precursors. In contrast, ~80% of the initial capacity was retained by the pristine LCO. Each of these studies were performed at a current density of 0.6 mA cm^{-2} with a rate of 3C for a voltage range of 3.0 to 4.25 V (vs Li/Li^+). These results indicated that thin coatings of MgF_2 were insufficient to enhance the cell performance. In contrast, a separate study indicated that a coating of MgF_2 on a $LiMn_2O_4$ spinel decreased the discharge capacity but enhanced the cyclability of this cathode material when the coating content was 3 wt% MgF_2 (when prepared by a precipitation method).[185] At a rate of charge of 1C at 55 °C, the $LiMn_2O_4$ cathode material coated with 3 wt% MgF_2 retained 77% of its initial capacity, which was significantly higher than the retained capacity of the uncoated spinel. In another study, a binary coating was prepared from MgF_2 and C on a cathode of $Li_3V_2(PO_4)_3$ (or LVP), which resulted in an enhancement to the electrochemical properties of the LVP materials.[186] These improvements were attributed to the synergistic effects of the two components within these coatings to prevent dissolution of the vanadium and to improve the conductivity of the coatings, respectively.

Zirconium tetrafluoride, ZrF_4, a heat and corrosion resistant material coated $Li(Li_{0.2}Ni_{0.17}Mn_{0.56}Co_{0.07}]O_2$ cathodes at a loading of 0.5, 1, 2, or 3 wt% ZrF_4 (each prepared by wet coating method) were observed to not significantly impact the performance of these cathode materials.[187] The coatings prepared from a 1 wt% ZrF_4 exhibited the most optimal discharge capacity (i.e., 194 $mA{\cdot}h{\cdot}g^{-1}$) of this series of materials after 100 cycles at 4.8 V (vs Li/Li^+). Due to the electrochemical inactivity of the ZrF_4, this layer can suppress the growth of the SEI and can also maintain a consistent charge transfer resistance upon potential cycling. Excess ZrF_4 can, however, reduce the electrochemical performance of the cathode materials by hindering the Li^+ ion transport. In a separate study, a zirconium

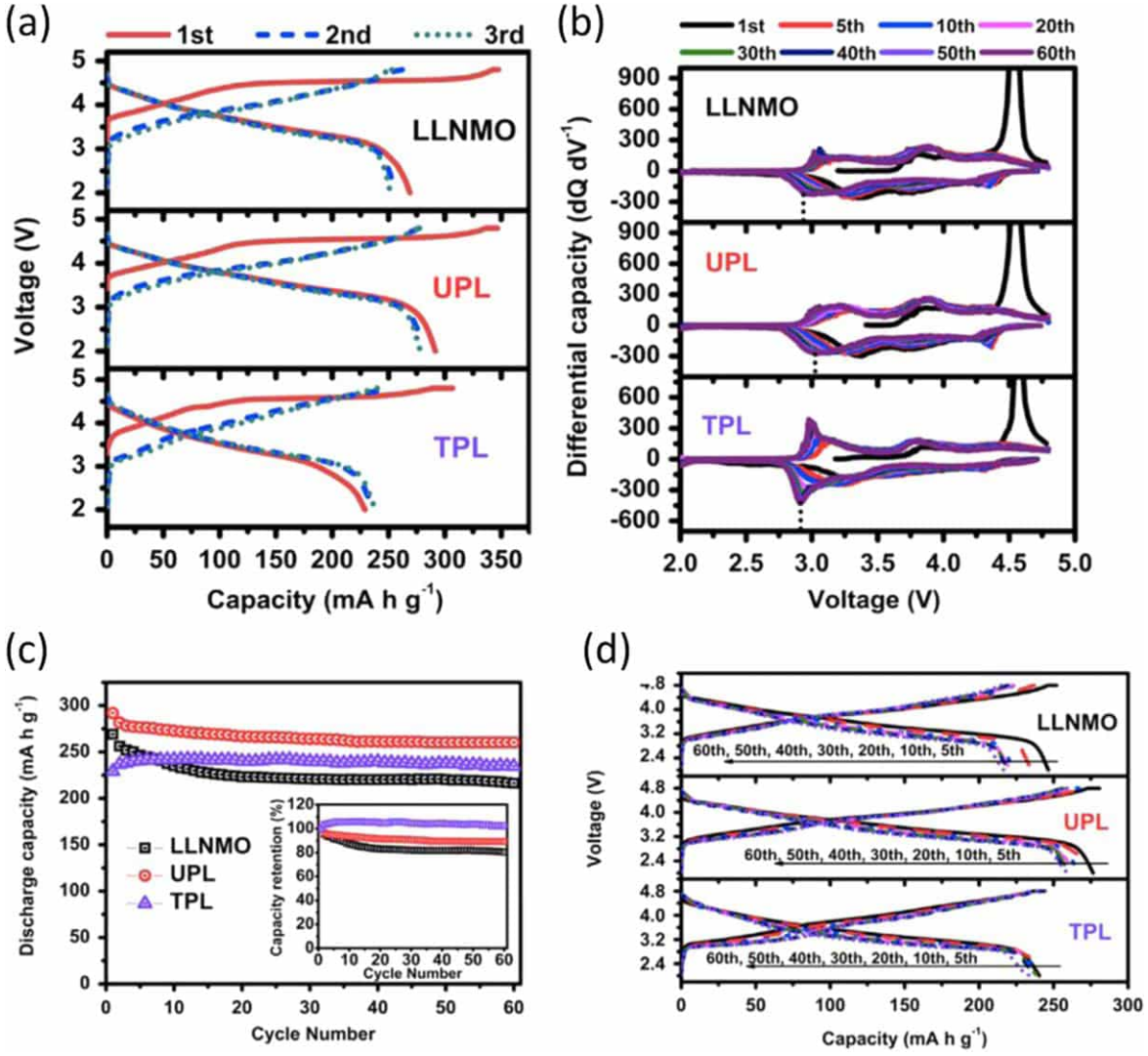


Figure 14. Electrochemical performance of pristine LLNMO and LLNMO coated with an ultrathin protective layer (UPL) prepared from a 1 wt% loading of LiF/FeF_3 and a thick protective layer (TPL) created from a 5 wt% loading of LiF/FeF_3: (a) charge/discharge profiles of each material obtained at 0.1C; (b) differential capacity curves at various cycles as noted in the legend; (c) capacity retention up to 60 cycles at 0.1C; and (d) charge/discharge profiles obtained over 60 cycles; reproduced with permission.[192]

oxyfluoride (ZrO_xF_y) was coated onto LCO.[152,168,188] At voltages below 4.6 V (vs Li/Li^+) the discharge capacities for the coated and pristine LCO cathodes were 195.6 $mA{\cdot}h{\cdot}g^{-1}$ and 188.4 $mA{\cdot}h{\cdot}g^{-1}$, respectively, at a rate of 1C. A severe capacity loss was observed when the cells were charged to 4.6 V; the coated and pristine samples exhibited a capacity retention of 33% and ~11%, respectively, after charging to 4.6 V at 1C.

Iron trifluoride, FeF_3, is a relatively stable compound that can also react with Li through the following transformation:[189]

$$FeF_3 + 3\,Li \rightarrow Fe + 3\,LiF \quad [13]$$

The FeF_3 has a theoretical capacity of 237 $mA{\cdot}h{\cdot}g^{-1}$ between 2.0 and 4.5 V (vs Li/Li^+) through the following intercalation reaction:

$$FeF_3 + Li \rightarrow LiFeF_3 \quad [14]$$

A composite of FeF_3 and reduced-graphene oxide exhibited an enhanced stability to electrochemical cycling between 1.5 and 4.5 V (vs Li/Li^+) and a discharge capacity of up to 202 $mA{\cdot}h{\cdot}g^{-1}$ at 0.1C after 50 cycles from 2.0 to 4.5 V.[189] A FeF_3 coated $Li(Li_{0.2}Ni_{0.13}Mn_{0.54}Co_{0.13})O_2$ prepared by solution-phase methods resulted in the formation of a 5-nm to 15-nm thick coating.[190] This FeF_3 coated cathode retained 95% of its capacity (i.e., 190 $mA{\cdot}h{\cdot}g^{-1}$) after 100 cycles at 0.5C when cycled from 2.0 to 4.8 V (vs Li/Li^+). The FeF_3 coated cathode exhibited a longer lifetime, a greater stability to potential cycling, and a better rate capability than the pristine cathode. Coatings of FeF_3 of different thickness, prepared using 0.25, 0.5 and 1.0 wt% solutions, on NMC 111 cathode materials suggested that the coating prepared from 1.0 wt% FeF_3 on NMC 111 offered the best protection against electrolyte-based degradation of these transition metals within the NMC cathodes.[191] The 1.0 wt% FeF_3 coated on NMC 111 retained 84% of the initial capacity whereas the 0.25 wt% FeF_3 coated on NMC 111 retained only 50% of its initial capacity after 50 cycles for the potential range from 3.0 to 4.6 V (vs Li/Li^+).

In another study, a process was demonstrated that used an aqueous solution to epitaxially grow layers of LiF/FeF_3 on $Li(Li_{0.2}Ni_{0.2}Mn_{0.6})O_2$ cathode materials.[192] The coin cell testing of these coated cathodes revealed an improved rate performance (e.g., 129.9 $mA{\cdot}h{\cdot}g^{-1}$ at 20C) and a complete retention of its initial capacity over the voltage range from 2.0 to 4.8 V (vs Li/Li^+). The coatings of LiF/FeF_3 on the cathode were compared at both a relatively high loading (5 wt%) and a low loading (1 wt%) of LiF/FeF_3 to performance of the uncoated or pristine cathodes (Fig. 14).

Epitaxial coatings of LiF/FeF_3 were sought to establish a relatively high capacity of 712 $mA{\cdot}h{\cdot}g^{-1}$ at an average potential of ~2.7 V (vs Li/Li^+) to enable the transformation outlined in Eq. 12. The LiF and Fe products were sought to serve as protective barriers against electrolyte decomposition. Another fluoride-based coating, also derived from a solution-phase process, was CaF_2 coated onto NMC 111. This coated cathode was able to retain ~94% of its capacity when prepared from a 1.0 wt% loading of CaF_2 on the NMC 111 in comparison to a retention of 68% of the initial capacity for the pristine cathode material.[193] Fluoride based coatings have also been proven to be protective against water absorption. An example is the protection of olivine phosphate when exposed to ambient levels of humidity. For example, SiF_4 coated $LiMn_{0.80}F_{0.20}PO_4$/carbon (or LMFP) were prepared to generate hydrophobic coatings that could protect the cathodes from moisture attack.[194] The SiF_4 treated LMFP retained 89% of its capacity after 450 cycles from 2.5 to 4.25 V (vs Li/Li^+) at a rate of C/10. In comparison, the uncoated LMFP retained 87% of its initial capacity. Each of these materials did, however, exhibit a similar performance after 450 cycles with a retention of 84% of their capacity.

Another fluoride derived from lanthanum (i.e., LaF_3) was coated onto LCO. This LaF_3 coating was reported to exhibit an initial discharge capacity of 177.4 $mA{\cdot}h{\cdot}g^{-1}$ between 2.75 and 4.5 V (vs Li/Li^+) at a rate of 0.2C, and retained 62% of its capacity after 50 cycles.[195] The tolerance to overcharging of the LaF_3 coated LCO was higher than that of the pristine LCO. A more recent study performed a systematic comparison of ten (10) fluoride coatings on NMC 532 cathodes: (i) BaF_2; (ii) ZnF_2; (iii) NiF_2; (iv) CeF_2; (v) ZrF_4; (vi) YF_3; (vii) BiF_3; (viii) PrF_3; (ix) SmF_3; and (x) AlF_3.[196] Of these coatings, the AlF_3 coated NMC 532 exhibited less stability to potential cycling, which could be due to the electrochemical activity of the Ni^{2+}. It was hypothesized that for metal fluorides derived from metals of a +3-oxidation state that the pH of the fluoride suspension and the ionic radius of the metal cations were prominent factors for determining the electrochemical activity of the coatings and the coated NMC 532 cathodes. For example, a high pH might not sufficiently dissolve all the Li species present in the solution (e.g., LiOH, Li_2CO_3) and those species dissolved in solution could react with acidic $LiPF_6$. In contrast, use of a low pH solution could degrade the surfaces of the NMC 532 particle. It can be concluded that the interface stability is dependent on the properties of the metal fluorides. A protective fluoride coating could be achieved by tailoring the pH of a fluoride containing suspension and using relatively small metal cations in the creation of the metal fluoride.

Phosphate coatings.—Phosphate based compounds often have strong P=O bonds that can enhance the thermal stability polyanions and inhibit the direct contact of the cathode materials with electrolytes. The inclusion of phosphate groups can inhibit oxygen release from the cathode lattices even at elevated temperatures, which is attributed to the strong affinity of phosphorus towards oxygen. For example, $Mn_3(PO_4)_2$ coatings prepared by a solution-phase sol-gel process on NMC 622 exhibited discharge capacities of 149 $mA{\cdot}h{\cdot}g^{-1}$ after 50 cycles at 25 °C, and 160 $mA{\cdot}h{\cdot}g^{-1}$ after 50 cycles at 60 °C.[197] In comparison, the pristine or uncoated cathode achieved discharge capacities of 153 $mA{\cdot}h{\cdot}g^{-1}$ after 50 cycles at 25 °C and 142 $mA{\cdot}h{\cdot}g^{-1}$ after 50 cycles at 60 °C. Additionally, the thermal decomposition of these cathode materials shifted from 275 °C to 292 °C upon coating the cathode with $Mn_3(PO_4)_2$. The corresponding heats of decomposition were 1882 J g^{-1} and 1170 J g^{-1}, respectively, which further indicated an improved thermal stability of the coated NMC 622 materials. In a separate study, an NMC 442 coated with $MnPO_4$ prepared from a 2 wt% solution also improved the capacity retention (i.e., 85%) of these cathodes, which were found to be independent of the discharge rates even at temperatures up to 60 °C and were also independent of the loading of active material.[198] The $MnPO_4$ coating on the NMC 422 cathodes also extended their operational potentials up to 4.5 V (vs Li/Li^+). A separate study investigated $MnPO_4$ coated NMC 622 and found that a coating prepared from a solution of 1 wt% $MnPO_4$ could substantially enhance the electrochemical performance of these Ni-rich cathodes with an excellent cycle stability.[199] The $MnPO_4$ coated NMC 622 could retain up to 93%, ~95%, and 98% of their capacity following 100 cycles at 0.1C, 2C, and 10C, respectively (Fig. 15). At 60 °C the coated NMC 622 retained 83% of its capacity after 100 cycles (10C), in contrast to a retention of 69% capacity for the uncoated, pristine NMC 622. At 10C and 60 °C, no capacity was retained for the uncoated NMC 622, but with the $MnPO_4$ coated cathode retained 71% of its initial capacity.

Lithium phosphate coatings have also been pursued for stabilizing cathode materials.[3,19,42] The Li^+ ion conductivity in Li_3PO_4 (e.g., 10^{-6} S m^{-1}) may facilitate charge transfer reactions across the electrode/electrolyte interface.[200] In one example, the surfaces of Ni-rich NMC 622 were coated with Li_3PO_4 derived from a H_3PO_3 precursor.[200] The reduction of lithium compounds such as LiOH or Li_2CO_3 in response to the oxidation of phosphorous acid could result in an increased capacity for the Li_3PO_4 coated NMC 622 cathodes. In addition, better rate capabilities and a slower change in impedance of the coated NMC 622 were attributed to the absorption of water by the Li_3PO_4 coating. This water management could lead to less HF production upon $LiPF_6$ decomposition, which could protect the active material from HF attack during the charge and discharge

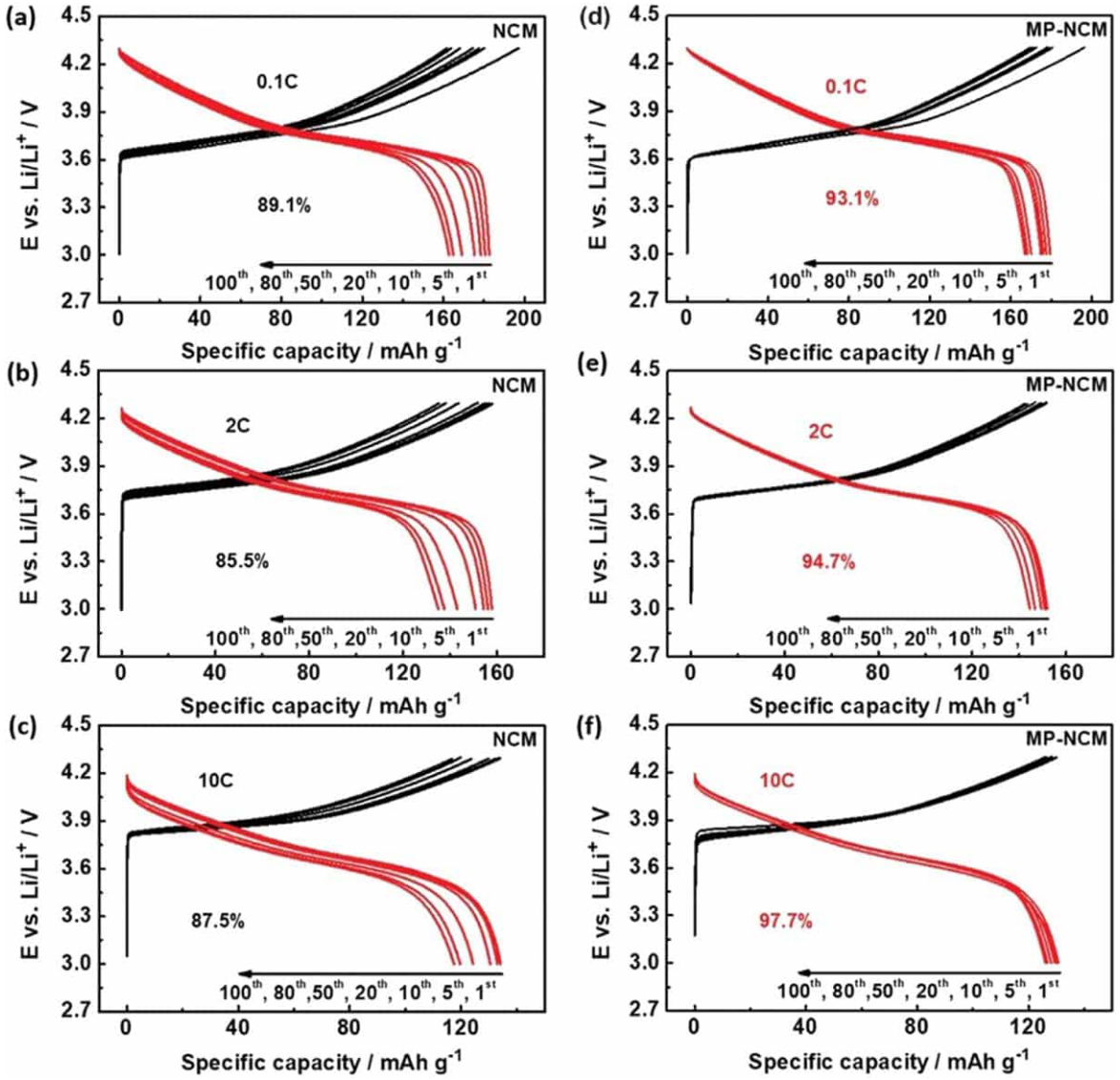


Figure 15. Charge/discharge profiles for electrodes at various C rates up to 100 cycles for: (a) pristine NMC 622 at 0.1C; (b) NMC 622 at 2C; (c) NMC 622 at 10C; (d) $MnPO_4$ coated NMC at 0.1C; (e) $MnPO_4$ coated NMC at 2C; and (f) $MnPO_4$ coated NMC at 10C; reproduced with permission.[199]

processes. In addition, a Li_3PO_4 coated $Li_{1.18}Ni_{0.15}Mn_{0.52}Co_{0.15}O_2$ cathode can be prepared by a precipitation method (Fig. 16) that produces surfaces free of Li_2O_3 impurities.[201]

At a 1 wt% coating of Li_3PO_4 on the cathode, the discharge capacity was 272.5 $mA{\cdot}h{\cdot}g^{-1}$ at 0.4C and 12.1 $mA{\cdot}h{\cdot}g^{-1}$ at 10C in comparison to 248.6 $mA{\cdot}h{\cdot}g^{-1}$ at 0.4C and 70.5 $mA{\cdot}h{\cdot}g^{-1}$ at 10C for the pristine cathode materials. Increasing the coating thickness by loading the cathode materials with 3 wt% Li_3PO_4 increases the energy loss and exhibits a decay in performance at lower voltages, which indicates that the larger amount of Li_3PO_4 can hinder electron and Li^+ ion transport. The TEM images in Fig. 16 indicate a corresponding formation of an amorphous Li_2CO_3 impurity layer on the pristine cathodes with a thickness around 3 nm. As the Li_3PO_4 content during the coating procedure increased, the coating layer also increased in its thickness. The resulting coating was, however, non-uniform and resulted in a partial encapsulation of the cathode particles.

A composite containing layers of a lithium rich oxide ($Li_{1.2}Ni_{0.13}Mn_{0.54}Co_{0.13}O_2$) was coated with Li_3PO_4 through a synthetic processing using polydopamine as a template.[202] This composite achieved a capacity of 118 $mA{\cdot}h{\cdot}g^{-1}$ at 5C, in comparison to 45 $mA{\cdot}h{\cdot}g^{-1}$ for the oxide without the Li_3PO_4 coating. A coating of Li_3PO_4 on NMC 622 was also derived using a citric acid assisted sol-gel method, which was observed to suppress the formation of Li_3PO_4 in solution (as opposed to on the surfaces of the NMC particles).[203] These Li_3PO_4 coated NMC 622 exhibited a capacity retention of 80% after 100 cycles with a cut-off voltage of 4.7 V (vs Li/Li^+), in comparison to 64% for the bare NMC 622. Additionally, a smaller R_{ct} was also observed for the Li_3PO_4 coated NMC 622 particles. In another example, Li_3PO_4 coated onto NMC 811 through a solution-phase process increased the capacity retention of these cathodes; the coated NMC 811 retained up to ~93% of its capacity at 25 °C and 1C after 100 cycles in comparison to 86.1% for the bare NMC 811.[204] While increasing the cycle number from 1 to 100 the R_{ct} of the pristine NMC 811 increased from 50.6 Ω to 511.1 Ω, while that for the coated cathode increased from 36.6 to 290.7 Ω. The Li^+ ion diffusion coefficients were measured to be 8.16×10^{-12} cm^2 s^{-1} and 1.68×10^{-11} cm^2 s^{-1} for the pristine NMC 811 and the Li_3PO_4 coated NMC 811, respectively, indicating an enhanced electrochemical performance for the coated cathode material.

Iron phosphates have also been prepared as coatings on cathode materials for LIBs in the search for improved stability and enhanced performance. For example, NMC 111 coated with a nanotextured

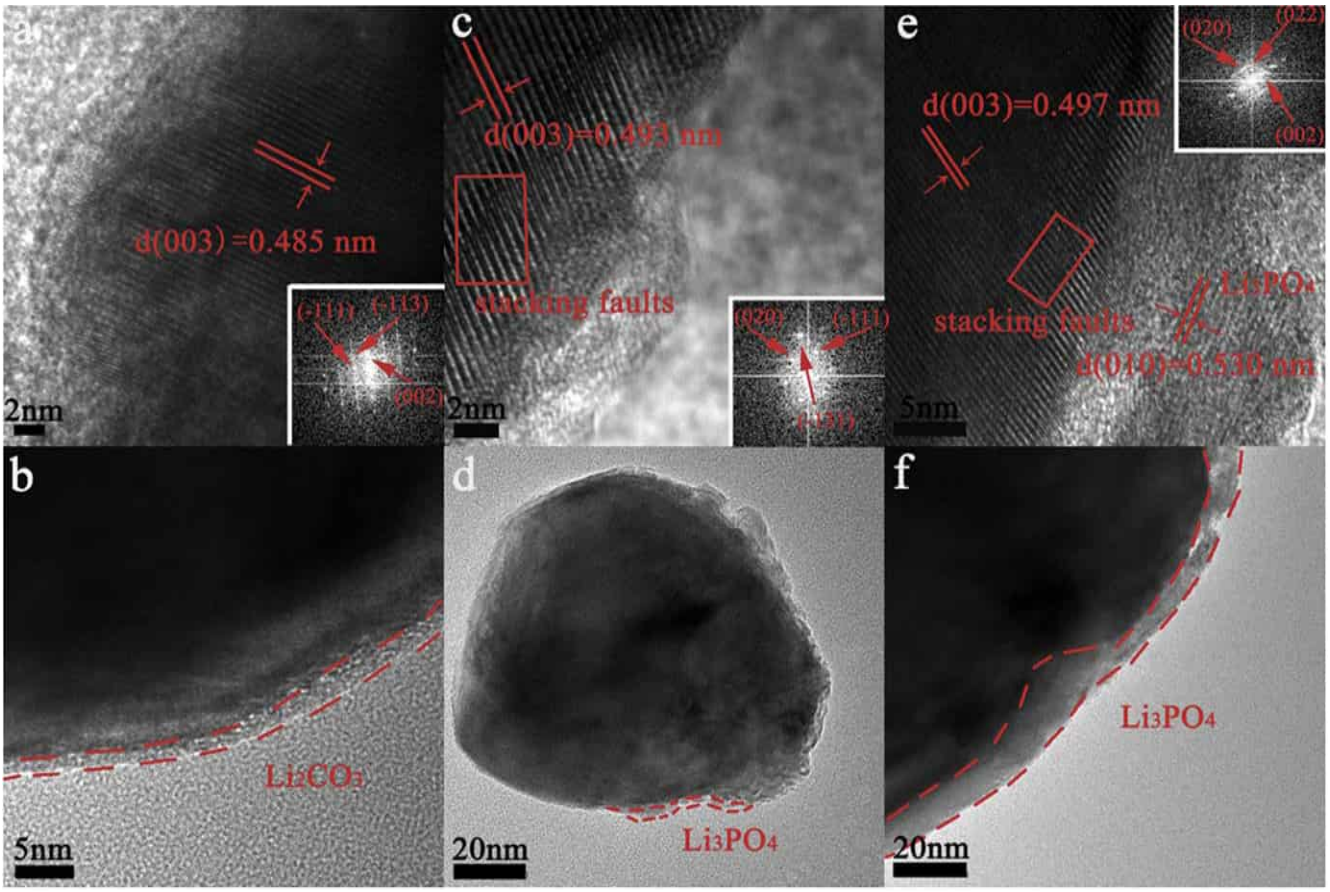


Figure 16. A series of HRTEM images of $Li_{1.18}Ni_{0.15}Mn_{0.52}Co_{0.15}O_2$ materials: (a,b) in a pristine state; (c,d) after coating with 1.0 wt% Li_3PO_4; and (e,f) after coating with 3.0 wt% Li_3PO_4; reproduced with permission.[201]

layer of 2 wt% $FePO_4$ using a co-precipitation method exhibited a capacity retention of up to 88% after 100 cycles for a voltage range of 2.8 to 4.5 V (vs Li/Li^+).[205] The discharge capacities for the $FePO_4$ coated NMC 111 (prepared from a 2 wt% solution) after heat treatment at 400 °C was 143.5 $mA{\cdot}h{\cdot}g^{-1}$, which was considerably higher than the 103.2 $mA{\cdot}h{\cdot}g^{-1}$ capacity attained for the pristine NMC 111 after 100 cycles (from 2.8 to 4.5 V at 1C). A heat treatment of 600 °C had a negative influence on the performance of the $FePO_4$ coated NMC 111 cathode materials. It was hypothesized that the coating layer might diffuse into the cathode and affect its crystalline lattice at these temperatures, which would negatively impact the Li^+ ion migration between the electrolyte and the electrode. In contrast, at lower process temperatures the resulting contact between the cathode and this coating might not be very strong. A heat treatment at 400 °C was determined to be near optimal based on the electrochemical performance of these materials. Modifying the surfaces of LCO with $FePO_4$ using a co-precipitation method has also been pursued to stabilize these cathode materials.[206] A $FePO_4$ coating of LCO, prepared from a 3 wt% solution of the iron phosphate precursor, delivered an initial discharge capacity of 146 $mA{\cdot}h{\cdot}g^{-1}$ at 4.3 V (vs Li/Li^+) and 155 $mA{\cdot}h{\cdot}g^{-1}$ at 4.4 V while retaining 89% and 83%, respectively, of their capacity after 400 cycles. As an alternative approach, microwave-based processing has been used to prepare $FePO_4$ coated LCO.[207] These coatings stabilized the LCO up to 50 cycles at higher voltages (e.g., 4.7 V vs Li/Li^+). These $FePO_4$ coated LCO cathodes retained 92% of their capacity after 50 cycles in comparison to 40% retention of capacity by the bare cathode materials treated using the same electrochemical conditions. Pristine LCO can become polarized after 50 cycles due to an increased impedance (due to an increase in both the capacitance and resistance terms) that results in an overall loss of capacity. The $FePO_4$ coating on LCO helped to suppress this degradation in performance. An ALD process has also been demonstrated for preparing $FePO_4$ coatings on LNMO samples.[208] This sample was able to improve the capacity retention as a function of the number of cycles. Coating the LNMO with 40 ALD cycles could enhance the stability of the LNMO but also decreased its capacity, possibly due to the low ionic conductivity of $FePO_4$. Conclusively, $FePO_4$ coating prevents the side-reaction at the electrode/electrolyte interface and suppresses an increase in charge transfer resistance increase upon charge discharge cycling. Additionally, it stabilizes the cathode surfaces due to the strong interactions between the PO_4 polyanions and Fe^{3+} ions.[205–207] It also decreases the activation energy of the charge transfer process thereby enhancing the charge transfer processes at the electrode/electrolyte interface.

Another distinct phosphate-based coating that has been sought are aluminum phosphates ($AlPO_4$). The surfaces of $Li[Li_{0.2}Fe_{0.1}Ni_{0.15}Mn_{0.55}]O_2$ cathode materials have been modified with a 3, 5, and 7 wt% $AlPO_4$ through a co-precipitation technique.[209] The 5 wt% $AlPO_4$ coating on this cathode yielded the best cycling performance of this series of materials with a capacity retention of 74% at 220.4 $mA{\cdot}h{\cdot}g^{-1}$ after 50 cycles at 0.1C. This sample also exhibited a good rate capability with a capacity of 120.2 $mA{\cdot}h{\cdot}g^{-1}$ after 100 cycles at 10C. The PO_4^{3-} polyanion paired with Al^{3+} provided a protective layer that resisted interfacial reactions between the electrolyte and the electrode. A separate study investigated the influences of temperature (e.g., 400 °C and 700 °C) on $AlPO_4$ coated NMC 111.[210] At 400 °C, the $AlPO_4$ reacted with NMC 111 to form Li_3PO_4. When heated at 700 °C, the spinel phases of $CoAl_2O_4$, Co_2NiO_4, and $CoMnAlO_4$ are expected to form at the interface between the coating and the cathode material ($M'_1M_2O_4$,

M = Ni/Co/Mn and M′ = Al). The surface resistances of the uncoated NMC 111 and the $AlPO_4$ coated NMC 111 that were heat treated to 400 °C both increased nearly 2 times after 50 cycles (at 4.6 V vs Li/Li^+), whereas the resistance of the $AlPO_4$ coated NMC 111 that was heat treated to 700 °C remained relatively stable after the same potential cycling. Each of these samples exhibited a similar morphology, depicting little influence from the coatings and heat treatment on the particle's appearance and surface roughness.

Cobalt phosphates have also been pursued as Li-reactive coatings. For example, $Co_3(PO_4)_2$ coatings have been applied to an $LiNi_{0.8}Co_{0.16}Al_{0.04}O_2$ cathode.[211] After annealing at 700 °C, a Li_xCoPO_4 coating formed upon these cathode materials. The $Co_3(PO_4)_2$ can react with surface impurities, which can be used to minimize unwanted side reactions. After an extended period of charging the cathode at 4.3 V (vs Li/Li^+) and 90 °C, the pristine cathode transformed into a spinel structure, whereas the coated cathode could maintain its layered phase. This result indicated that the coating was effective in preventing Ni^{4+} ions from dissolving into the electrolytes. A coating of $Co_3(PO_4)_2$ was also applied to $Li(Li_{0.2}Ni_{0.15}Mn_{0.55}Co_{0.1})O_2$ through a combustion method.[212] It was determined from this study that a 3 wt% $Co_3(PO_4)_2$ annealed at 800 °C yielded a cathode material with the best electrochemical performance. It was also hypothesized that these processing conditions also yielded the most homogeneous distribution of phosphorus species on the surfaces of these materials. The Ni and Co species had almost the same distribution within these surfaces after creating the $Co_3(PO_4)_2$ coating and applying this heat treatment. Possibly the Li_xCoPO_4 diffused into the bulk material during the heat treatment and/or the interdiffusion of species was promoted due to an incomplete coating (e.g., forming an initially less-dense coating). Coating $Co_3(PO_4)_2$ onto LiV_3O_8 cathode materials by solution-phase processes demonstrated the ability to stabilize these cathode materials during prolonged potential cycling possibly due to reducing the phase transition of LiV_3O_8 and side-reactions.[213] A separate study compared the influence of Al/Fe/Co derived phosphate coatings on $LiNi_{0.8}Mn_{0.05}Co_{0.15}O_2$ cathodes.[214] The electrochemical performance of these coated cathodes was correlated to the metal used to prepare the coating and the ratio of metal cation to PO_4^{3-}. For example, the ratio of Al^{3+} to PO_4^{3-} could be tuned to prepare a coating on NMC of an optimal performance, whereas tuning the ratio of Fe^{3+} to PO_4^{3-} to prepare coatings on NMC had little effect on altering the performance of these materials. A coating derived from a 1:1 mole ratio of Co^{3+} to PO_4^{3-} was the most effective surface modification for the NMC cathodes as it increased the capacity retention by up to 3% after 50 cycles at 1C.

A series of other phosphate-based coatings have also been explored for coating cathode materials. A nickel phosphate or $Ni_3(PO_4)_2$ coated NMC 111 retained 99% of its capacity following potential cycling between 2.7 and 4.6 V (vs Li/Li^+) after 10 cycles at 5C.[215] The specific capacities of pristine NMC 111 and $Ni_3(PO_4)_2$ coated NMC 111 were 80.5 $mA{\cdot}h{\cdot}g^{-1}$ and 91.3 $mA{\cdot}h{\cdot}g^{-1}$ at 5C. Lanthanum phosphate, $LaPO_4$, has also been applied as a coating to NMC 811 cathodes.[216] These $LaPO_4$ coated NMC 811 cathode materials achieved a diffusion coefficient of 142×10^{-11} $cm^2\ s^{-1}$ in comparison to 3.84×10^{-12} $cm^2\ s^{-1}$ for the pristine NMC 811 cathode.[217] In addition, the $LaPO_4$ coated samples retained a higher capacity (i.e., 91%) in comparison to a retention of 76% for the uncoated cathode at 1C after 100 cycles from 3.0 to 4.3 V (vs Li/Li^+). A yttrium phosphate, YPO_4, has also been used as an additive along with Al_2O_3 to modify the surfaces of a layered LCO.[218] The addition of Al_2O_3 and the YPO_4 yield a similar thermal performance, when added individually. An enhanced thermal stability of these coated materials was attributed to the formation of a solid solution of $Li_xM_yCo_{1-y}O_2$ (M = Al/Y) covering the surfaces of the layered LCO.

Lithium composite coatings to achieve fast ion conduction.—Fast ion conductors offer superior electrochemical performance over inert coatings such as oxides and fluorides. Fast ion conductors can be used directly as cathode materials. These materials have a relatively large space within their crystal lattice and a disordered lithium sub-lattice, which leads to relatively high rates of ion migration. Materials such as Li_2ZrO_3, Li_2TiO_3, $LiAlO_2$, $LiNbO_3$ and Li_2SiO_3 have been widely investigated as the coating materials and fast ion conductors.[3–6,12,14]

Lithium aluminate ($LiAlO_2$) coatings on NMC 811 have been prepared by a process of hydrolysis through a hydrothermal treatment.[219] A lithium aluminate coating layer stabilizes the interface between the cathode and the electrolyte, and also significantly improves the rate capability of the cathode materials. The improved rate capabilities were attributed to the excellent Li^+ conducting nature of $LiAlO_2$.[87,219,220] The NMC particles were almost entirely covered by the $LiAlO_2$ coating with a thickness of 8 to 12 nm. These $LiAlO_2$ coated NMC 811 materials retained ∼94% of their capacity after 100 cycles. Their capacity changed from 181.2 $mA{\cdot}h{\cdot}g^{-1}$ after the first cycle to 169.5 $mA{\cdot}h{\cdot}g^{-1}$ after the 100th cycle (1C from 2.7 to 4.3 V vs Li/Li^+). The pristine sample could retain ∼82% of its capacity after 100 cycles and the discharge specific capacity decreased from 181.8 $mA{\cdot}h{\cdot}g^{-1}$ for the first cycle to 148.3 $mA{\cdot}h{\cdot}g^{-1}$ for the 100th cycle. In another study, it was concluded that $LiAlO_2$ coated NMC 622 exhibited a significant improvement in performance when compared to Al_2O_3 coated NMC 622 at high cut-off voltages of 4.5 and 4.7 V (vs Li/Li^+).[87] These $LiAlO_2$ coated NMC 622 retained a capacity of 142 $mA{\cdot}h{\cdot}g^{-1}$ at 3C and 206.8 $mA{\cdot}h{\cdot}g^{-1}$ at 0.2C, in comparison to the Al_2O_3 coated NMC 622 with a capacity of 131.9 $mA{\cdot}h{\cdot}g^{-1}$ at 3C and 196.9 $mA{\cdot}h{\cdot}g^{-1}$ at 0.2C. Additionally, the $LiAlO_2$ coated NMC 622 materials can maintain a reversible capacity of 149 $mA{\cdot}h{\cdot}g^{-1}$ after 350 cycles with a decay of 0.08% per cycle. In another study, $LiAlO_2$ coated $Li_{1.2}Ni_{0.2}Mn_{0.6}O_2$ layered oxide exhibited a better performance and stability to potential cycling at room temperature and elevated temperatures in comparison to pristine $Li_{1.2}Ni_{0.2}Mn_{0.6}O_2$.[221] At 55 °C the $LiAlO_2$ coated sample had an initial discharge capacity of 201.2 $mA{\cdot}h{\cdot}g^{-1}$ in comparison to 190.2 $mA{\cdot}h{\cdot}g^{-1}$ for the uncoated sample. After 80 cycles these capacities reduced to 184.1 $mA{\cdot}h{\cdot}g^{-1}$ for the coated cathode and 119.8 $mA{\cdot}h{\cdot}g^{-1}$ for the pristine, uncoated electrode. The $LiAlO_2$ coating applied to NMC 811 through a solution-phase method exhibited a decrease in the electrode resistance relative to the pristine NMC 811 materials through suppression of undesirable side reactions between the electrolyte and electrode, which also hindered formation of the SEI.[222] A series of samples were also prepared with different coating thicknesses (0, 0.5, 1.0 and 2.0 wt%). From this series of samples, the 1 wt% coating of $LiAlO_2$ on NMC 811 exhibited the highest performance.

Each of these coatings of $LiAlO_2$ on NMC 811 exhibited a similar morphology and an average particle size of 11 μm (Fig. 17). These coated particles had a rough surface that changes with a higher loading of the coating material—as the thickness increased it becomes harder to distinguish between the granular features of the particles. It was determined that a small amount of Al^{3+} diffuses into these cathode particles during their calcination. The 1 wt% loading of $LiAlO_2$ on the NMC 811 cathode particles possessed the highest discharge capacity, achieving a capacity of 179.7 $mA{\cdot}h{\cdot}g^{-1}$ at 5.0C, retaining 86% of its original capacity. The charge transfer resistance of the $LiAlO_2$ coated cathode was also suppressed after 50 cycles, which suggested that the migration of Al^{3+} into the lattice of the NMC particles may have increased the structural stability of these materials.

Lithium titanate, Li_2TiO_3, has also been sought to stabilize cathode materials including a coating on NMC 811 cathode materials. Monoclinic Li_2TiO_3 is isostructural to Li_2MnO_3 with a strong Ti–O bond relative to the Mn–O bond, and Li_2TiO_3 is electrochemically stable over a wide range of voltages exhibiting excellent structural stability in organic electrolytes. Nanosized monoclinic Li_2TiO_3 has a high AC conductivity of 10^{-3} S cm^{-1}, much higher than that (i.e., 10^{-6} S cm^{-1}) of the layered Mn-based oxides containing an excess of Li.[223–226] The lithium titanate based coating on NMC 811 was able to retain 98% of the initial capacity in

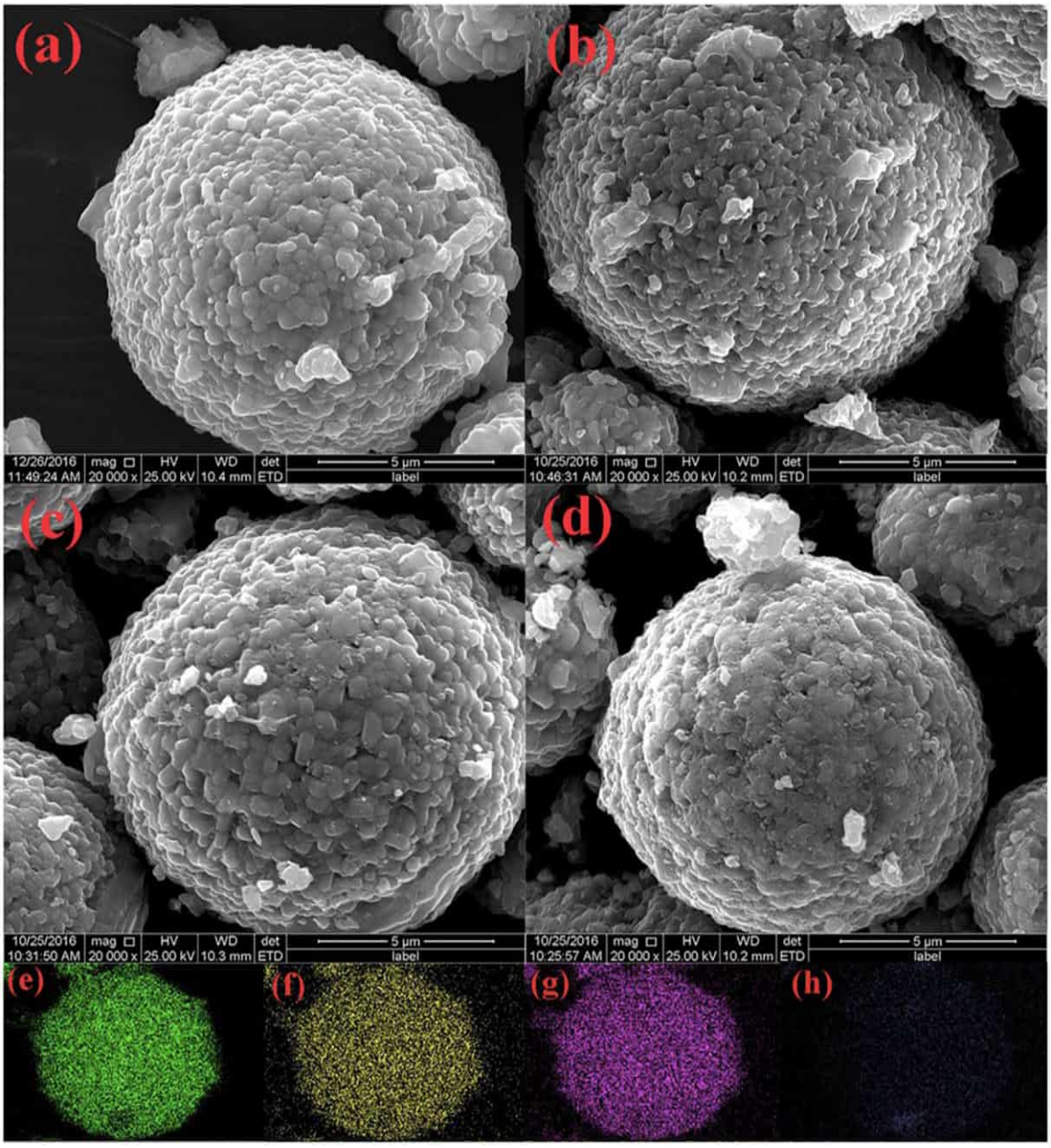


Figure 17. FESEM images of: (a) pristine NMC 811; (b) NMC 811 coated with 0.5 wt% $LiAlO_2$; (c) NMC 811 coated with 1.0 wt% $LiAlO_2$; and (d) NMC 811 coated with 2.0 wt% $LiAlO_2$. A series of EDS maps depict the distribution of: (e) Ni; (f) Co; (g) Mn; and (h) Al within the NMC 811 coated with 1.0 wt% $LiAlO_2$; reproduced with permission.[222]

comparison with the uncoated NMC cathode that retained only ~81% of its capacity after 70 cycles at 1C.[223] The surface film resistance (R_{sf}) increased upon cycling from 121.1Ω (10th cycle) to 146.5Ω (100th cycle) for the pristine NMC 811, but the Li_2TiO_3 coated NMC 811 didn't exhibit much change in R_{sf} (81.25 Ω at the 10th cycle, to 85 Ω at the 100th cycle). This result suggested that the CEI (cathode electrolyte interface) for the coated NMC particles was stabilized during the potential cycling. Another study prepared a series of $Li_4Ti_5O_{12}$ (LTO) coatings on NMC 811 particles with a range of thicknesses. The $Li_4Ti_5O_{12}$ has also been extensively investigated as an anode material as their spinel structure provides ample channels for Li^+ ion transport and stability for voltages up to 5.5 V (vs Li/Li^+) without the formation of an SEI.[224] The $Li_4Ti_5O_{12}$ coated samples exhibited a better rate capability and stability to potential cycling than the uncoated materials. The Li^+ diffusion coefficients were 8.77×10^{-15} cm^2 s^{-1}, 8.37×10^{-15} cm^2 s^{-1}, and 4.21×10^{-15} cm^2 s^{-1} for a 2 wt% LTO loading on NMC 811, 1 wt% LTO loading on NMC 811, and the pristine NMC 811, respectively. These results indicated a bit enhanced mobility of Li^+ ions through this coating. A strategy of both coating with Li_2TiO_3 and doping with Zr of $Li_{1.2}Ni_{0.2}M_{0.6}O_2$ cathode materials has also been investigated.[226] It was observed that the metal-to-oxygen bond length increased and the energy barrier to Li^+ ion diffusion decreased as a result of the reduced repulsive interactions between the Li^+ ions and the metal ions within the lattice of these coatings. These changes facilitated Li^+ ion diffusion within these materials. Pristine $Li_{1.2}Ni_{0.2}M_{0.6}O_2$ suffered from a more severe fade in capacity than the coated cathode particles. The bare $Li_{1.2}Ni_{0.2}M_{0.6}O_2$ had an initial discharge capacity of 133.5 $mA{\cdot}h{\cdot}g^{-1}$, which decreased to 92.2 $mA{\cdot}h{\cdot}g^{-1}$ after 200 cycles for a retention of 69% of the initial capacity. In contrast, the retention capability of the Li_2TiO_3 coated and Zr-doped $Li_{1.2}Ni_{0.2}M_{0.6}O_2$ was

~185% greater than that achieved by the bare $Li_{1.2}Ni_{0.2}M_{0.6}O_2$. In another study, a 3 wt% loading of Li_2TiO_3 onto the surfaces of $Li(Li_{0.2}Ni_{0.19}Mn_{0.51}Co_{0.1})O_2$ revealed a capacity retention of 169.9 $mA{\cdot}h{\cdot}g^{-1}$ at 2C, and 149.1 $mA{\cdot}h{\cdot}g^{-1}$ at 5C.[225] This coated cathode also achieved a discharge capacity of 207.1 $mA{\cdot}h{\cdot}g^{-1}$ at 0.5C after 100 cycles (from 2.0 to 4.8 V vs Li/Li^+), in comparison to a discharge capacity of 190.3 $mA{\cdot}h{\cdot}g^{-1}$ for the uncoated sample.

Lithium zirconate or Li_2ZrO_3 has been sought as a cathode coating as this material is stable in non-aqueous electrolytes and has a structure that promotes Li^+ ion diffusion. For example, Li_2ZrO_3 coated NMC 442 has exhibited an improvement in the rate performance, discharge capacity, and capacity retention particularly at an elevated temperature of 50 °C.[227] When the calcination temperature was increased to 750 °C, the coating was not as apparent as observed by electron microscopy techniques and its surfaces appeared to be relatively smooth. The results of this heat treatment suggested that the coating layer might diffuse into the crystalline lattice of the NMC 442, forming a solid solution at elevated temperatures. In another study, a 1wt% loading of Li_2ZrO_3 on NMC 532 was prepared that exhibited a capacity retention of 87% after 100 cycles at 1C in comparison to retaining 73% for the pristine cathode.[228] The initial discharge capacity of the pristine sample was 187.7 $mA{\cdot}h{\cdot}g^{-1}$, which decreased to 136.6 $mA{\cdot}h{\cdot}g^{-1}$ after 100 cycles. The 1 wt% loading of Li_2ZrO_3 on the cathode materials, on the other hand, decreased from 193.6 $mA{\cdot}h{\cdot}g^{-1}$ to 168.6 $mA{\cdot}h{\cdot}g^{-1}$ after 100 cycles. The thermal stability also improved for the coated materials. For example, exothermic transformations for the pristine sample were observed at 283.2 °C (765 J g^{-1}) but similar transformations for the coated NMC 532 shifted to 294.7 °C (484 J g^{-1}). A different approach was pursued in one example of coating Li_2ZrO_3 onto NMC 811 cathodes.[229] The coating process was carried out simultaneous to the preparation of the cathode particles, rather than being applied as a coating on the product. A loading of 2 wt% Li_2ZrO_3 on these NMC 811 cathode materials achieved a capacity retention of ~95% after 200 cycles at 1C, and a retention of ~83% of their specific capacity under same cycling conditions, whereas the pristine NMC maintained only 71% of its initial capacity. The specific capacity for the base cathode material was 107.4 $mA{\cdot}h{\cdot}g^{-1}$ at 10C (from 3.0 to 4.3 V vs Li/Li^+), which was lower than the specific capacity of 144.3 $mA{\cdot}h{\cdot}g^{-1}$ for the Li_2ZiO_3 coated NMC 811 under the same operating conditions.

Lithium silicates have also been sought after for their use as fast ion conductors and coatings on cathode materials. One example was Li_2SiO_3 that contained staggered chains of SiO_4 tetrahedra that were held together by Li^+ ions. The Li^+ ions diffuse through the (001) and (010) planes of the Li_2SiO_3 lattice. In one study, it was determined that Li_2SiO_3 coated $Li_{1.13}Ni_{0.30}Mn_{0.57}O_2$ prepared by a co-precipitation method improved the rates of Li^+ ion diffusion, as well as the cycle stability, rate capability, and polarization relative to the uncoated samples.[230] The Li_2SiO_3 coated $Li_{1.13}Ni_{0.30}Mn_{0.57}O_2$ achieved a discharge capacity of 152 $mA{\cdot}h{\cdot}g^{-1}$, whereas the bare cathode attained a capacity of 79 $mA{\cdot}h{\cdot}g^{-1}$ after 100 cycles (from 2.0 to 4.8 V vs Li/Li^+) at a current density of 100 mA g^{-1}. In a separate study, an NMC 811 cathode was coated with Li_2SiO_3, which retained 78% of its capacity after 50 cycles with a cut-off voltage of 4.6 V in comparison to 57% of retained capacity for the pristine sample under the same operating conditions.[231] The Li_2SiO_3 coating effectively minimized the electrolyte decomposition and side reactions, along with enhancing the structural stability of the Ni-rich electrodes upon removal of the Li^+ ions at high voltages. In another example, $Li_{1.2}Ni_{0.13}Mn_{0.54}Co_{0.13}O_2$ was coated with Li_2SiO_3 using an isochronous lithium source and this method demonstrated no significant changes in structure or morphology of the samples with the preparation of the coating.[232] Coating the electrode with a 3 wt% loading maintained a discharge capacity of 142 $mA{\cdot}h{\cdot}g^{-1}$ and exhibited a capacity retention of 85%, in comparison to 121.9 $mA{\cdot}h{\cdot}g^{-1}$ and ~78%, respectively, for the pristine cathode after 100 cycles at 1C. The diffusion coefficient for Li^+ ions within the cathode loaded with 3 wt% Li_2SiO_3 was 8.57×10^{-12} cm^2 s^{-1}, which was higher than the 1 wt% and 4.5 wt% coated samples.

Lithium tungstate (Li_2WO_4) has been pursued as the coating material for cathode materials due to its fast ion conductivity. In one example, Li_2WO_4 was coated onto NMC 811 through a one-step synthesis followed by a high temperature calcination. This coated NMC 811 cathode could maintain a discharge capacity of 146 $mA{\cdot}h{\cdot}g^{-1}$ after 100 cycles at 1C after being stored in air for 60 d, which was a 36% higher capacity than the bare electrode materials handled and tested under the same conditions.[233] The diffusion coefficient for Li^+ ions was 2.637×10^{-10} cm^2 s^{-1} and 1.479×10^{-10} cm^2 s^{-1} for the tungstate coated and bare cathode materials, respectively. These results indicated that the tungstate coating had a higher but comparable capacity for Li^+ ion diffusion as the NMC 811 cathode. The Li_2WO_4 has also been used as a dopant to increase cathode performance.[234] A 5 wt% addition of Li_2WO_4 within an NMC 622 electrode could achieve a reversible capacity of 199.2 $mA{\cdot}h{\cdot}g^{-1}$, and could retain 73% of its capacity after 200 cycles at 1C.

Lithium niobate or $LiNbO_3$ is a conventional electrolyte with an excellent thermal stability and ionic conductivity.[235,236] It has the potential to considerably enhance the interfacial stability of cathode materials. In one example, $LiNbO_3$ was applied as a coating to NMC 811 cathodes.[236] It was determined that the highly crystalline $LiNbO_3$ can effectively suppress structural changes to these cathode materials by providing strain relaxation due to the promotion of Li^+ intercalation and de-intercalation to and from the lattice.

Glass coatings.—Glasses have also been investigated as coating materials due to their relative inertness to electrochemical and chemical processes, their flexibility in terms of their composition, and their cost effectiveness relative to other coating materials. Glasses contain an open random network, which is advantageous for Li^+ ion diffusion.[237–239] The relatively open structure within a glass is attributed to non-bridging oxygen atoms within its network due to its unique structural properties and stability. Lithium and boron containing compounds such as Li_2O-B_2O_3 (LBO) have been widely used as coating materials because lithium and boron effectively reduce electrolyte decomposition in comparison to metal oxide-based coatings.[240] It is expected that the LBO glass would evenly coat the surfaces of cathode materials due to the relatively low viscosity of its precursors and their good wetting properties.[237,240] A layered $LiNi_{0.8}Co_{0.2}O_2$ cathode coated with a Li_2O–$2B_2O_3$ glass reduced the self-discharge of this cathode, and increased its reversible capacity and stabilized its cycling performance.[240,241] Different loadings of Li_2O–$2B_2O_3$ glass on NMC 811 were prepared using a heat treatment method. It was determined that a 0.3 wt% of LBO coated on NMC 811 exhibited a retention of 82% of its capacity in contrast to the pristine NMC 811 that retained 51% of its initial capacity.[242,243] All of the LBO coated NMC 811 exhibited better Coulombic efficiencies and discharge capacities than the pristine samples (Fig. 18). The surfaces of the NMC 811 were severely damaged upon cycling to 4.5 V, but the LBO coated NMC 811 exhibited a greater stability at these potentials.

Another study compared coatings of Al_2O_3, ZrO_2, and Li_2O–$2B_2O_3$ on NMC 811 each prepared using solution-phase methods.[153] The results of this study indicated that cycle performance and stability of the resistance of the LBO coated NMC 811 were slightly better than those properties observed for the Al_2O_3 and ZrO_2 coated cathodes. The retained capacity and an increase in cathode resistance observed for the LBO coated, ZrO_2 coated, and Al_2O_3 coated cathodes and the pristine cathode were 99.9%, 99.8%, 99.2%, and 99.5%, respectively, and 12.2 mΩ, 13.6 mΩ, 14.0 mΩ, and 19.6 mΩ, respectively. In another study, a 3 wt% loading of LBO on $Li(Li_{0.2}Ni_{0.13}Mn_{0.54}Co_{0.13})O_2$ retained 92% of its capacity after 100 cycles (at 1C from 2.5 to 4.6 V vs Li/Li^+), which was much better than observed for its pristine counterpart (i.e., only 70% retention of capacity under the same operating conditions).[244] The NMC 811 cathode coated with a 1 wt% loading of Li_2O–B_2O_3

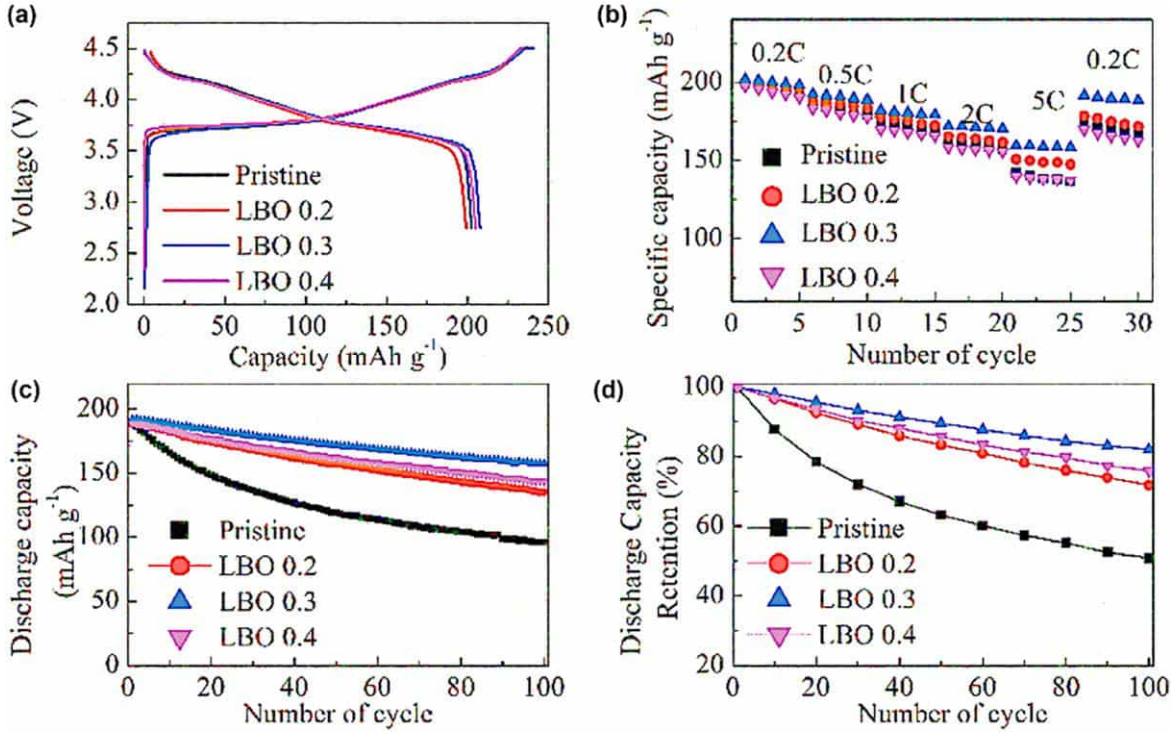


Figure 18. Electrochemical properties between 2.75 and 4.5 V (vs Li/Li^+) of pristine NMC 811 and the same cathode materials after coating with 0.2 wt% LBO, 0.3 wt% LBO, or 0.4 wt% LBO. (a) Initial charge and discharge curves obtained at 0.1C for capacities up to ~200 mA·h·g ^{1}. (b) Rate capabilities of these samples at various current densities. (c) Cycle performance at 1C with an initial discharge capacity of 180 mA·h·g ^{1}. (d) Relative discharge capacity retained at 1C; reproduced with permission.[242]

yielded an improved electrochemical performance in comparison to the 0.5 and 2 wt% loadings on NMC 811, and relative to the base NMC 811 cathode material.[245] The bare NMC 811 cathode had a specific capacity of ~182 $mA{\cdot}h{\cdot}g^{-1}$, whereas the NMC 811 coated with 0.5, 1, and 2.0 wt% $Li_2O–B_2O_3$ yielded specific capacities of ~150, 198 and 159 $mA{\cdot}h{\cdot}g^{-1}$ after 20 cycles at 0.2C over the voltage range from 3.0 to 4.3 V (vs Li/Li^+).

A glassy lithium phosphate or GLP has also been sought as a coating, such as on LFP prepared using magnetron sputtering techniques.[246] The cycle performance and rate capability of the GLP coated LFP gradually improved with an increase in the duration of sputter deposition time. These properties did not improve beyond 20 min of deposition, suggesting that deposition time (and likely both film thickness and its uniformity) plays an important role in optimization of these coatings. Initial discharge capacities of 152.6 $mA{\cdot}h{\cdot}g^{-1}$ and 165.8 $mA{\cdot}h{\cdot}g^{-1}$ at 1C were achieved for the bare cathode and coated LFP, respectively. After 100 cycles, the capacity and Coulombic efficiency for the GLP coated LFP and the bare LFP were 159.1 $mA{\cdot}h{\cdot}g^{-1}$ and 99.7%, and 135.7 $mA{\cdot}h{\cdot}g^{-1}$ and 99.1%, respectively. The amorphous nature of GLP might have reduced the anisotropy in the surface properties of the LFP cathode, which could enhance the Li^+ ion migration through the bulk material. Additionally, GLP could serve to cross-link the networks between particles and to reduce the resistance to electron and ion transfer between LFP particles. The GLP could, therefore, create more conductive paths for both electrons and Li^+ ions and enhance the electro-active regions within these coated cathodes.

A series of glasses based on LVSB or 20 li_2O 30 V_2O_5 (50 x) SiO_2 xB_2O_3 (x = 10, 20, 30, 40 mol%) have also been studied as potential cathode materials for LIBs. From one series of samples, the material with x = 10 mol% exhibited the best cycling capacity, which was attributed to the high ratio of V^{4+} yielding more polaron hopping, and hence an enhanced conductivity.[247] During 1st cycle, all samples show a low charge capacity less than 50 mA $h{\cdot}g^{-1}$. The discharge capacities of the LVSB10 (x = 10 mol%), LVSB20, LVSB30 and LVSB40 samples were 123.7 mA $h{\cdot}g^{-1}$, 51.5 mA $h{\cdot}g^{-1}$, 37.9 mA $h{\cdot}g^{-1}$ and 19.5 mA $h{\cdot}g^{-1}$, respectively (15 to 4.2 V). Ball milling was used to reduce the size of these particles. Impedance spectroscopy results suggested that the ball-milled samples effectively decreased the charge transfer resistance of these materials.

Other coatings.—Many other types of materials have also been pursued as coating materials on cathodes for LIBs, such as polymers, lithium rich materials, metals, reduced carbon, and additional composites. A PPy (polypyrrole) polymer coated $LiMn_2O_4$ spinel achieved a high capacity.[248] In another example, poly (3, 4-ethylenediozythiophene) or PEDOT coated $LiMn_2O_4$ exhibited a capacity fade of 22% to 24% over 100 cycles at 1C while held at 32 °C, which is slightly lower than that of conventional $LiMn_2O_4$ cathode.[249] It has been proposed that PEDOT could have a beneficial influence on the properties and utility of metal oxide cathodes, but its energy barriers are still insufficient for the life-cycle targets of LIBs. Poly(diallyldimethyl-ammonium chloride) or polyDDA coated $LiMn_2O_4$ spinel were prepared in a separate study using an adsorption process to inhibit the surface degradation of the spinel and Mn^{2+} dissolution.[250] Performance of these coated cathode materials was dependent on the processing temperature during synthesis and the amount of adsorbed polymer. Although minor changes to the surface topography were observed because of potential cycling at room temperature, it was observed that the stability and cell performance improved for the polyDDA coated cathodes. Many of the cathode materials lack strong bonding interactions with the polymer coatings. Although these coatings are non-specific and are relatively loosely adhered to the cathodes, they can still exhibit beneficial properties. For example, a mixture of polyaniline (PANI) and polyvinyl pyrrolidone (PVP) coated NMC 811 have an initial discharge capacity of 200 $mA{\cdot}h{\cdot}g^{-1}$ and retain 89% of this capacity after 100 cycles, as well as a capacity of 152 $mA{\cdot}h{\cdot}g^{-1}$ at 1000 $mA{\cdot}g^{-1}$ when cycled from 2.8 to 4.3 V (vs

Li/Li^+).[251] In other reports, it is revealed that polypyrole coated $LiMn_2O_4$ exhibited an initial capacity of 165.5 $mA{\cdot}h{\cdot}g^{-1}$ at 0.2C between 2.7 and 4.5 V (vs Li/Li^+).[252,253] Compared to the inorganic coating materials, conducting polymers [e.g., polyaniline (PANI)] possess advantages of low cost and high electronic conductivity, which can enhance cyclic stability and improve the rate capability of cathode materials.[251,252] However, coating a homogeneous conducting polymer layer on the cathode surface due to lack of bonding effects is still a topic of consideration.

A templating method was used to form a composite containing a lithium rich oxide ($Li_{1.2}Ni_{0.13}Mn_{0.54}Co_{0.13}O_2$) and Li_3PO_4.[202] The composite achieved a capacity of 118 $mA{\cdot}h{\cdot}g^{-1}$ at 5C, compared to 45 $mA{\cdot}h{\cdot}g^{-1}$ for the oxide without the Li_3PO_4 coating. A 1 wt% $ZnAl_2O_4$ coating on a lithium rich $Li_{1.2}Ni_{0.2}Mn_{0.6}O_2$ exhibited an initial discharge capacity of 254.3 $mA{\cdot}h{\cdot}g^{-1}$, and a capacity of 84 $mA{\cdot}h{\cdot}g^{-1}$ following a high rate of discharge at 10C. This coated cathode material retained ~99% of this capacity after 50 cycles at 10C when cycled from 2.0 to 4.8 V (vs Li/Li^+), demonstrating the spinel was a suitable coating material.[161] Metals have also been coated onto cathode materials to improve their electron conduction. Silver nanoparticles coated onto LFP cathode materials achieved an increase in initial discharge capacity from 128 $mA{\cdot}h{\cdot}g^{-1}$ (for the uncoated LFP) to 156 $mA{\cdot}h{\cdot}g^{-1}$ at 0.1C over the potential range from 2.0 to 4.5 V (vs Li/Li^+).[254] An analysis of a gold coated LNMO revealed that the method used for preparing the coating plays a dominant factor in determining the battery performance.[255] This noble metal is stable toward reactive compounds such as HF and could protect cathode particles against degradation while also improving the electronic conductivity of the electrode. At low rates of charge and discharge, such as C/6 and C/4, the capacity increased by 20% with the gold coating relative to the base cathode material, but at high rates of charge and discharge (e.g., 2C and 4C) the electrolyte decomposition was significant and limited the rate capability of these materials.

Carbon-based coatings of cathode materials have included carbon, graphene oxide, reduced graphene oxide (RGO), graphite, and other forms of carbon materials.[256–262] For example, a study on LNMO spinel coated with carbon species determined that a 1 wt% loading of sucrose (mixed with cathode in a solvent mixture of ethanol and water) on this cathode material exhibited the best behavior.[256] After 100 cycles between 3 and 4.95 V (vs Li/Li^+), a capacity of 130 $mA{\cdot}h{\cdot}g^{-1}$ was achieved and 92% of the capacity could be retained at a discharge rate of 1C. A super P-carbon (SPB) coated NMC 811 revealed that this type of carbon coating did not alter the morphology of the cathode. And a 0.5 wt% loading of SPB on NMC 811 retained ~87% of its initial capacity at 2C, and also retained 88% of its capacity after 80 cycles for a voltage range from 3 to 4.3 V (vs Li/Li^+).[257] A composite of Li_2FeSiO_4 and C (e.g., derived from sucrose or L-ascorbic acid using acid catalyzed hydrolysis) yielded an initial discharge capacity of 135.3 $mA{\cdot}h{\cdot}g^{-1}$ at a rate of C/16.[258] The cathodes with a composite coating derived from L-ascorbic acid exhibited a higher electronic conductivity and an improved Li^+ ion diffusion coefficient than the pristine one, whereas the composite coatings derived from sucrose yielded a better stability to potential cycling and overall cell performance. In another study, an NMC 622 was coated with a composite of C and Al_2O_3, which exhibited a high degree of structural stability.[260] The C and Al_2O_3 composite improved the electrical conductivity of these materials and decreased its charge transfer resistance. The Al_2O_3 itself provided structural flexibility that favored Li^+ ion diffusion though its network. It is worthwhile to note that the improved electrochemical performances and structural stability could be due to the synergistic effect of the conductive coatings (e.g., carbon, conductive polymers) and amorphous oxides (e.g., Al_2O_3, ZrO_2). The characteristics of cathode materials for LIBs are highly dependent on the composition and structure of both their core material and the coatings on their surfaces. Coatings on the cathode materials can significantly influence the electrochemical performance and stability of the encapsulated material. In addition to the properties of the coating material itself, the methods used to prepare the coating also influential the observed performance of the coated cathode materials.[12–15,261,262] The thickness of the coating is a vital parameter that influences Li^+ ion diffusion. Thickness of the coating must be optimized to provide a protective layer against material degradation while also promoting Li^+ ion transport. Hence, the precursors, methodology, selection of the coating material and variables like pressure-temperature should be carefully chosen when developing high performance cathode materials.

Conclusions and Outlook

Critical insights are needed for understanding the structure, property relationships and components behavior under the working condition of LIBs as cathodes serve as the main component of LIBs. There are many challenges to the safety of LIBs such as solvent co-interaction and graphite exfoliation, structural disordering, particle cracking, internal short-circuit, SEI decomposition and precipitation, binder decomposition/contact loss, dendrite formation and transition meta dissolution. The overall cell performance in terms of rate capability, retention capability, reversible capacity and specific capacity are significantly affected by the chemistry and physical properties of its components. Hence, it becomes imperative to address these challenges for the enhanced stability and long-term uninterrupted operation of LIBs. The cathodes of LIBs tend to react with the electrolytes and, hence, undergo surface modifications accompanied by degradation. Researchers have modified electrolytes using various additives to obtain a stable interface between the electrolyte and electrodes. Another approach is to introduce a passivation coating layer that acts as a physical barrier to the unwanted reactions. Surface coatings help to improve the structure of the cathode, endowing it with enhanced mechanical, physical, and chemical properties. The present review includes progress in the field for coatings on cathode materials. The types of coatings that are reviewed in detail include oxides, fluorides, phosphates, composites, glasses, and dual coating materials for layered, spinel and polyanion materials. The coating materials are each assessed for progress towards improving cathode performance and following points can be elucidated as well:

- Coatings prepared from amphoteric oxides (capable of functioning as either an acid or base), such as ZnO, Al_2O_3, SnO_2, or ZrO_2, have ability to stabilize these cathode materials. Amphoteric oxides coatings could maintain 97% of initial capacity of the cathode after 50 cycles when compared to retaining 75% capacity in the uncoated electrode after the same electrochemical conditions. Coatings of Al_2O_3, TiO_2 and SiO_2 also improve the chemical stability of the interface along with providing pathways for Li^+ diffusion. ZrO_2 coating and the $LiMn_2O_4$ cathode particles could reduce the Mn^{3+}/Mn^{4+} redox shift at high potentials.
- Rare earth oxides like cerium oxide, ruthenium oxide have also been considered as good candidates for preparing coatings due to their ability to improve electrical conduction to the supported oxides and to promote electron transfer.
- Another type of coating has been the custom preparation of films using two distinct components or from a mixture of materials. One example of such custom coatings seeks to combine the advantages of fast ion conductors and electron conductors to boost cell performance at high voltages. Fast ion conductors offer superior electrochemical performance over inert coatings such as oxides and fluorides. Fast ion conductors can be used directly as cathode materials. These materials have a relatively large space within their crystal lattice and a disordered lithium sub-lattice, which leads to relatively high rates of ion migration. Materials such as Li_2ZrO_3, Li_2TiO_3, $LiAlO_2$, $LiNbO_3$ and Li_2SiO_3 have been widely investigated as the coating materials and fast ion conductors. Lithium niobate or $LiNbO_3$ is a conventional electrolyte with an excellent thermal stability and ionic conductivity.

• Another approach to improving the functionality of cathode materials is through both doping and coating of the cathode materials. Fluoride based coatings are also of interest as the high electronegativity of F^- drives the formation of LiF, which can improve the interfacial stability of cathode materials.

• Phosphate based compounds often have strong P = O bonds that can enhance the thermal stability polyanions and inhibit the direct contact of the cathode materials with electrolytes. The inclusion of phosphate groups can inhibit oxygen release from the cathode lattices even at elevated temperatures, which is attributed to the strong affinity of phosphorus towards oxygen.

• Glasses have also been investigated as coating materials due to their relative inertness to electrochemical and chemical processes, their flexibility in terms of their composition, and their cost effectiveness relative to other coating materials. Glasses contain an open random network, which is advantageous for Li^+ ion diffusion.

• Many other types of materials have also been pursued as coating materials on cathodes for LIBs, such as polymers, metals, reduced carbon, and additional composites. A PPy (polypyrrole) polymer coated $LiMn_2O_4$ spinel achieved a high capacity. Metals especially silver nanoparticles have also been coated onto cathode materials to improve their electron conduction. Carbon-based coatings of cathode materials have included carbon, graphene oxide, reduced graphene oxide (RGO), graphite, and other forms of carbon materials.

The coating morphology and cathode performance is highly dependent on conditions that include the coating technique, cathode particle size, pH of the precursors, the synthesis temperature, and cathode morphology. For instance, increasing the operating temperature affects the cell performance via two mechanisms: (i) improved lithium ion and electron transport at elevated temperatures, which increases their electrochemical performance; and (ii) a faster Mn dissolution and electrolyte decomposition, which deteriorates their electrochemical performance. Assessments included herein for each coating material demonstrate the recent achievements in the cathode performance using these materials. The details on and limitations of each of these coatings covered in this review are aimed to serve as a guide and benchmark for future improvements to cathode materials for LIBs. Research efforts are still underway in the field to further improve the characteristics of the cathode for providing LIBs with outstanding performance metrics to fulfill the ever-increasing power needs.

Acknowledgments

This work is supported in part by Natural Sciences and Engineering Research Council (NSERC) of Canada (Discovery Grant No. RGPIN-2020-06522) and M. Hildred Blewett Fellowship of the American Physical Society (APS). Authors are highly thankful to the 4D LABS for access to the research facilities and instrumentation therein, and to CMC Microsystems for financial assistance (MNT Grant No. 9338).

ORCID

Gurbinder Kaur
Byron D. Gates

References

1. A. Manthiram, Nat. Commun., 11, 1 (2020).
2. N. Mohamed and N. K. Allam, RSC Advances, 10, 21662 (2020).
3. N. Nitta, F. Wu, J. T. Lee, and G. Yushin, Mater. Today, 18, 252 (2015).
4. C. Liu, Z. G. Neale, and G. Cao, Biochem. Pharmacol., 19, 109 (2016).
5. L. Lu, X. Han, J. Li, J. Hua, and M. Ouyang, J. Power Sources, 226, 272 (2013).
6. B. Xu, D. Qian, Z. Wang, and Y. S. Meng, Mater. Sci. Eng. R Reports, 73, 51 (2012).
7. Z. Chen, W. Zhang, and Z. Yang, Nanotechnology, 31 (2020).
8. M. Li, J. Lu, Z. Chen, and K. Amine, Adv. Mater., 30, 1 (2018).
9. K. Mizushima, P. C. Jones, P. J. Wiseman, and J. B. Goodenough, Solid State Ionics, 3–4, 171 (1981).
10. M. Hu, X. Pang, and Z. Zhou, J. Power Sources, 237, 229 (2013).
11. Z. Gong and Y. Yang, Energy Environ. Sci., 4, 3223 (2011).
12. Z. Chen, W. Zhang, and Z. Yang, Nanotech., 31, 012001 (2020).
13. P. Guan, L. Zhou, Z. Yu, Y. Sun, Y. Liu, F. Wu, Y. Jiang, and D. Chu, J. Energy Chem., 43, 220 (2020).
14. Z. Chen, Y. Qin, K. Amine, and Y. K. Sun, J. Mater. Chem., 20, 7606 (2010).
15. K. Nie, Y. Hong, J. Qiu, Q. Li, X. Yu, H. Li, and L. Chen, Front. Chem., 6, 1 (2018).
16. C. Li, H. P. Zhang, L. J. Fu, H. Liu, Y. P. Wu, E. Rahm, R. Holze, and H. Q. Wu, Electrochim. Acta, 51, 3872 (2006).
17. W. Yan, S. Yang, Y. Huang, Y. Yang, and G. Yuan, J. Alloys Compd., 819, 153048 (2020).
18. D. Zuo, G. Tian, X. Li, D. Chen, and K. Shu, J. Alloys Compd., 706, 24 (2017).
19. X. Tan, M. Zhang, J. Li, D. Zhang, Y. Yan, and Z. Li, Ceram. Int., 46, 21888 (2020).
20. A. K. Rai, L. T. Anh, J. Gim, V. Mathew, and J. Kim, Ceram. Int., 40, 2411 (2014).
21. K. Mizushima et al., Prog. Solid State Chem., 5, 145 (2014).
22. A. W. Sleight, Mater. Res. Bull., 30, 1589 (1995).
23. C. Daniel, D. Mohanty, J. Li, and D. L. Wood, AIP Conf. Proc., 1597, 26 (2014).
24. J. B. Goodenough and K. S. Park, J. Am. Chem. Soc., 135, 1167 (2013).
25. L. X. Yuan, Z. H. Wang, W. X. Zhang, X. L. Hu, J. T. Chen, Y. H. Huang, and J. B. Goodenough, Energy Environ. Sci., 4, 269 (2011).
26. J. B. Goodenough and Y. Kim, Chem. Mater., 22, 587 (2010).
27. R. Hausbrand, D. Becker, and W. Jaegermann, Prog. Solid State Chem., 42, 175 (2014).
28. N. J. J. De Klerk and M. Wagemaker, ACS Appl. Energy Mater., 1, 5609 (2018).
29. J. Maier, Prog. Solid State Chem., 23, 171 (1995).
30. S. Kim, J. Fleig, and J. Maier, Phys. Chem. Chem. Phys., 5, 2268 (2003).
31. C. C. Chen and J. Maier, Phys. Chem. Chem. Phys., 19, 6379 (2017).
32. Lithium Battery Failures, http://mpoweruk.com/lithium_failures.htm.
33. Q. Wang, J. Sun, X. Yao, and C. Chen, J. Electrochem. Soc., 153, A329 (2006).
34. G. Venugopal, J. Power Sources, 101, 231 (2001).
35. D. P. Abraham, E. P. Roth, R. Kostecki, K. McCarthy, S. MacLaren, and D. H. Doughty, J. Power Sources, 161, 648 (2006).
36. X. Wu, K. Song, X. Zhang, N. Hu, L. Li, and W. Li, Front. Energy Res., 7, 1 (2019).
37. C. R. Birkl, M. R. Roberts, E. McTurk, P. G. Bruce, and D. A. Howey, J. Power Sources, 341, 373 (2017).
38. F. P. S. Cui et al., Adv. Energy Mater., 6, 1501309 (2016).
39. A. K. Shukla and T. P. Kumar, Wiley Interdiscip. Rev. Energy Environ. 2, 14 (2013).
40. H. Yu, R. Ishikawa, Y. G. So, N. Shibata, T. Kudo, H. Zhou, and Y. Ikuhara, Angew. Chemie - Int. Ed., 52, 5969 (2013).
41. G. Assat and J. M. Tarascon, Nat. Energy, 3, 373 (2018).
42. A. Manthiram, K. Chemelewski, and E. S. Lee, Energy Environ. Sci., 7, 1339 (2014).
43. H. D. Yoo, E. Markevich, G. Salitra, D. Sharon, and D. Aurbach, Mater. Today, 17, 110.
44. C. S. Yoon, D. W. Jun, S. T. Myung, and Y. K. Sun, ACS Energy Lett., 2, 1150 (2017).
45. T. Ohzuku, A. Ueda, and M. Nagayama, J. Electrochem. Soc., 140, 1862 (1993).
46. K. K. Lee, W. S. Yoon, K. B. Kim, K. Y. Lee, and S. T. Hong, J. Power Sources, 97–98, 321 (2001).
47. W. Li, J. N. Reimers, and J. R. Dahn, Solid State Ionics, 67, 123 (1993).
48. A. Rougier, I. Saadoune, P. Gravereau, P. Willmann, and C. Delmas, Solid State Ionics, 90, 83 (1996).
49. D. Caurant, N. Baffier, B. Garcia, and J. P. Pereira-Ramos, Solid State Ionics, 91, 45 (1996).
50. J. Cho, H. S. Jung, Y. C. Park, G. B. Kim, and H. S. Lim, J. Electrochem. Soc., 147, 15 (2000).
51. Z. Liu, A. Yu, and J. Y. Lee, J. Power Sources, 81–82, 416 (1999).
52. M. M. Thackeray, W. I. F. David, P. G. Bruce, and J. B. Goodenough, Mater. Res. Bull., 18, 461 (1983).
53. M. M. Thackeray, W. I. F. David, and J. B. Goodenough, Mater. Res. Bull., 17, 785 (1982).
54. R. J. Gummow, A. de Kock, and M. M. Thackeray, Solid State Ionics, 69, 59 (1994).
55. W. Choi and A. Manthiram, J. Electrochem. Soc., 153, A1760 (2006).
56. C. Zhan, J. Lu, A. Jeremy Kropf, T. Wu, A. N. Jansen, Y. K. Sun, X. Qiu, and K. Amine, Nat. Commun., 4, 1 (2013).
57. M. M. Thackeray, Y. Shao-Horn, A. J. Kahaian, K. D. Kepler, E. Skinner, J. T. Vaughey, and S. A. Hackney, Electrochem. Solid-State Lett., 1, 7 (1998).
58. J. Choa and M. M. Thackeray, J. Electrochem. Soc., 146, 3577 (1999).
59. O. K. Park, Y. Cho, S. Lee, H. C. Yoo, H. K. Song, and J. Cho, Energy Environ. Sci., 4, 1621 (2011).
60. E. Lee and K. A. Persson, Nanotechnology, 25 (2014).
61. J. B. G. A. K. Padhi and K. 5. Nanjundaswamy, J. Electrochem. Soc., 144, 1188 (1997).
62. R. Dominko, M. Bele, M. Gaberšček, A. Meden, M. Remškar, and J. Jamnik, Electrochem. Commun., 8, 217 (2006).
63. S. Franger, C. Benoit, C. Bourbon, and F. Le Cras, J. Phys. Chem. Solids, 67, 1338 (2006).
64. G. Chen, J. D. Wilcox, and T. J. Richardson, Electrochem. Solid-State Lett., 11, A190 (2008).
65. M. Tang, H. Y. Huang, N. Meethong, Y. H. Kao, W. C. Carter, and Y. M. Chiang, Chem. Mater., 21, 1557 (2009).

66. H. Ehrenberg, N. N. Bramnik, A. Senyshyn, and H. Fuess, Solid State Sci., 11, 18 (2009).
67. J. Wolfenstine and J. Allen, J. Power Sources, 142, 389 (2005).
68. A. R. West and F. P. Glasser, J. Solid State Chem., 4, 20 (1972).
69. M. V. Reddy, G. V. Subba Rao, and B. V. R. Chowdari, J. Power Sources, 195, 5768.
70. Z. L. Gong, Y. X. Li, G. N. He, J. Li, and Y. Yang, Electrochem. Solid-State Lett., 11, 2 (2008).
71. G. He, Y. Li, J. Li, and Y. Yang, Electrochem. Solid-State Lett., 13, 19 (2010).
72. R. Dominko, J. Power Sources, 184, 462 (2008).
73. R. Amin, P. Balaya, and J. Maier, Electrochem. Solid-State Lett., 10 (2007).
74. J. Barker, M. Y. Saidi, and J. L. Swoyer, J. Electrochem. Soc., 151 (2004).
75. J. Barker, M. Y. Saidi, R. K. B. Gover, P. Burns, and A. Bryan, J. Power Sources, 174, 927 (2007).
76. J. Barker, R. K. B. Gover, P. Burns, and A. J. Bryan, Electrochem. Solid-State Lett., 10, 130 (2007).
77. S. Okada, M. Ueno, Y. Uebou, and J. I. Yamaki, J. Power Sources, 146, 565 (2005).
78. M. Nagahama, N. Hasegawa, and S. Okada, J. Electrochem. Soc., 157, A748 (2010).
79. S. S. Fedotov, N. R. Khasanova, A. S. Samarin, O. A. Drozhzhin, D. Batuk, O. M. Karakulina, J. Hadermann, A. M. Abakumov, and E. V. Antipov, Chem. Mater., 28, 411 (2016).
80. N. Recham, J. Chotard, L. Dupont, C. Delacourt, W. Walker, M. Armand, and J. Tarascon, Nat. Mater., 9, 68 (2010).
81. L. Sebastian, J. Gopalakrishnan, and Y. Piffard, J. Mater. Chem., 12, 374 (2002).
82. A. Yamada, N. Lwane, Y. Harada, S. I. Nishimura, Y. Koyama, and L. Tanaka, Adv. Mater., 22, 3583 (2010).
83. V. Legagneur, Y. An, A. Mosbah, R. Portal, A. Le Gal La Salle, A. Verbaere, D. Guyomard, and Y. Piffard, Solid State Ionics, 139, 37 (2001).
84. W. C. West, J. Soler, M. C. Smart, B. V. Ratnakumar, S. Firdosy, V. Ravi, M. S. Anderson, J. Hrbacek, E. S. Lee, and A. Manthiram, J. Electrochem. Soc., 158, A883 (2011).
85. B. Han, T. Paulauskas, B. Key, C. Peebles, J. S. Park, R. F. Klie, J. T. Vaughey, and F. Dogan, ACS Appl. Mater. Interfaces, 9, 14769 (2017).
86. L. Liu, L. Chen, X. Huang, X.-Q. Yang, W.-S. Yoon, H. S. Lee, and J. McBreen, J. Electrochem. Soc., 151, A1344 (2004).
87. W. Liu et al., Nano Energy, 44, 111 (2018).
88. Y. S. Lee, W. K. Shin, A. G. Kannan, S. M. Koo, and D. W. Kim, ACS Appl. Mater. Interfaces, 7, 13944 (2015).
89. R. Zhao, J. Liang, J. Huang, R. Zeng, J. Zhang, H. Chen, and G. Shi, J. Alloys Compd., 724, 1109 (2017).
90. B. Han, B. Key, A. S. Lipton, J. T. Vaughey, B. Hughes, J. Trevey, and F. Dogan, J. Electrochem. Soc., 166, A3679 (2019).
91. S. Neudeck, A. Mazilkin, C. Reitz, P. Hartmann, J. Janek, and T. Brezesinski, Sci Rep., 9, 1 (2019).
92. J. W. Kim, D. H. Kim, D. Y. Oh, H. Lee, J. H. Kim, J. H. Lee, and Y. S. Jung, J. Power Sources, 274, 1254 (2015).
93. B. Han, A. R. Dunlop, S. E. Trask, B. Key, J. T. Vaughey, and F. Dogan, J. Electrochem. Soc., 165, A3275 (2018).
94. B. Han, B. Key, S. H. Lapidus, J. C. Garcia, H. Iddir, J. T. Vaughey, and F. Dogan, ACS Appl. Mater. Interfaces, 9, 41291 (2017).
95. J. Zhao and Y. Wang, Nano Energy, 2, 882 (2013).
96. S. K. Hu, G. H. Cheng, M. Y. Cheng, B. J. Hwang, and R. Santhanam, J. Power Sources, 188, 564 (2009).
97. D. Wang, X. Li, Z. Wang, H. Guo, Y. Xu, Y. Fan, and J. Ru, Electrochim. Acta, 188, 48 (2016).
98. B. Lin, Z. Wen, Z. Gu, and X. Xu, J. Power Sources, 174, 544 (2007).
99. W. Luo and J. R. Dahn, J. Electrochem. Soc., 158, A428 (2011).
100. Z. He, Z. Wang, H. Chen, Z. Huang, X. Li, H. Guo, and R. Wang, J. Power Sources, 299, 334 (2015).
101. S. M. Lee, S. H. Oh, J. P. Ahn, W. Il Cho, and H. Jang, J. Power Sources, 159, 1334 (2006).
102. Q. Liu, H. T. Kuo, R. S. Liu, C. H. Shen, D. S. Shy, X. K. Xing, and J. M. Chen, J. Alloys Compd., 496, 512 (2010).
103. H. Liu, Y. P. Wu, E. Rahm, R. Holze, and H. Q. Wu, J. Solid State Electrochem., 8, 450 (2004).
104. Y. J. Kim, J. Cho, T.-J. Kim, and B. Park, J. Electrochem. Soc., 150, A1723 (2003).
105. J. Z. Kong, S. S. Wang, G. A. Tai, L. Zhu, L. G. Wang, H. F. Zhai, D. Wu, A. D. Li, and H. Li, J. Alloys Compd., 657, 593 (2016).
106. J. Zhao, G. Qu, J. C. Flake, and Y. Wang, Chem. Commun., 48, 8108 (2012).
107. Z. Wang, C. Wu, L. Liu, F. Wu, L. Chen, and X. Huang, J. Electrochem. Soc., 149, A466 (2002).
108. Z. Wang, X. Huang, and L. Chen, J. Electrochem. Soc., 150, A199 (2003).
109. M. R. Laskar, D. H. K. Jackson, S. Xu, R. J. Hamers, D. Morgan, and T. F. Kuech, ACS Appl. Mater. Interfaces, 9, 11231 (2017).
110. F. Ma, Y. Wu, G. Wei, S. Qiu, and J. Qu, J. Solid State Electrochem., 2, 2213 (2019).
111. M. Mladenov, R. Stoyanova, E. Zhecheva, and S. Vassilev, Electrochem. Commun., 3, 410 (2001).
112. Y. Iriyama, H. Kurita, I. Yamada, T. Abe, and Z. Ogumi, J. Power Sources, 137, 111 (2004).
113. G. G. Amatucci, J. M. Tarascon, and L. C. Klein, Solid State Ionics, 83, 167 (1996).
114. H. Zhao, L. Gao, W. Qiu, and X. Zhang, J. Power Sources, 132, 195 (2004).
115. J. H. Shim, S. Lee, and S. S. Park, Chem. Mater., 26, 2537 (2014).
116. H. J. Kweon, J. J. Park, J. W. Seo, G. B. Kim, B. H. Jung, and H. S. Lim, J. Power Sources, 126, 156 (2004).
117. A. Kumar, R. Nazzario, L. Torres-Castro, A. Pena-Duarte, and M. S. Tomar, Int. J. Hydrogen Energy, 40, 4931 (2015).
118. P. Li, L. Xue, Y. Li, Q. Su, Y. Chen, G. Cao, T. Lei, J. Zhu, and S. Deng, Mater. Lett., 207, 217 (2017).
119. S. Tao et al., J. Alloys Compd., 705, 413 (2017).
120. X. Yuan, Q. Jie Xu, X. Liu, H. Liu, Y. Min, and Y. Xia, Electrochim. Acta, 213, 648 (2016).
121. S. J. Kim, M. C. Kim, D. H. Kwak, D. M. Kim, G. H. Lee, H. S. Choe, and K. W. Park, J. Power Sources, 304, 119 (2016).
122. A. Zhou, Y. Lu, Q. Wang, J. Xu, W. Wang, X. Dai, and J. Li, J. Power Sources, 346, 24 (2017).
123. D. Zhang, Y. Liu, L. Wu, L. Feng, S. Jin, R. Zhang, and M. Jin, Electrochim. Acta, 328, 135086 (2019).
124. H. Sun, Z. Cao, T. Wang, R. Lin, Y. Li, X. Liu, L. Zhang, F. Lin, Y. Huang, and W. Luo, Mater. Today Energy, 13, 145 (2019).
125. L. Ma et al., ACS Appl. Energy Mater., 1, 7052 (2018).
126. S. Bin Park, H. C. Shin, W. G. Lee, W. Il Cho, and H. Jang, J. Power Sources, 180, 597 (2008).
127. W. Chang, J. W. Choi, J. C. Im, and J. K. Lee, J. Power Sources, 195, 320 (2010).
128. S. M. Moon, W. Chang, D. Byun, and J. K. Lee, Curr. Appl Phys., 10, e122 (2010).
129. Z. Kong, C. Ren, G. A. Tai, X. Zhang, A. D. Li, D. Wu, H. Li, and F. Zhou, J. Power Sources, 266, 433 (2014).
130. G. Singh, R. Thomas, A. Kumar, R. S. Katiyar, and A. Manivannan, J. Electrochem. Soc., 159, A470 (2012).
131. B. Qiu, J. Wang, Y. Xia, Z. Wei, S. Han, and Z. Liu, ACS Appl. Mater. Interfaces, 6, 9185 (2014).
132. X. Dai, L. Wang, J. Xu, Y. Wang, A. Zhou, and J. Li, ACS Appl. Mater. Interfaces, 6, 15853 (2014).
133. Y. Wang, Y. Ren, X. Dai, X. Yan, B. Huang, and J. Li, R. Soc. Open Sci., 5, 1 (2018).
134. Z.-W. Fu, F. Huang, Y. Zhang, Y. Chu, and Q.-Z. Qin, J. Electrochem. Soc., 150, A714 (2003).
135. X. Shen, D. Mu, S. Chen, B. Wu, and F. Wu, ACS Appl. Mater. Interfaces, 5, 3118 (2013).
136. L. Liang, G. Hu, F. Jiang, and Y. Cao, J. Alloys Compd., 657, 570 (2016).
137. W. Cho, S. M. Kim, J. H. Song, T. Yim, S. G. Woo, K. W. Lee, J. S. Kim, and Y. J. Kim, J. Power Sources, 282, 45 (2015).
138. S. H. Lee, G. J. Park, S. J. Sim, B. S. Jin, and H. S. Kim, J. Alloys Compd., 791, 193 (2019).
139. F. Wu, M. Wang, Y. Su, L. Bao, and S. Chen, J. Power Sources, 195, 2362 (2010).
140. J. Yao, F. Wu, X. Qiu, N. Li, and Y. Su, Electrochim. Acta, 56, 5587 (2011).
141. J. Song, Y. Zhang, and G. Shao, J. Nanomater., 2013, 687501 (2013).
142. Y. Ge, X. Yan, J. Liu, X. Zhang, J. Wang, X. He, R. Wang, and H. Xie, Electrochim. Acta, 55, 5886 (2010).
143. K. Liu, G. L. Yang, Y. Dong, T. Shi, and L. Chen, J. Power Sources, 281, 370 (2015).
144. Y. S. Hu, Y. G. Guo, R. Dominko, M. Gaberscek, J. Jamnik, and J. Maier, Adv. Mater., 19, 1963 (2007).
145. J. Liu and A. Manthiram, J. Mater. Chem., 20, 3961 (2010).
146. R. Zhang, Y. Zhang, K. Zhu, F. Du, Q. Fu, X. Yang, Y. Wang, X. Bie, G. Chen, and Y. Wei, ACS Appl. Mater. Interfaces, 6, 12523 (2014).
147. H. Wang, H. Xia, M. O. Lai, and L. Lu, Electrochem. Commun., 11, 1539 (2009).
148. H. Wang, T. A. Tan, P. Yang, M. O. Lai, and L. Lu, J. Phys. Chem. C, 115, 6102 (2011).
149. Y. Wang, Y. Yang, X. Hu, Y. Yang, and H. Shao, J. Alloys Compd., 481, 590 (2009).
150. B. Song, M. O. Lai, and L. Lu, Electrochim. Acta, 80, 187 (2012).
151. Q. Pang, Q. Fu, Y. Wang, Y. Zhang, B. Zou, F. Du, G. Chen, and Y. Wei, Electrochim. Acta, 152, 240 (2015).
152. Z. Wang, Z. Wang, H. Guo, W. Peng, and X. Li, Ceram. Int., 41, 469 (2015).
153. H. Zhang, J. Xu, and J. Zhang, Front. Mater., 6, 1 (2019).
154. I. Cameán, A. B. García, I. Suelves, J. L. Pinilla, M. J. Lázaro, R. Moliner, and J. N. Rouzaud, Carbon N. Y., 50, 5387 (2012).
155. J. Li, L. Zhang, L. Zhang, W. Hao, H. Wang, Q. Qu, and H. Zheng, J. Power Sources, 249, 311 (2014).
156. N. Ravet, M. Gauthier, K. Zaghib, J. B. Goodenough, A. Mauger, F. Gendron, and C. M. Julien, Chem. Mater., 19, 2595 (2007).
157. X. Yang, Y. Mi, W. Zhang, B. Wu, and H. Zhou, J. Power Sources, 275, 823 (2015).
158. M. M. Doeff, J. D. Wilcox, R. Kostecki, and G. Lau, J. Power Sources, 163, 180 (2006).
159. H. Liu, L. Ren, J. Li, and H. Tuo, Electrochim. Acta, 212, 800 (2016).
160. Y. Liu, D. Liu, Q. Zhang, D. Yu, J. Liu, and G. Cao, Electrochim. Acta, 56, 2559 (2011).
161. Y. Liu, Z. Zhang, Y. Fu, Q. Wang, J. Pan, M. Su, and V. S. Battaglia, J. Alloys Compd., 685, 523 (2016).
162. M. M. Thackeray, C. Wolverton, and E. D. Isaacs, Energy Environ. Sci., 5, 7854 (2012).
163. F. Wu et al., Nano Lett., 14, 3550 (2014).
164. M. M. Thackeray, Adv. Energy Mater., 11, 2001117 (2021).
165. B. Zhang, P. Dong, H. Tong, Y. Yao, J. Zheng, W. Yu, J. Zhang, and D. Chu, J. Alloys Compd., 706, 198 (2017).

166. Q. Ran et al., Electrochim. Acta, 289, 82 (2018).
167. T. Watanabe et al., RSC Adv., 10, 13642 (2020).
168. Z. Wang, Z. Wang, H. Guo, W. Peng, X. Li, and J. Wang, Mater. Lett., 123, 93 (2014).
169. P. Sun, Y. Ma, T. Zhai, and H. Li, Electrochim. Acta, 191, 237 (2016).
170. Q. Hao, H. Ma, Z. Ju, G. Li, X. Li, L. Xu, and Y. Qian, Electrochim. Acta, 56, 9027 (2011).
171. H. Yang, K. Du, G. Hu, Z. Peng, Y. Cao, K. Wu, Y. Lu, X. Qi, K. Mu, and J. Wu, Electrochim. Acta, 289, 149 (2018).
172. S. Guo et al., Nano Energy, 58, 673 (2019).
173. J. Barker, M. Y. Saidi, and J. L. Swoyer, Solid State Ionics, 167, 413 (2004).
174. G. Hu, Z. Gan, Y. Cao, K. Du, Y. Du, and Z. Peng, Electrochim. Acta, 292, 502 (2018).
175. Y. X. Wang, K. H. Shang, W. He, X. P. Ai, Y. L. Cao, and H. X. Yang, ACS Appl. Mater. Interfaces, 7, 13014 (2015).
176. N. Owen and Q. Zhang, J. Appl. Electrochem., 47, 417 (2017).
177. M. Li, H. Wang, L. Zhao, F. Zhang, and D. He, J. Solid State Chem., 272, 38 (2019).
178. H. Sun, D. Zhu, Y. Chen, C. Xu, L. Huang, and H. Yang, J. Solid State Electrochem., 16, 2979 (2012).
179. Q. Wu, Y. Yin, S. Sun, X. Zhang, N. Wan, and Y. Bai, Electrochim. Acta, 158, 73 (2015).
180. Y. K. Sun, J. M. Han, S. T. Myung, S. W. Lee, and K. Amine, Electrochem. Commun., 8, 821 (2006).
181. Y. Bai, K. Jiang, S. Sun, Q. Wu, X. Lu, and N. Wan, Electrochim. Acta, 134, 347 (2014).
182. Y. Cho, J. Eom, and J. Cho, J. Electrochem. Soc., 157, A617 (2010).
183. J. Cho, Y. W. Kim, B. Kim, J. G. Lee, and B. Park, Angew. Chemie - Int. Ed., 42, 1618 (2003).
184. H. J. Lee and Y. J. Park, Solid State Ionics, 230, 86 (2013).
185. Y. Wang, X. Wang, S. Yang, H. Shu, Q. Wei, Q. Wu, Y. Bai, and B. Hu, J. Solid State Electrochem., 16, 2913 (2012).
186. C. Zhang, L. Shen, H. Li, N. Ping, and X. Zhang, J. Electroanal. Chem., 762, 1 (2016).
187. Y. Wang, X. Wang, S. Yang, H. Shu, Q. Wei, Q. Wu, Y. Bai, and B. Hu, Solid State Ionics, 284, 7 (2016).
188. K. Shimoda, M. Murakami, D. Takamatsu, H. Arai, Y. Uchimoto, and Z. Ogumi, Electrochim. Acta, 108, 343 (2013).
189. H. Jung, H. Song, T. Kim, J. K. Lee, and J. Kim, J. Alloys Compd., 647, 750 (2015).
190. C. D. Li, J. Xu, J. S. Xia, W. Liu, X. Xiong, and Z. A. Zheng, Solid State Ionics, 292, 75 (2016).
191. C. S. Kim, J. H. Cho, and Y. J. Park, Mater. Res. Bull., 58, 49 (2014).
192. T. Zhao, L. Li, R. Chen, H. Wu, X. Zhang, S. Chen, M. Xie, F. Wu, J. Lu, and K. Amine, Nano Energy, 15, 164 (2015).
193. K. Xu, Z. Jie, R. Li, Z. Chen, S. Wu, J. Gu, and J. Chen, Electrochim. Acta, 60, 130 (2012).
194. M. G. Theivanayagam, T. Hu, R. Ziebarth, S. Santhany, J. Goss, H. Maeda, A. Patel, M. Behr, M. Lowe, and A. Leugers, Solid State Ionics, 281, 82 (2015).
195. Z. Yang, Q. Qiao, and W. Yang, Electrochim. Acta, 56, 4791 (2011).
196. H. Xie, Z. Liang, D. Luo, Y. Zhang, X. Ding, J. Cui, Z. Zhang, and Z. Lin, Chem. Commun., 56, 12009 (2020).
197. W. Cho, S. M. Kim, K. W. Lee, J. H. Song, Y. N. Jo, T. Yim, H. Kim, J. S. Kim, and Y. J. Kim, Electrochim. Acta, 198, 77 (2016).
198. Z. Chen, G. T. Kim, D. Bresser, T. Diemant, J. Asenbauer, S. Jeong, M. Copley, R. J. Behm, and J. Lin, Adv. Energy Mater., 8, 1 (2018).
199. Z. Shen et al., J. Power Sources, 402, 263 (2018).
200. C. H. Jo, D. H. Cho, H. J. Noh, H. Yashiro, Y. K. Sun, and S. T. Myung, Nano Res., 8, 1464 (2015).
201. X. Bian, Q. Fu, X. Bie, P. Yang, H. Qiu, Q. Pang, G. Chen, F. Du, and Y. Wei, Electrochim. Acta, 174, 875 (2015).
202. D. Chen, F. Zheng, L. Li, M. Chen, X. Zhong, W. Li, and L. Lu, J. Power Sources, 341, 147 (2017).
203. S. W. Lee, M. S. Kim, J. H. Jeong, D. H. Kim, K. Y. Chung, K. C. Roh, and K. B. Kim, J. Power Sources, 360, 206 (2017).
204. J. Zhu, Y. Li, L. Xue, Y. Chen, T. Lei, S. Deng, and G. Cao, J. Alloys Compd., 773, 112 (2019).
205. X. Liu, H. Li, E. Yoo, M. Ishida, and H. Zhou, Electrochim. Acta, 83, 253 (2012).
206. G. Li, Z. Yang, and W. Yang, J. Power Sources, 183, 741 (2008).
207. K. C. Kim, J. P. Jegal, S. M. Bak, K. C. Roh, and K. B. Kim, Electrochem. Commun., 43, 113 (2014).
208. B. Xiao et al., Adv. Sci., 2, 4 (2015).
209. F. Wu, X. Zhang, T. Zhao, L. Li, M. Xie, and R. Chen, ACS Appl. Mater. Interfaces, 7, 3773 (2015).
210. J. H. Wang, Y. Wang, Y. Z. Guo, Z. Y. Ren, and C. W. Liu, J. Mater. Chem. A, 1, 4879 (2013).
211. Y. Kim and J. Cho, J. Electrochem. Soc., 154, A495 (2007).
212. S. H. Lee, B. K. Koo, J. C. Kim, and K. M. Kim, J. Power Sources, 184, 276 (2008).
213. L. L. Xie, L. Q. You, X. Y. Cao, C. F. Zhang, D. W. Song, and L. B. Qu, Electron. Mater. Lett., 8, 411 (2012).
214. K. Park, J. H. Park, B. Choi, J. H. Kim, S. G. Hong, and H. N. Han, Electrochim. Acta, 257, 217 (2017).
215. Y. Cui and S. Xu, Chinese J. Chem. Eng., 23, 315 (2015), h.
216. H. G. Song, K. S. Park, and Y. J. Park, Solid State Ionics, 225, 532 (2012).
217. H. Tong, P. Dong, J. Zhang, J. Zheng, W. Yu, K. Wei, B. Zhang, Z. Liu, and D. Chu, J. Alloys Compd., 764, 44 (2018).
218. Y. Bai, Y. Yin, N. Liu, B. Guo, H. Shi, J. Liu, Z. Wang, and L. Chen, J. Power Sources, 174, 328 (2007).
219. Z. Xiao, C. Hu, L. Song, L. Li, Z. Cao, H. Zhu, J. Liu, X. Li, and F. Tang, Ionics (Kiel)., 24, 91 (2018).
220. J. Zheng, S. Myeong, W. Cho, P. Yan, J. Xiao, C. Wang, J. Cho, and J. G. Zhang, Adv. Energy Mater., 7, 1601284 (2017).
221. L. L. Zhang, J. J. Chen, S. Cheng, and H. F. Xiang, Ceram. Int., 42, 1870 (2016).
222. B. Huang, Z. Zhao, Y. Sun, M. Wang, L. Chen, and Y. Gu, Solid State Ionics, 338, 31 (2019).
223. K. Meng, Z. Wang, H. Guo, X. Li, and D. Wang, Electrochim. Acta, 211, 822 (2016).
224. Y. Di Xu, W. Xiang, Z. G. Wu, C. L. Xu, Y. C. Li, X. D. Guo, G. P. Lv, X. Peng, and B. H. Zhong, Electrochim. Acta, 268, 358 (2018).
225. J. Z. Kong, C. Ren, Y. X. Jiang, F. Zhou, C. Yu, W. P. Tang, H. Li, S. Y. Ye, and J. X. Li, J. Solid State Electrochem., 20, 1435 (2016).
226. Y. Zhai, J. Zhang, H. Zhang, X. Liu, C.-W. Wang, L. Sun, and X. Liu, J. Electrochem. Soc., 166, A1323 (2019).
227. J. Ni, H. Zhou, J. Chen, and X. Zhang, Electrochim. Acta, 53, 3075 (2008).
228. D. Wang, X. Li, Z. Wang, H. Guo, Z. Huang, L. Kong, and J. Ru, J. Alloys Compd., 647, 612 (2015).
229. H. Liang, Z. Wang, H. Guo, J. Wang, and J. Leng, Appl. Surf. Sci., 423, 1045 (2017).
230. E. Zhao, X. Liu, H. Zhao, X. Xiao, and Z. Hu, Chem. Commun., 51, 9093 (2015).
231. E. Zhao, M. Chen, Z. Hu, D. Chen, L. Yang, and X. Xiao, J. Power Sources, 343, 345 (2017).
232. L. Zhou, Y. Wu, J. Huang, X. Fang, T. Wang, W. Liu, Y. Wang, Y. Jin, and X. Tang, J. Alloys Compd., 724, 991 (2017).
233. L. Wu, X. Tang, Z. Rong, X. Chen, J. Huang, T. Chen, X. Fang, Y. Wang, and W. Dang, Appl. Surf. Sci., 484, 21 (2019).
234. J. Fu, D. Mu, B. Wu, J. Bi, H. Cui, H. Yang, H. Wu, and F. Wu, ACS Appl. Mater. Interfaces, 10, 19704 (2018).
235. R. F. Ali and B. D. Gates, Chem. Mater., 30, 2028 (2018).
236. J. H. Kim, H. Kim, W. Choi, and M. S. Park, ACS Appl. Mater. Interfaces, 12, 35098 (2020).
237. G. Kaur, Solid Oxide Fuel Cell Components: Interfacial Compatibility of SOFC Glass Seals (Springer, New York, NY) (2015).
238. G. Kaur, F. Baino, J. C. Mauro, V. Kumar, G. Pickrell, N. Sriranganathan, and S. G. Waldrop, Biomaterials for Cell Encapsulation: Progress Toward Clinical Applications (Springer, New York, NY) (2017).
239. G. Kaur, V. Kumar, O. P. Pandey, and K. Singh, J. Electrochem. Soc., 159, 277 (2012).
240. W. Zhou, L. Wang, F. Zhou, and D. Johnson, US patent 2020, US 2020/0185709.
241. V. Kumar, G. Kaur, and G. R. Pickrell, Silica Nanospheres (Elsevier, London, UK) (2018).
242. M. Du, P. Yang, W. He, S. Bie, H. Zhao, J. Yin, Z. G. Zou, and J. Liu, J. Alloys Compd., 805, 991 (2019).
243. J. Ying, C. Wan, and C. Jiang, J. Power Sources, 102, 162 (2001).
244. M. Bai, Z. Wang, X. Li, H. Guo, Z. He, and J. Zhao, Solid State Ionics, 292, 66 (2016).
245. H. S. Kang, P. Santhoshkumar, J. W. Park, G. S. Sim, M. Nanthagopal, and C. W. Lee, Korean J. Chem. Eng., 37, 1331 (2020).
246. G. Tan, F. Wu, L. Li, R. Chen, and S. Chen, J. Phys. Chem. C, 117, 6013 (2013).
247. E. L. Zhao, S. X. Zhao, X. Wu, J. W. Li, L. Q. Yu, C. W. Nan, and G. Cao, J. Mater., 5, 663 (2019).
248. M. Nishizawa, K. Mukai, S. Kuwabata, C. R. Martin, and H. Yoneyama, J. Electrochem. Soc., 144, 1923 (1997).
249. C. Arbizzani, A. Balducci, M. Mastragostino, M. Rossi, and F. Soavi, J. Power Sources, 119–121, 695 (2003).
250. R. Vidu and P. Stroeve, Ind. Eng. Chem. Res., 43, 3314 (2004).
251. Q. Gan, N. Qin, Y. Zhu, Z. Huang, F. Zhang, S. Gu, J. Xie, K. Zhang, L. Lu, and Z. Lu, ACS Appl. Mater. Interfaces, 11, 12594 (2019).
252. A. Hynowska et al., Materials (Basel), 6, 4930 (2013).
253. M. R. Shin and J. T. Son, J. Nanosci. Nanotechnol., 17, 8869 (2017).
254. E. Meng, M. Zhang, Y. Hu, F. Gong, L. Zhang, and F. Li, Electrochim. Acta, 265, 160 (2018).
255. J. Arrebola, A. Caballero, L. Hernán, J. Morales, E. Rodríguez Castellón, and J. R. Ramos Barrado, J. Electrochem. Soc., 154, A178 (2007).
256. T. Yang, N. Zhang, Y. Lang, and K. Sun, Electrochim. Acta, 56, 4058 (2011).
257. S. J. Sim, S. H. Lee, B. S. Jin, and H. S. Kim, Sci Rep., 10, 1 (2020).
258. Z. Yan, S. Cai, L. Miao, X. Zhou, and Y. Zhao, J. Alloys Compd., 511, 101 (2012).
259. W. Luo, B. Zheng, and J. He, J. Alloys Compd., 705, 405 (2017).
260. J. Z. Kong, Y. Chen, Y. Q. Cao, Q. Z. Wang, A. D. Li, H. Li, and F. Zhou, J. Alloys Compd., 799, 89 (2019).
261. C. Dhand, N. Dwivedi, X. J. Loh, A. N. Jie Ying, N. K. Verma, R. W. Beuerman, R. Lakshminarayanan, and S. Ramakrishna, RSC Adv., 5, 105003 (2015).
262. R. W. Johnson, A. Hultqvist, and S. F. Bent, Mater. Today, 17, 236 (2014).

Annex 11 UL 9540A testing data

UNIT TEST REPORT
UL 9540A
Test Method for Evaluating Thermal Runaway Fire Propagation in Battery Energy Storage Systems (AACD)

Project Number. .....:	**12345678**
Date of issue.....:	**July 1, 2020**
Total number of pages .....:	**43**
UL Report Office .....:	**UL LLC, Northbrook, IL 60062 USA**
Applicant's name .....:	**ACME Energy Storage**
Address.....:	**Anywhere USA**
Test specification:	4th Edition, Section 7, November 12, 2019
Standard.....:	UL 9540A, Test Method for Evaluating Thermal Runaway Fire Propagation in Battery Energy Storage Systems
Test procedure .....:	9.1 – 9.8
Non-standard test method .....:	N/A

Copyright © 2020 UL LLC All Rights Reserved.

General disclaimer:

The test results presented in this report relate only to the sample tested.

UL LLC did not select the sample(s), determine whether the sample(s) was representative of production samples, witness the production of the test sample(s), nor were we provided with information relative to the formulation or identification of component materials used in the test sample(s).

The issuance of this report in no way implies Listing, Classification or Recognition by UL and does not authorize the use of UL Listing, Classification or Recognition Marks or any other reference to UL on the product or system. UL LLC authorizes the above named company to reproduce this Report provided it is reproduced in its entirety. UL's name or marks cannot be used in any packaging, advertising, promotion or marketing relating to the data in this Report, without UL's prior written permission.

UL LLC, its employees, and its agents shall not be responsible to anyone for the use or non-use of the information contained in this Report, and shall not incur any obligation or liability for damages, including consequential damages, arising out of or in connection with the use of, or inability to use, the information contained in this Report.

This is a sample report to demonstrate the content provided in a UL 9540A unit level test report. This sample report contains real measurements taken from UL 9540A testing of a non-proprietary example product fabricated by UL for the purposes of creating demonstration data.
This report has been created for the purposes of demonstrating a minimum level of information and data that should be provided for a UL 9540A unit level test report.

Test item description ……..:		
BESS Intended Installation **Non Residential:** outdoor ground mounted, indoor floor mounted, outdoor wall mounted, indoor wall mounted, roof top, open garage **Residential:** Outdoor ground mounted, indoor floor mounted, outdoor wall mounted, indoor wall mounted	Non residential – Indoor floor mounted	
Residential Indoor Use: Smallest volume room installations specified.	N/A	
BESS module configuration	9 S/1 P module configuration	
Number of modules in BESS	9 modules	
Module Manufacturer/Model No.:	Top Cell Manufacturer/ Model XYZ Module	
Module cell configuration (xS/yP) ……:	14 S/4 P cell configuration	
Number of cells in module.:	56 cells	
Cells in Module: •**Manufacturer Name** •**Part Number** •**Chemistry** •**Format**	Top Cell Manufacturer	
	Model ABC	
	NMC (Lithium Nickel Manganese Cobalt Oxide ($LiNiMnCoO_2$))	
	Prismatic	
BESS dimensions (X x Y x Z (mm))……:	370 mm wide x 610 mm deep x 1485 mm high	
BESS weight (kgs)…… :	2300kg	
BESS enclosure material…….. :	The systems were an open rack design with enclosures provided at the individual module level	
Original Equipment Manufacturer (OEM):	**ACME Energy Storage**	
Branding Manufacturer (if not OEM):	N/A	
Model No ……: **Ratings ……:**	Powersource ABC 480Vac, 355 A output current, 170 KVA max power output, 1,350Ah max output energy output	
Test item certified? ……:	Yes	
Standard test item certified to ……:	UL 9540	
Organization that certified test item …….:	UL LLC	
Organization that certified BESS:	UL LLC	
Testing Laboratory and testing location(s):		
Testing Laboratory:	UL LLC	
Testing location/ address…… :	333 Pfingsten Road Northbrook, IL 60062, USA	
Tested by (name, signature)…… :	Sam Jones	*Sam Jones*

Witnessed by (for 3rd Party Lab Test Location) (name, signature) ..... :	N/A	N/A
Project Handler (name, signature)..... :	John Smith	*John Smith*
Reviewer (name, signature) .....:	Joe Adams	*Joe Adams*

List of Attachments (including a total number of pages in each attachment):

Attachment A: Sample Charging, OCV and SOC Measurement Profiles - (*Pages 29 through 29*)

Attachment B: BESS (including module and any integral fire detection and suppression systems) Construction Photos/Diagrams - (*Pages 30 through 31*)

Attachment C: BESS and Equipment Instrumentation and Test Installation Layout Photos/Diagrams - (*Pages 32 through 32*)

Attachment D: Temperature Profiles and Heat Flux Measurements During Testing (Initiating Cell and Module, Target Modules, Wall Surfaces, etc. - (*Pages 33 through 38*)

Attachment E: BESS Unit Testing and Post Testing Photos - (*Pages 39 through 41*)

Attachment F: BESS Unit Test Datasheets - (*Pages 42 through 42*)

Attachment G: BESS Unit Gas Flow Rate and Heat Release and Smoke Release Profiles – (*Pages 43 through 43*)

Summary of cell testing:

Cell failure test method performed (summary of method and test clause):

☒ External heating using thin film with 4°C to 7°C thermal ramp.

☐ Nail Penetration

☐ Overcharge

☐ External short circuit (***X*** Ω *external resistance*)

☐ Others

Description of method used to fail cells if other than external thin film heater with thermal ramp, :

N/A

Test Results from Cell Level Test:	
Average cell surface temperature at gas venting, °C:	159°C (318°F)
Average cell surface temperature at thermal runaway, °C:	201°C (394°F)
Test Results from Module Level Test	
No of initiating cells failed to establish propagation at the module level	one
Flaming external to module, Location	Yes, from the top of the module
Peak Heat Release Rate:	81 kW
Gas Composition Pre-Flaming:	CO_2 (1 L); CO (1 L); THC (43 L); H_2 (0 L)
Gas Composition After Flaming:	CO_2 (259L); CO (181 L); THC (157 L); H_2 (56 L)

Description of components employed within the BESS unit that serve to suppress propagation (fire protection features).

: N/A

Summary of BESS Unit Test Results

Thermal Runaway Propagation:	Propagation through all modules in the initiating unit
External Flaming from BESS:	External flames were visible
Location(s) of Flame Venting:	Flames were visible from the vent opening of the initiating unit
Maximum Target BESS Temperature, °C	800°C on the target adjacent to the BESS
Maximum Wall Surface Temperature, °C	820°C at the wall surface above the initiating BESS
Peak Chemical Heat Release Rate, kW	1170
Peak Convective Heat Release Rate, kW	490
Smoke Heat Release Rate, m^2/s	12
Maximum Heat Flux on Target Modules, kW/m^2	41
Maximum Heat Flux of Egress Path, kW/m^2	26
Flying Debris:	No evidence of flying debris
Re-ignitions:	No re-ignitions
Gas Composition Pre-Flaming:	CO, CO_2, THC
Gas Composition After Flaming:	CO, CO_2, THC

Gas Analysis:

☒ **Flame ionization detection (FID)**

☒ **Non-Dispersive Infrared Spectrometer (NDIR)**

☒ **Fourier-Transform infrared Spectrometer**

☒ **Hydrogen Sensor (palladium-nickel, thin-film solid state sensor)**

☒ **White light source with photo detector (smoke release rate)**

Summary of Gas Analysis Data:

- **Gas Composition & Volume for Each Compound (Pre-flaming and After flame):**

Gas Compound	Gas Type	Pre-Flaming (L)	Flaming (L)
Total Hydro-carbons (Propane Equi-valent)	Hydro-carbons	1,370	2,450
Carbon Dioxide	Carbon Contain-ing	1,000	24,250
Carbon Monoxide	Carbon Contain-ing	1,200	1,250
Hydrogen	-	0	0

• **Smoke Release Rate (m^2/s)**	12
• **Total Smoke Released: (m^2)**	20
• **Peak Chemical Heat Release Rate: (kW):**	1170

☐ **Performance Criteria met in accordance with Clause 9.8:** Not compliant with unit level performance criteria

Photo(s) of BESS unit:



Test Item Charge/Discharge Module Specifications:	
• **Charge current, A:**	58.5
• **Maximum charge voltage, Vdc:**	75.6
• **Charge temperature range, °C:**	-30~60
• **End of charge current, A:**	24
• **Discharge current, A:**	58.5
• **End of discharge voltage, Vdc:**	60
• **Discharge temperature range, °C:**	-30~60

Test item particulars..... :	Powersource ABC
Possible test case verdicts:	
- test case does not apply to the test object.....:	N/A
- test object does meet the requirement.....:	P (Pass)
- test object does not meet the requirement.....:	F (Fail)
Testing.....:	
Date of receipt of test item .....:	2020-05-11
Date (s) of performance of tests.....:	2020-05-14
General remarks:	
"(See Enclosure #)" refers to additional information appended to the report. "(See appended table)" refers to a table appended to the report.	
Manufacturer's Declaration of samples submitted for test:	
The applicant for this report includes samples from more than one factory location and a declaration from the Manufacturer stating that the sample(s) submitted for evaluation is (are) representative of the products from each factory has been provided..... :	☒ **Yes** ☐ **Not applicable**
Name and address of factory (ies) .....:	Anywhere in China
General product information and other remarks: Details of Construction of BESS provided in Test Item Description above and Attachment B.	

UL 9540A, Edition 4,			
Clause	Requirement + Test	Result - Remark	Verdict

5.0	**CONSTRUCTION**		**Verdict**
5.3	**Battery energy storage system unit Construction**		—
5.3.1, 5.3.2	Construction information	See Test Item Description at the beginning of this report (page 2)	—
5.3.2	General layout of BESS unit contents	See Attachment B	—
5.3.3	Details of integral fire suppression system	NA	—
5.3.1	BESS certified to UL 9540		P
	Organization that certified BESS:	UL LLC	—
6.0	**PERFORMANCE**		**Verdict**
6.1	**General**		
9.1	**Sample and test configuration**		
9.1.1	The unit level test conducted with BESS units installed as described in the manufacturer's instructions.	See Attachment C for test installations Installation type:	P
9.1.2	The unit level test required one initiating BESS unit in which an internal fire condition in accordance with the module level test is initiated and target adjacent BESS units representative of an installation.	See Attachment C for test installations	P
	Tests conducted for indoor floor mounted installations are representative of both indoor floor mounted and outdoor ground mounted installations.	Intended for indoor use only	N/A
	Tests conducted indoors with fire propagation hazards and separation distances between initiating and target units representative of the installation.		P
	Testing conducted outdoors for outdoor only installations with following in place: a) Wind screens with wind speed of ≤ 12 mph; b) Temperature range is 10°C to 40°C (50°F to 104°F); c) Humidity is < 90% RH; d) Sufficient light to observe the testing; e) There is no precipitation; f) There is control of vegetation and combustibles in the test area; and g) There are protection mechanisms in place to prevent inadvertent access by unauthorized persons in the test area.		N/A

UL 9540A, Edition 4,			
Clause	Requirement + Test	Result - Remark	Verdict
9.1.3	Testing to determine fire characterization was done at the battery system level rather than a complete BESS		N/A
9.1.4	The initiating BESS contained components representative of a BESS unit in a complete installation.		P
	Combustible components that interconnect the initiating and target BESS units was included.		P
9.1.5	Target BESS units include the outer cabinet (if part of the design), racking, module enclosures, and components that retain cells components.		P
9.1.6	The initiating BESS was at the maximum operating state of charge (MOSOC).	See Table 2 and Attachment A	P
	After charging and prior to testing, the initiating BESS was at rest for a maximum period of 8 hours at room ambient.	See Table 2	P
9.1.7	The BESS unit included an integral fire suppression system.	No fire suppression system was employed.	N/A
9.1.8	Electronics and software controls such as the battery management system (BMS) are not relied upon for this testing.		P
	Included a fire suppression control in accordance with UL 864 that is external to the BESS.		N/A
9.2	**Test method – Indoor floor mounted BESS units**		
9.2.1	Test room ambient temperature within 10°C (50°F) to 32°C (90°F).	See Table 2	P
9.2.2	Access door(s) or panels on the initiating BESS unit and adjacent target BESS units were closed, latched and locked duration of the test.		P
9.2.3	The initiating BESS unit was positioned adjacent to two instrumented wall sections.	Attachment C	P
9.2.4	Instrumented wall sections extend not less than 0.49 m (1.6 ft) horizontally beyond the exterior of target BESS units.	the width of the instrumented wall was 3000mm - Depth of one unit : 610mm - Distance between the target 3 and the initiating unit : 915mm	P
9.2.5	Instrumented wall sections were at least 0.61-m (2-ft) taller than the BESS unit height, but not less than 3.66 m (12 ft) in height above the bottom surface of the unit.	Height of the tested units was 1485mm and the instrumented wall was 2100mm high	P

UL 9540A, Edition 4,			
Clause	Requirement + Test	Result - Remark	Verdict
9.2.6	The surface of the instrumented wall sections were covered with 16-mm (5/8-in) gypsum wall board and painted flat black.	See Attachment C	P
9.2.7	The initiating BESS unit was centered underneath an appropriately sized smoke collection hood of an oxygen consumption calorimeter.		P
9.2.8	The light transmission in the calorimeter's exhaust duct was measured using a white light source and photo detector. The smoke release rate was calculated.	See Table 12 See Attachment G	P
9.2.9	The chemical and convective heat release rates were measured for the duration of the test.	See Table 12 See Attachment G	P
9.2.10	The heat release rate measurement system was calibrated using an atomized heptane diffusion burner. The calibration was performed using flows of 3.8, 7.6, 11.4 and 15.2 L/min (1, 2, 3 and 4 gpm) of heptane.		P
9.2.11	The chemical heat release rate was measured using the following equipment: • Paramagnetic oxygen analyzer • Non-dispersive infrared carbon dioxide and carbon monoxide analyzer • Velocity probe • Type K thermocouple		P
9.2.12	The chemical heat release rate at each of the flows was calculated.		P
9.2.13	The physical spacing between BESS units (both initiating and target) and adjacent walls was representative of the intended installation.	See Attachment C	P
9.2.14	Separation distances were specified by the manufacturer for distance between: a) The BESS units and the instrumented wall sections; and b) Adjacent BESS units.	See Attachment C	P
9.2.15	Wall surface temperature measurements were collected	See Table 6 See Attachment D	P
	The intended installation is composed completely of non-combustible construction		P

UL 9540A, Edition 4,			
Clause	Requirement + Test	Result - Remark	Verdict
9.2.16	Wall surface temperatures were measured in vertical array(s) at 152-mm (6-in) intervals for the full height of the instrumented wall sections using No. 24-gauge or smaller, Type-K exposed junction thermocouples.		P
	The thermocouples for measuring the temperature on wall surfaces were horizontally positioned in the wall locations to receive greatest thermal exposure from the initiating BESS unit.		P
9.2.17	Thermocouples were secured to gypsum surfaces and the thermocouple tip was depressed into the gypsum so as to be flush with the gypsum surface at the point of measurement .		P
9.2.18	Heat flux was measured with at least two water-cooled Schmidt-Boelter gauges at the surface of each instrumented wall: a) Both are collinear with the vertical thermocouple array; b) One is positioned to receive the greatest heat from the initiating module; and c) One is positioned to receive the greatest heat flux during potential propagation within the initiating BESS unit.	Due to the location of Target 2, which was in the path of heat flux from the initiating unit to the gauge, the sidewall was not instrumented with a heat flux gauge.	P
9.2.19	Heat flux was measured with 2 water-cooled Schmidt-Boelter gauges at the surface of each adjacent target BESS units facing initiating BESS unit: a) One is positioned at the elevation estimated to receive the greatest heat flux from the initiating module; and b) One is positioned at the elevation estimated to receive the greatest surface heat flux due to initiating BESS.	Only one heat flux gauge was installed in each target unit at the elevation estimated to receive the greatest heat flux due to the thermal runaway of the initiating module. No secondary heat flux was installed because the distance between each target unit and the initiating unit is 0mm and based upon the engineering discretion the flame was expected near the initiating module and the right next to the initiating module was assumed to experience the greatest surface heat flux even in the thermal runaway of the initiating BESS	P
9.2.20	Heat flux was measured with the sensing element of at least one water-cooled Schmidt-Boelter gauge positioned in the center of the accessible means of egress.		P

UL 9540A, Edition 4,			
Clause	Requirement + Test	Result - Remark	Verdict
9.2.21	No. 24-gauge or smaller, Type-K exposed junction thermocouples were installed to measure the temperature of the surface proximate to the cells and between the cells and exposed face of the initiating module.	See Attachment C	P
	Each non-initiating module enclosure within the initiating BESS unit was instrumented with at least one No. 24-gauge or smaller Type-K thermocouple(s) within non-initiating modules.	See Attachment C	P
	Additional thermocouples were placed to account for convoluted geometries.		N/A
9.2.22	For residential use, the DUT was covered with a single layer of cheese cloth ignition indicator. The cheesecloth was untreated cotton cloth running 26 – 28 m2/kg with a count of 28 – 32 threads in either direction within a 6.45 cm^2 (1 in^2) area.	Non residential application	N/A
9.2.23	An internal fire condition in accordance with the module level test was created within a single module in the initiating BESS unit: a) The position selected to present the greatest thermal exposure to adjacent modules; and b) The setup was the same as that used to initiate and propagate thermal runaway within the module level test.	See Attachment C	P
9.2.24	The composition, velocity and temperature of the initiating BESS unit vent gases was measured within the calorimeter's exhaust duct. Composition, velocity and temperature instrumentation shall be collocated with heat release rate calorimetry instrumentation.		P
	Hydrogen gas shall be measured with a palladium-nickel thin-film solid state sensor.		P
	The hydrocarbon content of the vent gas may also be measured using a Fourier-Transform Infrared Spectrometer with a minimum resolution of 1 cm-1 and a path length of at least 2 m (6.6 ft), or equivalent gas analyzer.		P
9.2.25	The hydrocarbon content of the vent gas was measured using flame ionization detection.	See Tables 8, 9, 10 and 11	P
9.3	**Test method – Outdoor ground mounted units**		N/A

UL 9540A, Edition 4,			
Clause	Requirement + Test	Result - Remark	Verdict
9.3.1	Outdoor ground mounted non-residential use BESS for installation: test method described in Section 9.2 was used.		N/A
	Outdoor use only installations: the smoke release rate, the convective and chemical heat release rate and content, velocity and temperature of the released vent gases were not be measured.		N/A
9.3.2	Outdoor ground mounted residential use BESS: The test method described in Section 9.2 except as noted in 9.3.3 and 9.3.4.		N/A
	Heat flux measurements for the accessible means of egress were measured in accordance with 9.2.20.		N/A
	Outdoor use only installations: the smoke release rate, the convective and chemical heat release rate and content, velocity and temperature of the released vent gases were not be measured.		N/A
9.3.3	Test samples were installed as shown in Figure 9.2 in proximity to an instrumented wall section that is 3.66-m (12-ft) tall with a 0.3-m (1-ft) wide horizontal soffit (under surface of the eave shown in Figure 9.2).		N/A
	The sample was mounted on a support substrate and spaced from the wall in accordance with the minimum separation distances. The wall and soffit were constructed with 19.05-mm (3/4-in) plywood installed on wood studs and painted flat black.		N/A
	The instrumented wall extended not less than 0.49-m (1.6-ft) horizontally beyond the exterior of the target BESS units.		N/A
	If the manufacturer requires installation against non-flammable material, the test setup may include manufacturer recommended backing material between the unit and plywood wall.		N/A
	The No. 24-gauge or smaller, Type-K exposed junction thermocouple array on the walls extended to the surface of the soffit.		N/A
9.3.4	Target BESS were installed on each side of the initiating BESS in accordance with installation specifications. The physical spacing between BESS units (both initiating and target) were the minimum separation distances specified.		N/A

UL 9540A, Edition 4,			
Clause	Requirement + Test	Result - Remark	Verdict
9.4	Test Method – Indoor wall mounted units		N/A
9.4.1	Testing of indoor wall mounted BESS were in accordance with Section 9.2, except as modified in section 9.4.		N/A
9.4.2	The test was conducted in a standard NFPA 286 fire test room, 3.66 × 2.44 × 2.44-m (12 × 8 × 8-ft) high, with a 0.76 × 2.13-m (2-1/2 × 7-ft) high opening.		N/A
	The room was constructed with 16-mm (5/8-in) gypsum wall board installed on wood studs and painted flat black.		N/A
9.4.3	The initiating BESS unit was positioned on the wall opposite of the door opening, with the center located 1.22-m (4-ft) above the floor, and halfway between adjacent walls.		N/A
9.4.4	Target BESS was installed on the wall on each side of the initiating BESS, at the same height above the floor as the initiating BESS. The physical spacing between BESS units (both initiating and target) were the minimum separation distances.		N/A
9.4.5	The wall on which the initiating and target BESS units were mounted were instrumented in accordance with Section 9.2.		N/A
9.4.6	The gas collection methods were in accordance with 9.2.		N/A
	For residential use systems, the gas collection data gathered in 9.2 was compared to the smallest room installation specified by the manufacturer to determine if the flammable gas collected exceeds 25% LFL in air.		N/A
9.4.7	For residential use BESS, the DUT was covered with a single layer of cheese cloth ignition indicator. The cheesecloth was untreated cotton cloth running 26 – 28 m2/kg with a count of 28 – 32 threads in either direction within a 6.45 cm2 (1 in2) area.		N/A
9.5	**Test Method – Outdoor wall mounted units**		N/A
9.5.1	Testing of outdoor wall mounted BESS were in accordance with Section 9.2, except as modified in section 9.5.		N/A

UL 9540A, Edition 4,			
Clause	Requirement + Test	Result - Remark	Verdict
	Intended for outdoor use only wall mount installations: the smoke release rate, the convective and chemical heat release rate; and the content, velocity and temperature of the released vent gases were not be measured.		N/A
9.5.2	Test samples were mounted on an instrumented wall section that is 3.66-m (12-ft) tall with a 0.3-m (1-ft) wide horizontal soffit. The wall and soffit were constructed with 19.05-mm (3/4-in) plywood installed on wood studs and painted flat black.		N/A
	The instrumented wall extended not less than 0.49-m (1.6-ft) horizontally beyond the exterior of the target BESS units.		N/A
	No. 24-gauge or smaller, Type-K exposed junction thermocouple array on the walls extended to the surface of the soffit.		N/A
9.5.3	The initiating BESS unit was positioned on the instrumented wall, with its center located 1.22-m (4-ft) above the floor, and halfway between wall edges.		N/A
9.5.4	Target BESS was installed on the wall on each side of the initiating BESS at the same height. The physical spacing between BESS units (both initiating and target) are the minimum separation distances specified.		N/A
9.5.5	The wall on which the initiating and target BESS units are mounted was instrumented in accordance with Section 9.2.		N/A
9.5.6	For residential use BESS: the DUT was covered with a single layer of cheese cloth ignition indicator. The cheesecloth was untreated cotton cloth running 26 – 28 m2/kg with a count of 28 – 32 threads in either direction within a 6.45 cm2 (1 in2) area .		N/A
9.6	**Rooftop and open garage installations**		N/A
9.6.1	Testing of BESS intended for non-residential use rooftop or open garage installations were in accordance with 9.2.		N/A
9.6.2	Intended for rooftop and open garage use only installations: the smoke release rate, the convective and chemical heat release rate and content, velocity and temperature of the released vent gases were not measured.		N/A

UL 9540A, Edition 4,			
Clause	Requirement + Test	Result - Remark	Verdict

9.7	**Unit level test report**		
9.7.1	Installation type tested:	Non-residential Indoor floor mounted	P
9.7.2	Testing is intended to represent more than one installation type.	See Test Item Description in beginning of this report.	
9.7.3	a. Unit manufacturer name and model number (and whether UL 9540 compliant);	Manufacturer : ACME Energy Storage Model Number : Powersource ABC UL 9540A Compliant	
	b. Number of modules in the initiating BESS unit	72 modules	
	c. BESS construction features;	See Attachment C See Critical Components Table See Also “Description of components employed within the module that impact propagation (fire protection features)” at the beginning of this report.	
	d. Fire protection features/ detection/ suppression systems within unit	Not applicable	
	e. Module voltages corresponding to the tested SOC;	See Attachment D	
	f. Thermal runaway initiation method used;	See Attachment C	
	g. Location of the initiating module within the BESS unit;	See Attachment C	
	h. Diagram and dimensions of the test setup including mounting location of the initiating and target BESS units, and the locations of walls, ceilings, and soffits;	See Attachment C	
	i. Observation of any flaming outside the initiating BESS enclosure and the maximum flame extension;	See Table 15	
	j. Chemical and convective heat release rate versus time data;	See Table 11 See Attachment G	
	k. Separation distances from the initiating BESS unit to target walls	See Attachment C	
	l. Separation distances from the initiating BESS unit to target BESS units	See Attachment C	
	m. The maximum wall surface and target BESS temperatures achieved during the test and the location of the measuring thermocouple;	See Tables 5 and 6	

UL 9540A, Edition 4,			
Clause	Requirement + Test	Result - Remark	Verdict
	n. The maximum ceiling or soffit surface temperatures achieved during the indoor or outdoor wall mounted test and the location of the measuring thermocouple;	See Table 6	
	o) The maximum incident heat flux on target wall surfaces and target BESS units;	See Table 7	
	p) The maximum incident heat flux on target ceiling or soffit surfaces achieved during the indoor or outdoor wall mounted test;	See Table 7	
	q. Flammable gas generation and composition data;	See Attachment G See Tables 7, 8, 9, and 10	
	r. Peak smoke release rate and total smoke release data.	See Table 12 See Attachment G	
	s. Indication of the activation of integral fire protection systems and if activated the time into the test at which activation occurred;	Table 13	
	t. Observation(s) of flying debris or explosive discharge of gases;	See Table 15	
	u. Observation of re-ignition(s) from thermal runaway events	See Table 16	
	v. Observation(s) of sparks, electrical arcs, or other electrical events;	See Table 15	
	w. Observations of the damage to: 1) The initiating BESS unit; 2) Target BESS units; 3) Adjacent walls, ceilings, or soffits;	See Table 16	
	x. Video of the test.	Provided to the client	
9.8	**Performance at Unit level testing**		F
9.8.1	Installation level testing in Section 10 was not required if the following performance conditions outlined in Table 9.1 are met during the unit level test.		
	Non-Residential Installations – Indoor floor mounted:		
	a) Flaming outside the initiating BESS unit is not observed;	Flaming outside the initiating BESS unit was observed;	F
	b) Surface temperatures of modules within target BESS units do not exceed the cell venting temperature;	The maximum temperature on the surface of modules within target BESS units was 800°C and the vent temperature at the cell level was 159°C	F

UL 9540A, Edition 4,			
Clause	Requirement + Test	Result - Remark	Verdict
	c) For BESS units intended for installation in locations with combustible constructions, surface temperature measurements on wall surfaces do not exceed 97°C (175°F) rise above ambient;	The maximum surface temperature measurements on wall surfaces was 820°C	F
	d) Explosion hazards are not observed, including deflagration, detonation or accumulation (to within the flammability limits in an amount that can cause a deflagration) of battery vent gases; and		P
	e) Heat flux in the center of the accessible means of egress did not exceed 1.3 kW/m^2.	Heat flux in the center of the accessible means of egress was 26kW/m^2	F
	Non-Residential Installations – Outdoor ground mounted: a) If flaming outside of the unit is observed, separation distances to exposures were determined by greatest flame extension observed during test. b) Surface temperatures of modules within target BESS units do not exceed the cell venting temperature; c) For BESS units intended for installation in locations near combustible construction, surface temperature measurements on wall surfaces do not exceed 97°C (175°F) rise above ambient; d) Explosion hazards are not observed, including deflagration, detonation or accumulation (to within the flammability limits in an amount that can cause a deflagration) of battery vent gases; and e) Heat flux in the center of the accessible means of egress did not exceed 1.3 kW/m^2.		N/A

UL 9540A, Edition 4,			
Clause	Requirement + Test	Result - Remark	Verdict
	Non-Residential Installations – Indoor Wall Mounted: a) Flaming outside the initiating BESS unit is not observed; b) Surface temperatures of modules within target BESS units do not exceed the cell venting temperature; c) For BESS units intended for installation in locations with combustible constructions, surface temperature measurements on wall surfaces do not exceed 97°C (175°F) rise above ambient; d) Explosion hazards are not observed, including deflagration, detonation or accumulation (to within the flammability limits in an amount that can cause a deflagration) of battery vent gases; and e) Heat flux in the center of the accessible means of egress did not exceed 1.3 kW/m^2.		N/A
	Non-Residential Installations – Outdoor Wall Mounted: a) Flaming outside the initiating BESS unit is not observed; b) Surface temperatures of modules within target BESS units do not exceed the cell venting temperature; c) For BESS units intended for installation in locations with combustible constructions, surface temperature measurements on wall surfaces do not exceed 97°C (175°F) rise above ambient; d) Explosion hazards are not observed, including deflagration, detonation or accumulation (to within the flammability limits in an amount that can cause a deflagration) of battery vent gases; and e) Heat flux in the center of the accessible means of egress did not exceed 1.3 kW/m^2.		N/A

UL 9540A, Edition 4,			
Clause	Requirement + Test	Result - Remark	Verdict
	Non-Residential Installations – Rooftop and Open Garages: a) If flaming outside of the unit is observed, separation distances to exposures were determined by greatest flame extension observed during test. b) Surface temperatures of modules within target BESS units do not exceed the cell venting temperature; c) For BESS units intended for installation in locations near combustible construction, surface temperature measurements on wall surfaces do not exceed 97°C (175°F) rise above ambient; d) Explosion hazards are not observed, including deflagration, detonation or accumulation (to within the flammability limits in an amount that can cause a deflagration) of battery vent gases; and e) Heat flux in the center of the accessible means of egress did not exceed 1.3 kW/m^2.		N/A
	Residential Installations – Indoor floor mounted: a) Flaming outside the initiating BESS unit is not observed as demonstrated by no flaming or charring of the cheesecloth indicator; b) Surface temperatures of modules within the target BESS units adjacent to the initiating BESS unit do not exceed cell venting temperature; c) BESS units intended for installation in locations with combustible construction, surface temperature measurements on wall surfaces do not exceed 97°C (175°F) of temperature rise above ambient; d) Explosion hazards are not observed, including deflagration, detonation or accumulation (to within the flammability limits in an amount that can cause a deflagration) of battery vent gases; and e) The concentration of flammable gas does not exceed 25% LFL in air for the smallest specified room installation size.		N/A

UL 9540A, Edition 4,			
Clause	Requirement + Test	Result - Remark	Verdict
	Residential Installations – Outdoor ground mounted: a) If flaming outside the unit is observed, separation distances to exposures shall be determined by greatest flame extension observed during test. b) Surface temperatures of modules within the target BESS units adjacent to the initiating BESS unit do not exceed the cell venting temperature; c) BESS units intended for near exposures, surface temperature measurements on wall surfaces do not exceed 97°C (175°F) of temperature rise above ambient; d) Explosion hazards are not observed, including deflagration, detonation or accumulation (to within the flammability limits in an amount that can cause a deflagration) of battery vent gases; and e) Heat flux in the center of the accessible means of egress2) shall not exceed 1.3 kW/m^2.		N/A
	Residential Installations – Indoor Wall Mounted: a) Flaming outside the initiating BESS unit is not observed as demonstrated by no flaming or charring of the cheesecloth indicator; b) Surface temperatures of modules within the target BESS units adjacent to the initiating BESS unit do not exceed cell venting temperature; c) BESS units intended for installation in locations near combustible construction, surface temperature measurements on wall surfaces do not exceed 97°C (175°F) rise above ambient; d) Explosion hazards are not observed, including deflagration, detonation or accumulation (to within the flammability limits in an amount that can cause a deflagration) of battery vent gases; and e) The concentration of flammable gas does not exceed 25% LFL in air for the smallest specified room installation size.		N/A

UL 9540A, Edition 4,			
Clause	Requirement + Test	Result - Remark	Verdict
	Residential Installations – Outdoor Wall Mounted: a) Flaming outside the initiating BESS unit is not observed; b) Surface temperatures of modules within target BESS units do not exceed the cell venting temperature; c) For BESS units intended for installation in locations with combustible constructions, surface temperature measurements on wall surfaces do not exceed 97°C (175°F) rise above ambient; d) Explosion hazards are not observed, including deflagration, detonation or accumulation (to within the flammability limits in an amount that can cause a deflagration) of battery vent gases; and		N/A

TEST RESULT TABLES:

Table 1 – Specified Module charging and discharging parameters			
Charging:		**Discharging:**	
Current (CC), A	58.5	Current (CC), A	58.5
Max Charge Voltage (CV), Vdc	75.6	End of discharge voltage, Vdc	60
End of charge current, A	24	Discharging Test Ambient, °C	25
Refer to Attachment A for charge/discharge profiles.			

Table 2 - Test Initiation Details	
Test Date	2020-05-14
Test Start Time (HH:MM:SS)	11:24 AM
Initial Lab Temperature, °C	19°C
Initial Relative Humidity % RH	50 ± 25%
Module OCV at Start of Test, Vdc	75.0

UL 9540A, Edition 4,			
Clause	Requirement + Test	Result - Remark	Verdict

Table 3 – Approximate time of thermal runaway propagation through module						
Initiating Cell(s) Numbers	5	1	4	2	6	7
Thermal Runaway Time (HH:MM:SS)	0:24:30	0:30:34	0:30:54	0:31:13	0:41:48	0:50:03

UL 9540A, Edition 4,			
Clause	Requirement + Test	Result - Remark	Verdict

Table 4 – Test overview timeline		
Time (HH:MM:SS)	**Event**	**Description**
00:00:00	Test Start	Heater energized for cell.
00:24:30	Thermal runaway of initiating cell	Cell at 111°C, gas venting observed from front vent.
00:24:30-00:57:49	Propagation through initiating module	Propagation through initiating module, observed through cell temperatures, gas release.
00:35:00	Ignition of vent gases	Ignition observed in vent gases in the vicinity of the initiating module.
00:40:00	Propagation to Module 9	Propagation to target Module 9 in the initiating rack.
00:40:30	Propagation to Module 8	Propagation to target Module 8 in the initiating rack.
00:41:45	Propagation to Module 7	Propagation to target Module 7 in the initiating rack.
00:42:00	Propagation to Module 6	Propagation to target Module 6 in the initiating rack.
00:42:05	Ignition of gas cloud	Ignition of battery gas plume.
00:48:00	Propagation to Module 4	Propagation to live Module 4 in the initiating rack.
00:55:45	Propagation to Module 1	Propagation to target Module 1 in the initiating rack.
00:58:30	Propagation to Module 5	Propagation to live Module 5 in the initiating rack.
1:04:15	Propagation to Module 2	Propagation to live Module 2 in the initiating rack.
1:43:00	Test termination	Manual suppression of fire with water. Data collection stopped.

UL 9540A, Edition 4,			
Clause	Requirement + Test	Result - Remark	Verdict

Table 5 - Maximum Temperatures in Target Units					
Cell vent temperature from cell test data, °C				98°C	
Target Unit 1		**Target Unit 2**		**Target Unit 3**	
Module Location No.	Temper-ature (°C)	Module Location No.	Temper-ature (°C)	Module Location No.	Temper-ature (°C)
Module 1	437	Module 1	346	Module 1	151
Module 2	603	Module 2	513	Module 2	218
Module 3	645	Module 3	808	Module 3	211
Module 4	800	Module 4	690	Module 4	281
Module 5	789	Module 5	742	Module 5	312
Module 6	455	Module 6	801	Module 6	301
Module 7	179	Module 7	780	Module 7	300
Module 8	156	Module 8	787	Module 8	300
Module 9	148	Module 9	785	Module 9	300

Table 6 - Maximum Temperatures on Instrumented Wall					
Ambient Temperature: 19 °C					
UL 9540A performance criteria, Ambient + 97°C: 116 °C					
Height , mm	Maximum Temperature (°C)	Height, mm	Maximum Temperature (°C)	Height	Maximum Temperature (°C)
6 in.	542	54 in.	808	102 in.	523
12 in.	469	60 in.	796	108 in.	784
18 in.	792	66 in.	804	114 in.	761
24 in.	760	72 in.	756	120 in.	761
30 in.	750	78 in.	748	126 in.	813
36 in.	813	84 in.	740	132 in.	818
42 in.	820	90 in.	738	138 in.	761
48 in.	755	96 in.	754	-	-
Note: Temperatures are measured constantly and then averaged every 60-seconds					

UL 9540A, Edition 4,			
Clause	Requirement + Test	Result - Remark	Verdict

Table 7 – Heat Flux Measurements			
Summary of maximum heat flux in target units		Summary of maximum heat flux measured on instrumented wall	
Maximum Heat Flux, kW/m^2			
Target Module 1.:	24	Heat Flux Gauge No.	kW/m^2
Target Module 2.:	41	1	38
Target Module 3.:	9	2	33
Egress path measurement:	28		

Table 8 – Gases measured and measurement methods used in unit level testing#			
Measurement Method	**Gases Measured**	**Chemical Formula**	**Gas Type**
Flame Ionization Detection (FID) Non-dispersive infrared spectroscopy (NDIR) Solid-state Hydrogen Sensor Fourier-Transform Infrared Spectrometer (FTIR)	Acetylene	C_2H_2	Hydrocarbons
	Ethylene	C_2H_4	Hydrocarbons
	Methane	CH_4	Hydrocarbons
	Methanol	CH_3OH	Hydrocarbons
	Propane	C_3H_8	Hydrocarbons
	Formaldehyde	CH_2O	Hydrocarbons (Aldehydes)
	Hydrogen Bromide	HBr	Hydrogen Halides
	Hydrogen Chloride	HCl	Hydrogen Halides
	Hydrogen Fluoride	HF	Hydrogen Halides
	Carbon Dioxide	CO_2	Carbon Containing
	Carbon Monoxide	CO	Carbon Containing
	Ammonia	NH_3	Nitrogen Containing
	Hydrogen Cyanide	HCN	Nitrogen Containing
	Total Hydrocarbons	-	Hydrocarbons
	Hydrogen	H_2	-
# - This table was modified to reflect the gases measured during testing.			

UL 9540A, Edition 4,			
Clause	Requirement + Test	Result - Remark	Verdict

Table 9 - Gas generation periods	
Time	**Condition**
00:24:30 to 00:34:58	Pre-Flaming
00:34:58 to 01:43:00	Flaming
External Flaming of Gas	
Condition	**Duration (minutes)**
External Flaming of Vent Gases:	68

Table 10 – Summary of battery gas volumes identified during thermal runaway in unit test			
Gas Component	**Gas Type**	**During Pre-flaming (L)**	**During Flaming (L)**
Carbon Dioxide	Carbon Containing	1,000	24,250
Carbon Monoxide	Carbon Containing	1,200	1,250
Ethylene	Hydrocarbons	1,100	875
Methane	Hydrocarbons	1,000	875

Table 11 – Summary of battery gas volumes for deflagration hazard calculations			
Gas Component	**Gas Type**	**During Pre-flaming (L)**	**During Flaming (L)**
Total Hydrocarbons (Propane Equivalent)	Hydrocarbons	1,370	2,450
Carbon Dioxide	Carbon Containing	1,000	24,250
Carbon Monoxide	Carbon Containing	1,200	1,250
Hydrogen	Hydrogen	0	0

Table 12 – Smoke and heat release rate			
Heat Release Rate (HRR)		**Smoke Release Rate (SRR)**	
Peak Chemical HRR (kW)	1170 kW	Maximum SRR (m^2/s)	12
Peak Convective HRR, (kW)	490 kW	Total Smoke Released (m^2)	20

UL 9540A, Edition 4,			
Clause	Requirement + Test	Result - Remark	Verdict

Table 13 – Integral Fire suppression system Details of Operation		
Time of operation of Sprinklers/Suppression System:	Time of Operation Start (HH:MM:SS)	Length of Operation (HH:MM:SS)
Sprinkler No. 1		
Sprinkler No. 2		
Sprinkler No. 3		
Sprinkler No. 4		
Fire Suppression System Operation		

Note : Integral fire suppression system was not employed for the product under test.

Table 14 -Module OCV voltage measurement comparison before and after testing	
Module Location In Rack	OCV Prior to Test (V)
1	75.66
2	75.70
3	75.70
4	75.28
5	75.60
6	75.58
7	75.59
8	75.19
9	75.64

Table 15 – Other Observations during Unit test			
	Observed, Yes/No	Comments/Location	
Flaming outside of Unit	Yes	Length of flame:	Not determined as no flaming was allowed for indoor use.
Flying debris	Yes		
Explosive discharge of gas	Yes		
Sparks or electrical arcs	Yes		

Table 16 - Post Test Observations	
Thermal runaway behavior	
Re-ignitions	No re-ignition
Explosions	No explosion
Other Observations	

UL 9540A, Edition 4,			
Clause	Requirement + Test	Result - Remark	Verdict

	TABLE: Critical components information				
Object / Part No.	**Manufacturer/ trademark**	**Type / model**	**Technical data**	**Standard**	**Mark(s) of conformity[1)]**
Cell	Top Cell Manufacturer	ABC	80Ah, 3.8V	UL1642	UL
Module	Top Cell Manufacturer	XYZ	320Ah, 53.2V	UL1973	UL
Battery Management System (BMS)	Top Cell Manufacturer	UVW	320 V, 355 A, 12 V, 20A	UL 1973. (UL 991, 1998)	UL
Unit Enclosure	UnitE Co.	GHI	SUS304, 4mm thickness	UL1973	UL
Rack Assembly	RakAssy.Ltd	JKL	Carbon Steel	UL50E	UL
Internal Wiring	Wirewire LLC	MNO	18AWG	UL62	UL
Thermal Insulating Materials	TIM Inc	PQR	3mm thickness	UL 746C	UL

List of test equipment used:

A completed list of used test equipment shall be provided in the Test Reports when a Customer's/Third Party Testing Facility has been used.

Clause	Measurement / testing	Testing / measuring equipment / material used, (Equipment ID)	Range used	Last Calibration date	Calibration due date

Note: Testing was done at the UL facility located in 333 Pfingsten Rd Northbrook Illinois, United States of America. Equipment specification and calibration information are maintained on UL's Laboratory Equipment Record System (LERS) database, which is subjected controls in accordance with ISO 17025.

Attachment A: Sample Charging, OCV and SOC Measurement Profiles - (*Pages 29 through 29*)

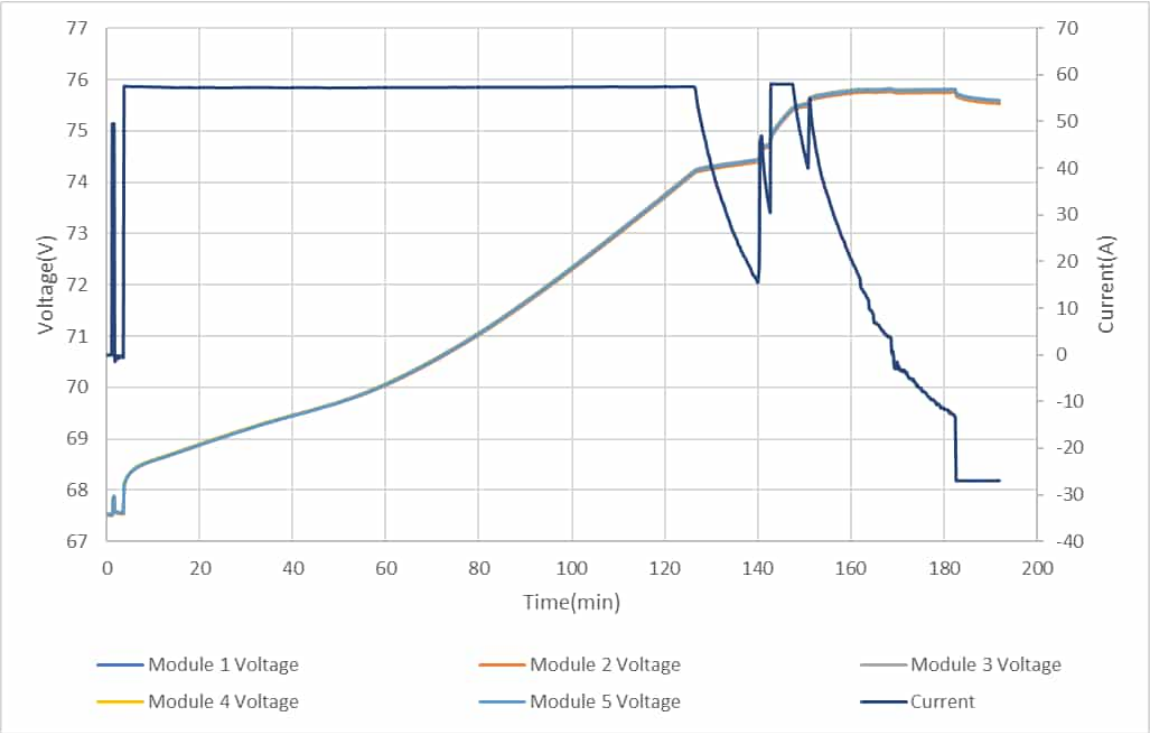


Figure 1 – Plot of module 1 – 6 charge data. Modules connected in series

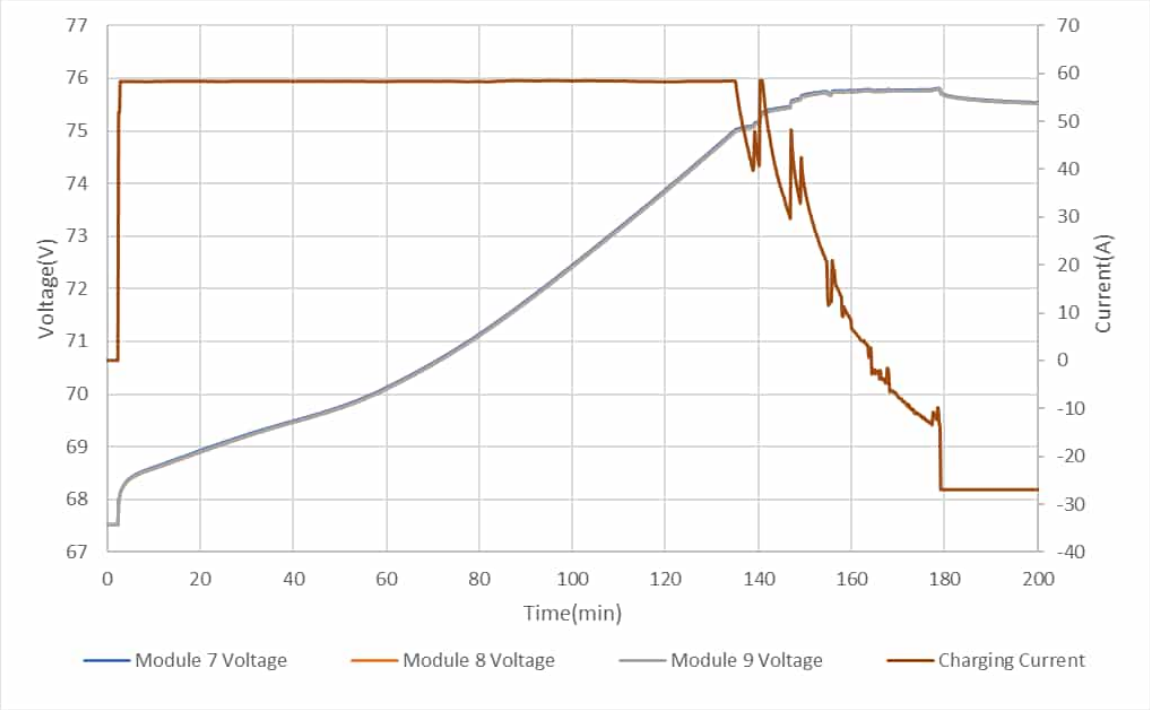


Figure 2 – Plot of module 7 – 9 charge data. Modules connected in series

Attachment B: BESS (including module and any integral fire detection and suppression systems) Construction Photos/Diagrams - (*Pages 30 through 31*)

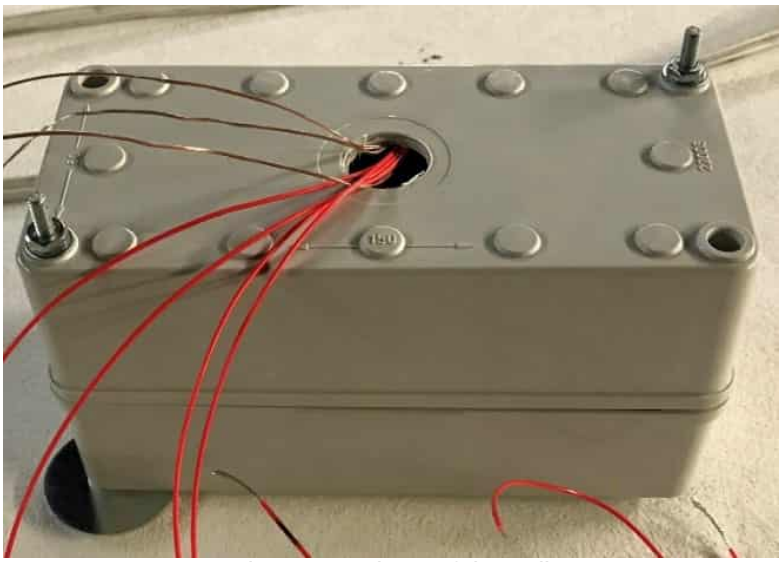


Figure 3 – Photo of the cell



Figure 4 – Photo of the module



Figure 5 – Photo of the unit

Attachment C: : BESS and Equipment Instrumentation and Test Installation Layout Photos/Diagrams - (*Pages 32 through 32*)

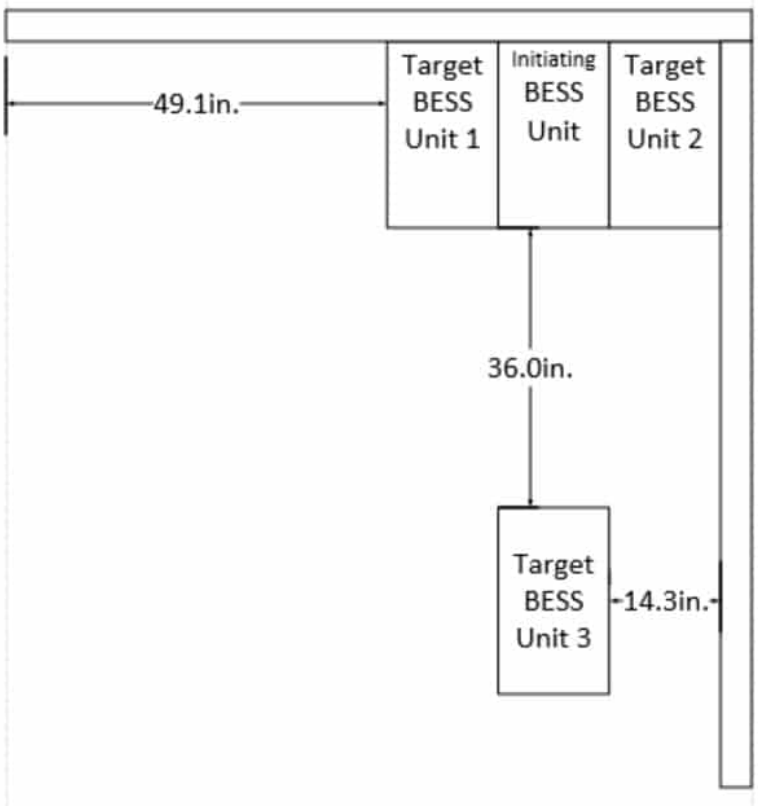


Figure 6 – Test configuration and unit spacing

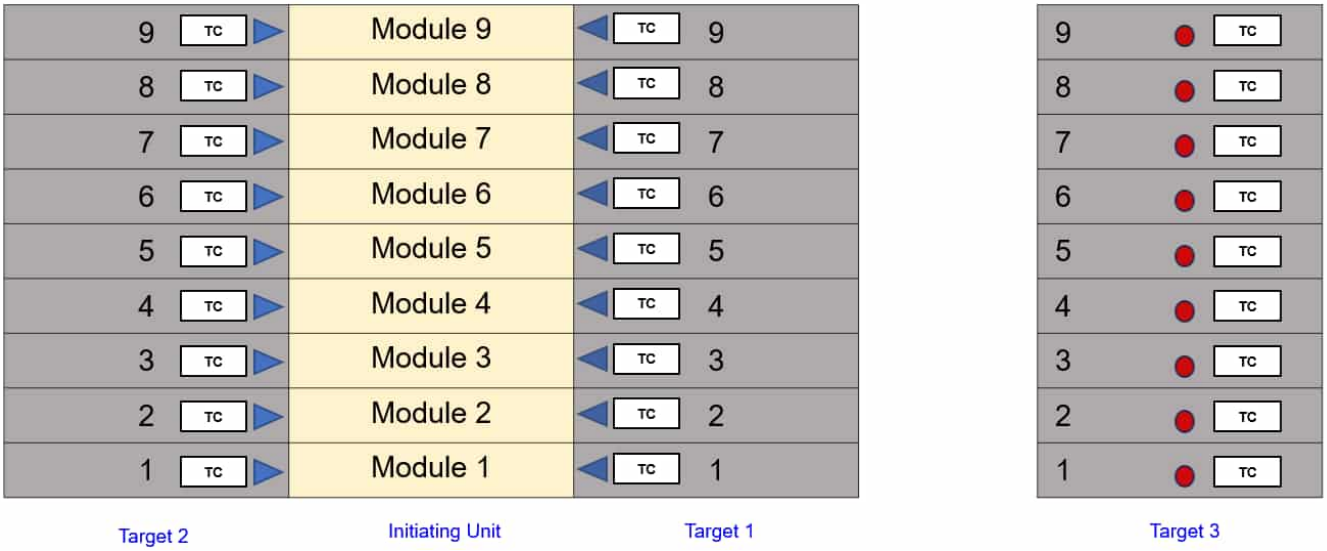


Figure 7 - Equipment Instrumentation

Attachment D: Temperature Profiles and Heat Flux Measurements During Testing (Initiating Cell and Module, Target Modules, Wall Surfaces, etc. - (*Pages 33 through 38*)

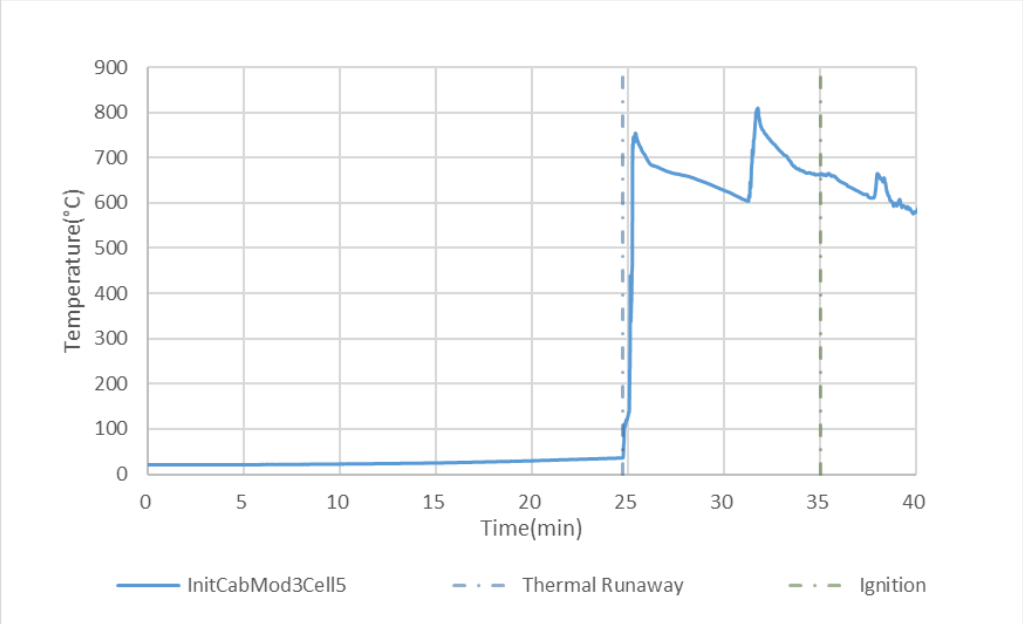


Figure 8 – Surface temperature measured on the initiating cell during the unit level test

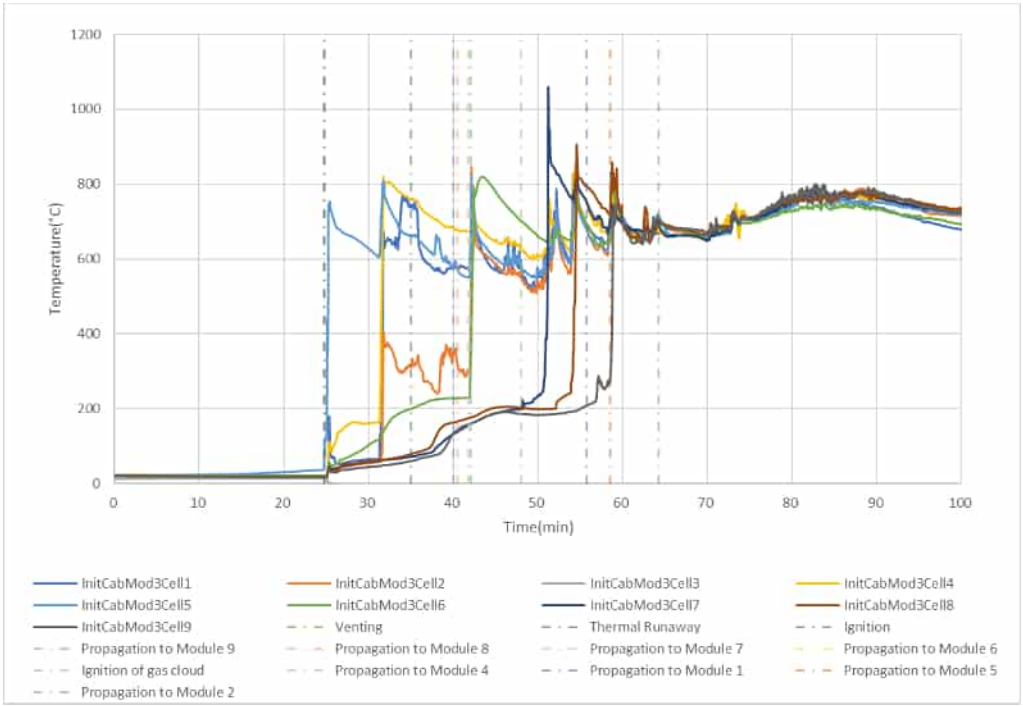


Figure 9 - Temperature measurements in the initiating module describing cell-to-cell propagation

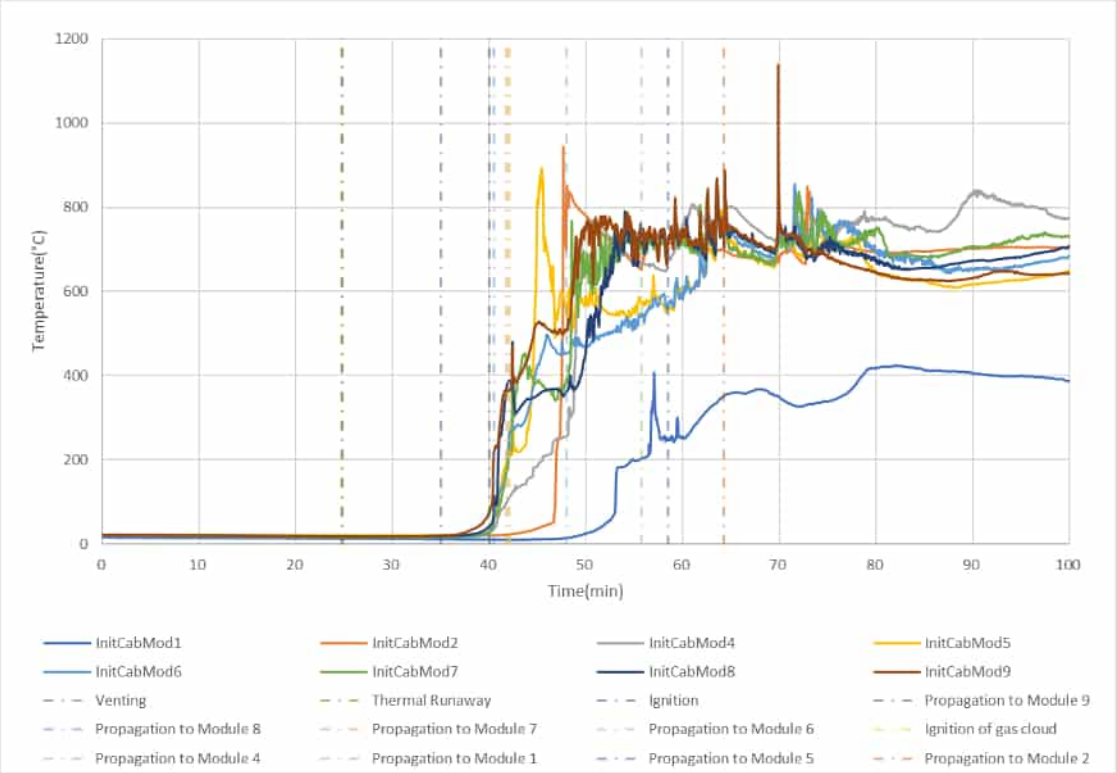


Figure 10 - Temperature measurements in the initiating unit

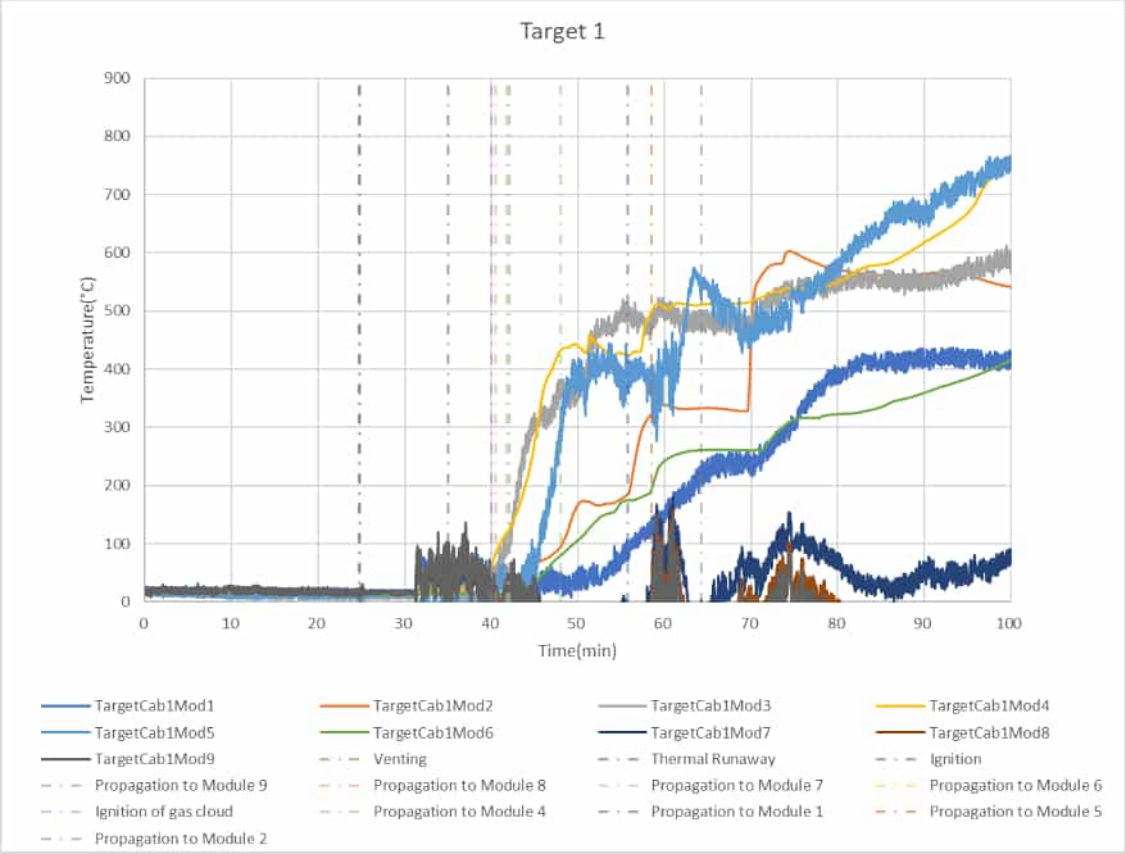


Figure 11 – Target Unit 1 Module temperature

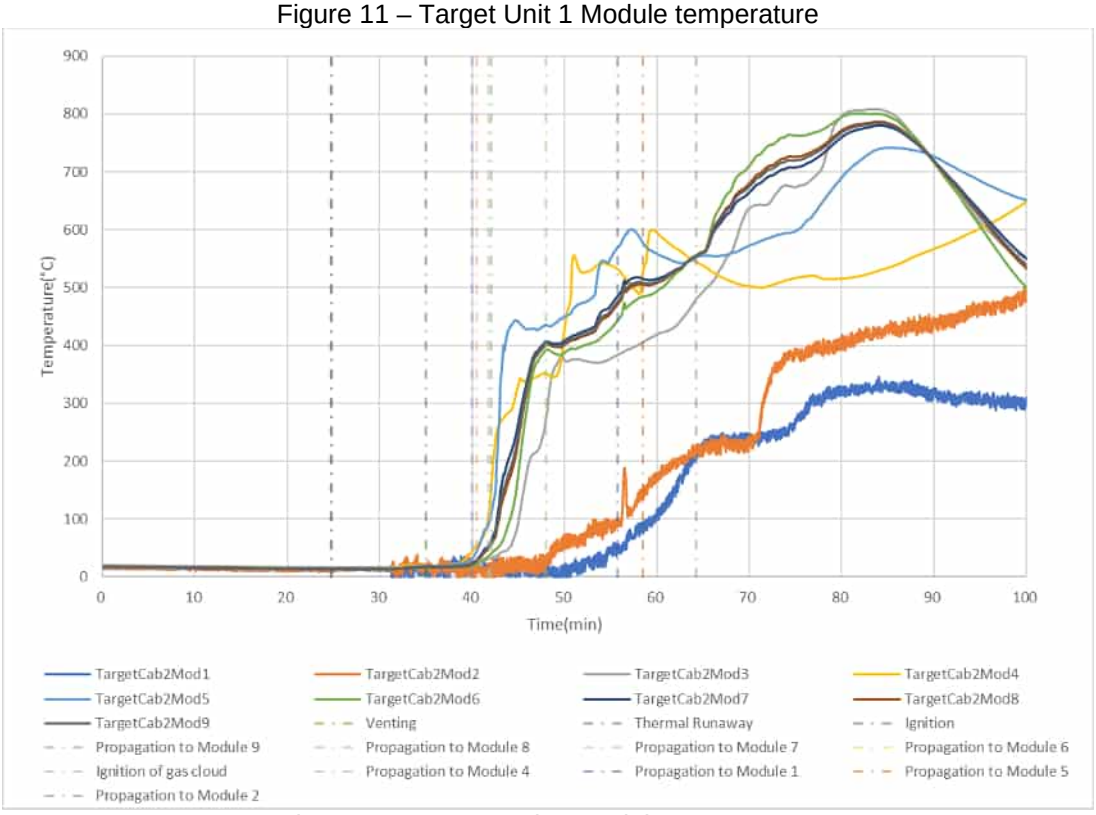


Figure 12 - Target Unit 2 Module temperature

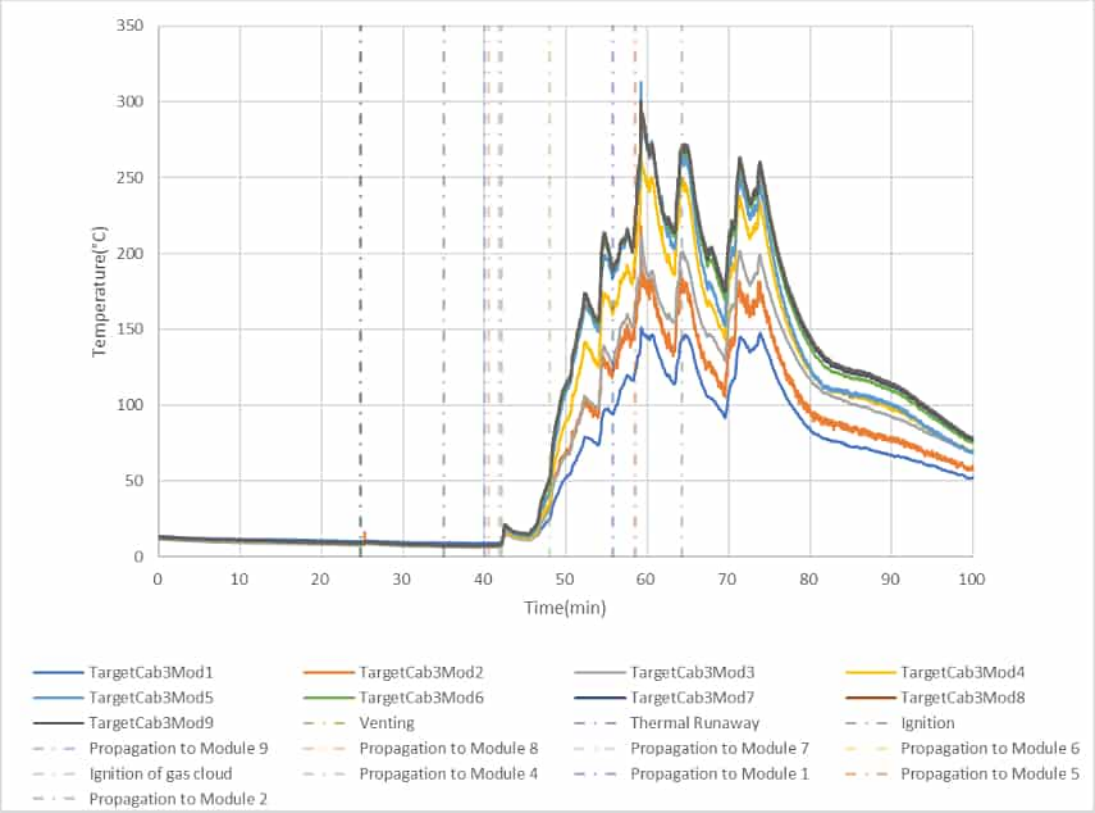


Figure 13 – Target 3 module temperature

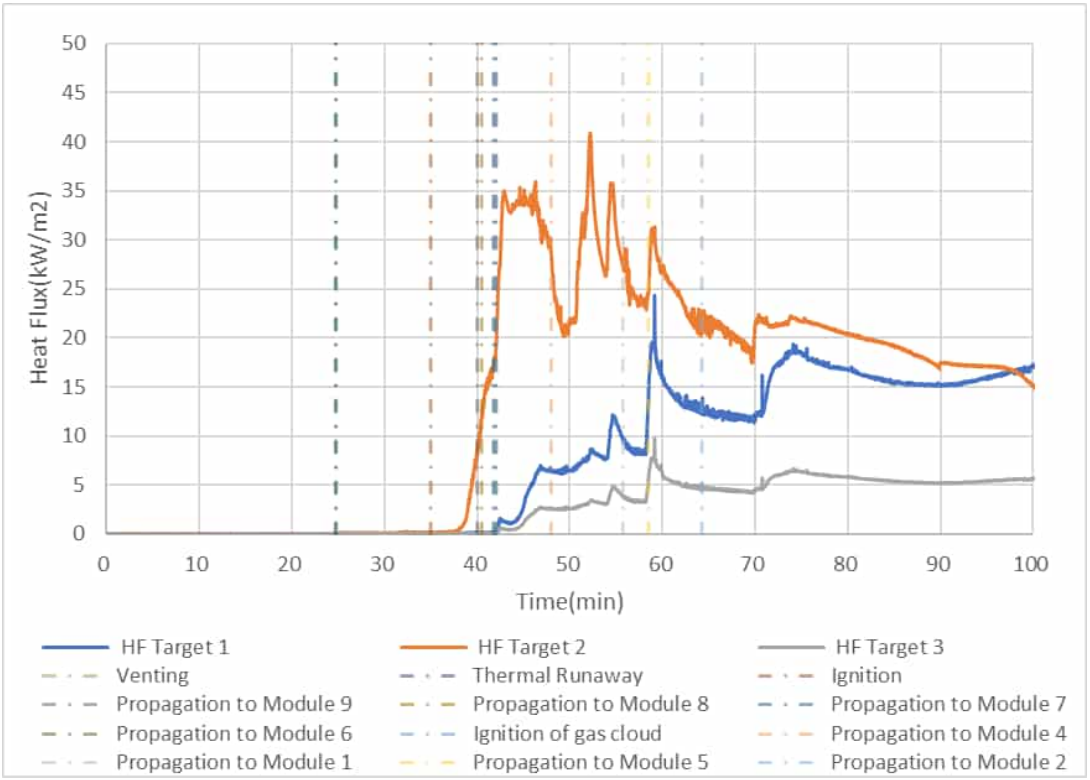


Figure 14 – Heat flux measurements for target units

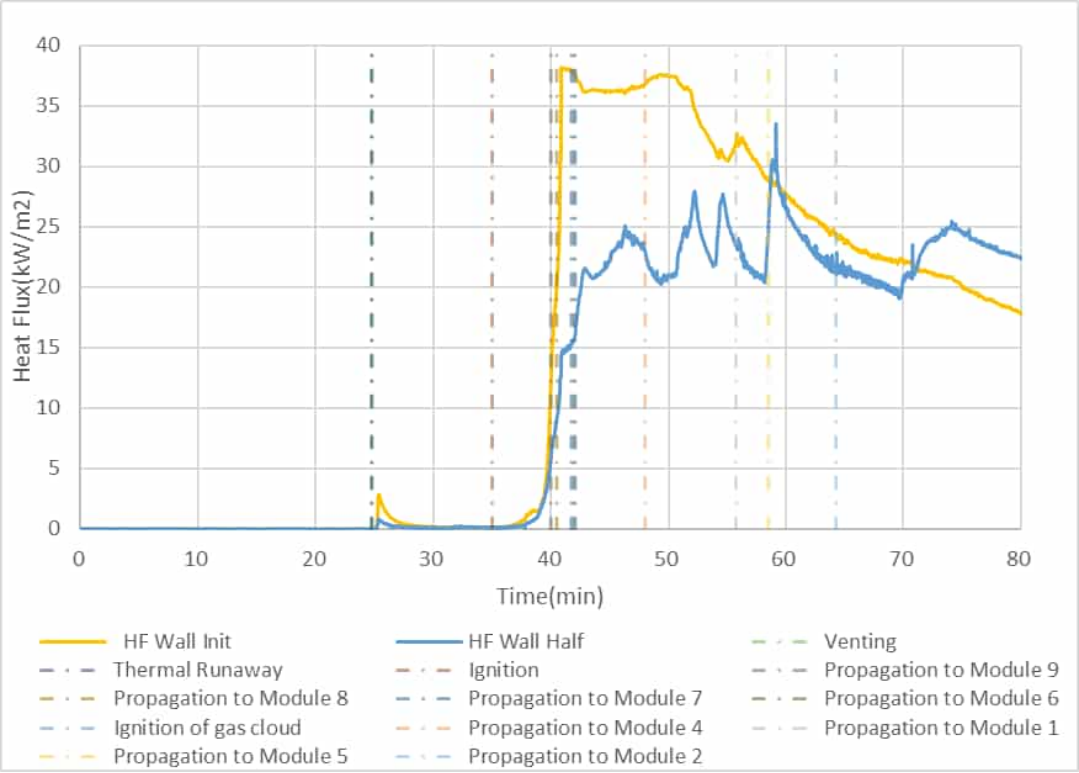


Figure 15 – Heat flux measurements on the instrumented wall

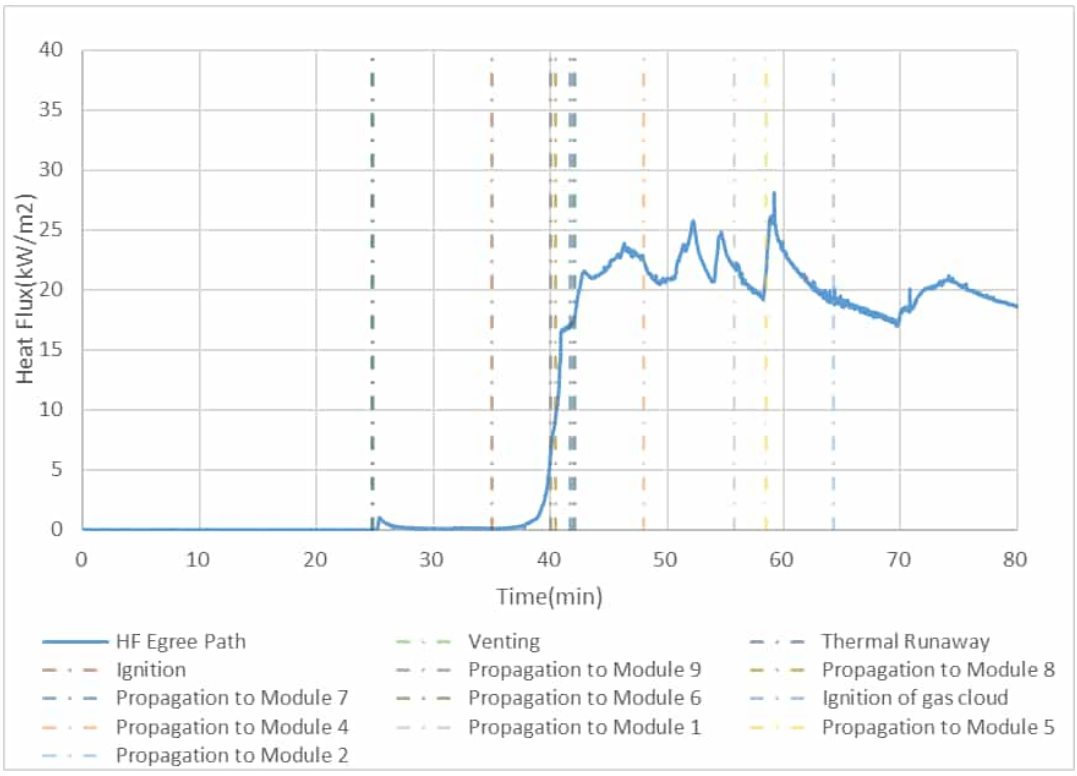


Figure 16 – Heat flux measurements for the egress path

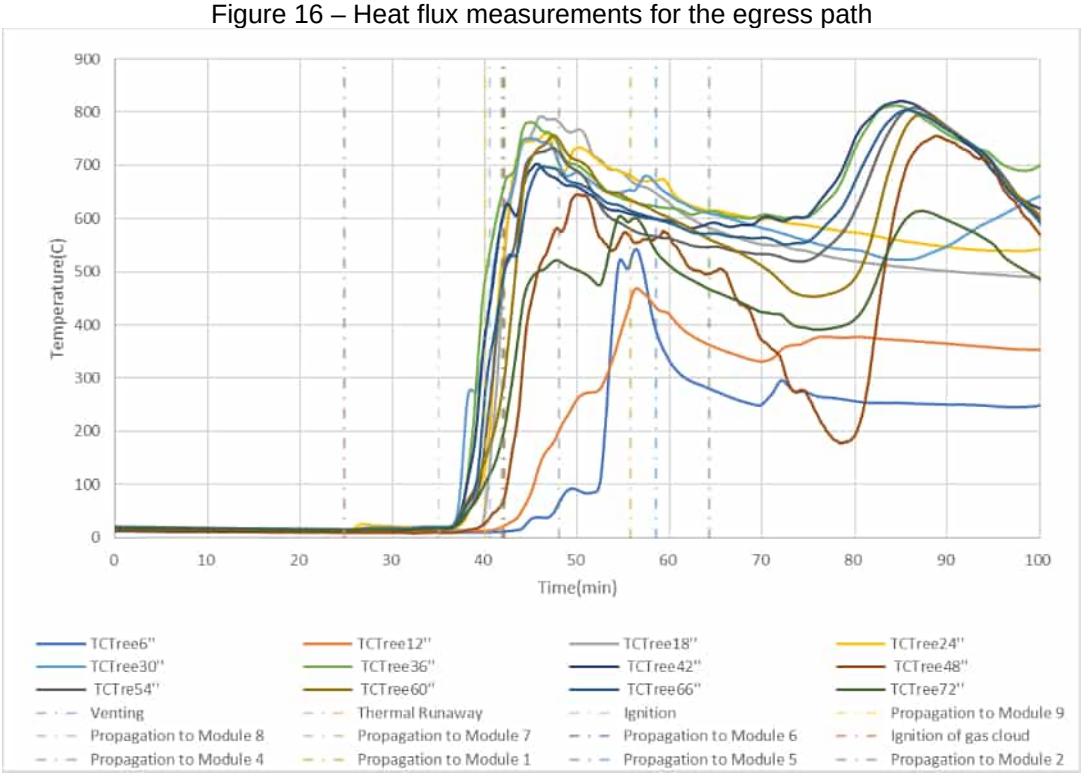


Figure 17 – Temperatures on the target wall, presented with a 60 second running average (6 to 72 inches)

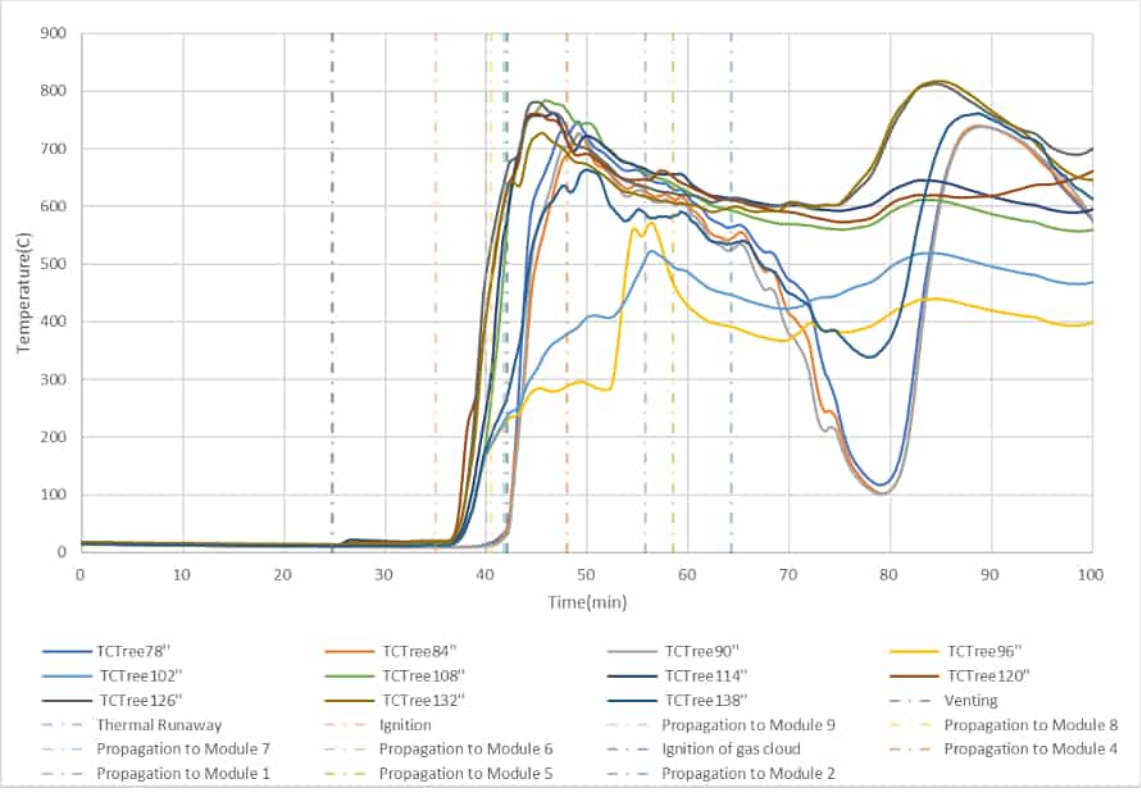
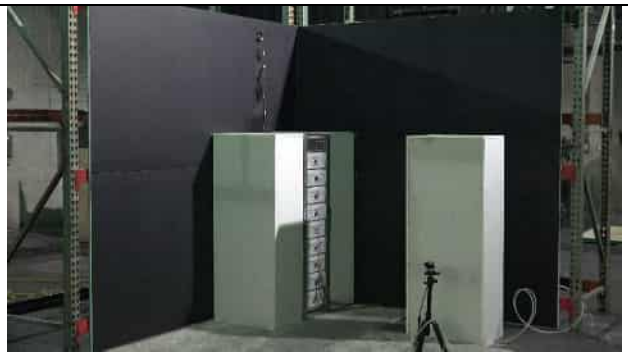


Figure 18 - Temperatures on the target wall, presented with a 60 second running average (78 to 138 inches)

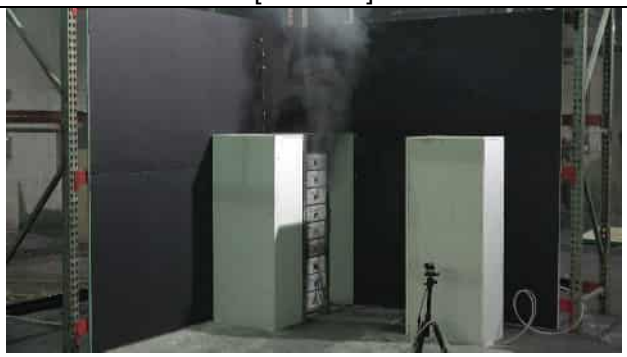
Attachment E: BESS Unit Testing and Post Testing Photos - (*Pages 39 through 41)*



(a) Test start [00:00:00]



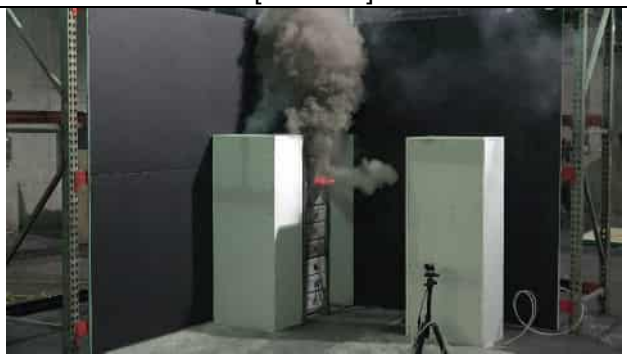
(b) Thermal runaway of initiating cell and propagating through module [00:26:51]



(c) Ignition of Vent gases near module [00:35:00]



(d) Propagation to Module 9 [00:40:00]



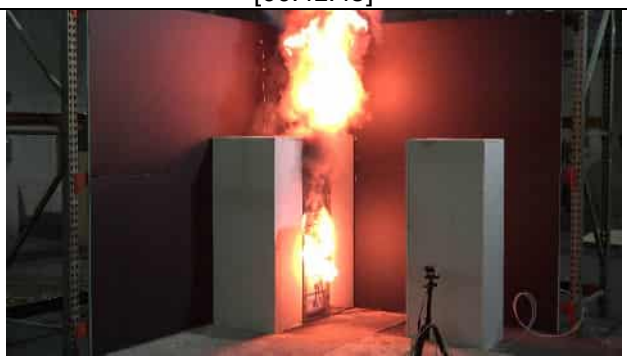
(e) Propagation to Module 8 [00:40:30]



(f) Propagation to Module 7 [00:41:45]



(g) Propagation to Module 6



(h) Ignition of gas cloud

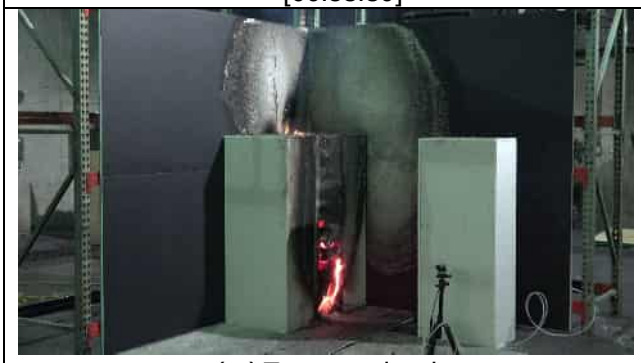
[00:42:00]	[00:42:05]
 (i) Propagation to Module 4 [00:48:00]	 (j) Propagation to Module 1 [00:55:45]
 (k) Propagation to Module 5 [00:58:30]	 (l) Propagation to Module 2 [01:04:15]
 (m) Test termination [01:43:00]	

Figure 19 – Test highlights

		
Target Unit 1	Target Unit 2	Target Unit 3

Figure 20 – Photos of damage to target units after the test



Figure 21 – Condition of instrumented target walls after the test

Attachment F: BESS Unit Test Datasheets - *(Pages 42 through 42)*

☐ Datasheets associated with this project are stored on UL's online project database

Attachment G: BESS Unit Gas Flow Rate and Heat Release and Smoke Release Profiles - (*Pages 43 through 44*)

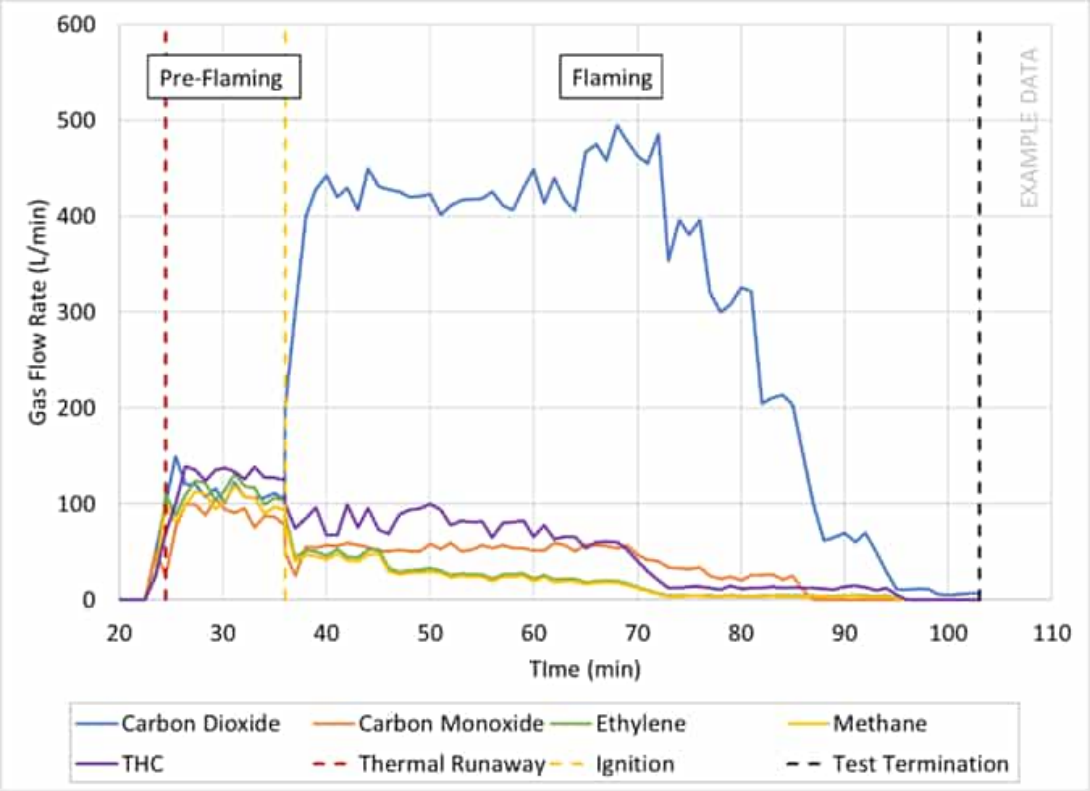


Figure 22 – Volumetric flow rates of gases over the duration of the unit test

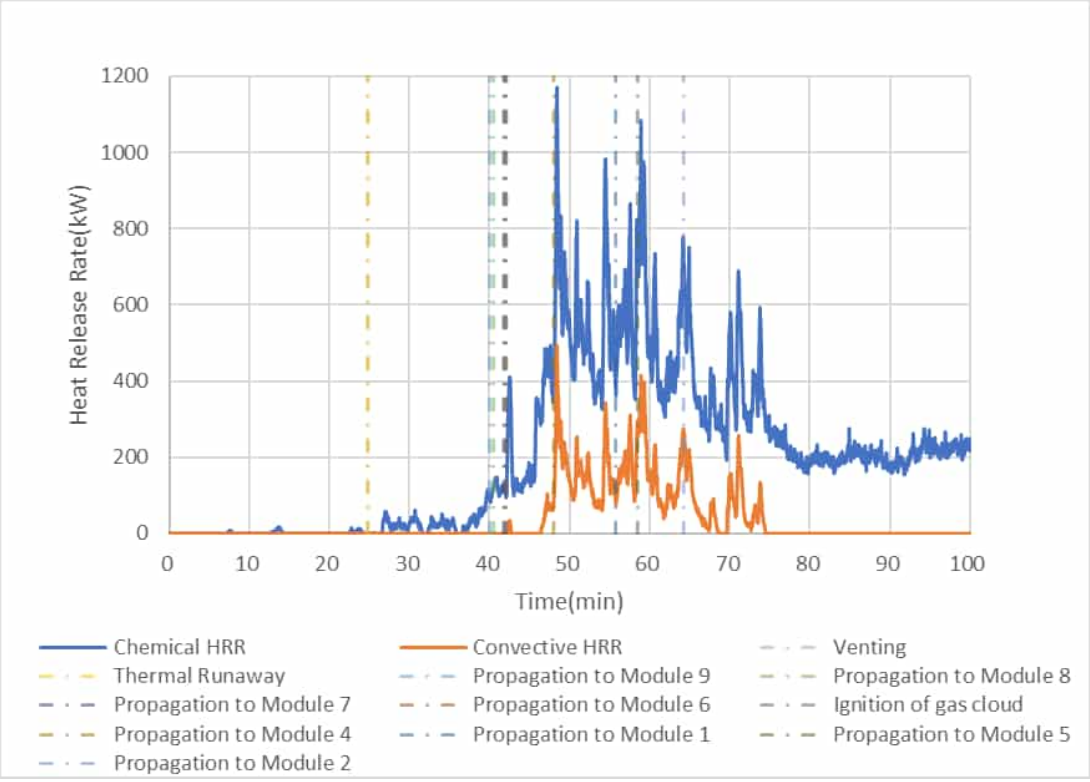


Figure 23 – Chemical and convective heat release rate

UL 9540A Installation Level Research Tests - Safety Considerations for Outdoor Containerized Li-Ion ESS

April 20, 2021 | Adam Barowy
Research Engineer, Fire Research & Development

Energy Storage Systems Safety and Reliability Forum

Empowering Trust®

Copyright 2021 UL Inc. All rights reserved



Agenda

1. Objectives
2. Test Setup
3. Results
4. Key Findings
5. Tactical Considerations
6. Future Test Method R&D

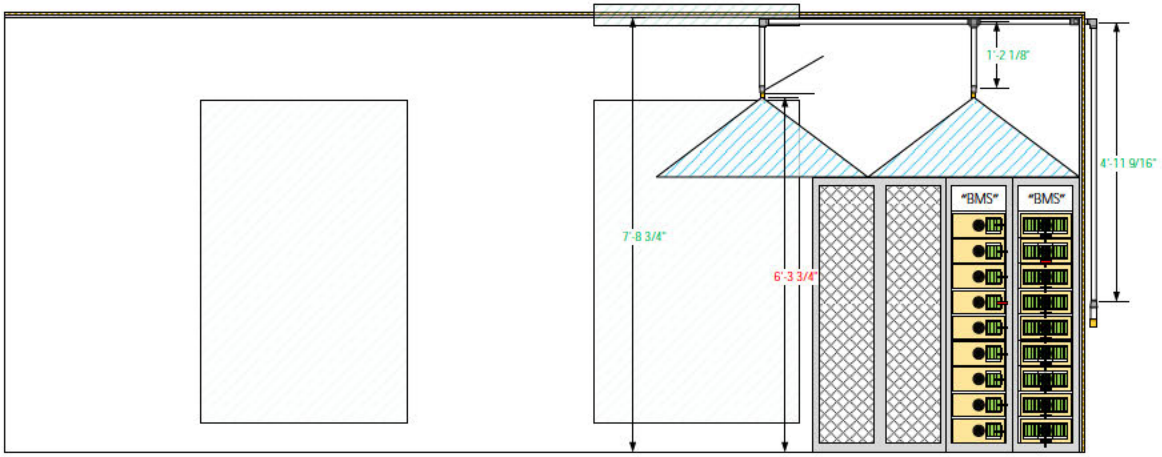
Objectives - UL 9540A Demonstration Series

1. Develop nonproprietary UL 9540A installation test data with representative lithium-ion battery products, with and without active fire protection systems.
2. Develop fire service size-up considerations using typical fire service hazard evaluation equipment under anticipated li-ion ESS thermal runaway use conditions.

Test Setup - Installation Level Test Configurations

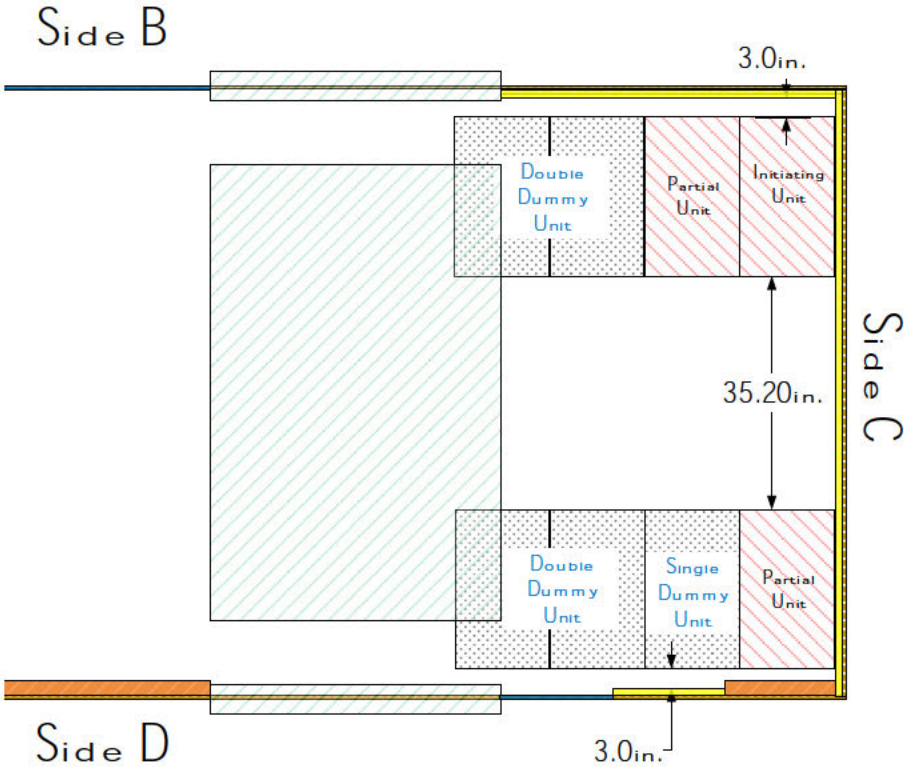
- Test 1 – Without any provision for fire protection.
- Test 2 – With Novec 1230 total flooding clean agent system (8 v% concentration).
- Test 3 – With 0.5 gpm/ft^2 density water spray system (from ceiling).





Operation pressure 0.5 psig; vent area calculation based on NFPA 68, *Standard on Explosion Protection by Deflagration Venting*

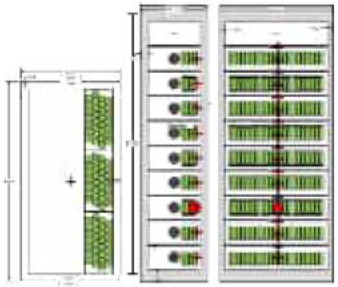
Test Setup – ESS Unit Construction and Spacing



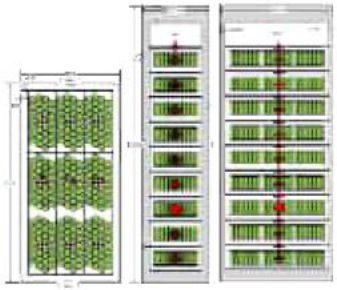
Dimension	Spacing
Aisle	35”
Unit side to wall	0”
Unit rear to wall	3”
Unit to unit	0”

Test Setup – ESS Unit Construction

Left Target Unit
780 qty 18650 cells



Initiating Unit
2,430 qty 18650 cells



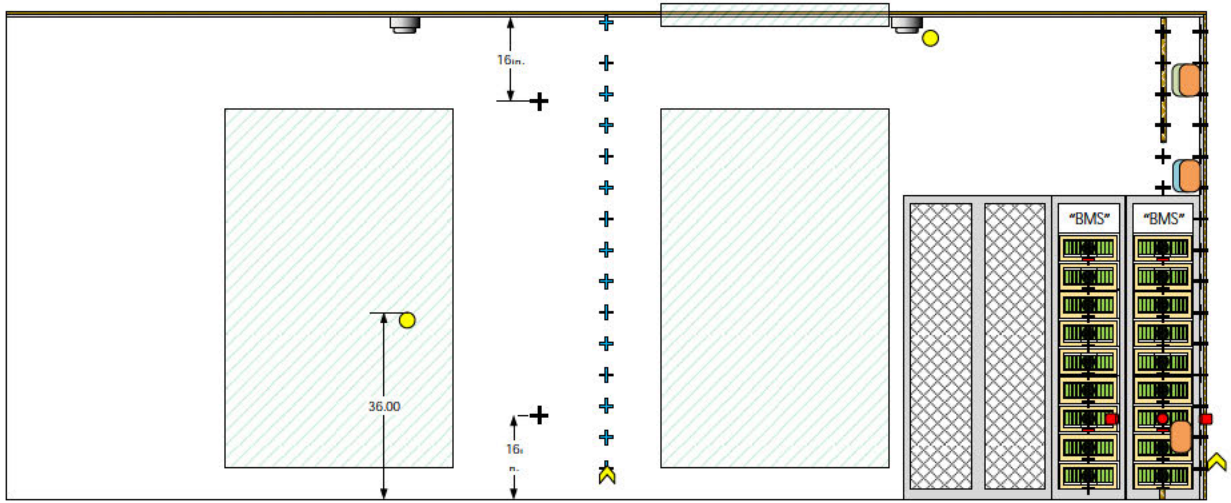
Front Target Unit
780 qty 18650 cells





Test Setup - Instrumentation (Elevation View, Long Axis)

- Pressure Transducers
- Wall Surface Thermocouple
- Gas Temperature Thermocouple
- Battery Temperature Thermocouple
- Vertical Thermocouple Array (in plan view)
- Smoke Detector
- Smoke Obscuration Meter
- Gas Measurement Probe
- Hydrogen Gas Detector
- LEL Gas Detector
- Carbon Monoxide Detector
- Heat Flux Gauge
- Deflagration vent
- Live batteries
- Dummy unit area
- Expanded metal unit door



Test Results

Results - Test 1, Timeline of Major Events



Smoke accumulation
[TR + 00:00:31]



Ignition
[TR + 00:00:31]



TR propagation
for 3 hours
[TR + 00:11:54]



Flaming outside container
[TR + 00:47:18]



Partial volume deflagration
[TR + 00:00:31]

Results - Test 2, Timeline of Major Events



Novec 1230 discharge
[TR + 00:00:58]



Smoke stratification before ignition [TR + 00:26:51]



Ignition [TR + 00:28:32]



Flashover and flaming from open door[TR + 02:09:48]

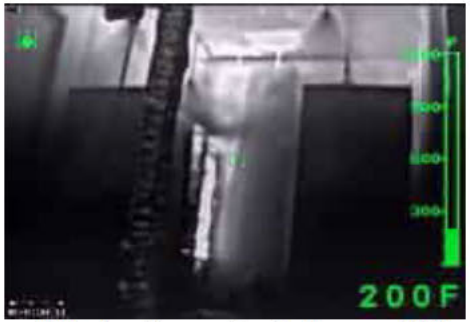


Deflagration
[TR + 00:44:39]

Results - Test 3, Timeline of Major Events



Ignition, sust. flaming
[TR + 00:08:49]



Waterflow @ 0.5 gpm/ft^2
[TR + 00:10:13]



TR propagation after water flow off
[TR + 01:13:05]



TR propagation continues after water flow restart [TR + 01:49:54]



Deflagration
[TR + 00:42:02]

Key Findings



Key Findings – Gas Detection

Common combustible gas/hydrogen detectors:

1) **Effective for detecting that thermal runaway has occurred.**

2) **Not reliable for ongoing hazard assessment.**

Advantages:

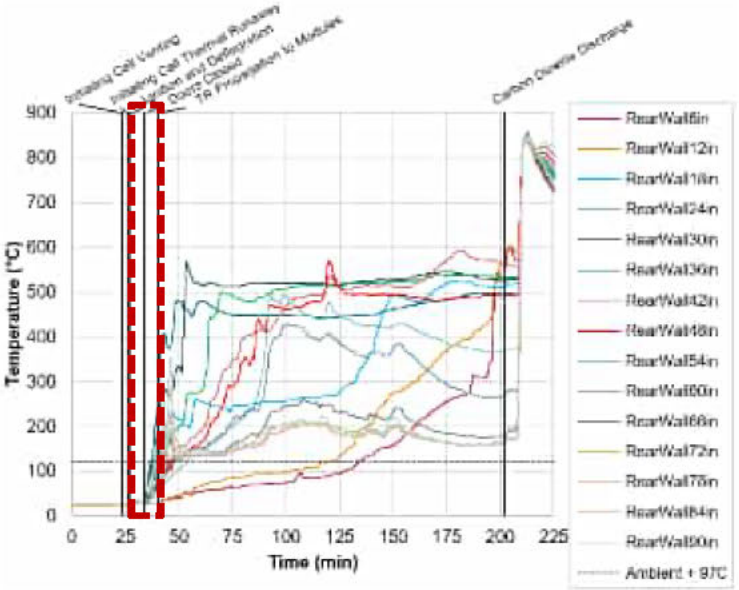
- All detectors responded within seconds when exposed to battery gas.
- Nuisance activation unlikely given measurands (e.g., H_2, CO, LEL).

Limitations:

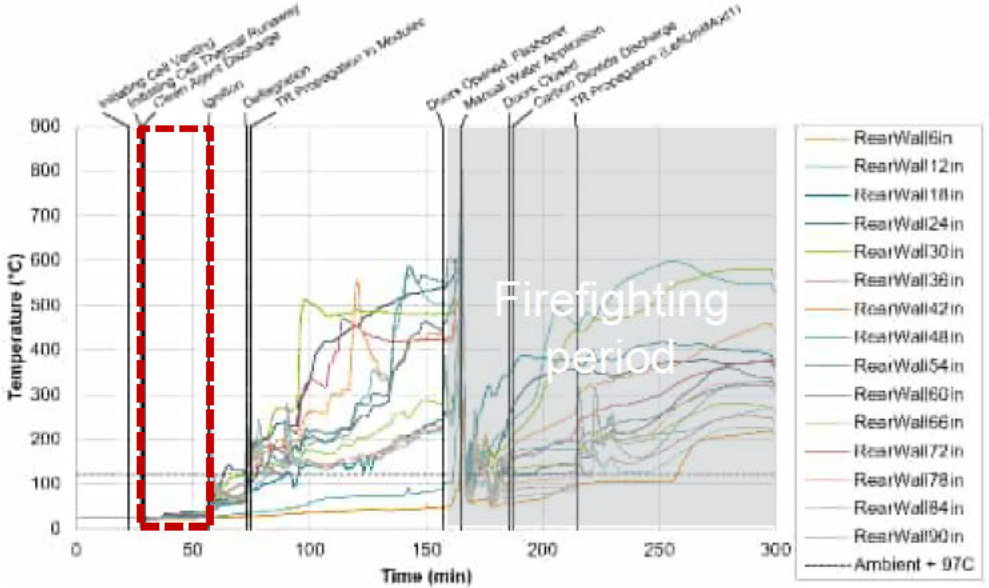
- Detection time dependent on positioning. Positional dependency was not within test scope.
- Cross sensitivity diminishes electrochemical sensor accuracy
- Catalytic bead:
  - Imprecise measurements of flammable gas mixtures,
  - Requires > 10% O_2 for proper operation,
  - "Poisoned" by halogen exposure.

Key Findings – Novec 1230 Total Flooding System

When simulating a total flooding system approach, Novec 1230 did not deliver sufficient cooling to prevent propagation of thermal runaway or to prevent thermal exposure to combustible construction materials.



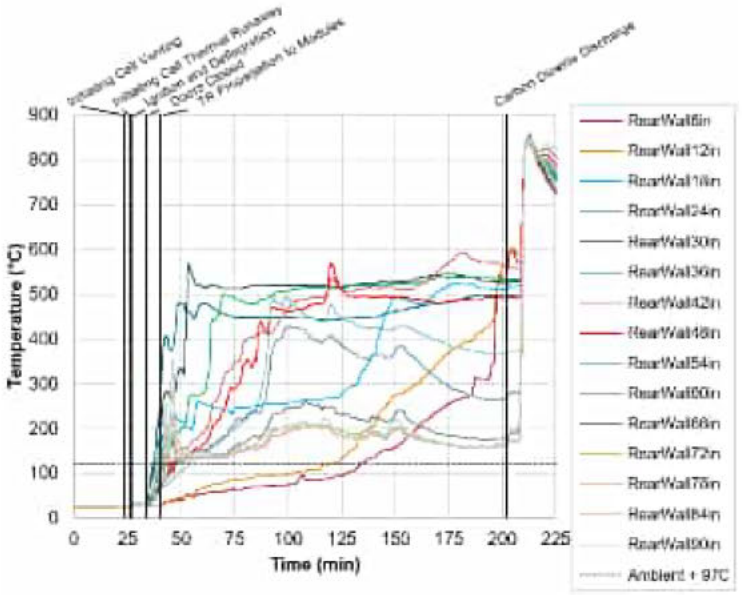
Rear Wall – No Novec 1230



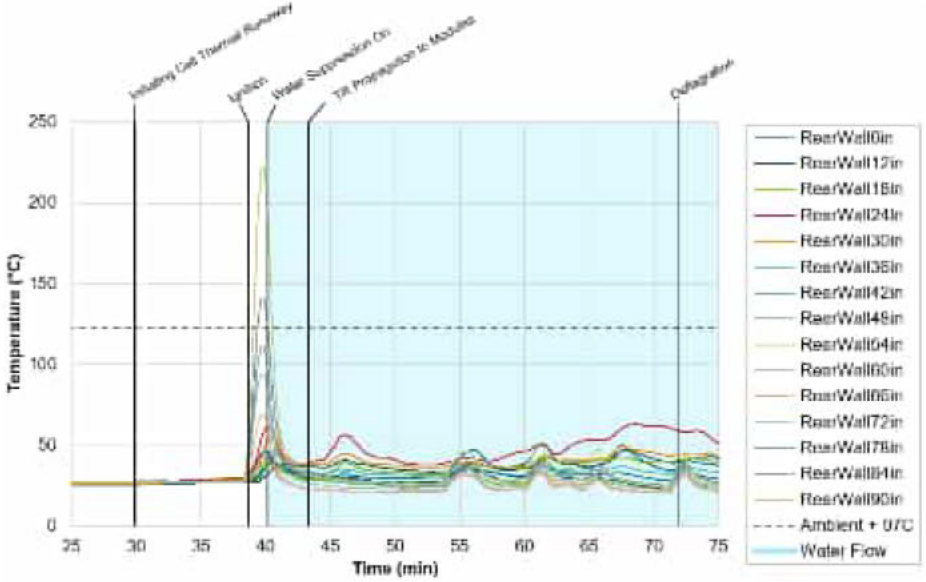
Rear Wall – w/ Novec 1230

Key Findings – Water Spray Suppression System

Ceiling-based water spray suppression system prevented unit-to-unit propagation, cooled surfaces adjacent to initiating ESS unit. Limited effectiveness to prevent module-to-module thermal runaway propagation within initiating unit.



Rear Wall – No Water



Rear Wall – w/ Water

Key Findings – Deflagration Protection System

The generation and accumulation of battery gases created an explosion hazard and was mitigated with an engineered deflagration protection system.



Test 1 - Baseline



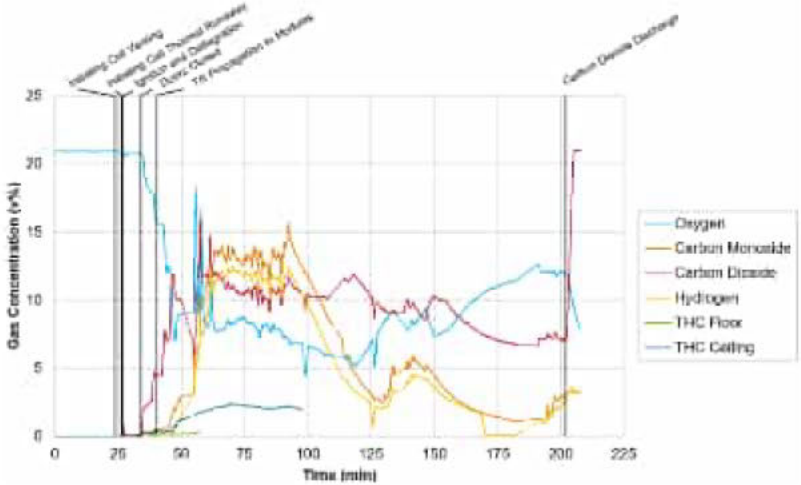
Test 2 – Novec 1230



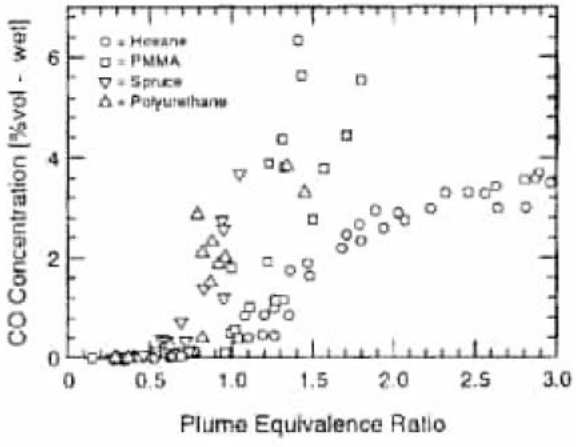
Test 3 – 0.5 gpm/ft^2

Key Findings – Comparison to Room and Content Fires

Propagating thermal runaway events generate more severe flammability and toxicity hazards than typical room and content fires.



- THC: ~3 v%
- H_2: > 10 v%
- CO: 12 v% - 15 v%
- CO_2: ~10%



- H_2 = 0 v%
- CO: ~6 v%
- CO_2: ~10%

Gottuk, D, Beyler, C., Roby, R., Peatross, M., "Carbon Monoxide Production in Compartment Fires", J. of Fire Prot Eng. **4**, 4, 1992

Tactical Considerations



Tactical Consideration – Ventilation

Ventilation of an ESS installation may result in a deflagration or rapid transition to flashover.

UL Tests - Flashover



$\Delta t = 21$ s

Surprise, AZ – Deflagration*



$\Delta t \approx 3$ min

*M. B. McKinnon, S. DeCrane and S. Kerber, "Four Firefighters Injured In Lithium-Ion Battery Energy Storage System Explosion - Arizona," UL Firefighter Safety Research Institute, Columbia, MD, 2020.

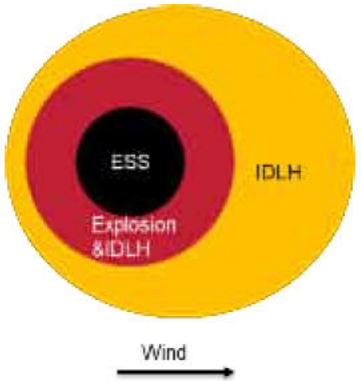
Tactical Considerations

- **Using portable gas meters to evaluate interior conditions or the gases/vapors leaking from an ESS places firefighters in an explosion hazard area.**
- **Portable gas meter measurement of battery gas is likely to be compromised by clogging and cross-sensitivity to battery gas mixture species.**
- **A deflagration event is hard to predict, even with good quality gas concentration data.**
- **Responding firefighters should consider using portable gas meters and visual observations to define an exclusion zone, while wearing full structural PPE (Level D Ensemble) with full SCBA.**
- **Additional tactical considerations and detail available in the full report:**

[redacted]

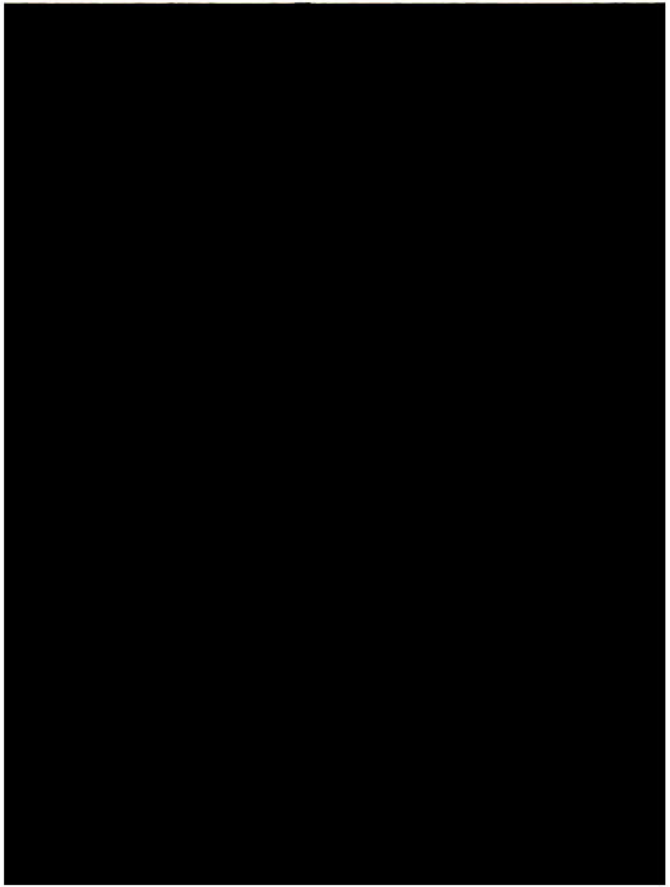
Future Needs:

1. **Better understanding and ID of ESS deflagration precursors are needed for incident size-up.**
2. **Responding firefighters need access to ESS instrumentation data, particularly gas measurement, through a remote monitoring panel and to personnel who can aid in interpretation.**



Enclosure Explosion Safety Test Method Development

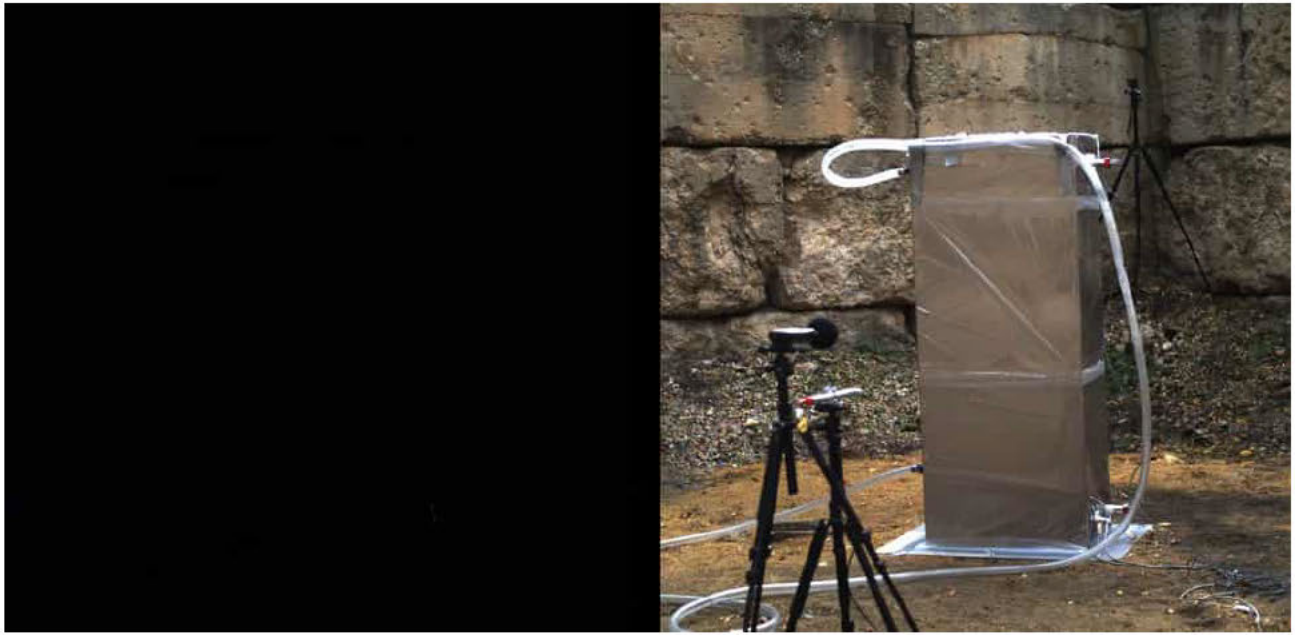
- Test methodology, performance criteria needed to evaluate safety performance of ESS enclosures designed to contain deflagration pressures or control deflagration pressure relief.
- Deflagration venting systems cannot be evaluated unless a deflagration occurs during test.
- Deflagration severity during a UL 9540A test is dependent on gas conditions at the time of ignition.
- Evaluation ESS product explosion hazards should not be conducted by unqualified persons.



Enclosure Explosion Safety Test Method Development

Methodology under development to evaluate explosion hazards:

- ESS enclosure rupture
- Blast waves and projectiles
- Direction of energy release





Thank you for your time. Questions?

Adam Barowy
[redacted]

Annex 12 Tesla BESS system testing information

Table of Contents

EXECUTIVE SUMMARY 9

1 INTRODUCTION 10

2 TEST SETUP 10
2.1 Test Plan 10
2.2 Equipment and Sensors 13
2.3 Test Setup – Outdoor Installation 15
2.4 Sensor Placement 17

3 OBJECTIVES 19

4 RESULTS 20
4.1 Outdoor Installation Test 20
4.1.1 Temperature Data 21
4.1.2 Heat Flux Data 29
4.1.3 Gas Data and Venting Pictures 34

5 CONCLUSION 40

Figures

Figure 2-1 Top view of test layout 10
Figure 2-2 Cartridge heater positions within the initiating module 11
Figure 2-3 Front view of the Powerpack initiator 12
Figure 2-4 Rendering of open Powerpack fully populated with initiator pack thermocouple placement 13
Figure 2-5 Gas analysis setup 14
Figure 2-6 Signal breakout board, NI cDAQ and control laptop 14
Figure 2-7 Wide view of test setup from the south with heat flux gauges 15
Figure 2-8 Tight view of Powerpacks with wall thermocouples 16
Figure 2-9 East wall sensor diagram 16
Figure 2-10 North wall sensor diagram 17
Figure 2-11 Target pack module internal thermocouple setup 17
Figure 2-12 Target pack module external thermocouple setup 18
Figure 2-13 External sensor placement through initiator Powerpack 18
Figure 2-14 Heat flux gauge external setup 19
Figure 4-1 Ceiling temperatures above DUT (fire side) 21
Figure 4-2 North wall, fire side temperatures 21
Figure 4-3 East wall, fire side temperatures 22
Figure 4-4 East wall, back side temperatures 22
Figure 4-5 Fire from DUT on east wall 23
Figure 4-6 North wall, back side temperatures 24
Figure 4-7 Temperatures inside the initiating module in DUT 25
Figure 4-8 Temperatures in the adjacent modules to the initator 25
Figure 4-9 Additional DUT temperatures 26
Figure 4-10 DUT initiator module external temperatures 26
Figure 4-11 Temperatures inside center module of neighbors 27
Figure 4-12 Temperatures on the outside of center module of neighbors 28
Figure 4-13 Temperatures inside the upper module in the neighbors 28
Figure 4-14 Temperatures on the outside of the upper module in the neighbors 29
Figure 4-15 East wall heat flux 30
Figure 4-16 North wall heat flux 30

Figure 4-17 West neighbor heat flux....31
Figure 4-18 Heat fluxes in front of unit at 8 and 10ft....32
Figure 4-19 Heat fluxes in front of unit at 15 and 20ft....32
Figure 4-20 Heat fluxes to side of unit at 4, 8 and 12ft....33
Figure 4-21 Test during peak heat release rate....33
Figure 4-22 LEL during test....34
Figure 4-23 Hydrogen gas concentration during test....34
Figure 4-24 Flammable hydrocarbon gases during test....35
Figure 4-25 Halides and hydrogen cyanide during test....36
Figure 4-26 Benzene and Toluene levels during test....36
Figure 4-27 Several seconds after initial gas venting....37
Figure 4-28 Continued gas production....38
Figure 4-29 Smoke and gas emanating from unit moments before deflagration....39
Figure 4-30 Combustion seconds after the door opening deflagration....39
Figure 4-31 Pressure inside DUT modules....40

List of abbreviations

BESS	Battery energy storage system
CO	Carbon monoxide
CO_2	Carbon dioxide
DAQ	Data acquisition system
DNV GL	DNV GL Energy Insights, LLC
DUT	Device under test
FMEA	Failure mode and effects analysis
FTIR	Fourier transform infrared gas analyzer
IDLH	Immediately dangerous to life and health
IFC	International Fire Code
HCl	Hydrogen chloride
HCN	Hydrogen cyanide
HF	Hydrogen fluoride
LEL	Lower explosive limit
NFPA	National Fire Protection Association
NMC	Nickel manganese cobalt oxide battery
PPE	Personal Protective Equipment
PPM	Parts per million
SCBA	Self-contained breathing apparatus
SME	Subject matter expert
SOP	Standard operating procedure

EXECUTIVE SUMMARY

On October 17th, 2018, DNV GL conducted large scale fire testing for Tesla Inc on their Powerpack energy storage system (ESS). The testing saw four units, one fully populated test pack (16 modules) and three "dummy" packs with only two modules, placed at typical installation spacing, subject to fire originating from within the test pack. To achieve this, multiple cells in the center module of the test pack were sent into thermal runway to ensure a propagating fire. This fire spread through the initial module, creating a fire which ultimately escaped the module. The module burned for a period of time before stopping, likely as a result of consuming its fuel. Following this cessation of combustion, heat transfer ultimately allowed the module fire to eventually propagate to adjacent modules, and ultimately the full pack. Multiple takeaways with respect to fire code requirements were observed, and are listed below:

- Though the test pack was completely consumed, the fire did not propagate to adjacent packs at the test spacing, which was 4" on the sides and 2" to the pack on the back.
- On the other side of the test pack, 18" away, a two-hour fire resistance rated wall saw no breaching. Additionally, no adverse temperatures on the back side of the wall were observed.
- The ceiling, which was comprised of two layers of 5/8" Type-X drywall also saw no breaching.
- Heat flux measurements around the test setup were taken during testing. Heat flux in the egress pathways were observed and are provided with timelines.
- No water or other suppression was applied to the system during testing. The system was allowed to burn itself out completely which resulted in the end of test.

1 INTRODUCTION

Tesla Inc has retained DNV GL to perform large scale fire testing on their modular, large scale energy storage product, the Tesla Powerpack, to satisfy code requirements specified by the 2018 edition of the International Fire Code (IFC) and the 2018 NFPA Fire Code Chapter 52. Chapter 12 of the International Fire Code lays out a number of requirements for energy storage systems in the built environment.

2 TEST SETUP

2.1 Test Plan

The test plan, proposed initially by Tesla and which was the inspiration for UL9540A, is shown as an overview shot below in Figure 2-1. This layout, intended to demonstrate the ability of systems at this spacing to resist pack to pack propagation, was also intended to determine the effectiveness of a two hour rated fire wall to resist the heat and even flame impingement.

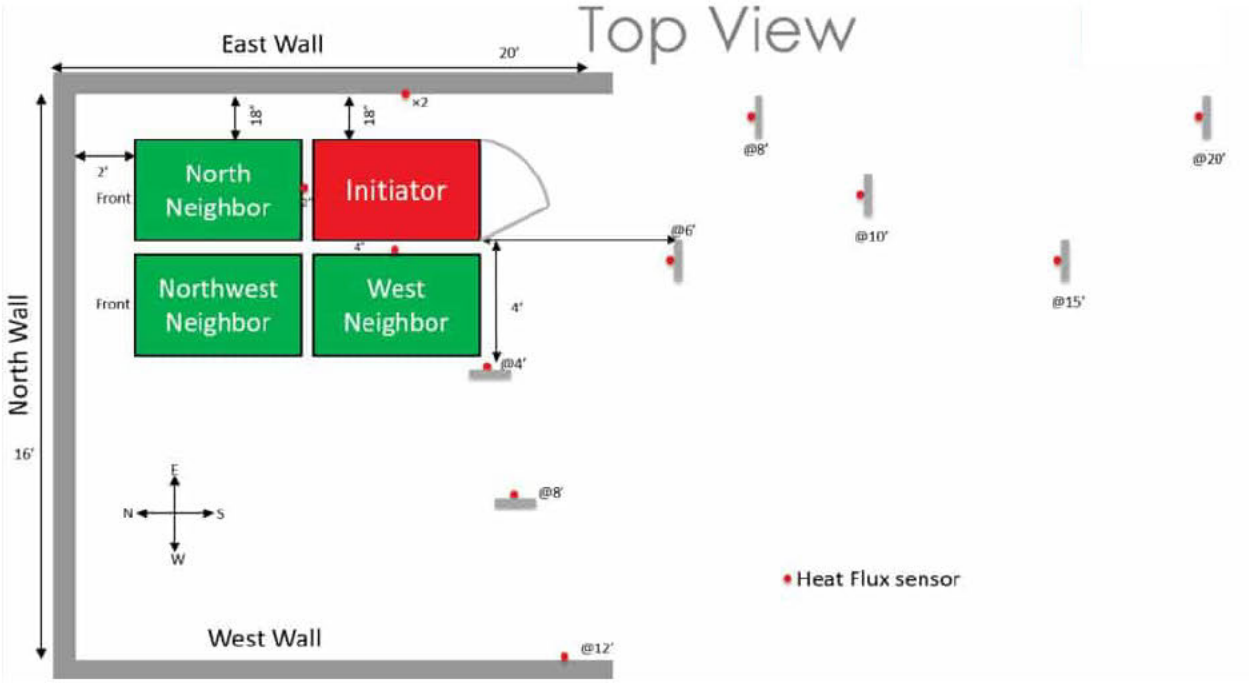


Figure 2-1 Top view of test layout

The initiator unit, shown in red above, is populated completely with 16 modules, the seventh from bottom of which is fitted with a number of cartridge heaters placed amongst the cells which are intended to drive the cells into thermal runaway (Figure 2-2). To ensure a complete failure of the module via cell to cell propagation, Tesla has placed numerous heaters within a grouping of cells with a backup location should the primary location fail to achieve propagation. When the test is performed, these heaters are run in a pre-engineered cycle to increase the likelihood of propagating failure.

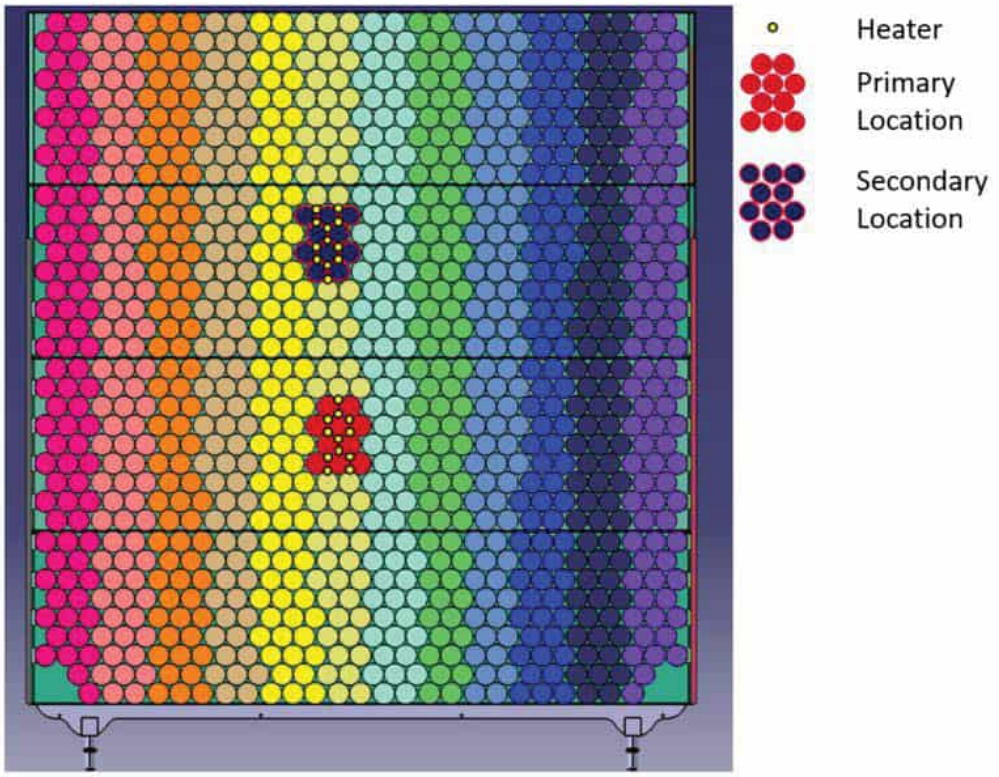


Figure 2-2 Cartridge heater positions within the initiating module

Figure 2-3 shows the front view of the initiator Powerpack for testing. This unit contained a fan and radiator setup on the front door, but it was not operational for testing. Figure 2-4 shows a rendered view of inside the Powerpack with captions describing the placement of the 20 thermocouples inside the initiator unit. The modules are numbered from the bottom with module 7 being the initiating module.

Three target, or dummy, packs were placed around the initiator unit with the intent of assessing internal temperatures within the packs as well as within the modules. Inside the target Powerpacks, only module 7 and 16 are in position, with the remaining space left empty. Temperature inside the packs and modules was observed with the intent of staying below a critical temperature setpoint. Additionally, should even a single cell within one of the target packs go into thermal runway, which would result in the production of smoke from a target exhaust duct, the test would be considered a fail at this spacing.



Figure 2-3 Front view of the Powerpack initiator

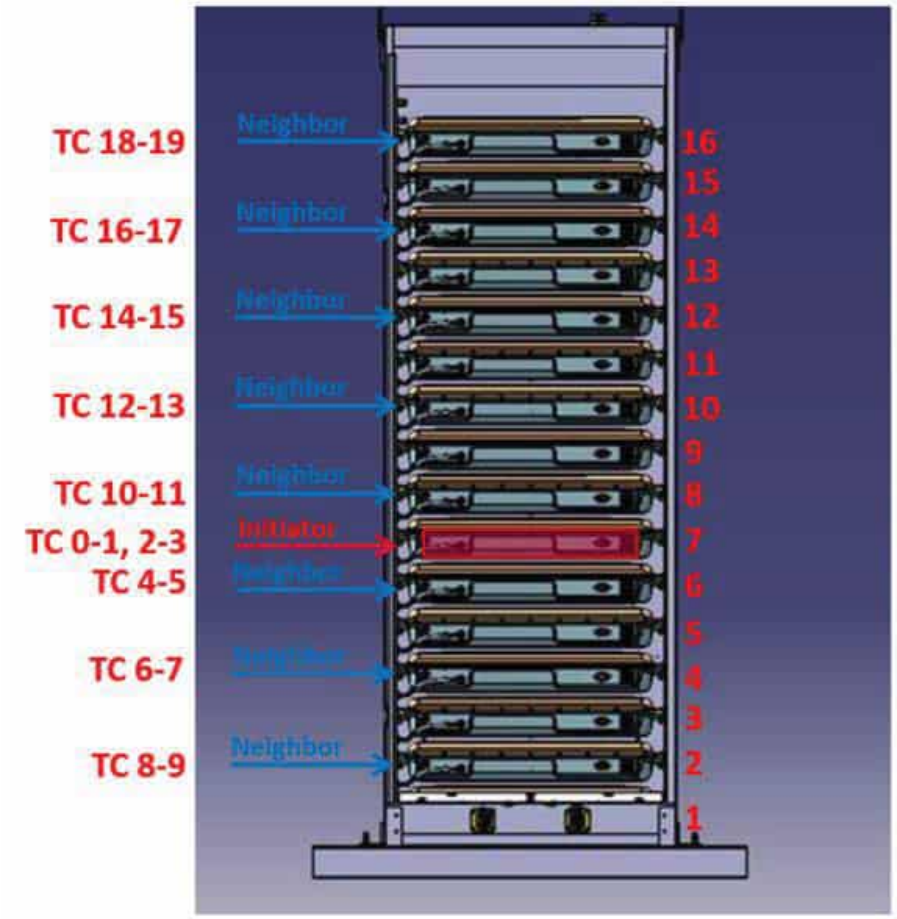


Figure 2-4 Rendering of open Powerpack fully populated with initiator pack thermocouple placement

2.2 Equipment and Sensors

To provide data necessary to assess deflagration hazards when installed inside rooms and spaces and to provide information generally on gases generated for the purpose of responding to AHJ inquiries, DNV GL measured a number of gases coming from the test using three different sensors. The primary sensor, who's air handling unit also provides temperature and humidity control as well as filtering for the other sensors, was the Gasmet DX-4000 FTIR (Fourier Transform Infrared) gas analyzer. As FTIR analysis is not capable of detecting diatomic gases, the sensor is fitted a with a crystalline oxygen sensor in the air handler and is supplemented by an MSA Optima-X catalytic bead LEL (lower explosive limit) sensor as well as a Hy-Scan 720B hydrogen sensor. The LEL sensor is propane calibrated and reports a 0-100% range while the hydrogen sensor reports a 0-5% hydrogen. The following gases were analyzed during testing:

Water Vapor (H2O, %)
Nitrogen Monoxide (NO, ppm)
Methane (CH4, ppm)
Hydrogen Chloride (HCl, ppm)
Benzene (ppm)
Methanol (ppm)
Hydrogen (H2%)
Carbon Dioxide (CO2, %)
Nitrogen Dioxide (NO2, ppm)
Ethane (ppm)
Hydrogen Fluoride (HF, ppm)
Toluene (ppm)
Propane (ppm)
LEL (%)
Carbon Monoxide (CO, ppm)
Acetonitrile (ppm)
Ethylene (C2H4)
Hydrogen Cyanide (HCN, ppm)
Ethanol (ppm)
Oxygen (O2, %)

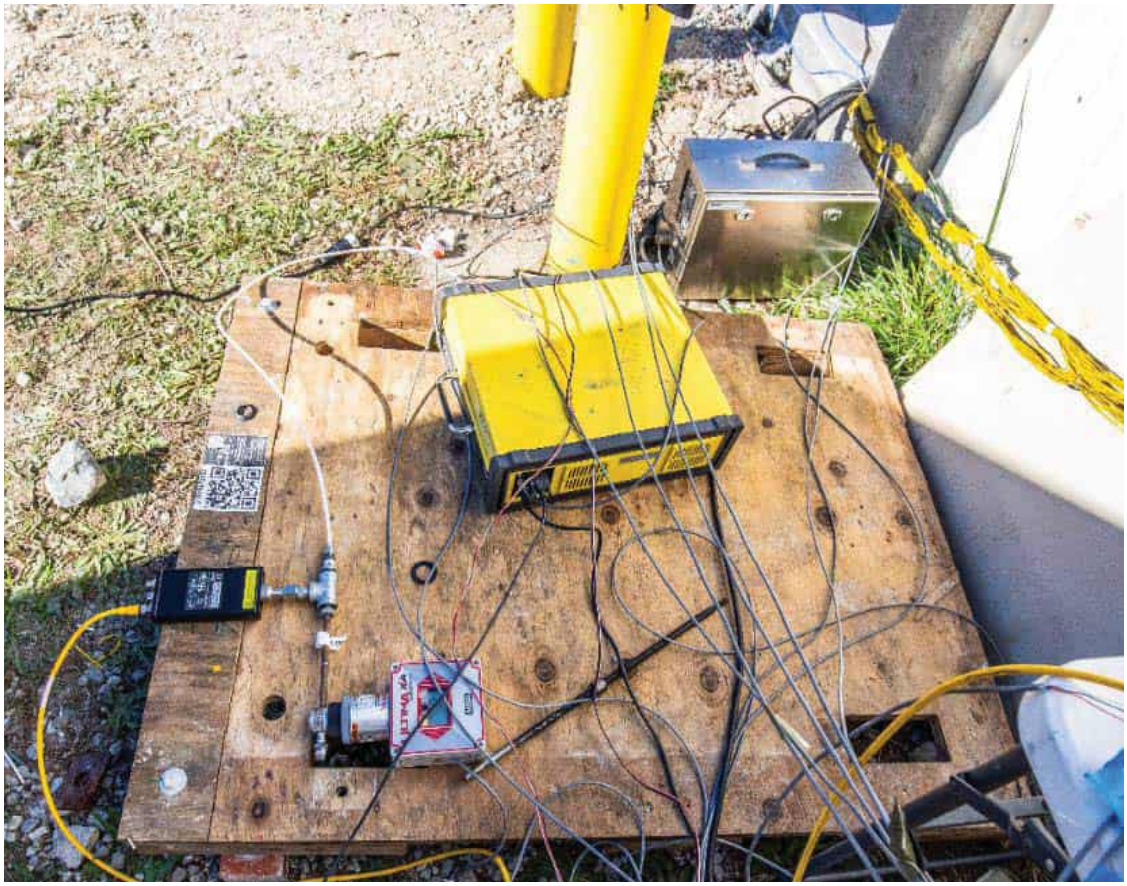


Figure 2-5 Gas analysis setup

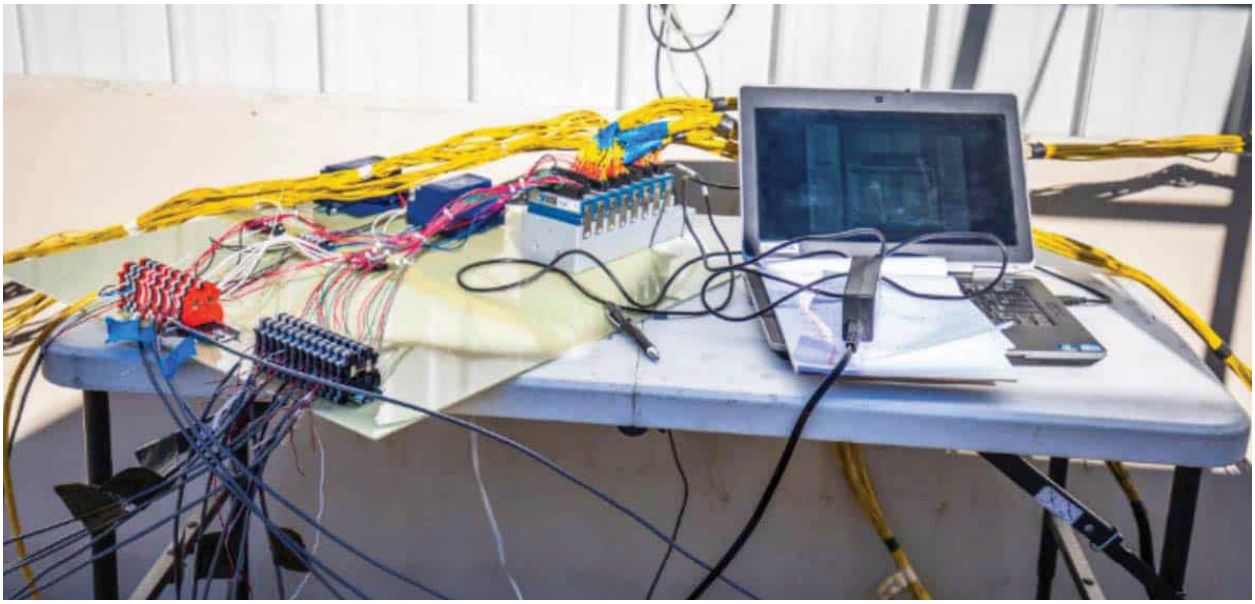


Figure 2-6 Signal breakout board, NI cDAQ and control laptop

In addition to the gas analysis. Numerous heat flux gauges, pressure sensors, thermocouples and other measurements were collected via an eight channel National Instruments cDAQ. These wires were sent to a custom built breakout board for ease of collection and wire management. The cDAQ

was run from National Instrument's LabVIEW software. In addition to these measurements, numerous cameras were placed around the test setup including two thermal IR cameras.

2.3 Test Setup – Outdoor Installation



Figure 2-7 Wide view of test setup from the south with heat flux gauges

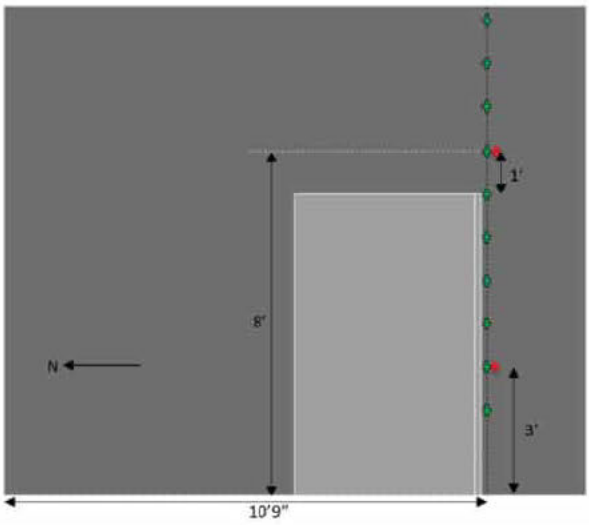
As Tesla currently aims to install systems outdoors, upon rooftops, and in open parking garages, the primary purpose of testing was to ensure a lack of pack to pack propagation based on the tested spacing of 4" between laterally adjacent units and 2" between the unit behind. As a secondary objective, Tesla sought to demonstrate the effectiveness of two hour-rated fire walls and to demonstrate a lack of other unforeseen effects when experiencing failure in open atmosphere. A large black room was constructed with double layer 5/8" Gypsum Type-X drywall as shown below. Per UL standards, the effectiveness of the wall was determined based on temperatures recorded on the back side.



Figure 2-8 Tight view of Powerpacks with wall thermocouples

East Wall

- Walls and ceiling are 2hr fire rated backed by wood studs spaced 16" apart.



- As shown 10 TCs are on the *exposed side* of the wall.
- There will be 10 TCs collocated with these TCs on the *unexposed side*.
- TC numbering and updated figure to be provided by the ATL.

Key:

-Schmidt-Boelter Total Heat Flux
-Type K Thermocouple (24 ga.) +

Figure 2-9 East wall sensor diagram

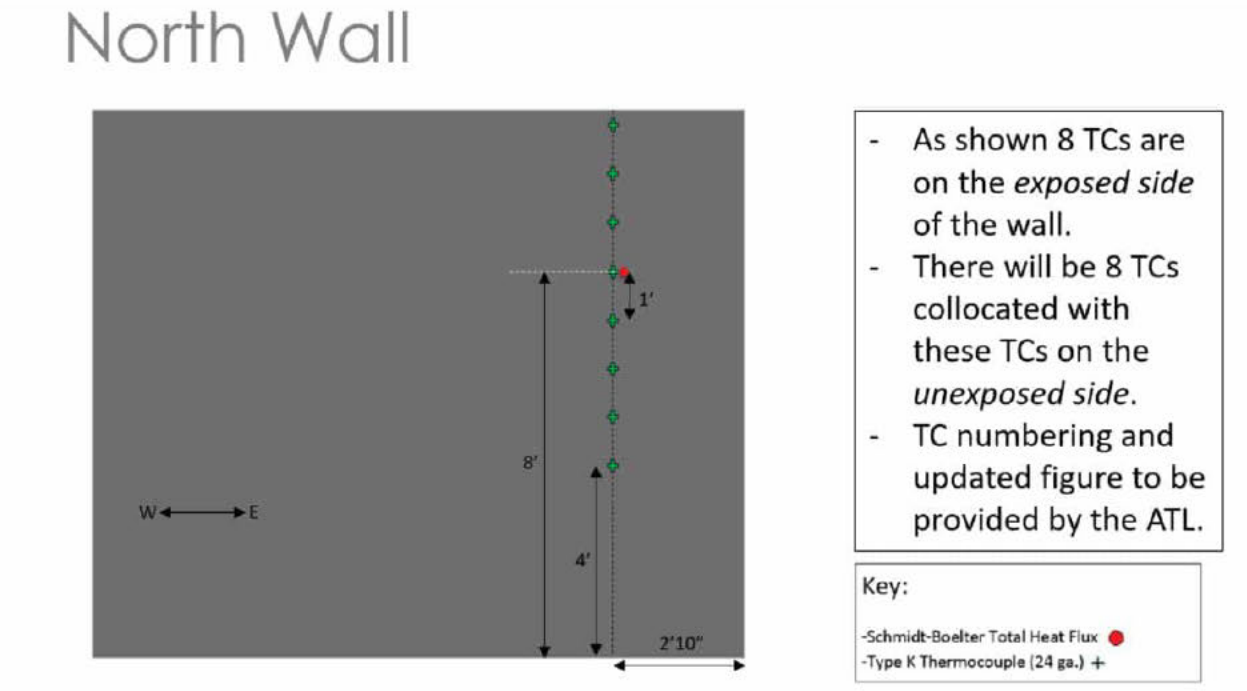


Figure 2-10 North wall sensor diagram

To demonstrate walls with simulated 2-hour fire-resistance-ratings can withstand an event of this magnitude, and to collect as much useful data as possible, thermocouples were placed in vertical arrays along the walls as shown. On the east wall (Figure 2-9), starting at 3′, thermocouples were placed every 12″ up to the ceiling. This was done on both the fire side as well as on the unexposed back side, where the opposing side of the wall was drywalled within the appropriate bay between the studs, which were spaced a typical 16″. On the north wall (Figure 2-10), a similar placement and construction was used, though the thermocouples started at 4′ instead of 3′. The heat flux gauges were located colinearly within this instrument line at the appropriate heights.

2.4 Sensor Placement

Thermocouples were placed through the target Powerpacks to determine the heat transfer into the units during the test unit's combustion. Two thermocouples were placed within each module in the

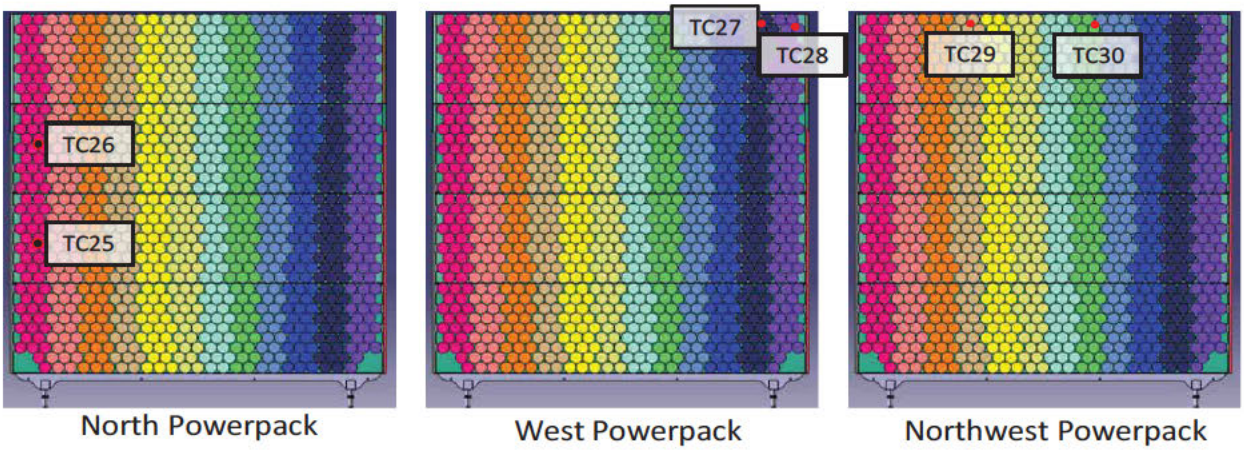


Figure 2-11 Target pack module internal thermocouple setup

target Powerpacks. Two were placed internally (Figure 2-11) while a single thermocouple was placed on the exterior of the module directionally toward the initiator unit (Figure 2-12).

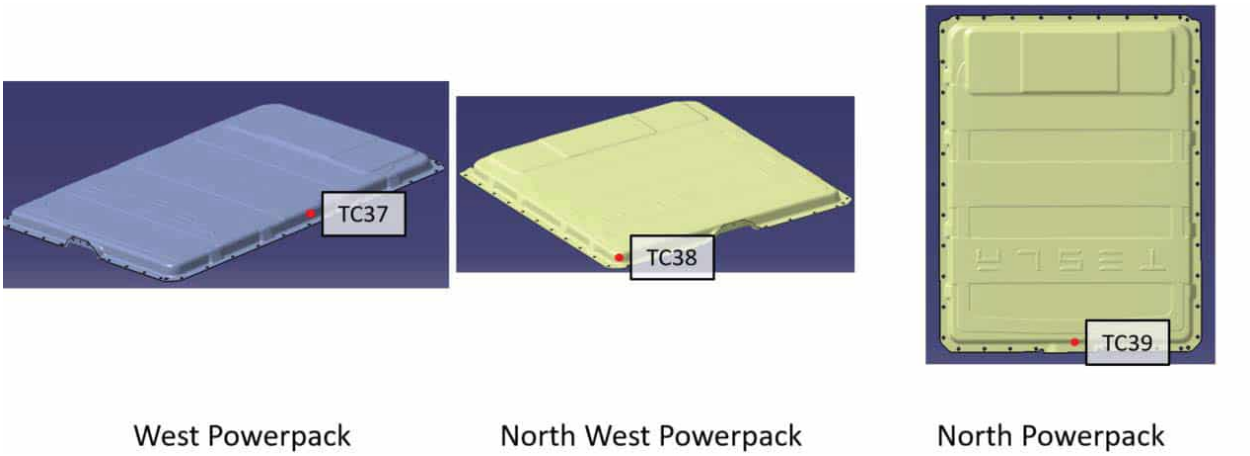


Figure 2-12 Target pack module external thermocouple setup

Four additional thermocouples were placed through the outer rack—but still within the enclosure—of the initiator Powerpack. These are shown below in Figure 2-13 along with the placement of the four pressure transducer probe inlets.

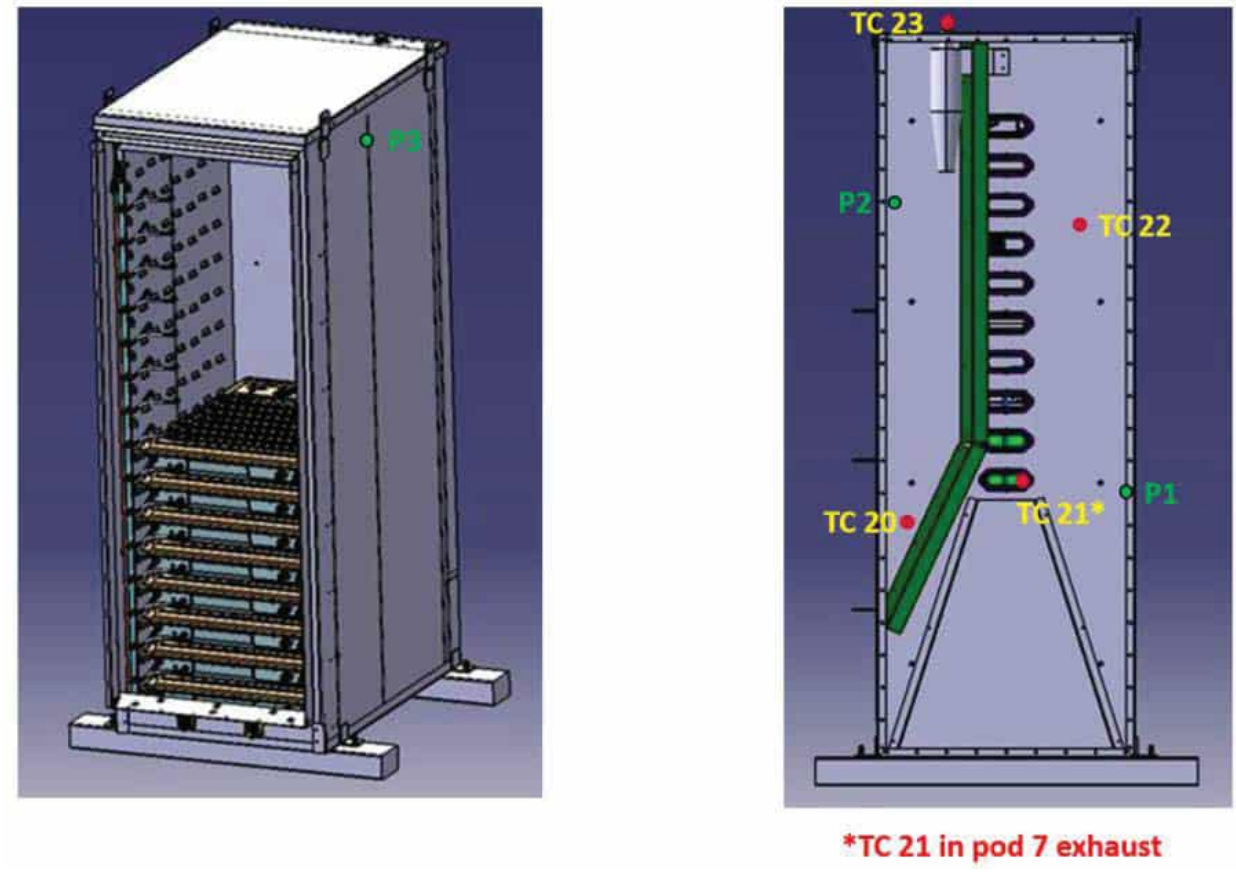


Figure 2-13 External sensor placement through initiator Powerpack



Figure 2-14 Heat flux gauge external setup

As per Figure 2-1, a number of Schmidt-Boelter heat flux gauges were also placed to the front and to the side of the initiator pack. These water-cooled gauges were placed on stands at 4' elevation. All gauges were carefully aimed at the front center of the initiator pack. The gauges ranged from 10-100kW/m^2 based on expected heat fluxes at each distance. Though not pictured, one heat flux gauge was also placed in the back and side wall appropriately of the adjacent target packs. Shown in Figure 2-1 but not pictured, these gauges were placed at 6' from the floor.

3 OBJECTIVES

The objective of the test was to demonstrate, via large scale testing by an approved laboratory, that the Tesla Powerpack, when subjected to internal thermal runaway sufficient to propagate module to module:

1. Does not pose a propagation risk to neighboring units or exposures based on the spacing observed in testing, even when no suppression or water is applied over the entire course of the event.
2. May be contained and sufficiently blocked by two hour fire resistance rated walls which do not show appreciable temperature rise on their back sides relative to the fire exposure.
3. Generate data via heat flux and temperature that allows for the modelling of thermal exposure from the unit for the purpose of assessing spacings necessary relative to exposures identified by relevant codes and standards language.

4 RESULTS

4.1 Outdoor Installation Test

Testing was performed on the morning of October 17th, 2018. Weather was clear with temperatures in the mid 50s°F with winds out of the west-southwest blowing 15-20mph with gusts up to 25mph. These winds were blowing into and along the open side of the test area. Prior to testing, a final check of all data acquisition was performed along with a safety briefing with all personnel on site. Table 4-1 below shows the time of relevant events during testing.

Cartridge heaters inside the unit were powered as part of a ten minute "pre-warming" period before which time they were turned to full power. During the initial combustion event, a single audible pop was heard during combustion, but the event failed to impact the DUT. Following cessation of the initial combustion event, the DUT sat idle for almost 90 minutes before the heat transfer within the DUT allowed the failure to propagate to neighboring modules. This resulted in a small deflagration event which succeeded in opening the already fire exposed front door of the DUT. Once the fire propagated to neighboring modules within the DUT, it burned one module at a time for approximately 45 minutes before reaching a point at which multiple modules began burning simultaneously and which resulted in a more violent conflagration.

In the plots below showing the results, a blue vertical dashed line is shown in most figures indicating the first thermal runaway. A second red vertical dashed line is shown to indicate the first visible flame from the unit.

Table 4-1 Test time stamps

Event	Time	Minutes after	
DAQ Start	11:17:50	DAQ Start	First Thermal Runaway
Heater Start	12:12	55	N/A
First audible event (thermal runaway)	12:24	67	0
First visible flame (door open)	12:42	85	18
2nd Module Ignition	14:14	177	110
End of Test	15:43	266	199

4.1.1 Temperature Data

4.1.1.1 Ceiling and Wall Temperatures

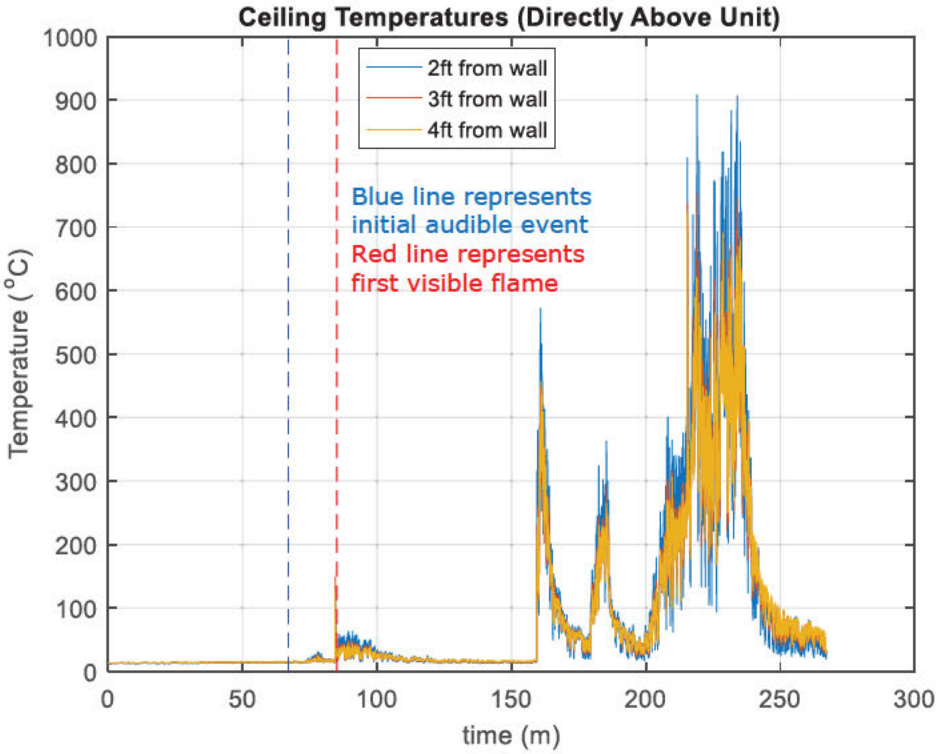


Figure 4-1 Ceiling temperatures above DUT (fire side)

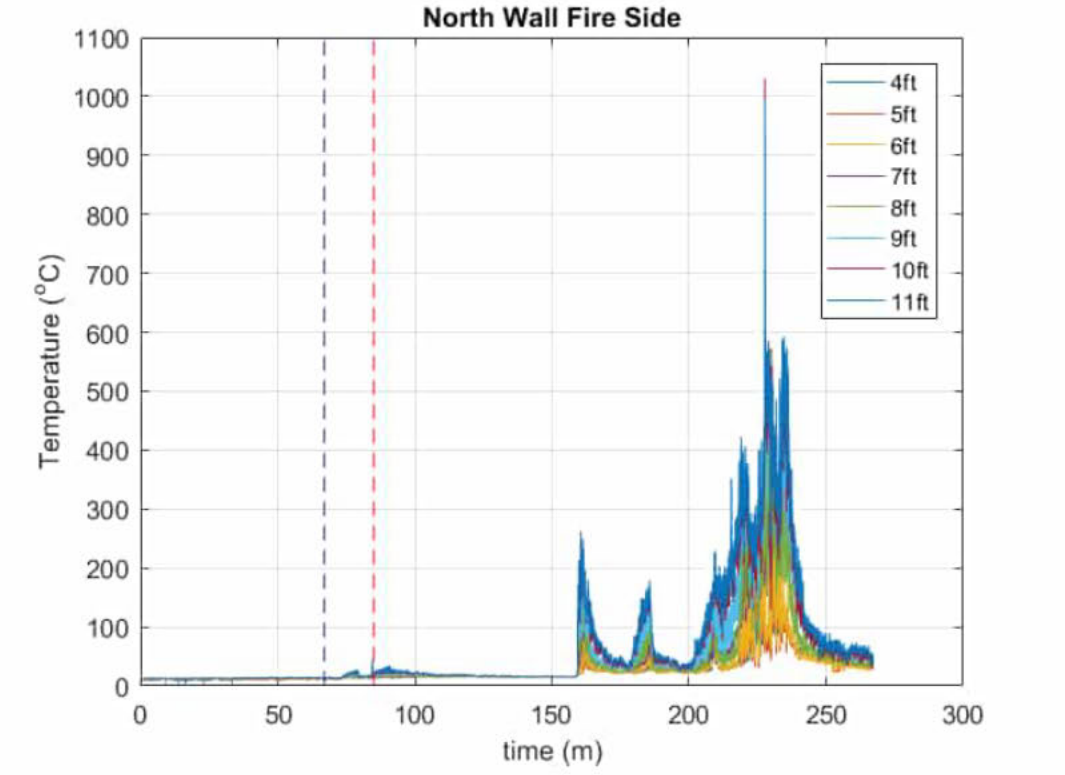


Figure 4-2 North wall, fire side temperatures

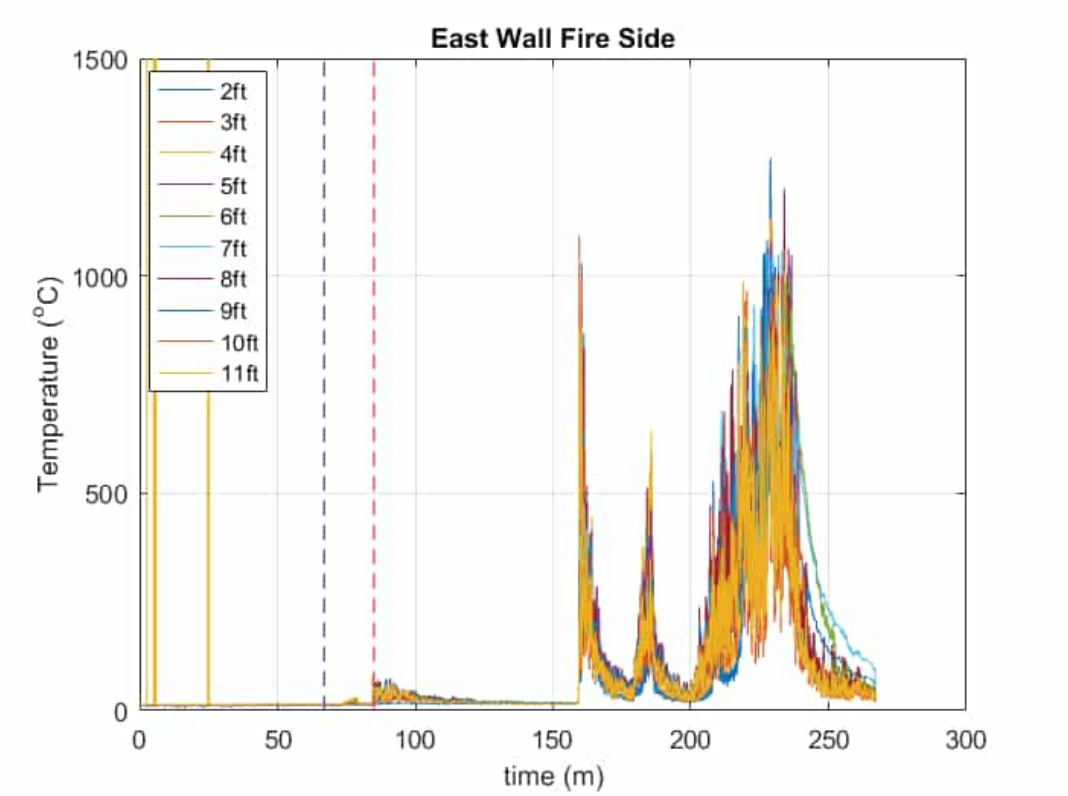


Figure 4-3 East wall, fire side temperatures

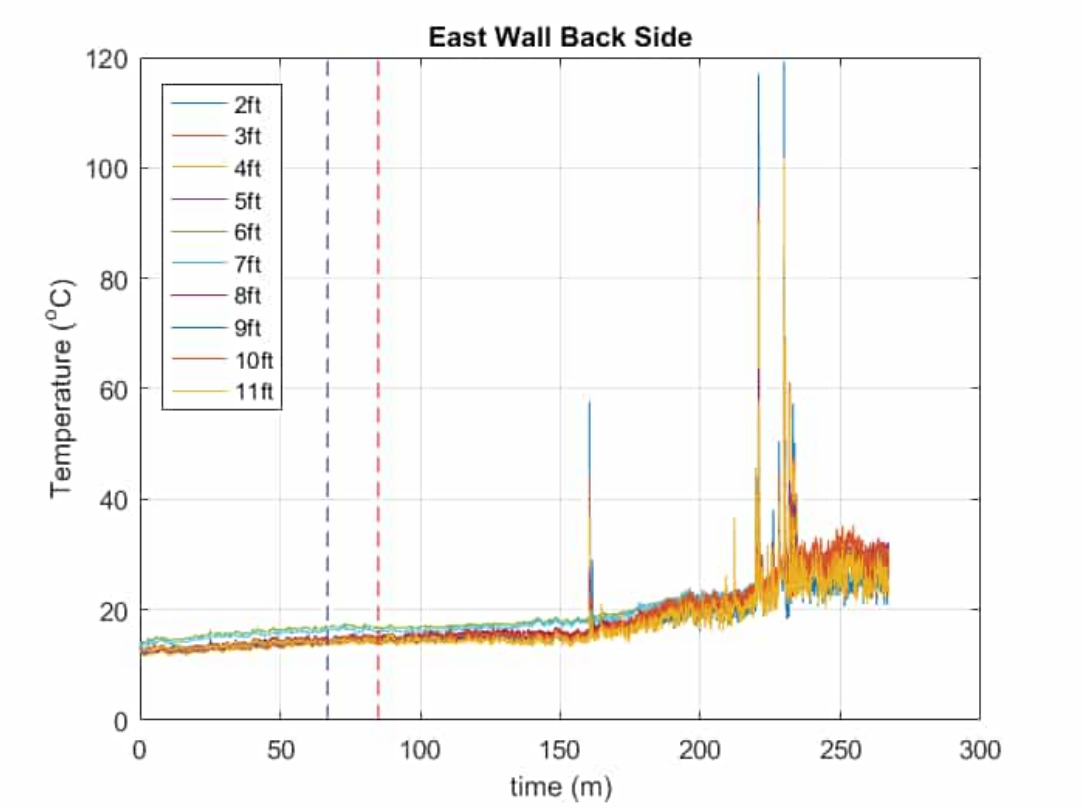


Figure 4-4 East wall, back side temperatures

The figures above show temperatures recorded on the fire side, and in one case on the back side, of the drywall walls during testing. The ceiling above the device saw high temperatures as would be expected from an event directly below, however, it was the east wall, that nearest the DUT, which saw the highest fireside temperatures. This was a result primarily on the geometry of the unit and test setup, where the open door directed flames out of the unit towards the wall as well as overall proximity. An example of this is below, in Figure 4-5.



Figure 4-5 Fire from DUT on east wall

Despite the high temperatures on fire side of the east wall, temperatures on the back side of the two-hour fire resistance rated wall remained safe, not exceeding 35°C (95°F), as shown in Figure 4-4. Despite being oriented away from the fire and with the exhaust hood pulling ventilation above, the fire side of the north wall saw higher than expected temperatures, likely as a result of roll over across the ceiling and of the westerly winds pushing heat back into the test area. Though one side of the test area was open to atmosphere and fire was directed that way, and though the exhaust hood with several thousand CFM of exhaust was above the DUT, temperatures on the back wall still reached nearly 600°C (~1100°F), as seen in Figure 4-2. Like the east wall though, the back side of the north wall saw temperatures raise less than 10°C above ambient at their peak, again providing confidence as to the ability of the two-hour fire resistance rated fire wall to protect adjacent rooms and areas from the high heat load.

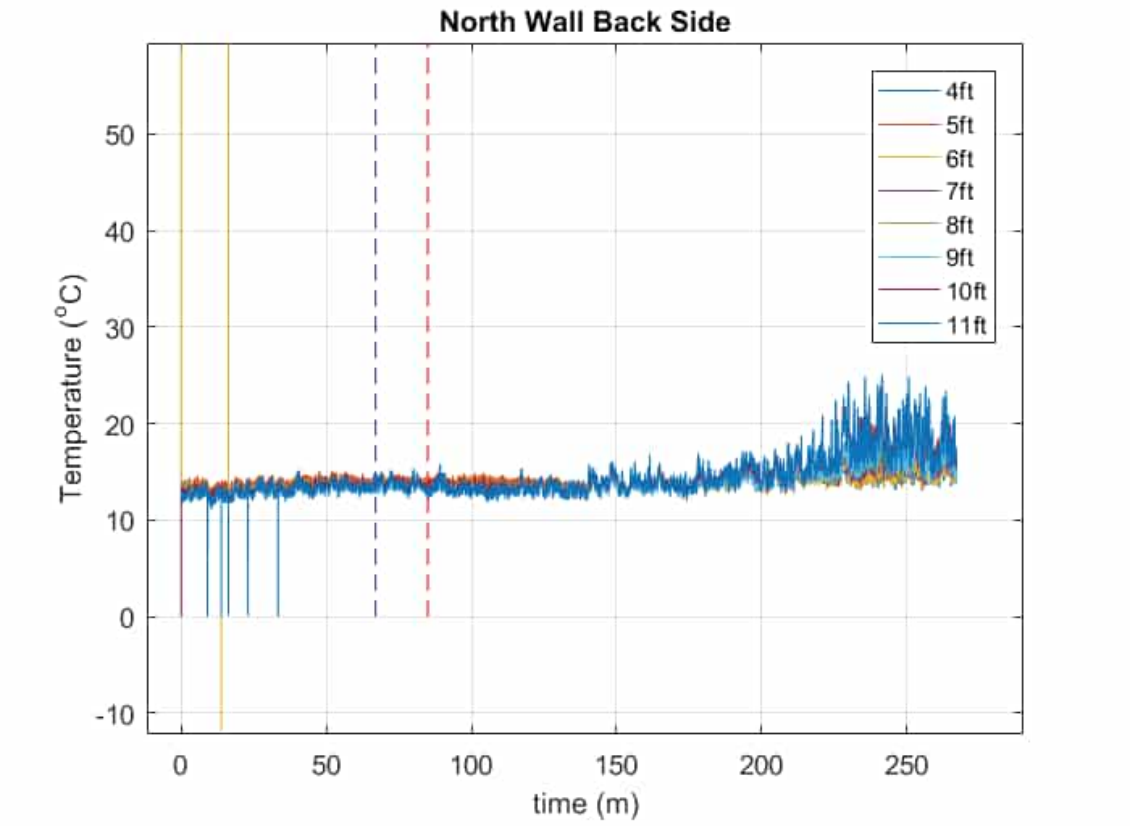


Figure 4-6 North wall, back side temperatures

4.1.1.2 DUT Temperatures

Though visually the fire appeared intense, with internal temperatures briefly exceeding 1500°C at times, external temperatures failed to exceed even half that, staying below 700°C. Though internal temperatures in excess of 1000°C are common for lithium ion battery fires, data for the external temperatures on the unit show that was mostly retained inside the unit or, much like the visual flame, was directional. This is evident through high ceiling temperatures as well as east side wall temperatures, which exceeded 700°C or more while the north wall, despite heat roll over from the ceiling, stayed below 600°C.

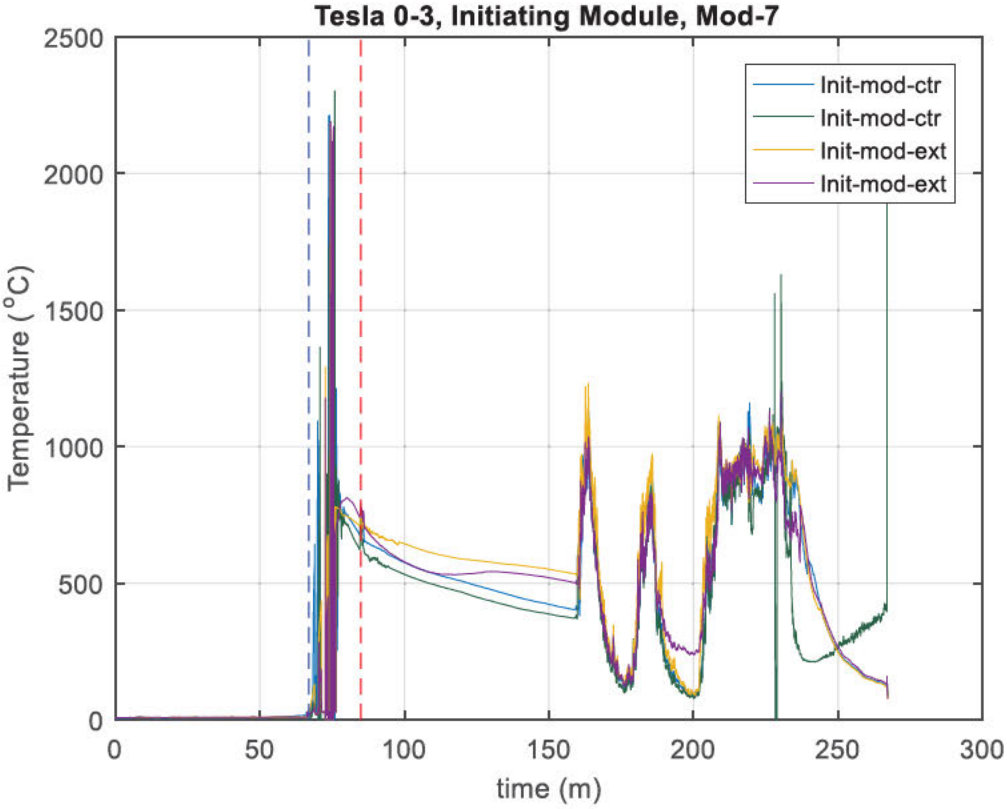


Figure 4-7 Temperatures inside the initiating module in DUT

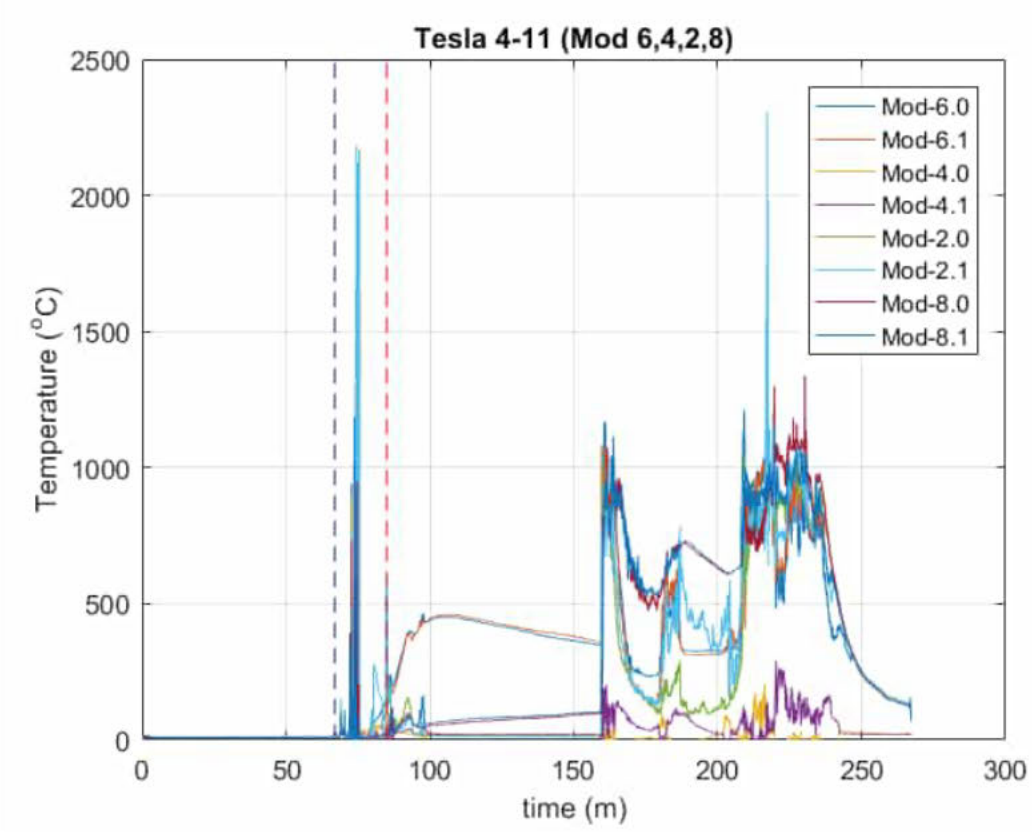


Figure 4-8 Temperatures in the adjacent modules to the initator

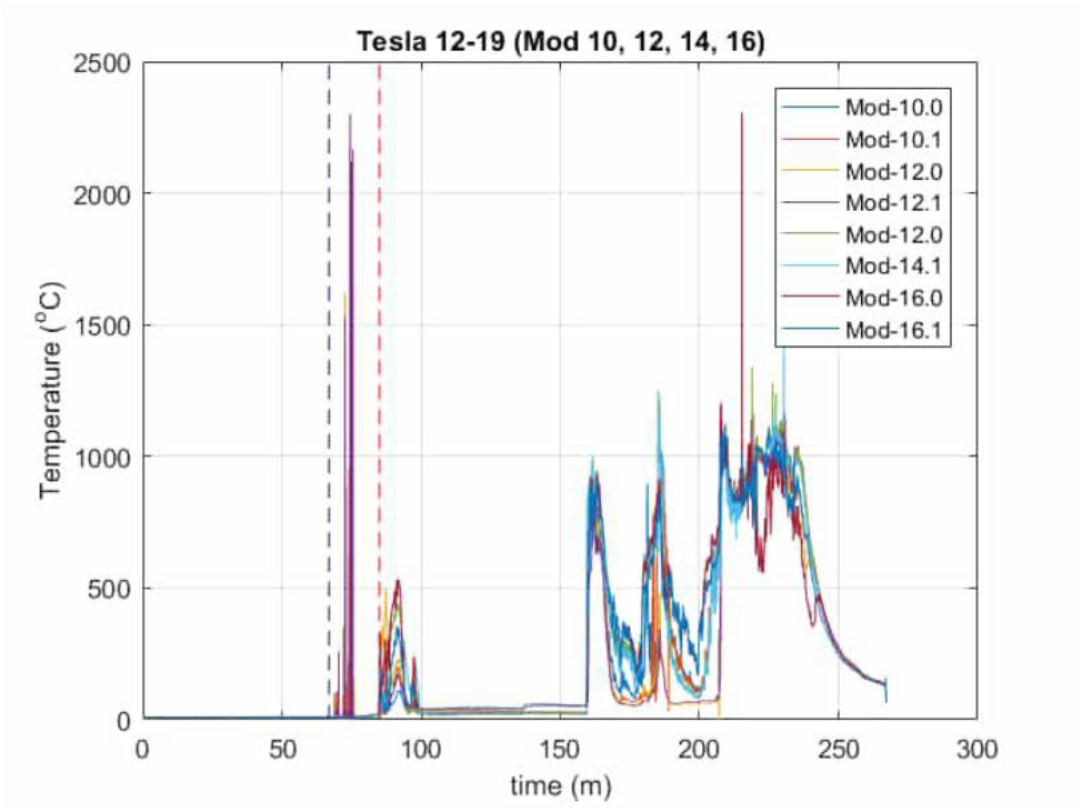


Figure 4-9 Additional DUT temperatures

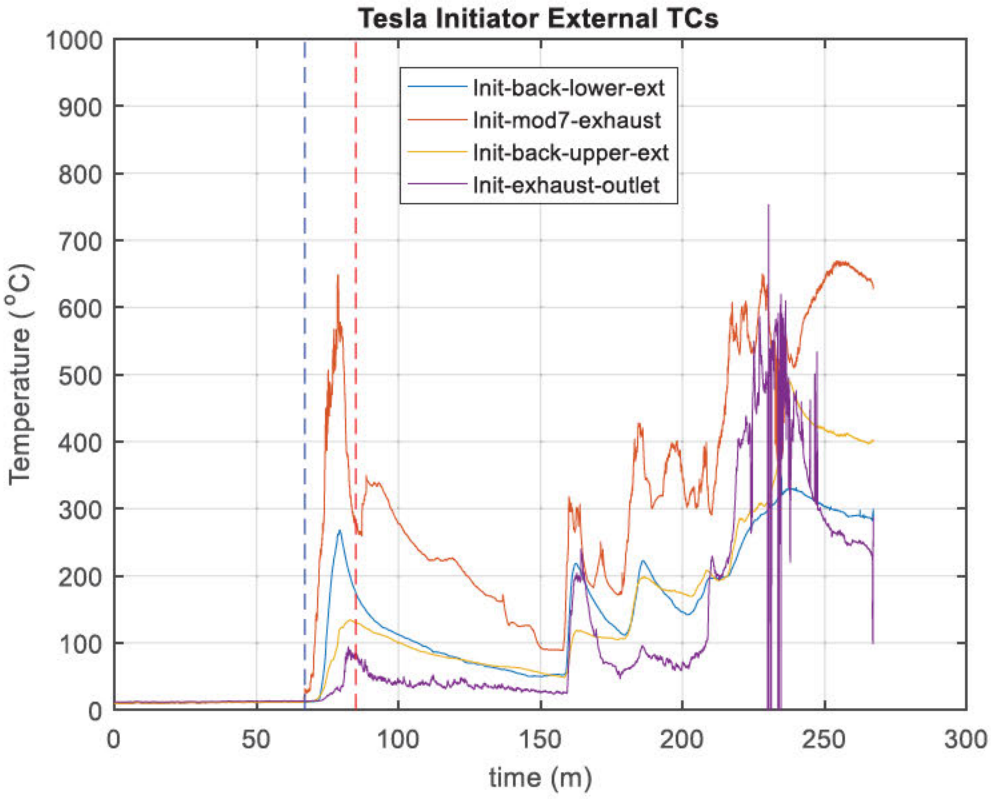


Figure 4-10 DUT initiator module external temperatures

4.1.1.3 Adjacent Powerpack Temperatures

Near the end of the test, fire impingement on some of the thermocouple cables resulted in open circuit failures, which show a value of approximately 2200°C, but are not real. To that end, Figure 4-11 and Figure 4-12, which show the errors, in reality saw essentially no noticeable temperature increase in or on module 7 in the adjacent systems. Figure 4-13 indicates that the upper module in the adjacent units was briefly exposed to high temperatures, likely a result of brief environmental effects, but in general saw no adverse temperature increase within the modules. Finally, Figure 4-14 shows that within the Powerpacks, but outside the modules, temperatures did begin to increase after exposure to the fire, and in two cases did become exceedingly hot. However, it can be assumed that this was from hot air passing over the thermocouple, as the sensor indications cooled quickly and this did not translate to an increase in internal temperature.

Ultimately, there was no propagation of the fire from the test Powerpack to the neighboring Powerpacks.

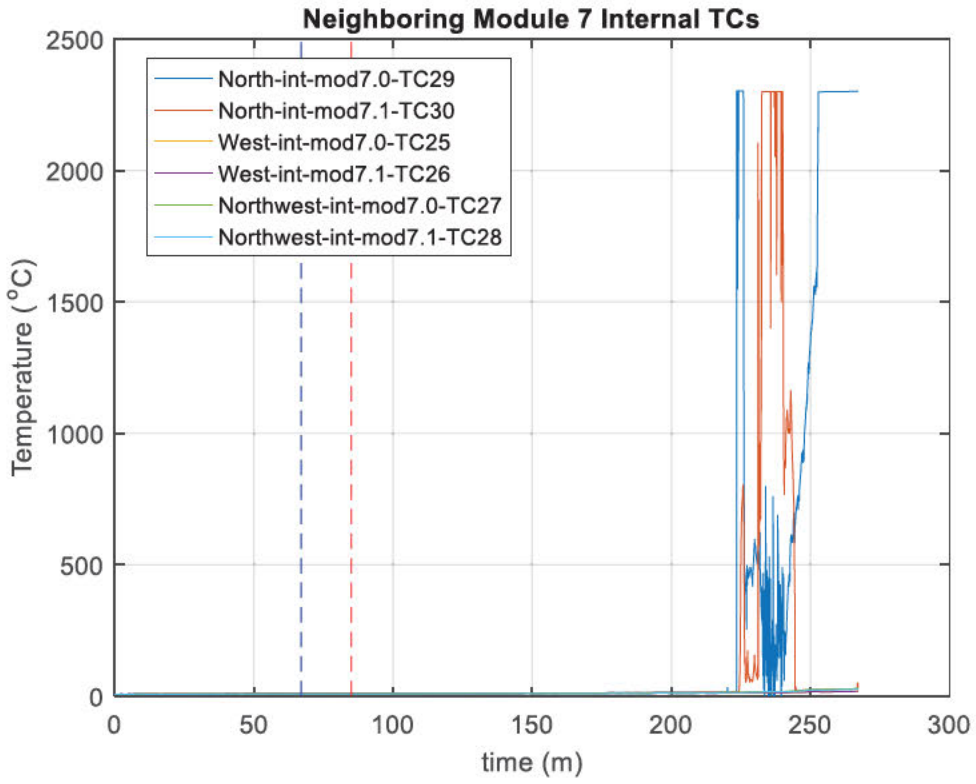


Figure 4-11 Temperatures inside center module of neighbors

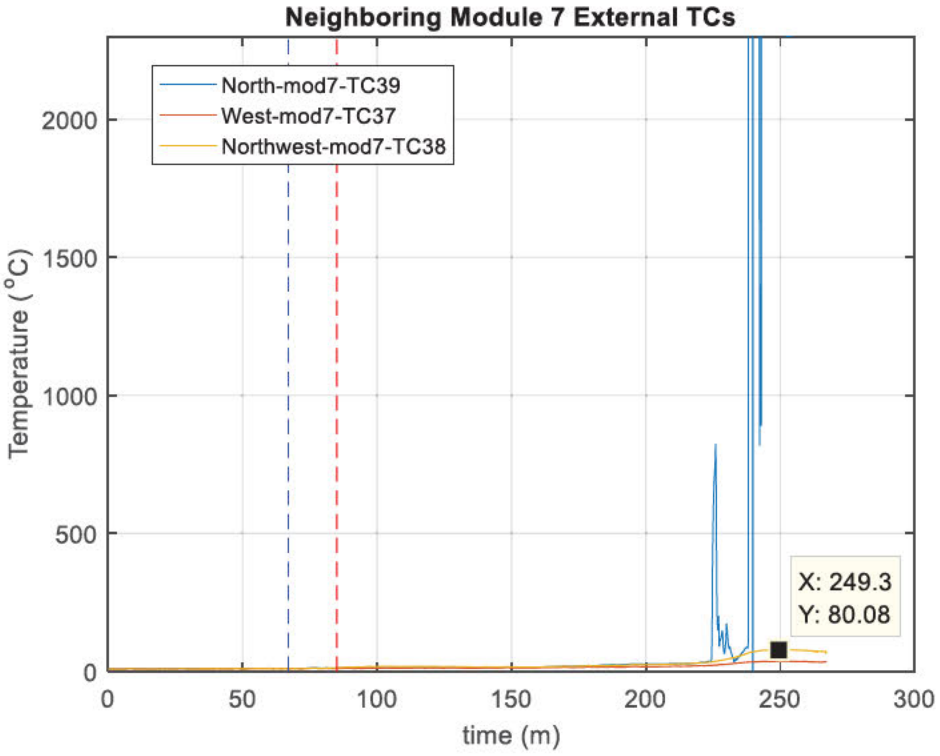


Figure 4-12 Temperatures on the outside of center module of neighbors

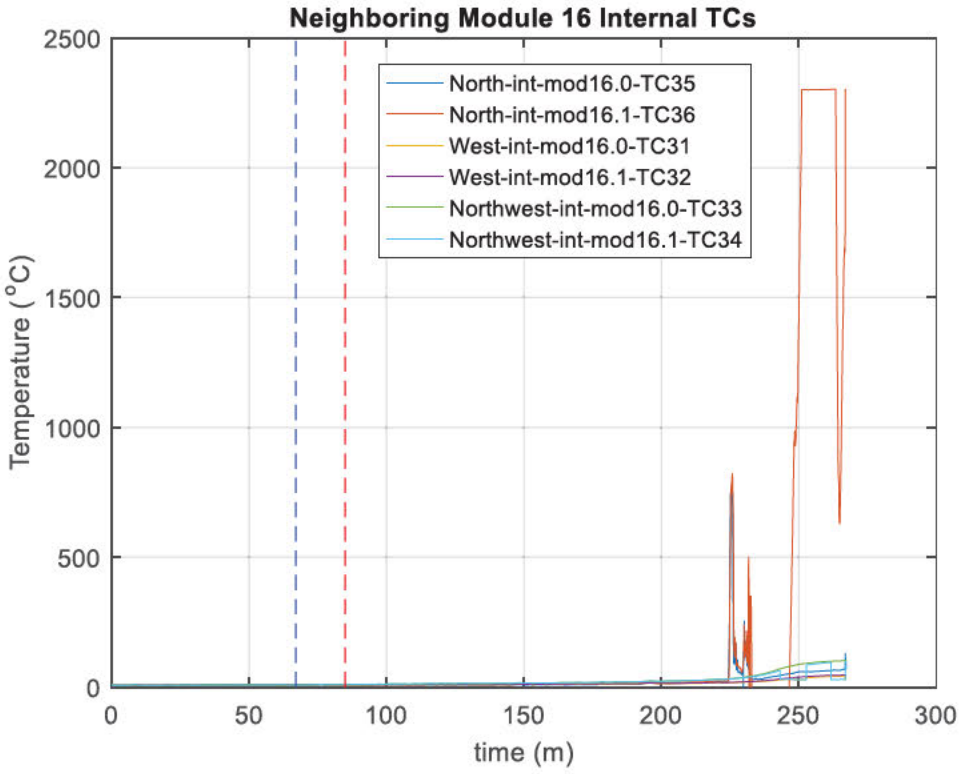


Figure 4-13 Temperatures inside the upper module in the neighbors

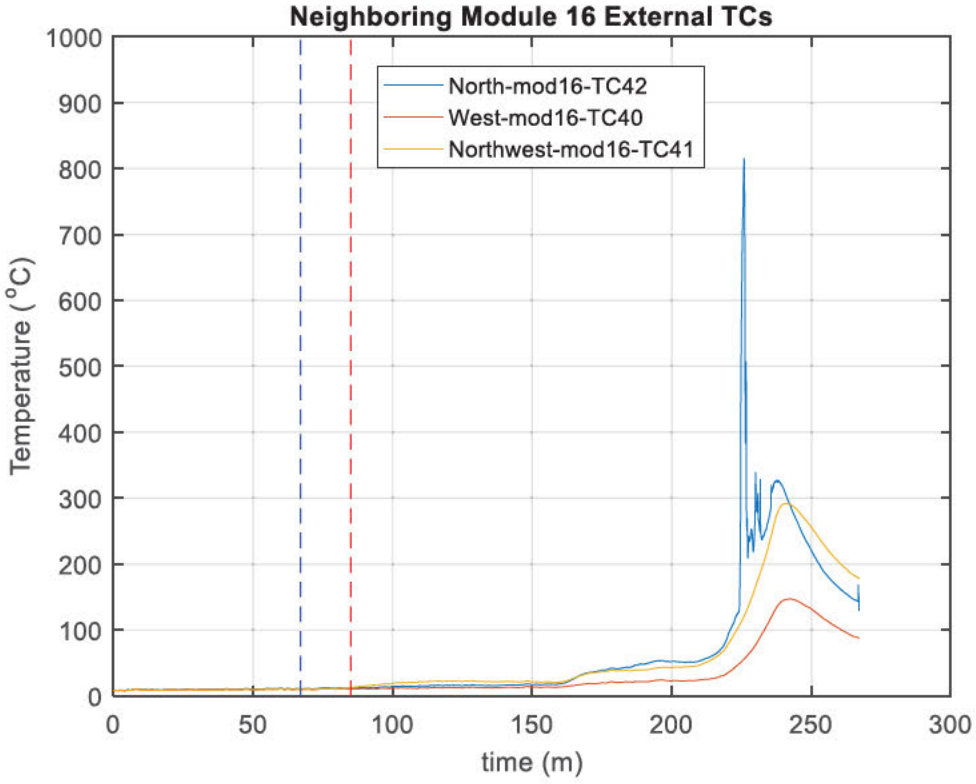


Figure 4-14 Temperatures on the outside of the upper module in the neighbors

4.1.2 Heat Flux Data

In addition to temperature measurements, the heat flux from the DUT was taken at multiple points with a particular focus on egress pathways and adjacent exposures. As expected, heat flux against the east wall (Figure 4-15) was the highest, exceeded only by the heat flux at 6ft in front of the unit, which was hit by a large initial heat and pressure wave that damaged the sensor.

Heat flux along the north wall, again oriented opposite from the opening of the DUT, briefly exceeded 5kW/m^2. This result would not be expected in a true open air atmosphere, whereas in this case the ceilings are believed to have aided in reflecting heat; as would also be the case for units placed under a ceiling or covering. It is also of note that this value was seen for only a few brief seconds several minutes after the initial thermal runaway and smoke release (and when the unit was clearly emitting flame) and was not seen again until nearly three hours after the initial thermal runaway when the system reached full flame involvement.

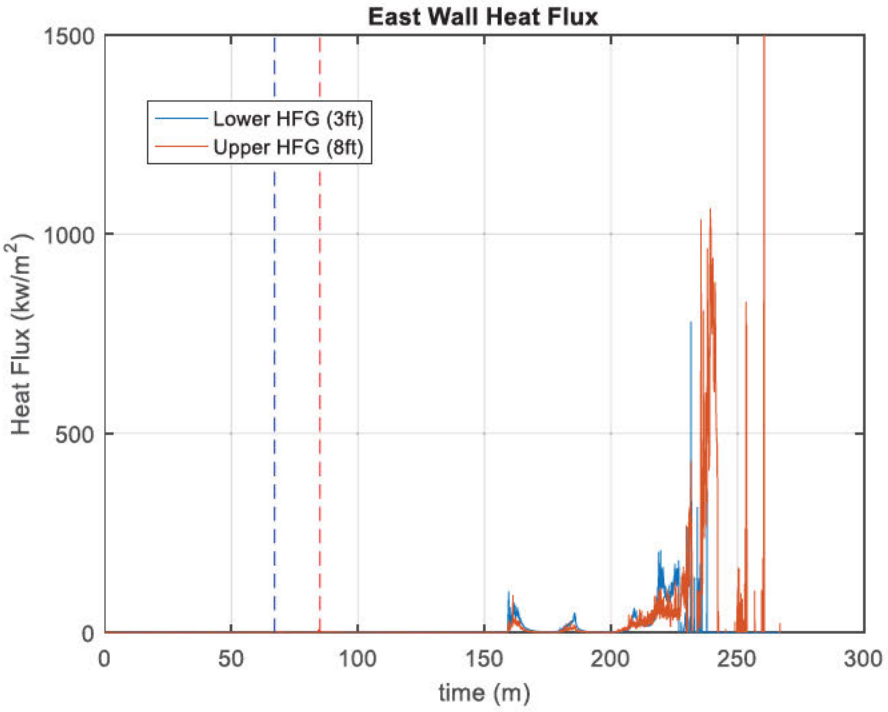


Figure 4-15 East wall heat flux

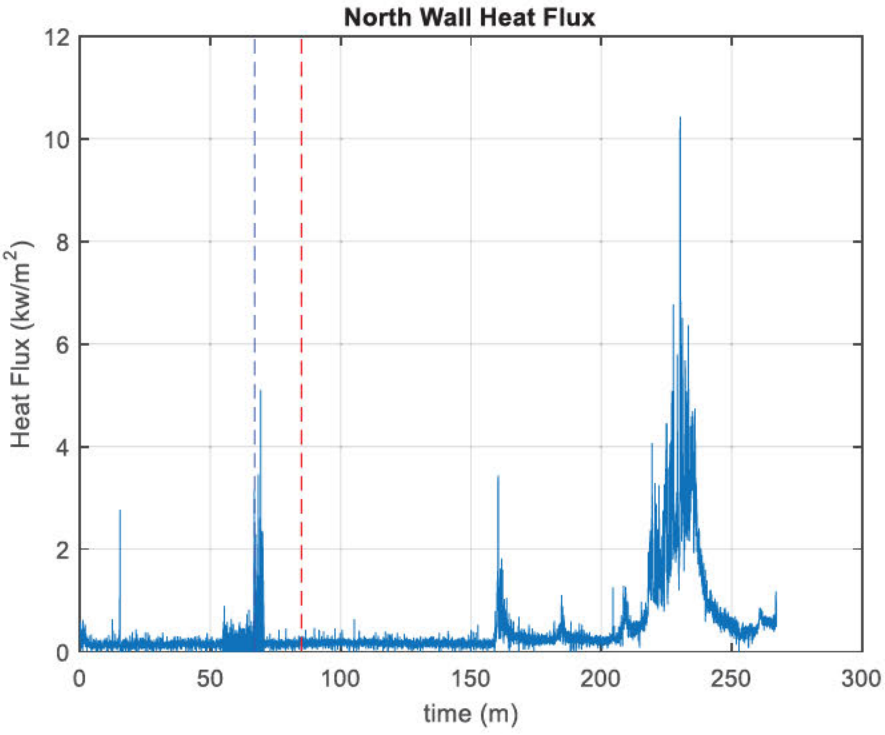


Figure 4-16 North wall heat flux

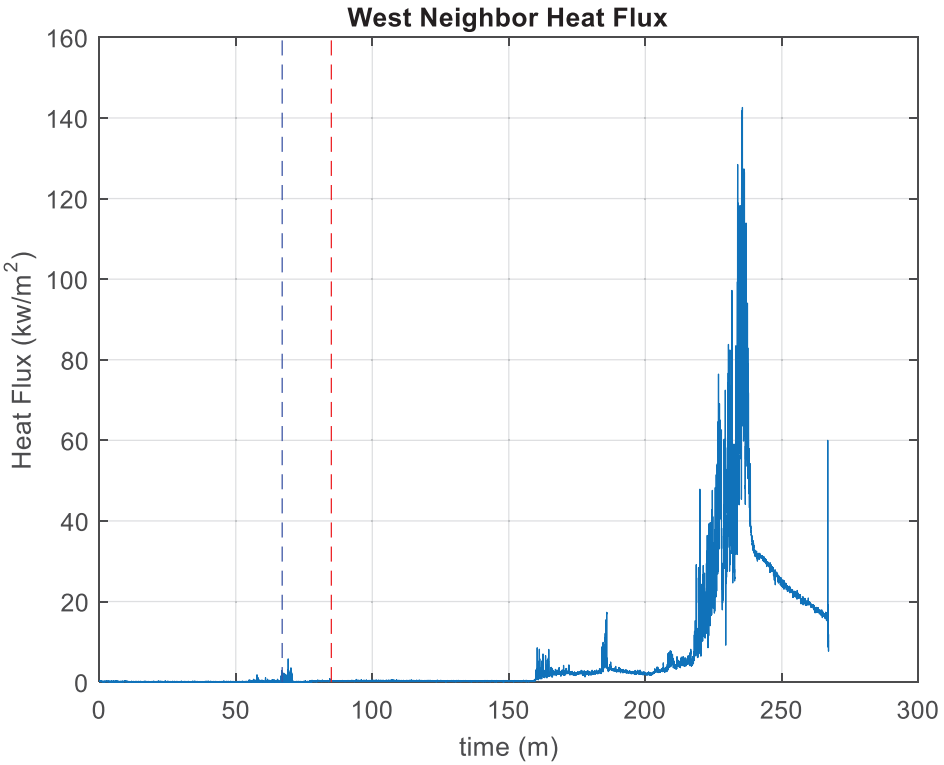


Figure 4-17 West neighbor heat flux

With expectedly high heat fluxes at the adjacent walls and neighbour, in part due to proximity of the test unit, heat flux emanating from the front of the unit is considered a key factor, as both the fire is directed that way and likely paths of egress will cross in front of it. To that end, multiple heat flux gauges were placed in front and to the side of the unit, as discussed above. Early in testing, the closest heat flux gauge, six feet from the front door, was damaged almost as soon as thermal activity began, negating the results from the device. High quality data was obtained from all other units though and is presented below in Figure 4-18, Figure 4-19, and Figure 4-20.

As expected, the heat flux at 8 and 10ft measured consistently once a fully involved fire developed and was sustained by the unit nearly two and a half hours after initial thermal runaway (minute 210). At these distances, the heat flux exceeded 20 and 10kW/m^2 respectively for sustainable periods of time.

Likewise, the heat flux at 15 and 20ft also showed sustained values after extensive indication of smoke and fire from the unit. Despite very short lived pulses of high heat flux prior to these sustained events, DNV GL believes that the unit provides ample indication of thermal risk prior to reaching high heat flux levels and thus practical egress pathways are sufficient for escape from the area until flame has developed, at which point further distances or alternative routes will be necessary.

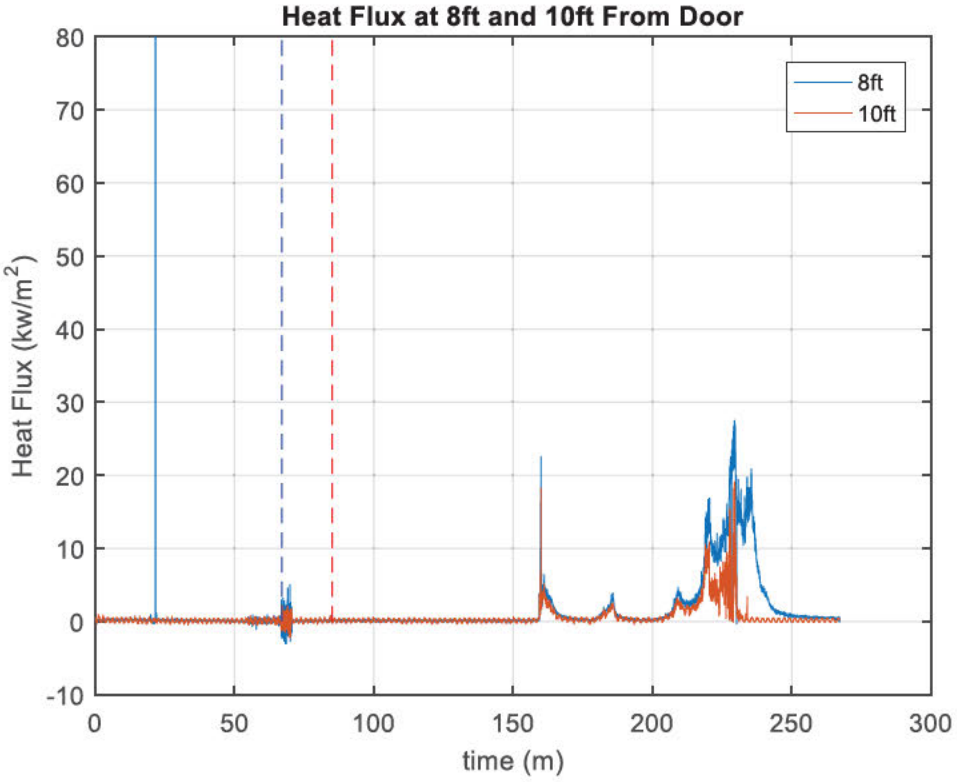


Figure 4-18 Heat fluxes in front of unit at 8 and 10ft

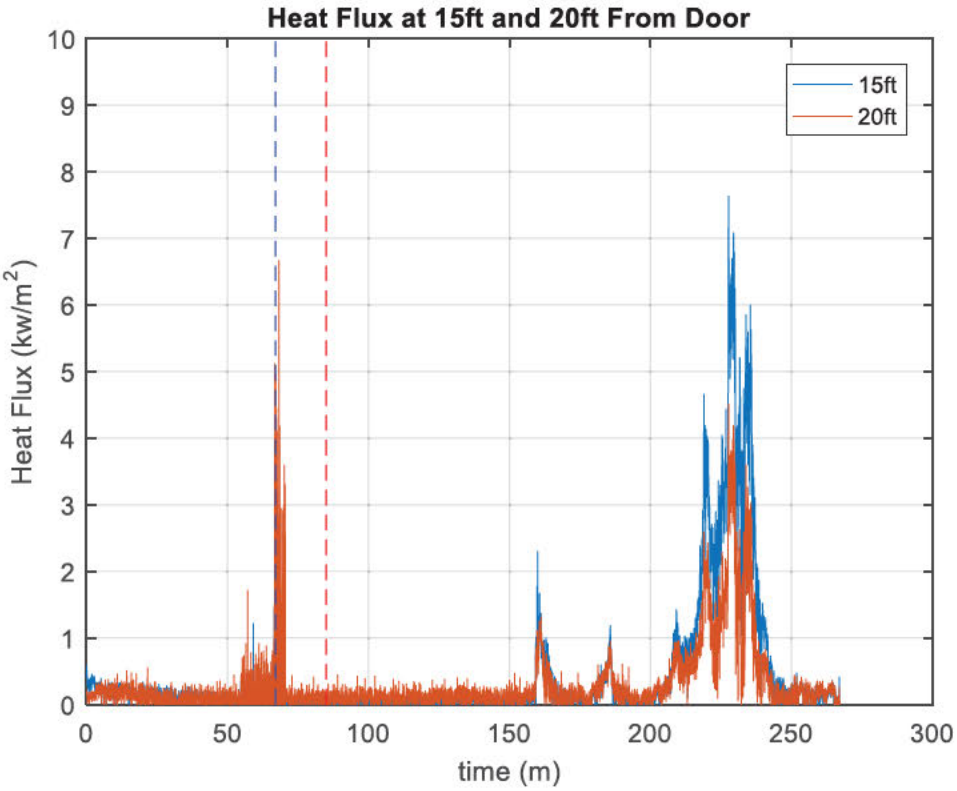


Figure 4-19 Heat fluxes in front of unit at 15 and 20ft

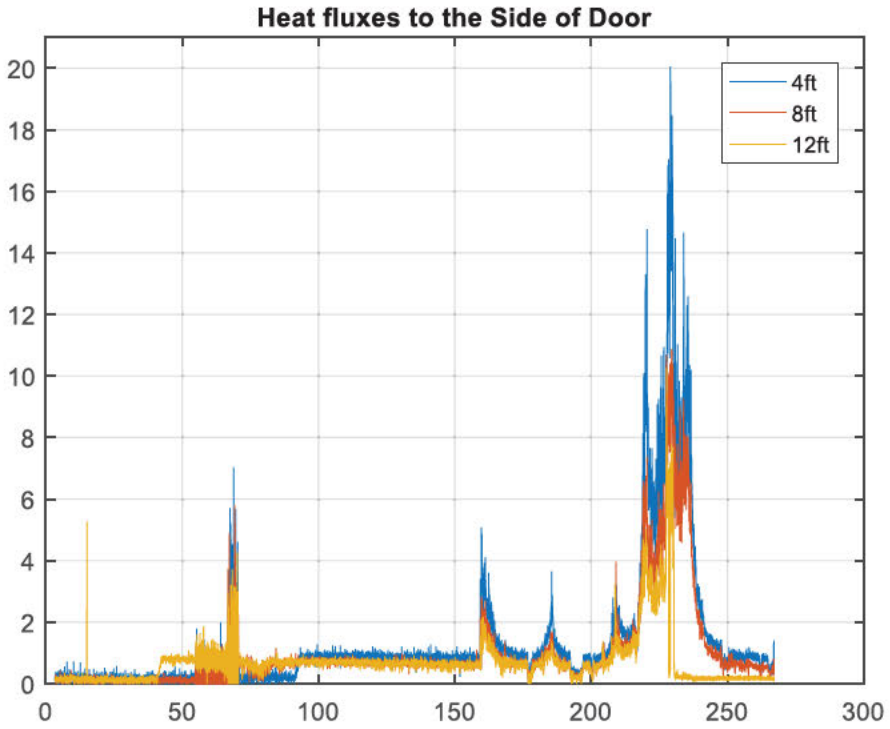


Figure 4-20 Heat fluxes to side of unit at 4, 8 and 12ft



Figure 4-21 Test during peak heat release rate

4.1.3 Gas Data and Venting Pictures

Following the initial thermal runaway, the unit began emitting flammable gas. It released a quantity of gas which exceeded 100% LEL within three minutes and saturated the sensor for the remainder of the test.

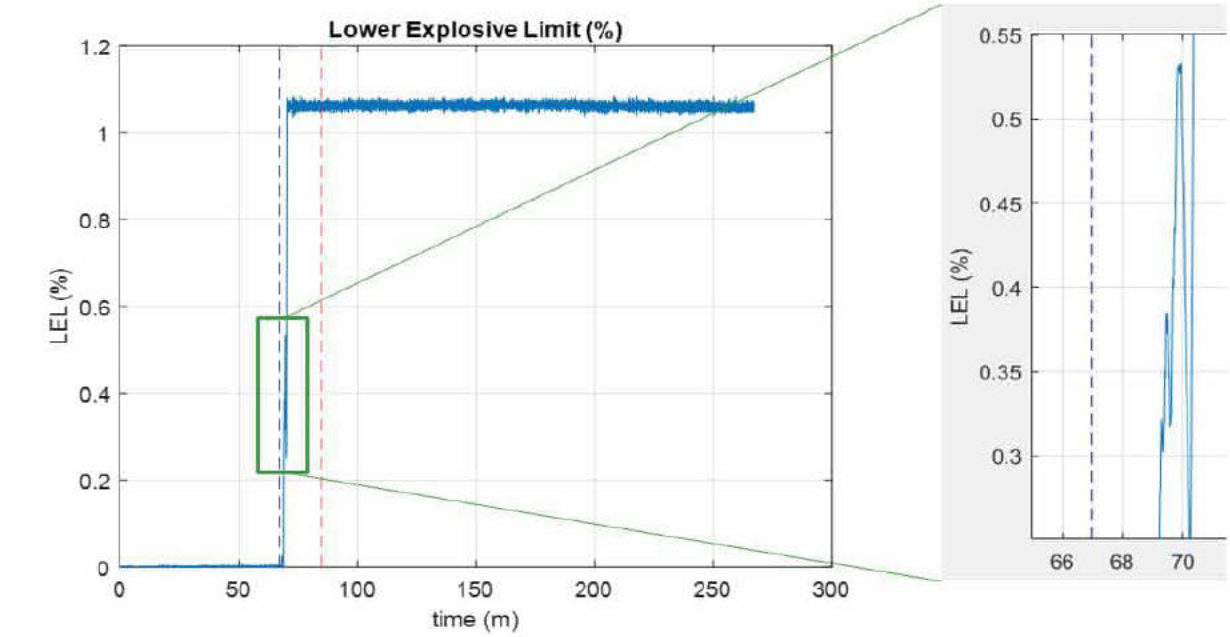


Figure 4-22 LEL during test

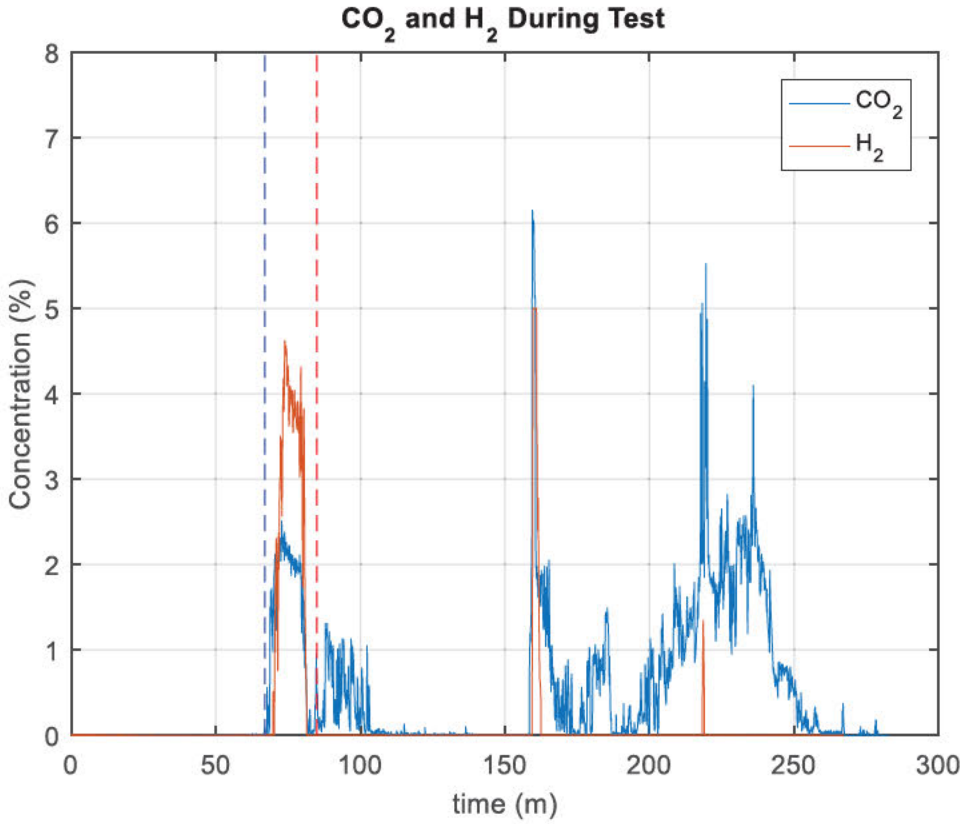


Figure 4-23 Hydrogen gas concentration during test

With hydrogen detection, one can see its presence in the offgas of the battery prior to the ignition event in Figure 4-23, exceeding the explosive limit of hydrogen at the onset of fire from the DUT. Once fire and high temperatures are observed within the system, hydrogen levels quickly drop as the gas is autoignited within the system. Initially increased CO levels were seen similarly at the onset of gas release, but, as with hydrogen, diminished greatly once steady combustion was obtained as the gas was consumed in the conflagration, as shown in Figure 4-24.

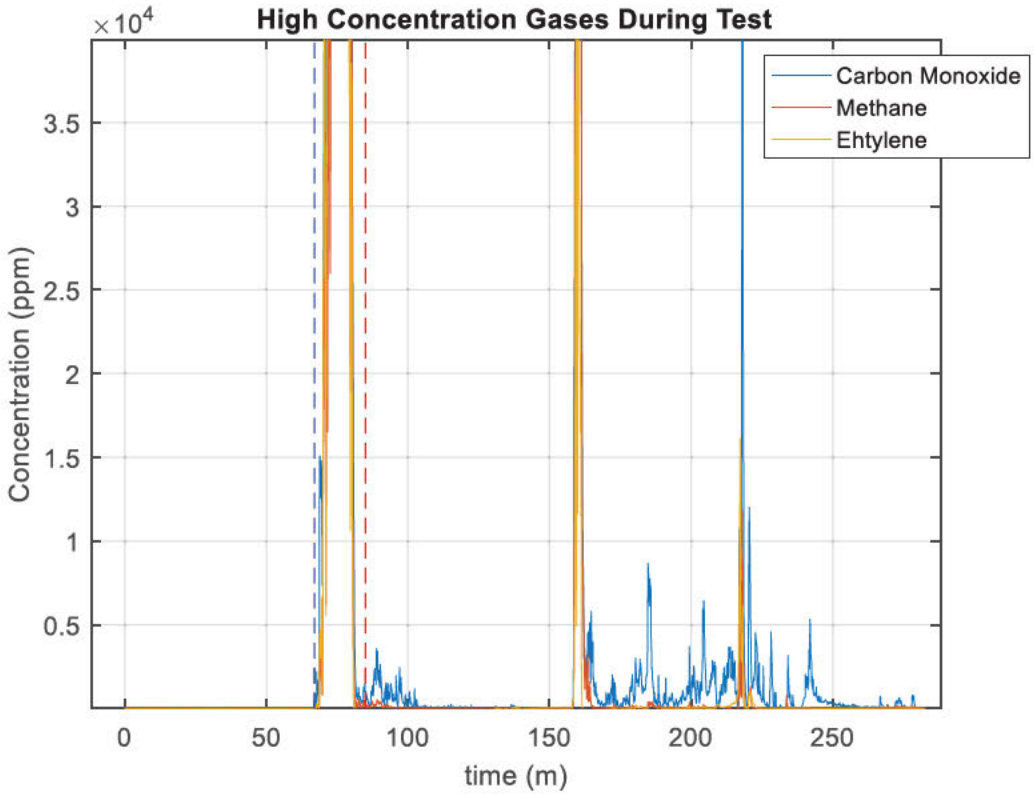


Figure 4-24 Flammable hydrocarbon gases during test

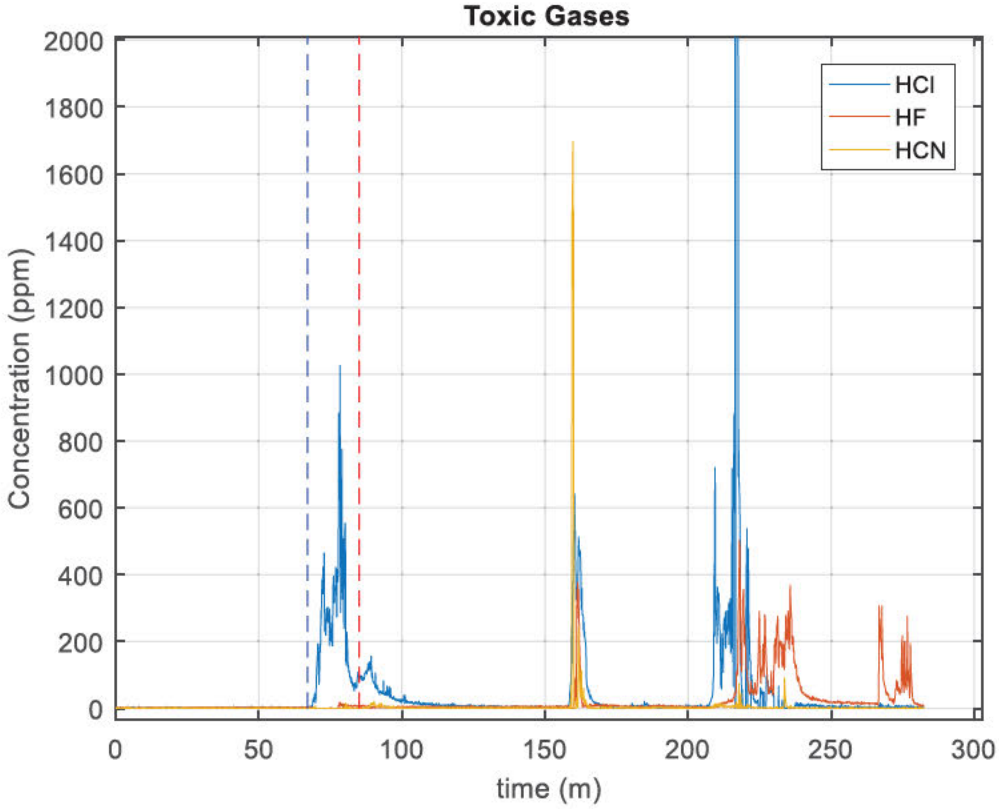


Figure 4-25 Halides and hydrogen cyanide during test

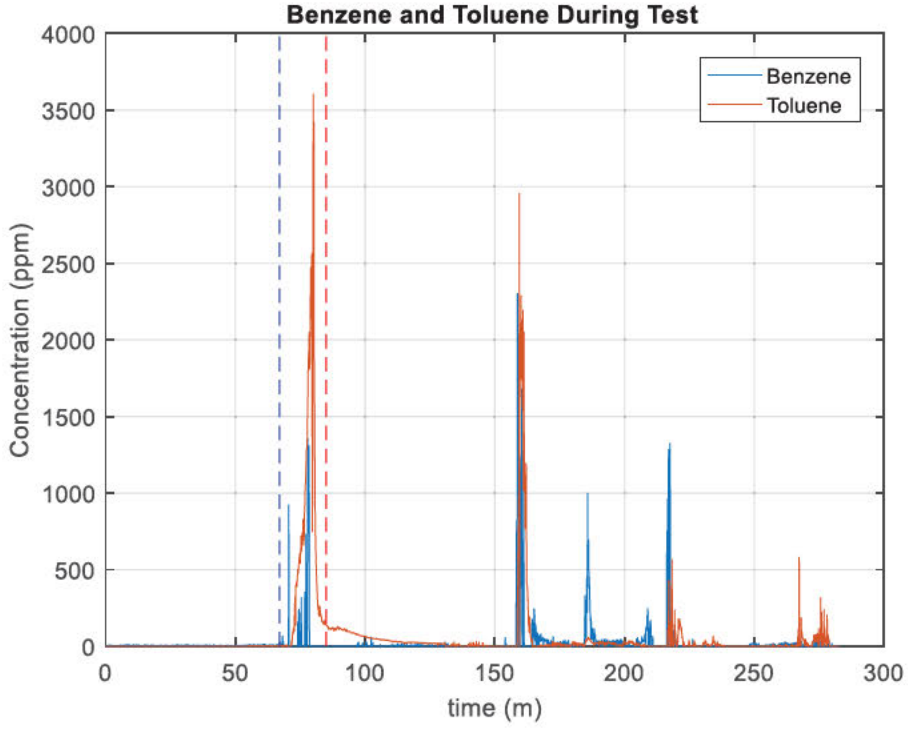


Figure 4-26 Benzene and Toluene levels during test



Figure 4-27 Several seconds after initial gas venting

Figure 4-27 above shows gas production several seconds after initial visible smoke production following the first thermal runaway. Initially 100% of gas escapes from the vent. Overtime, smoke accumulates in the area as production from the vent increases. Though most smoke is escaping through the exhaust hood overhead or out the front of the test area, some smoke lingers or sinks lower into the test area, as shown in Figure 4-28. Ultimately, as gas production within the unit continues and increases, smoke escapes from the sides and front of the unit. This gas, which also collects inside the unit, was ignited and expanded shortly after Figure 4-29 was taken. This expansion, while mild, did generate enough force to further open the front door of the unit, which had already released from the hinge following the earlier heat exposure. Following this event, most of the generated off gas was consumed via combustion as seen in Figure 4-30 Combustion seconds after the door opening deflagration Figure 4-30.

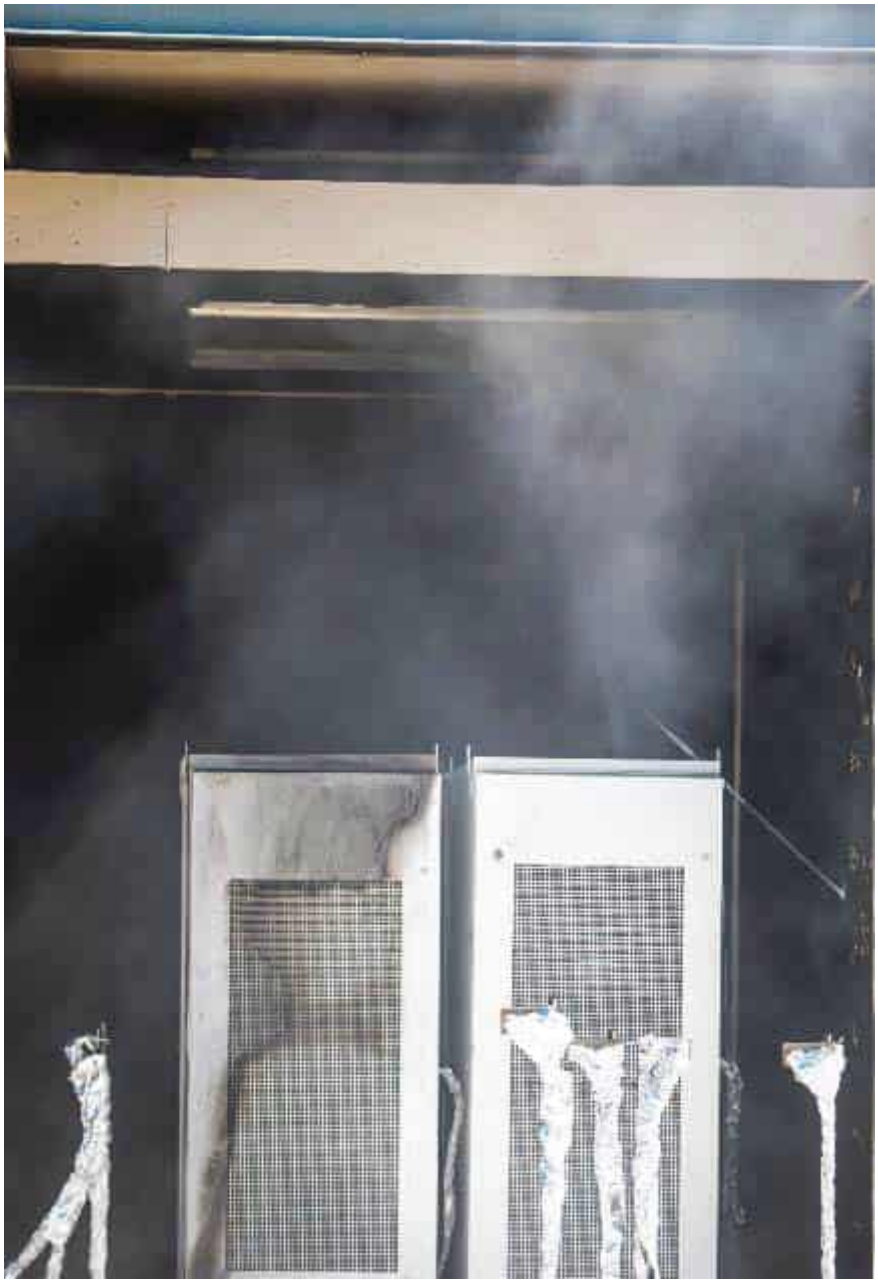


Figure 4-28 Continued gas production



Figure 4-29 Smoke and gas emanating from unit moments before deflagration



Figure 4-30 Combustion seconds after the door opening deflagration

4.1.3.1 Pressure Data

With the exception of two small deflagrations within the DUT at the onset of testing, no noticeable explosions occurred. While fire production was intense and directional, it too failed to create a dangerous pressure situation within the enclosure.

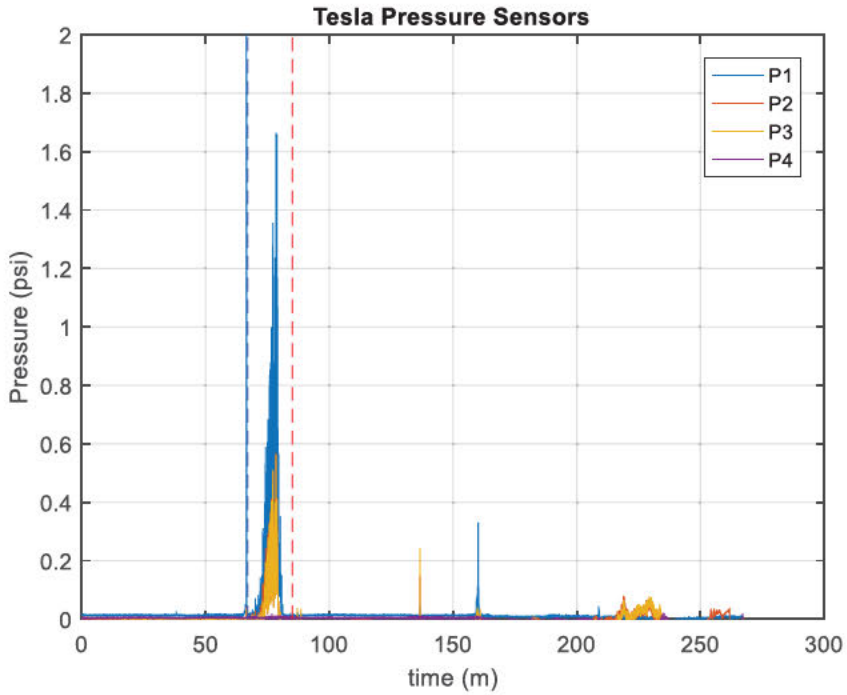


Figure 4-31 Pressure inside DUT modules

5 CONCLUSION

A single large scale, test of the Tesla Powerpack was performed. A completely live pack, consisting of 16 modules, was place in a square formation adjacent three target packs. Within the test pack, the center module was outfitted to induce thermal runaway within a number of cells ensuring a fire capable of propagating following a pre-engineered period of heat exposure. While individual cell thermal runaways are audible during the test early on, one potential deflagration exceeded the audible level of the cells failures. A second, mild overpressure event occurred which resulted in the opening of the test pack door. Following this event, a steady conflagration from the center module burned for some time before stopping. Eventually, heat transfer resulted in propagation of the event to adjacent modules, resulting in a second conflagration which lead to the complete consumption of all cells within the pack over nearly four hours.

The test showed that for outdoor installations or installations with limited adjacent exposure, pack to pack propagation for the Tesla Powerpack can be limited with sufficient spacing between packs. As one minor audible event was heard and a second deflagration event visually observed, deflagration risk is not completely absent. Test results indicate this risk would be higher for installations in confined, poorly ventilated spaces. The observed deflagration events did not result in physical damage to adjacent units or pressures that would cause damage to adjacent exposures and resulted merely in opening the test unit's door. The fire that followed the door opening proceeded to burn to completion over a nearly three and half hour period which saw one significant lull following combustion in the first

module before propagation to the next module occurred approximately an hour and a half later. That fire ultimately propagated through the entire system over the remainder of the test.

.

APPENDIX A

Gas Data at Select Times

Table 2A Gas data at select points during testing

Time		Water vapor (%)	Carbon dioxide CO2 (%)	Carbon monoxide CO	Nitrogen monoxide NO	Nitrogen dioxide NO2	Methane CH4	Ethane C2H6	Ethylene C2H4	Propane C3H8	Hydrogen chloride HCl	Hydrogen fluoride HF	Hydrogen cyanide HCN	Benzene	Toluene C7H8	Ethanol C2H6O	Methanol CH4O	Acetonitrile C2H3N	Oxygen (%)
12:25:41	1:07:46	-0.05	0.56	2198.87	0	54	218.83	64.33	308.48	19.7	3.49	1.92	1.49	0	0	0	0	0	14.26
12:25:48	1:07:53	-0.05	0.24	1305.93	0	41.88	126.51	49.62	182.55	15.46	3.21	2.5	0	18.15	0	0	0	0	15.94
12:25:55	1:08:00	-0.13	0.32	1501.53	0	42.93	146.02	50.71	220.83	15.42	8.43	2.68	0.31	0	0	0	0	0	14.23
12:26:02	1:08:07	-0.01	0.36	1646.68	0	49.32	163. 9	63.49	230.85	18.53	3.85	0	0	61.47	0	0	0	0	14.67
12:26:08	1:08:13	-0.0	0.16	977.06	0	32.13	72.48	45	149.27	11.9	4.99	0.99	0	67.13	0	0	0	0	15.64
12:26:15	1:08:20	-0.01	0.01	561.22	0	19.23	96.97	28.74	95.72	7.88	0.16	3.01	0.31	7.65	6.2	0	0	0	16.13
12:26:22	1:08:27	-0.09	0.05	341.8	0	7.83	60.05	18.59	64	5.99	0	1.71	0.69	32.89	6.61	0	0	0	16.36
12:26:29	1:08:34	-0.14	0.05	216.89	0	10.67	26.07	13.54	48.04	3.19	2.82	1.89	1.19	11.93	3.61	0	12.3	0	16.46
12:26:35	1:08:40	-0.69	0.22	1092.44	0	21.6	115.66	34.08	180.34	11.01	2.7	3.19	0	0	0	0	0	0	13.83
12:26:42	1:08:47	-0.01	1.5	14812.56	0	312.1	2334.23	408.5	4448.12	194.18	16.72	1.23	0	0	0	0	84.22	0	7.54
12:26:49	1:08:54	-0.01	1.33	15087.58	0	552.95	1707.32	425.8	3606.88	123.	22.62	0.77	0	0	0	0	85.72	0	10.15
12:26:56	1:09:01	-0.01	1.69	14495.43	0	539.35	3217.61	441.96	4702.53	217.11	30.35	0	0	0	0	0	127.13	0	7.86
12:27:02	1:09:07	-0.01	1.39	12589.42	0	531.81	1950.56	384.55	2999.3	118.31	20.46	1.99	2.81	0	3.98	0	95.28	0	11.45
12:27:09	1:09:14	-0.01	1.39	13 66.77	0	335.09	2193.74	316.5	3356.3	143.8	29.65	1.64	0	0	0	0	107.88	0	8.15
12:27:16	1:09:21	-0.01	1.72	14 95.97	0	842.23	3275.35	516.17	3569.6	193.22	29.83	0	0	0	0	245.39	143.7	0	8.68
12:27:23	1:09:28	-0.01	1.1	14388.41	0	714.76	4398.39	678.25	6582.35	200.15	45.18	0.8	3.62	0	0	0	227.38	0	7.37
12:27:29	1:09:34	-0.01	1.4	12614.77	0	386.15	2187.93	370.42	3601.0	205.93	33.47	0.14	0	0	0	157.48	136.19	0	9.38
12:27:36	1:09:41	-0.01	1.08	10939.3	0	489.61	1414.22	318.35	2242.93	105.8	28.67	0	7.52	0	11.31	0	87.34	0	11.16
12:27:43	1:09:48	-0.02	0.98	7339.49	0	348.32	792.48	218.76	827.03	77.5	17.2	2.38	0	0	0	136.24	36.53	593.21	11.83
12:27:50	1:09:55	-0.01	1.62	12983.3	0	664.94	3320.29	429.86	4179.51	109.38	30.87	0	0	0	0	313.21	128.17	0	4.68
12:27:56	1:10:01	-0.01	1.4	21615.61	0	3855.64	12346.31	1017.3	16786.65	191.65	66.78	0	0	0	0	1759.53	388.6	0	2.69
12:28:03	1:10:08	-0.01	1.81	25126.15	0	3941.13	16063.02	1437.05	24356.85	347.6	93.86	0.11	0	0	0	3110.58	532.51	0	0.98
12:38:58	1:21:03	0.54	1.18	6104.49	0	902.39	1759.2	526.93	0	277.3	143.68	8.1	5.03	0	596.4	7 9.3	489.53	2260.39	7.16
12:39:05	1:21:10	0.5	0.8	3986.06	0	621.09	720.62	389.77	0	272.38	120.97	11.09	0.86	0	489.88	877.6	389.63	1694.5	7.89
12:39:12	1:21:17	0.48	0.68	3162.58	0	563.89	658.9	291.41	0	303.04	129.09	7.63	4.33	0	441.21	1406.18	376.38	3122.82	8.44
12:39:19	1:21:24	0.56	0.45	2065.63	0	515.13	550.7	237.69	0	256.96	109.4	7. 6	0	0	381.58	1316.09	325.89	2892.12	9.14
12:39:25	1:21:30	0.51	0.32	1523.2	0	337.51	0	299.02	0	167.91	113.81	6.09	5.95	0	361.13	74.32	306.32	1969.2	9.58
12:39:32	1:21:37	0.49	0.28	1235.66	0	301.45	211.81	1 6.6	0	197.59	112.65	7.23	0	0	330.16	0	211.83	3188.99	10.09
12:39:39	1:21:44	1.33	0.08	943.86	0	136.57	432.26	209.87	0	133.42	93.08	7.96	2.1	0	279.04	408.04	266.97	582.43	10.56
12:39:46	1:21:51	1.35	0.03	669.76	0	110.14	269.26	189.44	0	115.62	96.21	8.09	0	0	240.2	0	266.99	2 92.21	11.08
12:39:52	1:21:57	0.55	0.02	710.92	0	186.01	69.38	134.71	0	144.44	92.44	9.09	1.2	0	269.44	0	140.75	2833.52	11.28
12:39:59	1:22:04	0.54	0.03	646.82	0	148.24	102.64	118.76	0	133.8	91.76	9.13	1.46	0	252.	257.49	144.19	0	11.85
12:40:06	1:22:11	1.29	0.05	528.38	0	59.32	62.8	146.12	0	87.31	6.88	6.87	0	0	197.36	195.31	82.38	60	12.13
12:40:13	1:22:18	0.52	0.18	907.73	0	157.69	155.12	106.78	0	118.95	92.83	8.65	1.81	0	230.59	308.15	119.82	0	12.24
12:40:19	1:22:24	0.45	0.03	697.79	0	105.8	214.06	95.93	0	113.26	85.59	8.25	0	0	221.79	272.45	109.29	751.91	12.63
12:40:26	1:22:31	0.48	0.3	1260.81	0	162.51	411.87	134	0	126.6	77.5	5.24	1.78	0	259.36	57.15	104.13	101.72	11.85
12:40:33	1:22:38	0.49	0.2	1050.28	0	175.46	565.44	133.48	0	122.43	78.87	5.67	0.76	0	249.75	0	62.49	1653.3	12.47
12:40:40	1:22:45	1.43	0.04	720.37	0	42.33	182.34	171.78	0	73.1	66.42	6.92	0	0	198.5	0	181.49	71	12.65
12:40:46	1:22:51	0.6	0.01	711.17	0	124.64	224.2	113.08	0	103.28	0.98	4.66	0.15	0	212.33	0	81.72	2285.63	13.15
12:40:53	1:22:58	0.4	0.01	518.14	0	107.22	373.18	91.01	0	95.3	74.21	6.36	0	0	201.42	88.55	56.23	939	13.44
12:41:00	1:23:05	0.5	0.02	632.81	0	102.12	331.98	82.02	0	93.72	68	8.26	0	0	192.42	120	90.13	1368.26	13.54
12:41:07	1:23:12	0.62	0.04	712.11	0	86.76	105.51	99.46	0	85.79	74.1	6.89	0	0	190.43	92.85	65.3	1081.63	13.33
12:41:13	1:23:18	1.43	0.02	449.89	0	0	159.91	128.06	0	59.9	52.36	7.01	0.92	0	161.79	9.04	62.75	0	13. 6
12:41:20	1:23:25	0.61	0.05	364.55	0	66.61	51.13	73.22	0	75.71	67.75	9.39	0.61	0	168.08	142.26	88.19	780.	14.25
12:41:27	1:23:32	0.5	0.06	319.16	0	57.35	107.36	65.44	0	70.94	64.27	9.58	0	0	161.1	188.05	31.48	570.13	14.46
12:41:34	1:23:39	0.5	0.01	467.92	0	53.04	176.41	68.05	0	73.2	6.41	9.14	0	0	162.29	138.24	47.82	631.4	14.26
12:41:41	1:23:46	0.51	0.06	354.5	0	62.99	65.75	66.5	0	66.7	64.51	6.56	0	0	153.81	136.35	32.41	726.3	14.55
12:41:47	1:23:52	0.56	0.05	356.23	0	61.63	102.07	64.45	0	63.1	61.72	6.22	0	0	147.53	135.54	51.9	812.76	14.63
12:41:54	1:23:59	0.5	0.06	418.42	0	66.07	117.47	67.76	0	62.29	69.67	8.15	0	0	146.83	124.27	4.2	08.46	14.43
12:42:01	1:24:06	0.48	0.0	356.16	0	48.63	244.07	59.29	0	62.79	60.77	7.97	0	0	141.59	111.62	57.75	01.75	14. 6
12:42:08	1:24:13	0.48	0.05	561.84	0	66.67	263.88	68.65	0	65.24	62.96	5.05	0	0	151.73	91.51	31.88	1074.34	14.38
13:56:19	2:38:24	-0.0	0	488.33	0	41.39	191.99	765.15	517.84	99.51	12.51	5.74	5.32	820.9	0	0	57.47	0	16.26
13:56:26	2:38:31	-0.02	1.03	4988.1	0	167.26	1161.1	827.71	468.59	127.12	17.62	6.74	0	0	0	0	0	2098.14	14.65
13:56:32	2:38:37	-0.02	1.04	13801.65	0	2056.18	3258.46	1788.82	2674.1	59.28	43.81	3.97	0	0	34.81	7631.48	8.95	12293.63	11.67
13:56:39	2:38:44	-0.01	1.2	25071.59	8258.35	275559.91	14902.94	3245.98	5843.32	0	47.63	6.44	0.61	2302.53	253.86	7631.48	174.91	12293.63	6.37
13:56:46	2:38:51	-0.01	1.09	26027.4	7887.79	414760.19	14374.63	3930.01	6051.61	0	54.6	7.72	0	2069.13	376.82	7631.48	237.56	12293.63	7.15
13:56:53	2:38:58	-0.03	1.3	49637.47	15822.95	563588.31	21765.98	4320.56	14176.96	0	77.22	3.29	15.59	1706.55	606.08	7631.48	273.75	12293.63	1.9
13:56:59	2:39:04	-0.04	1.42	38904.64	20981.35	828478.13	48810.41	1000.27	20018.93	0	71.04	5.83	35.42	1852	650.59	7631.48	332.56	12293.63	0.86
13:57:06	2:39:11	-0.1	1.95	63742.32	10864.46	1650311.38	153394.25	0	36237.59	0	118.7	0	66.75	1758.31	979.32	7631.48	686.36	12293.63	0
14:12:59	2:55:04	-0.05	0	120.9	0	0	23.42	22.08	5. 6	20.72	4.31	8.27	2.1	23.24	26.1	0	0	0	16.67
14:13:05	2:55:10	-0.01	0.04	307.31	0	0	59.01	58.16	19.74	31.1	3.01	7.58	0.52	30.71	0	0	3.63	0	16.33
14:13:12	2:55:17	0	0.06	322.96	0	0	45.31	65.29	14.87	36.05	2.94	6.95	0.84	0	0	0	0	0	16.45
14:13:19	2:55:24	-0.01	0.04	216.5	0	0	37.48	49.79	6.67	31.78	0.61	8.16	1.46	10.28	0	0	0.39	0	16.63
14:13:26	2:55:31	-0.01	0.03	177.01	0	0	28.96	48.8	3.33	31.06	0.86	7.83	0.18	23.45	0	0	0	0	16.74
14:13:32	2:55:37	-0.01	0.02	112.94	0	0	27.09	33.56	0	27.4	1.66	8.8	0	12.3	13.15	0	5.75	0	16.96
14:13:39	2:55:44	-0.06	0.01	93.59	0	0	5.22	25.02	0	23.8	2.18	9.55	0	4.7	15.9	0	21.81	0	17.05
14:13:46	2:55:51	-0.26	0.03	104.48	0	0	0	32.31	0	19.13	1	8.28	1.83	18.3	13.0	0	0	0	16.94
14:13:53	2:55:58	-0.01	0.14	364.99	0	0	54.97	51.24	9.69	30.69	4.26	6.24	1.49	16.24	0	0	0	0	16.45
14:37:58	3:20:03	-0.01	0.16	747.05	0	0	53.58	46.43	8.15	42.04	8.77	3.86	0	0	30.61	0	19.21	0	16.95
14:38:05	3:20:10	-0.01	0.55	1113.16	0	0	49.96	45.65	16.55	41.85	8.61	1.92	0	0	23.8	0	15.43	0	16.73
14:38:12	3:20:17	0	1.13	1962.42	0	0	93.75	51.98	38.26	42.52	2.24	3.65	0	0	20.63	0	0	0	16.23
14:38:18	3:20:23	0	1.04	1943.91	0	0	113.95	56.64	46.28	45.84	10.05	5.34	1.6	0	10.18	0	0	0	16.45
14:38:25	3:20:30	-0.01	0.83	1504.41	0	0	83.39	52.71	34.37	44.06	2.82	5.99	0	28.11	16.38	0	0	0	16.56
14:38:32	3:20:37	0	0.66	1276.57	0	2.69	85.13	46.05	44.14	45.53	2.74	3.85	0	0	15.73	0	9.69	0	16.43
14:38:39	3:20:44	0	0.89	1361.36	0	0	110.35	46.1	26.88	48.09	4.92	4	0	0	20.59	0	0	0	16.73
14:38:45	3:20:50	-0.01	1	1611.63	0	0	73.33	40.72	21.56	44.96	2.15	2.84	6.04	4.3	20.19	0	0	0	16.55
14:38:52	3:20:57	0	0.68	2554.16	0	0	123.06	66.92	54.16	50.85	1.55	3.65	3.34	0	15.59	0	5.53	0	16.24
14:58:01	3:40:06	3.54	3.14	71.88	190.44	0	0	66.22	18.71	141.32	0	183.19	0.73	9.77	10.1	27.44	165.7	242.8	10.44
14:58:07	3:40:12	2.8	2.16	3939.43	176.56	0	454.49	124.54	443.44	142.34	240.22	155.64	3.15	50.64	0	0	180.36	609.55	9.66
14:58:14	3:40:19	2.32	2.01	7718.5	192.4	0	657.25	183.29	732.11	131.26	278.88	118.98	6.43	27.5	0	0	0	491.79	9.57
14:58:21	3:40:26	2.12	2.09	10717.88	229.83	449.34	963.92	107.53	912.37	131.61	418.27	117.87	6.39	0	61.4	0	0	433.88	9.13
14:58:28	3:40:33	1.88	2.11	12014.38	247.42	894.05	822.62	138.66	987.96	128.6	479.37	115.37	0	0	26.58	0	0	372.8	9.16
14:58:34	3:40:39	1.34	1.86	10312.93	244.22	1156.78	1007.87	187.81	991.18	142.32	538.26	98.77	11.4	0	79.22	0	266.35	325.38	9.57
14:58:41	3:40:46	1.22	1.91	9266.5	254.26	1615.07	1046.72	252.6	1043.85	155.76	2.97	80.68	12.62	0	179.96	0	166.86	334.49	9.35
14:58:48	3:40:53	1.21	1.8	6041.56	236.89	1441.47	1185.3	293.65	931.73	171.54	0	81.38	3.02	0	137.64	0	212.35	334.4	9.56

Annex 13 US Navy fire and mitigation test program

Naval Research Laboratory
Washington, DC 20375-5320

NRL/FR/6104--14-10,262

Lithium Battery Fire Tests and Mitigation

Frederick W. Williams
Senior Scientific Staff Office
Chemistry Division

Gerard G. Back
Hughes Associates
Baltimore, Maryland

August 25, 2014

Approved for public release; distribution is unlimited.

REPORT DOCUMENTATION PAGE

Form Approved
OMB No. 0704-0188

Public reporting burden for this collection of information is estimated to average 1 hour per response, including the time for reviewing instructions, searching existing data sources, gathering and maintaining the data needed, and completing and reviewing this collection of information. Send comments regarding this burden estimate or any other aspect of this collection of information, including suggestions for reducing this burden to Department of Defense, Washington Headquarters Services, Directorate for Information Operations and Reports (0704-0188), 1215 Jefferson Davis Highway, Suite 1204, Arlington, VA 22202-4302. Respondents should be aware that notwithstanding any other provision of law, no person shall be subject to any penalty for failing to comply with a collection of information if it does not display a currently valid OMB control number. **PLEASE DO NOT RETURN YOUR FORM TO THE ABOVE ADDRESS.**

1. REPORT DATE *(DD-MM-YYYY)*	**2. REPORT TYPE**	**3. DATES COVERED** *(From - To)*
25-08-2014	Formal Report	September 2013 – December 2013

4. TITLE AND SUBTITLE

Lithium Battery Fire Tests and Mitigation

5a. CONTRACT NUMBER

5b. GRANT NUMBER

5c. PROGRAM ELEMENT NUMBER

6. AUTHOR(S)

Frederick W. Williams and Gerard G. Back*

5d. PROJECT NUMBER

5e. TASK NUMBER

5f. WORK UNIT NUMBER
61-8513-K-3-5

7. PERFORMING ORGANIZATION NAME(S) AND ADDRESS(ES)

Naval Research Laboratory
4555 Overlook Avenue, SW
Washington, DC 20375-5320

8. PERFORMING ORGANIZATION REPORT NUMBER

NRL/FR/6104--14-10,262

9. SPONSORING / MONITORING AGENCY NAME(S) AND ADDRESS(ES)

Office of Naval Research
One Liberty Center
875 North Randolph Street
Suite 1425
Arlington, VA 22203-1995

10. SPONSOR / MONITOR'S ACRONYM(S)

ONR

11. SPONSOR / MONITOR'S REPORT NUMBER(S)

12. DISTRIBUTION / AVAILABILITY STATEMENT

Approved for public release; distribution is unlimited.

13. SUPPLEMENTARY NOTES

*Hughes Associates, 3610 Commerce Drive, Suite 817, Baltimore, MD 21227

14. ABSTRACT

More than 100 lithium battery casualty tests were conducted to characterize the conditions produced during a range of both unmitigated and mitigated casualties. Both primary and secondary batteries were tested. This report summarizes the data and findings from these tests, including methods of mitigating thermal runaway of these cells under casualty conditions.

15. SUBJECT TERMS

Lithium batteries
Heat propagation
Failure
Mitigation

16. SECURITY CLASSIFICATION OF:			**17. LIMITATION OF ABSTRACT**	**18. NUMBER OF PAGES**	**19a. NAME OF RESPONSIBLE PERSON**
a. REPORT	**b. ABSTRACT**	**c. THIS PAGE**			Frederick W. Williams
Unclassified Unlimited	Unclassified Unlimited	Unclassified Unlimited	Unclassified Unlimited	68	**19b. TELEPHONE NUMBER** *(include area code)* [redacted]

Standard Form 298 (Rev. 8-98)
Prescribed by ANSI Std. Z39.18

This page
intentionally
left blank

CONTENTS

ACRONYMS v

EXECUTIVE SUMMARY E-1

1 INTRODUCTION 1

2 DEFINITIONS 1

3 BATTERY TUTORIAL 2

3.1 General 2
3.2 Chemistries 3
3.3 Cell Construction/Configuration 5
3.4 Battery Packs 6

4 BATTERY CASUALTY CHARACTERIZATION TESTS — OVERVIEW 7

5 COMMERCIALLY AVAILABLE BATTERY/CELL DESCRIPTIONS 8

6 REACTION DESCRIPTIONS (SINGLE CELL) 10

6.1 Initiating Events 10
6.2 General Types of Casualties 10
6.3 Observed Cell Casualties 11
6.4 SOC Effects on Reaction Types (Li-Ion Only) 15

7 REACTION PRODUCTS TESTING AND RESULTS (SINGLE CELL) 18

7.1 Reaction Products Test Description 18
7.2 Reaction Products for Cells at 100% SOC 18
7.3 SOC Effects on Reaction Products 23
7.4 Reaction Products at Low Oxygen Levels 23
7.5 Acid Gas Production 23
7.6 Gas Volume Production 23

8 HEAT RELEASE RATE TESTS AND RESULTS (SINGLE CELL) 24

8.1 Heat Release Rate Test Description 24
8.2 Heat Release Rate Test Results 25

9 HEAT RELEASE RATE TESTS AND RESULTS (GROUPS OF CELLS) 27

9.1 Burning Characteristics of Commercially Available Battery Packs/Modules 27
9.2 SOC Effects on Combustion Energy Released 32
9.3 Combustion Energy as a Function of Electrical Energy 33
9.4 HRRs of Bulk Storage Configurations 34

10 SAFE STORAGE AND CASUALTY MITIGATION OF MULTICELL LITHIUM BATTERIES 35

10.1 Battery Storage Locker (BSL) Development History 35

10.2 Detection System Development History 37
10.3 Suppression System Development History 37
10.4 Mitigation Test Results 39
10.5 Suppression Summary 44
11 UNMITIGATED BATTERY PACK REACTIONS INSIDE A PRESSURE VESSEL 44
11.1 BSL Worst-Case Thermal Conditions 45
11.2 Gas Production 49
12 BATTERY CASUALTY CLASSIFICATION 49
13 SUMMARY 50
REFERENCES 52
APPENDIX — Video Clips from Lithium Single Cell and Multicell Battery Casualties 53

ACRONYMS

Ah	Ampere Hours
BCS	Battery Charging Station
BCCT	Battery Casualty Characterization Tests
BLEVE	Boiling Liquid Expanding Vapor Explosion
BSC	Battery Stowage Compartment
BSL	Battery Storage Locker
C	Celsius
CAS	Chemical Abstract Service
CBD	Chesapeake Bay Detachment
COTS	Commercial Off The Shelf
F	Fahrenheit
ft	Feet
FTIR	Fourier Transform Infrared Spectroscopy
GC-MS/IR	Gas Chromatography–Mass Spectroscopy/Infrared
HMS	Hazard Mitigation Suite
HMT	Hazard Mitigation Test
HRR	Heat Release Rate
HSD	Heat Sensing Device
kW	Kilowatts
kWh	Kilowatt Hours
LBCMS	Lithium Battery Casualty Mitigation System for Lithium Battery Fires
LEL	Lower Explosive Limit
MCE	Maximum Credible Event
MW	Megawatts
NRL	Naval Research Laboratory
PHA	Preliminary Hazard Analysis
PHRR	Peak Heat Release Rate
SHA	System Hazard Analysis
SOC	State of Charge
VOC	Volatile Organic Compound

This page
intentionally
left blank

EXECUTIVE SUMMARY

Lithium batteries can pose a significant hazard during an acute casualty. Potential causes of such casualties include an electrical or mechanical short, overcharging the battery, exposure to excess heat, physical abuse, or spontaneous failure due to a latent defect. During this reaction, the battery may violently vent or rupture, releasing combustible, toxic, and/or acidic vapors and aerosols, and/or incandescent metal particles or carbon. These may result in a major fire or explosion and release of large quantities of toxic and acidic gases. More than 100 battery casualty and mitigation tests were conducted from 2009 to 2012 by the Naval Research Laboratory (NRL) aboard the research test ship ex-USS *Shadwell*. This report summarizes the results of these tests based on specific battery chemistries.

Primary and secondary lithium batteries with a range of chemistries, form factors, and capacities were tested. Lithium batteries may be made up of layers of anode (copper foil coated with a specialty carbon) and cathode (typically aluminum foil coated with a lithiated metal oxide or phosphate) separated by a microporous polyolefin film referred to as a separator. An electrolyte composed of an organic solvent and dissolved lithium salt provides the medium for lithium ion transport. A cell is constructed by stacking alternating layers of electrodes (typical for high-rate capability prismatic cells), or by winding long strips of electrodes into a "jelly roll" configuration (typical for cylindrical cells).

The lithium battery chemistries currently used throughout the industry produce cell voltages ranging from 3.2 to 4.2 V. The capacity of the cell (measured in ampere-hours) varies widely and is a function of the number of layers of electrodes in a prismatic cell or the length of the strip in a cylindrical cell. The commercial industry combines a large number of cells wired together in series and in parallel to produce battery packs and modules with a desired voltage and capacity. These packs can contain hundreds of cells.

NRL battery casualty tests were conducted on individual cells and on a variety of battery packs. The cell chemistries studied are $Li/LiCoO_2$, $Li/Li_{0.5}CoO_2$, $Li/SOCl_2$, $Li/LiFePO_4$, Li/CF_x, Li/MnO_2, Li/SO_2Cl_2-$SOCl_2$, and $Li/NiCoAlO_4$ All tests reported here were conducted on commercially available battery cells.

Based on the tests conducted, single cell reactions can be described using six terms: vent, smoker, flare, burner, explosive, and fireball. Smaller, lower capacity solid cathode cells typically vent and/or smoke and medium to higher capacity cells (specifically the oxyhalides) either ignite and burn or explode. Intuitively, one expects the type of reaction to be a function of the amount of energy contained in the cell at the time of the event. Therefore, the type of reaction should be a function of both the battery capacity and the state of charge (SOC) at the time of the event. Based on a very limited data set (not statistically valid), it appears that the threshold between a venting and a flaming reaction lies in the 10 to 20 watt-hour range. Battery pack configurations can significantly alter these single cell results.

The reaction products measured when a cell vents (without ignition) are electrolyte constituents, such as carbonates or oxyhalides. These are organic solvent gases and aerosols with flammable constituents and the potential to ignite. In some instances, the carbonates break down upon release to produce high levels of CO_2, CO, and a range of hydrocarbons. When a cell burns in a casualty, the electrolyte burns fairly efficiently, producing primarily CO_2 as the by-product. Acid gas can also be produced and is directly related to cell chemistry (and appears to be related to cell capacity): cells that

contain sulfur (e.g., $Li/SOCl_2$) produce sulfuric acid, cells that contain fluorine (e.g., $LiPF_6$) produce hydrofluoric acid, and cells that contain chlorine (e.g., $Li/SOCl_2$) produce hydrochloric acid. There is not enough data to develop a quantitative relationship between cell energy and acid gas production, but for a given cell chemistry, the amount of acid gas produced is expected to be directly proportional to the cell energy.

The mean heat release rate (HRR) for the small commercial cells (such as the AA size) is typically on the order of 10 kW. The larger commercial cells can produce mean heat release rates approaching 100 kW. The more reactive cell chemistries (i.e., $Li/SOCl_2$ and Li/SO_2Cl_2-$SOCl_2$) produce violent/explosive type reactions approaching 500 kW.

Tests conducted with multiple-cell packs demonstrate that single cell data for a specific cell type may not be indicative of the reactions of battery packs made up of those same cells: single cell tests and battery pack tests yielded different types of reactions. Specifically, except for the iron phosphate cells, all the packs/modules produced burning reactions, while many of the single cells only vented and never caught fire. This difference was attributed to the greater amount of electrical energy contained in a pack that could contribute to the severity of the reaction and provide an ignition source. In addition, during almost every unmitigated pack/module test, all the cells reacted and the casing materials were completely consumed.

The heat release rate of the multicell packs was a function of the propagation rate from cell to cell within the battery pack and the contribution of the battery pack casing material. The propagation rate from cell to cell ranged from seconds to minutes depending of the type of cell and the battery pack configuration. Some of the smaller packs were consumed in a few minutes while some of the larger packs reacted/burned for over an hour.

Combustion energy of a battery pack was shown to be proportional to the electrical energy contained in the pack after adjusting for the contribution of the packaging material. Some battery packs have metal casings that provide little if any contribution to the fire, whereas some packs have thick hard plastic casings that provide a significant contribution to the fire. After adjusting the combustion energies to account for the case material, the combustion energy is typically about six times the electrical energy potential of the battery.

With respect to suppression, the results from these tests demonstrate that it is virtually impossible to stop a reaction within a lithium cell once it has begun. Consequently, the objective of a fire suppression system should be to thermally manage the conditions in the space and try to cool adjacent cells in an attempt to slow or prevent cell-to-cell propagation. Suppression of the packaging material is also desired. Water appears to be the best suppression agent.

The ability of a suppression system to prevent secondary cell reactions within a complex battery pack is, in part, a function of the openness of the battery pack housing. If the battery housing is fairly open, a fast acting suppression system may be able to reduce the exposures to the adjacent cells within the housing to below the critical temperature value (below the level at which adjacent cells react). The best way to achieve this objective is to rapidly submerse the battery pack in water. The severity of the initial reaction, the proximity of the adjacent cells, and the vulnerability of adjacent cells are variables associated with achieving this performance objective. If the cells are contained within a closed housing (air tight, water tight, or even just a fairly tight enclosure), the suppression system will not be able to contain the reaction to the initial cell, and in most scenarios, all the cells within the pack will react, even if submersed under water. Battery pack submersion does prevent the spread to other packs.

A water spray/sprinkler system (versus a flooding system) has the ability to thermally manage the conditions around the pack of origin, but is unlikely to be effective in preventing the complete consumption/reaction of that initial pack. In some instances, passive thermal barriers between battery packs combined with the thermal management provided by a water spray/sprinkler system is the best approach to mitigate the overall hazard/risk. Two such configurations of a mitigation suite, called the Lithium Battery Casualty Mitigation System, were developed and tested.

There are currently no established criteria for classifying the hazards associated with a lithium battery casualty. Although the data presented here and historical data show that lithium batteries have the potential to ignite and cause a fire, the primary hazard associated with a battery casualty appears to be the gases produced during the reaction. These gases have been determined to be toxic and/or flammable. The concentration of toxic and/or flammable gases produced is a function of the battery chemistry, the number of cells involved in the reaction, the type of reaction (i.e., burning or venting), and the size of the compartment in which the reaction occurs. Since copious amounts of gases are produced during the reaction of larger batteries and battery packs, it must be assumed that any battery casualty will render the storage compartment untenable for unprotected personnel (personnel not wearing a breathing apparatus). During a venting scenario, the resulting mixture could be in the flammable range. A delayed ignition of these gases could produce a large fireball and overpressures that could produce structural damage and additional battery casualties. The consequences from such a scenario could be catastrophic.

The results presented here provide a general understanding of the hazards associated with lithium batteries and approaches to minimize the risk. The reaction characteristics and lessons learned provide a starting point for the development of a database that can be used both to conduct analytical assessments of lithium battery hazards and to develop battery packs for future applications.

This page
intentionally
left blank

LITHIUM BATTERY FIRE TESTS AND MITIGATION

1 INTRODUCTION

Lithium batteries can pose a significant hazard during an acute casualty. Potential causes for such casualties include an electrical or mechanical short, overcharging the battery, exposure to excess heat, physical abuse, or spontaneous failure due to latent defect. During this reaction, the battery may violently vent or rupture, releasing combustible, toxic, and/or acidic vapors and aerosols, and/or incandescent metal particles or carbon. These may result in a major fire or explosion and release of large quantities of toxic and acidic gases.

The Naval Research Laboratory (NRL) recently participated in several major research programs initiated to characterize and mitigate lithium battery fire hazards. The overall goal is to be able to safely handle, store, and charge this class of energy sources. More than 100 battery casualty tests were conducted between 2009 and 2012 to characterize the conditions produced during a range of both unmitigated and mitigated casualties, and to evaluate different containment and suppression systems. This report summarizes the results of these tests. The discussion is divided into data for single cells and data for groupings of cells that comprise what is termed a battery pack. Video clips of some of the tests are presented in the Appendix (on enclosed DVD).

2 DEFINITIONS

The following definitions apply to this report:

Battery: A power source designed to meet the specific needs of an application (voltage, current, power output/duration), containing one or more cells.

Battery pack: A group of cells permanently wired together.

Capacity: The quantity of electrical charge delivered by a battery under specific conditions. It is usually expressed in ampere-hours (Ah).

Casing: The outer shell of a cell or a battery.

Casualty: A scenario consisting of one or more cell reactions leading to a cell failure.

Cell: The smallest individual constituent energy storage unit of a battery.

Electrolyte: Any substance containing free ions that make the substance electrically (ionically) conductive. Most of the electrolytes assessed in this report are liquid and are mixtures of covalent organic and inorganic solvents containing dissolved ionic lithium salts. Where the electrolytes are not organic esters/carbonate mixtures, they are inorganic oxyhalides, usually with sulfur components.

Hazard: An existing or potential condition that can result in a mishap.

Housing: A structure that surrounds the battery pack that is an integral part of the battery. The battery casing and battery housing may be synonymous terms.

Manuscript approved June 17, 2014.

Large form cell: A single cell larger in form than two "D" size cells.

Lithium battery: For the purpose of this report, lithium batteries include all cells or batteries in which lithium metal, any lithium alloy, or any form of lithium in a supporting matrix serves as the active anodic component.

Lithium-ion battery: Lithium-ion batteries are comprised of cells that use lithium intercalation compounds as the positive and negative electrodes. As the battery is cycled, lithium ions (Li+) exchange between the positive and negative electrodes. Lithium-ion batteries are a subset of "lithium battery."

Primary battery: A battery designed to be discharged only once, i.e., not designed to be recharged; also called a nonrechargeable battery.

Reaction: A cell-level event resulting from one of the following: electrical abuse (shorting or overcharging), thermal abuse, or physical damage.

Secondary battery: A battery in which the electrochemical reaction is thermodynamically reversible and is designed to be recharged in use. Common secondary batteries include the lead-acid, nickel-cadmium, and lithium-ion batteries common to many consumer products. A secondary battery may also be referred to as a rechargeable battery.

Thermal runaway: An internal reaction within a cell or battery that generates enough heat to cause the cell to fail in one or more of the following modes: vent aerosols or smoke, jet incandescent particles, jet fire, explode, or ignite/catch fire. The intrinsic nature of thermal runaway is thermal acceleration of nearby cells to form a cascading event.

3 BATTERY TUTORIAL

3.1 General

Lithium batteries are a family of cells that consist of a lithium anode (negative terminal) and a variety of different types of cathodes (positive terminal) and electrolytes [1]. Lithium batteries are grouped into two general categories: primary and secondary batteries. Primary lithium batteries are comprised of single-use cells containing metallic lithium anodes and cannot be recharged. Secondary lithium-ion batteries are comprised of rechargeable cells containing an intercalated lithium compound for the anode and cathode. In this report, nonrechargeable (primary) lithium batteries are referred to as "lithium primary" batteries (often referred to as simply "lithium" batteries in the battery industry), and rechargeable (secondary) lithium batteries are "lithium-ion" or "Li-ion" batteries.

Lithium primary batteries can be classified into several categories based on the type of electrolyte (or solvent) and cathode material used. These classifications include soluble-cathode cells, solid-electrolyte cells, and solid-cathode cells.

Soluble-cathode cells use liquid or gaseous cathode materials, such as sulfur dioxide (SO_2) or thionyl chloride ($SOCl_2$), that dissolve in the electrolyte or are the electrolyte solvent. These soluble cathode lithium cells are used for low to high discharge rate applications. The high-rate designs, using large electrode surface areas, are noted for their high power density and are capable of delivering the highest current densities of any active primary cell.

Solid-electrolyte cells are noted for their extremely long storage life, in excess of 20 years, but are capable of only low-rate discharge in the microampere range. They are used in applications such as

memory backup, cardiac pacemakers, and similar equipment where current requirements are low but long life is critical. This battery type was not evaluated in the programs reported here.

Solid-cathode cells are the most commonly used type of lithium primary cell. They are designed, generally, for low- to medium-rate applications such as memory backup, security devices, portable electronic equipment, photographic equipment, watches, calculators, and small lights. Although a number of different solid-cathode lithium batteries have been developed, the lithium/manganese dioxide (Li/MnO_2) battery was one of the first to be used commercially and is still the most popular. It is relatively inexpensive, has excellent shelf life, has good high-rate and low-temperature performance, and is available in coin and cylindrical cells. The lithium/carbon monofluoride ($Li(CF)_n$) battery is another of the early solid-cathode batteries and is attractive because of its high theoretical capacity and flat discharge characteristics. It is also manufactured in coin, cylindrical, and prismatic configurations. The higher cost of polycarbon monofluoride has affected the commercial potential of this system but it is finding use in biomedical, military, and space applications. The construction of these primary cells is similar to that of the secondary (lithium-ion) cells described next.

Secondary/lithium-ion batteries are used across a range of portable applications ranging from consumer electronics to medical technology to military systems. They are characterized by medium to high energy density and are being developed in a variety of chemistries. In a lithium-ion cell, layers of anode (copper foil coated with a specialty carbon) and cathode (typically aluminum foil coated with a lithiated metal oxide or phosphate) are separated by a microporous polyolefin film referred to as a separator. An electrolyte composed of an organic solvent and dissolved lithium salt provides the medium for lithium ion transport. A cell can be constructed by stacking alternating layers of electrodes (typical for high-rate capability prismatic cells), or by winding long strips of electrodes into a “jelly roll” configuration (typical for cylindrical cells). Lithium ions move from the anode to the cathode during discharge and are intercalated into the cathode (i.e., inserted into voids in the crystallographic structure). The ions reverse direction during charging, as shown in Fig. 1.

3.2 Chemistries

The most common type of lithium-ion cell contains an intercalated lithium (lithium alloy) anode and lithiated cobalt dioxide as cathode. These batteries are inexpensive and have medium to high energy densities, but can self-discharge (begin a thermal runaway reaction) at temperatures in the 60 °C range. Since lithium ions are intercalated into host materials during charge or discharge, there is no free lithium metal within a lithium-ion cell. Consequently, if a cell ignites due to external flame impingement or due to an internal short, “metal fire” (e.g., lithium, sodium, or magnesium) suppression equipment and techniques are neither appropriate nor cost effective for controlling the fire.

Other chemistries, principally primary chemistries, that are being actively pursued/developed by the battery industry include thionyl chloride, sulfuryl chloride, sulfur dioxide, carbon monofluoride, and manganese dioxide. These cells have the highest energy densities (about twice that of Li-ion cells) but are more expensive based on total deliverable energy and useable life. The solid-electrode group of batteries is comprised of “specialty” type cells used primarily in the medical profession. These cells include silver, copper, iron, and lead (oxides and sulfides) chemistries. These cells are highly reliable, very expensive, and have limited current capacities. The automotive industry is aggressively pursuing higher energy density chemistries that may eventually be adopted for the commodity type usages.

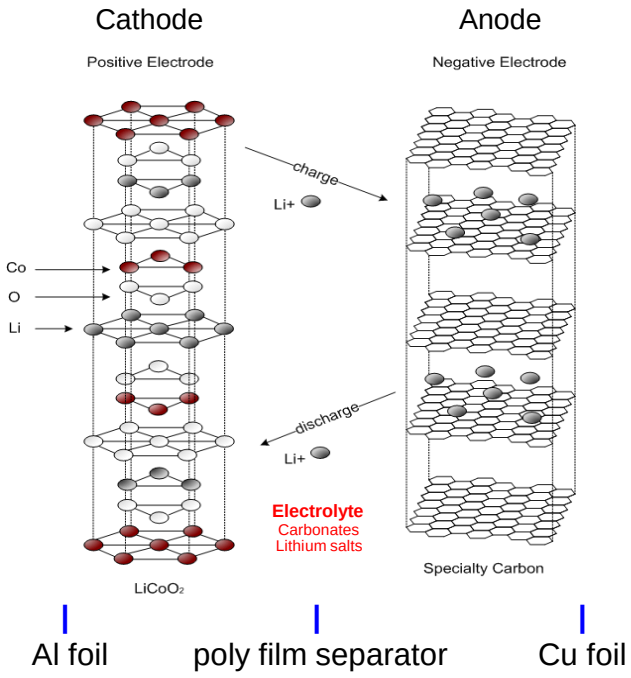


Fig. 1 — Generalized Li-ion cell components/configuration

The electrolyte in a lithium-ion cell is typically a mixture of a lithium salt dissolved in organic carbonates such as ethylene carbonate or diethyl carbonate. The compounds vary depending upon desired cell properties. For example, a cell designed for low-temperature applications will likely contain a lower viscosity electrolyte than one optimized for room temperature applications.

The flammability characteristics of common carbonates used in lithium cell electrolytes in a neat state are provided in Table 1. These characteristics apply only to liquefied carbonates. During a cell venting scenario, when the electrolyte may be released as an aerosol with partial decomposition to lower molecular weight species, both the flash point and the auto-ignition temperature may be lower.

The lithium-ion electrolyte solution contains solvated lithium ions, which are provided by lithium salts, most commonly lithium hexafluorophosphate ($LiPF_6$). At elevated temperatures, $LiPF_6$ decomposes to release hydrofluoric acid (HF) during a battery casualty if the resulting materials are exposed to moisture. The higher energy density primary cells also produce acid gases (sulfuric and hydrochloric) during high-temperature reaction processes if exposed to moisture in the air.

Table 1 — Flammability Characteristics of Typical Electrolyte Compounds

Compound	CAS Registry Number	Molecular Formula	Flash Point	Boiling Point	Auto-Ignition Temperature	Heat of Combustion
Diethyl Carbonate (DEC)	105-58-8	$C_5H_{10}O_3$	25°C 77°F	126°C 259°F	445°C 833°F	−20.9 kJ/ml −5.0 kcal/ml
Dimethyl Carbonate (DMC)	616-38-6	$C_3H_6O_3$	18°C 64°F	91°C 195°F	458°C 856°F	−15.9 kJ/ml −3.8 kcal/ml
Ethylene Carbonate (EC)	96-49-1	$C_3H_4O_3$	145°C 293°F	248°C 478°F	465°C 869°F	−17.2 kJ/ml −4.1 kcal/ml
Ethyl Methyl Carbonate (EMC)	623-53-0	$C_4H_8O_3$	25°C 77°F	107°C 225°F	440°C 824°F	−19.2 kJ/ml −4.6 kcal/ml
Propylene Carbonate (PC)	108-32-7	$C_4H_6O_3$	135°C 275°F	242°C 468°F	455°C 851°F	−20.1 kJ/ml −4.8 kcal/ml
Tetrahydrofuran (THF)	109-99-9	C_4H_8O	−14°C 6°F	65°C 149°F	321°C 610°F	−31.2 kJ/ml −7.5 kcal/ml
Dimethylether	115-10-6	C_2H_6O	−41°C −42°F	−23.7°C 11°F	350°C 662°F	−51.3 kJ/ml −12.3 kcal/ml
1,3-Dioxolane	646-06-0	$C_3H_6O_2$	2°C 35°F	75°C 167°F	?	−24.4 kJ/ml −5.8 kcal/ml
1,2-Dimethoxyethane (Ethylene Glycol)	110-11-4	$C_4H_{10}O_2$	104°C 232°F	83°C 197.5°F	400°C 752°F	−21.3 kJ/ml −5.1 kcal/ml
Acetonitrile (Methyl Cyanide)	75-05-8	CH_3CN	6°C 42°F	81.6°C 179°F	524°C 975°F	−23.9 kJ/ml −5.7 kcal/ml
Thionyl Chloride	7719-09-7	$SOCl_2$	?	78.8°C 174°F	?	?

Source: [redacted]

3.3 Cell Construction/Configuration

There are three basic lithium battery cell designs: coin shaped, cylindrical, and prismatic (Fig. 2). Coin shaped cells (sometimes referred to as button cells) are low-current cells used in watches, calculators, and remote keyless entry systems for cars, to name a few examples. They are available in many sizes and capacities, with a common variety being the 3 V manganese variety. Cylindrical cells incorporate the same design parameters that have been the standard for alkaline cells for years (A, AA, AAA, C, and D cells) with the option of spiral or bobbin internal construction. Prismatic cells include standard 9 V battery designs. A prismatic variety referred to as “pouch” cells are typically used in laptop computers.

Cell construction is a major variable affecting the severity of a battery mishap. The severity of a reaction is in part related to the buildup and release of pressure from inside the cell. Some cells have pressure relief vents and these typically produce less severe reactions than unvented cells that contain the pressure.



Fig. 2 — Typical cell designs. Top row: prismatic, cylindrical. Middle row: pouch (prismatic). Bottom row: coin.

3.4 Battery Packs

A lithium battery pack is made from two or more individual cells packaged together. The cells are connected/wired together to achieve a desired voltage and capacity. Connecting cells in parallel increases pack ampere-hour and discharge capacity, while connecting cells in series increases pack voltage. The cylindrical cell form factor 18650 is the “workhorse” of the lithium-ion battery industry and is used in a majority of commercially available battery packs. The “18” refers to the diameter of the cell and the “65” refers to the length of the cell, both in millimeters. Examples of battery packs produced with cylindrical cells are shown in Fig. 3.

In large format battery packs, cells may be connected together in series and/or in parallel to form battery modules, which may then be connected in series and/or in parallel to make larger battery packs to meet desired voltage and capacity requirements. Modules are used to facilitate different configurations and easy replacement of faulty portions of large battery packs (a module is a Lowest Replaceable Unit, LRU). Large format battery pack architecture can be significantly more complex than small consumer electronics battery packs which typically contain series connected elements consisting of two or more parallel connected cells. Many larger battery packs have built-in circuitry used to monitor charging and control the discharge cycle of the battery (i.e., shut down the battery when the charge level drops below a specified value). These large battery packs are used in the automotive industry.



Fig. 3 — Example battery packs

4 BATTERY CASUALTY CHARACTERIZATION TESTS — OVERVIEW

For U.S. Navy applications, the Navy requires that all lithium batteries are reviewed and formally approved in the context of each application. The Navy has adopted requirements and protocols for certifying lithium batteries that include Preliminary Hazard Analysis (PHA), Battery Casualty Characterization Tests (BCCT), Hazard Mitigation Tests (HMT), and a final System Hazard Analysis (SHA).

The BCCTs are typically conducted in two phases: single cell tests and all-up battery pack tests. The rationale is to quantify the reaction on a smaller, manageable scale, then increase the size and severity once the magnitude of the reaction has been bounded. A summary of the types of tests and associated parameters that make up the BCCT is provided below.

Battery casualty initiation: A key parameter of the BCCT is the method used to initiate the battery casualty. The method(s) used during the BCCT is typically determined in the PHA. For example, the most likely and most severe scenario for a lithium-ion battery results from being overcharged. Other potential initiating events include an internal manufacturer's defect, physical damage, and an external heat source.

Reaction products analysis: Tests are conducted to characterize the products released during the cell/battery casualty. A comprehensive approach is required that includes an initial qualitative study to assess the nature of the expected chemical species and relative concentration ranges. Ultimately, the products are assessed in terms of acidity, corrosiveness, toxicity, and aerosol particle composition. Real-time analysis is done via electrochemical sensors and optical methods (in situ Fourier transform infrared spectroscopy, FTIR). Samples are also collected using gas sampling canisters, sorbent tubes, and impingers. These grab samples are analyzed using a gas chromatography–mass spectrometry/infrared (GC-MS/IR) technique.

Heat release rate (HRR): The heat release rate is determined for each type/model of cell and battery. The HRR may determine whether there will be a cascading effect in a casualty. A hood calorimeter is used to make these measurements through an assessment of combustion products. This may also be done in an apparatus that allows the measurement of oxygen consumption during the casualty. When

measuring the HRR for a specific battery, in most cases there is an acceleration of the HRR, termed the peak heat release rate, PHRR.

Thermal exposures: The thermal exposure produced during the casualty (near field) is measured using both radiometers and calorimeters. These measurements provide information on exposures to items intimate with the casualty and provide an indication of the likelihood of a cascading event (reactions of adjacent batteries). “Mock collateral casualty exposure items” may be used in addition to radiometers and calorimeters to determine significant heating of local items to a casualty event.

Smoke generation: The amount of smoke/aerosols produced during the casualty is determined using an optical density meter. The measurement is typically made in the stack (hood exhaust ductwork) just below the gas sampling probe and in the test compartment.

Pressure transients: Pressure transients are recorded during these tests (both near field and far field). The pressure release may be a moderate and sustained pressure rise from low-order combustion to deflagration of battery components internal to the cell(s). The pressure release may also be sudden and abrupt stemming from a sudden failure of pressure containment of battery cell cases or battery pressure containment vessels.

Fragmentation of the cell and/or battery casing: Debris may be ejected from the article under test at high velocities. The location of flying debris (a debris map) is documented after each test. This debris may include small to large portions of the cell and/or battery casings, battery enclosures, or pressure vessel housings. Video recorded during each test is analyzed (frame by frame) to assess whether the debris is burning/flaming while it is ejected. Alternate measurement techniques include witness plates to capture the debris thrown or impact sensors. Burning incandescent debris provides a secondary ignition source that can result in fire spread and/or other battery casualties.

5 COMMERCIALLY AVAILABLE BATTERY/CELL DESCRIPTIONS

The battery cells that were tested during these programs are described in Tables 2 through 5. All are commercially available cells. A number of these cells were assessed for heat release rate only in a battery pack configuration, not individually.

Table 2 — A/AA and Pouch-size Commercially Available Cells Tested

Cell Manufacturer	**A**	**B-1**	**B-2**	**C-1**	**D-1**	**E**
Type	Secondary	Secondary	Primary	Secondary	Secondary	Secondary
Form Factor	Pouch cell	AA Cell	AA Cell	18650	18650	18650
Chemistry	$Li/LiCoO_2$	$Li/Li_{0.5}CoO_2$	$Li/SOCl_2$	$Li/LiFePO_4$	$Li/LiFePO_4$	$Li/Li_{0.5}CoO_2$
Voltage	3.7 V	3.7 V	3.6 V	3.3 V	3.2 V	3.7 V
Capacity	3.3 Ah	0.16 Ah	2.0 Ah	1.1 Ah	1.5 Ah	2.2 Ah
Energy	12.2 Wh	0.6 Wh	7.2 Wh	3.6 Wh	4.8 Wh	8.1 Wh
Mass	95 g	19 g	18 g	39 g	46 g	48 g

Table 3 — C-size Commercially Available Cells Tested

Cell Manufacturer	**F**	**H-1**	**D-2**	**C-2**
Type	Secondary	Primary	Secondary	Secondary
Form Factor	C Cell	5/4 C Cell	5/4 C Cell	5/4 C Cell
Chemistry	Li/CF_x	Li/MnO_2	$Li/LiFePO_4$	$Li/LiFePO_4$
Voltage	3.0 V	3.3 V	3.2 V	3.3 V
Capacity	5.0 Ah	6.1 Ah	3.2 Ah	1.1 Ah
Energy	15.0 Wh	20.1 Wh	10.3 Wh	3.6 Wh
Mass	42 g	71 g	82 g	70 g

Table 4 — D-size Commercially Available Cells Tested

Cell Manufacturer	**K**	**G**	**H-2**	**B-3**	**B-4**
Type	Primary	Primary	Primary	Primary	Primary
Form Factor	DD Cell	D Cell	D Cell	D Cell	D Cell
Chemistry	Li/CF_x	$Li/SOCl_2$	Li/MnO_2	$Li/SOCl_2$	Li/SO_2Cl_2-$SOCl_2$
Voltage	3.6 V	3.6 V	3.3 V	3.6 V	3.9 V
Capacity	40.0 Ah	19.0 Ah	11.1 Ah	19.0 Ah	16.5 Ah
Energy	144.0 Wh	68.4 Wh	37.0 Wh	68.4 Wh	64.4 Wh
Mass	320 g	100 g	115 g	93 g	100 g

Table 5 — Large Form and Pouch Commercially Available Single Cells Tested

Cell Manufacturer	**I-1**	**I-2**	**J**	**I-3**
Type	Secondary	Secondary	Secondary	Secondary
Chemistry (Cathode)	Lithium Nickel Cobalt Aluminum Oxide	Lithium Nickel Cobalt Aluminum Oxide	Lithium Polymer Format Lithium Cobalt Oxide	Lithium Nickel Cobalt Aluminum Oxide
Voltage	3.6 V	3.6 V	4.2 V	3.6 V
Capacity	4.0 Ah	33.0 Ah	53.0 Ah	52.0 Ah
Energy	14.4 Wh	118.8 Wh	222.6 Wh	187.2 Wh
Mass	340 g	940 g	1200 g	1000 g

6 REACTION DESCRIPTIONS (SINGLE CELL)

6.1 Initiating Events

The primary failure mode of a lithium battery is associated with a flaw or damage to the thin porous electrical insulation layer that separates the anode and the cathode (the separator). This is typically a microporous polyolefin layer 15 to 40 micrometers in thickness for the Li-ion cells and a glass or ceramic paper for oxyhalide cells. A flaw/damage to the separator can result in an internal short circuit that produces enough heat to vaporize the electrolyte and result in a boiling liquid expanding vapor explosion (BLEVE) type reaction. The separator can fail due to internal defects (production issues), physical damage (handling issues), exposure to high temperature (fire), and in the case of secondary cells, overcharging resulting in bridging of the separators. Once an internal short develops, a sudden release of stored energy can occur that may result in thermal runaway. This event can cascade to adjacent cells and throughout an entire battery pack and destroy the device the battery is serving. Fires involving lithium batteries can initiate within the product, which means that in storage, a fire can initiate deep within a battery pack or piece of equipment, beyond the influence of conventional fire protection systems.

The potential for manufacturers' defects was emphasized during the 1st Battery Safety Conference conducted November 2011 in Boston. In the presentation "Advances in System Design, Integration and Testing for Safety and Reliability," keynote speaker Dr. Brian Barnett (of TIAX LLC, a technology advancement company) presented the conclusions of an extensive study that found the probability of a manufacturer's defect is 10^{-6}. This failure rate is not bad when compared to other baseline probabilities such as electrical equipment failure (10^{-4}) and human error (10^{-2} to 10^{-3}). However, 10^{-6} is large when considering the number of cells produced per year (10^{10}) and increasing each year through wider use of these popular energy sources. This translates into the possibility of thousands of defects/failures per year.

6.2 General Types of Casualties

The experimental data suggest that the severity of a casualty reaction is a function of a number of parameters including battery size, chemistry, construction, and the charge level of the battery. In almost every battery casualty test conducted to date, the same hazardous components have been observed: flammable by-products (aerosols, vapors, and liquids), toxic gases, and flying debris (some burning), and in some instances, sustained burning of the electrolyte and casing material. The following sections provide a general terminology for describing cell level reactions.

During a runaway reaction within a cell, a significant amount of gas is produced that causes an increase in pressure within the cell housing. The mechanism of release of this pressure is dependent on the rate of the reaction and the configuration of the cell housing. For example, at a low state of charge (SOC), the event may consist of a small amount of liquid/aerosol sprayed through the overpressure vents (if available) or through a seam in the battery housing. The vented products are typically flammable and can be ignited if exposed to a flame.

At a high SOC (fully charged batteries), the venting is much more forceful and typically involves a much larger volume of liquid/aerosol. The flammable electrolyte liquid/aerosol can be ignited, forming small torch-like flames at the vent locations. During some instances, the electrolyte and battery contents may ignite with sustained burning, producing a moderate size, nonviolent fire.

In some cases, there can be a stronger, sometimes substantial, pressure pulse associated with this electrolyte release. Depending on the battery construction, flaming debris can be expelled (sprayed or thrown from the battery). Occasionally, the pressure release ports fail to operate correctly (or the battery is not equipped with vent ports), causing a buildup of pressure inside the cell casing until the casing fails.

When this occurs, the cell explodes, expelling the contents throughout the test chamber, producing a measurable pressure pulse. These explosive type reactions can vary from firecracker type bangs to as loud as shotgun blasts or greater. As with the slower venting scenarios, if the contents are flammable, the aerosol emitted can be ignited. Since the entire electrolyte content of the battery is released at once in these explosive type reactions, a substantial fireball occurs if the products are ignited. The ejected burning or incandescent material may start nearby fires or ignite the vapors being vented from the cell/battery. In these studies, the lithium-ion and solid cathode lithium cells use a flammable electrolyte.

In summary, single cell reactions can be described using the following six terms: vent, smoker, flare, burner, explosive, and fireball. Figure 4 shows photographs of all these scenarios except venting. Video clips are presented in the Appendix.



Fig. 4 — Single cell reaction classifications

6.3 Observed Cell Casualties

The reactions observed in the commercially available cells are described in Tables 6 through 9. In general, the smaller, lower capacity solid-cathode cells typically vented and/or smoked and the medium to higher capacity cells (specifically the oxyhalides) either ignited and burned or exploded.

Intuitively, one expects the type of reaction to be a function of the amount of energy contained in the cell at the time of the event. If this is the case, the type of reaction should be a function of both the battery capacity and the state of charge at the time of the event. Based on a very limited data set (i.e., not a statistically valid set of data), it appears that the threshold between a venting and a flaming reaction lies in the 10 to 20 Wh range. Battery pack configurations can significantly alter these single cell results.

Table 6 — A/AA/Pouch-size Commercially Available Cell Reaction Descriptions

Cell Manufacturer	**A**	**B-1**	**C-1**	**E**
Type	Secondary	Secondary	Secondary	Secondary
Form Factor	Pouch cell	AA Cell	18650	18650
Chemistry	Li/CoO_2	$Li/Li_{0.5}CoO_2$	$Li/FePO_4$	$Li/Li_{0.5}CoO_2$
Voltage **Capacity** **Energy**	3.7 V 3.3 Ah 12.2 Wh	3.7 V 0.16 Ah 0.6 Wh	3.3 V 1.1 Ah 3.6 Wh	3.7 V 2.2 Ah 8.1 Wh
SOC	100%	100%	100%	100%
Initiator	Calrod heater	Calrod heater	Calrod heater	Calrod heater
Reaction Type	Moderate venting	Moderate venting	Moderate venting	Venting/small flames
Reaction Description	Moderate venting for 1:12, no flames	Moderate venting for 0:22 followed by nonviolent rupture	Moderate venting for 0:48 followed by violent rupture, no flames	Moderate venting with small flames, short duration event (0:15)
Reaction Photograph				

Table 7 — C-size Commercially Available Cell Reaction Descriptions

Cell Manufacturer	**F**	**H-1**	**D-2**
Type	Secondary	Primary	Secondary
Form Factor	C Cell	5/4 C Cell	5/4 C Cell
Chemistry	Li/CF_x	Li/MnO_2	$Li/LiFePO_4$
Voltage **Capacity** **Energy**	3.0 V 5.0 Ah 15.0 Wh	3.3 V 6.1 Ah 20.1 Wh	3.2 V 3.2 Ah 10.3 Wh
SOC	100%	100%	100%
Initiator	Calrod heater	Calrod heater	Calrod heater
Reaction Type	Moderate flaming	Flare with sparks	Vent/Smoker
Reaction Description	3:45 venting, rupture with sparks, 1:30 burning	0:18 Roman candle, 0:57 moderate burning	Moderate venting of about one minute
Reaction Photograph			

Table 8 — D-size Commercially Available Cell Reaction Descriptions

Cell Manufacturer	**H-2**	**B-3**	**B-4**	**K**	**G**
Type	Primary	Primary	Primary	Primary	Primary
Form Factor	D Cell	D Cell	D Cell	DD Cell	D Cell
Chemistry	Li/MnO_2	$Li/SOCl_2$	Li/SO_2Cl_2	Li/CF_x	$Li/SOCl_2$
Voltage **Capacity** **Energy**	3.3 V 11.1 Ah 37.0 Wh	3.6 V 19.0 Ah 68.4 Wh	3.9 V 16.5 Ah 64.4 Wh	3.6 V 40.0 Ah 144.0 Wh	3.6 V 19.0 Ah 68.4 Wh
SOC	100%	100%	100%	100%	100%
Initiator	Calrod heater	Calrod heater	Calrod heater	Calrod heater	Propane flame
Reaction Type	Flare	Explosion	Explosion	Vigorous flaming	Rupture
Reaction Description	Fast venting with flaming combustion, long duration event (1:00)	Explosion, small fireball, no residual burning	Explosion, small fireball, no residual burning	Violent rupture with vigorous burning	Cell ruptured sometime during test (unnoticeable)
Reaction Photograph					

Table 9 — Large Form and Pouch Cell Reaction Descriptions

Manufacturer	I-1	I-2	J	I-3
Type	Secondary	Secondary	Secondary	Secondary
Chemistry	Lithium Nickel Cobalt Aluminum Oxide	Lithium Nickel Cobalt Aluminum Oxide	Lithium Polymer Format Lithium Cobalt Oxide	Lithium Nickel Cobalt Aluminum Oxide
Voltage **Capacity** **Energy**	~4 V ~5 Ah ~20 Wh	~4 V ~32 Ah ~128 Wh	~4 V ~53 Ah ~200 Wh	~4 V ~52 Ah ~208 Wh
SOC	100%	100%	100%	100%
Initiator	Calrod heater	Calrod heater	Calrod heater	Calrod heater
Reaction Type	Vent/Smoker	Smoker/flare	Fireball	Fireball
Reaction Description	Moderate venting for several minutes, no ignition/flames	Moderate venting that was ignited manually. Once ignited, flames jetted from end for several minutes.	Cell produced a 4–5 ft diameter fireball for about 30 seconds	Cell produced a 4–5 ft diameter fireball for about 30 seconds
Photograph				

6.4 SOC Effects on Reaction Types (Li-Ion Only)

A quasi-parametric assessment of the effects of SOC on cell level reactions was conducted on the large form and pouch cells. A detailed description of the reactions is provided in Table 10 and a summary in Table 11.

The lithium nickel cobalt aluminum oxide cells (~20 Wh, manufacturer I-1) produced significant amounts of smoke with very little flame and little if any HRR, regardless of SOC. These cells are classified as "vent/smokers." The same chemistry but larger capacity cells (~128 Wh, manufacturer I-2) vented/smoked at a low SOC (20%) but caught fire and readily burned at a higher SOC (100% and overcharged). These cells are considered "flares/burners." The lithium polymer format lithium cobalt oxide cells (~200 Wh, manufacturer J) burned slowly at a low SOC (20%) but produced fireballs at higher charge levels and are considered "burners" and "fireballs" depending on the SOC. The lithium nickel cobalt aluminum oxide cells (~200 Wh) exploded (hydraulic/pneumatic) at a low SOC (20%) but produced fireballs at higher charge levels and are considered "explosive" and "fireballs" depending on the SOC. All cells reacted more violently when initiated by deliberate overcharging.

As shown in Tables 10 and 11, the reaction severity tends to increase with the SOC of the battery. This is expected, since the higher the SOC, the more energy available in the cell to generate heat,

vaporize the electrolyte, and rupture the cell casing. As noted in Section 6.3, there appears to be a threshold between a venting and a flaming reaction in the 10 to 20 Wh range. Again, battery pack configurations can significantly alter these single cell results.

Although reaction severity increases with SOC, the HRR is not necessarily a function of the SOC. At lower SOC, there is less tendency for the cell to burn, thus less HRR; but if ignited at low SOC, the total HRR is about the same as at high SOC. This is shown in Section 8.2.

Table 10 — Large Form and Pouch Cell Reaction Descriptions for Various SOCs

Battery/ Cell Classification	**20% SOC**	**100% SOC**	**Overcharged**
I-1 **Vent/ Smokers** ~14.4 Wh 340 g	Battery vented (slow)/no fire PHRR <5 kW Avg. HRR <5 kW Fire duration – NA 	Battery vented (moderate)/ no fire (similar to previous test) PHRR <5 kW Avg. HRR <5 kW Fire duration – NA 	Battery jetted aerosol/smoke from one end for about 1 minute, no fire PHRR <5 kW Avg. HRR <5 kW Fire duration – NA 
I-2 **Burners/ Fireballs** ~120 Wh 940 g	Battery vented prolonged dense aerosol/no fire PHRR <5 kW Avg. HRR <5 kW Fire duration – NA 	Battery vented gases that were ignited by sparker followed by prolonged sustained burning PHRR <5 kW Avg. HRR <5 kW Fire duration – NA 	Battery produced a fireball (4–5 ft diameter) followed by sustained burning from both ends of the battery PHRR 120 kW Avg. HRR 50 kW Fire duration 40 sec 

Table 10 (cont.) — Large Form and Pouch Cell Reaction Descriptions for Various SOCs

Battery/ Cell Classification	**20% SOC**	**100% SOC**	**Overcharged**
J **Burners/ Fireballs** ~222 Wh 1200 g	Battery vented and burned slowly PHRR 55 kW Avg. HRR 27 kW Fire duration 80 sec 	Battery reacted producing a fireball (4–5 ft diameter) followed by sustained burning (smaller size) PHRR 120 kW Avg. HRR 50 kW Fire duration 35 sec 	Battery jetted aerosol then instantaneously ignited, producing fireball greater than 5 ft diameter PHRR 135 kW Avg. HRR 65 kW Fire duration 10 sec 
I-3 **Explosive/ Fireballs** ~190 Wh 1000 g	Sudden violent rupture spreading debris throughout the chamber, no fire, limited smoke PHRR <5 kW Avg. HRR <5 kW Fire duration – NA 	Battery violently ruptured into a fireball (4–5 ft diameter) followed by sustained burning (smaller size) PHRR 92 kW Avg. HRR 45 kW Fire duration 22 sec 	End blew off of battery, flames jetted (~ 5 ft) from open end PHRR 98 kW Avg. HRR 50 kW Fire duration 25 sec 

Table 11 — Summary of Large Form and Pouch Cell Reactions for Various SOCs

Cell	SOC	Reaction Description
I-1	20%	Minor off-gassing and contribution to heat release rate.
I-1	100%	Minor off-gassing and contribution to heat release rate.
I-2	20%	Minor off-gassing and contribution to heat release rate.
I-2	100%	Significant off-gassing and moderate contribution to heat release rate.
I-2	100%+	Major off-gassing and significant contribution to heat release rate, as cells jetted violently and exited the containment.
J	20%	Significant off-gassing and contribution to heat release rate. Surprisingly little damage to cell assemblies.
J	100%	Significant off-gassing and contribution to heat release rate. Surprisingly little damage to cell assemblies.
I-3	20%	Off-gassing and moderate contribution to heat release rate.
I-3	100%	Significant off-gassing and contribution to heat release rate. Battery left test table.
I-3	100%+	Major off-gassing and significant contribution to heat release rate, as cells jetted violently and exited the containment.

7 REACTION PRODUCTS TESTING AND RESULTS (SINGLE CELL)

7.1 Reaction Products Test Description

Reaction products were measured and documented using a range of standard analytical techniques. The reaction products tests were conducted in a 5 m^3 (177 ft^3) enclosure at the Naval Research Laboratory Chesapeake Bay Detachment test site located in Chesapeake Beach, Maryland. The casualty was typically initiated by heating the exterior of the cell using a cartridge heater (Calrod heater) fastened to the side of the cell. The products were assessed in terms of acidity, corrosiveness, and toxicity. Real-time analysis was done via electrochemical sensors and optical methods. Samples were also collected using gas sample canisters, sorbent tubes, and impingers. The collected samples were analyzed using gas chromatography–mass spectrometry/infrared (GC-MS/IR).

7.2 Reaction Products for Cells at 100% SOC

7.2.1 Reaction Products of Commercially Available Cells

The reaction products measured for the commercial cells are listed in Tables 12 through 14. When the cell vents (without ignition), the majority of the products released are aerosol electrolyte constituents (e.g., carbonates or oxyhalides). A significant amount of these organic solvent gases and aerosols have flammable constituents. This aerosol mixture was not further characterized in these tests, but a reaction products test chamber could be equipped with an oxygen analyzer and an explosive gas meter to measure the Lower Explosive Limit (LEL) of the gases within the chamber, and other equipment to measure aerosol concentrations (the flammability of aerosols are dependent on particle size and number density). In some venting scenarios, the carbonates break down upon release to produce high levels of carbon

dioxide (CO_2) and carbon monoxide (CO). When the cell burns during a casualty, the electrolyte burns fairly efficiently, producing primarily CO_2 as the by-product, as determined by in situ gas analyzers.

The production of acid gas is directly related to the cell chemistry (and appears to be related to cell capacity). Cells that contain sulfur produce sulfuric acid, cells that contain fluorine produce hydrofluoric acid, and cells that contain chlorine produce hydrochloric acid. There is not enough data to develop a quantitative relationship between cell energy and the amount of acid gas produced, but for a given cell chemistry, the amount of acid gas produced is expected to be directly proportional to the cell energy.

Table 12 — A/AA/Pouch-size Commercially Available Cell Reaction Products

Compounds	**A** Pouch cell 100% SOC	**B-1** AA cell 100% SOC	**C-1** 18650 100% SOC	**E** 18650 100% SOC
	mg	mg	mg	mg
Butyrolacetone				
Tetrahydrofuran			50	
Propene	175	24	5	
Benzene				
Hexafluoropropene				
Isoprene			10	
Methyl Carbonate			350	7
1,3 Butadiene	20			
Chlorobenzene			50	
1,2 Dimethoxyethane			10	
Isobutene	90			
Ethanol		33		
CO_2	5500			3300
CO	825			675
SO_2				37
Hydrochloric Acid				
Hydrofluoric Acid				
Propylene Carbonate				
1,2 Methoxyethane				
Dimethyl Carbonate	2200	825	1210	156
Ethylene Carbonate	2000		660	238
1,2 Dimethoxyethane	110			
Total (g)	**10.9**	**0.9**	**2.3**	**4.4**
Initial Mass of Cell (g)	**95**	**19**	**39**	**48**
Percentage (%)	**12**	**5**	**6**	**9**

Table 13 — C-size Commercially Available Cell Reaction Products

Compounds	**F** C Cell 100% SOC	**H-1** 5/4 C Cell 100% SOC	**D-2** 5/4 C Cell 100% SOC
	mg	mg	mg
Butyrolacetone	305		
Tetrahydrofuran	10		
Propene	13		5
Benzene	11		
Hexafluoropropene	7		
Isoprene	11		31
Methyl Carbonate		12	305
1,3 Butadiene			
Chlorobenzene			
1,2 Dimethoxyethane			
Isobutene			
H_2SO_4			88
CO_2	20350	14301	12310
CO	1232	2695	1865
SO_2	77	105	
Hydrochloric Acid			280
Hydrofluoric Acid	92		140
Propylene Carbonate		220	
1,2 Methoxyethane		1513	
Dimethyl Carbonate			75
Ethylene Carbonate			
1,2 Dimethoxyethane			
Carbonyl Sulfide			269*
Dimethyl Sulfide			406*
Ethyl Methyl Sulfide			113*
Total (g)	**22.1**	**18.9**	**15.9**
Initial Mass of Cell (g)	**42**	**71**	**82**
Percentage (%)	**53**	**27**	**19**

* Reaction produced moderate amounts of sulfide compounds

Table 14 — D/DD-size Commercially Available Cell Reaction Products

Compounds	**H-2** D Cell 100% SOC	**B-3** D Cell 100% SOC	**B-4** D Cell 100% SOC	**K** DD Cell 100% SOC
	mg	mg	mg	mg
Butyrolacetone				
Tetrahydrofuran	1752			
Propene	65			
Benzene	18	7	3	
Hexafluoropropene				
Isoprene				
Methyl Carbonate				15
1,3 Butadiene	13			
Chlorobenzene	27			
1,2 Dimethoxyethane	700			
Isobutene	27			
H_2SO_4		1050	390	600
CO_2	13750	26000	27500	
CO	2640	413	330	3465
SO_2	105	4455	4125	4950
Hydrochloric Acid		2200	1403	440
Hydrofluoric Acid				1193
Propylene Carbonate	633			
1,2 Methoxyethane				
Dimethyl Carbonate				
Ethylene Carbonate				
1,2 Dimethoxyethane	3080			
Carbon Tetrachloride		26	21	
Total (g)	**22.8**	**34.2**	**31.1**	**10.7**
Initial Mass of Cell (g)	**115**	**93**	**100**	**320**
Percentage (%)	**20**	**37**	**31**	**3**

7.2.2 Reaction Products of Large Form and Pouch Lithium-Ion Cells

The reaction products measured for the large form and pouch lithium-ion cells are listed in Table 15. When the cell vents (no ignition), the majority of the products released are electrolyte constituents (i.e., carbonates). Therefore, a significant amount of the gas has flammable constituents. In some instances, the carbonates break down upon release to produce high levels of CO and CO_2, especially under thermal runaway conditions at higher state of charge. When the cell burns, the electrolyte burns fairly efficiently, producing primarily CO_2 and water as the by-products.

Large form oxyhalide catholyte (primary) cells were not tested in these studies. The larger quantities of oxyhalide catholyte in these cells would likely produce higher levels of sulfur- and chloride-based compounds during venting and cell failures.

Table 15 — Large Form and Pouch Cell Reaction Products

Compound	**I-1** 100% SOC	**I-2** 100% SOC	**J** 100% SOC	**I-3** 100% SOC
	(mg)	(mg)	(mg)	(mg)
1,3 Butadiene	7	95	125	
1,4 Dioxane	34		25	
Benzene		145	25	43
Bromomethane	50	90	125	
CO_2	1265	8800	11825	13780
Chloromethane			48	37
Dimethyl Carbonate	1870	4125	4675	5225
Ethylbenzene		25	15	
Ethylene	94	495	1100	1100
Ethylene Carbonate	1018	1870	4235	4540
Hydrobromic Acid		6		
Hydrochloric Acid			60	60
Hydrofluoric Acid	99	55	630	550
Methane	550	2750	1375	1515
Methyl Butyrate	5500	18370	16225	
Methyl Fluoride	17	61	66	66
Phosphoric Acid	46		75	85
Propene	255	1000	1500	55
Styrene	37	65	10	
SO_2			1100	
Tetrahydrofuran		34	10	
Toluene	36	65	10	
*** Total (g)**	**11**	**38**	**43**	**27**
Initial Mass of Cell (g)	**340**	**940**	**1200**	**1000**
Percentage (%)	**3**	**4**	**4**	**3**

* These totals do not include the CO_2 values above, which would dramatically increase these totals.

7.3 SOC Effects on Reaction Products

The SOC of the cell affects the type of reaction. Low SOC cells tend to vent pneumatically or hydraulically. At higher SOC, cells tend to ignite. When the cell vents (with no ignition), the majority of the products released are electrolyte constituents (e.g., carbonates) or partial thermal breakdown products, including hydrogen and methane. A significant amount of these reaction products are flammable. In some instances, the carbonates break down upon release to produce high levels of CO_2 and CO. When the cell burns, the electrolyte burns fairly efficiently, producing primarily CO_2 and water vapor as the by-products.

Acid gas production appears to be higher in the burning reactions, and consequently, tends to be higher for higher SOC lithium batteries. Higher SOC also results in greater energy dissipation and heating or potential for incandescent materials such as metal foils and carbonaceous compounds being ejected.

7.4 Reaction Products at Low Oxygen Levels

At lower oxygen concentration, cells are less likely to ignite; they tend to vent only, and the reaction products are as previously described for venting reactions. For example, the H-1 cell at 21% oxygen vented and burned. At 12% oxygen, the cell only vented and sparked but did not ignite.

7.5 Acid Gas Production

The acid gas production is directly related to the cell chemistry, as noted above. For lithium oxyhalide catholyte cells, the acid gas formation can overwhelm the available water in the local atmosphere, or the addition of water vapor will increase the acid formation under these conditions.

7.6 Gas Volume Production

The volume of gas produced by each cell was estimated using the ideal gas law and the steady-state pressure in the test chamber after each test. These chamber pressures and associated gas volumes are listed in Table 16. The term steady-state used in the table means that these were the conditions measured after the gas temperature in the chamber enclosure had cooled back to ambient conditions. In many cases, the chamber pressure spiked higher than the values listed in Table 16 due to expansion of the gases as the temperature increased in the chamber during the reaction. For some oxyhalide cell chemistries, the apparent gas volume expansion will not make sense until the reaction products that are gaseous at high temperature fall below their boiling point and liquefy or solidify. Examples are lithium sulfide, lithium chloride, and aluminum chloride.

Additional work is needed to use these characterizations and this characterization technique. The electrolyte percentage in lithium-ion cells, for instance, is typically within 3% of the cell mass. For cells that vary by an order of magnitude in mass (cell E versus cell I-1) in a fixed volume chamber at similar SOC, statistically the final pressure is the same.

Table 16 — Cell Level Gas Production Quantities

Cell		SOC	Steady-State Pressure (atm)	Steady-State Gas Volume (m^3)
A	Pouch Cell	100%	1.00	Neg.
B-1	AA Cell	100%	1.00	Neg.
C-1	18650	100%	1.00	Neg.
E	18650	100%	1.05	0.017
F	C Cell	100%	1.10	0.034
H-1	5/4 C Cell	100%	1.08	0.027
H-2	D Cell	100%	1.13	0.044
B-3	D Cell	100%	1.06	0.020
B-4	D Cell	100%	1.15	0.051
K	DD Cell	100%	1.25	0.085
I-1	Large Form	100%	1.00	Neg.
I-2	Large Form	100%	1.05	0.017
J	Pouch Cell	100%	ND	ND
I-3	Large Form	100%	1.5	0.170

ND = no data; Neg. = negligible effects

8 HEAT RELEASE RATE TESTS AND RESULTS (SINGLE CELL)

8.1 Heat Release Rate Test Description

Heat release rate and related parameters were characterized on the U.S. Navy test ship ex-USS *Shadwell* located in Mobile, Alabama [2]. The heat release rate of the cell casualty was determined using a hood calorimeter. Four other types of measurements were made during the HRR tests: unburned hydrocarbons, smoke production (obscuration), thermal exposures (radiant and total), and overpressures. The energy contained in the unburned hydrocarbons was added to the HRR measured by the hood. Smoke production was assessed using an optical density meter installed in the compartment. The thermal exposures were determined by mapping the radiant and total heat fluxes in close proximity to the cell. Infrared and radiometric imaging cameras were also used to quantify hot gas release that may impinge on nearby objects. The overpressures were measured both local to the cell and globally in the test compartment.

The tests were conducted under a 1 MW hood calorimeter. The hood calorimeter was instrumented for gas temperature, gas velocity (volumetric flow rate), and typical fire/combustion gas concentrations (CO, CO_2, and O_2). The water vapor constituent of the combustion process was removed with an ice-water cold trap. In addition, explosive gas concentrations (Lower Explosive Limit) and potentially toxic and flammable gases (e.g., SO_2 and volatile organic compounds, VOCs) were measured. The test compartment and area below the hood were instrumented for temperature (five thermocouple trees), pressure, and smoke obscuration (using three optical density meters). The area around the test specimen/battery was instrumented to measure any localized exposures produced by the battery casualty. A computerized data acquisition system was used to collect and record the measurements during the test at a rate of one scan per second (1 Hz).

8.2 Heat Release Rate Test Results

8.2.1 HRRs of Commercially Available Cells

In general, the heat release rates of the commercially available cells were too low to measure using the 1 MW hood calorimeter on the ex-USS *Shadwell*. In future assessments, the heat release rates of the small commercial cells will be measured using a recently installed smaller hood calorimeter with a range from 10 to 100 kW.

Although the HRRs of the smaller commercial cells could not be measured using the 1 MW hood calorimeter, an estimation of the heat energy content of these cells was made based on the temperatures measured in the test chamber during reaction products testing at CBD. Specifically, the energy released was estimated by multiplying the mass of the gas in the CBD test chamber, an average specific heat for the gas(es), and the increase in temperature that occurred in the chamber during reaction. The resulting energies are listed in Table 17. The mean HRRs were determined by dividing the total energy released, by the duration of the reaction (determined based on measurements and visual observations). These values are also shown in Table 17.

Table 17 — HRRs of Commercially Available Cells

Cell	SOC	Delta-T (°C)	Mean HRR (kW)	Duration (sec)	Energy Released (kJ)
A Pouch Cell	100%	Neg.	Neg.	Neg.	Neg.
B-1 AA Cell	100%	Neg.	Neg.	Neg.	Neg.
C-1 18650	100%	Neg.	Neg.	Neg.	Neg.
E 18650	100%	5	0.4	70	27.5
F C Cell	100%	50	3.0	90	275
K DD Cell	100%	30	5.5	30	165
H-1 5/4 C Cell	100%	36	3.3	60	200
H-2 D Cell	100%	131	6	120	720
B-3 D Cell	100%	85	> 470	< 1	470
B-4 D Cell	100%	60	> 330	< 1	330

Neg. = negligible

8.2.2 HRRs of Large Form and Pouch Cells

The HRR data for large form and pouch cells are provided in Table 18. The cells were tested at three SOCs: 20%, 100%, and overcharged (listed in the table as 100%+). The cell/SOC combinations that show negligible HRRs produced venting reactions with little or no burning. These were measured using a special-purpose smaller hood and lower air flow interfaced to the 1 MW hood instrumentation. Special gas collection and air flow would be needed to achieve measureable HRRs and PHRRs for moderate size single cells of lithium primary (with organic) and lithium-ion cells.

Table 18 — HRRs of Large Form and Pouch Cells

Cell	SOC	Peak HRR (kW)	Mean HRR (kW)	Duration (sec)	Energy Released (MJ)
I-1	20%	Neg.	Neg.	-	-
I-1	100%	Neg.	Neg.	-	-
I-1	100%+	Neg.	Neg.	-	
I-2	20%	Neg.	Neg.	-	-
I-2	100%	Neg.	Neg.	-	-
I-2	100%+	50	~15	40	600
I-3	20%	Neg.	Neg.	-	-
I-3	100%	45	~10	22	220
I-3	100%+	50	~15	25	375
J	20%	27	~10	80	800
J	100%	50	~25	35	875
J	100%+	50	~50	25	1250

Neg. = negligible; - = Could not be accurately determined

9 HEAT RELEASE RATE TESTS AND RESULTS (GROUPS OF CELLS)

9.1 Burning Characteristics of Commercially Available Battery Packs/Modules

The commercially available battery packs/modules that were tested are described in Table 19 and the burning characteristics are summarized in Table 20. The first notable observation during testing was that the packs/modules reacted differently compared to the single cell tests. Specifically, except for the iron phosphate cells (discussed below), all the packs/modules produced burning reactions, while many of the single cells just vented and never caught fire. In addition, during almost every unmitigated pack/module test, all the cells in the module reacted and the casing materials were completely consumed.

Table 19 — Commercially Available Battery Packs Tested

No. of Cells **Cell Type** **Manufacturer**	10 D Cell **H-2**	10 D Cell Li-SO_2 *	24 18650 **E**	63 18650 **E**	32 5/4 C Cell **H-1**
Type	Primary	Primary	Secondary	Secondary	Primary
Voltage **Capacity** **Energy**	27 V 11.1 Ah 300 Wh	27 V 15.0 Ah 405 Wh	30 V 7.2 Ah 207 Wh	26 V 21.0 Ah 540 Wh	24 V 24.4 Ah 586 Wh
No. of Cells **Cell Type** **Manufacturer**	90 Li/MnO_2 *	6 Pouch **A**	4 18650 **C-1**	4 26650 **C-2**	
Type	Primary	Secondary	Secondary	Secondary	
Voltage **Capacity** **Energy**	24 V 30.0 Ah 720 Wh	22.2 V 3.85 Ah 85.5 Wh	13.2 V 1.1 Ah 14.5 Wh	13.2 V 2.3 Ah 30.4 Wh	

* These cells were not tested as single cells

Table 20 — Commercially Available Battery Pack HRRs

Pack/ Module Mfr. or Type	No. of Cells	Peak HRR (kW)	Mean HRR (kW)	Duration (sec)	Total Energy Released (MJ)	Fire Photograph
E	1 pack of 24	120	~35	60, 200	6.9	
	16 packs of 24	240	~150	560	85.0	
E	2 packs of 63	185	~60	100, 350	21.2	
H-1	1 pack of 32	135	~35	120, 320	11.4	
H-2	1 pack of 10	125	~50	250	13.2	
	2 packs of 10	115	~50	240, 540	25.5	
	3 packs of 10	165	~90	100, 350	32.5	
	10 packs of 10	inconclusive				
$LiMnO_2$	1 pack of 90	130	~60	120, 120	14.2	

Table 20 (cont.) — Commercially Available Battery Pack HRRs

Pack/ Module Mfr. or Type	No. of Cells	Peak HRR (kW)	Mean HRR (kW)	Duration (sec)	Total Energy Released (MJ)	Fire Photograph
Li-SO_2	1 pack of 10	35	20	300	6.0	
C-1	1 pack of 4 18650 cells	<5	Neg.	100, 350	Neg.	
C-2	1 pack of 4 26650 cells	<5	Neg.	100, 350	Neg.	
A	1 pack of 6 pouch cells	10	~5	175	0.9	

Neg. = negligible

The pack/module burning characteristics presented in Table 20 are the most severe measured during testing (for that specific set of conditions). There were many instances when the same test was conducted multiple times and produced significantly different results each time. Specifically, the heat release rate histories showed dramatic differences (i.e., lower intensity, longer duration burns sometimes); however, the total thermal energy released was typically in good agreement across the repeated tests.

An example of HRR variation is provided in Fig. 5, which shows the heat release rate histories of two tests conducted with two 63-cell 18650 (manufacturer E) $Li/Li_{0.5}CoO_2$ battery packs/modules at 100% SOC. The left graph shows a lower intensity (105 kW PHRR), longer duration event and the right graph shows a higher intensity (190 kW PHRR), shorter duration event. The two tests were conducted with identical conditions. The propagation from one pack to the receptor pack can be seen to initiate in

the slight double spike midway through the event. This transition (two distinct HRR contributions) is more clearly seen for the 20% SOC event in Fig. 9.

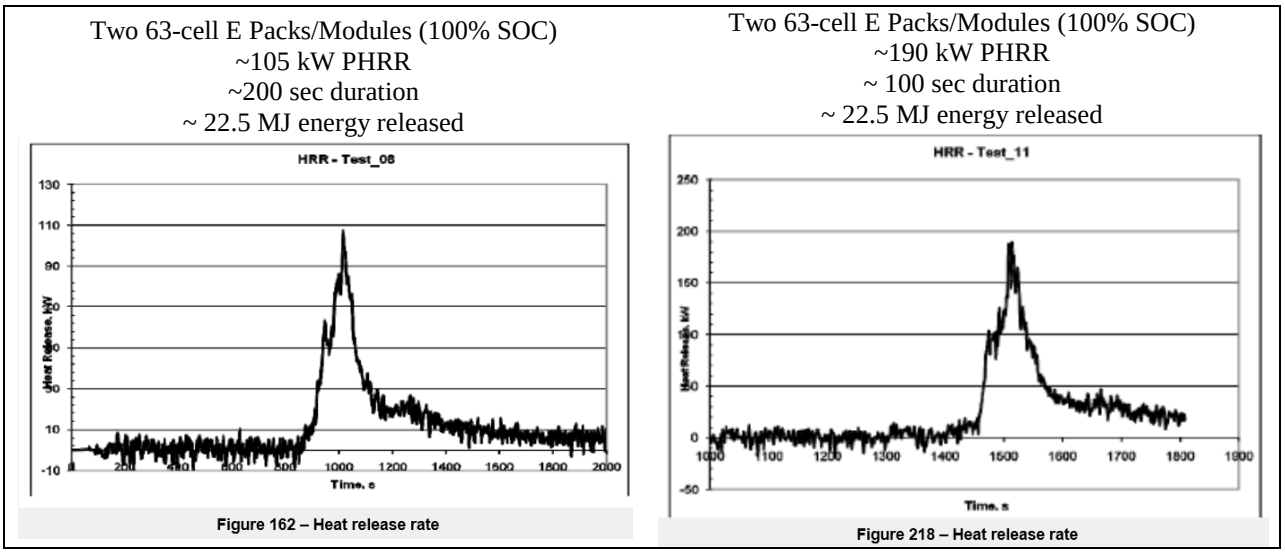


Fig. 5 — Example of variations in burning characteristics for identical tests

A typical single pack HHR plot is provided in Fig. 6. The plot shows a single spike representing the period during which all the cells within the pack vent and ignite. This period typically lasts 1 to 2 minutes, depending on the type and number of cells within the pack. After this rapid-growth-rate, high-intensity burning period, the reaction then decays to a small/steady fire that lasts 3 to 5 minutes as the combustible packaging, circuit boards, and wiring (insulation) is consumed.

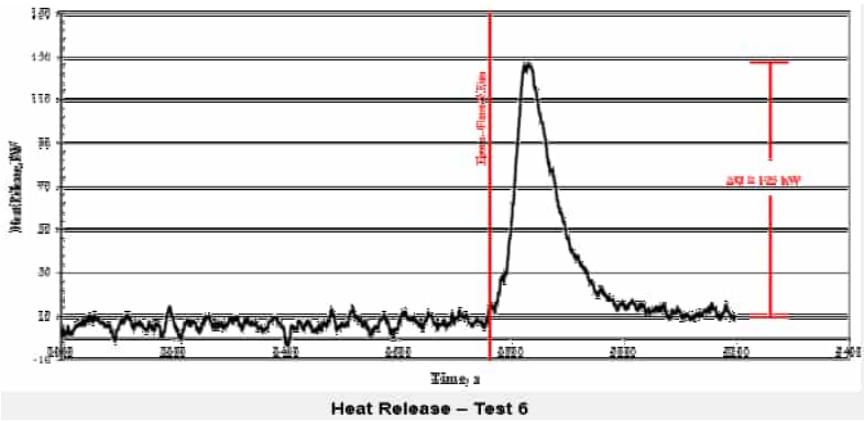


Fig. 6 — Typical HRR history for a single pack/module of lithium primary cells

For multiple packs/modules, the HRR history can have a single spike or multiple spikes, depending on how quickly the fire spreads to the adjacent pack (and the level of communication between packs). A typical multiple pack HHR plot with multiple spikes is shown in Fig. 7. The multiple spikes indicate the fire spreading to adjacent packs. The time between the spikes appears to be loosely related to the thermal inertia of the packaging. For example, the time between spikes is typically greater for the E and H-2 packs due to the thickness of the hard plastic battery case. Conversely, the time between spikes is shorter and typically less pronounced for thinner battery cases such as the shrink wrap used on the E battery packs/modules. In any case, after all the cells have reacted, the fire decays to a small/steady fire that lasts 3 to 5 minutes as the combustible packaging, circuit boards, and wiring (insulation) are consumed.

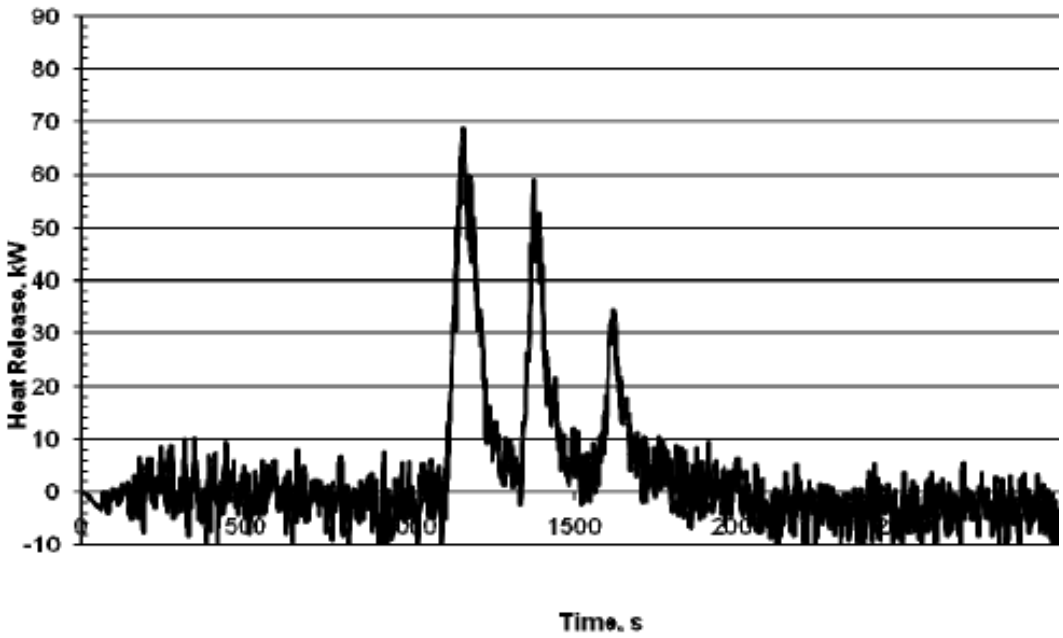


Fig. 7 — Typical HRR history for a group of packs/modules

As noted above, the phosphate-based lithium-ion packs/modules were the only ones tested that did not readily react to consume all the cells in the pack. Four tests were conducted with C-1 and C-2 battery packs (two 1100 mAh and two 2300 mAh). The results were similar for each of the four tests. In short, a single cell within each pack was heated until the cell achieved thermal runaway, but the reaction never spread to any of the adjacent cells. Figure 8 shows one of these packs being tested. Only one cell in the pack reacted.



Fig. 8 — Typical phosphate-based pack/module (C-1) under test

9.2 SOC Effects on Combustion Energy Released

Although the type of reaction, venting versus flaming, appears to be a function of SOC at the single cell level, the amount of combustion energy released during a burning reaction (the most common reaction at the pack/module level) appears to be constant regardless of SOC. An example of this is shown in Fig. 9. The left graph shows the HRR of two 63-cell E packs at 20% SOC and the right graph shows the HRR of two 63-cell E packs at 100% SOC. Although the peaks and the durations are different, the total combustion energy released during the two reactions is essentially identical (~22.5 MJ).

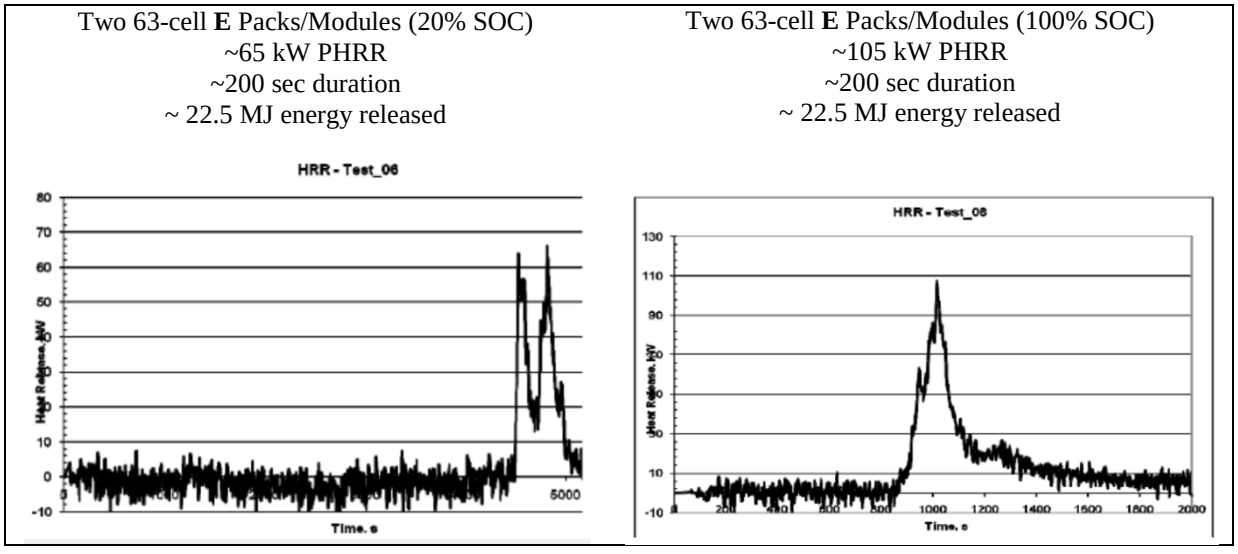


Fig. 9 — Example of two tests with equal amounts of energy released

9.3 Combustion Energy as a Function of Electrical Energy

Intuitively, one expects the combustion energy potential to be proportional to the electrical energy potential. The rationale is that the fuel load, i.e., the amount of combustibles (electrolyte and separator material), should be proportional to the electrical energy potential.

The published [1] electrical energy potential for each test configuration and the measured combustion energy released are shown in Table 21. The two right-hand columns show the ratio of the measured combustion energy to the published electrical energy.

At initial glance, there appears to be a fairly wide range in the ratios of combustion energy to electrical energy (5 to 12). However, the lithium-ion E battery packs have a hard plastic case with about 150 grams of plastic material. This plastic contributes about 30% of the total combustion energy for the pack. Similarly, the lithium manganese oxide H-2 battery packs have a hard plastic case with about 200 grams of plastic material. This plastic contributes about 40% of the total combustion energy for the pack.

After adjusting the combustion energies to account for the case material, there is fairly good agreement between the results of these tests, suggesting that the combustion energy is typically about six times the electrical energy potential of the battery.

Table 21 — Combustion Energy and Electrical Energy Comparison

Cell Type	No. of Cells	Combustion Energy Released (MJ)	Electrical Energy (Wh, MJ)	Ratio Comb./Elect.	Adjusted Ratio Comb./Elect.
E	1 pack of 24	6.9	207, 0.75	9.2	6.4
E	16 packs of 24 in a cardboard box	85.0	3312, 11.9	7.1	5.4
E	2 packs of 63	21.2	1080, 3.9	5.4	5.4
H-1	32	11.4	586, 2.1	5.4	5.4
H-2	1 pack of 10	13.2	300, 1.1	12	7.2
H-2	2 packs of 10	25.5	600, 2.2	11.6	6.9
H-2	3 packs of 10	32.5	900, 3.2	10.1	6.1
$LiMnO_2$	1 pack	14.2	720, 2.6	5.4	5.4

9.4 HRRs of Bulk Storage Configurations

Two HRR tests were conducted in bulk packing configurations such as might be encountered in shipping and storage. The first test consisted of 16 packs of 24 cells each of E type cells packed in a cardboard shipping box. The second test consisted of six 10-cell boxes of F cells. Pre-test photos and the HRR histories measured during the two tests are shown in Figs. 10 and 11. The 16 packs of E cells were triggered by exposure to a propane flame, and the six boxes of F cells were initiated by heat tape wrapped around the boxes.

A comparison between these results and the smaller scale tests suggests that for these two configurations, the cells tended to react sequentially rather than simultaneously. The peak HRRs were similar to the smaller battery configurations but the duration of burning was longer. These two tests provide only limited data; a rapidly growing reaction with numerous cells reacting simultaneously is easily conceivable.

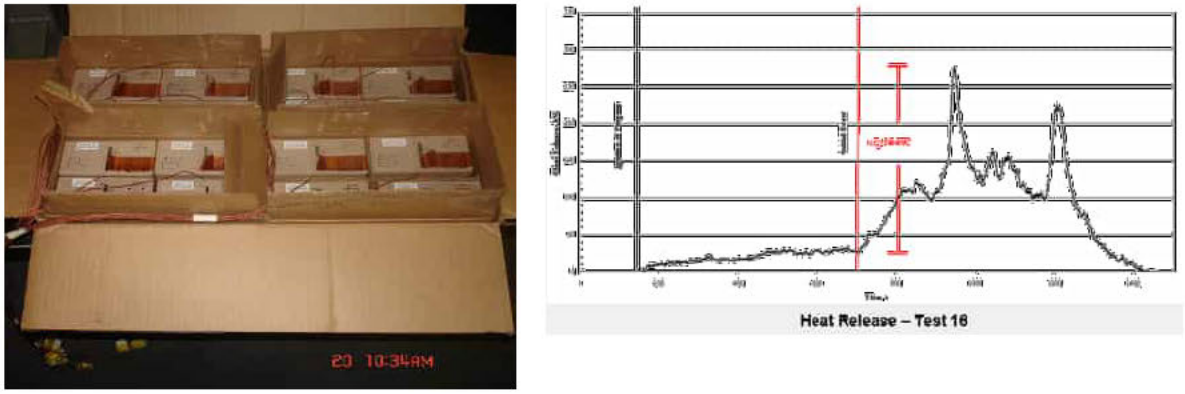


Fig. 10 — Bulk storage test, E type cells

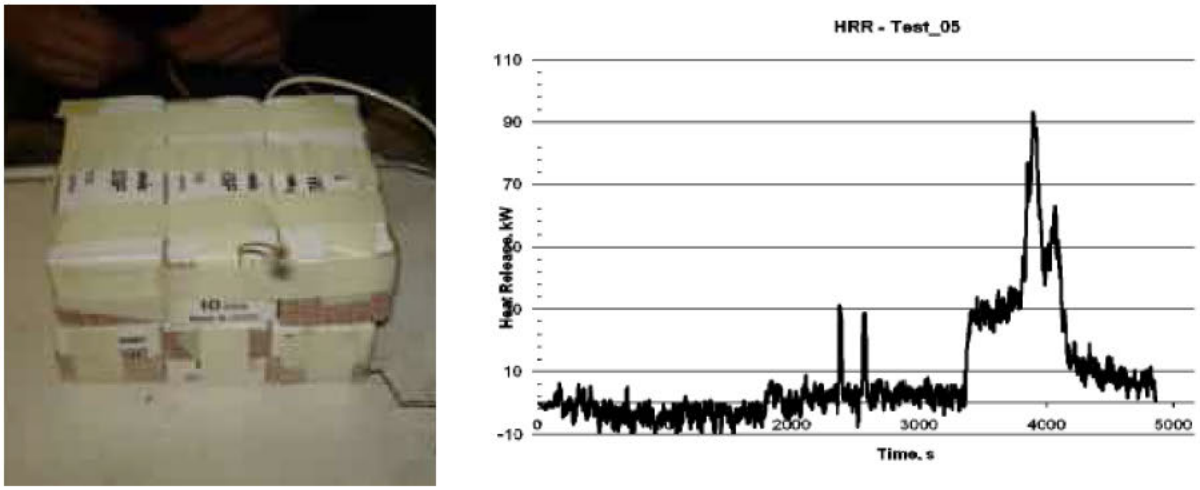


Fig. 11 — Bulk storage test, F type cells

10 SAFE STORAGE AND CASUALTY MITIGATION OF MULTICELL LITHIUM BATTERIES

One objective of the battery casualty test programs was to develop a facility to contain large lithium batteries and prevent a cascading casualty during storage and charging. The containment/mitigation structure developed is termed a Battery Storage Locker (BSL). In general terms, the BSL was designed to limit a casualty to the initial battery and to contain, to the maximum extent possible, the exposures (both thermal and products) produced by the event. The final mitigation system includes a pressure vessel housing to contain the gaseous products released during a casualty, a smoke detection system to notify personnel of the event, and a self-contained, closed head sprinkling system designed to suppress and ultimately extinguish a fire. The entire package is referred to as the Lithium Battery Casualty Mitigation System (LBCMS).

10.1 Battery Storage Locker (BSL) Development History

The initial approach was to develop a BSL similar to a commercial off-the-shelf (COTS) flammable liquid storage cabinet. Two series of tests were conducted to quantify the conditions produced in a prototype rectangular BSL and to assess/refine the design for the overall LBCMS. These conditions became the basis for the performance requirements for the system and components. Later, a cylindrical BSL was developed and tested (see Section 10.4.2).

The rectangular BSL design was based on a box-in-a-box concept. The inner box is the battery compartment. The battery compartment provides a passive barrier to contain the initial battery casualty and prevent direct exposures to and from adjacent battery packs. The battery compartment is also designed to contain the extinguishing agent (i.e., water) so that the battery can be completely submerged to aid in extinguishment and minimize cell-to-cell propagation within the battery. The battery compartment is equipped with a hinged lid (held closed by gravity, not secured) that is designed to vent the pressure and products of the initial battery casualty into the outer box. The outer box is a sealed unit that serves as a plenum to contain the reaction products.

The prototype BSL (Fig. 12) was constructed of 0.64 cm (0.25 in.) steel plate with dimensions of 46 cm × 46 cm × 1860 cm (18 in. × 18 in. × 73 in.). It contained three battery compartments and a plenum area located above and in front of each compartment. Each battery compartment was roughly 30 cm deep × 30 cm tall × 60 cm long (12 in. × 12 in. × 24 in.). The top of the BSL was also equipped with a hinged lid to provide access to the battery compartments. This lid was held shut using two latches located at the front of the BSL.

Each battery compartment was equipped with a closed head sprinkler to suppress and extinguish a casualty within the compartment. During development, a variety of detection technologies were installed in the plenum to aid in the downselect of the final technology.

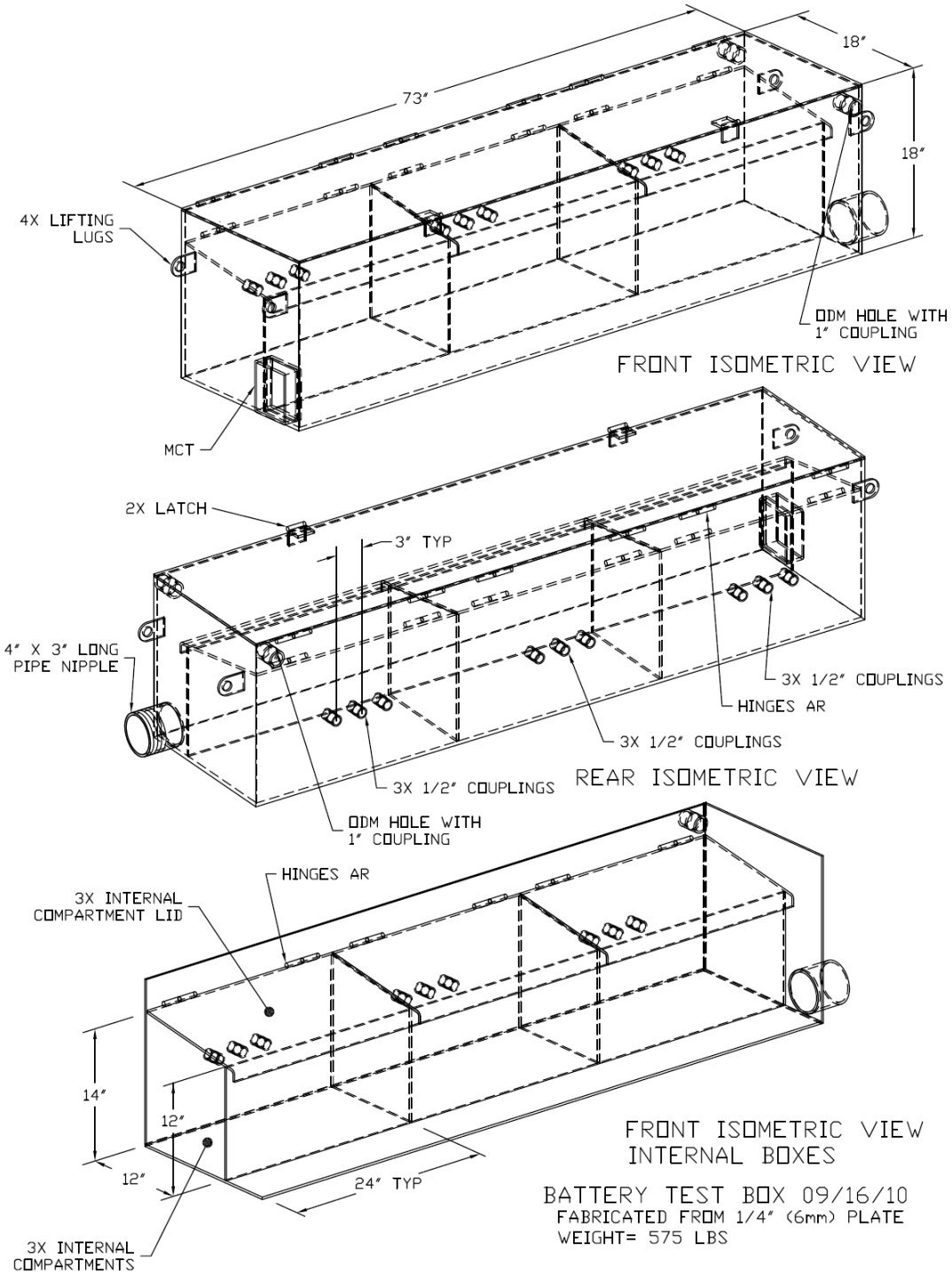


Fig. 12 — Prototype BSL schematic

10.2 Detection System Development History

During the development tests, the rectangular BSL was instrumented for both temperature and optical density so it could be determined if standard off-the-shelf heat and smoke detectors would be suitable for this application. In addition, two commercially available detectors were installed in the battery storage compartment: a heat sensing device (HSD) and an aspirated smoke detection system.

During the vast majority of the tests, there was no indication of the casualty outside the cell or pack prior to the event. Short-circuits or overcharge may produce sufficient local heating to be detected prior to the casualty if the battery pack is instrumented internally for temperature. A sudden increase or decrease in battery voltage may also indicate an ensuing battery casualty, but the voltage was not measured during these tests.

During the vast majority of the tests, the reaction of a single cell within the BSL produced effects that would be detectable using almost any of the available COTS technologies (i.e., heat and smoke). The battery compartment and the plenum space became obscure (80% to 100%) with smoke/aerosol particles during every casualty. COTS photoelectric type smoke detectors typically alarm when exposed to obscurations between 3% and 5%, making them a good option for this application. During many of the tests, there was a significant temperature increase (between 30 and 300 °C) in the battery compartment, indicating that temperature sensors would also work well in this application (i.e., inside the battery compartment to detect the battery casualty).

Ultimately, the results supported the selection of a photoelectric smoke detector for use as an early warning device to notify personnel.

10.3 Suppression System Development History

Table 22 provides an overview of the fire suppression systems considered and their anticipated capabilities for this application. Also included are a number of concerns associated with each technology/system.

Since a battery casualty typically cannot be detected prior to the first cell reaction (venting and/or fire), the suppression system for this application must be able to extinguish any fires in normal combustible materials, minimize the potential for secondary reactions (in adjacent cells and/or battery packs), and mitigate the hazards/exposures produced by the initial reaction (i.e., absorb the heat given off by the initial reaction, minimize the exposures to adjacent cells and batteries surfaces by cooling, and scrub some of the particles and compounds out of the vented gases).

Only water-based systems have the capabilities to meet these desired performance objectives. Gaseous agent systems have excellent fire extinguishing capabilities (they can extinguish most combustible materials in less than a minute of agent discharge) but have no cooling capabilities to help mitigate the hazard to adjacent cells or batteries.

The two systems that showed the most potential for this application were a water deluge (flooding) system and a sprinkling system. Additives such as foams would have been investigated if the “water only” systems could not meet the desired levels of performance. Ultimately, a closed head sprinkling system was selected for this application. The closed head sprinkling system has the advantage over other technologies of not needing a separate detection and activation system, making it the simplest, most cost effective, and easiest to maintain.

Table 22 — Suppression System Capabilities and Limitations

System	Capabilities	Limitations/Concerns
Seawater Flooding	Suppression, cooling, exposure protection	Shorting, collateral damage, electrolysis (hydrogen explosion)
Potable Water Flooding	Suppression, cooling, exposure protection	Shorting, collateral damage, electrolysis (hydrogen explosion)
Seawater Sprinkling	Cooling	Limited shorting collateral damage
Potable Water Sprinkling	Cooling	Limited shorting collateral damage
AFFF Sprinkling	Cooling	Limited shorting collateral damage
Medium Expansion or Compressed Air Foam	Suppression, cooling, exposure protection	Limited shorting collateral damage
High Expansion Foam	Suppression, cooling, exposure protection	Limited shorting collateral damage
Inert Gas	Suppression	No cooling
Halocarbons	Suppression	No cooling
Water Mist	Suppression, cooling	Limited shorting collateral damage
Powders/Aerosols	Suppression	No cooling
Aqueous Agents	Suppression, cooling	Limited shorting collateral damage

The suppression system chosen for the LBCMS consists of an individually thermally activated sprinkler (a closed head sprinkling system) installed above the center of each battery compartment. Standard Tyco pendent sprinkler heads (57 °C/135 °F) with k-factors of 80 lpm/bar^{½} (5.6 gpm/psi^{½}) were selected and tested for this application. Additional information on the sprinkler heads is provided in Table 23.

During the development and validation tests, the system was designed to fill the battery compartment with water in less than 20 seconds from activation. The system was secured (turned off) about 40 seconds after activation. This corresponds to twice the amount of water required to fill a single battery compartment.

Table 23 — Sprinkler Head Information

Manufacturer and Model	**Tyco Pendent Sprinkler Head**
K-Factor	80 lpm/bar^{½} (5.6 gpm/psi^{½})
Temperature Rating	57 °C (135 °F)
Response Time Index (RTI)	32 (m-s)^{½} (58 (ft-s)^{½})
Photograph	

10.4 Mitigation Test Results

10.4.1 Rectangular BSL Suppression Test Results

The capabilities of the suppression system installed in the rectangular BSL were assessed against two battery packs: 24 18650 type E cells and 10 D type H-2 cells. These batteries were selected because they produce a burning reaction that readily propagates to all the cells within the pack. Also, the individual cells are obstructed from direct water spray impingement from the sprinkler head due to packaging material. Table 24 describes these battery packs.

Table 24 — Battery Packs Tested in the Rectangular BSL

No. of Cells **Cell Type** **Manufacturer**	24 18650 **E**	10 D Cell **H-2**
Type	Secondary	Primary
Voltage **Capacity** **Energy**	30 V 7.2 Ah 207 Wh	27 V 11.1 Ah 300 Wh

During the first series of scoping tests, only one suppression test (H-2 pack) was conducted. The results suggested that a single individually thermally activated sprinkler head was a viable option for the battery compartment fire suppression system. During the second test series, four additional fire suppression tests and two baseline tests without suppression were conducted to further quantify the capabilities of the system. The results of these tests are summarized in Table 25.

Table 25 — Rectangular BSL Suppression System Test Results

Battery Description	Max. Battery Comp. Temp. (°C)	Max. Adjac. Battery Comp. Temp. (°C)	Max. Plenum Temp. (°C)	Sprinkler Activ. Time (sec)	Exting. Time* (sec)	No. of Cells that Reacted
One E pack of 24 cells	250	80	115	**5–10	NA	24 of 24
One E pack of 24 cells	165	25	30	5–10	~20	6 of 24
Three E packs, total 72 cells	200	30	85	5–10	~30	24 of 72
One H-2 pack of 10 cells	250	125	200	**5–10	NA	10 of 10
One H-2 pack of 10 cells	125	25	75	5–10	~15	4 of 10
Three H-2 packs, total 30 cells	145	175	***325	5–10	~35	15 of 30

* These are estimates due to the difficulty in determining the actual extinguishment time
** For this test, the water was not allowed to flow
*** The flammable electrolyte gases were burning outside of the battery compartment in the plenum

As shown in Table 25, three tests were conducted with each battery type: a single battery pack baseline test without suppression, a single battery pack test with suppression, and a test with three battery packs taped together to assess the ability of the system to prevent pack-to-pack propagation.

During the baseline tests, the casualty rapidly propagated through the entire pack(s), consuming all the cells in less than 2 minutes. In both cases (E and H-2), the plastic case continued to burn for another 2 to 3 minutes.

When repeated with the suppression system operational, the system activated within 10 seconds and the reaction was stopped before all the cells in the pack were consumed and before the battery case ignited (i.e., the fire was extinguished about 10 seconds after the start of discharge). Only 25% of the E cells were consumed and 40% of the H-2 cells were consumed.

When the tests were repeated with the three-pack configurations, the system again activated within 10 seconds and the reactions were stopped before all the cells in the pack of origin were consumed, but the fire did spread into one of the adjacent packs. This fire spread to the adjacent pack was an anomaly of the test configuration. Specifically, the wires/Calrod used to heat the cells in the center pack ran through the center of one of the adjacent packs. This wire run provided a path for the hot gases that were being released from the pack of origin to ignite the adjacent pack. However, in both three-pack tests, only one or two cells in the adjacent pack reacted prior to the suppression/extinguishment of the entire group of batteries. In both cases, the fire was extinguished less than 30 seconds after the start of discharge. Only 33% of the E cells were consumed and 50% of the H-2 cells were consumed in the pack of origin during these multiple pack tests.

With respect to thermal management, the sprinkler rapidly suppressed and extinguished the fires and prevented the spread of fire to batteries stowed in adjacent battery compartments (based on the temperatures measured in the adjacent areas).

10.4.2 Pressurizable Cylindrical BSL Suppression Test Results

Some lithium battery packs produce significant overpressure during a casualty. These pressures could not be contained in the rectangular design BSL. A pressurizable cylindrical BSL with three battery compartments was designed to handle up to 50 psig pressures with a vent.

The original battery pack intended to be stowed in the LBCMS, consisting of thionyl and sulfonyl chloride lithium cells (B-2, B-3, and B-4), was shown to be too energetic during casualty events to be contained within a reasonably designed BSL. Accordingly, notional battery packs were constructed using less energetic cells. These notional battery packs (referred to as Pack #1, Pack #2, and Pack #3) provide the necessary energy and power for some applications. The battery packs tested are described in Table 26.

Table 26 — Battery Pack Configurations

Battery Pack Designation (% of volume)	**Cell**	**Manufacturer**	**No. of Cells**	**Configuration**
Bulk	C	F	30	Three 10-cell boxes
1 Pack	18650	E	10	1 pack of 10 cells
Pack A	Large form	I-3	9	3 packs of 3 cells
Pack #1 – 25%	5/4 C	H-1	112	14 sticks of 8 cells
Pack #1 – 50%	5/4 C	H-1	224	28 sticks of 8 cells
Pack #1 – Full	5/4 C	H-1	416	52 sticks of 8 cells
Pack #2 – Full	18650	E	441	7 modules of 63 cells
Pack #3 – 25%	C	F	120	12 sticks of 10 cells
Pack #3 – 50%	C	F	250	25 sticks of 10 cells
Pack #3 – Full	C	F	480	48 sticks of 10 cells

The full battery pack configurations are shown in Fig. 13. In all cases, the cells that make up the pack were placed in an open-ended aluminum cylinder (8.5 in. internal diameter) to simulate the casing of a commercial battery pack. With respect to cell configuration/orientation, Pack #1 and Pack #3 consisted of a group of closely nestled cells packed end to end (in “sticks”) that were physically held connected together in series by a layer of shrink wrap PVC tubing to simulate a nominal battery assembler’s packaging. These “sticks” were secured to each other mechanically. Pack #2 consisted of seven 63-cell modules secured to each other by hot-melt glue.

Pack #1 – Full
H-1 5/4 C

Pack #2 – Full
E 18650

Pack #3 – Full
F C cell



Fig. 13 — Typical battery stick and 63-cell module loading configurations

For testing, the open-ended aluminum cylinder was placed inside a cylindrical battery compartment and into the pressure vessel (Fig. 14). In most tests, the open ends of the aluminum cylinder were partially sealed to simulate the potential water flow obstructions of an actual battery pack (i.e., to reduce the flow rate of water into the center of the pack).



Fig. 14 — Pressurizable containment configuration

Two series of suppression tests were conducted in the pressurizable BSL to assess the capabilities of the overall LBCMS. The first series tested against the reduced scale/partial battery packs (up to 50% of an all-up battery pack; see Table 26). In the second series, the capabilities were validated against the full battery packs (Table 26). Results of the ten tests are summarized in Table 27.

Table 27 — Cylindrical BSL Suppression System Test Results

Battery Pack Description (Pack #)	**Max. Battery Comp. Temp. (°C)**	**Max. Adjac. Battery Comp. Temp (°C)**	**Max. Plenum Temp. (°C)**	**Sprinkler Activ. Time (sec)**	**Exting. Time* (sec)**	**No. of Cells that Reacted**
30 F Cells	170	30	37	~90	~100	3
10 E Cells	80	30	36	<30	<30	4
9 I-3 Cells	135	35	110	7	16	1
112 H-1 Cells (#1, 25%)	65	25	29	10	10	2
** 224 H-1 Cells (#1, 50%)	325	70	260	15	10	28
416 H-1 Cells (#1, Full)	175	35	135	15	25	4
7 × 63 E Cells (#2, Full)	95	35	65	9	~60	16
120 F Cells (#3, 25%)	160	25	43	45	45	6
** 250 F Cells (#3, 50%)	385	55	125	15	15	100
480 F Cells (#3, Full)	95	35	80	10	37	6

* These are estimates due to the difficulty in determining the actual extinguishment time.
** The discharge of water was intentionally delayed to further challenge the LBCMS.

Specific findings of the ten tests are summarized as follows:

- The BSL (and installed systems) met all LBCMS requirements to contain the casualty to a single battery and prevent products of combustion from escaping the LBCMS.
- The smoke detector (photoelectric) installed in the BSL alarmed early into the casualty during every test and could be heard outside the pressure vessel.
- Only the sprinkler in/above the battery compartment of origin activated during any of these tests.
- The sprinkler head typically activated early in the casualty and within a few seconds of water discharge, stopped the reaction/casualty (with only a few cells reacting).
- For fast growing casualties, the sprinkler head typically activated about 15 seconds into the event.
- The maximum temperatures measured in the battery compartment of origin for normal LBCMS operation (i.e., no delay in water discharge) ranged from 65 °C to 175 °C.

- The maximum temperatures measured in the plenum for normal LBCMS operation (i.e., no delay in water discharge) ranged from 29 °C to 135 °C and the maximum temperatures measured in adjacent battery compartments (also called pigeon holes) ranged from 25 °C to 35 °C.
- For normal LBCMS operation (i.e., no delay in water discharge), the maximum pressure produced in the BSL was less than 10 psi overpressure (pressure due to both the gas generated during the casualty and the water injected to suppress the casualty).
- The two primary hazardous gases produced during these battery casualties were CO_2 and CO. During these suppression tests, the amount (mass) of CO_2 produced ranged from 0.02 to 0.08 kg. The amount (mass) of CO produced ranged from 0.01 to 0.05 kg.

10.5 Suppression Summary

The ability of a suppression system to prevent secondary cell reactions within a complex battery pack is, in part, a function of the openness of the battery pack housing. If the cells are contained within a closed housing (air tight, water tight, or even just a fairly tight enclosure), the mitigation system will not be able to contain the reaction to the initial cell within a single battery, and in most scenarios, all of the cells within the pack will react, even if submersed under water.

If the battery housing is fairly open, a fast acting mitigation system may be able to reduce the exposures to the adjacent cells within the housing below the critical value (below the level at which adjacent cells react). The best way to achieve this objective is to rapidly submerse the battery pack in water. The severity of the initial reaction, the proximity of the adjacent cells, and the vulnerability of adjacent cells are variables associated with achieving this performance objective. A water spray system (versus a flooding system) has the ability to thermally manage the conditions around the pack of origin, but is unlikely to be effective in preventing the complete consumption/reaction of the initial pack.

The data in Table 27 are from tests in which the individual cells were loosely packed and thus water could surround and cool each cell. This prevented total destruction of the battery pack in the BSL.

11 UNMITIGATED BATTERY PACK REACTIONS INSIDE A PRESSURE VESSEL

Three tests were conducted to validate the capabilities of the LBCMS (using the cylindrical BSL) against a number of worst-case scenarios: unabated reaction of an entire battery pack within the BSL and pressure vessel. These tests were conducted with all-up battery packs (full 100% packs) and are summarized in Table 28.

Table 28 — Conditions Produced Inside a Pressure Vessel

	7 × 63 E Cells	**416 H-1 Cells**	**480 F Cells**
Casualty Duration (sec)	300	96	162
No. Cells Reacted	441	416	480
Reaction Rate (cells/sec)	1.3	4.3	3.0
Max. Temp. Battery Storage Compartment (°C)	600	880	1000+
Max. Temp. Plenum (°C)	400	310	435
Max. Temp. Adj. Battery Storage Compartment (°C)	80	80	100
Volume of Gases Produced (m^3)	5.6	9.4	9.3
Volume of CO_2 Released (m^3)	5.1	6.1	6.1
Volume of CO Released (m^3)	0.5	3.3	3.2
Total Mass of CO_2 Produced (kg)	6.4	10.9	9.4
Total Mass of CO Produced (kg)	0.73	3.8	3.4

11.1 BSL Worst-Case Thermal Conditions

The maximum temperatures measured in the center battery compartment of the LBCMS (the one containing the battery casualty) ranged from 600 °C to over 1000 °C. The maximum temperatures measured in the plenum ranged from 310 °C to 435 °C and the maximum temperatures measured in adjacent battery storage compartments ranged from 80 °C to 100 °C. Although some of the batteries in the adjacent battery storage compartments showed moderate thermal damage, none of the batteries stowed in the adjacent battery storage compartments reacted during any of these worst-case tests.

Figures 15 and 16 show the worst-case thermal conditions produced in the BSL during these tests, which occurred in the test conducted with 480 F cells. The reaction began about 61 minutes into the test. The battery compartment containing the casualty exceeded 1000 °C about 3 minutes into the casualty. The aluminum cylinder used to house the cells (surrogate battery case) was significantly damaged with only the bottom half remaining at the end of the test. The plenum temperature above the battery storage compartment reached 435 °C. The adjacent battery storage compartments remained below 100 °C for the entire test.

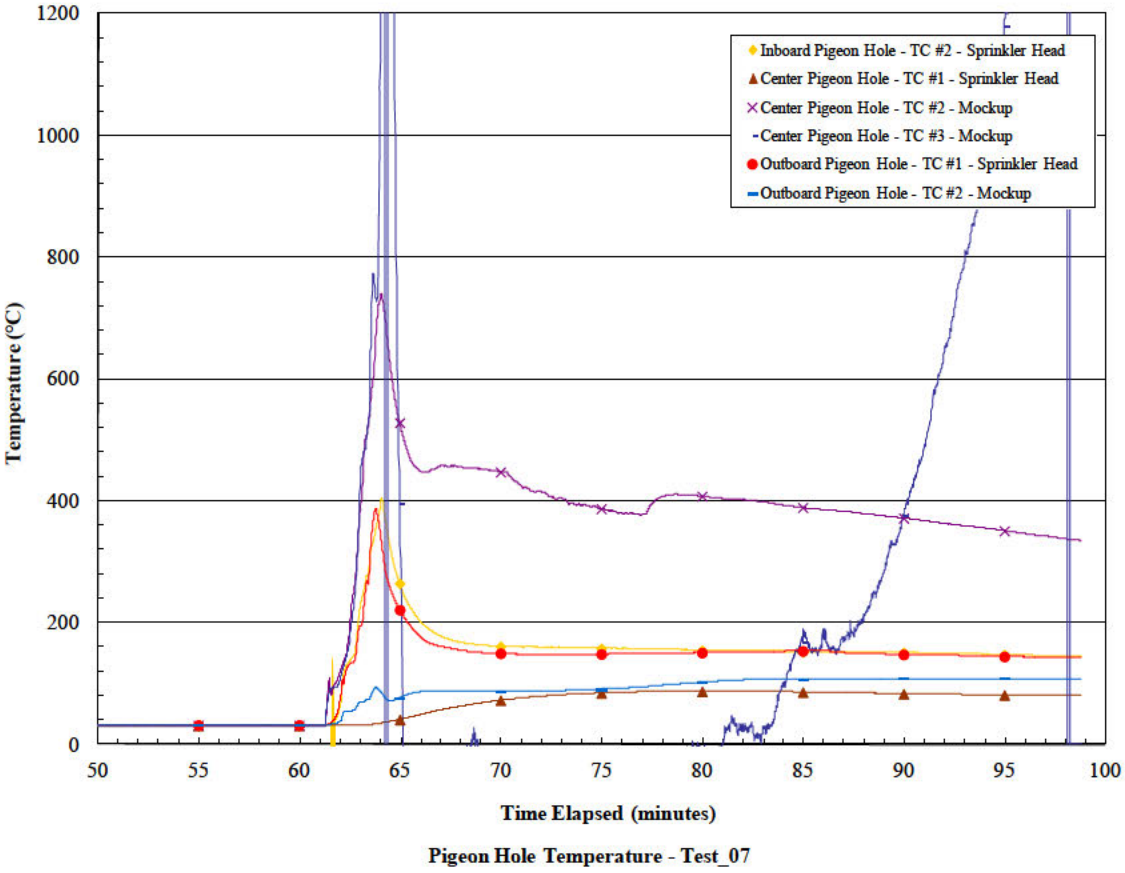


Fig. 15 — BSL worst-case thermal conditions in the compartment containing the battery (480 cells) (TC = thermocouple)

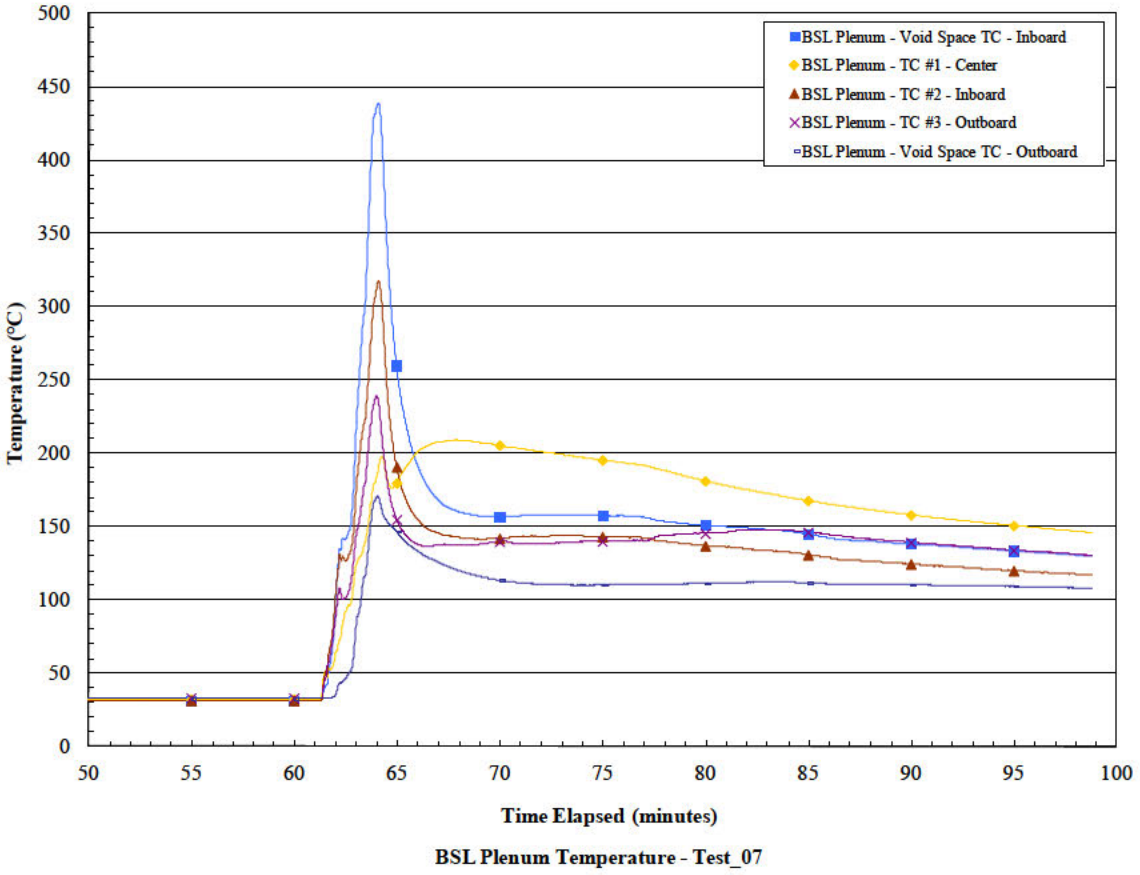


Fig. 16 — BSL worst-case thermal conditions in the plenum (480 cells) (TC = thermocouple)

The reactions of the battery pack significantly damaged the aluminum cylinder used to simulate a representative battery housing. Table 29 shows pre-test and post-test photographs of the battery packs and aluminum housings. As can be seen, some of the packs/cells released enough heat to completely destroy the housing.

The data collected during these tests provide valuable information on the reaction rates (cell-to-cell propagation) of a battery casualty in a confined space, involving a battery containing a large number of cells. The unabated cell-to-cell propagation rates (shown in Table 28) ranged from 1.3 to 4.3 cells per second. Surprisingly, the reactions continued inside the BSL even though there was no oxygen to support combustion of the vented products. It was assumed that the heat logged in the BSL prior to the complete consumption of oxygen was adequate to continue the reaction of the remaining cells in the pack. The reaction of these remaining cells still logged additional heat energy inside the BSL in the absence of combustion. Reactions of cells at low oxygen levels and the mechanism driving cell-to-cell propagation are topics that should be further investigated.

Table 29 — Damage Photographs

Battery	Pre-Test Photograph	Post-Test Photograph
7 × 63 E Cells		
416 H-1 LiMnO4 Cells		
480 F Cells		

11.2 Gas Production

During these worst-case tests, the volume of combustion gases released/produced during the reaction inside the BSL ranged from 5.6 to 9.4 m^3. About 65% of this gas was CO_2 and remaining was CO. On a mass basis, the amount of CO_2 produced ranged from 6.4 to 10.9 kg and the amount of CO produced ranged from 0.7 to 3.8 kg.

A significant quantity of unburned hydrocarbons was also produced but the amount could not be quantified with the instruments installed in the BSL and test compartment during these tests.

The cylindrical BSL was designed to vent the reaction gases when the pressure in the BSL reached 50 psi. Therefore, it was estimated that 85% of this gas vented outside the LCBMS.

12 BATTERY CASUALTY CLASSIFICATION

There are currently no established criteria for classifying the hazards associated with a lithium battery casualty. Table 30 provides a simplified approach to characterizing these events. A general description of these hazards follows.

Table 30 — Battery Hazard Classifications (Simplified Approach)

Hazard Parameter	Significant	Moderate	Insignificant
Explosion and Fragments	Will cause injury to unprotected personnel within the compartment of origin with compartment overpressures >1 PSIG or or release of any fragment with >15 ft/sec velocity or >20 ft-lb impact loading	Could cause injury to unprotected personnel in close proximity to the battery with compartment overpressures >0.25 PSIG or release of any fragment with >5 ft/sec velocity	Unlikely to cause injury (<0.05 PSIG overpressure) and no debris greater than 0.2 ft from battery
Fire/Thermal – HRR	PHRR > 100 kW for any duration	100 kW > PHRR >10 kW	PHRR < 10 kW
Fire – Fragments	Flaming fragments projected > 3 ft	Flaming fragments projected up to 3 ft	No flaming fragments
Aerosol Products	Loss of visibility within the compartment of origin and/or the production of explosive mixtures	Loss of visibility in close proximity to the battery (3 ft)	No loss of visibility
Gaseous Products (F)	Flammable concentrations within the compartment of origin	Flammable concentrations in close proximity to the battery	No flammable gases produced
Gaseous Products (T)	Toxic/hazardous concentrations within the compartment of origin for protected personnel	Toxic/hazardous concentrations in close proximity to the battery for unprotected personnel	No toxic/hazardous gases produced

PHRR = Peak Heat Release Rate (F) = Flammable (T) = Toxic

The same hazard parameters are typically produced during every reaction but to varying degrees: flammable by-products (aerosols, vapors, and liquids), toxic gases, flying debris (some burning), and sustained burning.

On a local scale, the exposures produced by the reaction are a function of the battery chemistry, the number of cells involved in the reaction, and the distance between the battery and the item of concern. On a global scale, the exposures produced by the reaction are a function of the battery chemistry, the number of cells involved in the reaction, and the size of the compartment in which the reaction occurs.

In the case of immediate ignition of gases as they discharge from a battery, the thermal exposures produced by the casualty are localized to a region around the reaction and significantly decrease with distance away from the battery/battery pack. Therefore, thermal exposures to equipment and personnel are only a concern in the region in close proximity to the battery (within a few feet of the battery). The main concern associated with these localized thermal conditions is the exposures to adjacent cells within the pack and adjacent batteries/battery packs within the storage device.

There is also a separate concern associated with nearby combustible materials. Based on limited data, it may be assumed that flaming debris from a battery casualty could cause ignition of combustible materials anywhere within the fragment zone/volume. Precautions should be taken to avoid or limit the storage of combustible materials near lithium batteries.

The primary hazard associated with a battery casualty appears to be the gases produced during the reaction. These gases have been determined to be toxic and in some cases flammable. The concentration of toxic and/or flammable gases is a function of the battery chemistry, the number of cells involved in the reaction, and the size of the compartment in which the reaction occurs. Due to the production of copious amounts of gases during the reaction of larger batteries and battery packs, it must be assumed that any battery casualty will render the storage compartment untenable for unprotected personnel (personnel not wearing a breathing apparatus).

Another significant concern is the production of a flammable mixture of gases (explosive mixture) within the storage compartment. If the resulting mixture is in the flammable range, the delayed ignition of the gases in the space can produce a large fireball and overpressures that could produce structural damage and additional battery casualties. In this scenario, the thermal exposure would be on a large scale, resulting in a hazard to personnel from thermal exposure, overpressures, and flying debris.

13 SUMMARY

The Naval Research Laboratory recently participated in, and completed, several major research programs initiated to characterize and mitigate lithium battery fire hazards for a number of applications. More than 100 battery casualty tests were conducted to characterize the conditions produced during a range of both unmitigated and mitigated casualties. This report summarizes the results of these tests.

The primary failure mode of a lithium battery is associated with a flaw or damage to the thin porous electrical insulation layer that separates the anode and the cathode (the separator). This is typically a microporous polyolefin layer in the Li-ion cells and a glass or ceramic paper in oxyhalide cells. Damage to the separator can result in an internal short circuit that produces enough heat to vaporize the electrolyte or in the case of a primary metallic lithium anode, melt and allow massive internal shorting and direct anode-catholyte reactions that result in a violent venting or explosive reaction. The separator can fail due to internal defects (production issues), physical damage (handling issues), exposure to high temperature (fire), and in the case of secondary cells, overcharging resulting in bridging of the separators. Once an internal short develops, a sudden release of stored energy occurs, commonly referred to as thermal

runaway. This event can cascade to adjacent cells and throughout an entire battery pack and ultimately destroy the device the battery is installed in and catastrophically impact the platform and personnel.

The requirements the U.S. Navy has adopted for the lithium battery safety program include a Preliminary Hazard Analysis, Battery Casualty Characterization Tests, Hazard Mitigation Tests, and a final Systems Hazard Analysis (SHA). There are two general types of tests conducted to characterize the battery casualty: reaction products testing and burning characteristics testing (heat release rate).

In the testing reported here, the reaction products were characterized for 19 different cells covering a range of chemistries, form factors, and capacities.

In general, when a cell casualty can be described as a venting reaction (no ignition), the majority of the products released are electrolyte constituents (i.e., carbonates or oxyhalides). These flammable gases and aerosols can accumulate and have the potential to produce an explosive atmosphere (explosion hazard). Explosive environments can be prevented by rapidly ventilating the space.

For the oxyhalides, the resulting dispersion generates an immediate risk to personnel from the acid gases (HCl, H_2SO_4, and HF). These products are also hazards to electronic equipment and have long-term effects on materials of construction.

For cell casualties that result in a burning reaction, the organic based electrolytes burn efficiently, producing CO_2 as the primary by-product, provided sufficient oxygen is available in the supporting atmosphere. Other products include CO and some amount of acid gases. Complete combustion is not assured, as the electrolyte and constituents are dense and may consume the limited oxygen in the cell, shifting the combustion products toward incomplete combustion with a large production of CO.

The acid gas production is directly related to the cell chemistry (and appears to be related to cell capacity and overall thermal effects), especially in the presence of high water vapor. Cells that contain sulfur produce sulfuric acid, cells that contain fluorine produce hydrofluoric acid, and cells that contain chlorine produce hydrochloric acid. It is proposed that for a given cell chemistry, the amount of acid gas produced should be directly proportional to the cell energy.

The heat release rates of the majority of the single cells were too low to measure using the 1 MW hood calorimeter on the ex-USS *Shadwell*. For future assessments, the heat release rates of the small commercial cells will be measured using a smaller hood calorimeter (10 to 100 kW). Ultimately, the HRRs of many of these cells were determined based on the results of tests on battery packs.

A wide range of battery pack configurations, groups of battery packs, and groups of battery modules were tested during these programs. There were significant differences in the types of reactions observed in the pack/module tests compared to the single cell tests. Specifically, except for the iron phosphate cells, almost all the packs/modules produced burning reactions, while many of the single cells only vented and never caught fire. In addition, during almost every unmitigated pack/module test, all the cells in the battery pack/module reacted and the casing materials were completely consumed.

The combustion energy potential was shown to be proportional to the electrical energy potential. The rationale is that the amount of combustibles (electrolyte and separator material) should be proportional to the electrical energy potential. However, the battery pack casing can provide a significant amount of fuel/energy to the fire. After adjusting the combustion energies to account for the case material, there is fairly good agreement between the results of the tests, suggesting that the combustion energy is typically about six times the electrical energy potential of the battery. The effect of a plastic case and packaging mass was found to be as high as 70% of the overall HRR with low thermal effect cells. Iron phosphate

based cells were combined and tested with ruggedized shipping containers and found to be fairly benign compared to other lithium batteries tested.

With respect to the fire hazard, the fire produced by the battery packs assessed during these programs was fairly energetic, but as a whole, should not be overmatching for a standard, properly attired fire response team. Most of the battery packs assessed during this program, with the exception of the large format battery packs, produced fires equivalent to the size of a large trashcan fire (20 to 50 kW). The large format battery packs contained an amount of energy equivalent to a gallon or two of JP-5 fuel (200 to 700 kW). In either case, suited-out responding personnel should be able to approach a battery casualty consisting of one of these and suppress/extinguish the fire through the application of copious amounts of water. However, for unmitigated bulk storage configurations, the fire has the potential to rapidly spread and can produce flashover conditions within the room.

Fire spread to adjacent batteries can be prevented by stowing the battery in a metal case and/or a segregated metal cabinet/locker. Fire insulation may also be required depending on the battery casualty characteristics, the thickness of the metal structure, and proximity to adjacent combustibles or batteries. Limitations of air and replenishment air will limit fire spread and may serve as a passive suppression system, although there is a possibility of back draft explosion as air is reintroduced to a hot room.

The precepts for the rapid control and suppression of a battery casualty were based on the development of a Battery Storage Locker similar to a commercial off-the-shelf flammable liquid storage cabinet. Tests were conducted to quantify the conditions produced in a prototype rectangular BSL and to assess/refine the design of an overall LBCMS. These conditions became the basis for the performance requirements for the system and components. The final design was a pressurizable cylindrical BSL. Two series of tests were conducted to validate the capabilities of the cylindrical BSL and the overall LBCMS.

Thirty-seven mitigation tests were conducted, all of which included some form of detection and 13 of which included active suppression.

The detection test results show that there are no universal precursors to a battery casualty that can be used for early warning detection for all types of batteries and systems. However, the results demonstrated that a smoke detector works well for detecting a casualty early into the event (i.e., after the first cell or group of cells have vented and/or caught fire).

The suppression system results show that water, or water-based agents, have good capabilities for managing the heat released during a battery casualty and have the potential to stop fire spread to adjacent batteries. The results demonstrate that cell-to-cell propagation within a large multicell pack can be stopped if the pack is rapidly submersed in water if the water can penetrate the battery pack. The final BSL design includes a sprinkler head installed inside each battery storage compartment. If battery packs (of the type studied) are colocated in adjacent storage areas, it is recommended they be protected from radiative and convective heat transfer.

REFERENCES

1. D. Linden and T. Reddy, *Handbook of Batteries,* 3rd ed. (McGraw-Hill, 2002).

2. F.W. Williams, X. Nguyen, J. Buchanan, J.P. Farley, J.L. Scheffey, J.T. Wong, H.V. Pham, and T.A. Toomey, “Ex-USS Shadwell (LSD-15): The Navy’s Full Scale Damage Control RDT&E Facility,” NRL Memorandum Report NRL/MR/6180--01-8576, August 24, 2001.

APPENDIX

VIDEO CLIPS FROM LITHIUM SINGLE CELL AND MULTICELL BATTERY CASUALTIES

Video clips (MP4 files) are on the enclosed DVD

A1 SINGLE CELL BATTERY CASUALTY VIDEO CLIPS

B-1 Cells $Li/Li_{0.5}CoO_2$ AA Size

File	Camera	Date	Start Time	SOC, %	Insult
146	Clip 8	11/3/2009	?	100	Heater
147	Clip 11	11/4/2009	?	100	Heater

B-2 Cells $Li/SOCl_2$ AA Size

File	Camera	Date	Start Time	SOC, %	Insult
123	5	8/20/2009	11:35:25	100	Propane

B-3 Cells $Li/SOCl_2$ D Size

File	Camera	Date	Start Time	SOC, %	Insult
151		4/15/2010	?	100	Heater
118		8/3/2010	12:47:20	100	Heater
119		10/13/2010	13:26:45	100	Heater

B-4 Cells Li/SO_2Cl_2-$SOCl_2$ D Size

File	Camera	Date	Start Time	SOC, %	Insult
157		4/16/2010	use all	100	Heater
120		8/6/2010	13:01:50	100	Heater

C-1 Cells $LiFePO_4$ 18650 Size

File	Camera	Date	Start Time	SOC, %	Insult
73	Exterior	1/4/2010	13:21:00	~40	Heater
74	Exterior	1/5/2010	10:15:15	100	Heater
75	Exterior	1/8/2010	14:21:30	discharged	Heater

D-2 Cell $Li/LiFePO_4$ 26650 Size

File	Camera	Date	Start Time	SOC, %	Insult
141*	Outside Chamber	7/19/2011	10:41:45	100	Heater

*Note: the banner on the video clip describes a18650 form fit, when actually it is a 26650 form fit.

E Cell $Li/Li_{0.5}CoO_2$ 18650 Size

File	Camera	Date	Start Time	SOC, %	Insult
83	Exterior	8/2/2010	13:56:00	100	Heater

F Cells Li/CF_x C Size

File	Camera	Date	Start Time	SOC, %	Insult
142	Outside Chamber	4/12/2010	7:00	100	Heater
143	Outside Chamber	4/12/2010	3:40	100	Heater
163	Exterior	5/24/2010	10:31:00	100	Heater
86	Inside Box	8/2/2010	15:03:20	100	Heater
88	Outside Box	8/2/2010	15:03:16	100	Heater

H-1 Cell Li/MnO_2 5/4 C Size

File	Camera	Date	Start Time	SOC, %	Insult
159	Outside Chamber	4/14/2010	?	100	Heater

H-2 Cell Li/MnO_2 D Size

File	Camera	Date	Start Time	SOC, %	Insult
158	Outside Chamber	4/12/2010	?	100	Heater

I-1 Cells $LiNiCoAlO_4$ Large Form Size

File	Camera	Date	Start Time	SOC, %	Insult
91	Exterior	6/21/2010	11:36:50	20	Heater
92*	Exterior	6/21/2010	11:40:00	20	Heater
96	Exterior	12/7/2012	9:19:10	100	Burner
94	Exterior	6/21/2010	13:54:38	100	Heater

*This is a continuation of file 91 same test later time

I-2 Cells $LiNiCoAlO_4$ Large Form Size

File	Camera	Date	Start Time	SOC, %	Insult
98	Exterior	12/6/2010	14:07:20	20	Burner
100	Exterior	6/22/2010	9:34:00	20	Heater
102	Exterior	6/22/2010	11:22:10	100	Heater
106	Exterior	6/24/2010	14:43:30	100+	Overcharge

I-3 Cells $LiNiCoAlO_4$ Large Form Size

File	Camera	Date	Start Time	SOC, %	Insult
108	Exterior	6/22/2010	13:53:25	20	Heater
109	Exterior	12/7/2010	12:26:50	100	Burner
112	Exterior	12/8/2010	13:28:28	100	Burner
110	Exterior	6/23/2010	9:54:20	100	Heater
113	2	6/24/2010	12:14:40	100+	Overcharge

J Cells $LiCoO_2$ Polymer Pouch Size

File	Camera	Date	Start Time	SOC, %	Insult
78	Exterior	12/8/2010	11:56:00	100	Burner
79	Exterior	6/23/2010	14:49:19	100	Heater
81	Exterior	6/25/2010	11:02:45	100+	Overcharge

Li/MnO_2 cell 18650 Size

File	Camera	Date	Start Time	SOC, %	Insult
162	Outside Chamber	6/17/2010	11:57:55	100	Heater

A2 MULTICELL LITHIUM BATTERY CASUALTY VIDEO CLIPS

$Li/Li_{0.5}CoO_2$ 18650 Size

File	Camera	Date	Start Time	SOC, %	Insult
125		5/26/2010	14:-07:47	20	Heater
126		5/27/2010	9:45:04	100	Heater
127*			9:45:35		
128		5/28/2010	11:53:21	100	Heater
129**			11:53:54		

*Continuation of the test shown in File 126
**Continuation of the test shown in File 128

Simulated #3 Battery Li/CF_x (480 cells) C Size

File	Camera	Date	Start Time	SOC, %	Insult
52*		9/22/2011	11:44:40	100	heater

*Pressure vessel with the relief valve set at 50 psi.

$LiCoO_2$ Polymer Pouch Size

File	Camera	Date	Start Time	SOC, %	Insult
61	Exterior	1/7/2010	13:51:50	100	Heater
63	Exterior	1/7/2010	16:42:10	100	Heater
11	Exterior	12/15/2010	14:27:48	100+	Overcharge
12	Infrared	12/15/2010	14:27:48	100+	Overcharge

$Li/FePO_4$ 18650 Size

File	Camera	Date	Start Time	SOC, %	Insult
58	Exterior	1/5/2010	13:24:00	100	Heater

$Li/FePO_4$ 26650 Size

File	Camera	Date	Start Time	SOC, %	Insult
57	Exterior	1/14/2010	11:21:00	100	Heater
54	Exterior	1/7/2010	15:43:30	100	Heater

Li/MnO_2 5/4 C Size

File	Camera	Date	Start Time	SOC, %	Insult
68	2	8/4/2010	14:07:00	100	Heater
69	3	8/5/2010	9:55:15	100	Heater

$LiNiCoAlO_4$ Large Form Size

File	Camera	Date	Start Time	SOC, %	Insult
26	Passageway	12/16/2010	10:07:20	100+	Overcharge

CHAPTER 4 – DESIGN PRECEPTS

In addition to the design guidance provided in NAVSEA TM S9310-AQ-SAF-010, this chapter defines additional guidance for the design of lithium battery systems where use on Navy platforms is anticipated. Failure to meet one or more of these functional safety requirements may necessitate alternative risk mitigation efforts, or result in residual risk that must be accepted by increasing levels of authority.

4-1 PREVENTION/MITIGATION OF ENERGY RELEASE.

The battery system shall be designed in such a manner that the unexpected, uncontrolled release of energy in any form (thermal, mechanical, or electrical) is mitigated to a point acceptable by the appropriate authority.

4-1.1 THERMAL ENERGY RELEASE.

The battery system shall be constructed in such a manner that it either insulates cell-level thermal events to prevent thermal failure propagation to adjacent cells, or such that it conducts heat away from adjacent cells and modules with sufficient speed and efficiency to prevent sympathetic cell failure and propagation. The ability to prevent cell failure propagation shall be verified by test in accordance with section 5-2 of this manual, at the temperature extremes of the intended usage and/or storage environments. A detailed thermal analysis may be necessary, using an appropriate computational model to further ensure that in the event of cell thermal runaway, propagation from one cell or module to another is mitigated for the various possible modes of operation (e.g., with battery in air or in water). Such analyses should also be used to determine the fidelity of temperature sensors placed at various locations for the early detection of thermal runaway.

4-1.1.1 Thermal Impact.

Provisions shall be made to accommodate and mitigate – in a safe manner – the thermal impact of all ejecta (solids, gases, particulate, aerosols, etc.) from a battery failure that may be released to the platform. Gases venting from burning lithium cells may include a variety of hazardous materials, including Hydrogen Fluoride (HF). Furthermore, these gases are hot enough and corrosive enough to cut through a variety of construction materials. Therefore, a conscious effort shall be made by designers to prevent the direct impingement of hot gases from cell vents on critical structural components of Navy platforms in the event of a battery fire. Furthermore, the thermal impact caused by combustion or explosion of any flammable ejecta shall be mitigated.

4-1.2 MECHANICAL/PRESSURE/KINETIC ENERGY RELEASE.

Catastrophic failure of a lithium-based battery will result in the evolution of large volumes of gases. For battery systems housed within pressure vessels, these gases must be either safely contained or relieved such that the pressure vessel itself does not become a hazard.

Upon characterization of the gas volumes and heat generated by a battery failure, an analysis shall be performed to determine if the pressure vessel meets the PASS requirements of Table I of NAVSEA

TM S9310-AQ-SAF-010 (Aug 2004 Rev).

For battery systems housed within pressure vessels that do not meet the Pass/Fail requirements of Table I of NAVSEA TM S9310-AQ-SAF-010 (Aug 2004 Rev), detailed mitigation plans shall be developed and verified to prevent a hazardous release of pressure.

The pressure vessel shall incorporate intentional failure points/mechanisms to prevent material failure of the housing itself. The mechanisms shall be designed to release the volumes of gas expected based on testing detailed within this manual. Examples of pressure relief devices include, but are not limited to:

- Belleville washers on pressure vessel bulkhead fasteners.
- Urethane springs on pressure vessel bulkhead fasteners.
- Shear-pin bolts on pressure vessel bulkhead fasteners.
- Pressure relief discs/ports/flapper valves on the pressure vessel.

The pressure relief mechanism chosen in the design shall be evaluated and tested to ensure particulates or other materials released during a battery failure will not cause failure/blockage of the pressure relief mechanism. Note: Lithium cells can eject up to half of their mass as particulate during failure, and can eject larger pieces of internal components (e.g., current collector foils) as well.

Provisions shall be made to accommodate and mitigate the mechanical impact of all ejecta (solids, gases, particulate, aerosols, etc.) released to the platform during a battery failure. Furthermore, the mechanical impact caused by combustion or explosion of any flammable ejecta shall be mitigated.

4-1.3 ELECTRICAL ENERGY RELEASE.

Battery systems shall be designed with mitigations to limit the release of electrical energy resulting from a battery failure.

The battery system shall be designed such that failure of any battery component does not create an electrical short circuit that causes cell failure, cell failure propagation, or other hazards, including uncontrolled release of energy in any form. Battery cables, connectors, and interconnects must be secure and capable of withstanding fire without creating loose power cables inside battery bottles and housing.

The battery system shall be designed such that short circuit paths that can be created by inadvertent operator error or system faults are mitigated via the use of electrical interruption devices and/or physical designs/layouts that prevent operator injury and catastrophic damage to the cells or battery.

Electrical Safety Devices (ESDs) (e.g., contactors, fuses, circuit breakers, diodes, Positive Temperature Coefficient [PTC] Devices, Current Interrupt Devices [CIDs], etc.) shall be tested and proven at voltages and currents that can be encountered during operation or during failure. Failure of such electrical devices shall not permit or create catastrophic cell or battery failure. The behavior and failure of such devices at the intended system voltages, currents, and operating environments shall be tested and well understood before acceptance and implementation as a system safety device.

In addition to software-based and user-initiated overvoltage/overcharge protection, to the extent possible, the battery shall be designed with passive hardware-based overvoltage/overcharge protection.

4-1.4 INADVERTENT ENVIRONMENTAL STRESS OR ABUSE.

Design requirements for tolerance to inadvertent abuse such as drop, impact shock, electrical abuse, thermal abuse etc., shall be established and reviewed by the program office and NAVSEA 05.

4-2 BATTERY MANAGEMENT SYSTEM (BMS).

4-2.1 BATTERY MONITORING.

For the purposes of this manual, the design goal of the BMS is to provide effective detection and mitigation of any condition that can lead to energetic or catastrophic failure of the battery. The battery system shall be equipped with an automated BMS capability that is commensurate with the potential hazards and levels of risk posed to the platform by failure of the battery.

The BMS shall provide, to the operator and to any automated battery control system and/or platform damage control system, all data necessary to assess the health of the battery and to make real-time decisions regarding control, continued use, and failure response/mitigation. The BMS shall be capable of providing data during all operational phases of charge, discharge, and open circuit, and during non-operational phases, including storage and handling, as appropriate.

Examples of data and capabilities that may be required include but are not limited to:

- The capability to monitor the temperature of cells and detect the presence of anomalous heating within a cell.
- The capability to monitor individual cell voltages and detect individual cell voltage excursions.

- For battery systems housed within a vessel, the capability to monitor ambient air/gas temperature and detect air/gas temperature excursions.

- For battery systems housed within a pressure vessel, the capability to monitor the pressure within the vessel and detect pressure excursions.
- For battery systems housed within a pressure vessel, the capability to monitor and detect the potential for a combustible environment.
- For battery systems housed within a pressure vessel and intended for underwater use, the capability to monitor and detect seawater leakage.
- The capability to provide both audible and visual alarms to the operator.
- The capability to report alarm status information to an area of the platform that is continuously manned and monitored.
- The capability and algorithms to determine State of Charge (SOC) of the battery and of individual cells.
- The capability to detect and report battery system and cell self-discharge characteristics.

Primary battery systems greater than 1 kWh shall contain a battery monitoring system.

4-2.2 BATTERY CONTROL.

Via a combination of operator input and automated intervention, the BMS shall be capable of safely securing the battery system and limiting potential damage to the host platform.

4-2.3 CONTROL OF BATTERY CHARGE (FOR RECHARGEABLE BATTERIES).

The operator shall be capable of manually halting charge or discharge of the battery system at any time. The BMS shall be capable of automatically halting charge and discharge based on critical sensor readings (e.g., cell temperature, voltage, pressure, current, etc.).

Battery charging shall be a closely monitored evolution where an operator is required to monitor battery charging outputs either in real time or through an automated charging system. Verbatim compliance to all charging precautions and approved initial conditions (wet or dry environment, specific volume flows surrounding the charge, etc.) shall be required. Software specifically designed for charging shall be installed and tested only by an approved activity and shall have NAVSEA-approved documentation for any changes. The SSA shall ensure battery charging software changes are approved and comply with the software safety requirements of this manual.

.

CHAPTER 5 – TESTING AND ANALYSES

All lithium batteries are subject to the standard safety test protocols in NAVSEA TM S9310-AQ-SAF-010, which include but are not limited to: short circuit, ESD testing, overcharge, over-discharge, and thermal abuse. The program office and system developer shall collaborate with NAVSEA 05 and NOSSA to establish a TP that defines which casualty characterization tests in Chapter 5 of this manual are required, based on the hazards and mitigations identified for the program. Tests required to satisfy the needs of both NAVSEA TM S9310-AQ-SAF-010 and this manual (NAVSEA TM SG270-BV-SAF-010) shall be identified, to avoid unnecessary duplication of efforts. Furthermore, the database being compiled by NAVSEA 05 should also be used to avoid unnecessary additional testing in those situations where sufficiently similar batteries have already been characterized.

The applicability of the specific test paragraphs of Chapter 5 of this manual derive directly from the System Safety Program Plan, from the specific hazards identified in the program's PHA and SHA, and from the mitigations proposed for each hazard.

NAVSEA TM S9310-AQ-SAF-010 tests may be conducted as precursory events or in parallel with the tests required by this manual as shown in Figure 5-1.

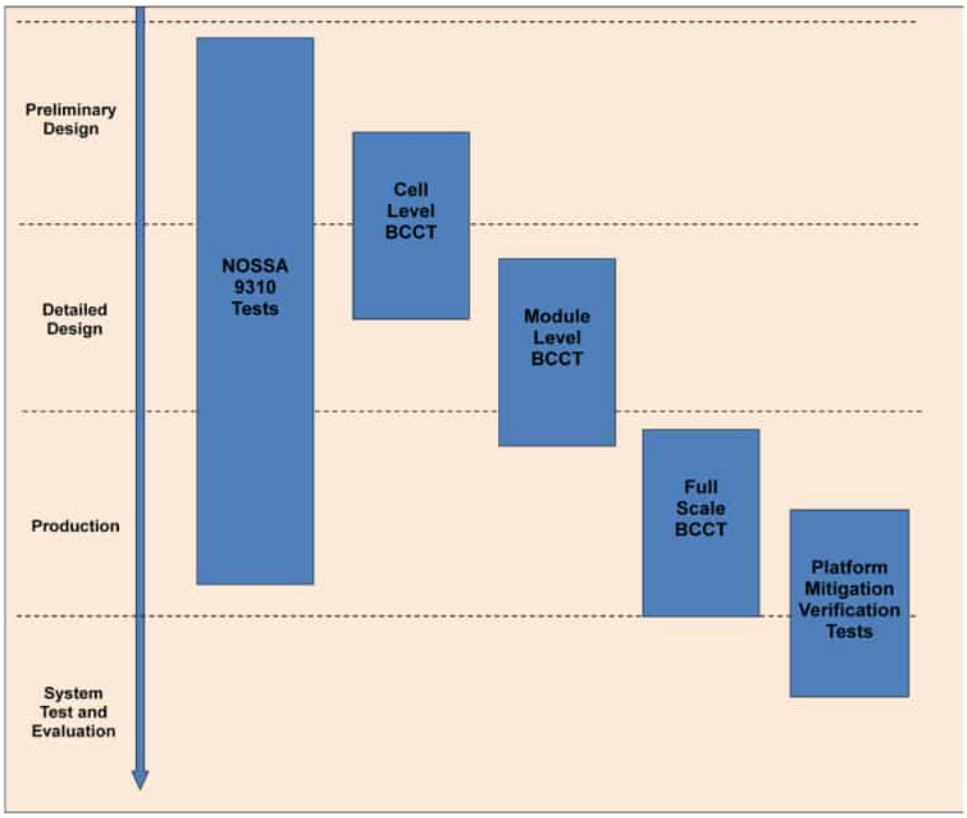


Figure 5-1. Notional Phasing and Coordination of Tests Called out by NAVSEA TM S9310-AQ-SAF-010 and NAVSEA TM SG270-BV-SAF-010.

5-1 GENERAL REQUIREMENTS.

NAVSEA TM SG270-BV-SAF-010 testing is necessary to characterize the hazards (corrosive and toxic gas production, heat release rates, debris ejection, pressure transients, propagation risk, etc.) from individual cells, groupings of cells, and batteries and in turn, to understand the risks that these hazards pose to personnel, systems, and platforms carrying or associated with the battery. Tests shall be conducted on individual cells; groupings of cells such as cell branches, modules, or Lowest Replaceable Units (LRUs); and full-scale batteries as defined in the TP and approved by NAVSEA 05.

NAVSEA TM SG270-BV-SAF-010 testing is designed to characterize the impact to the platform of the Worst Credible Event (WCE) involving a lithium battery casualty, and to evaluate the planned mitigation techniques. Battery testing shall be conducted in three categories:

- Cell and Battery Casualty Characterization Testing (BCCT) (see paragraph 5-3).
- Platform Characterization and Mitigation Testing (see paragraph 5-4).
- Platform Level Survivability/Recoverability and Environmental Testing (see paragraph 5-5).

The parameters of these tests shall be determined on a case-by-case basis as justified by the PHA, SHA, CONOPS, battery size and energy content, battery chemistry, and the potential sympathetic and collateral damage that a battery casualty may cause to the host platform.

Note: Test characterizations discussed in this section are intended to address all potential hazards and risks associated with the battery, the system, and the platform during any phase of use. For example, while the size, energy content, and chemistry of the battery are some of the most important drivers in characterizing failure energetics, it may also be important to include battery "shipping" or "packaging" material in casualty characterization tests because of the potential for such materials to act as fuel in the event of a fire. Also, in some battery chemistries, aerosols of organic electrolytes may be produced. The characterization of these aerosols is important, as they may present their own unique flammability or explosion hazards. The objective, therefore, is to characterize all relevant hazards, whether directly or indirectly associated with the battery.

5-1.1 TEST PLAN (TP) APPROVAL.

A TP shall be developed to address the known and unknown (or previously uncharacterized) hazards posed by the battery and system to personnel and to Navy facilities and platforms. This TP must be approved by NAVSEA 05 and/or their technical agents prior to execution. Tests to determine the platform hazards may be conducted without NAVSEA 05 pre-concurrence, but such tests are done at the risk that the data may be rejected or that additional tests may be required. The Platform Characterization and Mitigation section of the TP may be expected to evolve and undergo revision based on the emerging results of BCCT testing. All revisions to the TP must also be approved by NAVSEA 05 and/or their technical agents prior to execution.

5-1.2 TP CONTENT.

The PHL, PHA, SHA, FMEA, CONOPS, and any hazards and mitigations defined therein shall be used to determine the scope of the required tests, test methodologies, and test conditions. Hazards and failure modes identified in those documents shall be used to determine any data that must be gathered – whether specifically cited and required by this manual or not – to understand and characterize the behavior and potential risks of a battery casualty, both mitigated and unmitigated. Special consideration shall be given to the TP for any hazard determined to have an unmitigated HRI of 17 or lower.

Tests shall be conducted at the cell, module, LRU, full-scale assembly and system levels, as necessary to characterize the rate and magnitude of any heat, effluents, or ejecta generated by a cell or battery casualty. Chemical composition and quantities of gases or vapors evolved shall be characterized.

Tests shall subject assets to potential electrical, mechanical, and thermal influences that can cause significant battery events or failures. The potential for inadvertent environmental abuse such as mechanical shock or crushing events shall also be considered, and where not already covered under NAVSEA TM S9310-AQ-SAF-010, shall be included in the TP as agreed upon by the program manager and NAVSEA 05. For example, uncontrolled dropping, puncture, or crushing by a forklift or by

handling/loading equipment are examples of events that are not explicitly covered by NAVSEA TM S9310-AQ-SAF-010, but may be expected to occur with some, albeit low, frequency in shipboard environments.

The TP shall include the type and number of tests to be performed, the test conditions, orientation, and criteria for each proposed test, and the number of assets required. The TP shall define the data collection methods proposed, any test fixtures and equipment required, the location and facilities proposed, and the conceptual instrumentation arrangements and test layouts. The TP shall highlight and justify any off-scale, modularized, partial, or non-directly comparable test methods and test facilities proposed in lieu of required full-scale tests.

5-1.3 TEST CONDITIONS.

The TP shall address all aspects of CONOPS for system and battery support across the full life cycle. The full life cycle includes system development; system test and evaluation; system use and deployment; shipboard carriage, storage, maintenance, and handling of spares and replacement units; and disposal. Where not specifically directed otherwise by the TP, tests shall be performed under standard local environmental conditions. Non-ambient test conditions shall be given consideration and shall be included when driven by the CONOPS across the full life cycle. Temperature, pressure, and humidity shall be noted and recorded for each test in the test report.

5-1.4 SCALE AND FIDELITY.

When approved by NAVSEA, full-scale BCCT and platform-level survivability/ recoverability and environmental testing may be conducted at a reduced scale from whole batteries and systems (e.g., at the module scale or LRU scale) provided there is sufficient information to enable scaling factors to be accurately applied to the test results. When reduced scales are used, the reduction of fidelity and any potential underestimations of experimental error and/or scaling error shall be analyzed, discussed, and accounted for in the test report. When off-scale testing is conducted, the error associated with the off-scale test, and the error imparted by test facilities that are not fully comparable to the intended platform use, shall be assessed to the more severe levels. In other words, if the test system error of measurement is 10 percent of the total measurement, the hazard characterization shall be reported at the UPPER/HIGHER value. These results may be used to calibrate and validate predictive models.

5-1.5 SPECIAL CONDITIONS.

Unique test configurations and conditions beyond the tests described herein may be required to characterize special hazards where they are a concern, such as hull overpressure and underwater implosions or concussions. Where CONOPS/Logistics require recovery/storage/handling of systems at partial SOC, special testing at partial SOC may be required for lithium primary and secondary batteries to assess and characterize the hazards posed at cell-level and module-level to support final hazard analyses.

5-2 TEST METHODS AND REQUIREMENTS.

This section outlines general test methods and data-collection requirements. The methods outlined here shall be applied selectively to the various levels of cell, intermediate (LRU, module), or full-scale battery tests as appropriate to accomplish the required hazard characterization at that scale (i.e., not all tests listed in section 5-2 apply to all levels of test). Table 5-1 demonstrates how the hazard characterizations described below might apply to the various stages and levels of test.

Note that section 5-2 defines “what” tests may be required for a given application. Additional details regarding “how” these tests should be executed (e.g., the test techniques and the specifics of the measurements required for each characterization) are included in Appendix B.

Table 5-1. Hazard Characterizations Potentially Applicable to Different Levels of Test.

Battery Casualty Hazard Characterization Test	Cell-Level BCCT	Intermediate Module-Level BCCT	Full-Scale Assembly-Level BCCT	Platform Hazard Characterization and Mitigation Verification
5.2.1.2 Quantitative Off-Gas Production Analysis.	X			
5.2.1.2.1 Real-time and Continuous Monitoring of Gases.	X			
5.2.1.2.2 Grab Samples for Toxic and Corrosive Gases.	X	X	X	X
5.2.1.3 Volatile Off-Gas Ignition.	X	X	X	X
5.2.1.4 Thermal, Volumetric, and Pressure Impacts of Off-Gas Ignition.		X	X	X
5.2.1.5 Gas Velocity Measurements.		X	X	X
5.2.1.6 Heat Release Rate and Thermal Flux.	X	X	X	X
5.2.1.7 Pressure and Pressure Transients.	X	X	X	X
5.2.1.8 Incandescent Debris and Shrapnel.	X	X	X	X
5.2.1.9 Aerosol Analysis.	X			
5.2.1.10 Smoke Generation.		X	X	X
5.2.1.11 Metal and Material Exposure.	X	X		
5.2.1.12 Cell Failure Propagation Tests.		X	X	X
5.2.1.13 Mitigation Verification Tests.		X	X	X

5-2.1.1 Cell and/or Battery Failure Initiation Requirements.

Tests shall be designed to reliably initiate a cell and/or battery failure. The method of initiation of the cell and/or battery failure shall be determined from the PHA and should represent the WCE. The method of failure initiation shall be fully described in the TP and shall be approved by NAVSEA 05.

5-2.1.2 Quantitative Off-gas Production Analysis.

Cell and/or battery failure shall be initiated, causing the cell and/or battery to undergo thermal runaway with gaseous release.

Off-gas analysis shall be performed to fully characterize the quantity of gas produced, the rate of gas production, and the composition of the gas produced. Two methods shall be used to measure gas composition:

- Real-time online analysis to characterize bulk generation and decay rates of key bulk gas constituents.
- Whole gas analysis on grab samples to characterize finer details of gas component ratios and trace materials that might be toxic or corrosive.

Additional details on methods, techniques, accuracy required, and types of gases expected are included in Appendix B.

Hazard characterization tests and the corresponding gas analyses shall be conducted in both air environments and in inert environments if the battery is packaged or housed in such an environment, unless otherwise agreed to by NAVSEA 05.

5-2.1.3 Volatile Off-gas Ignition Requirements.

Where the battery electrolyte contains an organic solvent or other liquid that might exothermically react or combust upon contact with air, a triggerable gas ignition device shall be included in the test setup to provide a means of reliably igniting the vapors, fumes or aerosols produced by a battery venting.

In all mitigated and unmitigated BCCT characterizations, tests shall be conducted with the ignition device operated in both the ENABLED (active) and SECURED (off) mode to contrast the variability in results both with and without ignition and combustion of off-gasses produced by a battery failure. If a system produces potentially flammable gases and aerosols but these do not normally ignite during the casualty event, these gases SHALL BE triggered to evaluate the potential explosiveness of fuel-air mixtures. Tests shall be initially conducted with the ignition system SECURED. If the failure event itself does not automatically trigger combustion of the gases vented from the cell or battery module, tests shall then be conducted with the ignition source enabled and operating to acquire the necessary data from the secondary combustion of fumes, gases and aerosols.

5-2.1.4 Thermal, Volumetric, and Pressure Impacts of Off-gas Ignition.

A significant portion of the thermal casualty assessment is based on the sensible and radiant heat released from combustible sources in the area of the casualty. Hazard characterization tests and assessments shall therefore quantify the potential sensible and radiant heat from combustion of flammable gases or aerosols released from the battery, as described below.

Hazard characterization tests and assessments shall also quantify the amount of additional gas volume created by the battery casualty, and to characterize the "breathing" associated with the combustion processes. Dynamic pressures shall be measured during these test events, and estimates shall be provided regarding the total volume of gases produced in excess of the primary volume of gases released from the battery.

5-2.1.5 Gas Velocity Measurements.

When required by NAVSEA, the gas velocity of the casualty exiting the shipboard compartment shall be recorded. The gas volume, pressure, and temperature can be useful in determining how quickly gases may spread to other compartments of a ship. Additional details on methods, techniques, and accuracy required are included in Appendix B.

5-2.1.6 Heat Release Rate and Thermal Flux.

The heat release rate shall be characterized for the battery system under question. Characterization tests shall be devised to quantify the total heat released to the platform during battery failure, either as radiant heat, or as sensible heat due to conduction, convection, or combustion of evolved gases and/or aerosols. Additional details on methods, techniques, accuracy required, and special guidance for partially or fully oxygen starved environments are included in Appendix B.

5-2.1.7 Pressure and Pressure Transients.

Pressure transients may be produced by a cell or battery undergoing a casualty. Hazard characterization tests shall measure absolute pressure and rapid pressure transients within the test chamber or test compartment during test. Additional details on methods and accuracy required are included in Appendix B.

5-2.1.8 Incandescent Debris and Shrapnel.

Cells and batteries undergoing induced casualty failures may produce shrapnel and eject incandescent particles. Fragmentation of battery cases under casualty conditions shall be considered a potential hazard for co-located equipment. Cell and battery module tests shall therefore include witness plates, impact plates, and video coverage of the gas-analysis tests to assess impact of these ejecta on co-located equipment, if this has not already been accomplished during NAVSEA TM S9310-AQ-SAF-010 tests. Additional details on methods and accuracy required are included in Appendix B.

5-2.1.9 Aerosol Analysis.

A battery that contains an organic electrolyte or other flammable liquid may produce an aerosol that (depending on the particle size) could form an explosive-air mixture. This extends to electrolyte-solvent solutions that in a liquid state would not normally be characterized as flammable. Therefore, when required by NAVSEA, or recognized as a casualty failure mode, aerosol analysis shall be conducted. Additional details on aerosol measurements and the analyses required are included in Appendix B.

5-2.1.10 Smoke Generation.

The density of the smoke shall be determined and recorded in percent transmittance or extinction factor. Measurements shall be made using American Society for Testing and Materials (ASTM) standards or comparable methods.

5-2.1.11 Metal and Material Exposure.

When required by NAVSEA, representative metal and composite material coupons shall be prepared by cleaning and distributing in the chamber. After exposure during characterization tests, they are rinsed, weighted and visually inspected, to help determine the post-fire cleanup that would be necessary and the systemic material damage that would be caused by a casualty.

5-2.1.12 Mitigation Verification Tests.

Mitigation tests shall be conducted to verify that proposed mitigations are effective. Mitigation testing may be appropriate at the cell level, the module level, the full-scale assembly level, and at the platform integration level.

5-2.1.13 Cell Failure Propagation Tests.

Propagation tests shall be conducted to determine the effects of a critical failure of one cell to neighboring cells and/or from one grouping of cells to neighboring groupings of cells. The tests shall be conducted in a fashion that simulates the real system's physical constraints (i.e., cell/sub-system module spacing and orientation, free volume, packing material, wiring, etc). The PHA and CONOPS shall be evaluated to determine the best triggering event. Intermediate-scale tests may be conducted to understand the potential propagation hazards prior to testing at full-scale or in simulated platform compartments and enclosures. The goal of every program is to prevent cell to cell propagation.

5-3 BATTERY CASUALTY CHARACTERIZATION TEST (BCCT).

It is the objective of this general test series to subject the cells and battery in question to their worst-case failure scenario(s) in order to characterize the maximum unmitigated risk to the system, platform, and personnel. It is the intent of the unmitigated BCCT to cause and ascertain the unmitigated failure events and behaviors of batteries and battery systems described in the PHA and SHA. Tests which produce effects less severe than worst-case events may also be necessary and shall be outlined in the TP.

The results of the unmitigated tests shall be used to formulate and assess potential risk mitigation, firefighting, and casualty recovery techniques.

Tests shall be conducted on individual cells, groupings of cells, and full-scale batteries and systems to provide an accurate representation of the casualty.

5-3.1 CELL-LEVEL BCCT AND ANALYSES.

Tests shall be conducted in a sealed chamber to collect and analyze evolved gases and to measure the thermal effects of a casualty at the cell level. The results shall be further evaluated and used to provide data scalable to intermediate and a full-scale battery tests. The by-products of a cell casualty can be toxic or corrosive and as such need to be analyzed in order to appraise the hazard to platform and personnel.

The tests outlined in Table 5-1 may be required at the cell level.

5-3.2 INTERMEDIATE-LEVEL BCCT AND ANALYSES.

Intermediate-level testing may be conducted to increase fidelity and scalability of the data. Intermediate-level testing includes any testing that is more than one cell and less than a full-scale battery. Examples of intermediate groupings are cell branches, LRU, or sub-system modules. A properly crafted TP can utilize intermediate-level testing to greatly increase fidelity. The greatest benefit of intermediate-level testing is the ability to test for cell-to-cell propagation at a level less than full scale.

Intermediate-level tests may also include cell- and battery-level mitigation testing. This testing may be used as a design and verification aid. The mitigations explored at this level of test are those implemented within the battery itself, and might include variations in design parameters such as cell orientation and spacing, SOC, thermal barriers between cells, packaging of intermediate groupings, etc.

The tests outlined in Table 5-1 may be required at the intermediate or module level.

5-3.3 FULL-SCALE BATTERY AND SYSTEM-LEVEL BCCT.

While some scaling can be conducted using the single cell and intermediate-level test data, further unmitigated and mitigated BCCT shall be conducted on full-scale batteries and systems in their storage/operational configurations in order to gauge the true hazards to the system, platform, and personnel. In the event that full-scale batteries and systems cannot be used, modules or sub-modules shall be used in environments that are representative of the physical constraints and CONOPS of the actual system (materials of construction, packing materials, free volume inside packaging, co-located ordnance/flammable material, under pressure, etc) when approved by NAVSEA 05.

Mitigation techniques that are implemented on or within the battery itself (i.e., on or within the cell, intermediate assembly, or full-scale battery) shall be tested and evaluated at the full-scale during BCCT to verify their effectiveness. Examples might include variations in cell orientation and spacing, reduced SOC, thermal barriers between cells, packaging of intermediate groupings, etc. Verification test shall re-confirm all aspects of gas production, heat release, pressure effects, ejecta, etc., with mitigations in place.

Full-scale characterization tests shall be conducted in an appropriate enclosed space capable of representing the actual usage/stowage environment under controlled conditions to acquire and allow modeling of the hazard characteristics of a battery-system-platform interaction during a fire event. Test enclosures and full-scale tests shall simulate the nature and physical layout of the platform space, the sensitivity and criticality of the space, and other potential failures in the space. Examples of test space criticality and potential platform impact include but are not limited to: platform interaction with items in the torpedo room, lockout/lock-in chambers, dry deck shelters, external stowage trunks, and large-diameter tube stowage. The use of mock items or simulations (e.g., ordnance, valving, hydraulic piping, high-pressure gas bottles and feeds, personnel, personnel protective equipment) shall be considered based on location, size, and nature of the battery and system.

The tests outlined in Table 5-1 may be required at the full-scale battery assembly level.

5-4 PLATFORM-LEVEL HMT.

When identified by the TP or PHA, platform-Level HMT shall be conducted to develop and verify effectiveness of platform-level mitigation strategies and capabilities such as detection/alarms, automatic extinguishment/control, isolation/segregation, and casualty response procedures.

5-4.1 ENTRY CRITERIA.

At this stage, the following tasks shall have been completed to serve as the basis of the HMT:

- Hazards shall have been identified by the PHA.
- Level of unmitigated hazard shall have been quantified by the BCCT.
- Performance requirements of the mitigation technique shall have been defined.
- Potential mitigation techniques shall have been identified.
- A test methodology shall have been developed.

5-4.2 HAZARD MITIGATION TECHNIQUE SELECTION AND DEVELOPMENT.

Potential mitigation techniques identified during the PHA may include segregation, the use of storage containers, the installation of an early warning fire detection system, the installation of a fast response fire suppression system, manual intervention, or other techniques. If fresh water is used for firefighting a high-voltage system, it must be shown that explosive gas pockets are not formed. These techniques shall be assessed in terms of feasibility, ship impact and cost. Analyses must also demonstrate that the mitigation techniques do not introduce a secondary hazard. When higher level risks cannot be accepted

by the TWH without evaluation of further mitigation, a technique or combination of techniques shall be selected for further development and testing.

5-4.3 HAZARD MITIGATION EFFECTIVENESS.

Based on the discussions between the program manager, system developer, and NAVSEA 05, the safety TP shall include verification tests to assess the effectiveness of the proposed mitigation technique(s) and to quantify the resulting exposures produced during the test scenario. These exposures include the likelihood for fire spread, heat exposures to vital equipment, ordnance, and personnel, and chemical (toxic or corrosive gas) exposures to equipment and personnel. The tests shall be designed to challenge the mitigation technique(s). The tests may focus on a specific parameter identified during the PHA as undesirable or unacceptable. The effectiveness of the hazard mitigation technique(s) shall be evaluated versus the unmitigated BCCT tests conducted previously. The TP (including hazard mitigation test rationale) shall be approved by NAVSEA 05 prior to conducting the tests.

5-5 PLATFORM-LEVEL SURVIVABILITY/RECOVERABILITY AND ENVIRONMENTAL TESTING.

Other tests as required by the program's system specification may have a bearing on the safety and the design of the battery and its integration onto the platform. The following list is not exhaustive, but provides examples of scenarios where an environmental insult traceable to a system specification may induce a casualty of a battery system producing unexpected effects and results. NAVSEA and the program office shall review and agree upon the need for additional tests in this category, with consideration given to the impacts on platform and personnel under such conditions.

- Implosion.
- Hydrostatic crush.
- MIL-S-901 (shipboard shock).
- 40-foot drop.
- Bullet/fragmentation penetration.
- Fast cook-off/slow cook-off.
- MIL-STD-167 (shipboard vibration).

APPENDIX A – LITHIUM BATTERY-SPECIFIC CONTENT FOR HAZARD ANALYSES (PHA, SHA), FMEA, FMECA, HAZARD LOGS/RECORDS, SAFETY CRITICAL CRITERIA, AND SOFTWARE ANALYSES

A-1 HAZARD LOG AND RECORDS.

A Hazard Log comprising a collection of Hazard Records similar to the one shown in Figure A-1 shall be compiled and used as the master file to track, control, and communicate the technical and approval status of each hazard. A Hazard Record summarizes the key information relating to a specific hazard, including present status and history, failure mode and effects, mitigations, and associated risk assessments. Any pertinent information from the PHA, SHA, or other documentation that supports or bears upon the information summarized in the Hazard Record is referenced in the Hazard Record. The Hazard Log provides a concise and expedient vehicle for stakeholders to communicate and document the status of each hazard, as well as any agreements among stakeholders regarding risk assessments, and approvals of any tests or analyses that have been completed or are planned to verify mitigations. The Hazard Log is updated any time new information becomes available during the program's evolution. The Hazard Log and Hazard Records shall be placed under configuration control at the beginning of the Preliminary Design Phase, and shall contain as a minimum:

- Description of each hazard, to include associated HRI.
- Status of each hazard and control.
- Traceability of resolution on each Hazard Log item from the time the hazard was identified to the time the risk associated with the hazard was reduced to a level acceptable to the MA, including any interim approvals issued and the issuing authority.
- Identification of residual risk.
- Action person(s) and organizational element.
- The recommended controls to reduce the hazard to a level of risk acceptable to the MA.
- References to supporting design documentation, analyses, test data, etc., that verify the effectiveness of each recommended control or mitigation.
- The signature of the MA accepting the risk and thus effecting closure of the Hazard Log.

Hazard Record

Original Identification Date:

Project: System:

SHA Ref: Subsystem: Preparer:

Record#: Assembly: Reviewer:

Component: Designer:

History ID/Rev. Date	Status (Open/ Closed)	Risk Assessment:		HRI	Rating (Acceptable/ Unacceptable	Comments
		Severity	Probability			

Hazard Description:

Failure Mode:

Failure Effects:

Mitigating Actions:

Reference: Approval & Date:

Remarks:

Approval: Program Manager _____ Authorized SignatureDate

Approval: NAVSEA _____ Authorized SignatureDate

Figure A-1. Sample Hazard Record.

A-2 HAZARD ANALYSES (PHA, SHA).

A-2.1 GENERAL.

The overall objectives of the Hazard Analysis Program are to identify and evaluate hazards posed by the battery, to assess potential impacts to the system, platform, and personnel, and to evaluate the effectiveness of mitigations. The program office shall perform a PHA early in the program and an SHA later in the program as the system design matures and as results of BCCT and HMT become available.

Ultimately, the SHA shall verify the system compliance with system safety requirements and shall identify all hazards associated with subsystems, interfaces, and faults. The SHA will assess the risk associated with the total system design, including software. It will recommend actions necessary to eliminate identified hazards and/or control their associated risk to acceptable levels.

Hazard analyses shall be conducted following the requirements of MIL-STD-882.

A-2.2 CONTENT.

The hazard analysis shall include an overview of the primary components, interfaces, and functions of the system using the lithium battery (or batteries). The hazard analysis shall further describe the battery type, its characteristics, quantities to be stored or used, expected handling and usage protocols, intended platform or platforms, and specific locations of use, transport, or storage aboard the platform(s). Surrounding compartments adjacent and above the compartment containing the battery shall also be identified. The temperature ranges of the compartment during both storage and use shall be declared. If the battery system in question is to be charged onboard the platform, this shall be noted and the location of the battery during charging shall be declared. The hazard analysis shall identify planned co-location of the battery with other systems using similar batteries, co-location with flammable, combustibles or thermally sensitive materials, or co-location with ordnance (e.g., battery stowage in the torpedo room co-located with ordnance).

The hazard analysis shall include the results of any hazard or casualty characterization tests that may have already been performed on the battery.

A-2.3 HAZARD ANALYSIS ELEMENTS.

The hazard analysis should include the following elements:

- Characterize application, handling, and storage arrangements.
- Investigate fuel loading/chemical composition of the battery.
- Review historical usage and loss data.
- Perform FMEA.
- Evaluate environmental constraints, including operating environment.
- Identify possible casualty scenarios causing the basis of the threat.
- Identify how the battery reacts during each casualty scenario and quantify potential hazards to equipment and ship's personnel.
- Define hazard severity, probability, and HRI (see Chapter 6 and Appendix C of this manual).
- Develop application- and hazard-specific mitigations.
- Define test method(s) to characterize hazards and verify effectiveness of mitigations.
- Update the SHA, based on test results.
- Final risk assessment and submittal for program approval.

Each of these elements is described in detail as follows:

A-2.3.1 Characterize Application, Handling, and Storage Arrangements.

The conditions associated with the use, maintenance, and storage of the battery shall be characterized to serve as baseline conditions for the hazard analysis. The conditions to be characterized include compartment size, dimensions, configuration (contents/load-outs), ventilation, accessibility and fire protection features (detection, suppression, insulation), if any. Important parameters include contents of adjacent spaces, potential ignition sources, manning, and proximity of hazardous or energetic material or

systems such as flammable or combustible liquids, oxidizers, high pressure systems, ammunition and explosives, or vital equipment.

A-2.3.2 Investigate Fuel Loading/Chemical Composition of the Battery.

Battery equivalent fuel loading and oxidant content, including all construction materials, and including packaging materials if relevant, shall be defined prior to testing. This information shall be used to scope and develop test measurements required to characterize associated hazards. For example, the presence of an oxidizer in the battery will require additional testing to quantify the heat released by the battery during combustion (i.e., oxygen calorimetry will not provide an accurate measurement). Results from NAVSEA 9310-AQ-SAF-010 lithium battery safety tests should be incorporated, if available and applicable. The chemical composition shall also be used to predict the type of compounds that will be produced during combustion, which in turn will define the types of gas concentration measurements required during the test.

A-2.3.3 Review Historical Usage and Loss Data.

A review of the usage and fire loss history of similar batteries shall be conducted to help quantify the hazards. "Similar" batteries may be those used on U.S. Navy ships, in other DoD or Government applications, or even in commercial applications where data is pertinent and can be verified. Important areas to focus on when conducting this review include cause/origin of the fire, fire severity, fire loss (injury, loss of life, and cost), and effectiveness of mitigation systems and/or manual interventions.

A battery database being compiled by NAVSEA 05 for Navy battery applications should be utilized to the extent possible to support the hazard analyses. The database will be populated with the following information, as data become available:

Cell level:

- Manufacturer.
- Chemistry.
- Size and weight.
- Voltage.
- Charge/discharge rates.
- Capacity.
- Energy density.
- Safety devices.
- Mitigations.
- Testing and results.

Battery level:

- Assembling company, if different from cell manufacturer.
- Configuration of cells and modules.
- CONOPS.
- Size and weight.
- System energy density.
- System voltage.
- Mitigations.
- Testing and results.
- Field usage data.
- Fire loss data.
- Risk assessments.

This data will be useful in defining the failure modes and potential hazards and impacts for a program that proposes to use a lithium battery. Furthermore, if the proposed battery and its application are sufficiently similar to an example already in the database, then certain testing might be precluded if already performed, when approved by NAVSEA 05.

A-2.3.4 Perform FMEA.

FMEA shall be performed to understand and document how the battery can fail and what the impacts of the various failure modes will be. In the context of this manual, the objective of the FMEA is to identify those failure modes that result in potential safety hazards and to estimate their potential impacts. Additional discussion on FMEA is provided in section A-3 below.

A-2.3.5 Evaluate Environmental Constraints, Including Operating Environment.

Characterize environment and environmental stresses, including but not limited to: potential shock, vibration, drop, physical damage, ship motion, extreme temperatures and humidity, electromagnetic effects, and radiation that may affect the battery. These will be considered for all aspects of the battery life, from manufacturing to installment, operation, maintenance, and disposal.

A-2.3.6 Identify Possible Casualty Scenarios Forming the Basis of the Threat.

The information collected during the tasks above shall be used to develop the potential casualty scenarios that could result under conditions of storage, transport, or use. These scenario(s) shall be used to define the potential hazards, to identify the hazard characterization tests required (see Chapter 5), to define the test methodology, and to develop mitigation systems and techniques.

The hazard analysis shall include immediate hazards created by electrical, mechanical, and thermal abuses, and by excessive environmental conditions (e.g., scenarios involving local fire, MIL-S-901 mechanical shock, MIL-STD-167 vibration, transient exposure to seawater, operator or maintainer error, overcharge, etc). The PHA shall also include hazards that may emerge over time (e.g., scenarios involving emergent internal defects or wear-out failure modes).

A-2.3.7 Identify How the Battery Reacts During a Casualty Scenario and Quantify Potential Hazards to Equipment and Ship's Personnel.

The hazard analysis shall characterize the expected reactions of the battery during the casualty scenario (e.g., combustion, explosion, arcing, ejection of hot gases, fluids, or solids, etc.) and assess potential hazardous impacts to the host ship and personnel. Impacts should include the likelihood of fire spreading to adjacent equipment or compartments, of heat sufficient to damage vital equipment, of potential for initiation of nearby ordnance, of injury to personnel from toxic gas, and of chemical deterioration of equipment. The potential for the battery assembly to injure or kill personnel or to damage structures and equipment (e.g., due to battery pressure vessel explosion, where applicable, or battery cell explosion/fire) must also be addressed. This information should be used in planning the battery casualty characterization tests described in Chapter 5 of this manual.

A-2.3.8 Define Hazard Severity, Probability, and HRI.

Risks associated with a casualty involving the battery shall be assessed in accordance with Chapter 6 and Appendix C of this manual. This process results in an HRI based on assignment of severity and probability to each hazard.

A-2.3.9 Develop Application- and Hazard-specific Mitigations.

NAVSEA 05 will require that mitigations be developed for any safety hazards with severity level of "Critical" or "Catastrophic." Potential risk mitigation techniques, component design changes, or other (procedures, equipment, and fire protection features) should be identified. These may include segregation, the use of storage containers, the installation of an early warning fire detection system, the installation of a fast-response fire suppression system, and manual intervention.

Mitigation requirements can vary depending on the application and on the intended platform. Mitigations must therefore be application-specific (e.g., surface ship vice submarine, submarine host vice diving platform, open ocean vice under ice). Mitigation methods may be limited by the intended application and platform. For example, casualty mitigation for a battery on a surface ship may allow for aggressive firefighting methods and ventilation of smoke and toxic gasses overboard. However, the same mitigation techniques may not meet the requirements for a submarine atmosphere where gases cannot be vented overboard and where firefighting may be more limited.

A-2.3.10 Define Test Method(s) to Characterize Hazards and Verify Effectiveness of Mitigations.

Tests shall be defined to characterize the hazards (BCCT) and verify the effectiveness of the mitigations (HMT). The hazard analysis shall be updated with information from these tests as they are completed. Severity levels, probabilities, and HRIs shall be revised to reflect the result of these tests

A-2.3.11 Update the SHA based on Test Results.

The SHA will update and extend the battery-level PHA, and shall include the results and findings of the BCCT and HMT. The SHA shall compare the initial risk and residual risk to the host ship in accordance with Chapter 6. Comparing these two risks provides a measure of the effectiveness of the proposed mitigation technique(s).

At this point in the program, the following tasks should have been completed and will serve as the basis for the final SHA.

- The required level of hazard mitigation has been achieved.
- Potential additional mitigation techniques have been identified and tested or have been proposed.
- The final configuration for use on the ship has been identified.
- The exposures produced during a casualty when the battery/battery pack is installed in the proposed configuration have been quantified.

The SHA should document any resulting restrictions on battery location, safety equipment or procedures. Upon completion of HMT, the NAVSEA 05 TWH shall identify recommendations for refinements to battery stowage locations, safety equipment, and safe practices aboard the host ship. These recommendations may include but not be limited to: segregation, the use of storage containers, the installation of an early warning fire detection system, the installation of a fast response fire suppression system, and manual intervention.

A-2.3.12 Final Risk Assessment and Submittal for Program Approval.

The residual risks associated with a fire in the battery in the proposed application shall be documented and submitted to the appropriate level of programmatic authority for approval.

A-3 FAILURE MODES AND EFFECTS ANALYSIS (FMEA).

A-3.1 FMEA PROCESS.

FMEA shall be initiated as an integral part of early design process and incorporated into the PHA. The FMEA shall be updated as necessary to reflect design changes during the development. The FMEA shall be used to identify failure modes that may result in safety hazards. The following discrete steps shall be used in performing the FMEA:

- Define the system to be analyzed. Narratives of the system should include descriptions of each component in terms of functions to be performed.
- Construct functional block diagrams that illustrate the operation, interrelationships, and interdependencies of the functional components. All system interfaces shall be indicated.
- For each functional component or interface, identify all potential failure modes, their root cause, and their effects at the local level, the system level, and platform level by mission phase. Also identify any potential effects to personnel and environment.
- Evaluate each failure mode in terms of the worst-case hazard that may result. Estimate the probability that the event can and will occur, and the potential impact or severity.
- Identify failure detection methods, and record planned mitigations for each failure mode.
- Identify corrective design or other actions required to eliminate the failure or control the risk.
- Recommend hazard mitigations for unacceptable or undesirable risks.
- Estimate the effects of corrective actions and mitigations.
- Document the analysis, summarize any safety hazards that could not be corrected and mitigated by design, and identify the special controls which are necessary to reduce failure risk.

A-3.2 FMEA RISK ASSESSMENT.

The risk (HRI) associated with each component shall be determined using the risk evaluation system described in Chapter 6.

A-3.3 FMEA REPORT.

The results of the FMEA and other related analyses shall be documented in a report that identifies the level of analysis, summarizes the results, documents the data sources and techniques used in performing the analysis, and includes the system definition narrative, resultant analysis data, and worksheets. Interim reports shall be available at each design review to provide comparisons of alternative designs and highlight high-risk failure modes, potential single-failure points, and proposed design corrections. The final report shall reflect the final design and provide identification of the failure modes and single-point failures that could not be eliminated from the design.

A-3.4 FMEA SUMMARY.

The report shall contain a summary that provides the system developer's conclusions and recommendations based on the analysis. The system developer's interpretation and comments concerning the analysis and the initiated or recommended actions for the elimination or reduction of failure risks shall be included. A design evaluation summary of major problems detected during the analysis shall be provided in the final report. A list of items omitted from the FMEA shall be included, with rationale for each item's exclusion.

A-3.5 FMEA WORKSHEET.

A separate worksheet for each item with an HRI of 9 or less will be included in the FMECA. The worksheet will contain at minimum:

- In listed format: preparation date, preparer(s) name and title, item name, probability of failure, failure mode, and associated risk.
- In narrative format: function, failure mode description, possible causes, failure detection, system impact, mission impact, surroundings impact (e.g., storage area, host platform), mitigations, and recommendations.

A-4 FAILURE MODES EFFECTS AND CRITICALITY ANALYSIS (FMECA).

A-4.1 FMECA PROCESS.

FMECA is a bottom-up approach that expands upon the existing FMEA and includes a quantitative risk Criticality Analysis (CA). CA is a procedure to rank a failure mode according to the severity and probability of occurrence. A FMECA may not be applicable to all components of the battery, but it is appropriate for safety-critical electronics (e.g., battery management electronics) where a CA can be conducted utilizing reliable electronic component failure rate data. The FMECA results should be presented in a worksheet similar to the FMEA, with the additional CA included.

A-5 SYSTEM REQUIREMENTS DECOMPOSITION INTO ASSOCIATED SOFTWARE ANALYSES AND REQUIREMENTS.

A-5.1 SAFETY CRITICAL CRITERIA (SCC).

Unlike hardware, software does not fail due to wear-out or damage. Software fails due to flaws in the design and/or implementation, as well as its ability to handle Abnormal Conditions and Events (ACE). Therefore, it is important to establish the SCC early in the development so the system architecture and design can take the safety issues into consideration. The SCC is a joint effort between the Navy, the developer, and safety personnel to determine the safety concerns for the system.

A-5.2 SYSTEM CRITICAL FUNCTIONS (CFs), HAZARDS, AND BEST PRACTICES (BPs).

A system CF list, hazard list, and BP list are created that document all high-level system safety concerns that may have software impact within the system. The system hazard list is a list of hazards that have system involvement and may or may not have software involvement. The system hazard list comes

primarily from the PHA analysis. The system CF list is a list of functions whose correct performance is essential to the safe operation of the system. CFs usually respond to and/or control an actual or potential hazardous condition as opposed to preventing hazardous conditions. BPs are concerns with the development process and generation characteristics of the software rather than implementation of specific requirements. Check summing, strong data typing, and data initialization are examples of safety BPs.

A-5.3 COMPUTER PROGRAM CFs, HAZARDS, AND BPs.

System CFs, hazards, and BPs are examined to determine which ones are applicable to a specific computer program. Computer Program Critical Functions (CPCFs) are developed by taking the system-level CFs and determining which ones apply to each software program or CSCI. After determining a subset list of system CFs that apply, that subset list is expanded and further defined into more specifically derived CPCFs for each CSCI. The same process is used to determine computer program hazards and computer program BPs for each CSCI in the system.

A-5.4 SOFTWARE SAFETY REQUIREMENTS(SSRs).

SSRs are generated to document the specific concerns around each of the CPCFs, hazards, and system BPs. These SRs are the guidance for the safety analysis team. SRs are also used by the developers to ensure they are taking into account all the safety issues during the development of the system. Once the SRs are complete, a certification kickoff meeting is held with all pertinent parties to ensure consensus on the SRs and what safety tasks will be completed so each SR is met.

A-5.5 SOFTWARE SAFETY VERIFICATION REQUIREMENT (VR) DEVELOPMENT.

As software design features are further developed, VRs are created to give the code analyst and tester further insight into what must be verified for each SR. The number of VRs under any given SR will vary, depending on the complexity of the SR. Each VR will define the specific design details that must be verified for the SR and how that verification will be accomplished (test, analysis, etc.). Any VRs that are not capable of being verified through test must be verified through code analysis. Certain VRs might be verified by simple code inspection. For VRs that must ensure something does not happen, a fault tree or critical flow analysis approach may be required.

A-5.6 SOFTWARE SAFETY TEST/VERIFICATION.

During the Test and Evaluation Phase, all VRs must be verified to complete the safety analysis effort. The software safety test team shall document how each VR was verified and the results of the verification.

APPENDIX B – BATTERY CASUALTY CHARACTERIZATION (BCCT) TEST METHODS AND REQUIREMENTS

This appendix provides additional detail and guidance regarding test methods and data collection requirements for casualty characterization tests called out in Chapter 5.

B-1 CELL AND/OR BATTERY FAILURE INITIATION REQUIREMENTS.

Tests shall be designed to reliably initiate a cell and/or battery failure. The method of initiation of the cell and/or battery failure shall be determined from the PHA and should represent the WCE. Multiple methods may be used to initiate a cell casualty, and the method chosen will depend on the cell chemistry, cell failure response, and the hazard the casualty poses (as determined from the PHA/CONOPS). Potential methods to initiate a cell casualty include, but are not limited to: thermal abuse, overcharge, and puncture or crush. The use of a specialized donor cell that is purposely constructed to simulate a cell casualty due to a latent or emergent manufacturing defect (e.g., via an internal cell short initiated either external or internal to the cell) shall be used if available.

B-2 QUANTITATIVE GAS PRODUCTION ANALYSIS.

Cell and/or battery failure shall be initiated until the cell and/or battery undergoes thermal runaway with gaseous release. The test apparatus or compartment shall be capable of withstanding the pressures created from the rapid failure and disassembly of a cell and/or battery.

The chemical species released are expected to vary under different burning conditions, particularly with variations in the oxygen concentration. A comprehensive approach requires an initial qualitative study to assess the nature of the expected chemical species and relative concentration ranges. This will be followed by a targeted analysis that will provide quantitative results. Conditions will be varied to determine how changes in the burning conditions alter the chemical species that are released.

Gas analysis shall be performed to fully characterize the quantity of gas produced, the rate of gas production, and the composition of the gas produced. Two methods shall be used to measure gas composition:

- Real-time online analysis to characterize bulk generation and decay rates of key bulk gas constituents.
- Whole-gas analysis on grab samples to characterize finer details of gas component ratios and trace materials that might be toxic or corrosive.

B-2.1 REAL-TIME AND CONTINUOUS MONITORING OF GASES.

Oxygen (O_2), Carbon Monoxide (CO), and Carbon Dioxide (CO_2) shall be monitored and recorded real-time during the experiment. Real-time monitoring of other gases (e.g., Hydrogen [H_2], light hydrocarbons) may also be appropriate and will be determined on a case-by-case basis in the development of the TP by the test activity, with NAVSEA concurrence.

For cell-level tests, continuous sampling, based on cell chemistry, shall be conducted at a rate sufficient to characterize the evolution and decay of active species. A recommended real-time sampling rate is no less than once every five seconds. Chamber pressures shall also be recorded.

For intermediate-level and full-scale battery tests, gas analyses may be limited to real-time specific gas sensing and analysis using industrial-level, gas-specific sensors (i.e., not research-level trace gas sensitivity).

B-2.2 GRAB SAMPLES FOR TOXIC AND CORROSIVE GASES.

For cell-level tests, atmospheric grab samples from the chamber shall be taken prior to the start of the test, for a baseline. Samples shall also be taken periodically during the test at a rate sufficient enough to

characterize the progression of the event. It should be noted that samples may be required to be taken more frequently to support rapid battery events, as identified in the TP. Atmospheric grab samples for toxic gases will be acquired from the test chamber during battery testing in accordance with EPA guidelines for determination of toxic organic compounds in ambient air (EPA/625/R-96/010b), specifically methods TO-14, TO-15, and TO-17. Other techniques and protocols may be used when these protocols are industrial, medical or Navy standards and have been accepted for use as part of the TP. Examples other technique protocols include the National Institute for Occupational Safety and Health (NIOSH) and American Society for Testing and Materials (ASTM), or techniques developed for specific gas analysis.

Atmosphere samples shall be acquired and analyzed retrospectively to determine their chemical components. Analytic methods shall be selected based on the significant gas products expected for the specific battery chemistry being tested. Sampling systems shall be compatible with and be non-reactive with the materials to be measured, or the measurements must be completed in a time period that will minimize the loss of material by surface reactions. Depending on the cell chemistry, H_2, hydrocarbons and organic vapors, CO_2, CO, O_2, and HF may be expected during a fire but will likely not be the only chemical compounds generated. Battery by-products often contain Hydrochloric Acid (HCl), Carbon Tetrachloride (CCl_4), Hydrogen Sulfide (H_2S), and Sulfur Dioxide (SO_2). Additional gas products from high-temperature chemical reaction are expected and will be governed by the source cell or module chemical makeup and design. Partial decomposition of the battery could lead to the formation of some moderate molecular mass organics and polymeric species.

Corrosive gas production shall be determined to assess impact on the environment, component, and system materials and the host ship or vessel. The need for corrosive gas evaluation will depend on battery chemistry. Most corrosive gases are highly reactive by nature and make qualitative and quantitative analysis difficult. The type of testing to be performed should be adequate to provide needed data to allow hazard assessments. Real-time testing can be expensive and difficult, but it provides a much more complete picture of the timeline for generation of corrosive gas than end-of-test analysis. Corrosive gas analysis performed at the end of the test will provide data concerning the total amount of corrosive gas generated and is much less expensive or time-consuming.

NOTE: Sealed test chambers shall have sufficient humidification to allow full hydrolysis of all inorganic releases from a battery, unless otherwise directed and approved in the TP.

NOTE: The chamber atmosphere should be re-circulated at a rate that allows homogenous sampling unless such chamber circulation would hinder accurate analysis of expected hazards. Chamber circulation methods should be carefully considered to avoid biasing the sample away from expected actual environmental conditions. For example, circulation of the chamber atmosphere might properly represent shipboard ventilation but may not adequately represent battery storage in a poorly ventilated area. For poorly ventilated areas, consideration should be made concerning use of two sampling ports (one high and one low).

B-2.3 VOLATILE OFF-GAS IGNITION REQUIREMENTS.

The gaseous materials released from most lithium and lithium-ion batteries include combustible organics. Where the battery electrolyte contains an organic solvent or other liquid that might exothermically react or combust upon contact with air, a triggerable gas ignition device shall be included in the test setup to provide a means of reliably igniting the vapors, fumes or aerosols produced by a battery venting in all mitigated and unmitigated BCCT tests.

Tests shall be conducted with the ignition device operated in both the ENABLED (active) and SECURED (off) mode to contrast the variability in results both with and without ignition and combustion of off-gasses produced by a battery failure. If a system produces potentially flammable gases and aerosols but these do not normally ignite during the casualty event, these gases SHALL BE triggered to evaluate the potential explosiveness of fuel-air mixtures. Tests shall be initially conducted with the ignition system SECURED. If the failure event itself does not automatically trigger combustion of the gases vented from the cell or battery module, tests shall then be conducted with the ignition source enabled and operating, to acquire the necessary data from the secondary combustion of fumes, gases, and aerosols.

B-2.4 THERMAL, VOLUMETRIC, AND PRESSURE IMPACTS OF OFF-GAS IGNITION.

A significant portion of the thermal casualty assessment is based on the radiant heat released from combustible sources in the area of the casualty. Hazard characterization tests and assessments shall therefore quantify the potential radiant heat from combustion of flammable gases or aerosols released from the battery.

Hazard characterization tests and assessments shall also quantify the amount of additional gas volume created by the battery casualty, and to characterize the "breathing" associated with the combustion processes. Dynamic pressures shall be measured during these test events and estimates provided regarding the total volume of gases produced in excess of the primary volume of gases released from the battery.

B-2.5 GAS VELOCITY MEASUREMENTS.

When required by NAVSEA, the gas velocity of the casualty shall be recorded. The gas volume, pressure, and temperature can be useful in determining how quickly gases may spread to other compartments of a ship. Gas velocities shall be measured using differential pressure gages capable of 0.01" to 10" water column pressure differential measurements, or when a test chamber has a dedicated outlet and exhaust system, a density independent anemometer system may be used to determine the velocity through a dedicated opening. These data shall be acquired at 1 Hz minimum data rate.

B-2.6 HEAT RELEASE RATE (HRR).

The heat release rate shall be characterized for the battery system under question. Heat generation can occur by a variety of mechanisms, including but not limited to:

- Chemical heat due to internal electrochemical discharge reactions.
- Chemical heat due to chemical reactions between internal components inside a failing cell or battery.
- Chemical heat due to combustion of flammable cell internal components (electrolyte, separator, etc.).
- Chemical heat due to combustion of flammable battery components (cell restraints, cables, etc.).
- Resistive heat due to internal and/or external short circuit current flow.

Characterization tests shall be devised to quantify the total heat released to the platform during battery failure, either as sensible heat or as radiant heat.

Depending on the battery chemistry, characterization may involve calculation of fuel loadings being derived from internally oxidized fuels. When characterized by test, the atmospheric oxygen level shall be maintained to support effective combustion of fuel vapors, since depletion of oxygen in the global test environment will lead to under estimating the heat release rate, and a corresponding underestimation of the mitigation requirements. For some specific battery chemistries, overcharging can lead to the liberation of oxygen that generates an oxygen-enriched atmosphere in the vicinity of the battery, greatly affecting the burning rate, possibly making suppression more difficult. Such characteristics shall be accounted for. When a battery or battery system will be operating in an oxygen-deficient environment (e.g., a purged/inerted housing), special provisions shall be made to characterize the open (free air) HRR and thermal flux history in addition to that expected under the oxygen-deficient conditions, unless otherwise agreed to by NAVSEA 05. Heat release rates and measurements shall be scaled based on the battery.

B-2.6.1 Thermal Flux History.

Both radiometers and calorimeters shall be positioned a safe distance from the batteries yet close enough to capture the radiative, conductive, and convective heat emitted. The radiometers and calorimeters should be sized depending on the size of the battery being tested. For fires this would typically be in the ranges of 0-1, 0-5, or 0-10 BTU/ft2 sec. Large-scale systems may produce 100 BTU/ft2 events or greater. Data rates shall be 1 Hz minimum. As a minimum, the HRR calorimetry system used must be capable of less than a 10 percent error.

B-2.7 PRESSURE AND PRESSURE TRANSIENTS.

Pressure transients may be produced by a cell or battery undergoing a casualty. Hazard characterization tests shall measure absolute pressure and pressure transients within the test chamber or compartment during test. The pressure release may range from a moderate and sustained pressure rise due to low-rate combustion, to a rapid deflagration of battery components internal to the cell(s). The pressure release can be sudden and abrupt, stemming from a sudden failure of battery cell cases or battery pressure containment vessels. In the event of a sudden pressure transient, the data collection rate of any continuous monitoring device shall be sufficient to capture it, and/or the continuous method shall be supplemented by single-use devices which will capture or indicate a peak (transient) value. Specialized shock wave explosive transient recording is not required and is subject to erroneous analysis.

B-2.8 INCANDESCENT DEBRIS AND SHRAPNEL.

Cells and batteries undergoing induced casualty failures may produce shrapnel and eject incandescent particles. Fragmentation of battery cases under casualty conditions shall be considered a potential hazard for co-located equipment. Cell and battery module tests shall therefore include witness plates, impact plates, and video coverage of the gas analysis tests to assess impact of these ejecta on co-located equipment and personnel, if this has not already been accomplished during NAVSEA TM S9310-AQ-SAF-010 tests. Impact force assemblies may be used to determine lethal radius of shrapnel and debris.

NOTE: The use of shrapnel and incandescent ejecta debris protection for sampling and analysis equipments may cause shifts in other wise free “atmosphere” interactions by increasing the local reaction temperatures and reducing quenching of the cell casualty “fireball.” When such a reaction is expected (e.g., oxyhalide cells or high-temperature reactions from lithium-metal primary batteries using carbon monofluoride or manganese dioxide) within a protective shield, tests shall be conducted with the shield in place and removed with protection of equipment accomplished by the best means possible. Preference to gas accumulation space shall be given to the condition that most replicates the potential system failure modes. If mitigation techniques use open air storage, although a battery may be stored in a system, the set of tests shall include both constrained and open cell/battery-module casualty gas analysis.

B-2.9 AEROSOL ANALYSIS.

When required by NAVSEA or recognized as a casualty failure mode, aerosol analysis shall be conducted. Aerosols of electrolyte or supporting fluids in pressure-compensated battery systems pose hazards that depend on the battery chemistry and design. A battery that contains an organic electrolyte may produce an aerosol that (depending on the particle size) could form an explosive-air mixture. This includes electrolyte-solvent solutions which in a liquid state would not be characterized as flammable. The flammability rating, aerosol chemistry, particle size with respect to human exposure, and what is adsorbed and absorbed on and in the aerosol shall be determined.

B-2.9.1 Flammability and Flash Point Rating.

The flammability and flash point of the electrolyte shall be determined, to put the electrolyte on a comparative scale with other flammable liquids such as Diesel Fuel Mixture (DFM), hydraulic fluid, and kerosene. The resulting analysis will be used to provide guidance on how to deal with an aerosol exposure.

B-2.9.2 Aerosol Characteristics.

Aerosol production shall be determined. Vapor analysis will not give an indication of the hazard of an aerosol. Two issues are the size of the particles with respect to human exposure, and what is adsorbed and absorbed on and in the aerosol. Knowing the nature of the aerosol will give indication of the gas-free engineering required.

B-2.10 SMOKE GENERATION.

The density of the smoke shall be determined and recorded in percent transmittance or extinction factor. Measurements shall be made using ASTM standard or comparable methods. Systems that are calibrated prior to use are acceptable, (e.g., an Optical Density Meter [ODM]). Multiple wavelength and location

monitoring may be used at the test facility's preference. Monitoring of extinction values at various heights in the test facility may be used to identify behavior.

APPENDIX C – LITHIUM BATTERY-SPECIFIC METHODS AND RULES FOR ESTIMATION OF FAILURE PROBABILITY AND HAZARD SEVERITY

C-1 BATTERY-SPECIFIC METHODS TO ESTIMATE FAILURE PROBABILITY.

In general, the intent of this section is to focus on the probability of hardware and/or software failures that can cause catastrophic failure of a cell or battery, with uncontrolled and/or unexpected release of energy. Performance failures, such as failure to meet capacity requirements or cycle life requirements due to other "graceful" degradation modes, while also important, are not discussed in this section. Where failure to meet such a performance requirement can result in a safety hazard for the system (e.g., loss of life or equipment), these types of hazards shall be addressed as part of the SHA and System Reliability Analysis and battery-specific tests (in addition to those called out in this document) and shall be performed as needed to ensure the performance reliability of the battery over its intended life is maintained through the application of appropriate levels of redundancy and margin.

Table C-1. Failure Probability Levels and Maximum Allowable Failure Rates.

Description	Level	Environment, Safety, and Health Result Criteria	Fleet or Inventory
Frequent	A	Likely to occur often in the life of the item, with a probability of occurrence greater than 10^{-1} in that life.	Continuously experienced.
Probable	B	Will occur several times in the life of an item, with a probability of occurrence less than 10^{-1} but greater than 10^{-2} in that life.	Will occur frequently.
Occasional	C	Likely to occur sometime in the life of an item, with a probability of occurrence less than 10^{-2} but greater than 10^{-3} in that life.	Will occur several times.
Remote	D	Unlikely but possible to occur in the life of an item, with a probability of occurrence less than 10^{-3} but greater than 10^{-6} in that life.	Unlikely, but can reasonably be expected to occur.
Improbable	E	So unlikely, it can be assumed occurrence may not be experienced, with a probability of occurrence less than 10^{-6} in that life.	Unlikely to occur, but possible.

- Estimates of battery-related failure probability shall not be lower (i.e., shall not be more optimistic) than what is proven and supported by test, inspection, or other OQE.
- The objective in the Hazard Analysis is to estimate the "WCE." The primary objective in estimating the probability of failure shall therefore be to estimate the highest credible failure probability, and not the lowest credible failure probability.
- Calculation of a range of failure probabilities that includes the highest and lowest credible failure probabilities is acceptable, and sometimes informative, but in all cases the highest credible failure probability shall be calculated, communicated, and used in HRI estimates and in decisions where acceptance of residual risk is required.

- For Commercial/Off the Shelf (COTS) battery cells, manufacturer test data, and commercial use data can be used to estimate failure probability. However, because the safety of a cell is directly related to a specific manufacturer's design and manufacturing QA process, one manufacturer's data shall not be used to calculate and represent the probability of failure for another manufacturer's cells, unless additional verifications are done to prove that the cells and manufacturing processes of one manufacturer are comparable to another.
- Because the safety of a battery cell is directly related to the conditions and environment of its use, manufacturer's commercial use data or other test data shall not be used to directly estimate catastrophic failure probability unless the conditions and environment of use for the targeted application are proven to be equal to, or less stressful than, those for the manufacturer's commercial data.
- Estimates of catastrophic failure probability for primary lithium batteries can be derived from test data. Activation and discharge test of a primary battery renders it unusable for further cycle tests. Therefore, the test of a large number of samples can be required to develop acceptably low failure probability estimates using only this approach. For COTS primary lithium batteries that are sold commercially, representative commercial test data may be used to augment the data pool, under the limitations noted above.
- Rechargeable batteries are often subject to "wear out" failure modes that can result in "emergent defects" which may not manifest themselves until after many hundreds of cycles or years of use. Estimates of catastrophic failure probability for rechargeable batteries can be calculated from cycle test data, but to estimate the probability of failure due to emergent defects, test samples must be tested for at least as many cycles as the expected field use in order to provide valid results (e.g., 100 cells tested for 10 cycles is not the same as 10 cells tested for 100 cycles).
- Effect of Mitigations: For primary and rechargeable cells, additional reductions in catastrophic failure probability estimates may be applied if mitigations that reduce probability of a catastrophic failure are implemented, and if the effectiveness of those mitigations (i.e., the probability of failure of the mitigation itself) can be quantified and properly factored into the fault tree analysis described below. Mitigating methods to reduce failure probability, if proven and verified, might include:
    - X-ray tomography examination of cells to detect and characterize the frequency and magnitude/size of manufacturing defects and contaminants inside cells that can lead to catastrophic failure modes. This method is non-destructive and can be applied to 100 percent of cells intended for field service, when program requirements warrant, in order to reduce residual risk. In the fault tree analysis, the probability of failure of the X-ray examination mitigation shall be estimated and adjusted based on the resolution of the X-ray equipment, the percentage of the fielded cells examined, and the probability of operator oversight/error.
    - DPA of cells to detect and characterize the frequency and magnitude/size of manufacturing defects and contaminants inside cells that can lead to catastrophic failure modes. This method is destructive and can only be applied to representative samples from cell production lots. In this approach, the frequency and magnitude of defect data collected on the sample cells shall be used to calculate a probability distribution that is normalized to some representative design or manufacturing feature of the cell (e.g., the cumulative square area of electrode material in the sample cells if normalizing the frequency of debris or defects between electrodes, or the number of welds in the cell if normalizing weld defects). This normalized value shall then be extrapolated to the battery level (e.g., cumulative area of electrode materials in the fielded system, or cumulative number of welds) to calculate the probability and size of defects possible in the fielded system. Note that this approach will result in some real probability of larger defects and contaminants than observed in any of the cells undergoing DPA.
    - Manufacturing process quality control audits to verify manufacturing methods and controls that reduce the probability of cell or battery defects and contaminants.
    - Additional stress screening tests applied to cells for service, such as accelerated life tests to prove that cells are robust against emergent defects. Examples may include excess vibration tests and extended cycle tests.
- In calculating failure probability, a parametric approach to fault tree analysis shall be used and shall consider all relevant parameters that could bear upon the probability of failure, including but not limited to: cell and battery design, safety critical software design and complexity,

manufacturing processes and quality control, operator error, ancillary equipment failure, and unintended stresses related to the usage environment.

- Where required, for each identified battery failure hazard, the final event (e.g., thermal runaway) shall be analyzed to determine the various different fault pathways that can lead to the final event. Two logic gates are used in fault tree analysis. The "OR" gate is used where any one of the input events can, in and of itself, cause the output event. Fault or failure probabilities for each input event in the "OR" functions are added together to estimate the probability of the output event. The "AND" gate is used where the output event occurs only when all of the input events occur first. Probabilities for each input event in an "AND" function are multiplied together to estimate the probability of the output event.
- Pathways that are defined entirely by "OR" functions constitute potential single-point failures.
- When mitigating features are implemented, the mitigation is normally the "AND" function with the fault it seeks to mitigate. The probability that the mitigation itself will fail must be estimated and included in the analysis to determine the mitigated probability of the output event.
- An example of a top-level fault tree analysis is shown in Figure C-1 for three of the failure modes that can lead to thermal runaway in a rechargeable lithium-ion battery. Note that the fault tree analysis clearly identifies an internal cell short and abuse as potential single-point failures.
- Fault trees are further developed for each of the three failure modes in Figure C-2, Figure C-3, and Figure C-4.
- NOTE: Figures Figure C-1 through C-4 are meant to serve as examples of how a fault tree is constructed and are not to be interpreted as exhaustive representations of all potential faults and linkages.
- As shown in Figure C-2 through Figure C-4, the potential cause of a fault can be traced back as far as necessary (e.g., back to the raw material defects, back to manufacturing process quality issues, back to system design flaws, back to subpar test and verifications of hardware and software, etc.) to determine the probability that a defect might be present in the cell or battery or operating procedures, etc. In this fashion, the fault tree analysis provides the method by which data from manufacturing audits, inspections, and other mitigating activities can be folded into the estimate of failure probability.

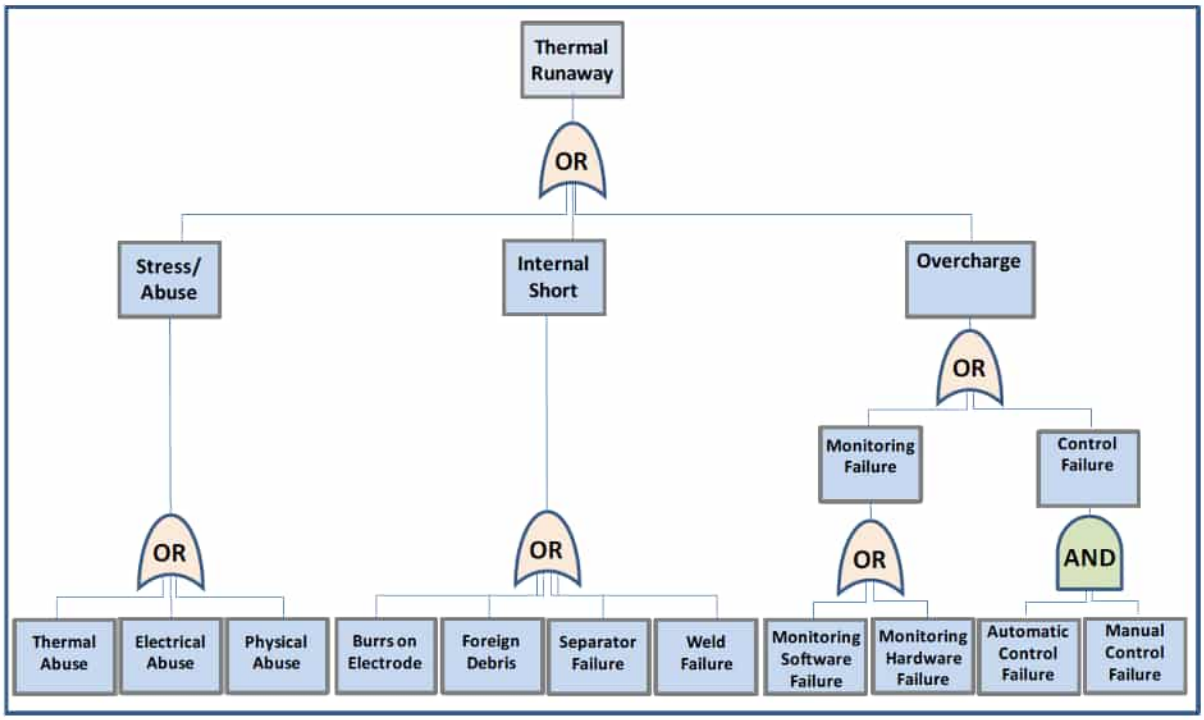


Figure C-1. Example of Top-level Fault Tree Analysis for Rechargeable Lithium-Ion Battery.

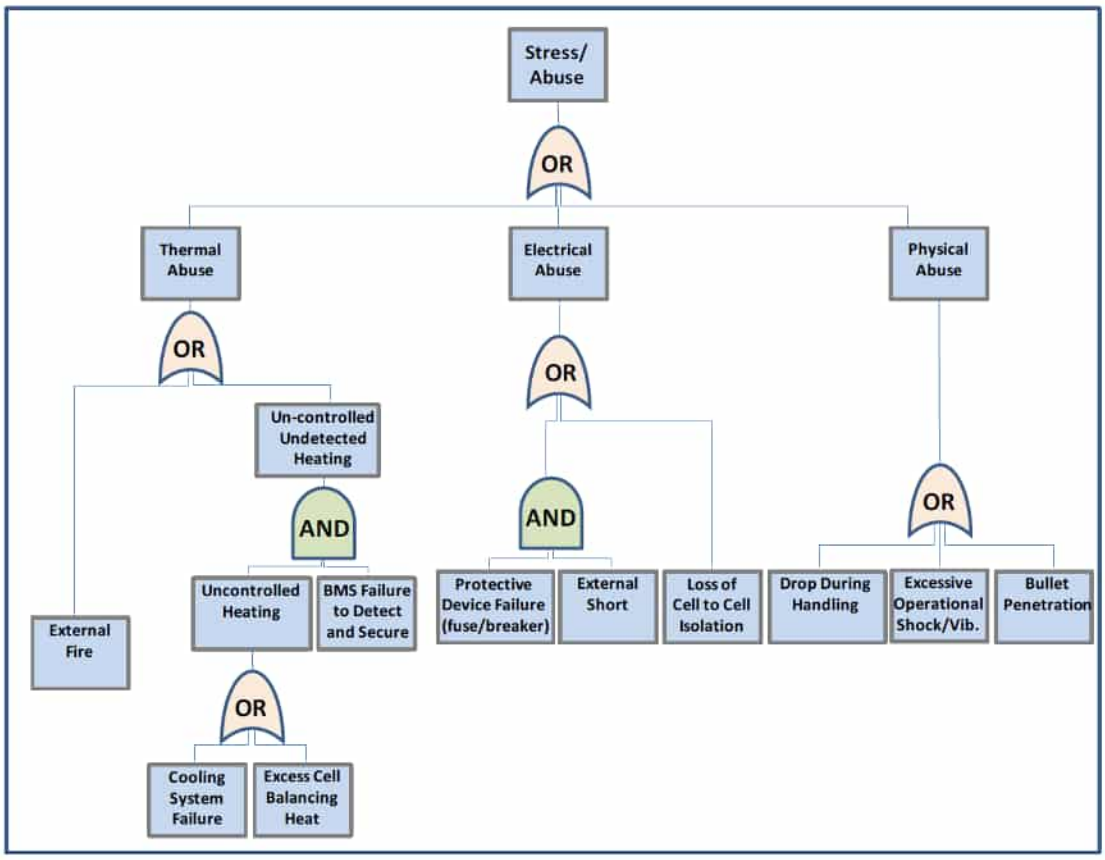


Figure C-2. Extension of Stress/Abuse Leg of Fault Tree Analysis for Rechargeable Lithium-Ion Battery.

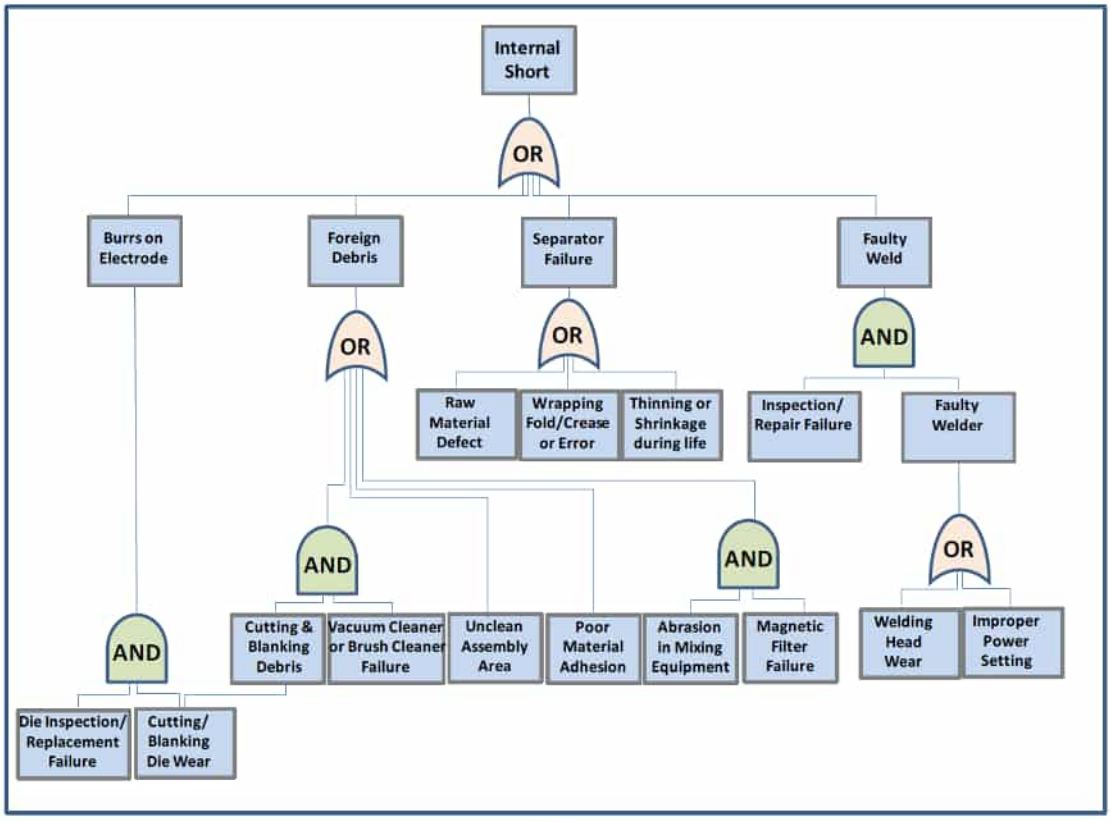


Figure C-3. Extension of Internal Short Leg of Fault Tree Analysis for Rechargeable Lithium-Ion Battery.

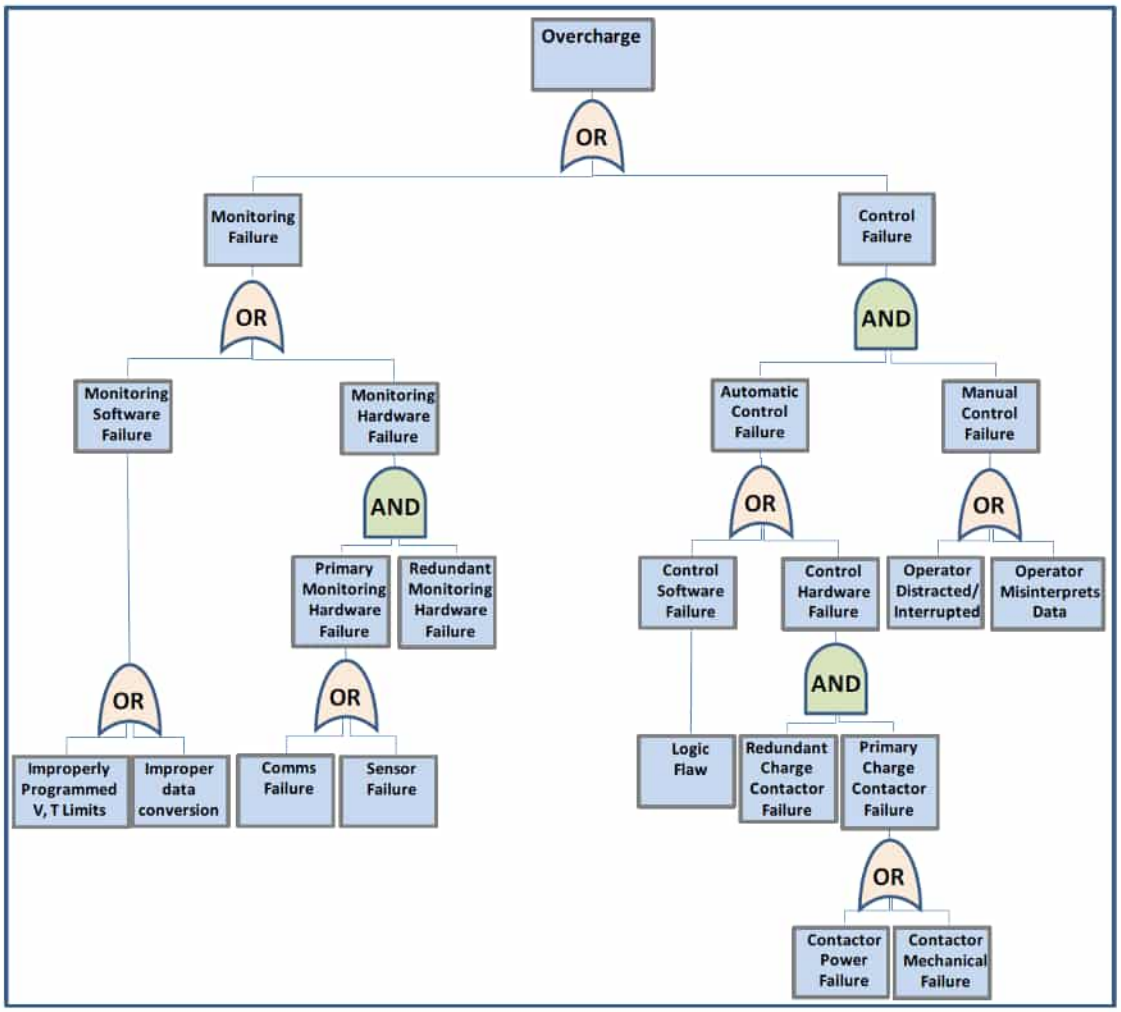


Figure C-4. Extension of Overcharge Leg of Fault Tree Analysis for Rechargeable Lithium-Ion Battery.

C-2 BATTERY-SPECIFIC METHODS FOR HAZARD SEVERITY ESTIMATES.

Hazard severity categories shall be defined as in Table C-2 for WCE that can result from personnel error, environmental conditions, design inadequacies, procedural deficiencies, and system, subsystem, or component failure or malfunction related to the battery.

Table C-2. Hazard Severity Categories from MIL-STD-882.

Description	Category	Environment, Safety, and Health Result Criteria
Catastrophic	I	Could result in death, permanent total disability, loss exceeding $1 million, or irreversible severe environmental damage that violates law or regulation.
Critical	II	Could result in permanent partial disability, injuries or occupational illness that may result in hospitalization of at least three personnel, loss exceeding $200,000 but less than $1 million, or reversible environmental damage causing a violation of law or regulation.
Marginal	III	Could result in injury or occupational illness resulting in one or more lost work day(s), loss exceeding $10,000 but less than $200,000, or mitigatible environmental damage without violation of law or regulation where restoration activities can be accomplished.
Negligible	IV	Could result in injury or illness not resulting in a lost work day, loss exceeding $2,000 but less than $10,000, or minimal environmental damage not violating law or regulation.

For each battery-related failure mode, hazard severity ranking shall be estimated based on the cell and battery testing and analyses outlined in Chapter 5. Hazard severity rankings shall be reviewed by the program manager and by NAVSEA 05 to ensure agreement that the severity rankings properly represent the WCEs.

Unless otherwise directed by the program manager, hazard severity rankings in the "Negligible" category will normally not require fault tree analysis to estimate failure probability.

Hazard severity rankings in the "Marginal" category may require fault tree analysis, and the level of analysis shall be determined by the program manager and NAVSEA 05.

Hazard severity rankings in the "Critical" and "Catastrophic" categories shall require fault tree analysis to quantify probability, if the decision authorities justify their decisions based on such probability estimates.

NOTE: Each software-dependent hazard takes its severity from the system hazard's severity category. The software severity categories are identical to the HRI severity categories shown in Figure 6-2 and Table C-2. The software risk also categorizes severity versus the SCC (i.e., level of software functional autonomy or lack of user interactive control), as shown in Table 6-1.

For primary and rechargeable cells and batteries, reductions in hazard severity estimates may be applied if mitigations that reduce the severity of a catastrophic failure are implemented, and if the effectiveness of those mitigations can be proven through test. In such cases, the probability of failure of the mitigation itself shall be quantified and properly factored into the fault tree analysis described above. Mitigating methods to reduce severity, if proven and verified, might include:

- Automated fire suppression systems.
- Modifications of CONOPS to reduce stored energy and the exposure of personnel, equipment, and platform to the effects of a failure.
- Efforts to reduce severity by preventing cell or battery failure propagation, as for example might be accomplished by providing adequate separation between multiple batteries in stowage.

APPENDIX D – BATTERY INTEGRATOR ON-SITE SURVEY PLAN AND STANDARD OPERATING PROCEDURE

D-1 FUNCTIONAL AREAS SUBJECT TO REVIEW.

- QA plan and procedures.
- Material control process.
- In-process demonstrations.
- Configuration control, including drawing and document revision control.
- Work planning and control process.
- System Safety Program.
- Management oversight.
- Test execution and control.
- Non-destructive testing.
- Instrument calibration.
- Plant/process cleanliness.

D-2 SURVEY STANDARD OPERATING PROCEDURES.

D-2.1 PRE-SURVEY ACTIVITIES.

Surveys will be scheduled by mutual agreement between the program manager and the applicable battery developer. The survey will be announced at least two weeks in advanced by NAVSEA letter, which will also identify the team members and any special administrative support needed. Survey teams will be staffed by one team leader and four to eight team members. Team members will have backgrounds in QA or engineering, with experience in complex battery design and specifications, and manufacturing. The activity being surveyed will arrange for badging prior to team arrival.

D-2.2 ON-SITE SURVEY ACTIVITIES.

Surveys will normally be scheduled for Tuesday through Thursday of the agreed-upon week. Upon team arrival, the activity will provide a one- to two-hour overview of the local processes and practices and will identify specific points of contact. The team leader will hold a brief meeting before close of business each day to summarize progress and identify emergent issues needing assistance to resolve. The team leader will convene an out brief to summarize findings and present a draft survey report on the final day of the survey. The team leader will provide the activity a draft set of cards (findings) prior to departure.

D-2.3 POST-SURVEY ACTIVITIES.

A soon as practical upon return to NAVSEA (Friday or Monday after survey) the team leader will brief the findings to NAVSEA 05Z and the system program manager. He/she will also provide an overview assessment as to the health of the activity safety and QA processes and any major systemic problems. The team leader will incorporate comments resulting from this brief and produce a final report for issue by NAVSEA 05Z letter.

D-2.4 SURVEY FINDINGS.

Findings will be one of two types: non-compliance issues or program improvements:

- Non-compliance findings document lack of compliance with either government requirements or implementing local procedures and processes. All non-compliance findings require a formal response from the activity to NAVSEA that provides an assessment of root cause of the finding, corrective action taken to resolve the problem, and corrective action taken that will prevent recurrence. Resolution of non-compliance findings will be tracked individually by the audited activity, with status reporting to NAVSEA every six weeks.
- Program improvement findings are items that team members recommend for increased program efficiency, better consistency, or more refined interpretations of requirements. Program improvement items require a written response from the surveyed activity, but there is flexibility

as to how the activity assesses the item and whether auditor recommendations are adopted. If the activity desires to implement a program improvement they feel justifies an equitable adjustment of the contract, the appropriate change clauses of the contract must be complied with before implementation of the change.

Survey findings will be documented one finding to a survey card (see Figure D-1) and cards will be uniquely numbered to allow tracking of finding resolutions. Each card will contain a concise one- or two-sentence statement of the finding and a narrative discussion of the finding. The discussion will include reference to the specific requirement violated and citing the specific documents the team member reviewed in determining the non compliance. The discussion will also contain a statement of whether the team member thinks the finding is an isolated case or part of a systemic problem. The cards will include the team members name and the name of the activity personnel with whom the finding was reviewed.

D-2.5 STAFFING OF SURVEY FINDINGS.

Once a team member has identified a finding, he/she will promptly draft the associated survey card. It is the team member's responsibility to review the finding with the cognizant activity's point of contact and document the name of the person on the survey card. The card will then be turned in to the team leader for processing. Once the team leader has edited the card, a designated activity management representative will initial that he/she has read and understands (but not necessarily agrees with) the finding. In cases where the team member and the activity point of contact cannot agree as to the validity of a finding, adjudication will be attempted by the team leader and the management representative. If agreement can still not be reached, the draft card will be briefed to NAVSEA.

Upon completion of immediate corrective action and establishment of long-term corrective action (if appropriate), these actions will be documented and endorsed by the activity QA manager. The response will then be forwarded to the NAVSEA 05Z survey team leader for approval. The team leader will be responsible for obtaining proper reviews within NAVSEA program and technical offices to support acceptance of the corrective action. NAVSEA 05Z will provide documentation of acceptance or rejection of survey correctives actions. In the event the Government rejects an activity response, the basis for the rejection will be documented, along with actions considered necessary to accept the response when resubmitted.

D-3 AUDIT AREAS.

Examples of processes and controls that should be evaluated during a manufacturing audit of a lithium-ion cell manufacturing facility are listed below. Auditors should collect in-process samples and take measurements to characterize compliance at all stages of production.

- Degree of Statistical Process Control (SPC).
- Frequency and level of integration of Quality Control checks.
- Shared anode and cathode production equipment and potential for cross-contamination.
- Processes that use metal-to-metal contact, and therefore provide the potential to create metal particulate.
- Control of particulate transfer by clothing, shoes, hair, tools, or other items that may enter/leave clean areas.
- Particulate and metallic contamination levels in production areas and in or around production equipment.
- Particulate and metallic monitoring and cleaning operations (magnets, brushes, vacuums) at the parts level, and the resulting contamination levels observed in the finished product.
- Production-area humidity and airborne particulate control systems and procedures.
- Moisture control for cell components prior to and during cell assembly, filling, formation, and sealing.
- Moisture control of any tools or materials that come into contact with cell components prior to or during cell assembly.
- Viscosity, thickness, drying, coating uniformity, and weight-loading controls during electrode coating operations.
- Handling and temporary storage of electrode rolls, separator rolls, or other components and potential for damage during such operations.
- Cutting and blanking operations and controls/inspections that ensure burrs, flakes of active materials, and current collector debris are not present in the final assembly.
- Separator application methods and equipment and the potential for folds, creases, misalignment, and improper tension levels.
- Welding operations and the potential for debris or splatter.
- Rework and repair procedures.
- Tracking of frequency of non-conformances and scrap/reject rates, and integration and use of this data to drive corrective action processes.
- Failure analysis processes and integration with corrective action processes.
- Continuous Improvement Process philosophy and commitment at all employee levels.
- Level of operator training and proficiency.
- Level of operator authority to identify, label, and scrap non-conforming material.

APPENDIX E – GLOSSARY OF ACRONYMS AND DEFINITIONS

ACRONYM LIST

ACAT	Acquisition Category
ACE	Abnormal Conditions and Events
ACN	Advance Charge Notice
AOA	Analysis of Alternatives
ASN(RDA)	Assistant Secretary of the Navy, Research, Development, and Acquisition
ASTM	American Society for Testing and Materials
BCCT	Battery Casualty Characterization Tests
BMS	Battery Management System
BP	Best Practices
BTU	British Thermal Unit
CA	Criticality Analysis
CCl_4	Carbon Tetrachloride
CDR	Critical Design Review
CID	Current Interrupt Device
CO	Carbon Monoxide
CO_2	Carbon Dioxide
CF	Critical Function
COTS	Commercial/Off the Shelf
CONOPS	Concept of Operations
CPCF	Computer Program Critical Functions
CSCI	Computer Software Configuration Item
DDS	Dry Deck Shelter
DFM	Diesel Fuel Mixture
DoD	Department of Defense
DON	Department of the Navy
DOSF	Deep Ocean Simulation Facility
DPA	Destructive Physical Analysis
DSC	Differential Scanning Calorimetry
DSS	Deep Submergence System
EDAX	Energy Dispersive Analysis with X-rays
EFI	Electric Field Intensity
EIS	Electrochemical Impedance Spectroscopy
EMI	Electromagnetic Interference
ESD	Electrical Safety Device
FA	Failure Analysis
FMEA	Failure Modes and Effects Analysis
FMECA	Failure Modes Effects and Criticality Analysis
FT	Fourier Transform
FTIR	Fourier Transform Infrared Spectroscopy
GCMS/LCMS	Gas/Liquid Chromatography with Mass Spectrometry
H	Hydrogen

ACRONYM LIST (Cont)

H_2S	Hydrogen Sulfide
HCl	Hydrochloric Acid
HECSSO	High Energy Chemical Storage Safety Office
HEMP	High-altitude Electromagnetic Pulse
HERO	Hazards of Electromagnetic Radiation to Ordnance
HESSSG	High Energy System Safety Steering Group
HF	Hydrogen Fluoride
HLR	Hazard Log Records
HM&E	Hull, Maintenance, and Electrical
HMT	Hazard Mitigation Tests
HRI	Hazard Risk Index
IIPRT	Internal Independent Peer Review Team
IOC	Initial Operating Capability
ISEA	In Service Engineering Agent
ITP	Index of Technical Publications
kWh	Kilowatt hour
LRU	Lowest Replaceable Unit
MA	Managing Authority
MDA	Milestone Decision Authority
mm	Millimeter
MOA	Memorandum of Agreement
NFESC	Naval Facilities Engineering Service Center
NAVSEA	Naval Sea Systems Command
NIOSH	National Institute for Occupational Safety and Health
nm	Nanometer
NOSSA	Naval Ordnance Safety and Security Activity
O&SHA	Operating and Support Hazard Analysis
OCV	Open Circuit Voltage
ODM	Optical Density Meter
O-Level	Organizational Level (of maintenance)
ONR	Office of Naval Research
OQE	Objective Quality Evidence
ORD	Operational Requirements Documents
O_2	Oxygen
PEO	Polyethylene Oxides
PHA	Preliminary Hazard Analysis
PHL	Preliminary Hazard List
PIA	Platform Integration Agent
PTC	Positive Temperature Coefficient
QA	Quality Assurance
R&D	Research and Development
RFI	Radio Frequency Interference
S&T	Science and Technology
SAR	Safety Analysis Report

ACRONYM LIST (Cont)

SCC	Safety Critical Criteria
SEAL	Sea, Air, and Land
SEM	Scanning Electron Microscopy
SHA	System Hazard Analysis
SHCM	Software Hazard Criticality Matrix
SO_2	Sulfur Dioxide
SOC	State of Charge
SPC	Statistical Process Control
SR/VR	Safety Requirements/Verification Requirements
SSGN	Submersible, Ship, Guide, Nuclear
SSA	Software Safety Activity
SSP	System Safety Plan
SSR	Software System Requirements
SSSA	System Software Safety Activity
TLR	Top Level Requirement
TMDER	Technical Manual Deficiency/Evaluation Report
TMMA	Technical Manual Maintaining Activity
TP	Test Plan
TWH	Technical Warrant Holder
UAV	Underwater Autonomous Vehicle
UUV	Unmanned Underwater Vehicle
VR	Verification Requirement
WCE	Worst Credible Event
XRD	X-ray Diffraction

LIST OF DEFINITIONS

B

BATTERY CELL VENDOR – Vendor that provides cells as raw materials for use in assembling battery modules or entire systems.

BATTERY CASUALTY CHARACTERIZATION TESTS – Tests designed to determine the likelihood, severity, and by-products of a battery failure. Tests are conducted at multiple levels, from individual cells to full-scale batteries.

BATTERY MANAGEMENT SYSTEM (BMS) – An electronic system designed for a secondary (rechargeable) battery that monitors the charging cycle to protect the individual cells of a battery from overcharging. A BMS may also be used to control/monitor discharge of individual cells in either a primary (non-rechargeable) or secondary (rechargeable) battery. Also known as Battery Monitoring Systems.

BATTERY MONITORING DEVICE – Provides detection and mitigation of any condition with potential for causing energetic or catastrophic failure of the battery.

BATTERY SYSTEM VENDOR – The entity tasked with design and production of a specific battery system, usually including BMS, electrical components, container, control system, and vehicle/system interfaces.

C

CELL – An individual unit of a battery consisting of a container, anode, cathode, separator, and electrolyte.

CHROMATOGRAPHY WITH MASS SPECTROMETRY (GCMS/LCMS) – An analytical chemistry technique that combines the physical separation capabilities of liquid chromatography with the mass-analysis capabilities of mass spectrometry to detect and identify chemicals in complex mixtures.

COMPUTER SOFTWARE CONFIGURATION ITEM (CSCI) – A group of software elements treated as a single entity by a configuration management system.

D

DESTRUCTIVE PHYSICAL ANALYSIS (DPA) – The systematic, detailed examination of electronic components, systems, and materials. Tests are conducted at joint DoD-approved laboratories for the performance of DPA, FA, and CA.

DIFFERENTIAL SCANNING CALORIMETRY (DSC) – Thermoanalytical technique in which the difference in the amount of heat required to increase the temperature of a sample and reference is measured as a function of temperature. The term DSC also describes the instrument allowing precise measurement of heat capacity.

E

ELECTROLYTE – The conductive material within a battery that allows charged species to move between anode and cathode so that the cell reaction may proceed and ionic current will flow. Most electrolytes are liquid and are solutions of an ionic material (e.g., salts or acids, such as potassium hydroxide or sulfuric acid) in a poor/non-conductive solvent (e.g., water). Non-liquid examples are PEO plastics that have been doped with lithium salts, or various ceramics or glasses doped with sodium or lithium oxides and hydroxides. Liquid, non-aqueous electrolytes are limited to molten, ionic salt mixtures, which require no additives to improve conductivity (usually operated at high temperatures), or mixtures of covalent organic or inorganic solvents, which require the addition of ionic salt additives.

ENERGY DENSITY – The quantity of energy stored by a battery per unit weight or unit volume; typical units include watt-hours per pound or watt-hours per cubic inch. To be most useful, energy densities must be measured at a specific discharge rate and temperature.

ENERGY DISPERSIVE ANALYSIS WITH X-RAYS (EDAX) – A variant of X-ray fluorescence spectroscopy used for chemical characterization of a sample via a high-energy beam of charged particles focused onto the sample.

F

FOURIER TRANSFORM (FT) – Transformation of one complex-valued function of a real variable into another. FT decomposes a function into rhythmic functions and refers to both frequency domain and the formula for transforming one function into another.

FOURIER TRANSFORM INFRARED SPECTROSCOPY (FTIR) – A measurement technique where spectra are collected based on measurements of radiative sources. The term reflects that an FT is required to turn raw data into the actual spectrum.

FULL-SCALE BATTERY – For the purposes of this manual, a full-scale battery is a complete battery system as it would be employed in its intended system, including all of its cells, intermediate-level groupings, electronics, wiring, housing, safeties, and mitigations.

FULL-SCALE BCCT – Battery Casualty Characterization Tests conducted with full-scale batteries.

H

HAZARD RISK INDEX (HRI) – Estimates based on structured analysis of hazard severity and failure probability, ranked and compared with the standard Hazard Risk Matrix to arrive at an HRI value.

HIGH ENERGY CHEMICAL STORAGE SAFETY OFFICE (HECSSO) – The office established within NAVSEA 05 (SEA 05Z34) to specifically address safety aspects of large lithium batteries and other energy-dense systems.

HIGH ENERGY SYSTEM SAFETY STEERING GROUP (HESSSG) – An executive oversight group whose members include selected NAVSEA major program managers and deputy warranting officers. The group meets on a semi-annual basis to assess status and progress of HECSSO efforts.

I

INFRARED SPECTROSCOPY – The study of the interaction of matter with an infrared radiation, using electromagnetic waves from the long-wavelength limit of visible light (800 nm) to the shortest microwaves (1mm).

LIST OF DEFINITIONS (Cont)

I (Cont)

INTERMEDIATE-LEVEL/GROUPING – For the purposes of this manual, this is an intermediate-level battery or grouping consisting of a packaged collection of cells, multiples of which are necessary to create a full-scale battery. May also be called modules, submodules, or LRUs.

INTERNAL INDEPENDENT PEER REVIEW TEAM (IIPRT) – An independent peer review composed of Navy technical experts in energy systems and safety who are not directly affiliated with HECSSO.

IN SERVICE ENGINEERING AGENT (ISEA) – The maintenance activity for electronic, ordnance, and HM&E systems and equipment engineering support.

K

KINETIC ENERGY – Energy needed to accelerate the body of a given mass from rest to its current velocity.

L

LOWEST REPLACEABLE UNIT (LRU) – For the purposes of this manual, an LRU is the smallest collection of cells or intermediate-level battery that can be replaced during O-Level maintenance.

M

MAINTENANCE – Any service or upkeep required to repair and/or re-evaluate the battery or system and its performance, including but not limited to non-operational charging, discharging, physical inspection, disassembly, reassembly, and calibration of BMS components.

MASS SPECTROMETRY (MS) – Analytical technique that measures the mass-to-charge ratio of charged particles to determine particle mass or elemental composition of a sample or molecule, and for detailing the chemical structure of molecules in chemical compounds.

MITIGATION VERIFICATION TEST – Verification of the effectiveness of platform-level mitigation strategies and capabilities such as detection/alarms, automatic extinguishment/control, isolation/segregation, and casualty response procedures.

N (Cont)

NON-OPERATIONAL TRANSPORT – Movement of the battery or system from one location to another while in a non-operating state.

O

OBJECTIVE QUALITY EVIDENCE (OQE) – A statement of face – either quantitative or qualitative – pertaining to the quality of a product or service, based on observation, measurement, or tests that can be verified.

P

PLATFORM – A vessel owned or leased by the Navy. Specifically excluded are range support craft operating within U.S. territorial waters. Platform impact includes situations where the Navy platform is host to ancillary vehicles containing large lithium batteries.

PLATFORM-LEVEL HAZARD MITIGATION AND VERIFICATION TESTS (HMT) – Tests conducted after the BCCT tests have determined the hazard to the platform in order to assess the effectiveness of the platform's mitigation techniques.

PLATFORM INTEGRATION AGENT (PIA) – Provides project oversight for systems containing lithium batteries for use on Navy platforms. Unless specifically approved by NAVSEA 05Z34, the PIA is the platform major program office in NAVSEA.

PRESSURE-RELEASE DEVICE – A failure-point mechanism designed to prevent material failure of the battery housing by releasing controlled volumes of gas.

PRIMARY BATTERY – A battery designed to be discharged only once (i.e., it is NOT designed to be recharged). Also called a non-rechargeable battery.

PROPAGATION – When the failure of a single cell or battery leads to the failure of neighboring cells or batteries, most commonly because of thermal or electrical energy transfer, known as cascading.

R

RADIOGRAPHY – Technique for producing photographic interior images or opaque specimens through radiation by gamma ray, X-ray, neutrons, or changed particles.

S

SAFETY CRITICAL CRITERIA (SCC) – Criteria defined by the program office and NAVSEA 05 that must be met to mitigate safety hazards and the severity of a mishap.

SCANNING ELECTRON MICROSCOPY (SEM) – A type of electron microscope that images the sample surface by scanning with a high-energy beam of electrons in a raster scan (rectangular) pattern.

SECONDARY BATTERY – A battery in which the electrochemical reaction is thermodynamically reversible and is designed to be recharged after use. May also be referred to as a rechargeable battery.

SOFTWARE SAFETY ACTIVITY (SSA) – Responsible for assessing the safety level and severity of software applications associated with lithium batteries and their systems. The SSA maintains configuration control of the software and works with program management in assessing changes to the software and the need for future upgrades and testing of associated battery software.

SPECIFIC ENERGY – The ratio of the energy output of a cell or battery to its weight (see Energy Density).

STORAGE – Stowage of a battery system or systems in the designated area on the naval vessel while not in use.

SYSTEM DEVELOPER – The prime activity in the design, building, and integration of systems that include large lithium batteries.

SYSTEM-LEVEL BCCT – BCCT tests conducted with a full-scale battery configured on its intended system, or a representative mock-up thereof.

T

TEST ACTIVITY – The organization assigned with testing large lithium batteries and their components to characterize hazards associated with battery failure. The test activity may be assigned to be the system developer, warfare center, or independent activity.

THERMAL RUNAWAY – Any discharge or charge condition in which a battery's internal temperature buildup continues until a cell/battery failure occurs. Typical causes of thermal runaway events can be forced discharge of electrodes that are insufficiently wetted by electrolyte, or excessive discharge currents, as in an internal or external short circuit.

TEST PLAN (TP) – A document that specifies battery system testing required to mitigate risks as defined in the PHA and SHA.

U

USE – The action of exercising the battery or system, including but not limited to operational periods such as charge, discharge, open circuit periods, or operational transport.

W

WORST CREDIBLE EVENT (WCE) – The event that combines maximum severity with highest probability.

X

X-RAY DIFFRACTION (XRD) – The scattering of X-rays by matter, with accompanying variation in intensity due to interference effects. Used in solid-state chemistry to determine atomic arrangements in matter.

X-RAY TOMOGRAPHY – The use of energy waves to generate images on the inside of objects from a series of two-dimensional X-ray images taken around a single axis of rotations